

---

# Mechanistic Investigation of the Diastereodivergent Asymmetric Allylic Alkylation of Cyclobutenes

---

## Mechanistische Untersuchung der Diastereodivergenten Asymmetrischen Allylischen Alkylierung von Cyclobutenen

Zur Erlangung des Grades eines Doktors der Naturwissenschaften (Dr. rer. nat.)

genehmigte Dissertation von Johann Julius Primozic aus Berlin

Tag der Einreichung: 30. Oktober 2023, Tag der Prüfung: 18. Dezember 2023

Darmstadt – D 17

1. Gutachten: Prof. Dr. Christina M. Thiele (Technische Universität Darmstadt)
  2. Gutachten: Prof. Dr. Dorian Didier (Technische Universität Darmstadt)
  3. Gutachten: Prof. Dr. Nuno Maulide (Universität Wien)
- 



TECHNISCHE  
UNIVERSITÄT  
DARMSTADT

Fachbereich Chemie  
Clemens-Schöpf-Institut für  
Organische Chemie und Biochemie

---

Mechanistic Investigation of the Diastereodivergent Asymmetric Allylic Alkylation of Cyclobutenes  
Mechanistische Untersuchung der Diastereodivergenten Asymmetrischen Allylischen Alkylierung von  
Cyclobutenen

Genehmigte Dissertation von Johann Julius Primozic aus Berlin

1. Gutachten: Prof. Dr. Christina M. Thiele (Technische Universität Darmstadt)
2. Gutachten: Prof. Dr. Dorian Didier (Technische Universität Darmstadt)
3. Gutachten: Prof. Dr. Nuno Maulide (Universität Wien)

Tag der Einreichung: 30. Oktober 2023

Tag der Prüfung: 18. Dezember 2023

Darmstadt – D 17

Darmstadt, Technische Universität Darmstadt

Jahr der Veröffentlichung der Dissertation auf TUpriints: 2024

© Alle Rechte vorbehalten.



---

*Junge,  
Warum hast du nichts gelernt?  
Guck dir den Dieter an,  
Der hat sogar ein Auto.*

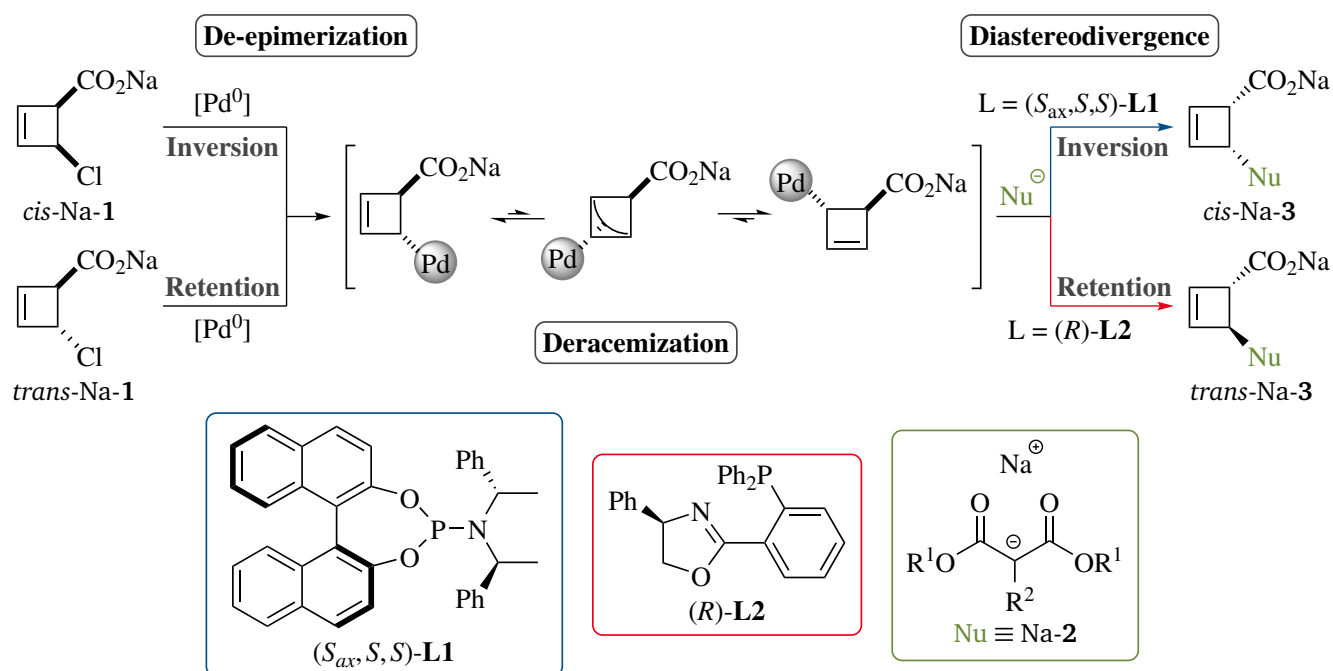
Die Ärzte – Junge

---



# Abstract

The Pd-catalyzed asymmetric allylic alkylation of cyclobutenes **1** with stabilized nucleophiles Na-**2** represents a unique example of a diastereodivergent deracemization and de-epimerization. In the present work, a comprehensive mechanistic analysis is reported, encompassing the preparation of putative Pd-allyl intermediates,  $^1\text{H}/^{31}\text{P}$ -NMR reaction monitoring,  $^2\text{H}$ -labeling studies, ESI-HRMS analysis of reaction mixtures, kinetic rate order determination, and  $^2\text{H}/^{13}\text{C}$ -KIE studies. As a result, an unprecedented mechanistic scenario with a stereochemical dichotomy for both oxidative addition and nucleophilic attack is proposed. Oxidative addition exhibits a convergent course, allowing for de-epimerization of *cis/trans*-**1** to a rapidly interconverting mixture of  $\eta^1$ - and  $\eta^3$ -coordinated Pd-allyl intermediates with the  $\eta^1$ -species as resting states of the reaction. This suprafacial  $\eta^1$ - $\eta^3$ - $\eta^1$  equilibrium enables deracemization via a dynamic kinetic asymmetric transformation type I. Nucleophilic attack of Na-**2** displays a ligand-controlled divergent behavior, establishing a diastereodivergent access to enantioenriched products *cis/trans*-**3**.



Die Pd-katalysierte asymmetrische allylische Alkylierung von Cyclobutensubstraten **1** mit stabilisierten Nucleophilen Na-**2** stellt ein einzigartiges Beispiel für eine diastereodivergente Deracemisierung und Deepimerisierung dar. In der vorliegenden Arbeit wird eine umfangreiche mechanistische Studie vorgestellt. Diese beinhaltet die Synthese mutmaßlicher Pd-Allylintermediate, Reaktionsverfolgung mittels  $^1\text{H}$ - und  $^{31}\text{P}$ -NMR, Experimente mit  $^2\text{H}$ -markierten Edukten, ESI-HRMS-Untersuchungen der Reaktionsmischungen, die Bestimmung kinetischer Reaktionsordnun-

---

gen sowie die Ermittlung von  $^2\text{H}$ - und  $^{13}\text{C}$ -KIEs. Basierend auf den Ergebnissen dieser Experimente wird ein beispielloses mechanistisches Szenario mit einer stereochemischen Dichotomie sowohl für die oxidative Addition als auch für den Angriff des Nucleophils vorgeschlagen. Die oxidative Addition weist dabei ein konvergentes Verhalten auf, wodurch die Deepimerisierung von *cis/trans*-**1** zu einer im schnellen Gleichgewicht stehenden Mischung aus  $\eta^1$ - und  $\eta^3$ -koordinierten Pd-Allylintermediaten mit den  $\eta^1$ -Spezies als Ruhezustand ermöglicht wird. Basierend auf diesem suprafacialen  $\eta^1\text{-}\eta^3\text{-}\eta^1$  Gleichgewicht wird die Deracemisierung von **1** über eine dynamisch-kinetische asymmetrische Umwandlung Typ I erreicht. Der nukleophile Angriff durch Na-**2** zeigt ein divergentes Verhalten, welches durch den Liganden kontrolliert wird und dadurch den Zugang zu enantiomerenangereicherten Produkten *cis/trans*-**3** eröffnet.

---

# List of Publications

Parts of this work have been submitted for publication or presented at international conferences.

## Research Articles

- J. J. Primožič, J. Ilgen, P. Maibach, M. Brauser, J. Kind, C. M. Thiele, **Pd-Catalyzed Asymmetric Allylic Alkylation of Cyclobutenes: From Double Inversion to Double Retention**, *J. Am. Chem. Soc.* **2023**, *145*, 15912–15923, DOI 10.1021/jacs.3c03590.

## Poster Presentations

- J. J. Primožič, C. M. Thiele, **Diastereodivergent Asymmetric Allylic Alkylation of Cyclobutenes: Kinetics and HPLC-MS Studies**, *International Symposium on Synthesis and Catalysis*, Évora/Portugal, **09/21**.
- J. J. Primožič, J. Ilgen, P. Maibach, C. M. Thiele, **Diastereodivergent Asymmetric Allylic Alkylation of Cyclobutenes: A Challenging Mechanistic Puzzle**, *Balticum Organicum Syntheticum*, Vilnius/Lithuania, **07/22**.
- J. Ilgen, J. J. Primožič, P. Maibach, M. Brauser, J. Kind, C. M. Thiele, **NMR Spectroscopic Investigation reveals Insights into the Mechanism of a unique Pd-Catalyzed Allylic Alkylation**, *SMASH*, Baveno/Italy, **09/23**.



---

# Acknowledgements

Intensive five years of Ph.D. studies are coming to an end, which have been marked by various different impressions and emotions, ranging from joy and motivation to frustration and exhaustion. Fortunately, I was never walking alone during this time, and many people have given me their support, both scientifically and mentally.

First and foremost, I am obliged to PROF. DR. CHRISTINA THIELE for giving me the chance to do my Ph.D. in her group. Thank you for the many in-depth discussions and for valuing my work. Moreover, I am grateful to the Fonds der Chemischen Industrie for financial support by awarding a Ph.D. fellowship to me.

I would furthermore like to express my gratitude to DR. VOLKER SCHMIDTS for his guidance and patience when I was struggling at the spectrometer or when my poor IT knowledge had come to its limits again. Please keep your constant kindness, helpfulness and openness, that make you the heart and soul of the group.

Many of my experiments required unconventional reaction conditions or challenging characterization techniques, that made me stuck more than one time. It was the invaluable advice by DR. JASON WILLIAMS (University of Graz) and DR. GUILHEM COUSSANES (University of Vienna) that enabled me to finally achieve the synthesis of cyclobutene substrates after a long trial-and-error process. The performance of sophisticated mass spectrometry analyses was only possible thanks to the great service of our routine measuring department operated by DR. ALEXANDER SCHIESSER and CHRISTIANE RUDOLPH. Furthermore, I would like to thank DR. JÖRG ENGSTLER for his kind help in realizing IR spectroscopic measurements under challenging conditions, and DR. CHRISTIAN RICHTER (Goethe University Frankfurt) for enabling me to spend two days at the Center for Biomolecular Magnetic Resonance to perform external measurements.

My Ph.D. project has strongly benefited from contributions by my colleagues DR. JULIAN ILGEN, DR. JONAS KIND and MATTHIAS BRAUSER, master students PATRICK MAIBACH and SONJA DÖLLER as well as project students PATRICK MANN and CARL VORBRUEGGEN. Thank you for your creativity, commitment and hard work.

I must extend my gratitude to all the other past and present members of the THIELE group: MICHAEL GÖLZ and RIMJHIM HOSSAIN for being a great company in the lab, JAN RETTIG and LUKAS LAUX for fun conversations and competent scientific advice, CHRISTOPHER ROSS for his broad technical knowledge and support, KILIAN HECKENBERGER for the shared passion for music, DR. MAX HIRSCHMANN, DR. MARCEL ALCARAZ JANSSEN, DR. DOMINIC SCHIRRA and DR. KEVIN KNOLL for initial help and guidance during my first months in the lab, SANDRA PACKMOHR and LAURA WERNER for keeping tiring paperwork away from us, and DOMINIK HEROLD, JENS NOWAG, EMANUELA BUA,

---

DR. MIRA SCHWAB, DR. FELIX ROTH, DR. MARTIN LEYENDECKER, DR. SHARON JEZIOROWSKI and SUSANN WEISSHEIT for enjoyable lunch breaks and group activities.

During my Ph.D., I could always rely on the strong mental support by my family and friends. I would like to thank my parents JANA and FRANK PRIMOZIC, my siblings JULIA LINGENBERG and JUSTUS PRIMOZIC, and my friends LOUNES MESSAOUDI, FLORIAN STAUBACH and MICHAEL MONATH for making my spare time enjoyable, thus helping me to unwind from my scientific problems. My deepest gratitude, however, goes to my fiancée and closest confidant LAURA KELLER. Thank you for your understanding when I had to stay longer in the lab and for listening to me when I needed someone to talk. You are the most important person in my life.



---

# Contents

<b>1</b>	<b>Introduction</b>	<b>1</b>
<b>2</b>	<b>State of the Art</b>	<b>5</b>
2.1	Transition Metal Catalyzed Allylic Substitution: General Considerations . . . . .	5
2.2	Regioselectivity and Memory Effects in Allylic Substitution Chemistry . . . . .	7
2.2.1	Influence of the Substrate Structure . . . . .	8
2.2.2	Influence of the Transition Metal . . . . .	10
2.2.3	Influence of Chloride Ions . . . . .	12
2.3	Stereospecificity of Allylic Substitutions . . . . .	14
2.3.1	Unbiased Stereospecificity . . . . .	14
2.3.2	Loss and Manipulation of Stereospecificity . . . . .	17
2.4	Enantioselectivity in Allylic Substitution Chemistry . . . . .	21
2.4.1	General Mechanisms of Enantiodiscrimination . . . . .	21
2.4.2	Key Interactions . . . . .	27
2.5	Allylic Substitution of Cyclobutenes . . . . .	31
<b>3</b>	<b>Motivation and Aims</b>	<b>39</b>
<b>4</b>	<b>Results and Discussion</b>	<b>43</b>
4.1	Synthesis of Starting Materials . . . . .	43
4.1.1	On the Preparation of Cyclobutene Substrates . . . . .	43
4.1.2	On the Preparation of Malonate Nucleophiles . . . . .	47
4.2	Stereoselectivity of Oxidative Addition and Nucleophilic Attack ( <i>Publication</i> ) . . .	49
4.3	Steric Influence of Nucleophile . . . . .	184
4.4	Towards the Possibility of an Inner-Sphere Mechanism for Nucleophilic Attack . .	186
4.5	Kinetic Analysis . . . . .	188
4.5.1	Model Reaction and Quantitative Reaction Monitoring . . . . .	188
4.5.2	Initial Rate Analysis . . . . .	191
4.5.3	Reaction Progress Kinetic Analysis (RPKA) . . . . .	199
4.5.4	Summary of Kinetic Analysis . . . . .	206
4.6	Kinetic Isotope Effects (KIEs) . . . . .	208
4.6.1	$^2\text{H}$ -KIEs for Allylic System by LC-MS Monitoring . . . . .	209
4.6.2	Relative $^2\text{H}$ -KIEs for Allylic System by $^1\text{H}$ -NMR Monitoring . . . . .	214

---

4.6.3	$^{13}\text{C}$ -KIEs for Nucleophile by $^{13}\text{C}$ -NMR Monitoring . . . . .	216
4.6.4	Summary of Kinetic Isotope Effect Studies . . . . .	220
4.7	Discussion of the Mode of Nucleophilic Attack . . . . .	224
<b>5</b>	<b>Conclusion and Outlook (<i>English</i>)</b>	<b>229</b>
<b>6</b>	<b>Zusammenfassung und Ausblick (<i>Deutsch</i>)</b>	<b>233</b>
<b>7</b>	<b>Experimental Part</b>	<b>239</b>
7.1	Synthesis of Malonates . . . . .	239
7.2	Allylic Alkylation Reactions . . . . .	246
7.3	Investigation of the Nucleophilic Nature of Malonate Nucleophiles . . . . .	256
7.4	Kinetic Analysis . . . . .	258
7.5	Determination of KIEs . . . . .	261
7.5.1	$^2\text{H}$ -KIEs by offline LC-MS Monitoring . . . . .	261
7.5.2	Relative $^2\text{H}$ -KIEs by offline $^1\text{H}$ -NMR Monitoring . . . . .	263
7.5.3	$^{13}\text{C}$ -KIEs by offline $^{13}\text{C}$ -NMR Monitoring . . . . .	264
	<b>Bibliography</b>	<b>267</b>
	<b>List of Abbreviations</b>	<b>293</b>
	<b>List of Figures</b>	<b>295</b>
	<b>List of Schemes</b>	<b>297</b>
	<b>List of Tables</b>	<b>301</b>

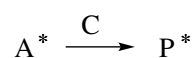
# 1 Introduction

The *in vivo* effect of biologically active compounds such as pharmaceuticals<sup>[1]</sup> or agrochemicals<sup>[2]</sup> often significantly depends on the three-dimensional structure, and two stereoisomers may at times even hold antithetic<sup>[3,4]</sup> properties. Hence, rigid stereocontrol is of pivotal importance for the synthesis of those compounds.

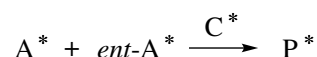
The selective preparation of diastereomers is, in theory, straightforward, due to an energetic difference of the competing diastereomorphous transition states (kinetic control) and the downstream diastereomeric products (thermodynamic control). Thus, diastereoselectivity can in many cases be achieved by appropriate choice of standard parameters such as temperature, solvent polarity or the steric and electronic properties of substrate and reagents.<sup>[5,6]</sup>

The synthesis of enantiomerically pure compounds, on the other hand, often requires more sophisticated approaches. From a strategic point of view, optically active products can be accessed by ex-chiral-pool synthesis (i.e. the use of an enantiomerically pure natural product as starting material),<sup>[7-9]</sup> the resolution of a racemic precursor,<sup>[10-12]</sup> or asymmetric synthesis (i.e. the stereoselective construction of a stereogenic unit using an achiral precursor),<sup>[13-15]</sup> as outlined in Scheme 1.1. The ex-chiral-pool strategy is only attractive if the synthetic route starting from a readily available enantiopure natural product such as an amino acid,<sup>[16,17]</sup> a carbohydrate,<sup>[18]</sup> or a terpene<sup>[19]</sup> is straightforward and does not involve a large number of additional steps compared to the corresponding racemic synthesis. Moreover, many chiral pool materials are only available in one absolute configuration, with the enantiomeric form – if accessible at all – requiring an additional inversion sequence.

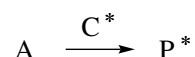
(a) Ex-chiral-pool Synthesis



(b) Resolution of a Racemate



(c) Asymmetric Synthesis



**Scheme 1.1:** General strategies for the synthesis of optically active products P\*: (a) Ex-chiral-pool synthesis using an enantiomerically pure natural product A\* as starting material; (b) resolution of a racemic mixture of enantiomeric precursors A\* and *ent*-A\*; (c) asymmetric synthesis starting from an achiral substrate A. The latter two approaches imply the use of a chiral, non-racemic catalyst or reagent C\*.

---

Therefore, the development of methods enabling late-stage enantioenrichment by resolution of racemic mixtures or asymmetric induction into achiral scaffolds has received considerable attention over the last decades.<sup>[20]</sup> The obvious drawback of classical racemate resolution techniques, that is, a maximum yield of 50 % by selective conversion of only one substrate enantiomer,<sup>[21]</sup> has been overcome by establishing alternative resolution approaches such as dynamic kinetic resolutions (DKRs)<sup>[22,23]</sup> and dynamic kinetic asymmetric transformations (DYKATs),<sup>[24–27]</sup> allowing for quantitative conversion of a racemic mixture into a single enantiomer.<sup>[28–30]</sup>

Asymmetric synthesis has become popular with the advent of chiral auxiliaries pioneered by EVANS.<sup>[31–35]</sup> This now well-established strategy requires pre-installation of a chiral function such as an oxazolidinone,<sup>[36]</sup> which allows for achieving enantioselectivity under substrate control and can be cleaved in the subsequent step.<sup>[37]</sup> As this sequence, however, requires additional protection/deprotection steps and stoichiometric amounts of the auxiliary, modern approaches rely on asymmetric induction under reagent or, more sustainable and cost-efficient, catalyst control,<sup>[20]</sup> thus aligning better with the principles of green chemistry<sup>[38,39]</sup> by maximizing the atom economy<sup>[40]</sup> and avoiding derivatization steps. A plethora of chiral, non-racemic catalysts such as enzymes,<sup>[41]</sup> organocatalysts<sup>[42]</sup> and transition metal complexes<sup>[43–46]</sup> has been developed, opening access to various chiral target structures via sustainable and cost-efficient routes.<sup>[47]</sup> While enzymes and many organocatalysts can be readily prepared from renewable feedstocks, their use is often limited to mild reaction conditions, a rather narrow range of substrates and only one kind of transformation. In contrast, transition metal based chiral catalysts, composed of a metal center and an enantiopure ligand, usually feature a better thermal and chemical robustness as well as a higher synthetic versatility, enabling use of the same catalyst for different reactions with an increased range of compatible substrates.

The development of modern catalytic asymmetric or deracemization protocols requires sound mechanistic understanding, ideally allowing for rational design rather than tedious trial-and-error approaches. In the field of enantioselective transition metal catalysis, allylic substitution has been established as a benchmark reaction for catalyst design, given the large number of highly selective asymmetric variants developed.<sup>[43,48]</sup> The reaction generally proceeds with a high level of chemo-, regio- and diastereoselectivity, and the intermediacy of a  $\eta^3$ -allyl complex readily allows for resolution of racemic (i.e. via a DYKAT),<sup>[24,49,50]</sup> or regioisomeric<sup>[51–53]</sup> substrates. According to the generally accepted mechanistic picture, enantioselectivity is controlled by the ligand, while diastereoselectivity is determined by the substrate's relative configuration and the electronic nature of the nucleophile.<sup>[54]</sup>

A highly remarkable exception from the established stereochemical mechanism of allylic substitution has been developed by MAULIDE and coworkers<sup>[55,56]</sup> using racemic cyclobutene substrates. This protocol allows for controlling diastereo- and enantioselectivity only by the choice of ligand and independent of the configuration of substrate, thus displaying the characteristics of a *diastereodivergent deracemization* and *de-epimerization*. Previous mechanistic studies have shone light

---

on the spatial structure of putative intermediates,<sup>[57,58]</sup> however, the origin of stereinduction remained speculative. In this work, a comprehensive mechanistic study is presented, aiming to disclose an overarching mechanism and to fully elucidate the driving forces responsible for stereoselectivity. The insights generated by this study may help synthetic organic chemists to design novel highly selective transition metal catalyzed reactions, thus enriching the toolbox of methods for the preparation of valuable chiral building blocks.

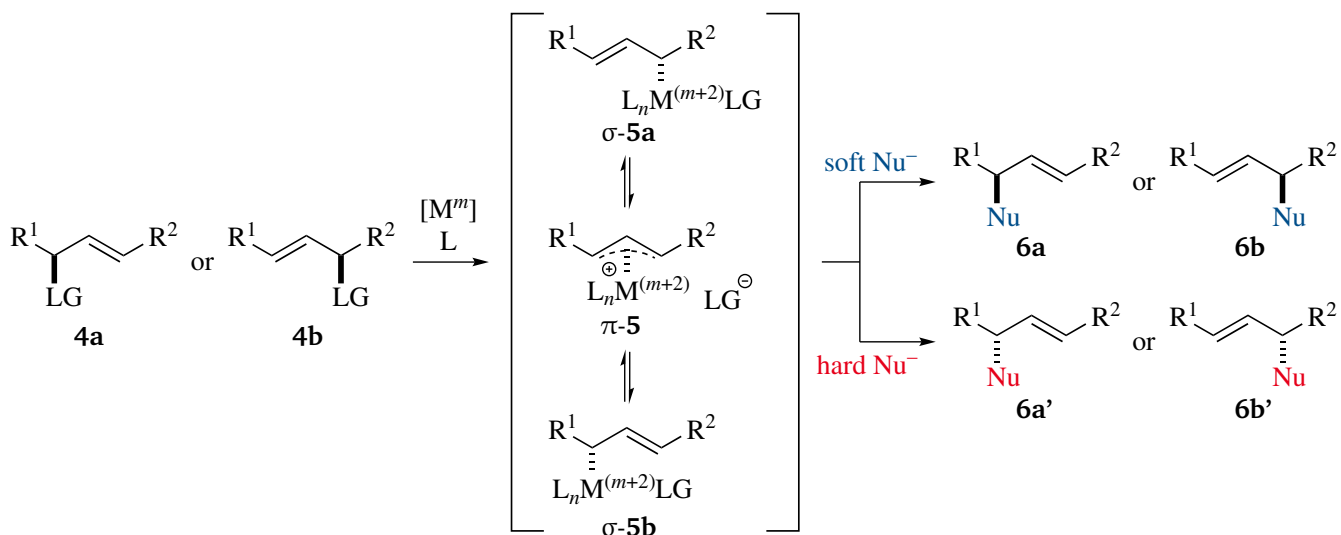


## 2 State of the Art

In this chapter, the allylic substitution chemistry relevant to this work will be outlined, centering on Pd-catalyzed variants as well as the use of soft nucleophiles. In particular, stereospecificity and stereoselectivity questions will be addressed.

### 2.1 Transition Metal Catalyzed Allylic Substitution: General Considerations

The transition metal catalyzed allylic substitution is a versatile methodology for the introduction of nucleophiles into allylic systems.<sup>[48,59,60]</sup> As shown in Scheme 2.1, the reaction proceeds from an allylic electrophile **4** undergoing oxidative addition to form an intermediate Pd complex **5**, which can readily interconvert between one or several, usually cationic  $\eta^3$ -coordinated species  $\pi$ -**5** and the corresponding  $\eta^1$ -bond species  $\sigma$ -**5a** and  $\sigma$ -**5b**.<sup>[61–65]</sup> For coordinating leaving groups such as chloride, additional  $\eta^3$ -species are possible where the leaving group occupies a coordination site (see also section 2.2.3).<sup>[66,67]</sup> Oxidative addition might be reversible<sup>[68,69]</sup> or irreversible,<sup>[70,71]</sup> depending on substrate structure and reaction conditions. Subsequent attack of a nucleophile  $\text{Nu}^-$  can furnish two regioisomeric products **6a** and **6b** (if  $R^1 \neq R^2$ ). The regioselectivity of this step is mainly determined by steric and electronic properties of substrate and ligand,<sup>[72,73]</sup> which will be outlined in more detail in section 2.2. As further described in section 2.3, the reaction exhibits overall retention of configuration with stabilized (“soft”)



**Scheme 2.1:** General reaction scheme of a transition metal catalyzed allylic substitution proceeding via complexes **5** as intermediates, with stereospecificities as usually observed.  $R^i$  denote organic moieties or hydrogen atoms,  $[M^m]$  is the catalyst precursor in the oxidation state  $m$ , and  $L$  represents the ligand employed.

nucleophiles, whereas inversion of configuration is observed when using non-stabilized (“hard”) nucleophiles.<sup>[54]</sup>

The leaving group (LG) is typically a carboxylate moiety such as acetate.<sup>[74–76]</sup> In addition, allylic halides<sup>[77,78]</sup> and carbonates<sup>[79–81]</sup> are common substrates as well. Apart from these readily reacting electrophiles, the use of unactivated substrates such as allylic alcohols,<sup>[82–85]</sup> ethers<sup>[85,86]</sup> and amines<sup>[87,88]</sup> has received increasing attention. These usually more stable and easier available starting materials require the presence of an activator (e.g. a LEWIS or BRØNSTED acid) to generate the reactive leaving group *in situ*.<sup>[89,90]</sup>

In its archetypal version, the reaction is performed under Pd catalysis, which has remained the most employed metal in allylic alkylation chemistry.<sup>[91,92]</sup> Alternatively, Ir,<sup>[93,94]</sup> Mo,<sup>[95,96]</sup> Rh,<sup>[97]</sup> Ru,<sup>[98]</sup> Cu,<sup>[99]</sup> Fe,<sup>[100]</sup> W,<sup>[96]</sup> Ni,<sup>[101]</sup> Co<sup>[102]</sup> and Pt<sup>[103]</sup> catalysts have been established. The choice of ligand is of pivotal importance for regio- and stereoselectivity. Most commonly, a monodentate organophosphorus(III) compound (e.g. a phosphine)<sup>[104]</sup> or a bidentate *P,P*<sup>[105]</sup> or *P,N*<sup>[106]</sup> ligand is employed. The application of chiral, non-racemic ligands allows for rendering the reaction asymmetric.

Most attention has been devoted to the use of C-centered nucleophiles like malonates,<sup>[74,76,81]</sup> enolates<sup>[107]</sup> or organometallics.<sup>[78,108,109]</sup> In this case, the reaction is more specifically termed as *allylic alkylation*, or TSUJI–TROST<sup>[110,111]</sup> reaction. Also, N-,<sup>[112,113]</sup> O-,<sup>[114,115]</sup> S-<sup>[116,117]</sup> or P-centered<sup>[118]</sup> heteroatom nucleophiles are compatible with this methodology.<sup>[119]</sup> The vast majority of allylic substitution procedures utilizes stabilized nucleophiles.<sup>[43,48]</sup> Conversely, the successful use of non-stabilized nucleophiles is more challenging, as they tend to undergo problematic side reactions such as  $\beta$ -hydride elimination.<sup>[120–122]</sup>

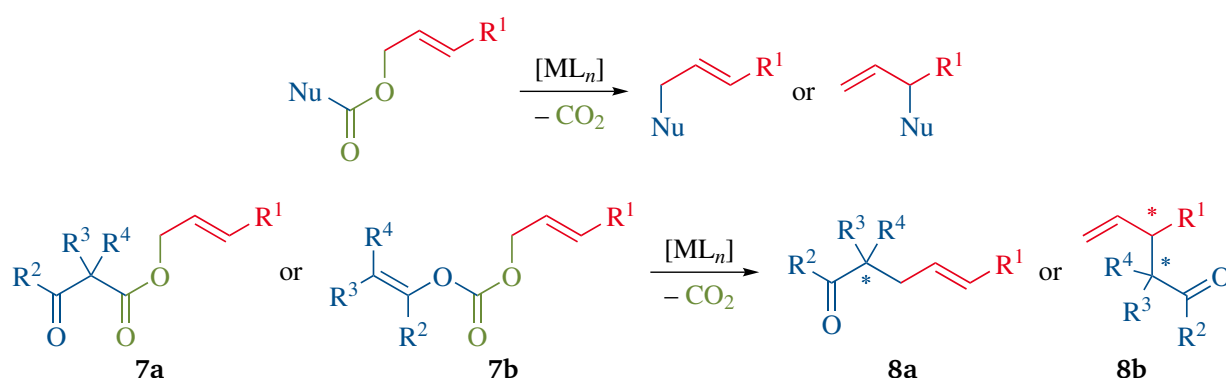
The  $\eta^3$ -coordinated oxidative addition products are usually lower in energy than their  $\eta^1$ -isomers. Various NMR spectroscopic, X-ray crystallographic and DFT computational studies have gained detailed insight into the structure of  $\eta^3$ -Pd-allyl complexes.<sup>[123–130]</sup> Exceptions where the  $\eta^1$ -species are energetically favored have been reported for complexes bearing pincer ligands.<sup>[131,132]</sup> Also, bidentate *P,N* ligands<sup>[133–135]</sup> or strained allylic systems such as cyclobutenes<sup>[57,58]</sup> can increase the relative stability of the  $\eta^1$ -complexes rendering them detectable.

For most metals including palladium, the intermediate  $\eta^3$ -species are considered as the reactive electrophile attacked by the nucleophile, whereas the isomeric  $\eta^1$ -complexes have been evidenced to be unreactive towards common nucleophiles.<sup>[66,136]</sup> Exceptions have been reported for amines as nucleophiles, which have been shown to directly react with  $\eta^1$ -coordinated Pd species via slow  $S_N2'$ -type displacement,<sup>[137,138]</sup> albeit at an approximately 100 times lower rate than the corresponding  $\eta^3$ -species.<sup>[137]</sup> In the presence of electrophiles,  $\eta^1$ -Pd species have been demonstrated to exhibit strongly nucleophilic behavior.<sup>[139,140]</sup> For Rh- and Fe-catalyzed allylic substitutions, on the other hand, conclusive experimental evidence has been reported for  $\eta^1$ -species being highly reactive electrophiles, undergoing facile displacement with various types of



soft nucleophiles.<sup>[141–144]</sup> The implications on the regio- and stereoselectivity of these systems is further described in sections 2.2 and 2.4.

For non-stabilized enolates, which have long been deemed as challenging nucleophiles in allylic alkylation chemistry,<sup>[145]</sup> yield and stereoselectivity can be drastically enhanced by making the enolate part of a carboxylate leaving group, rendering the reaction a decarboxylative process. As shown in Scheme 2.2, this variant typically converts an un- or  $\gamma$ -substituted allyl  $\beta$ -keto-carboxylate **7a** or allyl vinyl carbonate **7b** to rearranged products **8** upon cleavage of CO<sub>2</sub>, with *in situ* generation of the enolate nucleophile.<sup>[146]</sup> The use of prochiral enolate units in combination with a chiral, non-racemic ligand allows for construction of all-carbon stereocenters, which has emerged as a valuable strategy in for enantioselective natural product synthesis.<sup>[147]</sup>

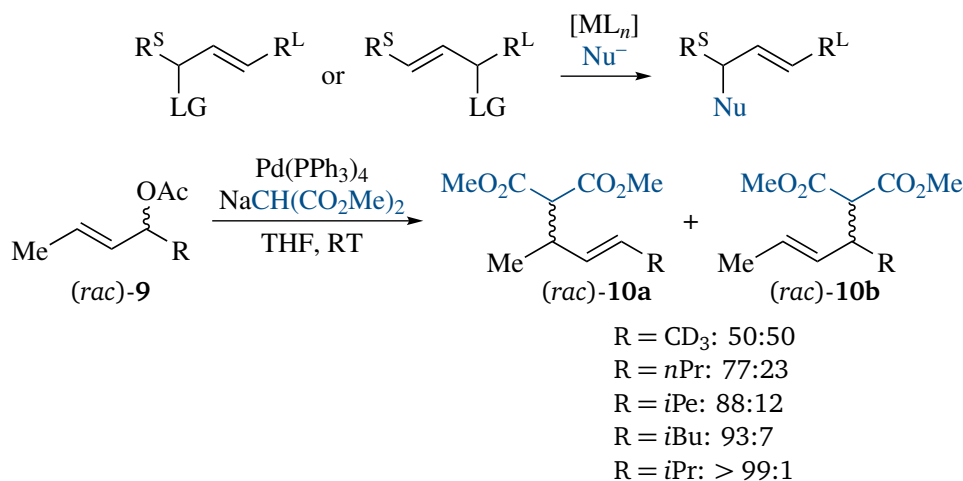


**Scheme 2.2:** Transition metal catalyzed decarboxylative allylic substitution: General reaction scheme (top) and most common variant (bottom). R<sup>i</sup> denote organic moieties or hydrogen atoms, [M] is the catalyst precursor and L represents the ligand employed.

This section has provided an introductory glance on the wide chemistry of allylic substitution reactions. The general structure of electrophile, intermediates and products has been introduced, and a preliminary overview of compatible transition metals, ligands and nucleophiles has been given. It has already been mentioned that the control of regio- and stereoselectivity is of particular interest in allylic substitution chemistry. Therefore, these issues will be discussed in more detail in the following subchapters.

## 2.2 Regioselectivity and Memory Effects in Allylic Substitution Chemistry

As has been outlined in the previous section, the allylic substitution usually proceeds via a  $\eta^3$ -complex  $\pi$ -5 as electrophilic intermediate, the formation of which acts as a scrambling event for the allylic termini.<sup>[148]</sup> This implies that for unsymmetrically substituted allylic systems regioisomeric products are possible. In this subchapter, the factors determining the regioselectivity will be discussed. Additionally, instances where full or partial regiospecificity is observed will be presented.

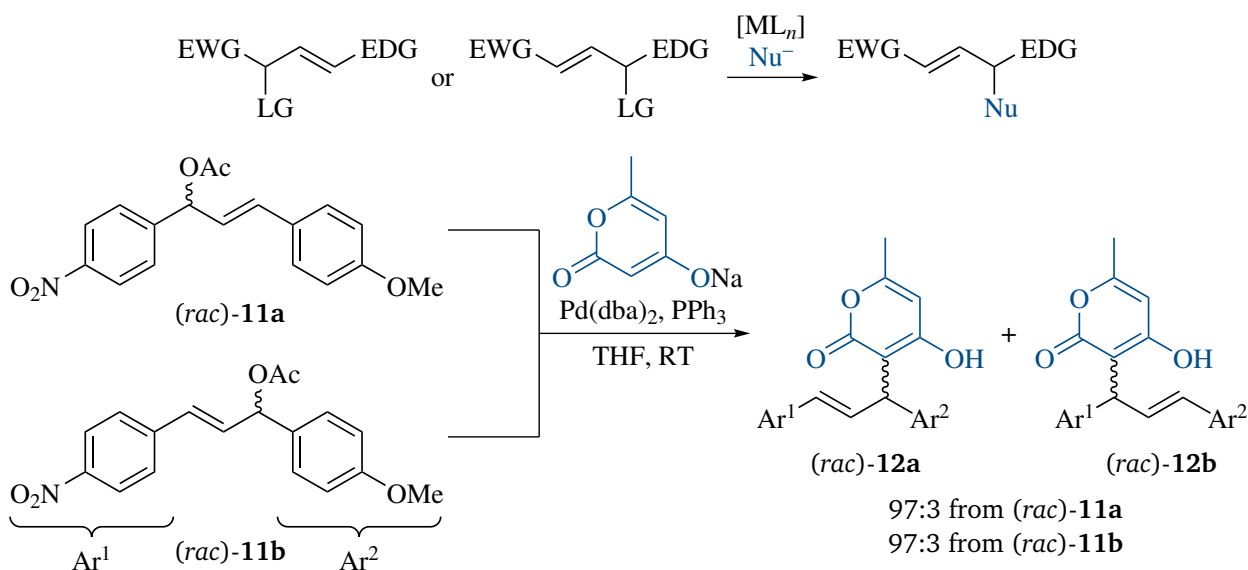


**Scheme 2.3:** Steric influence of substituents on the regioselectivity: General rule (top) and examples<sup>[150]</sup> (bottom).  $\text{R}^i$  denote organic moieties, with  $\text{R}^{\text{L}}$  being bulkier than  $\text{R}^{\text{S}}$ .

### 2.2.1 Influence of the Substrate Structure

In most cases, regioselectivity is mainly controlled by the steric and electronic properties of the allylic substituents.<sup>[72,73,149]</sup> As shown in Scheme 2.3, the nucleophile tends to attack the allylic terminus which is sterically better accessible. For instance, allylic alkylation of substrates (*rac*)-**9** gives a mixture of regioisomers (*rac*)-**10a** and (*rac*)-**10b**, and the selectivity for (*rac*)-**10a** increases with the difference in steric demand of the opposite allylic substituents.<sup>[150]</sup>

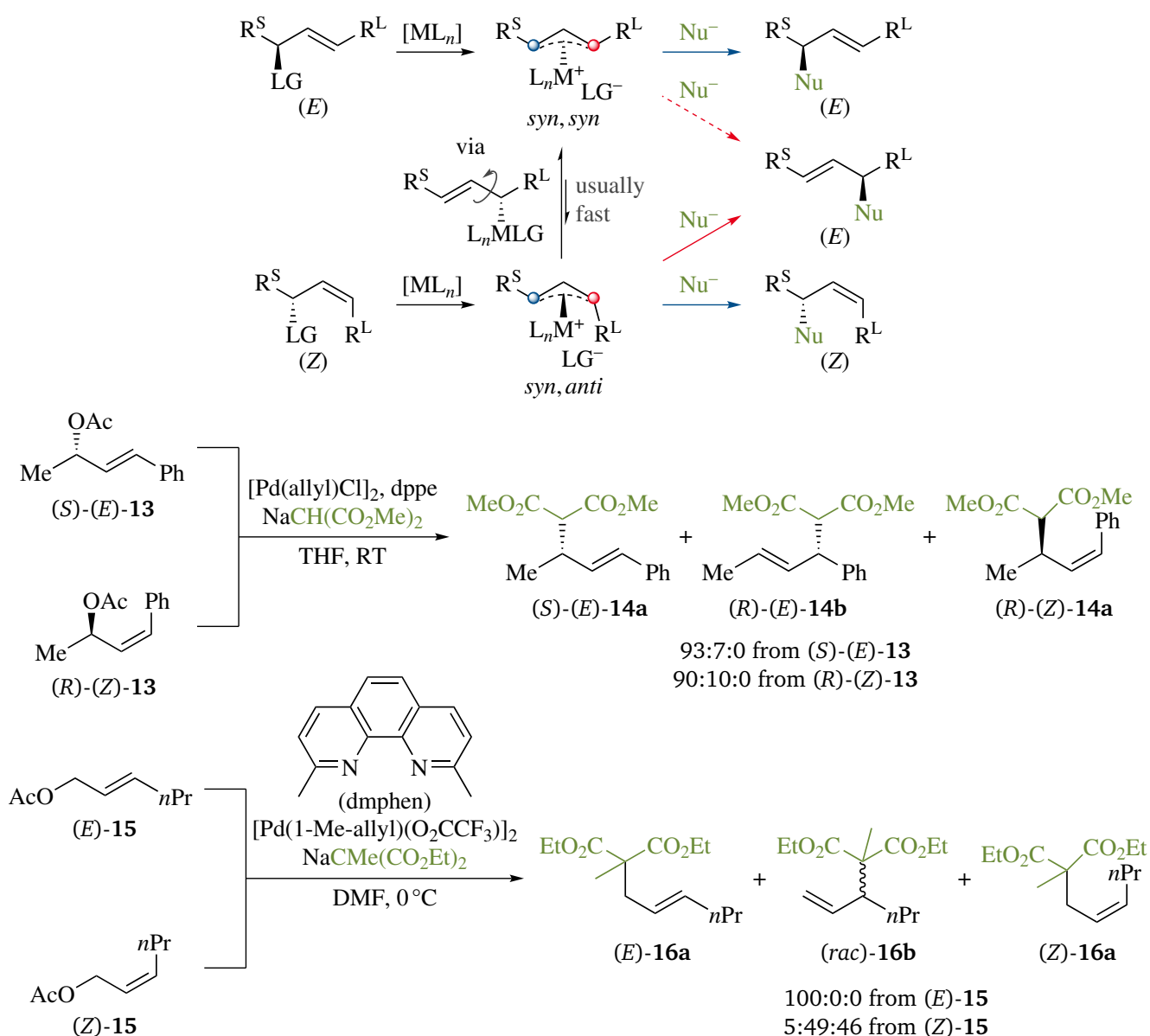
In addition to steric factors, electronic effects exerted by the allylic substituents have a significant influence on the regioselectivity. If none of the allylic termini is preferred for steric reasons, the terminus adjacent to the electronically stronger donating moiety is more reactive (Scheme 2.4).<sup>[72,73,149]</sup> This has been demonstrated by MORENO-MAÑAS and coworkers, using



**Scheme 2.4:** Electronic influence of substituents on the regioselectivity: General rule (top) and example<sup>[151]</sup> (bottom).

substrates (*rac*)-**11** which bear a *p*-methoxyphenyl moiety as electron donating group (EDG) and a *p*-nitrophenyl substituent as electron withdrawing group (EWG). Regardless of the substrate regioisomer (*rac*)-**11a** or (*rac*)-**11b** employed, product (*rac*)-**12a** substituted distal to the EWG was obtained selectively.<sup>[53,151]</sup> Density functional theory (DFT) calculations revealed that the allylic terminus closer to the most electron-withdrawing substituent has a shorter Pd–C bond, rendering the opposite terminus more exposed to nucleophilic attack.<sup>[152]</sup>

The influence of the substrate's double bond geometry is outlined in Scheme 2.5. Oxidative addition of (*E*)-configured substrates gives a *syn, syn*  $\eta^3$ -intermediate, whereas (*Z*)-substrates react to



**Scheme 2.5:** Influence of double bond configuration on the regioselectivity: General scenario with stabilized nucleophiles (top), example without significant influence<sup>[51]</sup> (middle) and example with significant influence<sup>[153]</sup> (bottom). The dashed arrow indicates a minor reaction path.  $\text{R}^{\text{S}}$  denotes an organic moiety or a hydrogen atom;  $\text{R}^{\text{L}}$  is an organic moiety bulkier than  $\text{R}^{\text{S}}$ .

the corresponding *syn, anti*-complex.<sup>[72,73,149]</sup> Both metal–allyl species can equilibrate via the well-established  $\pi$ – $\sigma$ – $\pi$  (or  $\eta^3$ – $\eta^1$ – $\eta^3$ ) mechanism.<sup>[61–65]</sup> Apart from exceptional cases,<sup>[154–157]</sup> the *syn, syn*-species is energetically strongly favored. The  $\pi$ – $\sigma$ – $\pi$  equilibrium is usually fast compared to the subsequent nucleophilic displacement, and the resulting regioselectivity is consequently independent of the double bond configuration. For example, allylic alkylation of diastereomers (*S*)-(*E*)- and (*R*)-(*Z*)-**13** has been reported to give the same product isomer (*S*)-(*E*)-**14a** with virtually identical regioselectivity.<sup>[51]</sup>

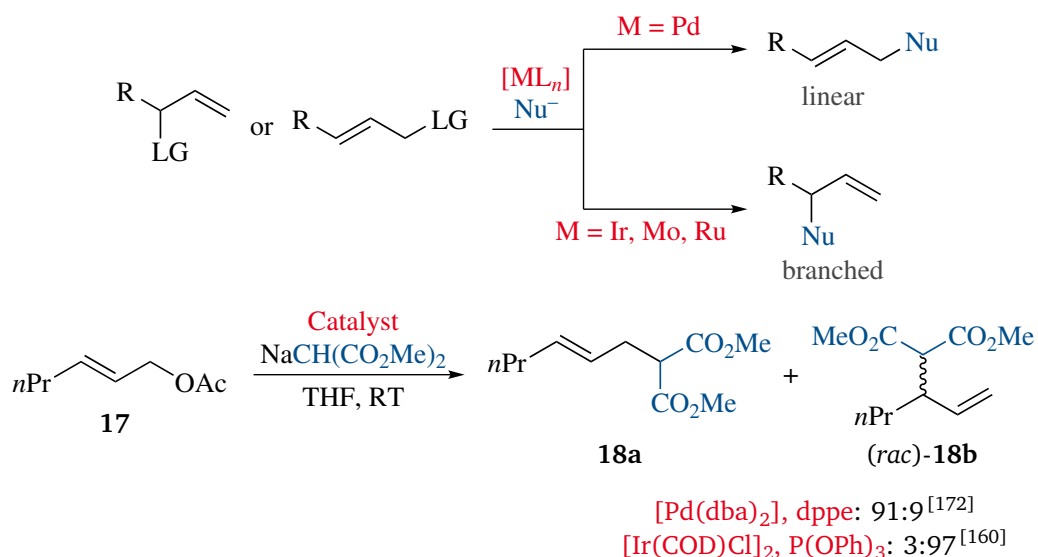
However, if  $\pi$ – $\sigma$ – $\pi$  equilibration is sufficiently slow, the *syn, anti*  $\eta^3$ -species formed from the (*Z*)-substrate might predominantly react directly with the nucleophile, leading to a different product distribution compared to the corresponding (*E*)-substrate. In the *syn, anti*-complex, the *anti*-configured allylic terminus has been shown to experience a boost in reactivity (Scheme 2.5, red path).<sup>[158]</sup> This might be attributed to the trajectory of the incoming nucleophile bringing it closer to the *syn*- than to the *anti*-position of the allylic terminus attacked, and hence a less bulky substituent in *syn*-position (e.g. hydrogen) facilitates nucleophilic attack.<sup>[159]</sup> Thus, attack at the *anti*-configured terminus might dominate, even if steric or electronic factors favor the opposite allylic terminus (blue path, favored in the *syn, syn*-complex).<sup>[72,73,149]</sup>

The equilibration between *syn, syn*- and *syn, anti*-complex can be rendered slow relative to the nucleophilic displacement step by employing a sterically demanding ligand.<sup>[153,156]</sup> For instance, Pd-catalyzed allylic alkylation of (*E*)-**15** in the presence of 2,9-dimethyl-1,10-phenanthroline (dmphen) cleanly furnishes product (*E*)-**16a**, whereas (*Z*)-**16a** gives an approximately 1:1 mixture of product isomers (*rac*)-**16b** and (*Z*)-**16a**.<sup>[153]</sup> Furthermore, the use of iridium as transition metal has been demonstrated to slow down  $\pi$ – $\sigma$ – $\pi$  equilibration, resulting in a different product distribution for (*E*)- and (*Z*)-configured substrates<sup>[160–163]</sup> even with non-bulky ligands such as P(OPh)<sub>3</sub>.<sup>[160,161]</sup>

### 2.2.2 Influence of the Transition Metal

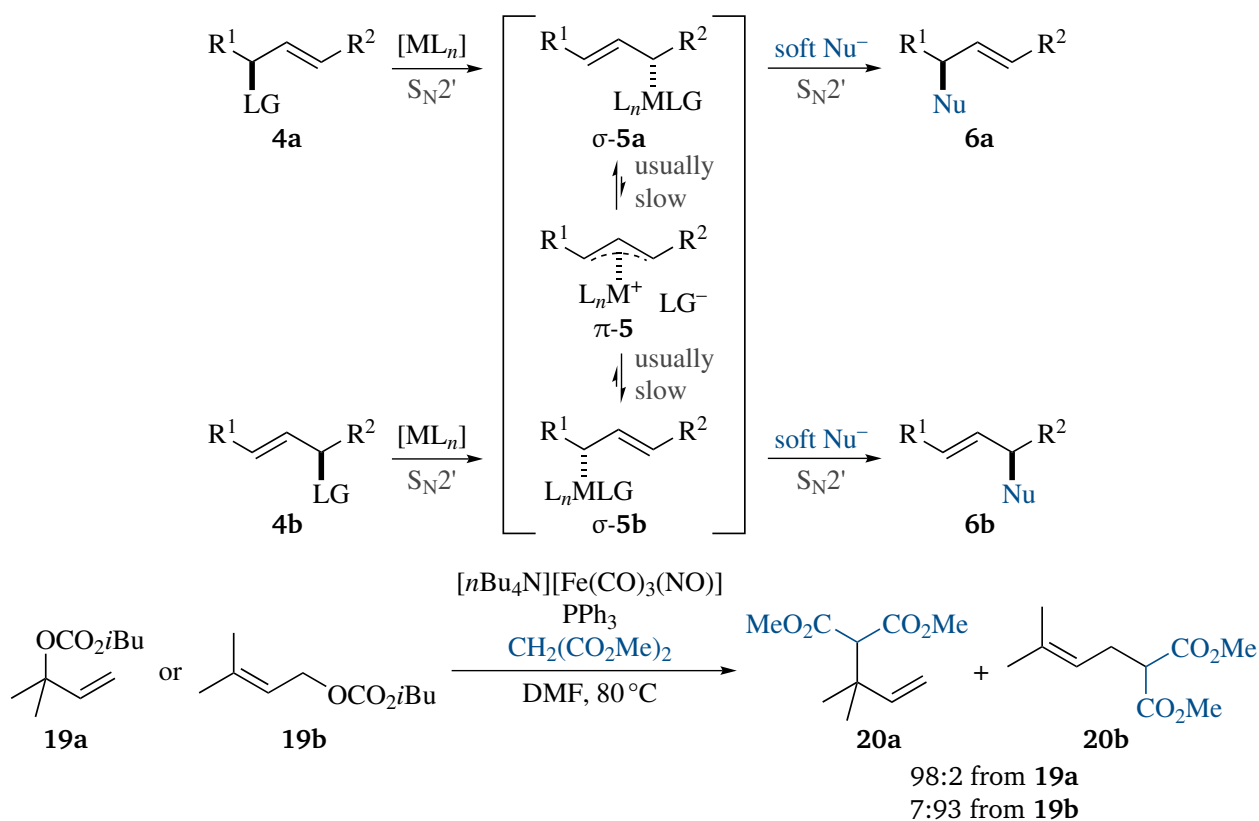
As outlined above, the regioselectivity is mainly determined by steric and electronic effects. In cases where the electronically favored allylic terminus is sterically disfavored, the transition metal may determine which effect dominates. In terminal allylic systems, the substituted terminus is electronically preferred, while the terminal position is sterically better accessible. As shown in Scheme 2.6, linear allylic substitution products are usually obtained under Pd catalysis,<sup>[164–166]</sup> whereas Ir,<sup>[160,167]</sup> Mo<sup>[168,169]</sup> and Ru<sup>[170,171]</sup> catalysts give branched products, independent of the regiochemistry of the substrate. For example, Pd-catalyzed allylic alkylation of terminal substrate **17** has been reported to yield linear product **18a** as main product.<sup>[172]</sup> Under Ir catalysis, on the other hand, branched product **18b** is obtained with high regioselectivity.<sup>[160]</sup>

For most transition metals, the primary oxidative addition product is commonly believed to be a  $\eta^3$ -complex  $\pi$ -**5**, which also represents the reactive electrophile. For iron and rhodium, in contrast, experimental data support a scenario where oxidative addition gives a  $\eta^1$ -coordinated



**Scheme 2.6:** Preference for linear or branched allylic substitution products dependent on the transition metal M employed: General rule (top) and examples<sup>[160,172]</sup> (bottom). R denotes an organic moiety.

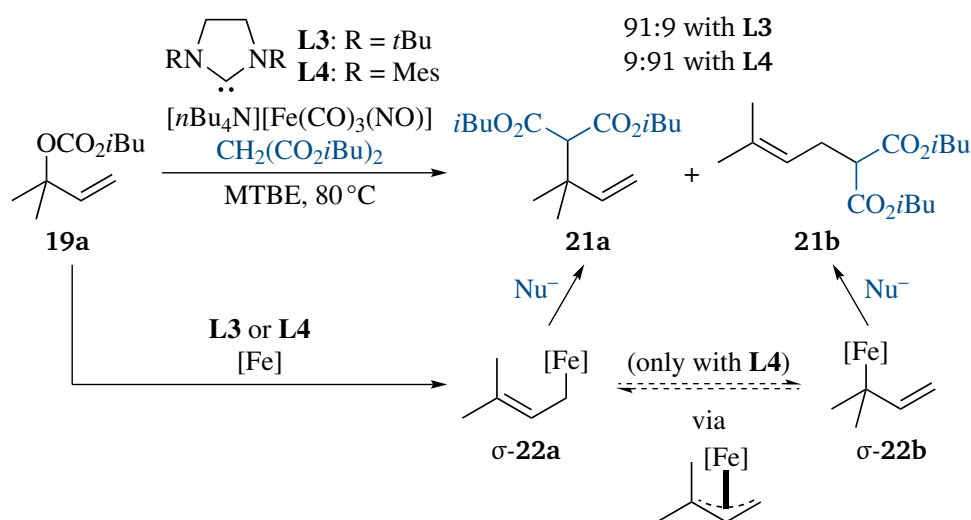
intermediate  $\sigma$ -5, which is subsequently attacked by the nucleophile (Scheme 2.7).<sup>[141–144]</sup> Both steps are believed to proceed in an  $S_N2'$  fashion with  $\sigma$ - $\pi$ - $\sigma$  equilibration usually being slow, which results in a regiochemical memory effect.<sup>[97,100,173]</sup> For instance, Fe-catalyzed



**Scheme 2.7:** Regiochemical retention observed in Fe- and Rh-catalyzed allylic substitution chemistry: General scenario (top) and example<sup>[144]</sup> (bottom). R<sup>i</sup> denote organic moieties or hydrogen atoms.

allylic alkylation of regioisomers **19a** and **19b** has been shown to proceed under retention of regiochemistry, giving *ipso*-substituted products **20a** and **20b**, respectively.<sup>[144]</sup>

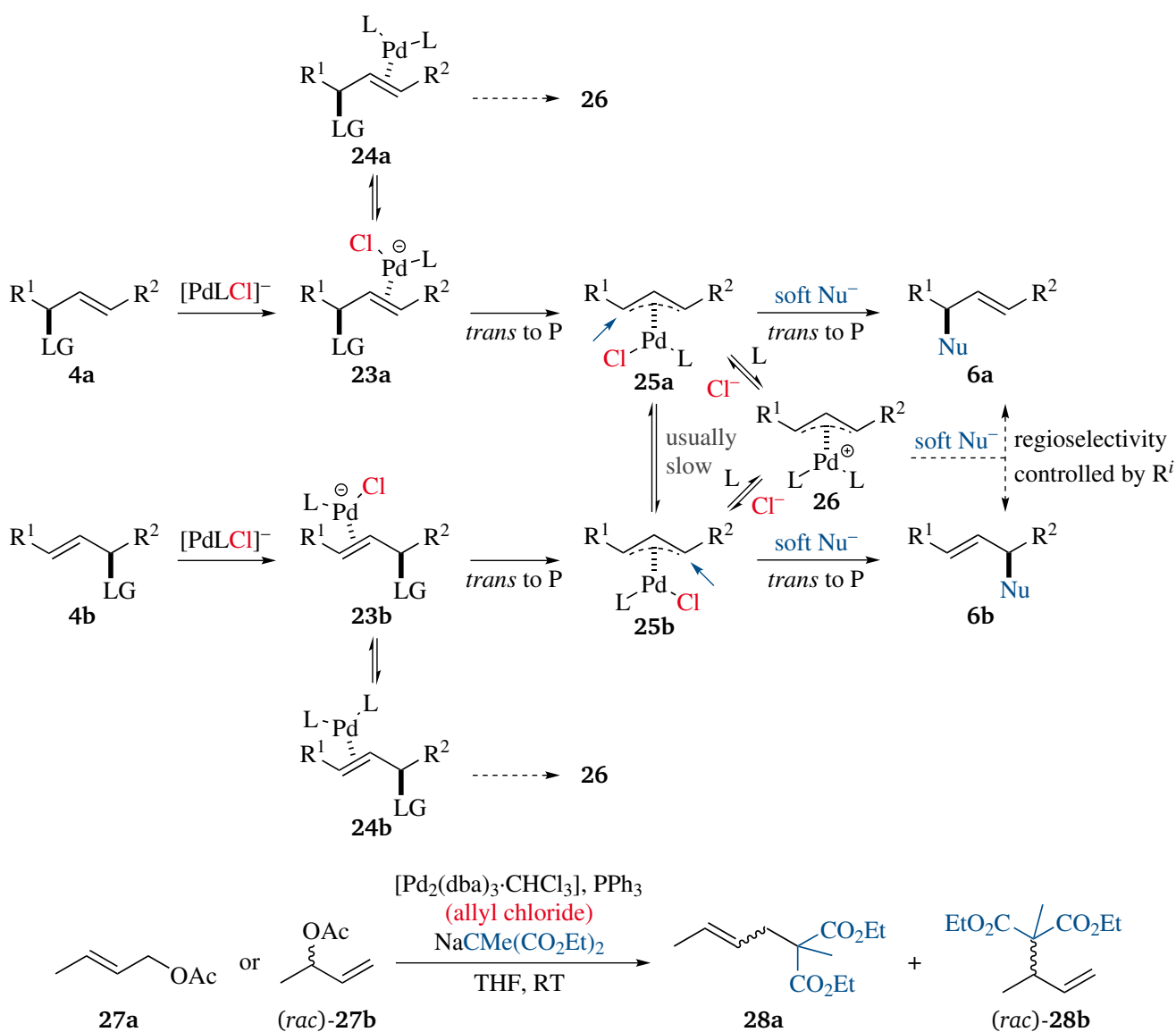
A remarkable variant of the Fe-catalyzed allylic substitution has been developed by PLIETKER *et al.*, using *N*-heterocyclic carbene (NHC) ligands **L3** (SI*t*Bu) and **L4** (SIMes). As demonstrated for allylic carbonate **19a**, the reaction exhibits a regiodivergent<sup>[174]</sup> behavior, selectively furnishing branched product **21a** with **L3** and linear product **21b** in the presence of **L4** (Scheme 2.8). Mechanistic experiments indicated the  $\sigma$ - $\pi$ - $\sigma$  equilibrium between regioisomeric complexes  $\sigma$ -**22a** and  $\sigma$ -**22b** to be suppressed with bulky ligand **L3**, whereas **L4** renders this exchange process fast enough for enabling full equilibration to the more easily attacked complex  $\sigma$ -**22b**.<sup>[143]</sup>



**Scheme 2.8:** Ligand-controlled regiodivergent Fe-catalyzed allylic alkylation developed by PLIETKER and coworkers.<sup>[143]</sup>

### 2.2.3 Influence of Chloride Ions

The presence of chloride anions is known to have a profound impact on selectivity<sup>[138,175–178]</sup> and kinetics<sup>[137,178]</sup> of Pd-catalyzed allylic substitutions.<sup>[179]</sup> These effects are based on the high palladophilicity of chloride. Reactions involving chloride as substrate leaving group, additive (e.g. LiCl) or part of the Pd source (e.g.  $[\text{Pd}(\text{allyl})\text{Cl}]_2$ ) typically exhibit partial retention of either regio- or stereochemistry, depending on whether the substrate is unsymmetrically or symmetrically substituted. This type of memory effect has been investigated experimentally and computationally by NORRBY, FRISTRUP, TANNER and coworkers for monodentate phosphine ligands, furnishing the mechanistic rationale shown in Scheme 2.9.<sup>[66,180,181]</sup> In agreement with earlier studies,<sup>[182–187]</sup> the reactive zerovalent palladium species was found to be  $[\text{PdLCl}]^-$  rather than  $[\text{PdL}_2]$ . It was further disclosed that  $\eta^2$ -substrate complex **23** and interconverting  $\eta^3$ -allyl intermediates **25** are ligated by one chloride and one phosphine ligand as well. The corresponding chloride-free complexes **24** and **26** were shown to be significantly less reactive towards oxidative addition and nucleophilic attack, respectively.<sup>[66]</sup> Computations established that chloride-ligated intermediates



Entry	Substrate	Allyl Chloride	Regioselectivity <b>28</b>	
			<b>28a (E:Z)</b>	<b>28b</b>
1	<b>27a</b>	–	84 (92:8)	16
2	<b>27b</b>	–	74 (81:19)	26
3	<b>27a</b>	5 mol%	83 (98:2)	17
4	<b>27b</b>	5 mol%	54 (80:20)	46

**Scheme 2.9:** Partial regiochemical retention observed in Pd-catalyzed allylic substitutions in the presence of chloride: General scenario<sup>[66,180,181]</sup> (top) and example<sup>[181]</sup> (bottom, reaction with strong memory effect marked in green). Dashed arrows indicate minor reaction paths. R<sup>i</sup> denote organic moieties or hydrogen atoms, L is a P-donating ligand. The small regioselectivity difference obtained from substrates **27a** and **27b** (entries 1 and 2) was attributed to concurrent formation of both *syn* and *anti* η<sup>3</sup>-intermediate from **28b**, with the latter having an increased propensity to react to the branched product (*rac*)-**28b** (cf. Scheme 2.5). Partial formation of an *anti* Pd–allyl species from **27b** also explains the higher (*Z*)-content of product **28a** (entries 2 and 4).<sup>[181]</sup>

---

**23** and **25** react *trans*-selectively with respect to the phosphine ligand in both steps.<sup>[66,181]</sup> Hence, product **6** might be obtained with some degree of regioselectivity, depending on the relative rate of equilibration between  $\eta^3$ -complexes **25a**, **25b** and **26**.<sup>[180]</sup>

The effect of added chloride was demonstrated using acetate substrate (*rac*)-**27b** (Scheme 2.9, bottom). Under chloride-free conditions, linear substitution product **28a** was obtained with 74:26 selectivity over the branched isomer (*rac*)-**28b**, close to the selectivity observed with the corresponding linear isomer **27a**. Addition of a catalytic amount of allyl chloride, on the other hand, significantly increased the extent of regioselectivity, giving a 54:46 mixture of products **28a** and **28b**.<sup>[181]</sup>

Apart from chloride anions, the use of bidentate, electronically unsymmetric ligands can lead to observation of regio- and stereochemical memory effects. For example, 2-(diphenylphosphanyl)-2'-methoxy-1,1'-binaphthalene (MOP) and 2'-dimethylamino-2-(diphenylphosphanyl)-1,1'-binaphthalene (MAP) ligands, which coordinate to palladium in a *P,C* fashion,<sup>[188]</sup> have been reported to exhibit strong memory effects when employed in allylic alkylation reactions.<sup>[127,189,190]</sup>

In this section, the basic factors determining the regiochemical outcome of allylic substitutions have been introduced. As described above, regioselectivity is usually predetermined by the steric and electronic properties of the substituents at the allylic termini. In case of opposite substituent effects, the choice of transition metal can serve as a handle to control which effect dominates. On the other hand, conditions under which regiochemical memory effects up to full regiospecificity can be observed have been discussed, namely the use of transition metals forming slowly equilibrating reactive intermediates, the use of bulky ligands and addition of chloride. Apart from effective opportunities for controlling the regiochemistry, an important feature of the allylic substitution is its inherent stereospecificity. The following subchapter describes the general stereochemical course of the reaction, as well as strategies how to manipulate it.

---

## 2.3 Stereospecificity of Allylic Substitutions

---

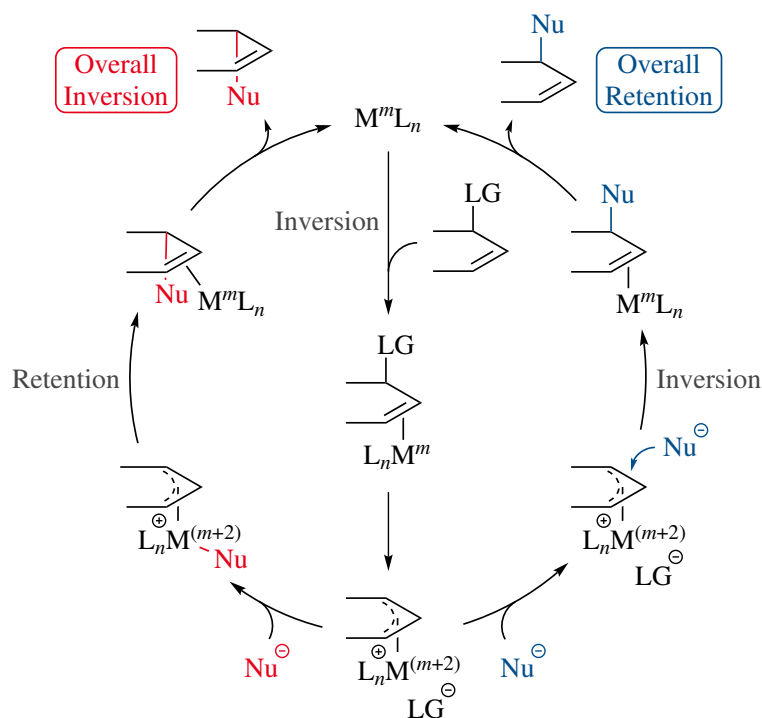
The ability of the allylic alkylation to effectively translate the substrate's stereochemical information into the product's configuration bases on a highly robust mechanism, with the overall specificity depending only on the nature of the nucleophile employed. This general catalytic cycle will be introduced hereinafter, as will be literature-known exceptions featuring altered stereospecificities.

### 2.3.1 Unbiased Stereospecificity

The stereospecificity of Pd-catalyzed allylic substitutions has been observed to be strikingly different for stabilized<sup>[165,191–193]</sup> and non-stabilized<sup>[194,195]</sup> nucleophiles. With soft nucleophiles, the product is obtained with overall retention of configuration, whereas the use of hard nucleophiles



affords stereochemical inversion. As a result of extensive mechanistic research, the catalytic cycle depicted in Scheme 2.10 has been established.<sup>[71,196,197]</sup> This mechanism, which fully accounts for the stereoselectivities experimentally observed, has later on been formally confirmed for iridium<sup>[198,199]</sup> and ruthenium,<sup>[116,200]</sup> and is likely to be operative for most other transition metals as well.

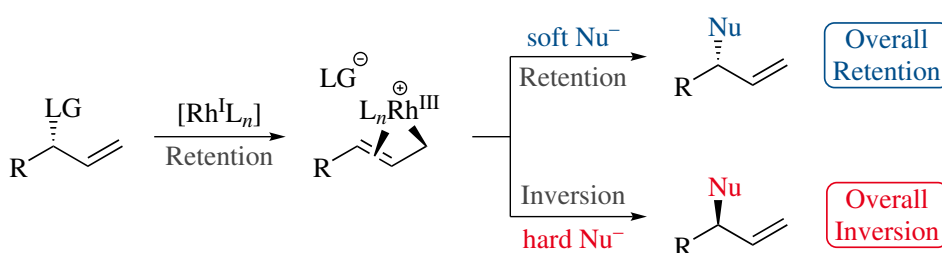


**Scheme 2.10:** General stereochemical mechanism of the transition metal catalyzed allylic substitution with either **stabilized** (right) or **non-stabilized** nucleophiles (left). This catalytic cycle has been evidenced experimentally for  $M = Pd$ ,<sup>[71,196,197]</sup>  $Ir$ ,<sup>[198,199]</sup>  $Ru$ <sup>[116,200]</sup> and is believed to be operative also for most other transition metals. L denotes the ligand employed.

According to the general stereochemical mechanism, olefin complexation of the allylic electrophile followed by oxidative addition gives the  $\eta^3$ -intermediate, featuring inversion of configuration. Stabilized nucleophiles ( $pK_a \lesssim 25$  for corresponding acid) subsequently react via outer-sphere  $S_N2$ -like displacement under inversion of configuration. The generated  $\eta^2$ -product complex eventually releases the final product. This sequence thus proceeds under overall retention of configuration, and is commonly referred to as ‘double inversion rule’. Non-stabilized nucleophiles ( $pK_a \gtrsim 25$ ), on the other hand, directly attack the metal center, followed by reductive elimination to give the product olefin complex, from which the product dissociates. This inner-sphere path proceeds under retention with respect to the  $\eta^3$ -intermediate, resulting in an overall inversion of configuration.<sup>[54]</sup>

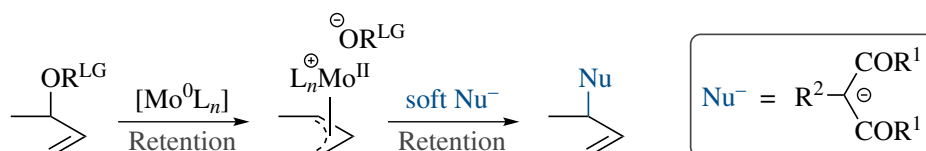
The Rh-catalyzed allylic substitution, which has been disclosed to follow a double  $S_N2'$ -type mechanism via a  $\eta^1$ -coordinated reactive intermediate,<sup>[141,142]</sup> also exhibits overall retention with stabilized nucleophiles<sup>[141,201–203]</sup> and overall inversion with non-stabilized nucleophiles.<sup>[201,204]</sup>

Hence, the stereospecificities of oxidative addition and nucleophilic displacement are likely to be identical as in the general mechanism (cf. Scheme 2.10), i.e. inversion–inversion for soft nucleophiles and inversion–retention for hard nucleophiles. Surprisingly, stereospecificity has also been observed for chiral substrates with a terminal double bond, although involving a terminal  $\eta^1$ -intermediate.<sup>[141,202–204]</sup> This was explained by intermediacy of a configurationally stable ( $\sigma + \pi$ ) or *enyl* species (Scheme 2.11),<sup>[141]</sup> a structural feature that has already been described earlier for Rh–allyl complexes.<sup>[205,206]</sup> In Fe-catalyzed allylic substitutions, which also proceed via  $\eta^1$ -intermediates,<sup>[143,144]</sup> the same kind of memory effect has been detected for the reaction of soft nucleophiles with terminal substrates, indicating that Fe–allyl complexes are stabilized by additional  $\pi$ -coordination as well.<sup>[207]</sup>



**Scheme 2.11:** Stereochemical mechanism proposed for the Rh-catalyzed allylic substitution with either **stabilized** or **non-stabilized** nucleophiles, accounting for the observation of stereospecificity with monosubstituted chiral substrates. R denotes an organic moiety, L is the ligand employed.

Mo-catalyzed allylic substitutions with stabilized malonate or  $\beta$ -diketone nucleophiles again proceed under retention of configuration.<sup>[208,209]</sup> However, in stark contrast to the standard mechanism outlined above, the reaction has been shown to follow a ‘double retention’ rather than a ‘double inversion’ mechanism (Scheme 2.12).<sup>[210–213]</sup> Investigation of the oxidative addition delivered evidence for a precoordination between the Mo(0) catalyst and the carboxylate or carbonate leaving group usually employed, which renders the oxidative addition *syn*-directed.<sup>[214,215]</sup> The nucleophilic displacement step was furthermore suggested to proceed via a retentive inner-sphere path, with the nucleophile undergoing monodentate Mo–O coordination prior to reductive elimination.<sup>[211]</sup>

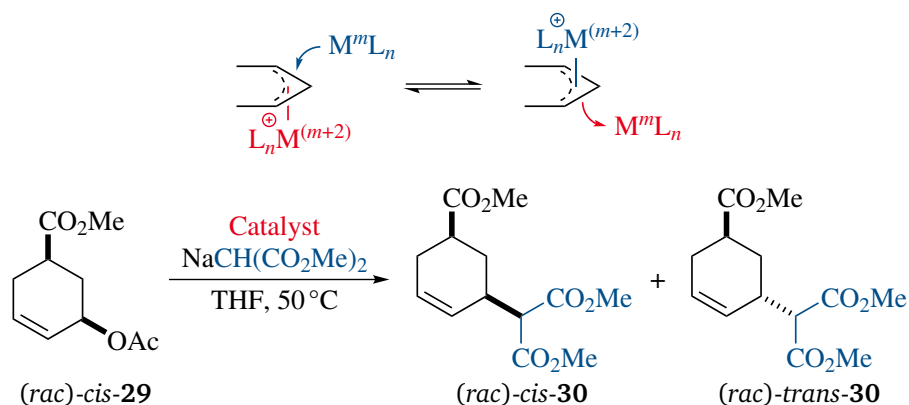


**Scheme 2.12:** Stereochemical mechanism for the Mo-catalyzed allylic substitution with malonate or  $\beta$ -diketone nucleophiles. The leaving group  $\text{OR}^{\text{LG}}$  is typically a carboxylate or a carbonate function.  $\text{R}^1$  denotes an organic moiety or an alkoxy group,  $\text{R}^2$  represents an organic substituent or hydrogen atom, and L is the ligand employed.

### 2.3.2 Loss and Manipulation of Stereospecificity

A number of exceptions from the normal stereospecificity has been reported, in which either the stereochemical course of oxidative addition is inverted or a (partial) isomerization of the intermediate  $\eta^3$ -species occurs.<sup>[216]</sup>

A widely known mechanism for the loss of stereospecificity, which can, in principle, occur in any allylic alkylation system, is the complete or partial equilibration of the  $\eta^3$ -intermediate through  $S_N2$ -like displacement by a second incoming metal center (Scheme 2.13). This scenario is well studied for palladium, and the interconversion rate (and thus the extent of stereochemical scrambling) has been shown to critically depend on catalyst concentration and the choice of ligand.<sup>[71,217,218]</sup> For instance, allylic alkylation of (*rac*)-*cis*-**29** catalyzed by Pd(PPh<sub>3</sub>)<sub>4</sub> has been demonstrated to be impacted by intermediate metal–metal displacement, reflected in the diastereomeric (*cis* : *trans*) ratio of substitution product **30** decreasing upon elevating the catalyst loading. Conversely, stereochemical scrambling by Pd–Pd displacement could be suppressed by using bidentate ligand dppe.<sup>[217]</sup> Also, the separation of Pd sites from each other by using solid supports has been reported to shut down undesired Pd–Pd displacement.<sup>[219]</sup> In a similar manner as known for  $\eta^3$ -Pd intermediates,  $\eta^1$ -allyl complexes of rhodium have been shown to undergo slow interconversion via a  $S_N2'$ -type mechanism.<sup>[142]</sup>



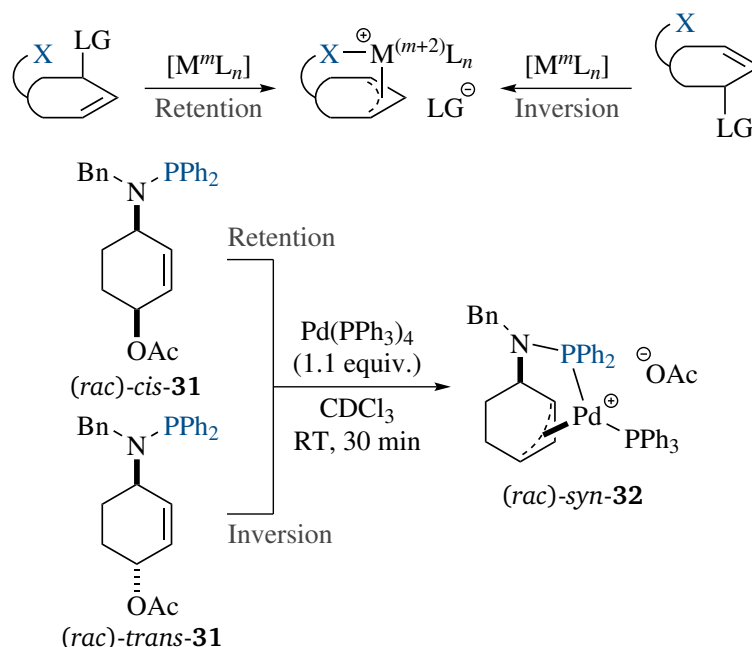
Catalyst	Pd loading <sup>[a]</sup>	<i>cis</i> - <b>30</b> : <i>trans</i> - <b>30</b>
Pd(PPh <sub>3</sub> ) <sub>4</sub>	5 mol%	95:5
Pd(PPh <sub>3</sub> ) <sub>4</sub>	24 mol%	92:8
Pd(dppe) <sub>2</sub>	5 mol%	> 99:1

[a] reactions performed at 125 mM substrate concentration

**Scheme 2.13:** Isomerization of  $\eta^3$ -intermediates via  $S_N2$ -like displacement with free catalyst: General scenario (top) and example<sup>[217]</sup> (bottom).

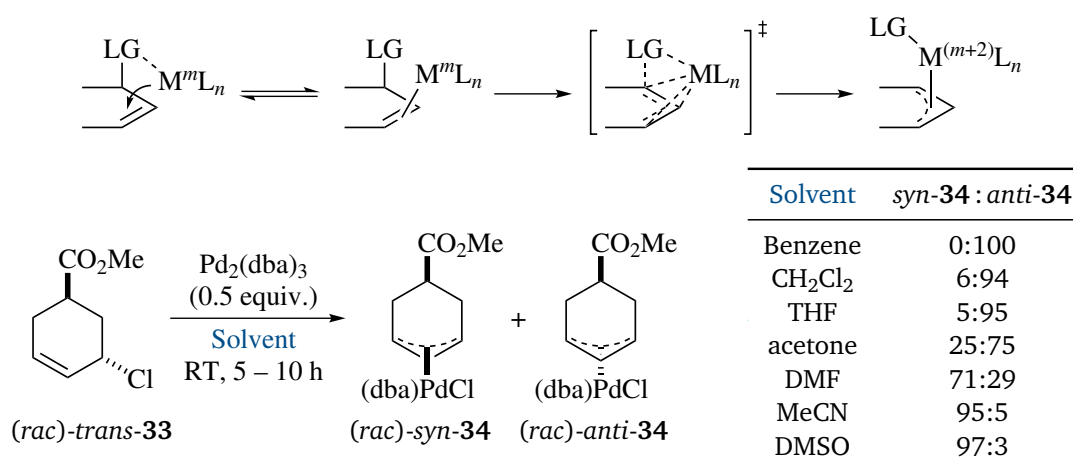
The stereochemical outcome of oxidative addition can be drastically changed by installing a directing group (e.g. a phosphine moiety)<sup>[220]</sup> in the substrate, which coordinates the catalyst prior to oxidative addition and stabilizes the intermediate  $\eta^3$ -allyl complex by internal chelation (Scheme 2.14). This strategy has been showcased by FARTHING and KOČOVSKÝ for diastereomeric

substrates (*rac*)-*cis*- and (*rac*)-*trans*-**31**, which were converted to the same Pd intermediate (*rac*)-*syn*-**32**.<sup>[220]</sup> Hence, precoordination by a directing group can dominate over the stereochemical preference of the starting material, thus giving a *syn*-configured intermediate independent of the substrate's relative configuration.



**Scheme 2.14:** Formation of a *syn*-configured  $\eta^3$ -intermediate by means of a directing group, independent of the substrate's relative configuration: General scenario (top) and example<sup>[220]</sup> (bottom). M denotes the metal, L is the ligand employed and X represents the coordinating group.

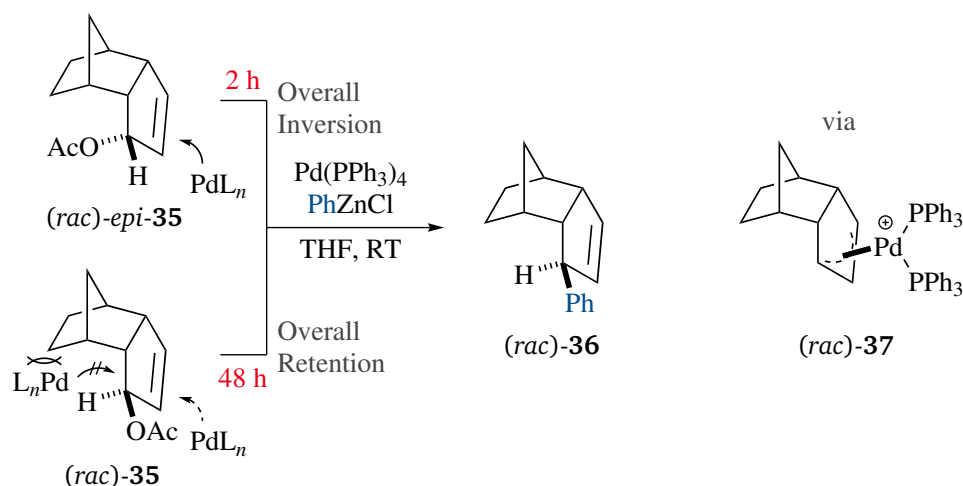
Another interaction that may render the oxidative addition retentive is an electronic attraction of the catalyst by a coordinating leaving group (Scheme 2.15). For palladium, this scenario has been shown to be possible for Cl,<sup>[221,222]</sup> and Br.<sup>[222]</sup> Also, (diphenylphosphino)acetate as a leaving group with a ligating site electronically separated from the allylic system has been reported



**Scheme 2.15:** Oxidative addition under retention promoted by a coordinating leaving group: General scenario (top) and example for solvent dependency<sup>[221]</sup> (bottom).

to facilitate oxidative addition under retention.<sup>[223]</sup> For allylic chlorides, experimental<sup>[221,222]</sup> and computational<sup>[224]</sup> investigations have revealed that the retentive path is promoted by low-dielectric solvents and withdrawing or weakly donating ligands. For instance, oxidative addition of chloride substrate (*rac*)-**trans-33** with dba as withdrawing ligand has been reported to selectively afford complex (*rac*)-*anti*-**34** (i.e. under retention of configuration) in non- and medium polar solvents such as benzene, CH<sub>2</sub>Cl<sub>2</sub> and THF, whereas polar media like MeCN and DMSO cleanly gave Pd species (*rac*)-*syn*-**34** (i.e. inversion of configuration).<sup>[221]</sup> For molybdenum, the described interaction between leaving group and catalyst has been proposed to be responsible for the general preference of these systems to undergo oxidative addition under retention, even with weakly coordinating leaving groups such as carboxylates and carbonates (see subsection 2.3.1).<sup>[211,212,214,215]</sup>

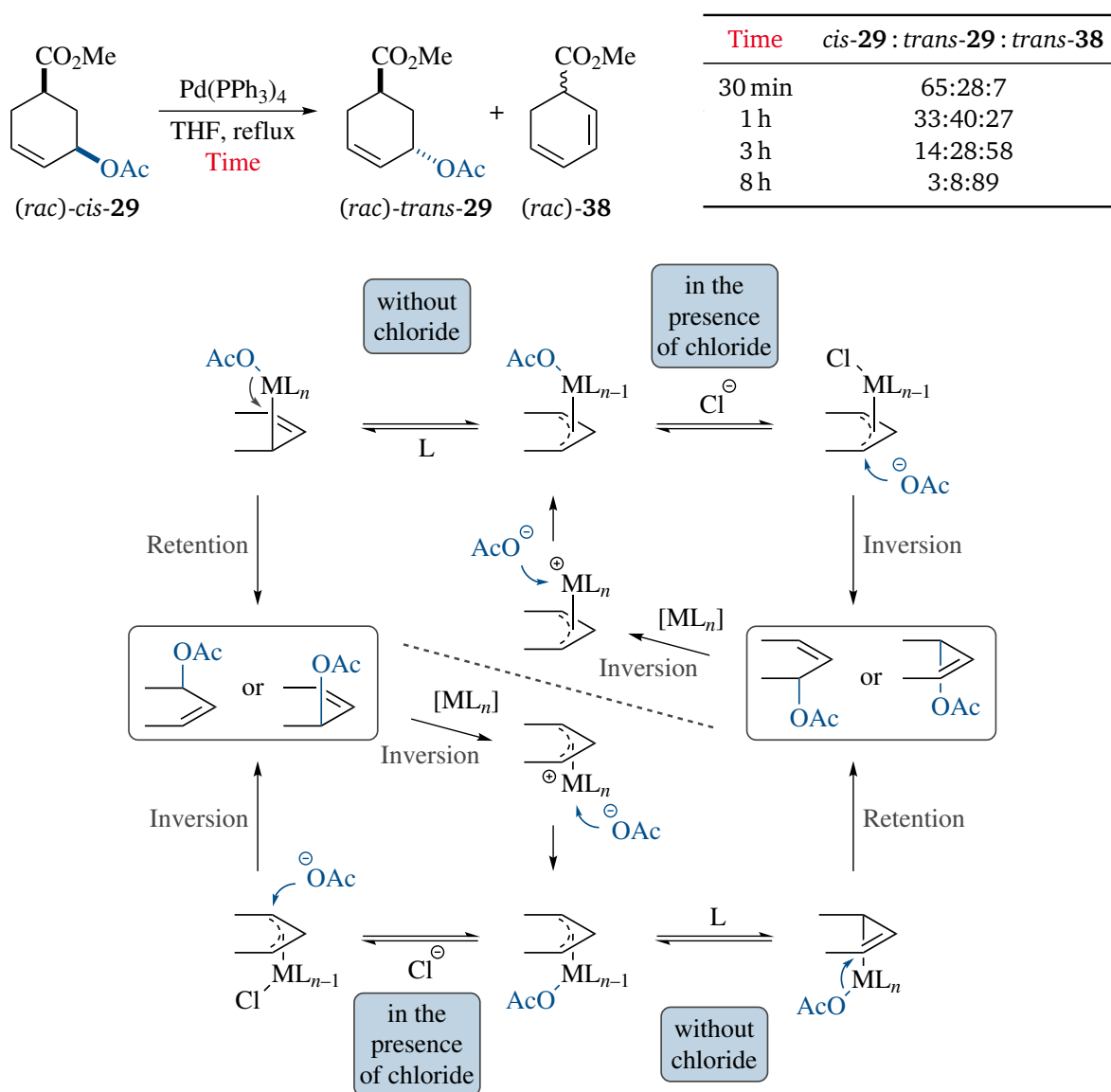
For substrates where the allylic face *anti* to the leaving group is sterically shielded, oxidative addition might be forced to proceed under retention. This has been demonstrated by Kočovský and coworkers, using *endo*-dicyclopentadiene and verbenol derived substrates.<sup>[223,225]</sup> Pd-catalyzed allylic alkylation of dicyclopentadiene derivative (*rac*)-**35** with hard nucleophile PhZnCl has been reported to afford the same product stereoisomer (*rac*)-**36** as its epimer (*rac*)-*epi*-**35**, with (*rac*)-**35** requiring significantly longer to reach full conversion (Scheme 2.16). It was concluded that for (*rac*)-**35** steric bias prevents oxidative addition under inversion, thus leaving slow formation of  $\eta^3$ -intermediate (*rac*)-**37** under retention as the only feasible reaction path.



**Scheme 2.16:** Inverted stereospecificity by using a sterically biased substrate (*rac*)-**35** that can only undergo slow oxidative addition under retention.<sup>[223]</sup>

Allylic acetates have been observed to undergo slow isomerization upon treatment with a Pd catalyst. As initially described by TROST *et al.*, heating of substrate (*rac*)-*cis*-**29** in the presence of Pd(PPh<sub>3</sub>)<sub>4</sub> gives the more stable diastereomer (*rac*)-*trans*-**29**, which undergoes consecutive elimination to (*rac*)-**38** (Scheme 2.17).<sup>[226]</sup> This indicates that acetate can not only act as leaving group, but also as a nucleophile. Extensive studies by BÄCKVALL and coworkers led to a mechanistic proposal where the acetate anion can re-enter the allylic system via either inner- or

outer-sphere attack. In the former case, which is favored by weakly coordinating ligands, acetate undergoes transient coordination to the  $\eta^3$ -coordinated oxidative addition product, followed by suprafacial shift to the corresponding  $\eta^1$ -complex and reductive elimination under retention to give the allylic acetate. The presence of chloride, on the other hand, was suggested to lead to displacement of acetate from the coordination sphere, thus facilitating outer-sphere attack under inversion. [227–230] A similar isomerization behavior has been disclosed for carbonate substrates. [231]



**Scheme 2.17:** Transition metal catalyzed isomerization of allylic acetates: Example [226] (top) and mechanistic scenario proposed by BÄCKVALL [227–230] (bottom).

As outlined in this subchapter, the allylic substitution usually proceeds stereospecifically, with the nature of the nucleophile (soft or hard) determining if the reaction exhibits overall retention or inversion. Exceptions that involve altered stereospecificity of the oxidative addition or isomerization of the  $\eta^3$ -intermediate have been discussed. The next section introduces the

---

main concepts of asymmetric allylic substitution, as well as key interactions responsible for enantioselectivity.

---

## 2.4 Enantioselectivity in Allylic Substitution Chemistry

---

The allylic substitution has been shown to be highly responsive towards asymmetric induction by using chiral, non-racemic ligands,<sup>[48,59]</sup> with the first enantioselective variant disclosed as early as 1977.<sup>[232]</sup> The peculiarity of this reaction is that every step in the mechanism (cf. Scheme 2.10) apart from the dissociation of product from the primarily formed  $\eta^2$ -product complex can be an enantiodiscriminating event. In this section, the general types of enantiodiscrimination will be introduced, followed by key mechanistic aspects related to enantioselectivity.

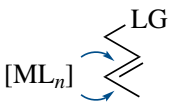
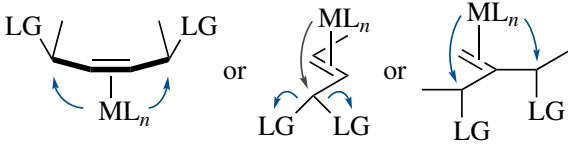

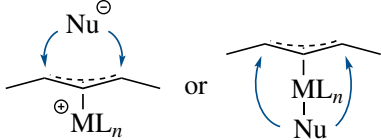
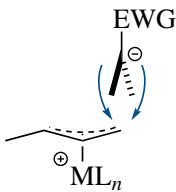
### 2.4.1 General Mechanisms of Enantiodiscrimination

Trost has defined five general mechanisms of enantiodiscrimination, based on the step in the catalytic cycle that is responsible for the preferred formation of one enantiomer. Accordingly, enantioselectivity can be achieved by enantiofacial differentiation at the double bond, desymmetrization of a substrate with two enantiotopic leaving groups, a transient enantiofacial exchange between stereoisomeric  $\eta^3$ -intermediates, discrimination of enantiotopic allylic termini in a symmetrically substituted system, or enantiofacial differentiation of a prochiral nucleophile (Table 2.1).<sup>[43,54,59,233]</sup>

For achiral (usually terminal) substrates with a non-symmetrically substituted double bond, the chiral catalyst may prefer one of the prochiral olefin faces over the other (Table 2.1, Mechanism A). This type of enantiodifferentiation is also operative in other catalytic enantioselective transformations of olefins such as asymmetric hydrogenation,<sup>[239,240]</sup> epoxidation<sup>[241,242]</sup> and dihydroxylation;<sup>[243,244]</sup> however, in Pd-catalyzed allylic substitution it only plays a minor role. This is because nucleophilic capture of the  $\eta^3$ -intermediate must be faster than  $\pi$ - $\sigma$ - $\pi$  equilibration, and formation of the branched product must be favored if a terminal substrate is employed, two prerequisites that are both difficult to meet under Pd catalysis.

Conversely, Ir-allyl intermediates are known to equilibrate slowly,<sup>[160–163]</sup> and to selectively afford branched rather than achiral linear products.<sup>[160,167]</sup> Hence, the discrimination of enantiotopic olefin faces constitutes an attractive strategy for Ir-catalyzed asymmetric allylic substitutions. For example, alkylation of terminal substrates **39** catalyzed by iridium and phosphoramidite ligand<sup>[245,246]</sup> ( $S_{ax}, S, S$ )-**L5** has been reported to furnish branched products **40** with high enantioselectivity (Scheme 2.18).<sup>[234]</sup> On the other hand, the corresponding branched racemic substrates gave only poor enantioselectivities (32 % e.e. upon slow addition of nucleophile). Since the latter type of substrates can only be deracemized by an intermediate enantiofacial exchange via  $\pi$ - $\sigma$ - $\pi$  interconversion (*vide infra*), but not by enantioselective olefin complexation, this result showcased that the enantioselectivity observed with **39** is indeed mainly based on

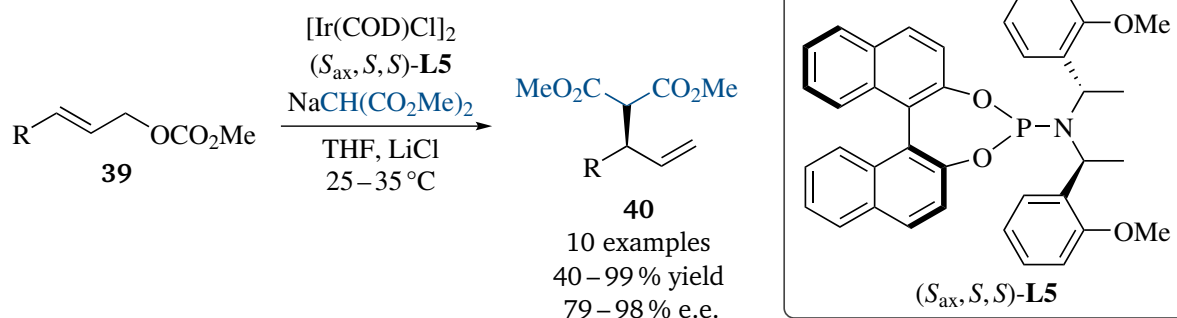
**Table 2.1:** General mechanisms for achieving enantioselectivity in allylic substitution chemistry.

Mechanism	Differentiated Sites	Enantioselectivity Controlling Step	Example
A	 enantiotopic olefin faces	complexation of substrate	[234]
B	 enantiotopic leaving groups	oxidative addition	[235]
C	 enantiotopic allylic faces	$\pi$ - $\sigma$ - $\pi$ interconversion	[236]
D	 enantiotopic allylic termini	nucleophilic attack	[237]
E	 enantiotopic faces of prochiral nucleophile	nucleophilic attack	[238]

enantiofacial discrimination at the double bond, with only small contributions by enantiofacial exchange between enantiomeric  $\eta^3$ -intermediates.<sup>[234]</sup>

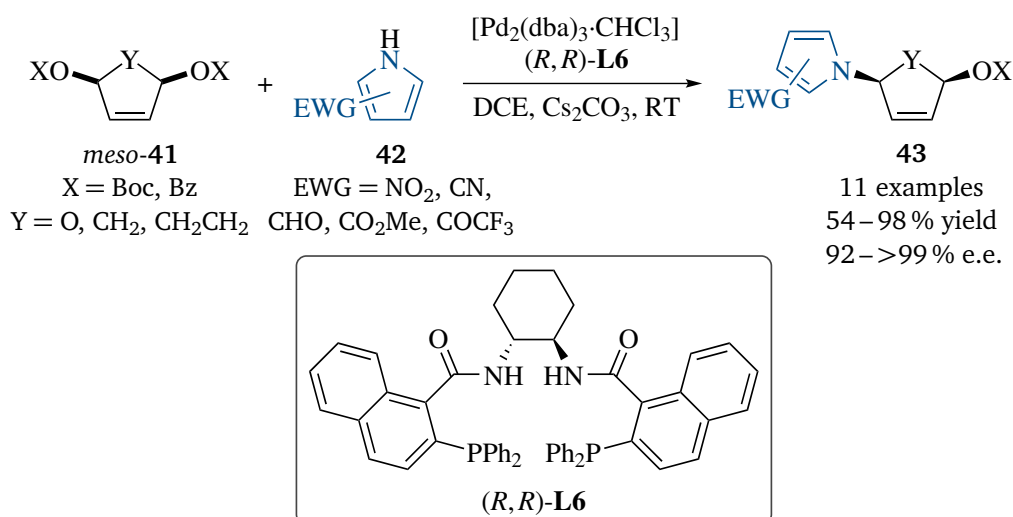
Bifunctional substrates with enantiotopic leaving groups can be desymmetrized upon oxidative addition (Table 2.1, Mechanism B). Most attention has been paid to five-membered *meso*-electrophiles as potential precursors for chiral biologically active compounds such as nucleosides<sup>[247]</sup> and carbanucleosides.<sup>[248–250]</sup> For instance, Trost and coworkers have developed a Pd-catalyzed allylic amination of bifunctional substrates *meso*-**41** with pyrrole nucleophiles **42** in





**Scheme 2.18:** Example for differentiation of enantiotopic olefin faces (cf. Table 2.1, Mechanism A) by Ir-catalyzed allylic alkylation.<sup>[234]</sup> Branched products **40** were obtained regioselectively, with <1–20 % of the linear isomer. R denotes an organic moiety (aryl for most examples).

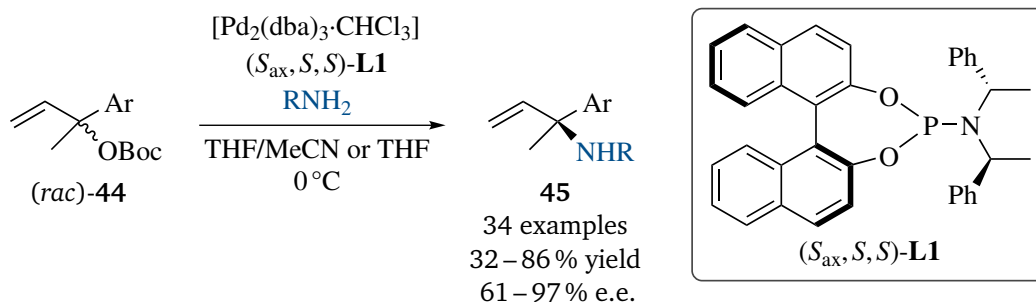
the presence of 1,2-diaminocyclohexane-*N,N'*-bis(2-diphenylphosphinobenzoyl) (DACH) derivative (*R,R*)-**L6**, affording desymmetrized products **43** as single regio- and diastereoisomers. A selected substitution product was subjected to a second allylic substitution and further converted to a ribonucleoside analogue.<sup>[235]</sup>



**Scheme 2.19:** Example for differentiation of enantiotopic leaving groups (cf. Table 2.1, Mechanism B) by Pd-catalyzed allylic substitution.<sup>[235]</sup> Substrates *meso*-**41** were used in slight excess (1.1 equiv.).

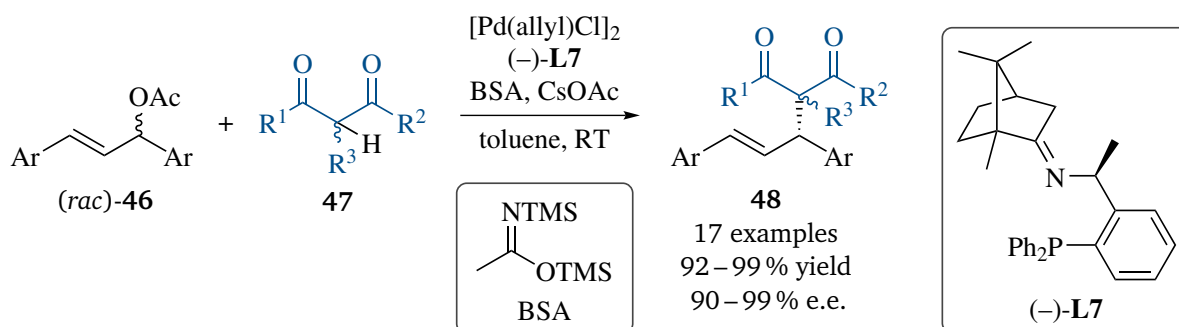
For substrates with a non-prochiral terminus (typically terminal allylic systems), the  $\eta^3$ -intermediate may exhibit enantiofacial exchange via a  $\eta^1$ -species with the metal bond to the non-prochiral terminus (Table 2.1, Mechanism C). C–C bond rotation in the transient  $\eta^1$ -complex allows the metal to choose between enantiotopic allylic faces. If this process is faster than subsequent nucleophilic attack, the product's e.e. is predetermined by the relative abundance of the interconverting  $\eta^3$ -species or their difference in reactivity towards the nucleophile. The substrate might be either chiral or achiral, depending on the position of the leaving group. In the latter case, enantiodifferentiating complexation (Table 2.1, Mechanism A) might be operative as well. For chiral substrates, an intermediate enantiofacial exchange allows for the

process to be designed as a DYKAT for the resolution of racemic starting material. For example, Pd-catalyzed allylic amination of racemates (*rac*)-**44** in the presence of phosphoramidite ligand (*S*<sub>ax</sub>, *S*, *S*)-**L1** has been disclosed to give access to optically active branched products **45**, along with only trace amounts of linear (i.e. achiral) products as usually obtained under Pd catalysis (Scheme 2.20).<sup>[236]</sup>



**Scheme 2.20:** Example for differentiation of enantiotopic allylic faces by intermediate  $\pi$ - $\sigma$ - $\pi$  interconversion (cf. Table 2.1, Mechanism C) in a Pd-catalyzed allylic substitution.<sup>[236]</sup> Ar denotes an aryl substituent, R is an organic moiety.

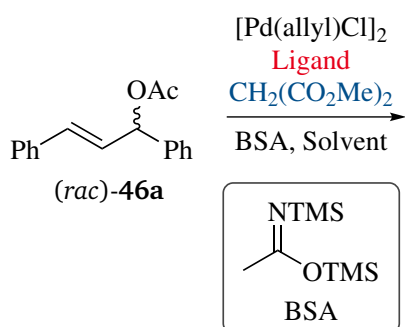
For chiral 1,3-disubstituted or (rather rarely) 1,1,3,3-tetrasubstituted substrates generating an allyl ligand with enantiotopic allylic termini upon oxidative addition, the nucleophilic attack can be directed to either of these termini, leading to enantiomeric products (Table 2.1, Mechanism D). This scenario generally allows for deracemization of racemic electrophiles. For instance, diaryl substrates (*rac*)-**46** can be efficiently resolved to enantioenriched products **48** when subjected to the action of palladium and *D*-camphor derived ligand (–)-**L7**,<sup>[237]</sup> with pronucleophiles **47** being activated *in situ* by use of *N,O*-bis(trimethylsilyl)acetamide (BSA)<sup>[251]</sup> and a catalytic amount of CsOAc (Scheme 2.21).



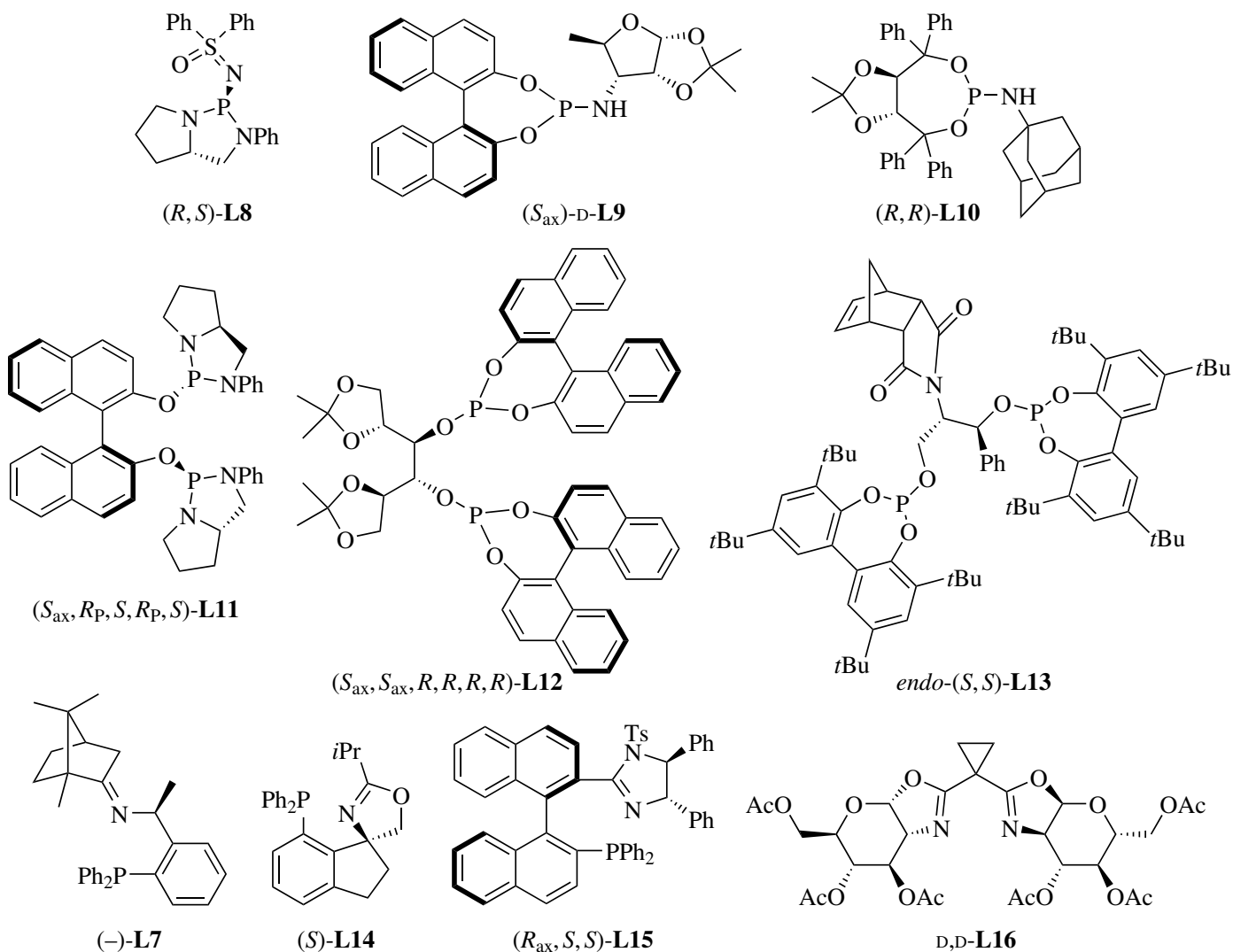
**Scheme 2.21:** Example for differentiation of enantiotopic allylic termini (cf. Table 2.1, Mechanism D) by Pd-catalyzed allylic alkylation.<sup>[237]</sup> Ar denotes an aryl substituent,  $\text{R}^i$  are organic moieties or hydrogen atoms (three examples were performed with unsymmetric racemic malonates **47**, i.e.  $\text{R}^1 \neq \text{R}^2$ , giving products **48** with d.r. = 63:37 – 50:50 and comparably high enantioselectivities for both diastereomers).

Among substrates competent for asymmetric induction by discrimination of enantiotopic allylic termini, (*rac*)-1,3-diphenylallyl acetate (*rac*)-**46a** has been extensively studied. Pd-catalyzed allylic alkylation of (*rac*)-**46a** with dimethyl malonate has been employed as benchmark system

for the design of new chiral ligands, with the e.e. of substitution product **48a** serving as indicator for ligand performance. Some recent examples are given in Scheme 2.22, including monodentate P-donors **L8** – **L10** [252–254] as well as bidentate *P,P* ligands **L11** – **L13**, [255–257] *P,N* ligands



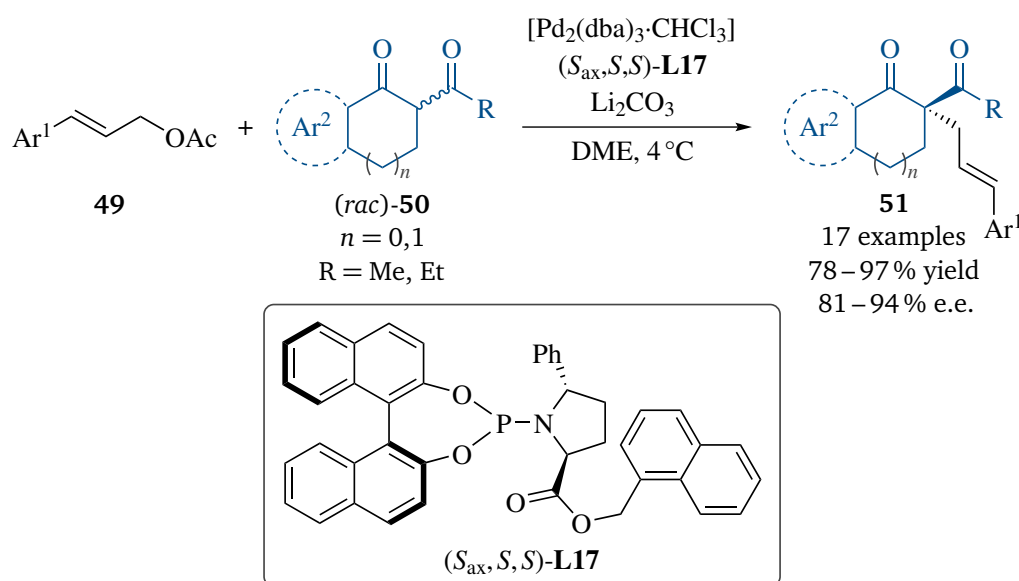
Ligand	e.e. / %	Reference
( <i>R,S</i> )- <b>L8</b>	96 ( <i>S</i> )	[252]
( <i>S</i> <sub>ax</sub> )- <b>D-L9</b>	96 ( <i>S</i> )	[253]
( <i>R,R</i> )- <b>L10</b>	92 ( <i>S</i> )	[254]
( <i>S</i> <sub>ax</sub> , <i>R</i> <sub>p</sub> , <i>S</i> , <i>R</i> <sub>p</sub> , <i>S</i> )- <b>L11</b>	99 ( <i>S</i> )	[255]
( <i>S</i> <sub>ax</sub> , <i>S</i> <sub>ax</sub> , <i>R</i> , <i>R</i> , <i>R</i> , <i>R</i> )- <b>L12</b>	93 ( <i>S</i> )	[256]
<i>endo</i> -( <i>S,S</i> )- <b>L13</b>	97 ( <i>S</i> )	[257]
(–)- <b>L7</b>	99 ( <i>R</i> )	[237]
( <i>S</i> )- <b>L14</b>	>99 ( <i>R</i> )	[258]
( <i>R</i> <sub>ax</sub> , <i>S</i> , <i>S</i> )- <b>L15</b>	96 ( <i>R</i> )	[259]
<b>D-L16</b>	98 ( <i>R</i> )	[260]



**Scheme 2.22:** Pd-catalyzed asymmetric allylic alkylation of (*rac*)-1,3-diphenylallyl acetate (*rac*)-**46a** with various ligands.

**L7,L14,L15** <sup>[237,258,259]</sup> and *N,N* ligand **L16**. <sup>[260]</sup> Comprehensive compilations of chiral ligands that have been subjected to this test system can be found in references [48] and [60].

Enantioselectivity can not only be achieved by means of a prochiral electrophile, but also by using a prochiral nucleophile. In this case, the  $\pi$ -allyl intermediate differentiates between enantiotopic faces of the nucleophile (Table 2.1, Mechanism E). This concept has been employed for the Pd-catalyzed deracemization of pronucleophiles (*rac*)-**50**, which become prochiral upon deprotonation. Using terminal allylic acetates **49** in combination with phosphoramidite ligand (*S*<sub>ax</sub>,*S,S*)-**L17**, substitution products **51** were obtained as single regioisomers with significant enantiomeric excess (Scheme 2.23). <sup>[238]</sup>



**Scheme 2.23:** Example for differentiation of enantiotopic faces of a prochiral nucleophile (cf. Table 2.1, Mechanism E) by Pd-catalyzed allylic alkylation. <sup>[238]</sup>  $\text{Ar}^i$  denote aryl moieties, with  $\text{Ar}^2$  being optional.

Allylic alkylation of a prochiral electrophile with a prochiral nucleophile opens up the possibility for achieving double stereoselectivity by combining differentiation of enantiotopic sites in the substrate (Table 2.1, Mechanisms A – D) with discrimination of enantiotopic faces in the nucleophile (Mechanism E). Respective examples have been developed by several groups, allowing for constructing and controlling two stereogenic centers in one reaction. <sup>[261–265]</sup> The potential of combining two prochiral starting materials has further been harnessed for the design of diastereodivergent <sup>[266]</sup> processes. Application of dual catalysis <sup>[267]</sup> to allylic alkylation chemistry has been shown to enable access to all four product stereoisomers with only one set of reaction conditions. <sup>[268–270]</sup>

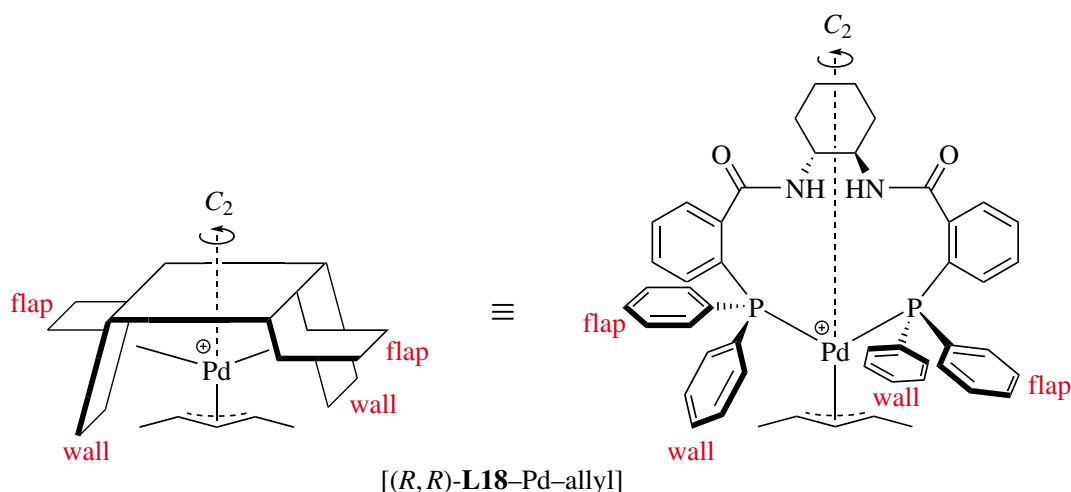
The realization of any of the five general mechanisms described requires fine tuning of a complex interplay of mechanistic interactions. These will be outlined in the following subsection, including stereochemical models that have been developed to rationalize enantioselectivity for two common ligand classes.

## 2.4.2 Key Interactions

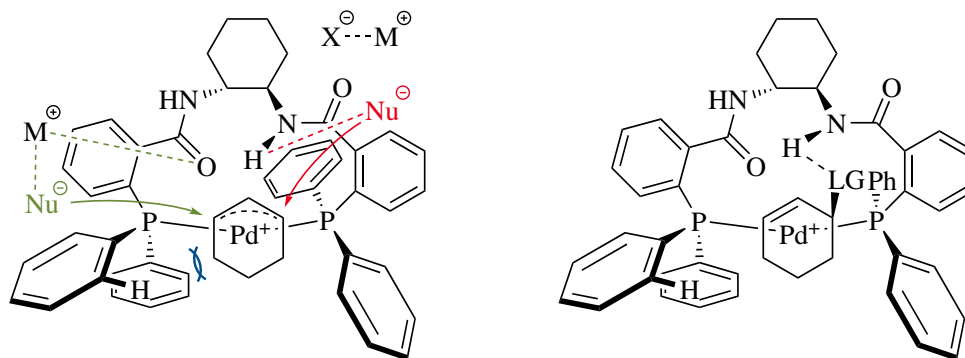
As a result of extensive mechanistic work,<sup>[69,123,124,271–278]</sup> three key interactions have been identified to govern enantioselectivity in allylic alkylation chemistry, constituting valuable design strategies for the development of novel chiral ligands. The first strategy implies the ligand to create a chiral cavity around the metal center, thus breaking the symmetry of the allylic system and disfavoring formation of one enantiomer. Secondly, the ligand may undergo a directing electronic interaction with the incoming nucleophile or – more rarely – with the departing leaving group, e.g. by means of a hydrogen bond, selectively facilitating formation of one enantiomer. The third rational applies mostly for chelate ligands and relies on electronic or steric interactions between ligand and allylic substrate, rendering one allylic terminus more reactive towards nucleophilic attack than the other. In most cases, enantioselectivity can not be fully explained by one of these models alone, but rather by a combination of several interactions which is individual for every ligand class.<sup>[48]</sup> The interactions described are usually of subtle nature, so that small changes regarding, for example, the counteraction of nucleophile,<sup>[279]</sup> the transition metal-to-ligand ratio<sup>[280]</sup> or a substituent at the ligand<sup>[281,282]</sup> can completely reverse the absolute configuration of the product, without changing the chirality of the ligand backbone.

For the popular DACH ligand series (also referred to as TROST ligands),<sup>[278,283]</sup> TROST has developed a rational relying on steric interactions in the reactive Pd-allyl intermediate,<sup>[278,284–286]</sup> which is depicted in Scheme 2.24 for the DACH standard ligand (*R,R*)-L18. Accordingly, the  $C_2$ -symmetric<sup>[287]</sup> ligand creates a chiral cavity, with two of the phosphine phenyl groups arranged approximately perpendicular ('wall') and the other two approximately parallel ('flap') to the allylic system. This 'wall-and-flap' model can be applied to all types of enantiodiscrimination (cf. Table 2.1) and has been employed for various examples of Pd-DACH catalyzed allylic substitutions to successfully predict the product's absolute configuration.<sup>[49,235,288–290]</sup> The basic idea is that – depending on which step is enantiodetermining – leaving group departure or nucleophilic attack will preferably proceed under one of the flap-type phenyl groups, as the opposite allylic terminus is sterically shielded by the walls (Scheme 2.24, bottom).<sup>[284]</sup>

A refined rational has been disclosed by LLOYD-JONES, NORRBY and coworkers,<sup>[124]</sup> including not only steric, but also electronic interactions into the mechanism of enantioselection. As result of a comprehensive NMR, isotopic labeling and computational study on a cyclohexenyl model system, the authors showed that the  $\eta^3$ -allyl chelate with DACH standard ligand (*R,R*)-L18 adopts a conformation with a concave ligand surface, in which one of the ligand's NH protons as well as the carbonyl group of the opposite amide unit are projected out of the concave surface in close vicinity of the allylic termini. As a consequence, enantioselectivity of nucleophilic attack is based on three main interactions (Scheme 2.25, left): a torquoselective steric bias analogous to the original wall-and-flap model disfavoring *pro-R* delivery (blue), a *pro-S* directing hydrogen bond between nucleophile and the proximate NH proton (red), and an electrostatic interaction



**Scheme 2.24:** Wall-and-flap model developed by TROST and coworkers<sup>[278,284-286]</sup> rationalizing the enantioselectivity of Pd-catalyzed allylic substitutions with DACH-type ligands: General cartoon of a Pd-allyl complex with DACH standard ligand (*R,R*)-L18 (top) and implications on the enantioselectivity of leaving group departure (bottom, left) and nucleophilic attack (bottom, right).

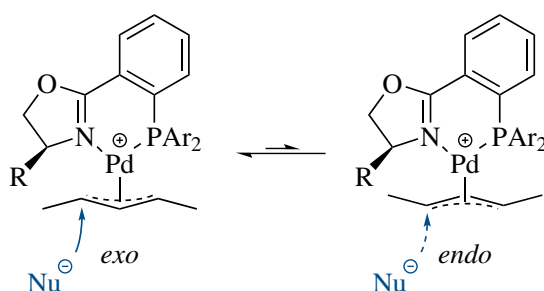


**Scheme 2.25:** Structural model disclosed by LLOYD-JONES, NORRBY and coworkers<sup>[124]</sup> rationalizing the enantioselectivity of Pd-catalyzed allylic substitutions with DACH standard ligand (*R,R*)-L18, using a cyclohexenyl model system and counterions  $M^+$  and  $X^-$ : Nucleophilic attack with *pro-R* disfavoring steric bias by interaction between one of the ligand's phenyl groups and the  $\eta^3$ -cyclohexenyl moiety, *pro-S* directing hydrogen bond between nucleophile and amide proton, and *pro-R* directing electrostatic interaction between  $M^+$  and an amide carbonyl function (left); kinetic resolution by hydrogen bond activation of the leaving group feasible only for the (*S*)-enantiomer of substrate (right).

between escort cation  $M^+$  and the concave oriented carbonyl group facilitating *pro-R* delivery (green). The dichotomy between the latter two interactions accounts for previous observations that enantioselectivity is dependent upon the identities of escort cation  $M^+$  and counterion  $X^-$  as well as the choice of solvent,<sup>[69,291,292]</sup> determining if  $M^+$  actively participates in the transition

state of nucleophilic attack or rather interacts with  $X^-$ . Also, the presence of a hydrogen bond acceptor in the nucleophile in 1,3-position relative to the nucleophilic site was disclosed to be crucial for formation of a *pro-S* directing hydrogen bond. Additionally, previous observations of a kinetic resolution to be operative for carboxylate<sup>[176,293–295]</sup> and carbonate<sup>[296,297]</sup> substrates with DACH-type ligands were rationalized by an activating hydrogen bond between the concave oriented NH proton and the leaving group in the  $\eta^2$ -substrate complex, which is only possible for the (*S*)-enantiomer of the cyclohexenyl substrate and thus selectively accelerates its oxidative addition (Scheme 2.25, right).<sup>[124]</sup>

While DACH ligands perform well on unhindered 1,3-disubstituted substrates, the phosphinooxazoline (PHOX) ligand series<sup>[298,299]</sup> has been established as ligands of choice for hindered 1,3-disubstituted electrophiles. Thus, both ligand classes have a complementary scope.<sup>[48]</sup> Pd-allyl complexes of PHOX ligands exist as a mixture of two rapidly equilibrating diastereomers in solution, with the *exo*-species typically being enriched (Scheme 2.26).<sup>[300]</sup> As the P-donor site exhibits a stronger *trans*-effect than the N-ligating function,<sup>[301]</sup> nucleophilic attack proceeds at the allylic terminus *trans* to P ( $> 10^4$  selectivity over attack *trans* to N<sup>[274]</sup>). The enantiomeric excess obtained usually exceeded the *exo:endo* ratios determined for the reactive  $\eta^3$ -intermediates, indicating that the *exo*-form is more reactive towards nucleophilic displacement.<sup>[300]</sup>

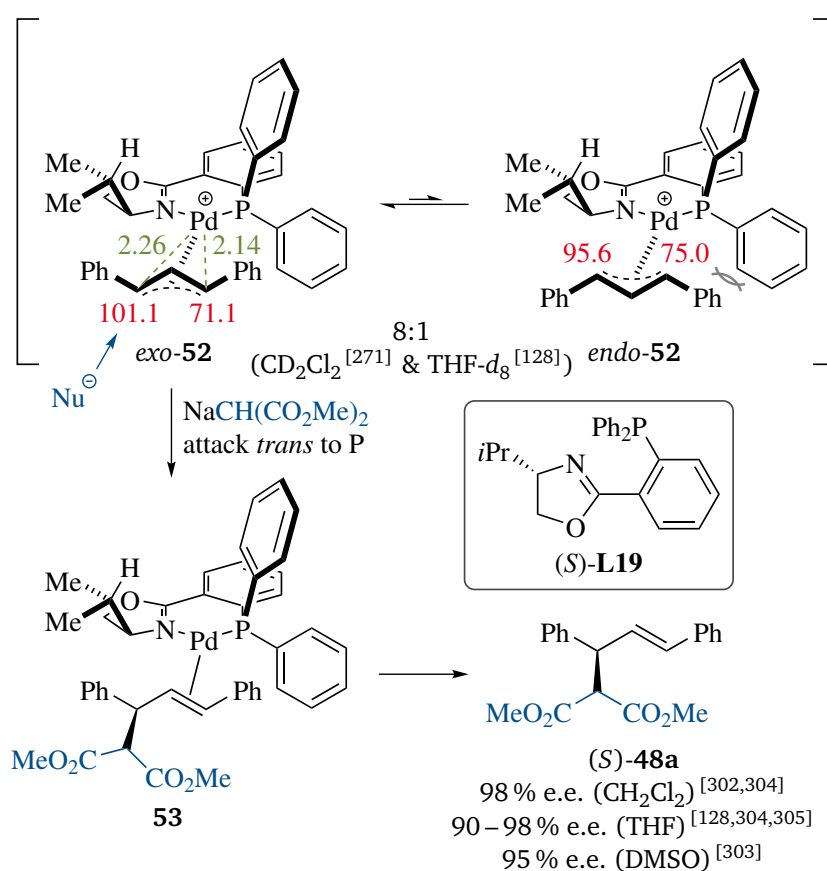


**Scheme 2.26:** General model for the enantioselectivity of Pd-PHOX catalyzed allylic substitutions enabled by a rapid equilibrium between diastereomeric  $\eta^3$ -intermediates, with the *exo*-form being enriched and more reactive towards nucleophilic attack *trans* to P (solid arrow) than the *endo*-species (dashed arrow). Ar denotes an aryl substituent, R is an organic moiety.

The mechanism of enantiodiscrimination has been studied in detail by the groups of HELMCHEN and BUNT, mainly using the 1,3-diphenylallyl model system in combination with *i*PrPHOX ligand (*S*)-L19 and a dimethyl malonate salt as stabilized nucleophile (Scheme 2.27). For the corresponding substitution product (*S*)-48a, consistently high enantiomeric excess of 90–98% have been reported in various solvents.<sup>[128,302–305]</sup> The oxidative addition products 52 have been characterized by solution NMR<sup>[128,271,274,306,307]</sup> and single-crystal X-ray diffraction.<sup>[128,274,307]</sup> In solution, an *exo:endo* ratio of 8:1 was determined at room temperature,<sup>[128,271]</sup> which even increases upon lowering the temperature.<sup>[306]</sup> This was ascribed to a destabilizing interaction of one of the phosphine phenyl groups with the proximate substrate substituent, which is



minimized in *exo*-**52**.<sup>[298,300]</sup> X-ray analysis of selectively crystallized *exo*-**52** revealed the Pd–C bond *trans* to P to be significantly longer than the Pd–C bond *trans* to N (2.26 Å vs 2.14 Å), confirming the strong *trans*-effect expected.<sup>[128,274]</sup> Furthermore, <sup>13</sup>C-NMR analysis showed that the difference  $\Delta\delta_C$  of <sup>13</sup>C-chemical shifts at the allylic termini is drastically higher for *exo*-**52** ( $\Delta\delta_C = 30.0$  ppm) than for its *endo*-diastereomer ( $\Delta\delta_C = 20.6$  ppm), indicating *exo*-**52** to display a stronger *trans*-effect and thus higher reactivity than *endo*-**52**.<sup>[271,307]</sup> HAMMETT<sup>[308,309]</sup> and SWAIN–LUPTON<sup>[310–312]</sup> analysis using electronically modified derivatives of (*S*)-**L19** disclosed that the *exo*-complex is less susceptible to electronic changes than its *endo*-form.<sup>[271]</sup> The  $\eta^2$ -product complex **53** arising from nucleophilic attack of sodium dimethyl malonate on *exo*-**52** at the carbon *trans* to P turned out to be metastable and could be characterized by low-temperature NMR analysis.<sup>[306,313]</sup>



**Scheme 2.27:** Summary of mechanistic studies on the enantioselectivity of Pd–PHOX catalyzed allylic substitutions, using the 1,3-diphenylallyl model system with *i*PrPHOX ligand (*S*)-**L19**:  $\eta^3$ -Allyl species **52** featuring an *exo*–*endo* equilibrium,<sup>[128,271]</sup> Pd–C distances determined by X-ray analysis of *exo*-**52** indicating a strong *trans*-effect (analyzed as SbF<sub>6</sub><sup>−</sup> salt, distances given in Å),<sup>[128,274]</sup> <sup>13</sup>C-NMR shifts of allylic termini suggesting the *trans*-effect to be significantly stronger for *exo*-**52** than for the *endo*-isomer (determined in CD<sub>2</sub>Cl<sub>2</sub>, given in ppm),<sup>[271]</sup> characterized  $\eta^2$ -product complex **53**,<sup>[306,313]</sup> and enantioselectivities determined for substitution product (*S*)-**48a**.<sup>[128,302–305]</sup>

In this section, the five general mechanisms of asymmetric induction in allylic substitution chemistry as defined by TROST<sup>[43,54,59,233]</sup> have been introduced. It has been shown that several steps in the catalytic cycle can be enantiodetermining, namely formation of the  $\eta^2$ -substrate



---

complex, oxidative addition,  $\pi$ - $\sigma$ - $\pi$  equilibration and nucleophilic attack. Either substrate or nucleophile can serve as chiral precursor, and a combination of both allows for achieving double stereoselectivity. Furthermore, the main interactions that govern enantioselectivity have been outlined, including sterically shielding and electronically directing interactions between ligand and incoming nucleophile or departing leaving group, as well as interactions between ligand and allylic system that render the allylic termini different in reactivity. Finally, key mechanistic work has been presented for two of the most widely used ligand classes (DACH and PHOX ligands). The next subchapter focuses on cyclobutenes as unusual substrates in allylic alkylation chemistry. Relevant enantioselective methods as well as mechanistic studies will be discussed.

---

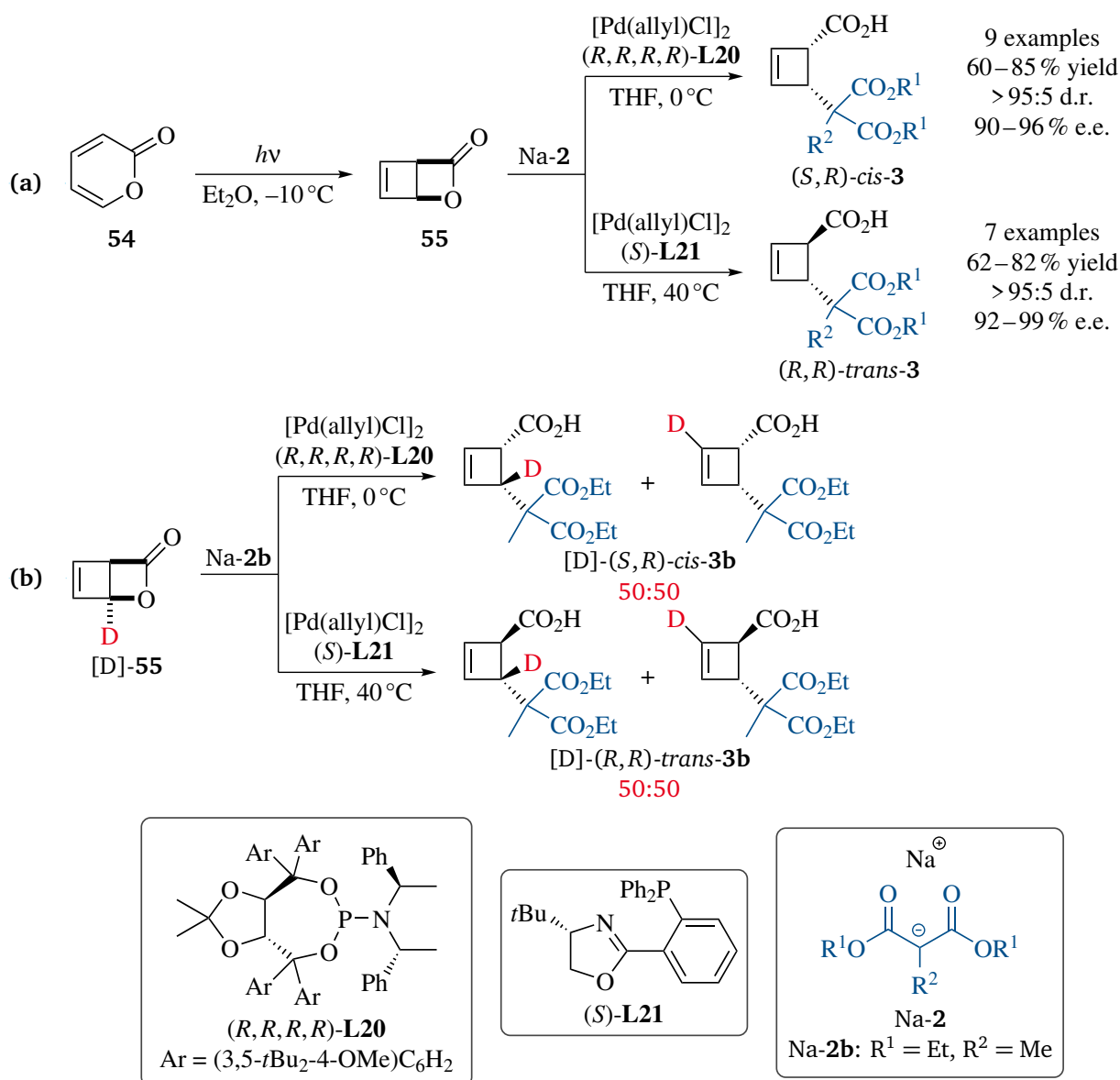
## 2.5 Allylic Substitution of Cyclobutenes

---

Substituted cyclobutenes are valuable synthetic intermediates for the preparation of polyene targets<sup>[314–317]</sup> and natural products with all-carbon four-membered rings,<sup>[318–322]</sup> exhibiting a rich chemistry with at times unexpected selectivities.<sup>[323–325]</sup> Their potential as substrates for asymmetric allylic substitutions has been harnessed by the MAULIDE and coworkers, who reported a number of stereoselective variants.<sup>[55,56,122,326,327]</sup>

Bicyclic lactone **55**,<sup>[328]</sup> prepared by 4- $\pi$ -photocyclization<sup>[329]</sup> from 2-pyrone **54** and handled as 0.1 – 0.2 M stock solution in Et<sub>2</sub>O, was found to be a suitable substrate for Pd-catalyzed allylic alkylation, featuring an internal leaving group.<sup>[326]</sup> With malonate nucleophiles Na-**2**, efficient deracemization of **55** could be achieved in the presence of tetraaryl-1,3-dioxolane-4,5-dimethanol (TADDOL) derived phosphoramidite ligand<sup>[330,331]</sup> (*R,R,R,R*)-**L20**, giving substitution products *cis*-**3** under retention of relative configuration (Scheme 2.28a). *t*BuPHOX ligand (*S*)-**L21** was found to promote highly selective deracemization of **55** as well. Strikingly, products *trans*-**3** were obtained with inversion of configuration, which is not in agreement with the selectivity expected according to the ‘double inversion rule’ valid for stabilized nucleophiles such as Na-**2** (cf. Scheme 2.10).<sup>[55]</sup> Thus, this protocol represents an example of diastereodivergent asymmetric catalysis.<sup>[332–334]</sup> When deuterated substrate [D]-**55** was subjected to both reaction conditions, products [D]-**3b** were obtained with full deuterium scrambling, showing that the reaction involves a transient symmetrization event for the allylic termini (Scheme 2.28b).<sup>[55]</sup>

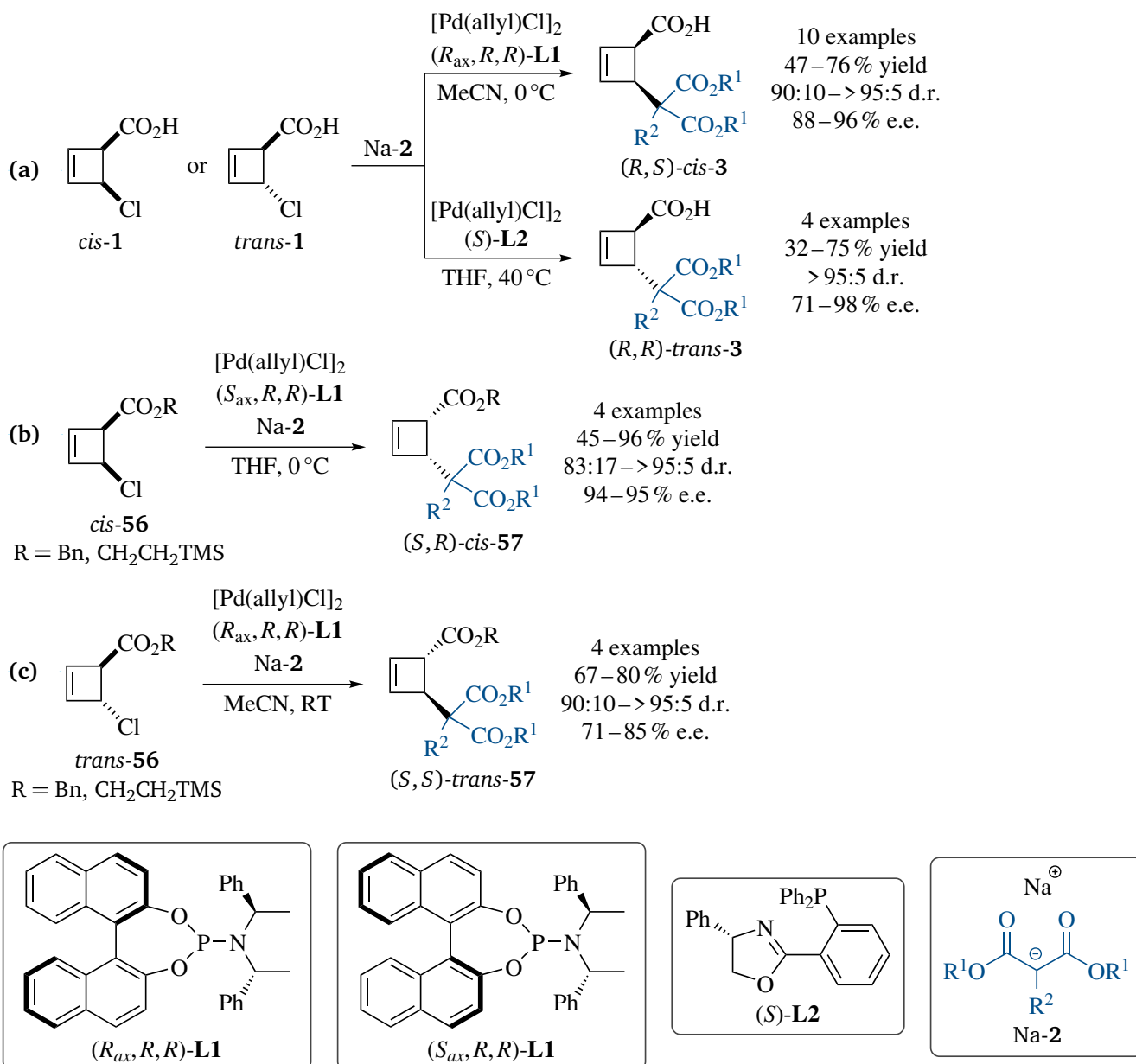
To further explore the uncommon stereoselectivity of this allylic alkylation system, *cis*- and *trans*-configured racemic acids **1**<sup>[335]</sup> were tested as substrates as well. Under somewhat modified reaction conditions, diastereodivergent deracemization could be accomplished again. By employing phosphoramidite ligand (*R*<sub>ax</sub>,*R,R*)-**L1**, *cis*-configured products *cis*-**3** were obtained, whereas PhPHOX ligand (*S*)-**L2** furnished the corresponding diastereomers *trans*-**3** (Scheme 2.29a). Surprisingly, the absolute and relative configuration of products **3** turned out to be independent of the relative configuration of substrate under both conditions, allowing this reaction to be used as de-epimerization.<sup>[56]</sup>



**Scheme 2.28:** Catalytic diastereodivergent deracemization of 2-oxabicyclo[2.2.0]hex-5-en-3-one **55**: (a) Preparation and Pd-catalyzed asymmetric allylic alkylation of **55**; (b) labeling studies exhibiting full deuterium scrambling for products [D]-**3b**.<sup>[55]</sup> R<sup>i</sup> denote organic moieties.

In stark contrast to acids **1**, allylic alkylation of the corresponding esters **56** in the presence of (*S*<sub>ax</sub>,*R,R*)-**L1** for *cis*-**56** and (*R*<sub>ax</sub>,*R,R*)-**L1** for *trans*-**56**, respectively, gave enantioenriched products **57** with retention of relative configuration, as expected from the ‘double inversion’ rule (Scheme 2.29b and c). Ligand (*S*)-**L2**, on the other hand, turned out not to be competent for these substrates.<sup>[56]</sup>

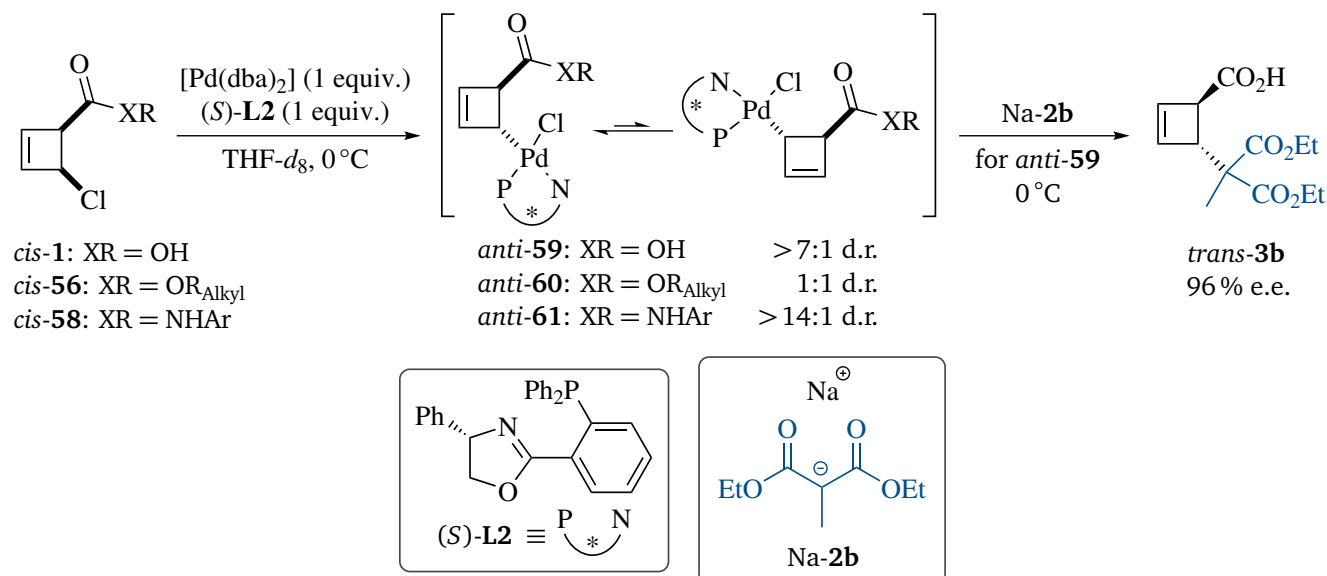
In order to shine light on the unusual stereochemical outcome furnished by cyclobutene substrates, further studies have been conducted, aiming to elucidate the structure of Pd intermediates.<sup>[57,58]</sup> When subjecting acid *cis*-**1**, esters *cis*-**56** and amide *cis*-**58** to stoichiometric reaction with a Pd<sup>0</sup> source and PHOX ligand (*S*)-**L2**, η<sup>1</sup>-complexes *anti*-**59**, *anti*-**60** and *anti*-**61** were obtained



**Scheme 2.29:** Catalytic deracemization of 4-chlorocyclobut-2-ene carboxylic acid **1** and corresponding esters **56**: (a) Pd-catalyzed asymmetric allylic alkylation of acid substrates *cis*- and *trans*-**1**, acting as diastereodivergent de-epimerization; Pd-catalyzed asymmetric allylic alkylation of (b) *cis*- and (c) *trans*-ester substrates **56**.<sup>[56]</sup> R<sup>i</sup> denote organic moieties.

instead of the  $\eta^3$ -species expected, with NMR spectroscopic data suggesting an *anti*-relationship of the cyclobutene substituents, i.e. oxidative addition under inversion (Scheme 2.30). For acid and amide complexes *anti*-**59** and *anti*-**61**, one of the two possible *anti*-diastereomers was found to be highly enriched, whereas ester complexes *anti*-**60** were obtained as rapidly interconverting diastereomeric 1:1 mixtures. DFT computations suggested a suprafacial  $\eta^1$ - $\eta^3$ - $\eta^1$  pathway to be operative for this equilibrium. When acidic  $\eta^1$ -species *anti*-**59** was treated with nucleophile Na-**2b**, the same product stereoisomer *trans*-**3b** was obtained as under catalytic conditions,

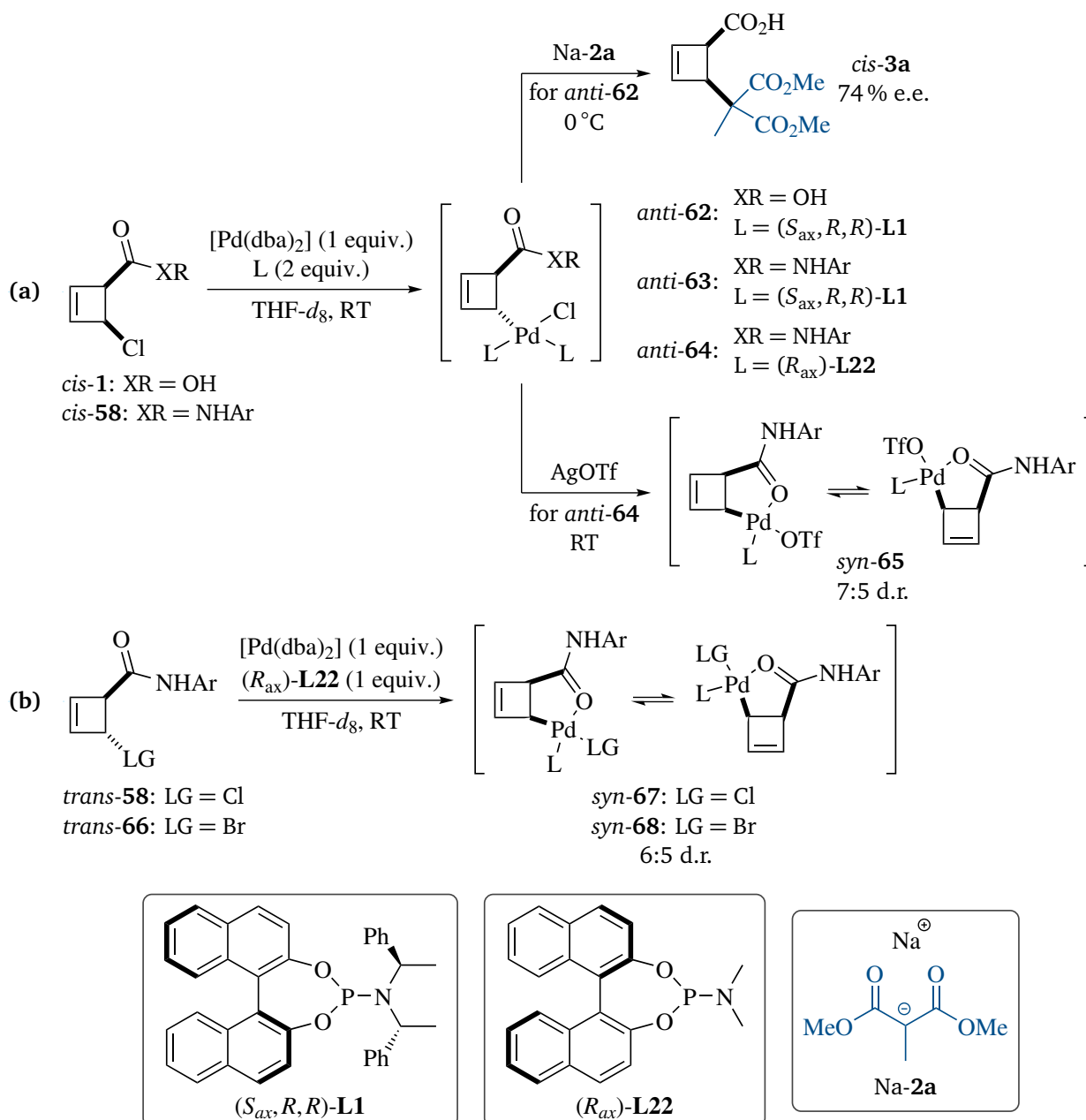
indicating *anti*-**59** to be a catalytically active intermediate. Amide complex *anti*-**61** turned out to be sufficiently stable for isolation. Single-crystal X-ray analysis of *anti*-**61** revealed the presence of a hydrogen bond between Cl and the NH proton, as well as a slightly distorted square-planar coordination geometry at the Pd center.<sup>[57]</sup>



**Scheme 2.30:** Preparation of  $\eta^1$ -coordinated Pd–cyclobutene complexes ligated by PhPHOX ligand (S)-L2 as putative allylic alkylation intermediates ( $R_{\text{Alkyl}}$  = Me, Bn,  $\text{CH}_2\text{CH}_2\text{TMS}$ ; Ar = *p*-tolyl), and reactivity of complex *anti*-**59** towards nucleophile Na-2b.<sup>[57]</sup>

In a subsequent collaboration with the THIELE group, the corresponding phosphoramidite complexes were investigated. Oxidative addition of both acid *cis*-**1** and amide *cis*-**58** with ligand ( $R_{\text{ax}}$ , *R*, *R*)-L1 or MonoPhos ( $R_{\text{ax}}$ )-L22 as less bulky model ligand proceeded under inversion, giving  $\eta^1$ -species *anti*-**62**, *anti*-**63** and *anti*-**64**, respectively, as single diastereomers (Scheme 2.31a). Acidic Pd complex *anti*-**62** responded productively upon addition of nucleophile Na-2a, furnishing enantioenriched substitution product *cis*-**3a** with the relative configuration consistent to the catalytic process. Addition of AgOTf to amide-MonoPhos complex *anti*-**64** resulted in an unexpected antarafacial exchange upon Cl–OTf ligand exchange to produce complex *syn*-**65** as a 7:5 mixture of interconverting diastereomers.<sup>[58]</sup>

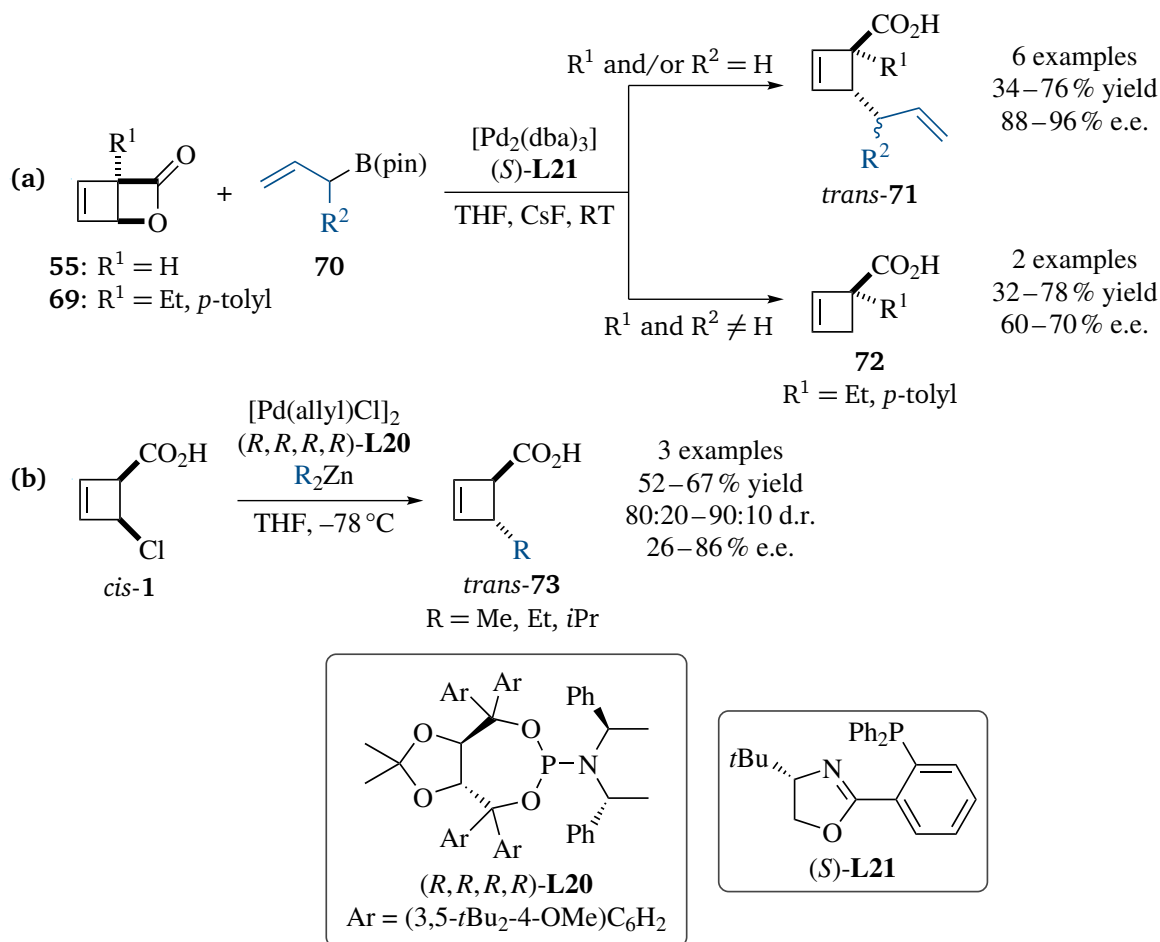
Like its *cis*-diastereomer, substrate *trans*-**58** as well as the corresponding bromide *trans*-**66** underwent oxidative addition under inversion upon addition of a Pd<sup>0</sup> source and ligand ( $R_{\text{ax}}$ )-L22 (Scheme 2.31b). The resulting Pd species *syn*-**67** and *syn*-**68** were obtained as diastereomeric, equilibrating 6:5 mixtures. DFT calculations again supported a facile  $\eta^1$ – $\eta^3$ – $\eta^1$  path to be responsible for this exchange process. All *syn*-configured complexes investigated (*syn*-**65**, *syn*-**67** and *syn*-**68**) were found to be stabilized by internal Pd–O coordination, as indicated by <sup>13</sup>C-NMR displaying strongly deshielded signals for the carboxylate carbons. The major diastereomer of *syn*-**68** could furthermore be selectively crystallized and analyzed by X-ray diffraction.<sup>[58]</sup>



**Scheme 2.31:** Preparation of  $\eta^1$ -coordinated Pd–cyclobutene complexes ligated by phosphoramidite ligands (*R*<sub>ax</sub>, *R*, *R*)-L1 or (*R*<sub>ax</sub>)-L22 as putative allylic alkylation intermediates: (a) Oxidative addition of *cis*-configured cyclobutene substrates and reactivity of *anti*-complexes obtained towards nucleophile Na-2a and facial exchange triggered by AgOTf; (b) Oxidative addition of *trans*-configured cyclobutene substrates giving internally chelated *syn*-complexes (Ar = *p*-tolyl; L denotes the respective ligand). The absolute configuration of substitution product *cis*-3a was not determined.<sup>[58]</sup>

Apart from stabilized nucleophiles, hard nucleophiles have also been explored as reaction partners in Pd-catalyzed asymmetric allylic alkylations of cyclobutene substrates.<sup>[122,327]</sup> Allyl boronate nucleophiles **70**, originally established by MORKEN and coworkers,<sup>[120,336,337]</sup> were successfully employed for the catalytic deracemization of lactone **55** and its  $\alpha$ -substituted derivatives **69** in the presence of ligand (*S*)-L21 (Scheme 2.32a). The chemoselectivity was found to depend

on the combination of starting materials: If either the allylic substrate or the boronate (or both) were unsubstituted, allylated cyclobutenes *trans*-71 were obtained under inversion of relative configuration, consistent with an inner-sphere mechanism, whereas sterically hindered electrophile-nucleophile combinations led to the formation of hydrodehalogenation products 72, presumably by  $\beta$ -hydride elimination from the transmetalated Pd intermediate.<sup>[327]</sup>



**Scheme 2.32:** Catalytic deracemization of cyclobutene substrates with hard nucleophiles: (a) Pd-catalyzed asymmetric allylic alkylation or halide reduction of lactones 55 and 69 with allyl boronates 70;<sup>[327]</sup> (b) Pd-catalyzed asymmetric allylic alkylation of acid *cis*-1 with dialkylzinc.<sup>[122]</sup>  $R^i$  denote organic moieties or hydrogen atoms. The absolute configurations of enantioenriched products 71 – 73 was not determined. When prochiral allyl boronates were used ( $R^2 \neq H$ ), products *trans*-71 were obtained as 1:1 epimeric mixtures.

Moreover, dialkylzinc reagents have been demonstrated to be competent nucleophiles for the Pd-catalyzed allylic alkylation of cyclobutene substrate *cis*-1. Using sterically congested ligand (*R,R,R,R*)-L20, deracemization of *cis*-1 could be achieved, giving alkylated products *trans*-73 with inversion of relative configuration (Scheme 2.32b).<sup>[122]</sup> This report represents a noteworthy exception from the commonly observed umpolung reactivity of Pd–allyl complexes in the presence of organozinc compounds,<sup>[338]</sup> as especially known from the Pd-catalyzed and dialkylzinc-mediated allylation of aldehydes.<sup>[339–344]</sup>

---

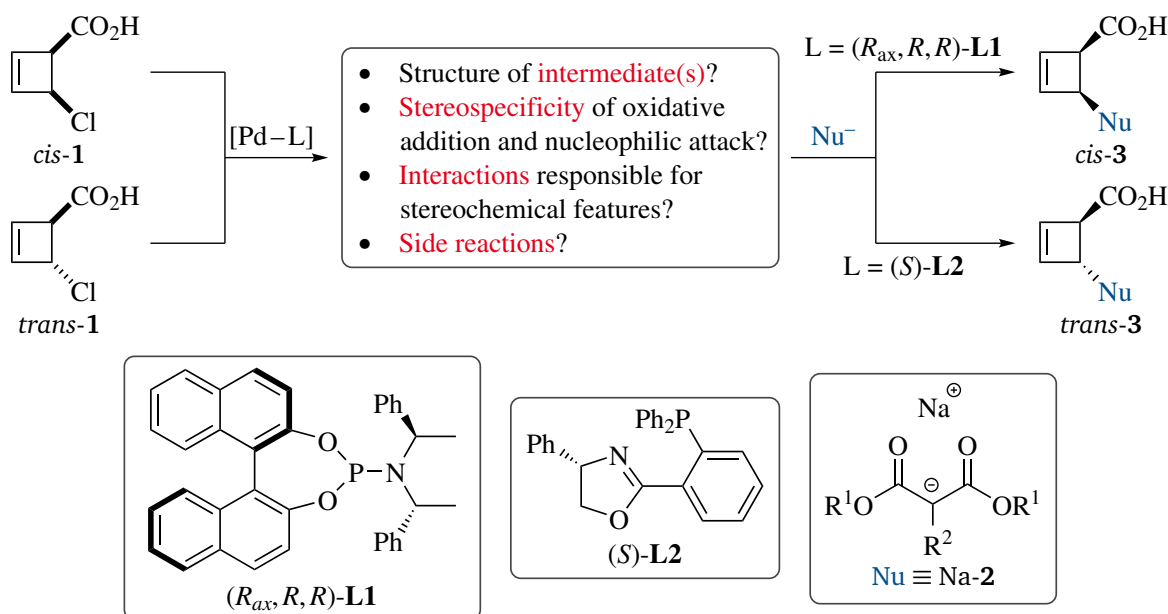
In summary, cyclobutene substrates can be efficiently deracemized by Pd-catalyzed allylic alkylation with both stabilized and non-stabilized nucleophiles. Highly remarkable chemo- and stereoselectivities have been reported, which have stimulated further mechanistic studies. These have revealed that cyclobutenes form fairly stable  $\eta^1$ -complexes upon oxidative addition, which can interconvert via a  $\eta^1$ - $\eta^3$ - $\eta^1$  equilibrium. However, a general model accounting for the unprecedented stereoselectivity has hitherto not been presented.





### 3 Motivation and Aims

The transition metal catalyzed allylic substitution appears at first glance to be a mechanistically simple reaction with seemingly well-understood stereospecificity and stereoselectivity. However, many decades after its discovery,<sup>[110,111]</sup> it continues to surprise and fascinate by emergence of novel variants with unconventional stereochemical outcome enabled by previously hidden mechanistic complexity.<sup>[48]</sup> One of the most remarkable contemporary developments in this area has undoubtedly been the Pd-catalyzed asymmetric allylic alkylation of racemic 3,4-disubstituted cyclobutene electrophiles, disclosed between 2011 and 2012 by the MAULIDE group.<sup>[55,56]</sup> This variant allows for selectively converting racemic and/or epimeric mixtures of cyclobutene substrate **1** into one out of four possible stereoisomers of substitution products **3**, with the ligand mediating between *cis*- and *trans*-selectivity (Scheme 3.1).<sup>[56]</sup> Thus, it represents a unique example of a one-step diastereodivergent deracemization combined with a de-epimerization.



**Scheme 3.1:** Pd-catalyzed asymmetric allylic alkylation of cyclobutene substrates **1** as reaction of interest for this work. R<sup>i</sup> denote organic moieties.

Subsequent mechanistic investigations have revealed that oxidative addition of cyclobutene substrates furnishes  $\eta^1$ - rather than  $\eta^3$ -configured Pd–cyclobutene species. Using predominantly amides as more stable model systems, the Pd–allyl complexes obtained were extensively characterized by NMR spectroscopy and X-ray diffraction. For all complexes investigated, the relative configuration with respect to the cyclobutene was opposite compared to the starting material, suggesting oxidative addition to proceed under inversion. Pd species with a *syn*-relationship

---

across the cyclobutene were found to be stabilized by internal chelation, which was speculated to be a driving force of the reaction. *anti*-Configured  $\eta^1$ -complexes reacted productively upon treatment with nucleophiles Na-2, whereas no such data were presented for the corresponding *syn*-species. Computational studies and complementary EXSY experiments indicated the presence of a suprafacial  $\eta^1$ - $\eta^3$ - $\eta^1$  pathway enabling facile exchange between diastereomeric  $\eta^1$ -species.<sup>[57,58]</sup>

Albeit these studies gained detailed insight into the structure and dynamics of putative Pd intermediates, they could not disclose a conclusive rationale explaining the stereoselectivity observed. Therefore, the present work aims to develop an overarching mechanistic proposal that fully explains the unusual stereochemical features of the reaction. More specifically, the objective is to identify the mechanistic events responsible for deracemization, de-epimerization and diastereodivergence, respectively, as well as the driving forces behind those.

In order to accomplish these goals, the reaction of interest shall be studied under conditions as close as possible to the synthetic ones. This especially includes reaction monitoring and kinetic experiments as well as isotopic labeling studies and the preparation and characterization of putative Pd intermediates. In contrast to previous mechanistic studies,<sup>[57,58]</sup> the latter experiments will focus on Pd-allyl complexes prepared from the actual electrophiles **1** rather than the corresponding amides, which are – from a preparative point of view – irrelevant as they are not competent to perform with a stereoselectivity comparable to **1**.<sup>[58]</sup>

In a first step, the single steps of the reaction shall be investigated. To this end, the oxidative addition of substrates **1** will be studied by both end-point analyses of the Pd-allyl complexes obtained and NMR reaction monitoring of their formation. In addition, the reactivity of these Pd-cyclobutene species towards nucleophilic displacement will be probed systematically. Preliminary results for this part of the project have already been disclosed in the Ph.D. thesis of JULIAN ILGEN.<sup>[345]</sup> The second step is to corroborate which of the Pd-cyclobutene species characterized are present under catalytic conditions. This might be achieved by reaction monitoring techniques that are competent to detect these catalytic species, e.g. <sup>31</sup>P-NMR or high resolution mass spectroscopy coupled with electrospray ionization (ESI-HRMS), and by complementary intermediate capture reactions. The results from all these experiments are anticipated to allow for concluding on the stereospecificity of oxidative addition and nucleophilic attack, and for disclosing in which mechanistic steps the stereochemical features deracemization, de-epimerization and diastereodivergence are anchored, respectively.

With this preliminary mechanistic outline in hand, the detailed mechanism of the key steps shall be further investigated. To examine whether stereoselectivity is governed by a steric interplay between the nucleophile and the reactive Pd complex, test reactions with a series of sterically different but electronically comparable derivatives of Na-2 will be carried out. A kinetic analysis<sup>[346]</sup> shall furthermore allow for determining the turn-over limiting step. The experiments planned also encompass the determination of <sup>2</sup>H- and <sup>13</sup>C-kinetic isotope effects (KIEs)<sup>[347]</sup>

---

for both substrate and nucleophile, which will be indicative for the transition states of key steps. These results shall be used for refining the mechanistic proposal, allowing for disclosing a comprehensive rationale that fully accounts for the astonishing stereoselectivity displayed by the asymmetric allylic alkylation of cyclobutenes.



---

# 4 Results and Discussion

---

## 4.1 Synthesis of Starting Materials

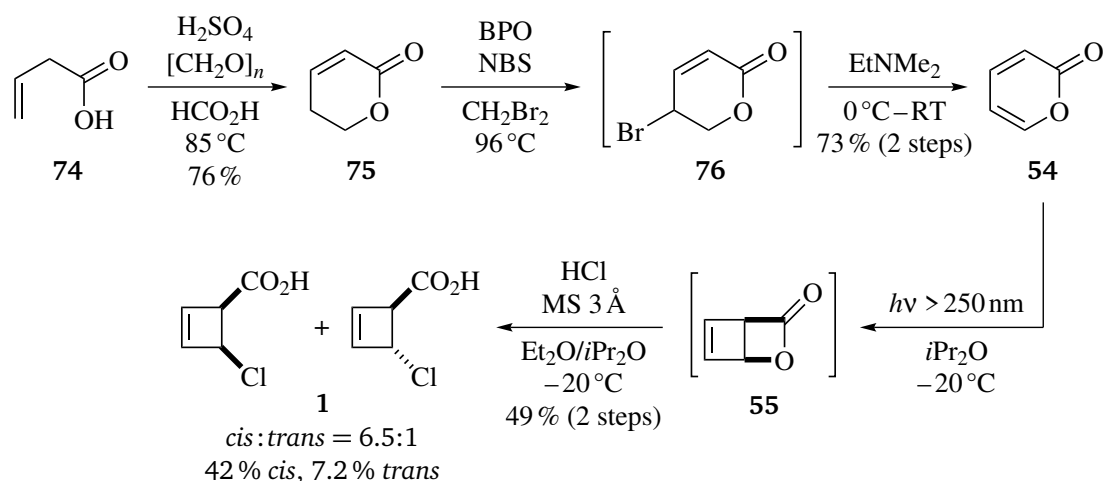
---

Prior to commencing with mechanistic experiments, the starting materials for the reaction of interest had to be synthesized from commercially available precursors. In the following, the preparation of cyclobutene substrates and malonate nucleophiles will be described briefly, including the synthesis of  $^2\text{H}$ - and  $^{13}\text{C}$ -labeled isotopologues.

### 4.1.1 On the Preparation of Cyclobutene Substrates

Cyclobutene acids **1** were synthesized starting from vinylacetic acid **74**, following modified literature procedures (Scheme 4.1). In the first step, **74** was cyclized with formaldehyde generated *in situ* from paraformaldehyde.<sup>[348]</sup> After optimization of solvent (formic acid instead of acetic acid) and temperature (85 °C instead of reflux), 5,6-dihydro-2-pyrone **75** was obtained with 76 % yield (literature:<sup>[348–350]</sup> 25 – 48 %).

**75** was then subjected to WOHL–ZIEGLER bromination<sup>[351–353]</sup> to give 5-bromo-5,6-dihydro-2-pyrone **76**. For this type of radical bromination, the choice of solvent is of critical importance, and  $\text{CCl}_4$  has been established as medium of choice due to its inert behavior against bromine radicals, a low solubility for the bromine source *N*-bromosuccinimide (NBS) and the by-product succinimide,<sup>[354]</sup> and a sufficiently high boiling point (77 °C<sup>[355]</sup>) required to overcome the relatively high activation barrier of this reaction.<sup>[356–358]</sup> However, environmental and toxicological concerns have strongly limited the availability of  $\text{CCl}_4$ , thus making it necessary to change to a less problematic alternative solvent for the large-scale bromination of **75**. After a series of unsuccessful test reactions in  $\text{CHCl}_3$ <sup>[359]</sup> (no reaction), cyclohexane<sup>[360]</sup> (bromination of solvent) and  $\text{CBrCl}_3$  (predominantly addition of  $\text{Br}_2$  to the double bond), selective allylic bromination could be achieved with  $\text{PhCl}$ <sup>[361,362]</sup> as reaction medium. However, due to its high boiling point (132 °C<sup>[363]</sup>), the use of  $\text{PhCl}$  as solvent turned out to be inconvenient on preparative scale. Eventually,  $\text{CH}_2\text{Br}_2$  (b.p. 97 °C<sup>[364]</sup>) was identified as equivalent alternative to  $\text{CCl}_4$ , giving allylic bromide **76** with only low amounts of side products formed by ionic addition of  $\text{Br}_2$  to the double bond or by a second allylic bromination of **76**. After elimination of  $\text{HBr}$  with  $\text{EtNMe}_2$  as base, 2-pyrone **54** was obtained with 73 % yield after two steps (literature:<sup>[348–350]</sup> 34 – 70 % in  $\text{CCl}_4$ ). The product was found to be a thermally and photochemically unstable compound, as, for instance, showcased by freshly distilled samples turning from colorless to brownish overnight when stored at  $\geq 4$  °C without light protection. Stable storage of **54** could be achieved at  $-20$  °C in a brown-glass flask.



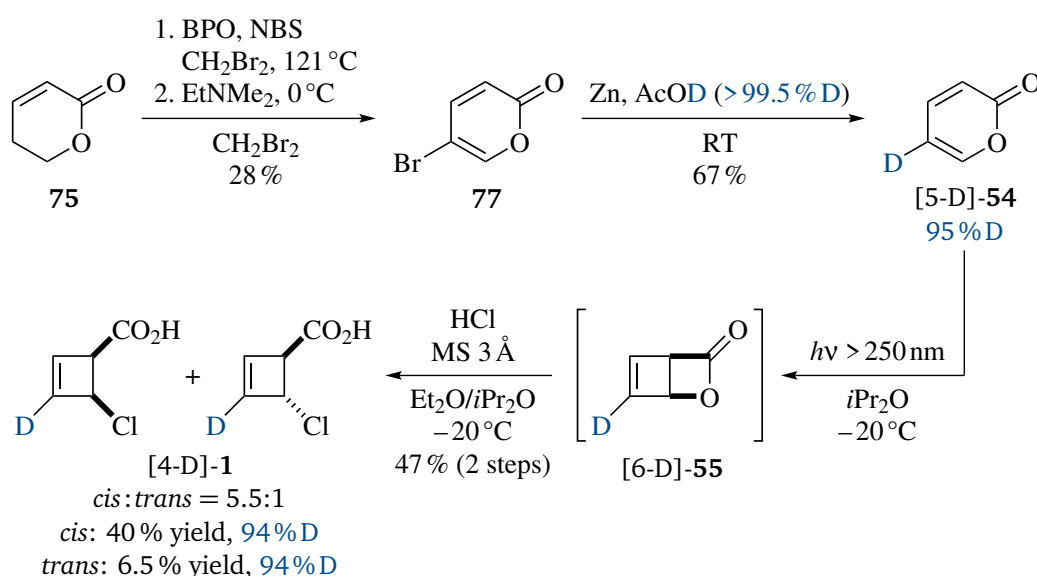
**Scheme 4.1:** Synthesis of cyclobutene substrates **1** (top) and images of the circulating flow photoreactor employed for the photocyclization of 2-pyrone **54** (bottom).

As a more step-efficient access to **54**, the thermal gas-phase decarboxylation of commercially available coumalic acid has been reported.<sup>[365,366]</sup> However, the harsh reaction conditions required for this one-step protocol (650–670 °C, < 7 mbar, continuous gas stream) could not be realized with the laboratory equipment available. Attempts to achieve protodecarboxylation of coumalic acid under milder conditions using a silver-catalyzed variant<sup>[367]</sup> were unsuccessful, as were test reactions employing BARTON<sup>[368,369]</sup> conditions. Also, an open-chain approach with a ring-closing esterification as final step remained unproductive, as described in more detail in the master's thesis of SONJA DÖLLER.<sup>[370]</sup>

2-Pyrone **54** was further subjected to photoisomerization under UV-irradiation giving a solution of bicyclic lactone **55**,<sup>[328]</sup> followed by partial ring-opening with HCl to furnish a diastereomeric mixture of cyclobutenes *cis*- and *trans*-**1**.<sup>[335]</sup> The photoisomerization of **54** has been reported

both in batch (with Et<sub>2</sub>O as solvent)<sup>[326,328,335,371]</sup> and under continuous flow conditions (in MTBE).<sup>[372]</sup> In general, irradiation has to be performed with an optical cut-off filter and under sufficient cooling, in order to avoid photochemical or thermal decomposition of **55**. For cost reasons, the flow variant was chosen, using a water-cooled mercury arc lamp surrounded by aqueous Na<sub>2</sub>WO<sub>4</sub> as 250 nm<sup>[373]</sup> cut-off filter. Since MTBE turned out not to be compatible with HCl used as reagent in the subsequent step, the solvent was changed to iPr<sub>2</sub>O. As already reported in the original flow procedure for the photoisomerization of **54**,<sup>[372]</sup> scale-out runs were plagued by fouling inside the reactor coil, which is a common problem in flow photochemistry.<sup>[374–377]</sup> This led to a successively decreasing irradiation efficiency and, as a consequence, incomplete conversion in the product solution collected. Quantitative conversion could be achieved by performing the reaction in a circulating-flow rather than a continuous-flow fashion, which allowed for continuing irradiation until reaching full conversion of **54**. After addition of HCl, product **1** was typically obtained with a *cis*:*trans* ratio of 6.5:1, and both diastereomers could be separated by careful flash column chromatography. Main product *cis*-**1** was obtained with a yield of up to 42% over two steps (best yield achieved by PATRICK MAIBACH as part of his master's thesis),<sup>[378]</sup> which is somewhat below the yields that have been reported using batch systems for the photoisomerization of **54** (44–83%<sup>[56,317,371]</sup>).

For labeling and KIE studies (see sections 4.2 and 4.6), the preparation of deuterated substrates [4-D]- and [5-D]/[3-D]-**1**<sup>[335]</sup> (deuterium scrambling as a result of the synthesis, *vide infra*) was envisioned. Both targets were synthesized by master student PATRICK MAIBACH.<sup>[378]</sup> Isotopologue [4-D]-**1** was prepared starting from 5,6-dihydro-2-pyrone **75** (Scheme 4.2), with the synthesis being literature-known apart from the last step.<sup>[335,379,380]</sup> WOHL–ZIEGLER dibromination under similar conditions as the corresponding monobromination (*vide supra*) followed by basic work-up

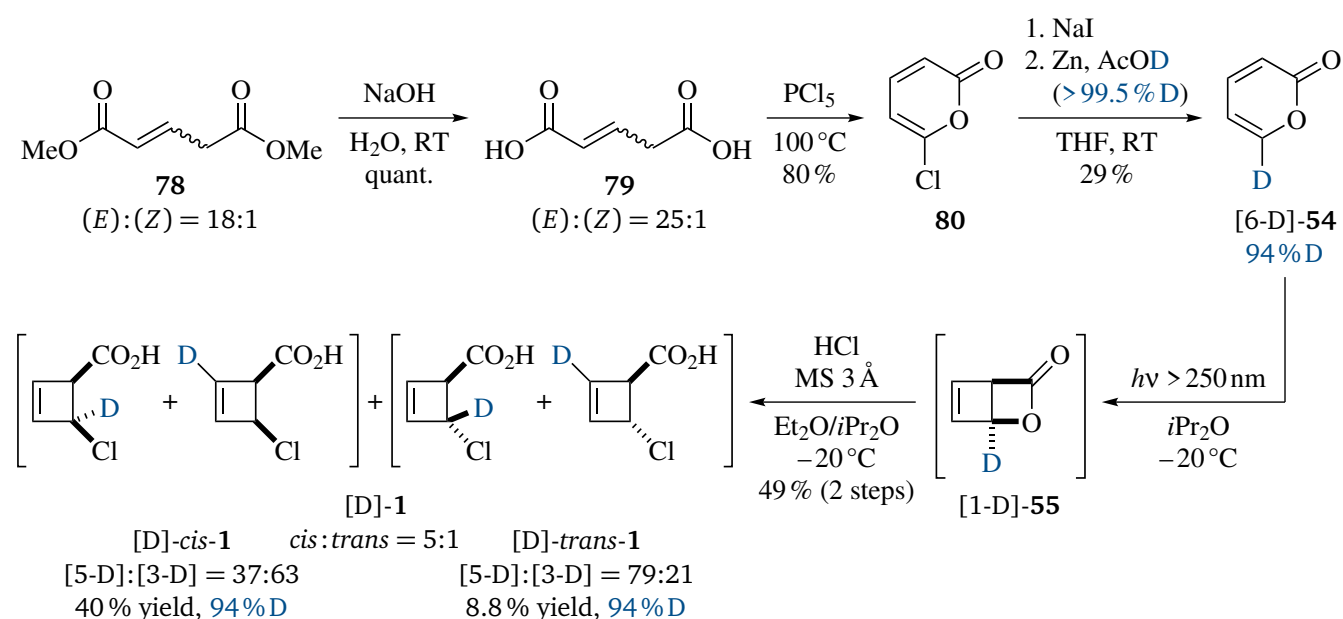


**Scheme 4.2:** Synthesis of deuterated cyclobutene substrates [4-D]-**1**, performed as part of a master's thesis related to this work.<sup>[378]</sup>



with EtNMe<sub>2</sub> gave 5-bromo-2-pyrone **77** in 28 % yield (literature: <sup>[350,380,381]</sup> 31 – 34 % in CCl<sub>4</sub>). In contrast to the monobromination of **75**, elimination of HBr proceeded spontaneously, as shown by NMR analysis of the reaction mixture, and a basic work-up was only required for ensuring facile separation of side products. A one-pot halogen–zinc exchange with AcOD as trapping agent for the transient zinc organyl <sup>[382]</sup> afforded selectively deuterated 2-pyrone [5-D]-**54** with improved yield (67 %) and isotopic purity (95 % D) compared to the literature procedure (30 % yield, 87 – 88 % D <sup>[379]</sup>). Photoisomerization and subsequent addition of HCl to the intermediate lactone [6-D]-**55** <sup>[335]</sup> furnished labeled substrates *cis*- and *trans*-[4-D]-**1** with an isotopic purity of 94 % D. <sup>[378]</sup>

The synthesis of [5-D]/[3-D]-**1** has been described in the literature <sup>[335,379]</sup> and was largely adopted (Scheme 4.3). Starting from a diastereomeric mixture of dimethyl glutaconate **78**, alkaline ester hydrolysis gave glutaconic acid **79**, <sup>[383]</sup> which was treated with PCl<sub>5</sub> to afford 6-chloro-2-pyrone **80**. <sup>[335,384]</sup> A FINKELSTEIN reaction <sup>[385]</sup> with NaI followed by halogen–zinc–deuterium exchange furnished 2-pyrone isotopologue [6-D]-**54** with somewhat lower yield (29 %) and isotopic purity (94 % D) as reported in the literature procedure (39 % yield, 96 % D <sup>[379]</sup>). 4- $\pi$ -Photocyclization afforded a solution of lactone [1-D]-**55**, <sup>[335]</sup> which was treated with HCl to give a 37:63 isotopomeric mixture of [5-D]- and [3-D]-*cis*-**1** along with a 79:21 mixture of [5-D]- and [3-D]-*trans*-**1**, both products featuring an overall isotopic purity of 94 % D. <sup>[378]</sup> These observations are not in full agreement with those of PIRKLE and coworkers, who reported a 50:50 scrambling for [5-D]/[3-D]-*cis*-**1** consistent with an S<sub>N</sub>1 mechanism and no detectable scrambling for [5-D]-*trans*-**1** indicating an S<sub>N</sub>2 path. <sup>[335]</sup> The [5-D]:[3-D] ratios reported herein suggest



**Scheme 4.3:** Synthesis of deuterated cyclobutene substrates [5-D]/[3-D]-**1**, performed as part of a master's thesis related to this work. <sup>[378]</sup>



---

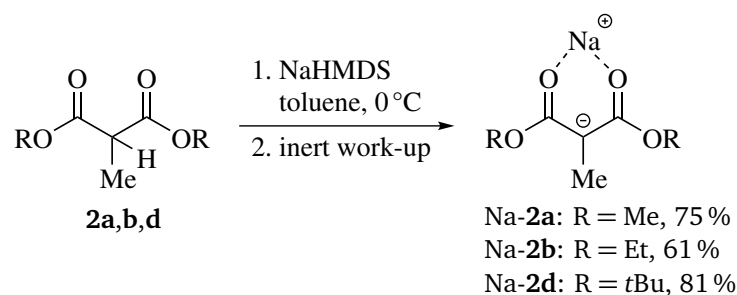
that both *cis*- and *trans*-**1** are not formed via one substitution mechanism alone, but rather by a combination of at least two paths, with S<sub>N</sub>1 (full scrambling), S<sub>N</sub>2 (formation of [5-D]-**1**) and S<sub>N</sub>2' (formation of [3-D]-**1**) as possible scenarios.<sup>[378]</sup> The experimental extent of deuterium scrambling is, however, of no relevance for the mechanistic experiments planned with substrates [5-D]/[3-D]-**1**, as the reaction investigated in this work includes a symmetrizing event for the allylic termini (cf. Scheme 2.28b, see also Scheme 4.15).

#### 4.1.2 On the Preparation of Malonate Nucleophiles

Malonate salts represent a versatile class of stabilized nucleophiles and have been employed for various C–C bond forming reactions.<sup>[386,387]</sup> Most commonly they are generated *in situ* by deprotonation of the parent acidic malonate diester, using a sufficiently strong base such as NaH,<sup>[388–392]</sup> an alkoxide<sup>[393–395]</sup> or the BSA/acetate system.<sup>[396–399]</sup>

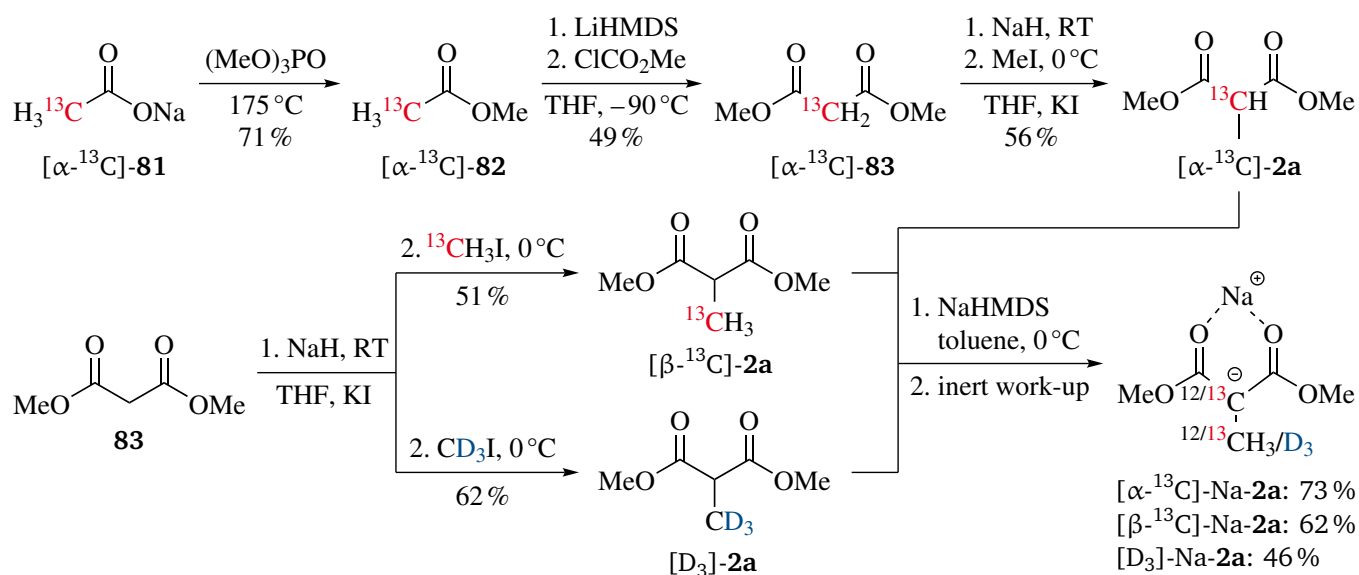
The reaction investigated in this work has been performed with alkylated sodium malonates Na-**2** as tertiary C-nucleophiles, prepared *in situ* by deprotonation of the corresponding malonate pronucleophiles **2** with NaH prior to addition of catalyst and substrate.<sup>[55–58]</sup> In order to facilitate reaction monitoring experiments and kinetic studies, the isolation of reactive nucleophiles Na-**2** was envisioned. Several reports describe the isolation of non-alkylated sodium malonates NaCH(CO<sub>2</sub>R)<sub>2</sub>,<sup>[400–403]</sup> however, analogous data for alkylated malonate salts MCR(CO<sub>2</sub>R')<sub>2</sub> are scarce. Sodium dimethyl methylmalonate NaCMe(CO<sub>2</sub>Me)<sub>2</sub> has been isolated by deprotonation of the corresponding neutral malonate with NaOMe in MeOH, followed by removal of the solvent.<sup>[400]</sup> However, no characterization data are given for the solid product obtained. Lithium diethyl alkylmalonates LiCR(CO<sub>2</sub>Et)<sub>2</sub> have been isolated and characterized after deprotonation with LiHMDS in THF followed by removal of solvent and HMDS.<sup>[404]</sup> For sodium<sup>[405]</sup> and potassium<sup>[406]</sup> as counterion, characterization data of *in situ* prepared alkylated diethyl malonate salts MCR(CO<sub>2</sub>Et)<sub>2</sub> have been reported using DMSO/DMSO-*d*<sub>6</sub> as solvent.

After some preliminary experimentation, NaHMDS<sup>[407]</sup> emerged as an ideal base for the isolation of alkylated sodium malonates, featuring commercial availability in sufficiently high purity, a low nucleophilicity and excellent solubility in common organic solvents. When dialkyl methylmalonates **2a,b,d** were subjected to a solution of NaHMDS in toluene, precipitation of a colorless solid was observed, which after inert filtration and anhydrous washing was identified as fairly pure deprotonated species Na-**2a,b,d** (Scheme 4.4). The isolated malonate salts turned out to be highly water-sensitive, undergoing mono- and dihydrolysis of the ester units upon contact with moisture. Nevertheless, the products could be stably stored and characterized under inert conditions. Malonate salts Na-**2a,b,d** were found to be highly soluble and stable in THF, but slowly decomposed in MeCN forming an insoluble precipitate. As model nucleophile for the forthcoming mechanistic analysis, sodium dimethyl methylmalonate Na-**2a** was chosen due to its simple NMR spectra. Inert recrystallization of Na-**2a** from THF/*n*-hexane gave highly pure material suitable for kinetic studies.



**Scheme 4.4:** Isolation of moisture-sensitive sodium malonate salts Na-2.

In order to allow for extraction of  $^{13}\text{C}$ -KIEs as well as for tracing of a potential  $\beta$ -hydride elimination (see sections 4.4 and 4.6), labeled nucleophiles  $[\alpha\text{-}^{13}\text{C}]$ -,  $[\beta\text{-}^{13}\text{C}]$ - and  $[\text{D}_3]$ -Na-**2a** were required. The preparation of deuterated dimethyl methylmalonate  $[\text{D}_3]$ -**2a** has been reported in the literature,<sup>[408]</sup> as has been the synthesis of diethyl analogues of  $^{13}\text{C}$ -labeled pronucleophiles  $[\alpha\text{-}^{13}\text{C}]$ - and  $[\beta\text{-}^{13}\text{C}]$ -**2a**.<sup>[409–411]</sup> Based on these procedures,  $[\alpha\text{-}^{13}\text{C}]$ -**2a** was prepared in three steps starting from labeled NaOAc  $[\alpha\text{-}^{13}\text{C}]$ -**81** (Scheme 4.5). Reactive distillation using  $(\text{MeO})_3\text{PO}$ <sup>[412]</sup> as methylating agent afforded highly volatile MeOAc isotopologue  $[\alpha\text{-}^{13}\text{C}]$ -**82**<sup>[410,413–415]</sup> (b.p.  $57^\circ\text{C}$ <sup>[413]</sup>), which was further converted the same day in order to prevent loss of material by evaporation. Deprotonation and subsequent reaction with methyl chloroformate furnished dimethyl malonate isotopologue  $[\alpha\text{-}^{13}\text{C}]$ -**83**,<sup>[410,411]</sup> which was sequentially treated with NaH and MeI to give labeled pronucleophile  $[\alpha\text{-}^{13}\text{C}]$ -**2a**.<sup>[409]</sup> Isotopologues  $[\beta\text{-}^{13}\text{C}]$ - and  $[\text{D}_3]$ -**2a** were prepared by methylation of unlabeled dimethyl malonate **83** with  $^{13}\text{CH}_3\text{I}$  and  $\text{CD}_3\text{I}$ , respectively.



**Scheme 4.5:** Synthesis of labeled malonates **2a** and transformation into their sodium salts Na-**2a**. All labeled products were obtained with an isotopic purity of  $\geq 99\%$ , matching the isotopic purity of the deuterium or  $^{13}\text{C}$  source used.

---

Labeled malonates [ $\alpha$ - $^{13}\text{C}$ ]-, [ $\beta$ - $^{13}\text{C}$ ]- and [ $\text{D}_3$ ]-Na-**2a** were converted into their sodium salts Na-**2a** by deprotonation with NaHMDS. In contrast to unlabeled Na-**2a**, however, all labeled malonate salts were obtained contaminated with various unidentified impurities, which could not be removed by recrystallization. This might be attributed to preparative differences, since labeled pronucleophiles [ $\alpha$ - $^{13}\text{C}$ ]-, [ $\beta$ - $^{13}\text{C}$ ]- and [ $\text{D}_3$ ]-**2a** were purified by flash column chromatography, whereas unlabeled **2a** was distilled prior to deprotonation. As the labeled malonate salts prepared could not be purified to a satisfying level, mechanistic experiments were performed using the corresponding pronucleophiles [ $\alpha$ - $^{13}\text{C}$ ]-, [ $\beta$ - $^{13}\text{C}$ ]- and [ $\text{D}_3$ ]-**2a** for *in situ* generation of reactive nucleophiles.

In this section, the synthesis of starting materials was outlined. Cyclobutene electrophiles were prepared via a 4- $\pi$ -photocyclization as key step, using a circulating flow photoreactor. Reactive malonate nucleophiles were isolated by deprotonation of the corresponding pronucleophile followed by inert work-up. Furthermore, the synthesis of several  $^2\text{H}$ - and  $^{13}\text{C}$ -labeled cyclobutenes and malonates was disclosed. The successful preparation of these materials sets the stage for the mechanistic experiments described in the following subchapters.

---

## 4.2 Stereoselectivity of Oxidative Addition and Nucleophilic Attack

---

The content of this section has been published:

J. J. Primožic, J. Ilgen, P. Maibach, M. Brauser, J. Kind, C. M. Thiele

**Pd-Catalyzed Asymmetric Allylic Alkylation of Cyclobutenes: From Double Inversion to Double Retention**, *J. Am. Chem. Soc.* **2023**, *145*, 15912–15923, DOI 10.1021/jacs.3c03590. Manuscript reprinted with permission, © 2023 American Chemical Society.

Compound numbers referring to structures given in the publication are quoted in brackets if differing from those used in this thesis.

The initial focus of mechanistic analysis was to elucidate the stereochemical course of the key reaction steps, i.e. oxidative addition and nucleophilic attack. As model reaction, the alkylation of cyclobutene substrates *cis*- and *trans*-**1** with sodium dimethyl methylmalonate Na-**2a** (Na-**2**) was chosen, using the reaction conditions developed by MAULIDE and coworkers.<sup>[56]</sup> Test reactions afforded enantioenriched substitution products **3a** (**3**), with stereoselectivities consistent with the literature.<sup>[56]</sup> Variation of the catalyst loading with racemic *cis*-**1** as electrophile did not display a significant influence on stereoselectivity. Since no erosion of the d.r. was observed at high catalyst concentrations, it can be presumed that stereochemical scrambling by intermediate Pd–Pd displacement<sup>[71,217,218]</sup> is not operative. Furthermore, these data indicate that potential formation of Pd–ligand oligomers, which have been described for DACH standard ligand (*R,R*)-**L18** and typically lead to a strong dependence of the e.e. on catalyst concentration,<sup>[124,416,417]</sup> is of no relevance here. With substrate *trans*-**1**, the same product stereoisomers were obtained as

---

from its diastereomer *cis*-**1**, in agreement with the literature.<sup>[56]</sup> Additionally, small to moderate amounts of *syn*-configured,  $\eta^1$ -coordinated Pd–cyclobutene complexes (*syn*-**Na-4**) were detected as stable side products.

The stereospecificity of oxidative addition was investigated by subjecting a range of cyclobutene substrates to stoichiometric oxidative addition with a Pd<sup>0</sup> source and ligand (*S*<sub>ax</sub>, *S*, *S*)-**L1** or (*R*)-**L2**, followed by in-solution characterization of the Pd–cyclobutene complexes obtained. These experiments were performed together with JULIAN ILGEN (acidic **L1**-coordinated complexes **4a**)<sup>[345]</sup> and PATRICK MAIBACH (acidic **L2**-bearing  $\eta^1$ -species **4b**). In line with previous mechanistic studies,<sup>[57,58]</sup> acid *cis*-**1** and the corresponding methyl ester (*cis*-**5**) underwent oxidative addition under inversion of relative configuration, giving  $\eta^1$ -bound Pd–allyl complexes with an *anti*-relationship between the cyclobutene substituents (*anti*-**4** and *anti*-**6**). The *trans*-diastereomers of both substrates, on the other hand, reacted under both inversion and retention to afford a mixture of *syn*- and *anti*-configured  $\eta^1$ -complexes, the former being stabilized by internal Pd–O chelation.<sup>[58]</sup> In general, both *syn*- and *anti*-configured Pd species were obtained as mixtures of two interconverting diastereomers, with ratios ranging from d.r. = 50:50 to d.r. > 95:5.

When substrate *trans*-**1** was deprotonated as it is under catalytic conditions and subsequently subjected to oxidative addition using phosphoramidite **L1** as ligand, the amount of *anti*-complex formed was significantly higher than in the analogous experiment without substrate deprotonation, indicating that the anionic charge of the carboxy group plays a crucial role for the stereoselectivity of oxidative addition. The same experiment with PHOX ligand **L2** instead afforded only *syn*-species along with large amounts of unidentified decomposition products, which was attributed to the corresponding anionic *anti*-complex being unstable.

The formation of Pd–cyclobutene complexes was further investigated by NMR reaction monitoring and subsequent analytical or numerical kinetic analysis, with the experimental conditions established by JULIAN ILGEN<sup>[345]</sup> and numerical treatment performed by JONAS KIND. Oxidative addition of *cis*-**1** with both **L1** and **L2** was disclosed to give the previously characterized *anti*-complexes (*anti*-**4**) as a diastereomeric 50:50 mixture, which then equilibrated towards enrichment of the major species. This unambiguously shows that the  $\eta^1$ -species are formed prior to  $\eta^1$ – $\eta^3$ – $\eta^1$  isomerization, which stands in contrast to the common assumption that under Pd catalysis the  $\eta^3$ -allyl complex is the primary oxidative addition product.<sup>[66,126,136,418]</sup> A similar behavior was found for the formation of **L1**-ligated *syn*-complexes (*syn*-**4a**) from substrate *trans*-**1**, albeit requiring significantly longer for reaching full equilibration. Conversely, *syn*-configured complexes coordinated by ligand **L2** (*syn*-**4b**) were formed with one diastereomer slightly enriched, followed by gradual equilibration to an end-point d.r. of 50:50. For all oxidative additions investigated, the reaction monitoring data could be accurately fitted using a kinetic model based on a second-order oxidative addition and a first-order equilibrium between the diastereomeric  $\eta^1$ -complexes.

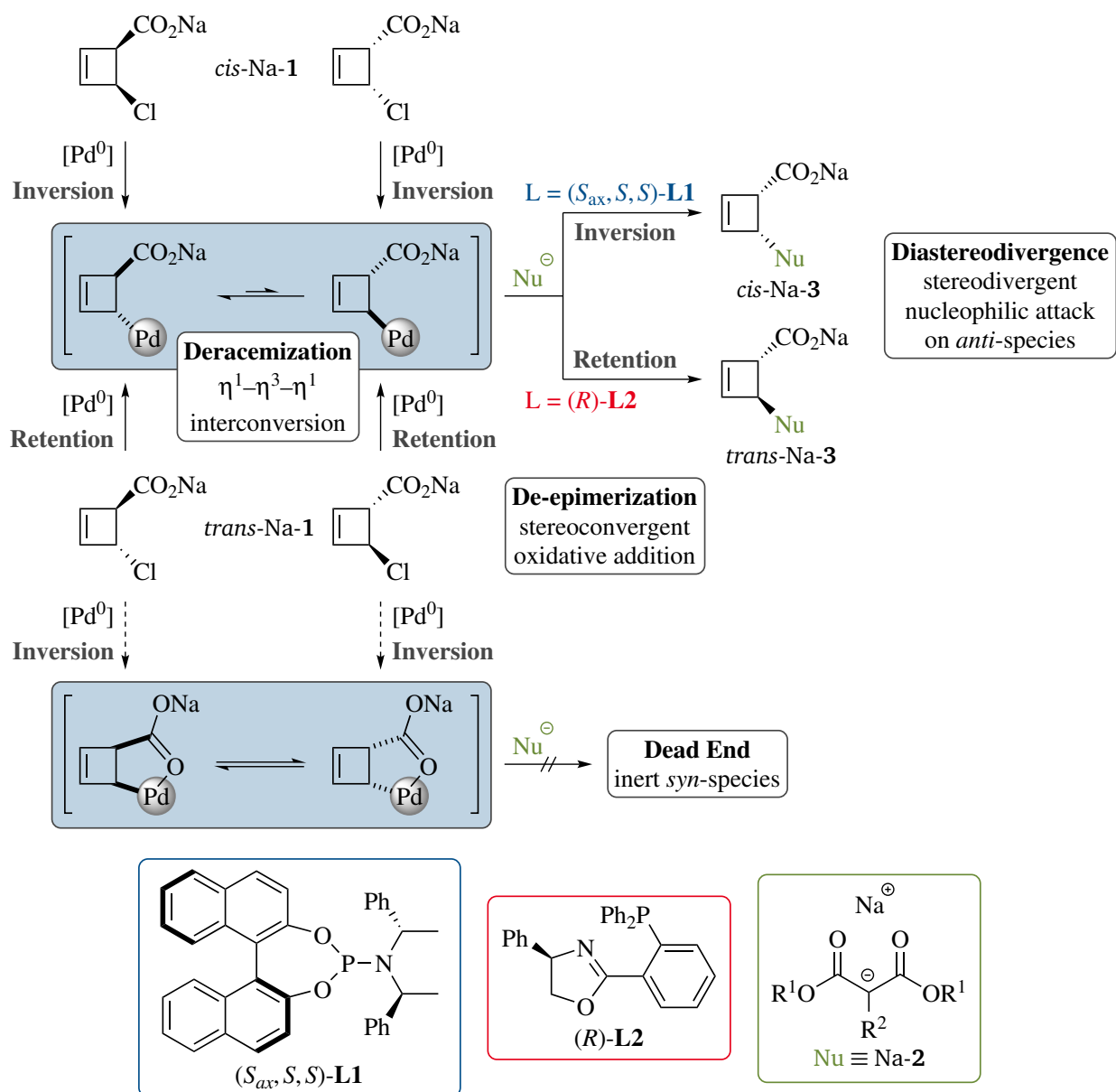
---

In order to probe the role played by the different Pd–cyclobutene complexes potentially involved, both *anti*- and *syn*-configured  $\eta^1$ -species prepared from **1** were treated with stabilized nucleophile Na-**2a** (Na-**2**). In agreement with previous studies,<sup>[57,58]</sup> *anti*-complexes (*anti*-**4**) underwent smooth nucleophilic substitution, giving the products of retention (with **L1**) and inversion (with **L2**), respectively, consistent with the stereoselectivities obtained under catalytic conditions. In stark contrast, the corresponding *syn*-configured Pd species (*syn*-Na-**4**) turned out to be entirely unreactive, which was attributed to stabilization by internal Pd–O coordination.

After having studied the single steps of the catalytic cycle, the question arose which of the Pd species characterized are actually present under catalytic conditions. Therefore, an intermediate capture experiment based on stereospecific  $\beta$ -hydride elimination<sup>[122,327]</sup> was designed, using deuterated substrates [5-D]/[3-D]-**1**<sup>[378]</sup> in combination with a suitable hard nucleophile. With both ligand **L1** and **L2**, substrate [5-D]/[3-D]-*cis*-**1** gave a product mixture consistent with the intermediacy of an *anti*-configured Pd–cyclobutene species. When [5-D]/[3-D]-*trans*-**1** was subjected to the same conditions, the elimination products of both *anti*- and *syn*-configured Pd species were obtained. These results show that the allylic alkylation of acids **1** generally proceeds via *anti*-configured Pd–cyclobutene intermediates (*anti*-Na-**4**), regardless of the substrate's relative configuration and the ligand employed. The corresponding *syn*-complexes (*syn*-Na-**4**), on the other hand, are only formed when *trans*-**1** is used as substrate. The general intermediacy of *anti*-configured  $\eta^1$ -complexes (*anti*-Na-**4**) could be confirmed by subjecting the model reaction (*vide supra*) to qualitative ESI-HRMS and <sup>31</sup>P-NMR analyses under reactive conditions, which allowed for observing these complexes as transient species (HRMS measurements performed with the help of ALEXANDER SCHIESSER and CHRISTIANE RUDOLPH).

Based on these findings, a preliminary mechanistic scenario was proposed rationalizing the unusual stereoselectivity observed (Scheme 4.6). Accordingly, the de-epimerization of substrates *cis*- and *trans*-**1** is based on a stereoconvergent behavior of oxidative addition, which proceeds under either inversion (with *cis*-**1**) or retention (with *trans*-**1**) to afford *anti*-configured Pd–cyclobutene species (*anti*-Na-**4**) as reactive intermediates. The altered stereoselectivity displayed by *trans*-**1** in this step was speculated to be based on a suprafacial electrostatic shielding by the anionic carboxy group, allowing the incoming Pd<sup>0</sup> catalyst to access the allylic system only from the opposite face. Substrate *trans*-**1** also undergoes oxidative addition under inversion as side reaction, giving *syn*-configured  $\eta^1$ -complexes (*syn*-Na-**4**). These are, however, unreactive due to strong internal coordination, preventing formation of undesired product stereoisomers.

The on-cycle, *anti*-configured  $\eta^1$ -intermediates (*anti*-Na-**4**) formed by oxidative addition as a diastereomeric 50:50 mixture rapidly interconvert via one or several undetected  $\eta^3$ -species, which is believed to be the deracemization enabling event. Subsequent nucleophilic attack on an *anti*-configured Pd–cyclobutene complex displays a stereodivergent course, proceeding under either inversion (with **L1**) or retention (with **L2**). This mechanistic dichotomy, which explains the diastereodivergence observed, must be based on different properties of the Pd–allyl intermediate



**Scheme 4.6:** Preliminary mechanism proposed for the Pd-catalyzed asymmetric allylic alkylation of cyclobutene substrates **1** with malonate nucleophiles Na-2. Dashed arrows indicate minor reaction paths.

attacked by the nucleophile. DFT-computations on the characterized acidic  $\eta^1$ -complexes (*anti*-**4**) performed by MATTHIAS BRAUSER revealed that ligands **L1** and **L2** create significantly different steric environments: While Pd-allyl complexes with highly bulky phosphoramidite **L1** seem to be accessible only at the opposite face, the rather slim PHOX ligand **L2** might retain the possibility of nucleophilic attack under retention. In addition, the anionic nature of the carboxy group that has been demonstrated to play a crucial role upon oxidative addition was anticipated to be of critical importance for the stereoselectivity of nucleophilic attack as well. Taking these aspects together, diastereodivergence was tentatively proposed to be based on a competition between

---

steric shielding by the ligand backbone and electrostatic repulsion by the anionic carboxy moiety, with the ligand determining which of these opposing effects dominates.

In conclusion, a stereochemical mechanism going far beyond the ‘double inversion rule’ has been disclosed, featuring an inversion–retention dichotomy for both oxidative addition and nucleophilic attack. However, question marks regarding the latter step have remained, as the results presented cannot distinguish if the Pd–cyclobutene species attacked by the nucleophile is  $\eta^1$ - or  $\eta^3$ -coordinated. Also, the data reported do not allow for rationalizing the unusual retentive stereospecificity of nucleophilic attack on **L2**-coordinated intermediates, which may proceed via either an inner-sphere mechanism or an anomalous outer-sphere path. These questions will be addressed in the following sections 4.3–4.6.



# Pd-Catalyzed Asymmetric Allylic Alkylation of Cyclobutenes: From Double Inversion to Double Retention

Johann J. Primožic, Julian Ilgen, Patrick Maibach, Matthias Brauser, Jonas Kind, and Christina M. Thiele\*



Cite This: *J. Am. Chem. Soc.* 2023, 145, 15912–15923



Read Online

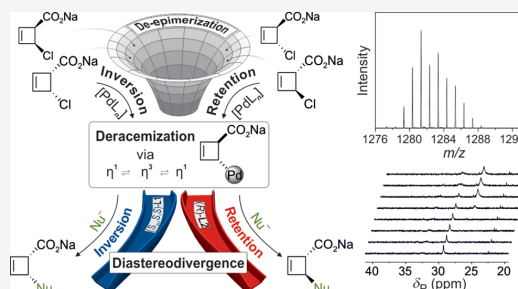
ACCESS |

Metrics & More

Article Recommendations

Supporting Information

**ABSTRACT:** The Pd-catalyzed allylic alkylation of 3,4-disubstituted, racemic cyclobutene electrophiles exhibits a highly unusual stereoselectivity that allows for controlling diastereo- and enantioselectivity only by the choice of ligand and independent of the configuration of the substrate. In order to shed light on the origin of stereoinduction, we performed a systematic mechanistic investigation, including preparation of various putative Pd-allyl intermediates,  $^1\text{H}/^{31}\text{P}$  NMR reaction monitoring,  $^2\text{H}$ -labeling studies, ESI–HRMS and  $^{31}\text{P}$  NMR analysis of reaction mixtures, and DFT structural computations. The mechanism disclosed exhibits several steps with stereospecificities deviating from the commonly accepted “double inversion rule”: oxidative addition was found to follow a stereoconvergent course, giving *anti*-configured  $\eta^1$ -Pd-cyclobutene species as detectable on-cycle intermediates irrespective of the configuration of starting material, while the subsequent nucleophilic attack features a stereodivergent behavior. In stark contrast to their highly reactive *anti*-analogues, *syn*-Pd-cyclobutene complexes that can be formed as side products are rendered entirely unreactive by strong internal Pd–O chelation, preventing the formation of undesired product diastereomers.



## INTRODUCTION

The transition-metal-catalyzed introduction of C-centered nucleophiles into allylic substrates represents a versatile and powerful tool for stereoselective C–C bond formation. A variety of asymmetric variants involving readily available chiral ligands has been developed, the vast majority relying on Pd catalysis.<sup>1–5</sup> Moreover, the reaction is highly stereospecific, which is commonly rationalized by the “double inversion rule” (Scheme 1a) valid for the predominantly used stabilized nucleophiles.<sup>6–9</sup> Accordingly, both oxidative addition and subsequent nucleophilic attack on the intermediate  $\eta^3$ -Pd-species proceed under inversion, giving the product with overall retention of configuration.

A remarkable exception from the “double inversion rule” has been developed by Maulide and co-workers,<sup>10,11</sup> using racemic cyclobutene<sup>12,13</sup> substrates such as carboxylic acid **1** (Scheme 1b). This protocol allows for controlling the absolute and relative configuration of substitution products only by the choice of ligand and independent of the relative configuration of the substrate (*cis* or *trans*), thus displaying the characteristics of diastereodivergent deracemization and de-epimerization.

The unprecedented stereoselectivity has stimulated further investigations,<sup>14,15</sup> which revealed that cyclobutene substrates form fairly stable  $\eta^1$ -rather than  $\eta^3$ -coordinated complexes<sup>16</sup> upon treating with a Pd<sup>0</sup> source and a chiral ligand. Oxidative addition was generally observed to proceed under inversion of configuration, and the Pd-complexes obtained were found to

interconvert between two diastereomeric  $\eta^1$ -species, with DFT calculations suggesting a  $\eta^1$ - $\eta^3$ - $\eta^1$  pathway<sup>17</sup> to be operative.<sup>14,15</sup> For *syn*-configured model complexes prepared from amide-derivatized *trans*-substrates with a structurally simplified surrogate of **L1** as ligand, spectroscopic data indicated stabilization by internal Pd–O coordination through the cyclobutene’s carbonyl group.<sup>15</sup>

Despite extensive characterization of putative  $\eta^1$ -Pd-intermediates, the origin of stereoinduction remained speculative. For this reason, we have conducted a comprehensive mechanistic study, aiming to disclose the driving forces responsible for stereoselectivity. We herein present our mechanistic findings obtained from systematic screening of the oxidative addition with different ligands and substrates, kinetic analysis of the  $\eta^1$ - $\eta^3$ - $\eta^1$  interconversion, reactivity screening and DFT computations of selected  $\eta^1$ -Pd-cyclobutene complexes prepared, intermediate capture experiments with deuterated substrates, and direct observation of Pd-intermediates by ESI–HRMS and  $^{31}\text{P}$  NMR analysis of

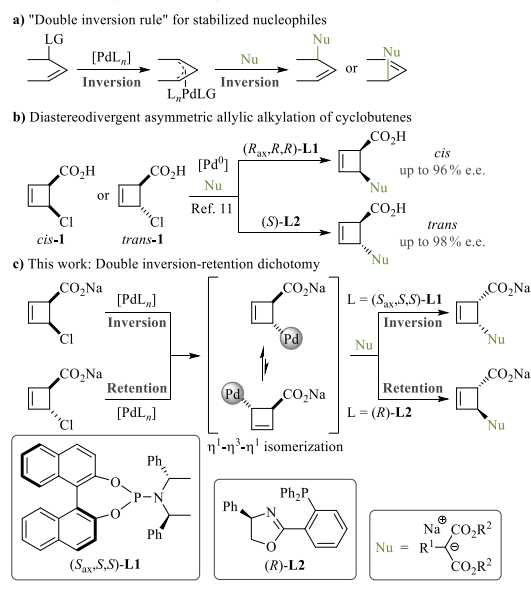
Received: April 11, 2023

Published: July 6, 2023





**Scheme 1. Placement of This Work in Allylic Alkylation Chemistry:** (a) Commonly Accepted Mechanism for Stabilized Nucleophiles; (b) Variant Developed for Cyclobutene Substrates; and (c) Mechanistic Scenario Disclosed by This Study



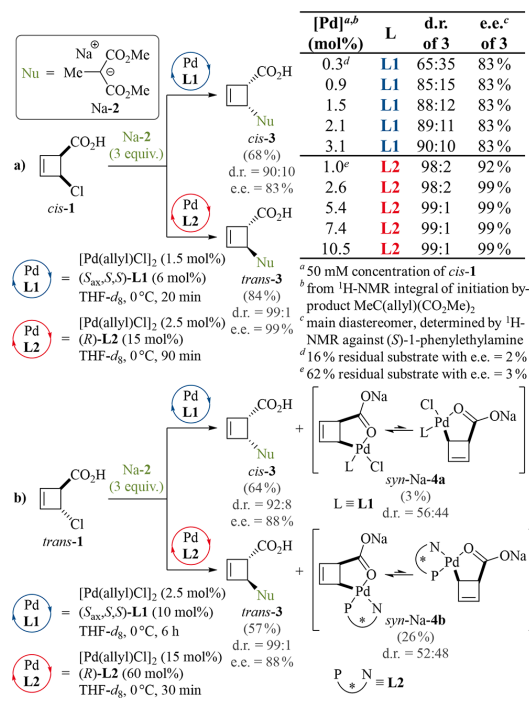
reaction mixtures. The mechanistic scenario derived features an unprecedented combination of a stereoconvergent oxidative addition and a stereodivergent nucleophilic displacement, allowing for rationalization of the stereoselectivity observed (Scheme 1c).

## RESULTS AND DISCUSSION

**Preliminary Studies.** We commenced our study by subjecting substrate *cis*-1<sup>18</sup> to the reaction conditions investigated, using pre-isolated malonate Na-2 as a nucleophile. Consistent with the stereoselectivities reported in the literature,<sup>11</sup> the use of the monodentate phosphoramidite<sup>19,20</sup> ligand (*S,S,S*)-L1 led to the formation of enantioenriched product *cis*-3, whereas stereoisomer *trans*-3 was obtained with bidentate phosphinoxazoline<sup>21–23</sup> ligand (*R*)-L2 (Scheme 2a). In the absence of the catalyst, very slow *trans*-selective background reactivity was observed (ca. 20% conversion after 46 h at 40 °C, d.r. ≈ 96:4).

Variation of the Pd loading over a wide range exhibited no significant influence on the stereoselectivity under both reaction conditions. The moderate increase of the d.r. observed with ligand L1 and the very small to negligible increase of d.r. and e.e. with ligand L2 can potentially be attributed to racemic background reactivity, which is independent of the catalyst loading. Since no erosion of enantioselectivity was observed at high Pd concentrations, it can be presumed that a potential oligomerization of the Pd-allyl intermediate, as has been reported for the Trost standard ligand,<sup>24–26</sup> is of no relevance here. At very low Pd loadings, reactions stalled at incomplete conversion, and the residual cyclobutene substrate was recovered as a racemate (e.e. ≤ 3%), indicating that no kinetic resolution is operative.

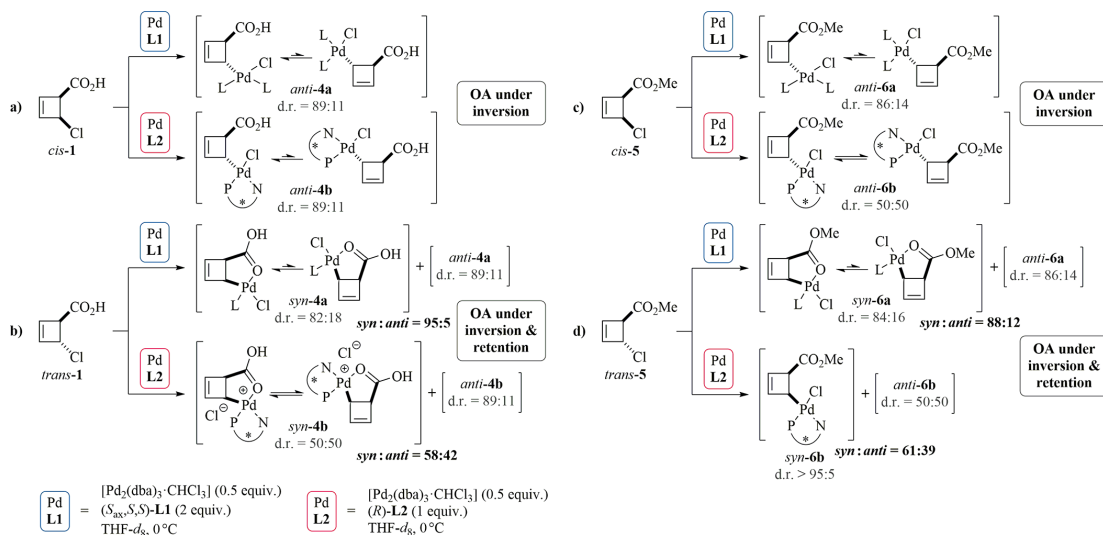
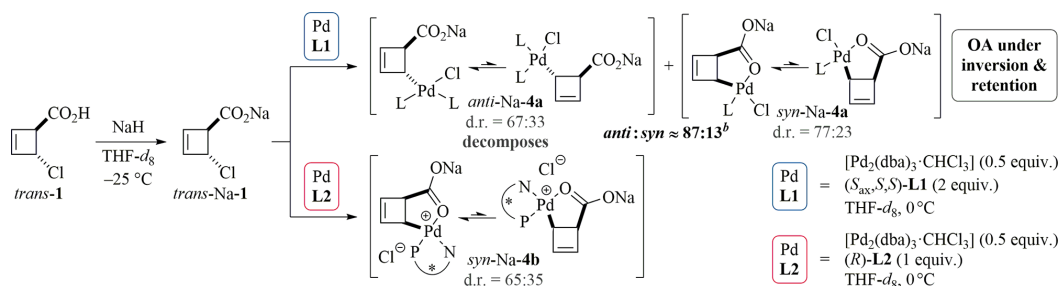
**Scheme 2. Allylic Alkylation Test Reactions with Substrate 1 (NMR Yields Determined against Internal Standard Given in Brackets)**



With substrate *trans*-1, the same stereoisomers of products 3 were obtained, albeit requiring an increased catalyst loading to reach quantitative conversion (Scheme 2b). Additionally, endpoint NMR and HRMS analyses of reaction mixtures revealed  $\eta^1$ -Pd-cyclobutene complexes *syn*-Na-4 to be formed as stable side products, which are believed to be stabilized by internal coordination (vide infra). The extent of this side reaction was particularly high with ligand L2 (26% NMR yield of *syn*-Na-4b).

**Screening of Oxidative Addition.** In order to investigate the stereospecificity of oxidative addition, a range of cyclobutene substrates was treated with stoichiometric amounts of a Pd<sup>0</sup> source and ligand L1 or L2, and the Pd-species obtained were extensively characterized by one- and two-dimensional <sup>1</sup>H, <sup>13</sup>C, <sup>31</sup>P, and <sup>15</sup>N NMR, including NOESY,<sup>27</sup> EASY-ROESY,<sup>28</sup> and diffusion-ordered spectroscopy<sup>29</sup> experiments, ESI–HRMS in positive- and negative-ion mode, and DFT computations (see Section 4 in the Supporting Information for details).

With both ligands employed, acid substrate *cis*-1 smoothly reacted under inversion of configuration to a diastereomeric mixture of two rapidly interconverting  $\eta^1$ -species *anti*-4, with one diastereomer highly enriched over the other and—as all other Pd-cyclobutene species prepared—without any detectable amount of the corresponding  $\eta^3$ -complexes (Scheme 3a). These observations are consistent with findings reported in earlier mechanistic studies.<sup>14,15</sup> Oxidative addition of *trans*-1, on the other hand, was found not to follow a clear stereospecificity, giving *syn*-configured complexes *syn*-4 along

Scheme 3. Oxidative Addition (OA) of (a) *cis*- and (b) *trans*-Configured Acid **1** and (c) *cis*- and (d) *trans*-Configured Ester **5** with Ligand **L1** and **L2**<sup>a</sup><sup>a</sup>d.r. and *syn:anti* values determined by <sup>1</sup>H or <sup>31</sup>P NMR.Scheme 4. Deprotonation and Subsequent Oxidative Addition (OA) of Substrate *trans*-**1** with Ligand **L1** and **L2**<sup>a</sup>d.r. and *syn:anti* values determined by <sup>1</sup>H- or <sup>31</sup>P NMR. <sup>b</sup>Determined by <sup>31</sup>P NMR monitoring and subsequent initial rate analysis.

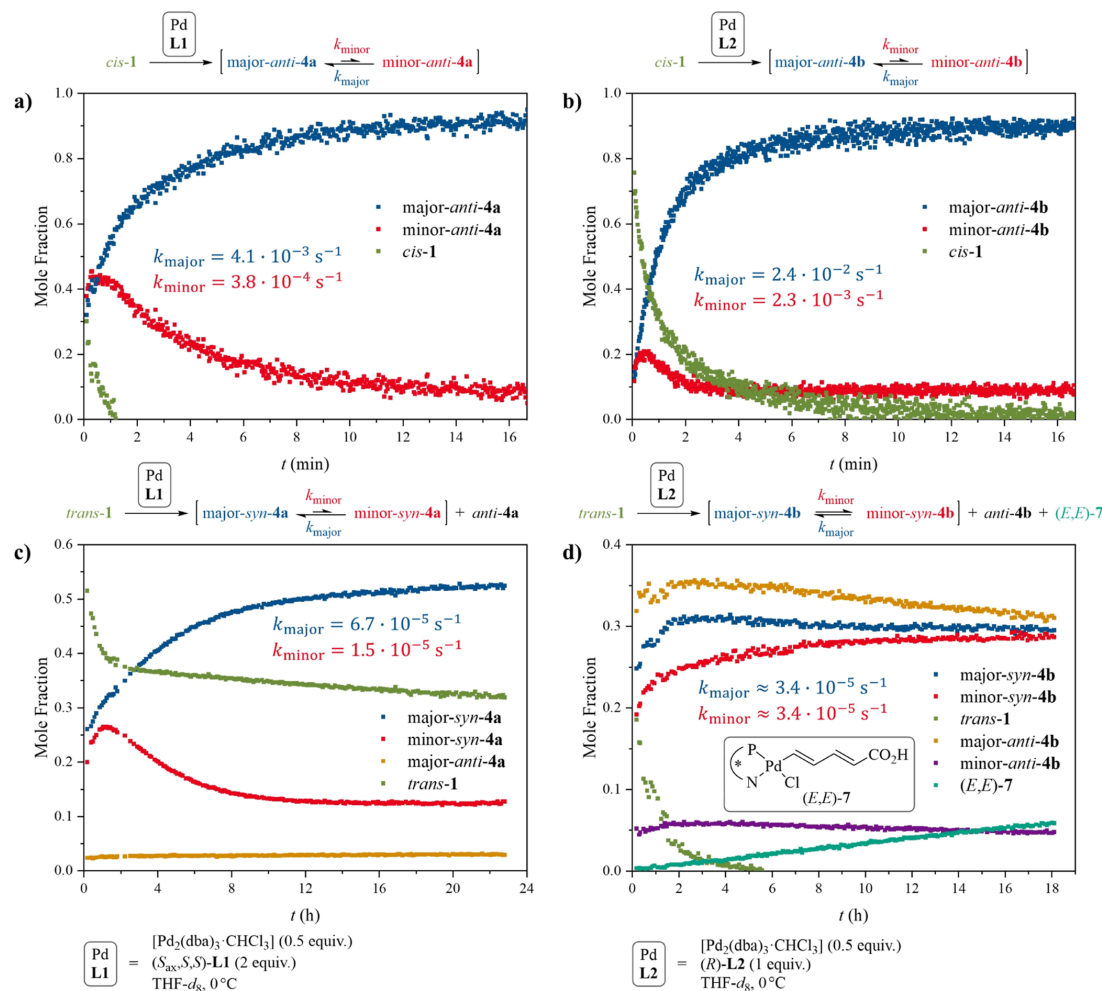
with 5% (with **L1**) and 42% (with **L2**) of their *anti*-analogues (Scheme 3b), respectively. Spectroscopic data suggest *syn*-**4** to be stabilized by internal Pd–O coordination.<sup>15</sup> Albeit complexes *syn*-**4** exhibited the same kind of suprafacial Pd-shift as *anti*-**4**, only complexes *syn*-**4a** prepared with ligand **L1** featured significant enrichment of one diastereomer.

In order to probe the role of the carboxy group of acid substrates **1**, which potentially allows for protonation/deprotonation events as well as hydrogen bond donation, the corresponding methyl esters **5** were subjected to oxidative addition under the same conditions. Like its parent acid *cis*-**1**, substrate *cis*-**5** underwent oxidative addition under inversion, giving pairs of interconverting  $\eta^1$ -complexes *anti*-**6** (Scheme 3c). Interestingly, complexes *anti*-**6a** coordinated by **L1** equilibrated to a similarly high d.r.<sup>30</sup> as the corresponding acidic species *anti*-**4a**, whereas complexes *anti*-**6b** bearing ligand **L2** were obtained as a diastereomeric 50:50 mixture.

With ester substrate *trans*-**5**, the oxidative addition products of both inversion and retention were obtained (Scheme 3d), with a *syn:anti* ratio similar to what had been observed with

acid substrate *trans*-**1**. Again, Pd-complexes *syn*-**6a** synthesized by using **L1** were found to behave similar to the parent acid complexes *syn*-**4a**, with the carbonyl group acting as an internal chelator and the equilibrium clearly favoring one diastereomer over the other. **L2**-coordinated complex *syn*-**6b**, on the other hand, was obtained as a single diastereomer and did not exhibit any evidence for internal Pd–O coordination, thus strongly differing from the properties of the corresponding acid complex *syn*-**4b**.

In comparing the results obtained by oxidative addition of acid **1** and ester **5**, it is noticeable that **L1**-bearing complexes **4a** and **6a** generally feature very similar d.r. values, whereas for **L2**-coordinated complexes **4b** and **6b**, a drastic change of the d.r. from  $\geq 89:11$  to 50:50 or vice versa was observed when replacing the substrate's carboxy function by an ester moiety. This indicates that the carboxy group seems to play a crucial role for energetic discrimination (i.e.,  $d.r. \neq 50:50$ ) between interconverting complex diastereomers with ligand **L2** but not with **L1**. Furthermore, the observation that oxidative additions of ester *trans*-**5** furnished a comparable extent of retention (i.e.,



**Figure 1.** Temporal mole fraction profiles for the oxidative addition of substrate *cis*-1 (top) and *trans*-1 (bottom) with ligand L1 (left) and L2 (right) to interconverting Pd-cyclobutene species **4** (cf. Scheme 3a,b), recorded by <sup>1</sup>H NMR reaction monitoring. Mole fractions were calculated from the corresponding integrals. The rate constants  $k_{\text{major}}$  and  $k_{\text{minor}}$  for the  $\eta^1$ - $\eta^3$ - $\eta^1$  equilibrium were determined by analytical first-order fitting of the corresponding temporal d.r. profiles or numerical fitting of temporal mole fraction profiles based on the reaction equations shown, using either <sup>1</sup>H or <sup>31</sup>P NMR data (see Section 5 in the Supporting Information for details).

the relative amount of *anti*-complexes obtained) as the analogous reactions with acid *trans*-1 suggests that it is not the acidity or hydrogen bond donating ability of *trans*-1 that is responsible for *trans*-substrates not exclusively reacting under inversion.<sup>31</sup>

In order to better simulate the catalytic conditions, under which acid substrate **1** is deprotonated, carboxylate substrate *trans*-Na-**1** (prepared by carefully treating *trans*-**1** with NaH)<sup>32</sup> was subjected to oxidative addition (Scheme 4). Strikingly, the stereochemical preference was inverted toward retention when using ligand L1, indicating that the anionic nature of the deprotonated carboxy group has a strong impact on the stereoselectivity of oxidative addition. Characterization was complicated by decomposition of complexes *anti*-Na-**4a** occurring readily upon formation, with a half-life of ca. 1 h.

The corresponding *syn*-species, on the other hand, turned out to be stable, potentially as a consequence of internal chelation. <sup>31</sup>P NMR monitoring and subsequent initial rate analysis revealed that oxidative addition proceeds with 87% retention and only 13% inversion for this system (*anti*:*syn* ratio = 87:13).

With ligand L2, complexes *syn*-Na-**4b** were obtained, along with large amounts of unidentified decomposition products, which can presumably be attributed to the corresponding *anti*-complexes being too unstable for characterization. Other than its protonated form, *syn*-Na-**4b** featured moderate enrichment of one diastereomer.

**Reaction Monitoring and Kinetic Analysis of  $\eta^1$ - $\eta^3$ - $\eta^1$  Interconversion.** The suprafacial exchange between diastereomeric Pd-cyclobutene species prepared from acid substrates **1** was further investigated by NMR reaction monitoring and

subsequent kinetic analyses. Oxidative addition of *cis*-1 with both L1 and L2 was found to proceed on a timescale of just a few minutes and was therefore monitored using a rapid-injection set-up<sup>33–35</sup> in combination with <sup>1</sup>H NMR series with spatially selective and frequency-shifted excitation.<sup>36</sup> The temporal mole fraction profiles obtained reveal that diastereomeric  $\eta^1$ -Pd-complexes *anti*-4 are initially formed as an approx. 50:50 mixture, which then equilibrates toward enrichment of the major species (Figure 1a,b). This clearly indicates that formation of the  $\eta^1$ -complexes precedes  $\eta^1$ - $\eta^3$ - $\eta^1$  isomerization<sup>37</sup> as direct formation of an intermediate  $\eta^3$ -species prior to isomerization to the more stable  $\eta^1$ -complexes would imply the d.r. of the  $\eta^1$ -species observed to be constant over time. Both substrate decay and equilibration between major- and minor- $\eta^1$ -species could be accurately fitted with rate laws derived from a kinetic model. Accordingly, the substrate enantiomers undergo second-order oxidative addition (first order in both substrate and Pd<sup>0</sup>) to diastereomeric  $\eta^1$ -complexes, which then interconvert via a first-order equilibrium (see Section 5 in the Supporting Information for further explanation of the kinetic model and full fitting details).

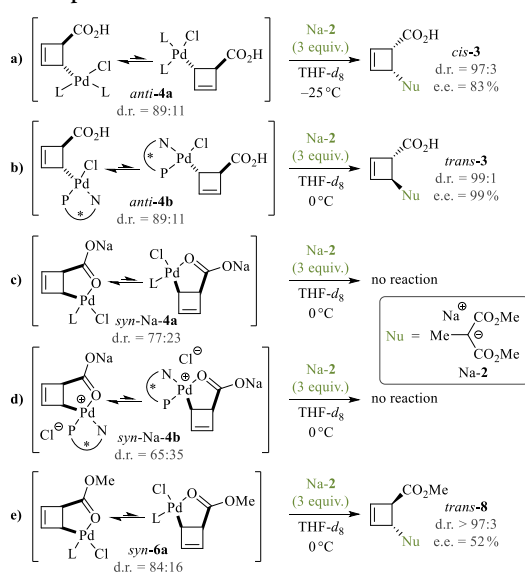
With substrate *trans*-1, oxidative addition and subsequent  $\eta^1$ - $\eta^3$ - $\eta^1$  isomerization of complexes *syn*-4 turned out to be much slower, requiring several hours for full equilibration. Thus, the reactions could be conveniently monitored with a series of alternating <sup>1</sup>H and <sup>31</sup>P NMR experiments after initiation outside the spectrometer. An opposite equilibration behavior was observed for L1-coordinated complexes *syn*-4a and L2-bearing species *syn*-4b (Figure 1c,d): While *syn*-4a exhibited a gradual enrichment of the major-species similarly to what had been observed with complexes *anti*-4, the diastereomers of *syn*-4b were formed with one species slightly enriched and then slowly equilibrated to an end-point d.r. of 50:50. Nevertheless, the same kinetic model could be applied for both systems as for reactions with substrate *cis*-1. The drastically decreased equilibration rates  $k_{\text{major}}$  and  $k_{\text{minor}}$  determined for complexes *syn*-4 compared to the corresponding *anti*-species are likely to be a consequence of internal Pd–O coordination, stabilizing the  $\eta^1$ -species toward isomerization.

During monitoring the equilibration of *syn*-4b, the concurrently formed *anti*-complexes underwent slow first-order electrocyclic ring-opening to the isomeric diene (*E,E*)-7<sup>14</sup> (Figure 1d, see Section 5 in the Supporting Information for details on kinetic analysis). Complexes *syn*-4b, on the other hand, were found to be stable against ring-opening, which underlines the stabilizing effect of internal chelation.

**Reactivity of  $\eta^1$ -Pd-Cyclobutene Complexes.** To further continue our investigation along the catalytic cycle, we turned our attention toward investigating the role played by the different  $\eta^1$ -complexes potentially involved. To this end, selected complexes that had been prepared by oxidative addition of cyclobutene substrates (vide supra) were treated with malonate nucleophile Na-2.

Complexes *anti*-4<sup>38</sup> were found to be highly reactive, giving substitution products 3 featuring stereoselectivities consistent with those obtained under catalytic conditions (Scheme 5a,b). These results are in line with experiments reported in previous studies,<sup>14,15</sup> suggesting nucleophilic attack to proceed under either inversion (with L1) or retention (with L2), depending on the ligand employed. Since attack under retention on a Pd-allyl intermediate has been established only for unstabilized nucleophiles reacting via an inner-sphere mechanism,<sup>7,9</sup> but not for stabilized nucleophiles such as Na-2, one might

**Scheme 5. Reactivity of Pd-Cyclobutene Complexes toward Nucleophile Na-2**



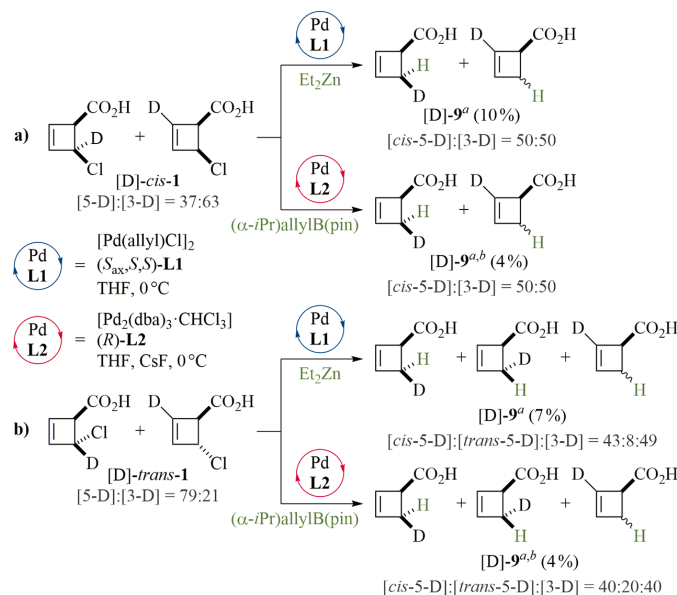
consider *anti*-Na-4b to undergo facial displacement<sup>8,39</sup> to *syn*-Na-4b prior to outer-sphere nucleophilic attack under inversion. However, *syn*-Na-4b and *syn*-Na-4a turned out to be entirely unresponsive toward nucleophile Na-2, even after prolonged reaction times (Scheme 5c,d).<sup>40</sup> These findings suggest complexes *syn*-Na-4 to act as dead-end species of the catalytic cycle rather than active intermediates.<sup>31</sup>

In stark contrast to acidic Pd-species *syn*-4a, the corresponding ester complexes *syn*-6a smoothly reacted under inversion to enantioenriched substitution product *trans*-8 (Scheme 5e). This experiment highlights that the carboxy group of 1 is crucial for rendering the internal Pd–O chelation present in both *syn*-4a and *syn*-6a sufficiently strong for shutting down the reactivity of acid complexes *syn*-4.<sup>41</sup>

**Capture of Intermediates.** After having extensively studied the formation, dynamics and reactivity of Pd-cyclobutene species, we proceeded by studying the reaction under catalytic conditions, focusing on the question which Pd-species are actually formed during turnover. Cyclobutene substrates have been reported to potentially undergo stereoselective  $\beta$ -H elimination when subjected to allylic alkylation with unstabilized nucleophiles such as dialkylzinc<sup>42</sup> and allyl boronates.<sup>43</sup> We attempted to employ this—usually undesired—side reaction to capture the Pd-species involved, using deuterated substrates [5-D]/[3-D]-1.<sup>18</sup>

When an isotopomeric 37:63 mixture of [5-D]- and [3-D]-*cis*-1 (partial deuterium scrambling as a result of the synthesis, see Section 2 in the Supporting Information) was subjected to the action of a suitable unstabilized nucleophile and catalytic amounts of [Pd–L1] or [Pd–L2], fully scrambled hydrodehalogenation product [*cis*-5-D]/[3-D]-9 was obtained (Scheme 6a). As  $\beta$ -H elimination generally proceeds under retention with respect to the Pd-allyl species,<sup>44</sup> the formation of [*cis*-5-D]-9 shows that *anti*-configured Pd-cyclobutene complexes *anti*-Na-4 have been captured. The quantitative deuterium scrambling at the allylic termini in the hydro-

Scheme 6. Capture of Pd-Species by Catalytic  $\beta$ -H Elimination, Using Deuterated Substrates [5-D]/[3-D]-1 (Unoptimized NMR Yields Determined against Internal Standard Given in Brackets)<sup>b</sup>



<sup>a</sup>As the reduced carbon in [3-D]-9 bears two (unlabeled) protons, the relative position of the hydride transferred from the nucleophile cannot be determined experimentally. <sup>b</sup>Obtained as a side product along with enantioenriched, fully scrambled allylated substitution product (20% from [D]-*cis*-1, 13% from [D]-*trans*-1, see Section 7 in the Supporting Information for details).

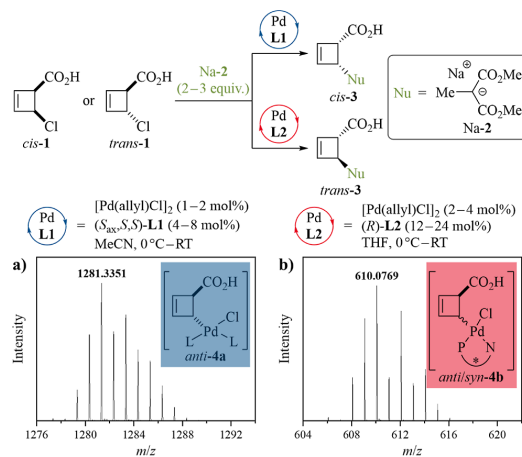
dehalogenation of [5-D]/[3-D]-*cis*-1 furthermore suggests  $\eta^1$ - $\eta^3$ - $\eta^1$  isomerization to be operative also under catalytic conditions as a symmetrizing event.

With substrate [5-D]/[3-D]-*trans*-1, reduced cyclobutenes [cis-5-D]- and [3-D]-9 were obtained again, along with small amounts of isotopomer [trans-5-D]-9 (Scheme 6b). The formation of both [cis-5-D]-9 and [trans-5-D]-9 corresponds to the presence of both *anti*- and *syn*-configured Pd-cyclobutene species. Hence, allylic alkylation of 1 generally involves complexes *anti*-Na-4, regardless of the substrate's relative configuration, whereas Pd-species *syn*-Na-4 seem to be present only when substrate *trans*-1 is employed.<sup>45</sup> This is consistent with the stereoselectivities observed in stoichiometric oxidative additions (vide supra).

**ESI–HRMS and <sup>31</sup>P NMR Analysis of Reaction Mixtures.** With unambiguous evidence in hand that complexes *anti*-Na-4 are generally present under catalytic conditions, we finally envisioned to detect these species as transient intermediates in running reactions. To this end, reaction mixtures of both substrate *cis*-1 and *trans*-1 were subjected to qualitative HPLC–ESI–HRMS analysis in the positive-ion mode, with a dead-time of <1 min for all reactions.

Ions consistent with [M – Cl]<sup>+</sup> fragments of Pd-cyclobutene species 4 were detected with both ligand L1 (Scheme 7a) and L2 (Scheme 7b). Comparison of the mass-selective HPLC traces recorded after initiation and after reaching full conversion confirmed these species to be present only during turnover (see Section 9 in the Supporting Information for full mass range and detailed spectral analyses). In the case of ligand L1, the Pd-fragment detected can be unambiguously assigned to complexes *anti*-4a (or their isomeric ring-opening product)

Scheme 7. ESI–HRMS Analysis of the Allylic Alkylation of Substrates 1 (Positive-Ion Mode): Characteristic MS Peaks of Pd-Cyclobutene Species with (a) L1 and (b) L2<sup>a</sup>



<sup>a</sup>MS data of reactions with substrate *cis*-1 shown, consistent data obtained with *trans*-1.

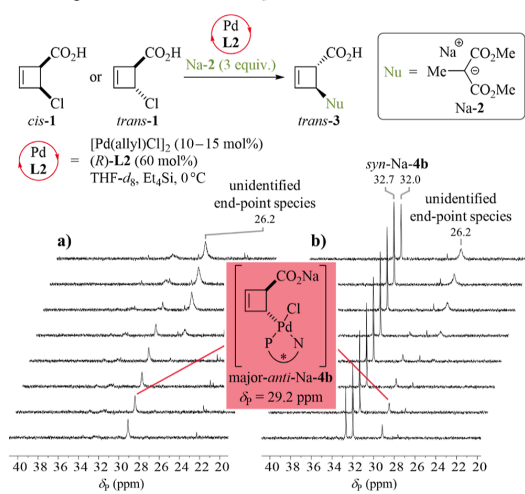
as the corresponding *syn*-complexes have been shown to coordinate only one equivalent of L1 (vide supra) and therefore have a lower molecular mass.<sup>46</sup>

The Pd-cyclobutene fragment detected with L2, on the other hand, is—in theory—consistent with both *anti*- and *syn*-4b, which prompted us to conduct complementary reaction



monitoring experiments using  $^{31}\text{P}$  NMR. At increased catalyst concentrations, a transient species could be observed at  $\delta_{\text{p}} = 29.2$  ppm with both substrate *cis*-1 (Scheme 8a) and *trans*-1 (Scheme 8b), which is consistent with the expected intermediate major-*anti*-Na-4b (experimental shift of corresponding acidic complex major-*anti*-4b:  $\delta_{\text{p}} = 29.0$  ppm).<sup>47</sup>

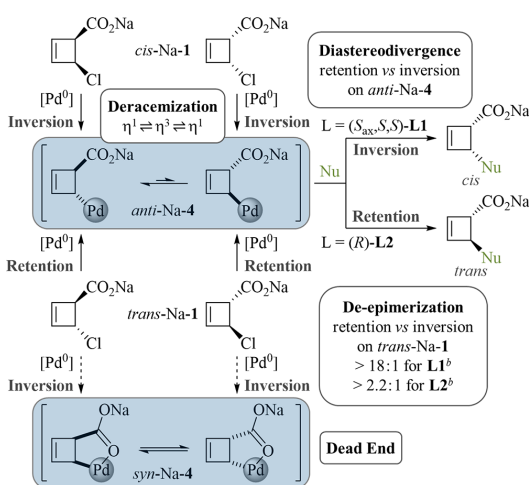
**Scheme 8.**  $^{31}\text{P}\{^1\text{H}\}$  NMR Monitoring of the Allylic Alkylation of Substrate (a) *cis*-1 and (b) *trans*-1 Using Ligand L2, with Signals of Pd-Cyclobutene Species *anti*- and *syn*-Na-4b Shown (Reactions Were Monitored Over (a) 60 and (b) 30 min, Respectively, with the Time Course Running from Bottom to Top)



**Mechanistic Implications.** Based on our results obtained from experiments under both stoichiometric and catalytic conditions, we propose the mechanistic scenario depicted in Scheme 9. As shown by a systematic screening of the oxidative addition and confirmed by intermediate capture experiments, substrate *cis*-Na-1 undergoes oxidative addition under inversion to  $\eta^1$ -complexes *anti*-Na-4, while *trans*-Na-1 can react under both retention (major path) and inversion (minor path), the latter producing internally chelated  $\eta^1$ -species *syn*-Na-4. Investigation of the reactivity of Pd-cyclobutene species revealed that the stabilizing internal coordination renders *syn*-Na-4 entirely unreactive. Hence, the de-epimerizing ability of the oxidative addition of *trans*-Na-1 (i.e. retention as major path), and product selectivity is further improved by the minor path leading to an inert Pd-species rather than to undesired product stereoisomers. Albeit formation of *syn*-Na-4 does not affect the overall stereoselectivity, it acts as both catalyst deactivation path and side reaction of the substrate, explaining the generally higher Pd loadings required with *trans*-1 as well as the lower product yields obtained compared to *cis*-1.

Reaction monitoring experiments showed that formation of on-cycle  $\eta^1$ -species *anti*-Na-4 is followed by their rapid interconversion via one or several undetected  $\eta^3$ -complexes. We believe this step to be the deracemization enabling event, given the ample literature precedence for discrimination of enantiotopic allylic termini based on upstream equilibration between isomeric Pd-allyl species.<sup>48–54</sup>

**Scheme 9.** Mechanistic Proposal Based on the Results of This Work<sup>47</sup>



<sup>a</sup>The undetected zerovalent Pd-intermediate  $[\text{Pd}^0]$  is likely to be anionic (i.e.,  $[\text{PdL}_n\text{Cl}]^-$ ) based on literature precedence.<sup>61–67</sup>  
<sup>b</sup>Selectivities refer to THF-*d*<sub>8</sub> as the solvent and were estimated by comparing the NMR yields of substitution products 3 and side products *syn*-Na-4 (cf. Scheme 2b).

As disclosed by investigation of the nucleophilic attack and corroborated by intermediate capture experiments as well as ESI-HRMS and  $^{31}\text{P}$  NMR analyses of reaction mixtures, *anti*-Na-4 can undergo productive substitution under either inversion (with L1) giving *cis*-configured alkylated cyclobutenes, or under retention (with L2) leading to *trans*-configured products. This surprising dichotomy rationalizes the diastereodivergent character of the reaction.

The interactions responsible for the unusual stereoselectivities of both oxidative addition and nucleophilic attack are hitherto speculative and will be subject of further studies. Altering the inherent stereospecificity of oxidative addition toward retention has been reported to be possible for substrates featuring a *syn*-directing group,<sup>55</sup> a pre-coordinating leaving group,<sup>56–60</sup> or an internal strong steric bias.<sup>58,59</sup> The carboxy group of Na-1 might be expected to act as a directing group, which would, however, imply formation of *syn*-Na-4 to be generally preferred, i.e., the opposite of what is observed. In the presence of palladophilic anions such as chloride, the reactive zerovalent Pd-species is known to be anionic, i.e.,  $[\text{PdL}_n\text{Cl}]^-$ .<sup>61–67</sup> Hence, a conceivable explanation for the stereospecificity obtained with *trans*-Na-1 would be a suprafacial electrostatic shielding by the anionic carboxy group, making the anionic catalyst attack from the opposite face in order to minimize electrostatic repulsion. This would be consistent with the drastically increased extent of retention observed in the stoichiometric oxidative addition of carboxylate substrate *trans*-Na-1 in comparison with neutral substrates *trans*-1 and *trans*-5 (cf. Schemes 3 and 4).

Regarding the C–C bond-forming step, we note that our results cannot distinguish if the nucleophile attacks the spectroscopically characterized  $\eta^1$ -species or the short-living, undetected  $\eta^3$ -intermediates.  $\eta^1$ -Coordinated Pd-complexes have been recognized as crucial intermediates for the  $\eta^3$ - $\eta^1$ - $\eta^3$

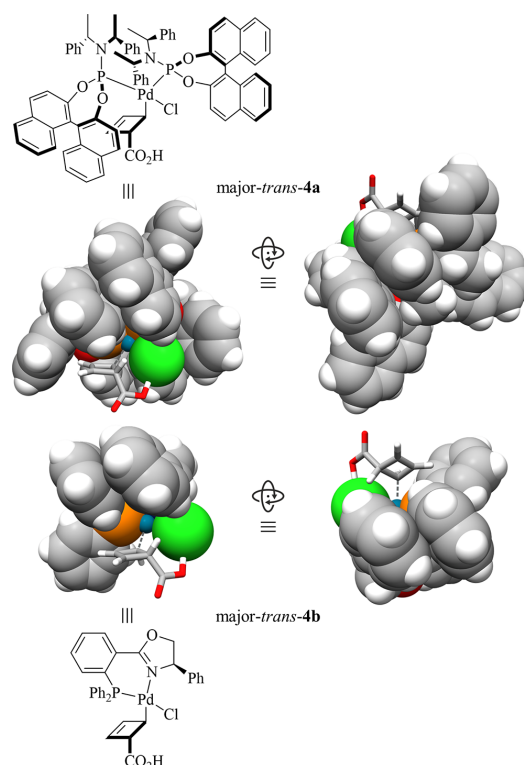
interconversion between stereoisomeric  $\eta^3$ -species<sup>17</sup> but are generally considered to be unreactive toward stabilized nucleophiles.<sup>61,68</sup> For Rh<sup>69</sup> and Fe<sup>70</sup> catalyzed allylic substitutions, in contrast, conclusive evidence has been reported for  $\eta^1$ -species being competent electrophiles that can directly be attacked by stabilized nucleophiles in an  $S_N2'$  fashion.<sup>71–74</sup> Thus, we do not exclude this possibility at this stage, given the spatially confined nature of cyclobutenes that may allow for interactions not possible in common allylic systems.

As for the uncommon retentive stereospecificity of nucleophilic attack on L2-ligated ( $\eta^1$ - or  $\eta^3$ -) intermediates, an obvious explanation would be a switch from the outer-sphere mechanism established for stabilized nucleophiles such as Na-2<sup>6–9</sup> to an inner-sphere path. In fact, evidence supporting an inner-sphere mechanism has been reported for the somewhat less stabilized enolate nucleophiles under Pd–PHOX<sup>68,75–77</sup> and Pd–NHC<sup>78</sup> catalysis. However, to the best of our knowledge, no such precedence exists for malonate nucleophiles under Pd-catalyzed conditions. Since our data do not allow for discerning between inner-sphere attack and an outer-sphere scenario with anomalous stereospecificity as rational for nucleophilic attack under retention, we can presently not make a definite conclusion on this point.

Regardless of the hapticity of the intermediate electrophile ( $\eta^1$  or  $\eta^3$ ) and the mechanism of nucleophilic attack (inner- or outer-sphere), we tentatively suggest the diastereodivergence observed to be based on a competition between steric hindrance by the ligand backbone and electrostatic repulsion by the cyclobutene's carboxylate moiety, with the ligand determining which effect dominates. This potential explanation becomes plausible by comparing the DFT-computed structures of neutral  $\eta^1$ -species major-*anti*-4 as more amenable model systems for the corresponding deprotonated complexes major-*anti*-Na-4 present under catalytic conditions (Figure 2): the high steric demand of L1 seems to make the allyl fragment of *anti*-4a only accessible at the opposite face, whereas coordination by the rather slim ligand L2 might retain the possibility of *anti*-4b to react under retention. Accordingly, sterically less demanding ligands such as L2 allow for circumventing electrostatic repulsion between carboxy group and incoming nucleophile by undergoing nucleophilic substitution under retention. This explanation should also be valid for the isomeric  $\eta^3$ -species as potential electrophiles. Although  $\eta^1$ - $\eta^3$  isomerization is likely accompanied by dissociation of the weakest ligand (chloride or one equivalent of L1) to accommodate an increase in allyl denticity, the preference for nucleophilic attack under either inversion or retention is not expected to change drastically since the steric environment is mainly determined by the bulkiness of the ligand.

## CONCLUSIONS

The Pd-catalyzed asymmetric allylic alkylation of acidic cyclobutene substrates **1** constitutes a rare example of a process combining an efficient deracemization with both diastereodivergence and a de-epimerization.<sup>11</sup> Previous mechanistic studies have reported detailed insights into the structure of  $\eta^1$ -complexes prepared by oxidative addition of cyclobutene substrates, mainly using amide derivatives as more stable model systems. These Pd-species have further been shown to interconvert via a suprafacial  $\eta^1$ - $\eta^3$ - $\eta^1$  pathway.<sup>14,15</sup> However, an overarching mechanism explaining the unprecedented



**Figure 2.** Computed structures for complexes major-*anti*-4, obtained at the BP86/def2-SVP (def2-TZVP on Pd)/CPCM (THF) level of theory, including van der Waals radii of ligands L1 and L2 (lowest energy conformers shown). The cyclobutene ligand is depicted in a stick representation. Color code: gray—C, white—H, red—O, orange—P, blue—N, green—Cl, and turquoise—Pd.

stereoselectivity could not be disclosed, which prompted us to perform a comprehensive mechanistic analysis, including systematic investigation of the single steps (oxidative addition,  $\eta^1$ - $\eta^3$ - $\eta^1$  isomerization, and nucleophilic attack) as well as verification of our findings under catalytic conditions.

The oxidative addition of *cis*-configured substrates generally proceeded under inversion of configuration, whereas *trans*-substrates reacted under both inversion and retention, giving mixtures of *anti*- and *syn*-configured Pd-cyclobutene species. A kinetic analysis employing fast reaction monitoring techniques revealed the  $\eta^1$ - $\eta^3$ - $\eta^1$  interconversion between diastereomeric  $\eta^1$ -species to be significantly faster for *anti*-configured Pd-species *anti*-4 than that for their *syn*-analogues. This was attributed to internal Pd–O coordination stabilizing complexes *syn*-4 against isomerization. The same structural feature is believed to be responsible for the striking difference in reactivity observed upon treatment with nucleophile: while *anti*-4 smoothly reacted to enantioenriched substitution products **3**, the corresponding *syn*-species turned out to be entirely unreactive. By means of a specially designed capture experiment, we were able to show that *anti*-configured Pd-species are generally involved under catalytic conditions, whereas dead-end species *syn*-Na-4 are only formed when using substrate *trans*-1. The transient intermediates *anti*-Na-4

could eventually be directly observed by ESI–HRMS and  $^{31}\text{P}$  NMR analysis under reactive conditions.

Our findings led us to propose an unconventional general mechanism, which allows for rationalizing the stereoselectivities observed. Accordingly, the oxidative addition exhibits a convergent stereochemical course, proceeding under either inversion (with *cis*-1) or retention (with *trans*-1), depending on the substrate's relative configuration. Complexes *syn*-Na-4 formed as side products from *trans*-1 are prevented by internal chelation from reacting to undesired product stereoisomers. Nucleophilic attack on intermediates *anti*-Na-4, on the other hand, displays a ligand-controlled divergent behavior, giving the substitution product of either inversion (with L1) or retention (with L2). Thus, the mechanism disclosed allows for full manipulation of the commonly accepted "double inversion rule", even enabling a "double retention" scenario as known for Mo-catalyzed allylic substitutions.<sup>79–81</sup> A mechanism that includes a stereochemical dichotomy for both oxidative addition and nucleophilic attack, without changing the metal or the nucleophile, is to the best of our knowledge unprecedented in allylic alkylation chemistry.

## ■ ASSOCIATED CONTENT

### Supporting Information

The Supporting Information is available free of charge at <https://pubs.acs.org/doi/10.1021/jacs.3c03590>.

Experimental procedures, characterization data and NMR spectra, additional discussion, further kinetic data and analysis, further MS and HPLC data, and full computational details (PDF)

Computed structures of the Pd-cyclobutene species with ligands FER and PHOX (ZIP)

Correlation plots of calculated and experimental chemical shifts (ZIP)

## ■ AUTHOR INFORMATION

### Corresponding Author

Christina M. Thiele – Clemens-Schöpf-Institute of Organic Chemistry and Biochemistry, Technical University of Darmstadt, 64287 Darmstadt, Germany; [orcid.org/0000-0001-7876-536X](https://orcid.org/0000-0001-7876-536X); Email: [cthiele@thielelab.de](mailto:cthiele@thielelab.de)

### Authors

Johann J. Primožic – Clemens-Schöpf-Institute of Organic Chemistry and Biochemistry, Technical University of Darmstadt, 64287 Darmstadt, Germany; [orcid.org/0000-0002-7525-2371](https://orcid.org/0000-0002-7525-2371)

Julian Ilgen – Clemens-Schöpf-Institute of Organic Chemistry and Biochemistry, Technical University of Darmstadt, 64287 Darmstadt, Germany

Patrick Maibach – Clemens-Schöpf-Institute of Organic Chemistry and Biochemistry, Technical University of Darmstadt, 64287 Darmstadt, Germany; [orcid.org/0009-0001-3910-2296](https://orcid.org/0009-0001-3910-2296)

Matthias Brauser – Clemens-Schöpf-Institute of Organic Chemistry and Biochemistry, Technical University of Darmstadt, 64287 Darmstadt, Germany; [orcid.org/0000-0002-0047-1481](https://orcid.org/0000-0002-0047-1481)

Jonas Kind – Clemens-Schöpf-Institute of Organic Chemistry and Biochemistry, Technical University of Darmstadt, 64287 Darmstadt, Germany; [orcid.org/0000-0001-8074-5552](https://orcid.org/0000-0001-8074-5552)

Complete contact information is available at:

<https://pubs.acs.org/10.1021/jacs.3c03590>

## Funding

J.J.P. and J.I. are obliged to the Fonds der Chemischen Industrie and to the Studienstiftung des Deutschen Volkes for being awarded Ph.D. fellowships. M.B. acknowledges funding by the Hans Messer Foundation. The research leading to these results has received funding from the German Research Foundation (TH1115/12-1). The authors gratefully acknowledge the computing time provided to them on the high-performance computer Lichtenberg at the NHR Centers NHR4CES at TU Darmstadt. This is funded by the Federal Ministry of Education and Research, and the state governments participating on the basis of the resolutions of the GWK for national high-performance computing at universities.

## Notes

The authors declare no competing financial interest.

## ■ ACKNOWLEDGMENTS

We are grateful to Prof. Dr. Nuno Maulide (University of Vienna), Dr. Guilhem Coussanes (University of Vienna), and Dr. Jason D. Williams (University of Graz) for initial discussion and for help with synthesizing the cyclobutene substrates. Furthermore, the invaluable analytical support by Dr. Alexander Schießer and Christiane Rudolph (Technical University of Darmstadt, MS department) is acknowledged.

## ■ ABBREVIATIONS

dba (*E,E*)-dibenzylideneacetone

Nu nucleophile

L ligand

## ■ REFERENCES

- (1) Pàmies, O.; Margalef, J.; Cañellas, S.; James, J.; Judge, E.; Guiry, P. J.; Moberg, C.; Bäckvall, J.-E.; Pfaltz, A.; Pericás, M. A.; Diéguez, M. Recent Advances in Enantioselective Pd-Catalyzed Allylic Substitution: From Design to Applications. *Chem. Rev.* **2021**, *121*, 4373–4505.
- (2) Helmchen, G.; Kazmaier, U.; Förster, S. Enantioselective Allylic Substitutions with Carbon Nucleophiles. In *Asymmetric Carbon-Carbon Bond-Forming Reactions*; Ojima, I., Ed.; John Wiley & Sons: Hoboken, 2010; pp 497–641.
- (3) Milhau, L.; Guiry, P. J. Palladium-Catalyzed Enantioselective Allylic Substitution. In *Transition Metal Catalyzed Enantioselective Allylic Substitution in Organic Synthesis*; Kazmaier, U., Ed.; Springer: Berlin, 2012; pp 95–154.
- (4) Trost, B. M.; Crawley, M. L. Asymmetric Transition-Metal-Catalyzed Allylic Alkylations: Applications in Total Synthesis. *Chem. Rev.* **2003**, *103*, 2921–2944.
- (5) Guerrero Rios, I.; Rosas-Hernandez, A.; Martin, E. Recent Advances in the Application of Chiral Phosphine Ligands in Pd-Catalyzed Asymmetric Allylic Alkylation. *Molecules* **2011**, *16*, 970–1010.
- (6) Trost, B. M.; Verhoeven, T. R. Allylic Substitutions with Retention of Stereochemistry. *J. Am. Chem. Soc.* **1976**, *41*, 3215–3216.
- (7) Hayashi, T.; Hagihara, T.; Konishi, M.; Kumada, M. Stereochemistry of Oxidative Addition of an Optically Active Allyl Acetate to a Palladium(0) Complex. *J. Am. Chem. Soc.* **1983**, *105*, 7767–7768.
- (8) Mackenzie, P. B.; Whelan, J.; Bosnich, B. Asymmetric Synthesis. Mechanism of Asymmetric Catalytic Allylation. *J. Am. Chem. Soc.* **1985**, *107*, 2046–2054.
- (9) Fiaud, J. C.; Legros, J. Y. New Method for the Classification of Nucleophiles in the Palladium-Catalyzed Substitution of Allylic Acetates. *J. Org. Chem.* **1987**, *52*, 1907–1911.



- (10) Luparia, M.; Oliveira, M. T.; Audisio, D.; Frébault, F.; Goddard, R.; Maulide, N. Catalytic Asymmetric Diastereodivergent Deracemization. *Angew. Chem., Int. Ed.* **2011**, *50*, 12631–12635.
- (11) Audisio, D.; Luparia, M.; Oliveira, M. T.; Klütt, D.; Maulide, N. Diastereodivergent De-Epimerization in Catalytic Asymmetric Allylic Alkylation. *Angew. Chem., Int. Ed.* **2012**, *51*, 7314–7317.
- (12) Misale, A.; Niyomchon, S.; Maulide, N. Cyclobutenes: At a Crossroad between Diastereoselective Syntheses of Dienes and Unique Palladium-Catalyzed Asymmetric Allylic Substitutions. *Acc. Chem. Res.* **2016**, *49*, 2444–2458.
- (13) Didier, D.; Reiners, F. Uncommon Four-Membered Building Blocks – Cyclobutenes, Azetines and Thietes. *Chem. Rec.* **2021**, *21*, 1144–1160.
- (14) Audisio, D.; Gopakumar, G.; Xie, L.-G.; Alves, L. G.; Wirtz, C.; Martins, A. M.; Thiel, W.; Farès, C.; Maulide, N. Palladium-Catalyzed Allylic Substitution at Four-Membered-Ring Systems: Formation of H<sup>1</sup>-Allyl Complexes and Electrocyclic Ring Opening. *Angew. Chem., Int. Ed.* **2013**, *52*, 6313–6316.
- (15) Xie, L.-G.; Bagutski, V.; Audisio, D.; Wolf, L. M.; Schmidts, V.; Hofmann, K.; Wirtz, C.; Thiel, W.; Thiele, C. M.; Maulide, N. Dynamic Behaviour of Monohaptoallylpalladium Species: Internal Coordination as a Driving Force in Allylic Alkylation Chemistry. *Chem. Sci.* **2015**, *6*, 5734–5739.
- (16) For related systems that were shown to involve a stable  $\eta^1$ -Pd-allyl intermediate, see (a) Sherden, N. H.; Behenna, D. C.; Virgil, S. C.; Stoltz, B. M. Unusual Allylpalladium Carboxylate Complexes: Identification of the Resting State of Catalytic Enantioselective Decarboxylative Allylic Alkylation Reactions of Ketones. *Angew. Chem., Int. Ed.* **2009**, *48*, 6840–6843. (b) Kollmar, M.; Helmchen, G. An (H1-Allyl)Palladium Complex of a Chiral Bidentate Ligand: Crystallographic and NMR Studies on a (H1-3,3-Diphenylallyl)-(Phosphinooxazoline)Palladium Complex. *Organometallics* **2002**, *21*, 4771–4775. (c) Braunstein, P.; Zhang, J.; Welter, R. Monohapto-allyl Pd(II) complexes with bidentate hybrid P,N ligands. *Dalton Trans.* **2003**, *2003*, 507–509.
- (17) For earlier investigations on equilibria between  $\eta^3$ - and  $\eta^1$ -species in Pd-allyl systems see for example (a) Hansson, S.; Norrby, P.-O.; Soegren, M. P. T.; Aakermark, B.; Cucciolito, M. E.; Giordano, F.; Vitagliano, A. Effects of phenanthroline type ligands on the dynamic processes of (eta.3-allyl)palladium complexes. Molecular structure of (2,9-dimethyl-1,10-phenanthroline)[(1,2,3-eta.)-3-methyl-2-butenyl]chloropalladium. *Organometallics* **1993**, *12*, 4940–4948. (b) Breutel, C.; Pregosin, P. S.; Salzmann, R.; Togni, A. An Unusual, Selective (eta.3-eta.1 Allyl Isomerization in a Chiral Allylic Alkylation Catalyst. *J. Am. Chem. Soc.* **1994**, *116*, 4067–4068. (c) Pregosin, P. S.; Salzmann, R.; Togni, A. 31P, 13C, and 1H NMR Studies on Chiral Allyl Ferrocenyldiphosphine Complexes of Palladium(II). *Organometallics* **1995**, *14*, 842–847. (d) Barloy, L.; Ramdeehul, S.; Osborn, J. A.; Carlotti, C.; Taulelle, F.; De Cian, A.; Fischer, J. H1- and H3-Allylpalladium(II) Complexes Bearing Potentially Tridentate Ligands: Synthesis, Solution Dynamics, and Crystal Structures. *Eur. J. Inorg. Chem.* **2000**, *2000*, 2523–2532. (e) Gatti, G.; López, J. A.; Mealli, C.; Musco, A. Structural and NMR Spectroscopic Characterization of H3-Benzyl Palladium(II) Complexes. *J. Organomet. Chem.* **1994**, *483*, 77–89. (f) Lloyd-Jones, G. C.; Stephen, S. C.; Murray, M.; Butts, C. P.; Vyskočil, Š.; Kočovský, P. Diastereoisomeric Cationic  $\pi$ -Allylpalladium-(P,C)-MAP and MOP Complexes and Their Relationship to Stereochemical Memory Effects in Allylic Alkylation. *Chem.—Eur. J.* **2000**, *6*, 4348–4357.
- (18) Synthesized by using a home-made flow photoreactor, set-up described in Section 2 in the [Supporting Information](#).
- (19) Teichert, J. F.; Feringa, B. L. Phosphoramidites: Privileged Ligands in Asymmetric Catalysis. *Angew. Chem., Int. Ed.* **2010**, *49*, 2486–2528.
- (20) Feringa, B. L. Phosphoramidites: Marvellous Ligands in Catalytic Asymmetric Conjugate Addition. *Acc. Chem. Res.* **2000**, *33*, 346–353.
- (21) Helmchen, G.; Pfaltz, A. Phosphinooxazolines - A New Class of Versatile, Modular P,N-Ligands for Asymmetric Catalysis. *Acc. Chem. Res.* **2000**, *33*, 336–345.
- (22) Pfaltz, A.; Drury, W. J., III. Design of Chiral Ligands for Asymmetric Catalysis: From C2-Symmetric P,P- and N,N-Ligands to Sterically and Electronically Nonsymmetrical P,N-Ligands. *Proc. Natl. Acad. Sci. U.S.A.* **2004**, *101*, 5723–5726.
- (23) Carroll, M. P.; Guiry, P. J. P,N ligands in asymmetric catalysis. *Chem. Soc. Rev.* **2014**, *43*, 819–833.
- (24) Fairlamb, I. J. S.; Lloyd-Jones, G. C. On the Effect of Catalyst Loading in Pd-Catalysed Allylic Alkylation. *Chem. Commun.* **2000**, 2447–2448.
- (25) Lloyd-Jones, G. C.; Stephen, S. C.; Fairlamb, I. J. S.; Martorell, A.; Dominguez, B.; Tomlin, P. M.; Murray, M.; Fernandez, J. M.; Jeffery, J. C.; Riis-Johannessen, T.; Guereziz, T. Coordination of the Trost Modular Ligand to Palladium Allyl Fragments: Oligomers, Monomers and Memory Effects in Catalysis. *Pure Appl. Chem.* **2004**, *76*, 589–601.
- (26) Butts, C. P.; Filali, E.; Lloyd-Jones, G. C.; Norrby, P.-O.; Sale, D. A.; Schramm, Y. Structure-Based Rationale for Selectivity in the Asymmetric Allylic Alkylation of Cycloalkenyl Esters Employing the Trost 'Standard Ligand' (TSL): Isolation, Analysis and Alkylation of the Monomeric Form of the Cationic H3-Cyclohexenyl Complex [(H3-c-C6H9)Pd(TSL)]<sup>+</sup>. *J. Am. Chem. Soc.* **2009**, *131*, 9945–9957.
- (27) Thrippleton, M. J.; Keeler, J. Elimination of Zero-Quantum Interference in Two-Dimensional NMR Spectra. *Angew. Chem., Int. Ed.* **2003**, *42*, 3938–3941.
- (28) Thiele, C. M.; Petzold, K.; Schleucher, J. EASY ROESY: Reliable Cross-Peak Integration in Adiabatic Symmetrized ROESY. *Chem.—Eur. J.* **2009**, *15*, 585–588.
- (29) Wu, D. H.; Chen, A. D.; Johnson, C. S. An Improved Diffusion-Ordered Spectroscopy Experiment Incorporating Bipolar-Gradient Pulses. *J. Magn. Reson.* **1995**, *115*, 260–264.
- (30) For the Pd-cyclobutene species prepared, the d.r. values given refer to the ratio of diastereomeric complexes featuring an identical relative configuration with respect to the cyclobutene, whereas the *syn/anti* ratios given are used for the ratio of Pd-species with a different relative configuration at the cyclobutene. Note that related *syn*- and *anti*-species might differ in their constitution, due to differences in the coordination sphere (e.g. by internal chelation).
- (31) Oxidative addition was generally observed to be irreversible and thus does not allow for interconversion between *anti*- and *syn*-Pd-species via substrate *trans*-1. Hence, unreactive *syn*-Na-4 cannot re-enter the catalytic cycle. For systems where oxidative addition has been shown to be reversible, see for example (a) Amatore, C.; Jutand, A.; Meyer, G.; Mottier, L. Evidence of the Reversible Formation of Cationic  $\pi$ -Allylpalladium(II) Complexes in the Oxidative Addition of Allylic Acetates to Palladium(0) Complexes. *Chem.—Eur. J.* **1999**, *5*, 466–473. (b) Evans, L. A.; Fey, N.; Harvey, J. N.; Hose, D.; Lloyd-Jones, G. C.; Murray, P.; Orpen, A. G.; Osborne, R.; Owen-Smith, G. J. J.; Purdie, M. Counterintuitive Kinetics in Tsuji-Trost Allylation: Ion-Pair Partitioning and Implications for Asymmetric Catalysis. *J. Am. Chem. Soc.* **2008**, *130*, 14471–14473.
- (32) When substrate *cis*-1 was subjected to the sequence shown in [Scheme 4](#), decomposition and formation of an insoluble precipitate was observed upon addition of NaH.
- (33) Mok, K. H.; Nagashima, T.; Day, I. J.; Jones, J. A.; Jones, C. J. V.; Dobson, C. M.; Hore, P. J. Rapid Sample-Mixing Technique for Transient NMR and Photo-CIDNP Spectroscopy: Applications to Real-Time Protein Folding. *J. Am. Chem. Soc.* **2003**, *125*, 12484–12492.
- (34) Pardo, Z. D.; Olsen, G. L.; Fernández-Valle, M. E.; Frydman, L.; Martínez-Álvarez, R.; Herrera, A. Monitoring Mechanistic Details in the Synthesis of Pyrimidines via Real-Time, Ultrafast Multidimensional NMR Spectroscopy. *J. Am. Chem. Soc.* **2012**, *134*, 2706–2715.
- (35) Kind, J.; Thiele, C. M. Still Shimming or Already Measuring? – Quantitative Reaction Monitoring for Small Molecules on the Sub Minute Timescale by NMR. *J. Magn. Reson.* **2015**, *260*, 109–115.

- (36) Wagner, G. E.; Sakhaii, P.; Bermel, W.; Zangger, K. Monitoring Fast Reactions by Spatially-Selective and Frequency-Shifted Continuous NMR Spectroscopy: Application to Rapid-Injection Protein Unfolding. *Chem. Commun.* **2013**, *49*, 3155–3157.
- (37) Kpante, M.; Wolf, L. M. Pathway Bifurcations in the Activation of Allylic Halides by Palladium and Their Influence on the Dynamics of H1 and H3 Allyl Intermediates. *J. Org. Chem.* **2021**, *86*, 9637–9650.
- (38) Although the cyclobutene's carboxylate group is deprotonated under catalytic conditions, protonated complexes *anti-4* rather than their sodium salts *anti-Na-4* were used for reactivity screening of Pd-cyclobutene species, as deprotonated complexes *anti-Na-4* are unstable.
- (39) Granberg, K. L.; Baecvull, J. E. Isomerization of ( $\pi$ -allyl) palladium complexes via nucleophilic displacement by palladium(0). A common mechanism in palladium(0)-catalyzed allylic substitution. *J. Am. Chem. Soc.* **1992**, *114*, 6858–6863.
- (40) When mixtures of *anti*- and *syn-4* were treated with Na-2, only complexes *anti-4* underwent productive substitution, whereas complexes *syn-4* were only deprotonated.
- (41) For all reactions shown in Scheme 5, no  $\eta^2$ -Pd-product complex could be detected by end-point NMR and HRMS analyses of reaction mixtures, suggesting that liberated substitutions products Na-3 are thermodynamically preferred over their corresponding  $\eta^2$ -complexes. Characterized examples of stable  $\eta^2$ -Pd-product complexes have been reported in (a) Steinhagen, H.; Reggelin, M.; Helmchen, G. Palladium-Catalyzed Allylic Alkylation with Phosphinoaryldihydrooxazole Ligands: First Evidence and NMR Spectroscopic Structure Determination of a Primary Olefin–Pd0 Complex. *Angew. Chem., Int. Ed.* **1997**, *36*, 2108–2110. (b) Junker, J.; Reif, B.; Steinhagen, H.; Junker, B.; Felli, I. C.; Reggelin, M.; Griesinger, C. Structure Determination of a Key Intermediate of the Enantioselective Pd Complex Catalyzed Allylic Substitution Reaction. *Chem.—Eur. J.* **2000**, *6*, 3281–3286.
- (42) Misale, A.; Niyomchon, S.; Luparia, M.; Maulide, N. Asymmetric Palladium-Catalyzed Allylic Alkylation Using Dialkylzinc Reagents: A Remarkable Ligand Effect. *Angew. Chem., Int. Ed.* **2014**, *53*, 7068–7073.
- (43) Niyomchon, S.; Audisio, D.; Luparia, M.; Maulide, N. Regio- and Enantioselective Cyclobutene Allylations. *Org. Lett.* **2013**, *15*, 2318–2321.
- (44) See Section 7 in the supporting information for further explanation.
- (45) Consistent results were obtained by intermediate capture experiments using unlabeled substrates **1** in combination with a  $\beta$ -deuterated unstabilized nucleophile, see Section 7 in the Supporting Information for details.
- (46) For all reaction mixtures investigated by HRMS, no dinuclear Pd(I)-allyl species could be detected, as has been reported for a different allylic alkylation system in Markert, C.; Neuburger, M.; Kulicke, K.; Meuwly, M.; Pfaltz, A. Palladium-Catalyzed Allylic Substitution: Reversible Formation of Allyl-Bridged Dinuclear Palladium(I) Complexes. *Angew. Chem., Int. Ed.* **2007**, *46*, 5892–5895.
- (47) With ligand LI, no transient species could be observed with both substrate *cis-1* and *trans-1*, data shown in Section 8 in the Supporting Information.
- (48) Kollmar, M.; Steinhagen, H.; Janssen, J. P.; Goldfuss, B.; Malinovskaya, S. A.; Vázquez, J.; Rominger, F.; Helmchen, G. ( $\eta^3$ -Phenylallyl)(phosphanyloxazoline)palladium Complexes: X-Ray Crystallographic Studies, NMR Investigations, and Ab Initio/DFT Calculations (Phosphanyloxazoline)palladium Complexes, Part II. Part I see: ref. 5. *Chem.—Eur. J.* **2002**, *8*, 3103–3114.
- (49) Johansson, C.; Lloyd-Jones, G. C.; Norrby, P.-O. Memory and Dynamics in Pd-Catalyzed Allylic Alkylation with P,N-Ligands. *Tetrahedron: Asymmetry* **2010**, *21*, 1585–1592.
- (50) Ramdeehul, S.; Dierkes, P.; Aguado, R.; Kamer, P. C. J.; van Leeuwen, P. W. N. M.; Osborn, J. A. Mechanistic Implications of the Observation of Kinetic Resolution in a Palladium-Catalyzed Enantioselective Allylic Alkylation. *Angew. Chem., Int. Ed.* **1998**, *37*, 3118–3121.
- (51) Boele, M. D. K.; Kamer, P. C. J.; Lutz, M.; Spek, A. L.; de Vries, J. G.; van Leeuwen, P. W. N. M.; van Strijdonck, G. P. F. Bulky Monodentate Phosphoramidites in Palladium-Catalyzed Allylic Alkylation Reactions: Aspects of Regioselectivity and Enantioselectivity. *Chem.—Eur. J.* **2004**, *10*, 6232–6246.
- (52) Pericàs, M. A.; Puigjaner, C.; Riera, A.; Vidal-Ferran, A.; Gómez, M.; Jiménez, F.; Muller, G.; Rocamora, M. Modular Bis(Oxazoline) Ligands for Palladium Catalyzed Allylic Alkylation: Unprecedented Conformational Behaviour of a Bis(Oxazoline) Palladium H3-1,3-Diphenylallyl Complex. *Chem.—Eur. J.* **2002**, *8*, 4164–4178.
- (53) Armstrong, P. B.; Dembicer, E. A.; DesBois, A. J.; Fitzgerald, J. T.; Gehrmann, J. K.; Nelson, N. C.; Noble, A. L.; Bunt, R. C. Investigation of the Electronic Origin of Asymmetric Induction in Palladium-Catalyzed Allylic Substitutions with Phosphinooxazoline (PHOX) Ligands by Hammett and Swain–Lupton Analysis of the <sup>13</sup>C NMR Chemical Shifts of the ( $\pi$ -Allyl)Palladium Intermediates. *Organometallics* **2012**, *31*, 6933–6946.
- (54) Widhalm, M.; Nettekoven, U.; Kalchauer, H.; Mereiter, K.; Calhorda, M. J.; Félix, V. Origin of Enantioselectivity in Palladium-Catalyzed Asymmetric Allylic Alkylation Reactions Using Amino-phosphine Ligands. *Organometallics* **2002**, *21*, 315–325.
- (55) Farthing, C. N.; Kočovský, P. The Stereochemical Dichotomy in Palladium(0)- and Nickel(0)-Catalyzed Allylic Substitution. *J. Am. Chem. Soc.* **1998**, *120*, 6661–6672.
- (56) Kurosawa, H.; Ogoshi, S.; Kawasaki, Y.; Murai, S.; Miyoshi, M.; Ikeda, I. Novel dependency of stereochemistry upon metal, ligand, and solvent in oxidative addition of allylic chloride to palladium(0) and platinum(0) complexes. *J. Am. Chem. Soc.* **1990**, *112*, 2813–2814.
- (57) Kurosawa, H.; Kajimaru, H.; Ogoshi, S.; Yoneda, H.; Miki, K.; Kasai, N.; Murai, S.; Ikeda, I. Novel Syn Oxidative Addition of Allylic Halides to Olefin Complexes of Palladium(0) and Platinum(0). *J. Am. Chem. Soc.* **1992**, *114*, 8417–8424.
- (58) Starý, I.; Kočovský, P. The first observation of *syn-anti* dichotomy in the formation of ( $\pi$ -allyl)palladium complexes. *J. Am. Chem. Soc.* **1989**, *111*, 4981–4982.
- (59) Starý, I.; Zajíček, J.; Kočovský, P. Stereochemistry of the Palladium-Catalyzed Allylic Substitution: The Syn-Anti Dichotomy in the Formation of ( $\pi$ -Allyl)Palladium Complexes and Their Equilibration. *Tetrahedron* **1992**, *48*, 7229–7250.
- (60) Wolf, L. M.; Thiel, W. Origin of Inversion versus Retention in the Oxidative Addition of 3-Chloro-cyclopentene to Pd(0)<sub>L<sub>n</sub></sub>. *J. Org. Chem.* **2014**, *79*, 12136–12147.
- (61) Fristrup, P.; Ahlquist, M.; Tanner, D.; Norrby, P.-O. On the Nature of the Intermediates and the Role of Chloride Ions in Pd-Catalyzed Allylic Alkylations: Added Insight from Density Functional Theory. *J. Phys. Chem. A* **2008**, *112*, 12862–12867.
- (62) Kozuch, S.; Amatore, C.; Jutand, A.; Shaik, S. What Makes for a Good Catalytic Cycle? A Theoretical Study of the Role of an Anionic Palladium(0) Complex in the Cross-Coupling of an Aryl Halide with an Anionic Nucleophile. *Organometallics* **2005**, *24*, 2319–2330.
- (63) Kozuch, S.; Shaik, S.; Jutand, A.; Amatore, C. Active Anionic Zero-Valent Palladium Catalysts: Characterization by Density Functional Calculations. *Chem.—Eur. J.* **2004**, *10*, 3072–3080.
- (64) Amatore, C.; Jutand, A.; Suarez, A. Intimate Mechanism of Oxidative Addition to Zerovalent Palladium Complexes in the Presence of Halide Ions and Its Relevance to the Mechanism of Palladium-Catalyzed Nucleophilic Substitutions. *J. Am. Chem. Soc.* **1993**, *115*, 9531–9541.
- (65) Amatore, C.; Azzabi, M.; Jutand, A. Role and Effects of Halide Ions on the Rates and Mechanisms of Oxidative Addition of Iodobenzene to Low-Ligated Zerovalent Palladium Complexes Pd0(PPh3)2. *J. Am. Chem. Soc.* **1991**, *113*, 8375–8384.
- (66) Amatore, C.; Jutand, A. Anionic Pd(0) and Pd(II) Intermediates in Palladium-Catalyzed Heck and Cross-Coupling Reactions. *Acc. Chem. Res.* **2000**, *33*, 314–321.

(67) Amatore, C.; Jutand, A. Mechanistic and Kinetic Studies of Palladium Catalytic Systems. *J. Organomet. Chem.* **1999**, *576*, 254–278.

(68) Cusumano, A. Q.; Stoltz, B. M.; Goddard, W. A., III. Reaction Mechanism, Origins of Enantioselectivity, and Reactivity Trends in Asymmetric Allylic Alkylation: A Comprehensive Quantum Mechanics Investigation of a C(Sp<sup>3</sup>)–C(Sp<sup>3</sup>) Cross-Coupling. *J. Am. Chem. Soc.* **2020**, *142*, 13917–13933.

(69) Turnbull, B. W. H.; Evans, P. A. Asymmetric Rhodium-Catalyzed Allylic Substitution Reactions: Discovery, Development and Applications to Target-Directed Synthesis. *J. Org. Chem.* **2018**, *83*, 11463–11479.

(70) Plietker, B. Iron-Catalyzed Substitution Reactions. In *Iron Catalysis in Organic Chemistry*; Plietker, B., Ed.; Wiley VCH: Weinheim, 2008; pp 197–215.

(71) Evans, P. A.; Nelson, J. D. Conservation of Absolute Configuration in the Acyclic Rhodium-Catalyzed Allylic Alkylation Reaction: Evidence for an Enyl ( $\sigma + \pi$ ) Organorhodium Intermediate. *J. Am. Chem. Soc.* **1998**, *120*, 5581–5582.

(72) Wucher, B.; Moser, M.; Schumacher, S. A.; Rominger, F.; Kunz, D. First X-Ray Structure Analyses of Rhodium(III)  $\eta^1$ -Allyl Complexes and a Mechanism for Allylic Isomerization Reactions. *Angew. Chem., Int. Ed.* **2009**, *48*, 4417–4421.

(73) Plietker, B.; Dieskau, A.; Möws, K.; Jatsch, A. Ligand-Dependent Mechanistic Dichotomy in Iron-Catalyzed Allylic Substitutions:  $\sigma$ -Allyl versus  $\pi$ -Allyl Mechanism. *Angew. Chem., Int. Ed.* **2008**, *47*, 198–201.

(74) Plietker, B. A. A Highly Regioselective Salt-Free Iron-Catalyzed Allylic Alkylation. *Angew. Chem., Int. Ed.* **2006**, *45*, 1469–1473.

(75) Keith, J. A.; Behenna, D. C.; Sherden, N. H.; Mohr, J. T.; Ma, S.; Marinescu, S. C.; Nielsen, R. J.; Oxgaard, J.; Stoltz, B. M.; Goddard, W. A., III The Reaction Mechanism of the Enantioselective Tsuji Allylation: Inner-Sphere and Outer-Sphere Pathways, Internal Rearrangements, and Asymmetric C–C Bond Formation. *J. Am. Chem. Soc.* **2012**, *134*, 19050–19060.

(76) Behenna, D. C.; Mohr, J. T.; Sherden, N. H.; Marinescu, S. C.; Harned, A. M.; Tani, K.; Seto, M.; Ma, S.; Novák, Z.; Krout, M. R.; McFadden, R. M.; Roizen, J. L.; Enquist, J. A., Jr.; White, D. E.; Levine, S. R.; Petrova, K. V.; Iwashita, A.; Virgil, S. C.; Stoltz, B. M. Enantioselective Decarboxylative Alkylation Reactions: Catalyst Development, Substrate Scope, and Mechanistic Studies. *Chem.—Eur. J.* **2011**, *17*, 14199–14223.

(77) Keith, J. A.; Behenna, D. C.; Mohr, J. T.; Ma, S.; Marinescu, S. C.; Oxgaard, J.; Stoltz, B. M.; Goddard, W. A., III The Inner-Sphere Process in the Enantioselective Tsuji Allylation Reaction with (S)-t-Bu-Phosphinoxazoline Ligands. *J. Am. Chem. Soc.* **2007**, *129*, 11876–11877.

(78) Bai, D.-C.; Yu, F.-L.; Wang, W.-Y.; Chen, D.; Li, H.; Liu, Q.-R.; Ding, C.-H.; Chen, B.; Hou, X.-L. Palladium/N-Heterocyclic Carbene Catalyzed Regio and Diastereoselective Reaction of Ketones with Allyl Reagents via Inner-Sphere Mechanism. *Nat. Commun.* **2016**, *7*, 11806.

(79) Lloyd-Jones, G. C.; Krska, S. W.; Hughes, D. L.; Gouriou, L.; Bonnet, V. D.; Jack, K.; Sun, Y.; Reamer, R. A. Conclusive Evidence for a Retention-Retention Pathway for the Molybdenum-Catalyzed Asymmetric Alkylation. *J. Am. Chem. Soc.* **2004**, *126*, 702–703.

(80) Hughes, D. L.; Lloyd-Jones, G. C.; Krska, S. W.; Gouriou, L.; Bonnet, V. D.; Jack, K.; Sun, Y.; Mathre, D. J.; Reamer, R. A. Mechanistic Studies of the Molybdenum-Catalyzed Asymmetric Alkylation Reaction. *Proc. Natl. Acad. Sci. U.S.A.* **2004**, *101*, 5379–5384.

(81) Dvořák, D.; Starý, I.; Kočovský, P. Stereochemistry of Molybdenum(0)-Catalyzed Allylic Substitution: The First Observation of a Syn-Syn Mechanism. *J. Am. Chem. Soc.* **1995**, *117*, 6130–6131.

## NOTE ADDED AFTER ASAP PUBLICATION

This paper was published on July 6, 2023. The abstract graphic has been updated and the revised version was re-posted on July 11, 2023.

## Recommended by ACS

### Divergent Catalysis: Catalytic Asymmetric [4+2] Cycloaddition of Palladium Enolates

Kaylin N. Flesch, Brian M. Stoltz, *et al.*

MAY 15, 2023  
JOURNAL OF THE AMERICAN CHEMICAL SOCIETY

READ 

### Regioselective and Geometrically Controlled Heck 1,1-Diarylation of Unactivated Aliphatic Alkenes

Yao Zhao, Xiaojin Wu, *et al.*

JUNE 05, 2023  
ORGANIC LETTERS

READ 

### Dual-Hydrogen-Bond Donor and Brønsted Acid Cocatalysis Enables Highly Enantioselective Protio-Semipinacol Rearrangement Reactions

Melanie A. S. Blackburn, Eric N. Jacobsen, *et al.*

JULY 10, 2023  
JOURNAL OF THE AMERICAN CHEMICAL SOCIETY

READ 

### Chiral Phosphoric Acid–Palladium(II) Complex Catalyzed Asymmetric Desymmetrization of Biaryl Compounds by C(sp<sup>3</sup>)–H Activation

Tatsuhiko Uchikura, Takahiko Akiyama, *et al.*

JULY 13, 2023  
JOURNAL OF THE AMERICAN CHEMICAL SOCIETY

READ 

Get More Suggestions >

---

## Supporting Information

### **Pd-Catalyzed Asymmetric Allylic Alkylation of Cyclobutenes: From Double Inversion to Double Retention**

Johann J. Primožic, Julian Ilgen, Patrick Maibach, Matthias Brauser, Jonas Kind, and Christina M. Thiele\*

Clemens-Schöpf-Institute of Organic Chemistry and Biochemistry, Technical University of Darmstadt, Alarich-Weiss-Straße 4, 64287 Darmstadt, Germany.

\* Email: [cthiele@thielelab.de](mailto:cthiele@thielelab.de)

---

## Table of Contents

<b>1</b>	<b>General Experimental Conditions</b> .....	<b>3</b>
<b>2</b>	<b>Synthesis of Starting Materials</b> .....	<b>4</b>
	Cyclobutene Substrates .....	4
	Nucleophiles.....	8
<b>3</b>	<b>Test Reactions Allylic Alkylation of Cyclobutenes</b> .....	<b>10</b>
<b>4</b>	<b>Preparation and Investigation of Pd-Cyclobutene Complexes</b> .....	<b>13</b>
	Oxidative Addition of Acid and Ester Substrates.....	14
	Oxidative Addition of Carboxylate Substrates .....	24
<b>5</b>	<b>Reaction Monitoring and Kinetic Fitting of Oxidative Addition and <math>\eta^1</math>-<math>\eta^3</math>-<math>\eta^1</math> Interconversion</b> .....	<b>28</b>
	Kinetic Model .....	28
	Oxidative Addition of Substrate <i>cis</i> - <b>1</b> and <i>trans</i> -Na- <b>1</b> (fast Reaction Monitoring).....	33
	Oxidative Addition of Substrate <i>trans</i> - <b>1</b> (slow Reaction Monitoring) .....	37
	Comparison .....	42
<b>6</b>	<b>Reactivity of Pd-Cyclobutene Complexes</b> .....	<b>43</b>
<b>7</b>	<b>Capture of Intermediates</b> .....	<b>45</b>
	Allylic Alkylation with Deuterated Substrates and Unstabilized Nucleophiles.....	45
	Allylic Alkylation with Deuterated Unstabilized Nucleophiles .....	49
<b>8</b>	<b><math>^{31}\text{P}\{^1\text{H}\}</math>-NMR Reaction Monitoring</b> .....	<b>51</b>
<b>9</b>	<b>ESI-HRMS Analysis of Reactive Mixtures</b> .....	<b>54</b>
<b>10</b>	<b>Computational Details</b> .....	<b>62</b>
<b>11</b>	<b>NMR Spectra of New Compounds</b> .....	<b>80</b>
<b>12</b>	<b>NMR Spectra with Chiral Solvating Agent</b> .....	<b>109</b>
<b>13</b>	<b>References</b> .....	<b>116</b>

## 1 General Experimental Conditions

### Chemicals

Unless stated otherwise, reagents and solvents were purchased from commercial sources (Sigma Aldrich, Fisher Scientific, Fluorochem, ABCR, Tokyo Chemical Industry or Cambridge Isotope Laboratories) and used without further purification. Anhydrous tetrahydrofuran (THF), THF-*d*<sub>8</sub>, MeCN and diisopropyl ether were obtained by distillation from freshly grounded CaH<sub>2</sub> and stored under argon until use. All other anhydrous solvents were purchased from Fisher Scientific in the grade *AcroSeal*<sup>TM</sup>. Molecular sieves were activated at 160 °C under high vacuum for at least 48 h prior to use.

### Nuclear Magnetic Resonance (NMR) Spectroscopy

NMR spectra were recorded on a Bruker AVANCE III HD 400 MHz spectrometer equipped with a broadband fluorine observe (BBFO) probe (<sup>1</sup>H, <sup>19</sup>F, BB<sup>2</sup>H), a Bruker AVANCE III 600 MHz spectrometer equipped with a triple resonance broadband inverse (TBI) probe (<sup>1</sup>H/<sup>31</sup>P, BB<sup>2</sup>H), or a Bruker AVANCE III HD 700 MHz spectrometer equipped with a quadruple resonance inverse (QCI) cryo probe (<sup>1</sup>H/<sup>19</sup>F, <sup>31</sup>P/<sup>13</sup>C/<sup>15</sup>N/<sup>2</sup>H). Unless reported otherwise, measurements were performed at a temperature of 300 K using 1D and 2D experiments available in the Bruker pulse sequence library (<sup>1</sup>H: zg, <sup>13</sup>C{<sup>1</sup>H} and <sup>31</sup>P{<sup>1</sup>H}: zgpg30, <sup>13</sup>C{<sup>1</sup>H} distortionless enhancement by polarisation transfer (DEPT): deptsp135, <sup>1</sup>H-<sup>13</sup>C heteronuclear single quantum coherence (HSQC): hsqcetgpsp.2, <sup>1</sup>H-<sup>13</sup>C heteronuclear multiple bond correlation (HMBC): hmbcetgp13nd, <sup>1</sup>H-<sup>15</sup>N- and <sup>1</sup>H-<sup>31</sup>P-HMBC: hmbcgpndqf, efficient adiabatic symmetrized (EASY) rotating frame Overhauser effect spectroscopy (ROESY): roesyadjsphpr,<sup>1</sup> Nuclear Overhauser effect spectroscopy (NOESY): noesygpphzs,<sup>2</sup> diffusion-ordered spectroscopy (DOSY): ledbpgp2s<sup>3</sup>) or in the literature (<sup>1</sup>H-<sup>1</sup>H- clean in-phase (CLIP) correlated spectroscopy (COSY),<sup>4</sup> pure shift yielded by chirp excitation to deliver individual couplings (PSYCHEDELIC)<sup>5</sup>). Spectrometers were operated with *TopSpin* (version 3.5pl7, Bruker BioSpin, 2017).

NMR spectra were analyzed using *TopSpin* (version 3.5pl7, Bruker BioSpin, 2017) or *MestReNova* (version 14.2.1, Mestrelab Research, 2021). Chemical shifts  $\delta$  are given in parts per million (ppm) and referred to tetramethylsilane (<sup>1</sup>H and <sup>13</sup>C), tetramethylsilane-*d*<sub>12</sub> (<sup>2</sup>H), BF<sub>3</sub>·Et<sub>2</sub>O (<sup>11</sup>B), liquid ammonia (<sup>15</sup>N), 0.1 M aq. NaCl (<sup>23</sup>Na), and 85 % aq. H<sub>3</sub>PO<sub>4</sub> (<sup>31</sup>P) as reference. <sup>15</sup>N-chemical shifts were extracted from <sup>1</sup>H-<sup>15</sup>N-HMBC experiments. <sup>1</sup>H, <sup>2</sup>H and <sup>13</sup>C{<sup>1</sup>H} shifts were corrected by referencing the residual signal of the solvent CDCl<sub>3</sub>/CHCl<sub>3</sub> (7.26 ppm for <sup>1</sup>H and <sup>2</sup>H, 77.16 ppm for <sup>13</sup>C), THF-*d*<sub>8</sub>/THF (1.72 ppm for <sup>1</sup>H and <sup>2</sup>H, 25.31 ppm for <sup>13</sup>C) or dimethyl sulfoxide-*d*<sub>6</sub> (DMSO-*d*<sub>6</sub>) (2.50 ppm for <sup>1</sup>H, 39.52 ppm for <sup>13</sup>C).<sup>6</sup> All <sup>13</sup>C resonances are assumed to be singlets, unless stated otherwise. Scalar coupling constants *J* are reported in Hz. Diffusion coefficients *D* extracted from DOSY experiments were not corrected for potential concentration dependence. ROE and NOE mixing time series were performed with 5 – 10 different mixing times between 50 and 500 ms, using published 1D ROE<sup>7</sup> or 1D NOE<sup>8,9</sup> pulse sequences. Intramolecular distances were extracted using the peak amplitude normalization for improved cross-relaxation (PANIC)<sup>10</sup> approach.

### High Resolution Mass Spectrometry (HRMS)

Electrospray ionization in positive or negative ion mode (ESI<sup>+</sup> and ESI<sup>-</sup>) data were recorded on a Bruker Impact II mass spectrometer using a quadrupole time-of-flight mass analyzer. Molecular ion peaks *M* are reported as mass numbers.

### Infrared Spectroscopy

Infrared (IR) spectra were recorded on a Bruker APLHA spectrometer equipped with a Platinum attenuated total reflection (ATR) unit. Characteristic absorption wavenumbers  $\nu_{\text{max}}$  were recorded in the range of 400 – 4000 cm<sup>-1</sup>.

### Melting points

Melting points (m.p.) were determined on a Stuart SMP10 capillary apparatus and are uncorrected.

### Reaction Conditions

For reactions requiring an inert atmosphere, a Schlenk line operating with argon and equipped with a high vacuum pump was used. Reaction flasks were flame-dried under high vacuum and allowed to cool down under argon. Moisture or air sensitive work was carried out in an argon-filled MBraun glove box.

Room temperature (RT) refers to 20 – 25 °C. Temperatures of 0 °C, –78 °C and –90 °C were realized by means of ice/water, dry ice/isopropanol and liquid-nitrogen isopropanol baths, respectively. Inside the glove box, reactions requiring low temperature were cooled with an *n*-hexane bath that was allowed to stand in a –25 °C freezer prior to use. Temperatures below RT that were desired to be constant overnight were realized with a Huber TC45E immersion cryostat. Reactions involving heating were performed using silicon oil baths and heating plates with magnetic stirrer connected to a contact thermocouple.



## Chromatography

Analytical thin-layer chromatography (TLC) was performed on Silica gel 60 F254 precoated aluminium-backed plates (Sil G/UV254, Macherey-Nagel). TLCs of cyclobutenes were gently heated for about 10 s prior to visualization, in order to convert the cyclobutene to the corresponding diene. Visualization was achieved using ultraviolet light (254 nm) and/or staining with solid iodine or either an acidic ethanolic anisaldehyde solution. Preparative flash column chromatography was performed using silica gel 60A (40 – 60  $\mu\text{m}$ , Acros Organics).

## NMR Yield, Diastereomeric Ratio and Enantiomeric Excess Determination

NMR yields were determined by  $^1\text{H}$ -NMR against a known, gravimetrically determined amount of  $\text{Et}_4\text{Si}$  (distilled from  $\text{CaH}_2$  prior to use) added to the crude product sample as internal standard. Diastereomeric ratios (d.r.) were determined by  $^1\text{H}$ -NMR analysis of the crude product. Enantiomeric excess (e.e.) values were determined against (*S*)-(-)-1-phenylethylamine ((*S*)-PEA, Alfa Aesar, 99.5 % e.e.) or europium(III) tris[3-(heptafluoropropylhydroxymethylene)-*d*-camphorate] ( $\text{Eu}(\text{hfc})_3$ , Aldrich Chemicals) as chiral solvating agent. For enantiodifferentiating analysis, (*S*)-PEA (>1.5 equiv.) or  $\text{Eu}(\text{hfc})_3$  (ca. 0.4 equiv.) was added to a product sample in  $\text{CDCl}_3$  at 0  $^\circ\text{C}$ , which was then loaded into the NMR spectrometer and allowed to magnetically equilibrate for two hours after wobbling and shimming at 273 K. The sample was then subjected to a full characterization ( $^1\text{H}$ ,  $^{13}\text{C}\{^1\text{H}\}$ ,  $^1\text{H}$ - $^1\text{H}$ -CLIP-COSY,  $^1\text{H}$ - $^{13}\text{C}$ -HSQC,  $^1\text{H}$ - $^{13}\text{C}$ -HMBC) in order to identify the resonances of both enantiomers, and the e.e. was determined from the  $^1\text{H}$ -NMR spectrum. If accurate manual integration of the resonances of product enantiomers was not possible due to signal overlap, signal deconvolution was performed instead.

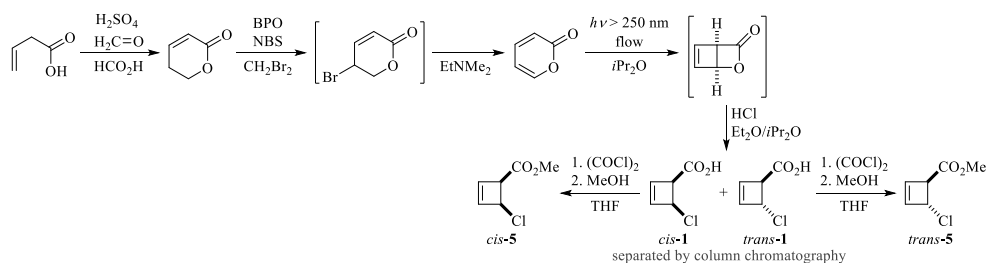
## Ligands

Phosphoramidite ligand ( $S_{ax},S,S$ )-**L1** was obtained commercially (TCI,  $\geq 98$  % e.e.) and used without further purification. Phosphinooxazoline (PHOX) ligand (*R*)-**L2** was prepared from *D*-phenylglycine according to a literature procedure.<sup>11</sup> After purification by flash column chromatography, the final product (*R*)-**L2** was recrystallized twice from hot *n*-hexane. Both ligands were stored under inert atmosphere to prevent decomposition.

## 2 Synthesis of Starting Materials

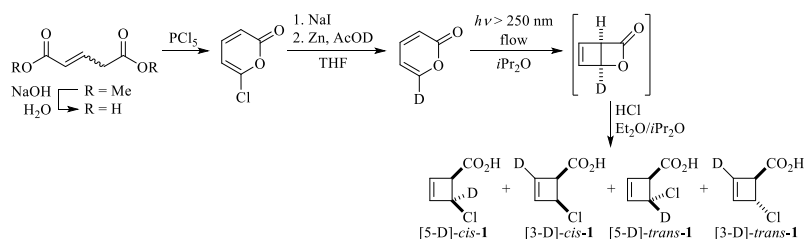
### Cyclobutene Substrates

Cyclobutene substrates **1** and **5** were synthesized according to modified literature procedures,<sup>12–16</sup> starting from vinylacetic acid (Scheme S1).



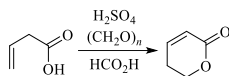
Scheme S1. Synthesis of cyclobutene substrates.

Deuterated cyclobutenes [5-D]/[3-D]-**1** were prepared according to modified literature procedures,<sup>14,15,17,18</sup> starting from a diastereomeric mixture of (*E*)- and (*Z*)-dimethyl glutaconate (Scheme S2).



Scheme S2. Synthesis of deuterated cyclobutene substrates.

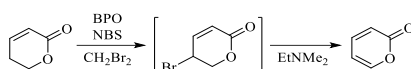
### 5,6-Dihydro-2H-pyron-2-one



The title compound was prepared following a modified literature procedure.<sup>12</sup> To a stirred solution of vinylacetic acid (48.51 g, 563.5 mmol, 1 equiv.) in formic acid (150 mL) was added paraformaldehyde (20.32 g, 676.7 mmol, 1.2 equiv.), followed by concentrated sulfuric acid (2.3 mL, 42.3 mmol, 7.5 mol%). The reaction mixture was heated at 85 °C overnight (15 h) and then allowed to cool down to RT. After addition of Na<sub>2</sub>CO<sub>3</sub> (18.0 g), the mixture was concentrated *in vacuo* at RT, diluted with water (80 mL) and brine (40 mL), carefully neutralized with Na<sub>2</sub>CO<sub>3</sub>, and extracted with CH<sub>2</sub>Cl<sub>2</sub> (3 × 160 mL). The combined organic layers were washed with brine (100 mL), dried over Na<sub>2</sub>SO<sub>4</sub> and concentrated *in vacuo* at RT to give the title compound as yellowish oil (41.91 g, 427.0 mmol, 76 %). The product was stored at 4 °C to prevent decomposition.

**R<sub>f</sub>** = 0.67 (CH<sub>2</sub>Cl<sub>2</sub>:EtOAc 7:3); **<sup>1</sup>H-NMR** (600 MHz, CDCl<sub>3</sub>): δ<sub>H</sub> = 6.93 (1H, dt, <sup>3</sup>J<sub>HH</sub> = 9.8, <sup>3</sup>J<sub>HH</sub> = 4.2, O=C-CH=CH-), 6.03 (1H, dt, <sup>3</sup>J<sub>HH</sub> = 9.8, <sup>4</sup>J<sub>HH</sub> = 1.9, O=C-CH=), 4.42 (2H, t, <sup>3</sup>J<sub>HH</sub> = 6.3, O-CH<sub>2</sub>-), 2.45 (2H, tdd, <sup>3</sup>J<sub>HH</sub> = 6.3, <sup>3</sup>J<sub>HH</sub> = 4.2, <sup>4</sup>J<sub>HH</sub> = 1.9, O-CH<sub>2</sub>-CH<sub>2</sub>-) ppm; **<sup>13</sup>C{<sup>1</sup>H}-NMR** (151 MHz, CDCl<sub>3</sub>): δ<sub>C</sub> = 163.6 (C=O), 145.0 (O=C-CH=CH-), 121.2 (O=C-CH=CH-), 66.4 (O-CH<sub>2</sub>-CH<sub>2</sub>-), 23.8 (O-CH<sub>2</sub>-CH<sub>2</sub>-) ppm. The spectroscopic data are consistent with those reported in the literature.<sup>12</sup>

### 2-Pyrene



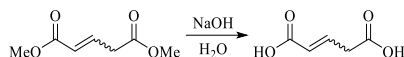
The title compound was prepared following a modified literature procedure.<sup>13</sup> A stirred solution of 5,6-dihydro-2H-pyron-2-one (4.91 g, 50.1 mmol, 1 equiv.), *N*-bromosuccinimide (10.25 g, 57.6 mmol, 1.15 equiv.) and benzoyl peroxide (75 w% aq. dispersion, 81 mg, 0.25 mmol, 0.5 mol%) in CH<sub>2</sub>Br<sub>2</sub> (50 mL) was heated to 96 °C. After complete consumption of starting material (ca. 16 h), the solution was concentrated *in vacuo* at 30 °C, to give crude 5-bromo-5,6-dihydro-2H-pyron-2-one as a brown oil, which was used in the next step without further purification.

**R<sub>f</sub>** = 0.75 (CH<sub>2</sub>Cl<sub>2</sub>:EtOAc 7:3); **<sup>1</sup>H-NMR** (600 MHz, CDCl<sub>3</sub>): δ<sub>H</sub> = 6.99 (1H, ddd, <sup>3</sup>J<sub>HH</sub> = 9.6, <sup>3</sup>J<sub>HH</sub> = 5.1, <sup>4</sup>J<sub>HH</sub> = 1.3, O=C-CH=CH-), 6.04 (1H, dd, <sup>3</sup>J<sub>HH</sub> = 9.6, <sup>4</sup>J<sub>HH</sub> = 0.3, O=C-CH=), 4.73 – 4.65 (2H, m, CBrH and -CBrH-CHH-), 4.59 (1H, ddd, <sup>2</sup>J<sub>HH</sub> = 12.9, <sup>3</sup>J<sub>HH</sub> = 3.2, <sup>4</sup>J<sub>HH</sub> = 1.3, -CBrH-CHH-O-) ppm.

The crude intermediate was cooled to 0 °C, dissolved in EtNMe<sub>2</sub> and stirred upon gradually reaching RT. After complete consumption of the bromide (ca. 16 h), the mixture was concentrated *in vacuo* at RT. The residue was taken up in aq. KHSO<sub>4</sub> (0.1 M, 50 mL) and extracted with CH<sub>2</sub>Cl<sub>2</sub> (5 × 60 mL). The combined organic layers were washed with brine and aq. KHSO<sub>4</sub> (0.1 M, 40 mL each), dried over Na<sub>2</sub>SO<sub>4</sub> and concentrated *in vacuo* at RT. The residue was purified by flash column chromatography on silica gel (*n*-pentane:Et<sub>2</sub>O 50:50 → 25:75) to give the title compound as a colorless oil (3.53 g, 36.7 mmol, 73 % over both steps). The product was stored at -30 °C under light protection to prevent decomposition.

**R<sub>f</sub>** = 0.69 (CH<sub>2</sub>Cl<sub>2</sub>:EtOAc 7:3); **<sup>1</sup>H-NMR** (600 MHz, CDCl<sub>3</sub>): δ<sub>H</sub> = 7.47 (1H, ddd, <sup>3</sup>J<sub>HH</sub> = 5.2, <sup>4</sup>J<sub>HH</sub> = 2.2, <sup>5</sup>J<sub>HH</sub> = 1.2, O-CH=), 7.31 (1H, ddd, <sup>3</sup>J<sub>HH</sub> = 9.5, <sup>3</sup>J<sub>HH</sub> = 6.4, <sup>4</sup>J<sub>HH</sub> = 2.2, O=C-CH=CH-), 6.31 (1H, ddd, <sup>3</sup>J<sub>HH</sub> = 9.5, <sup>5</sup>J<sub>HH</sub> = 1.2, <sup>4</sup>J<sub>HH</sub> = 1.1, O=C-CH-), 6.21 (1H, ddd, <sup>3</sup>J<sub>HH</sub> = 6.4, <sup>3</sup>J<sub>HH</sub> = 5.2, <sup>4</sup>J<sub>HH</sub> = 1.1, O-CH=CH-) ppm; **<sup>13</sup>C{<sup>1</sup>H}-NMR** (151 MHz, CDCl<sub>3</sub>): δ<sub>C</sub> = 161.8 (C=O), 152.1 (O-CH=), 142.9 (O=C-CH=CH-), 117.0 (O=C-CH=), 106.1 (O-CH=CH-) ppm; **HRMS** (ESI<sup>+</sup>): C<sub>8</sub>H<sub>5</sub>O<sub>2</sub> [M+H]<sup>+</sup> requires 97.0284, found 97.0283 (Δ = -1.2 ppm). The spectroscopic data are consistent with those reported in the literature.<sup>12,13</sup>

### Glutaconic acid



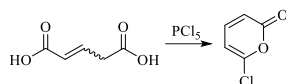
A diastereomeric mixture of dimethyl glutaconate (*E:Z* = 18:1, 24.61 g, 156.0 mmol, 1 equiv.) was suspended in water and cooled to 0 °C. NaOH (14.56 g, 364.0 mmol, 2.33 equiv.) was added slowly and the mixture was stirred at RT overnight (16 h). The reaction mixture was carefully acidified with conc. H<sub>2</sub>SO<sub>4</sub> (pH ≤ 2) and extracted with EtOAc (3 × 300 mL). The combined organic layers were dried over MgSO<sub>4</sub>, concentrated *in vacuo* at 40 °C and dried under high vacuum overnight to give the title compound as a colorless solid (*E:Z* = 25:1, 19.96 g, 153 mmol, 98 %).

**M.p.**: 134 °C {Lit.:<sup>19</sup> 136 °C (Et<sub>2</sub>O), *Z*-isomer; 138 °C (Et<sub>2</sub>O), *E*-isomer}; **<sup>1</sup>H-NMR** (600 MHz, DMSO-*d*<sub>6</sub>): δ<sub>H</sub> = 12.39 (2.08H, br. s, CO<sub>2</sub>H, both isomers), 6.81 (1H, dt, <sup>3</sup>J<sub>HH</sub> = 15.7, <sup>3</sup>J<sub>HH</sub> = 7.2, HO<sub>2</sub>C-CH=CH-, *E*-isomer), 6.39 (0.04H, dt, <sup>3</sup>J<sub>HH</sub> = 11.4, <sup>3</sup>J<sub>HH</sub> = 7.1, HO<sub>2</sub>C-CH=CH-, *Z*-isomer), 5.87 (1H, dt, <sup>3</sup>J<sub>HH</sub> = 15.7, <sup>4</sup>J<sub>HH</sub> = 1.6, HO<sub>2</sub>C-CH=CH-, *E*-isomer), 5.84 (0.04H, dt, <sup>3</sup>J<sub>HH</sub> = 11.4, <sup>4</sup>J<sub>HH</sub> = 1.9, HO<sub>2</sub>C-CH=CH-, *Z*-isomer), 3.62 (0.08H, dd, <sup>3</sup>J<sub>HH</sub> = 7.1, <sup>4</sup>J<sub>HH</sub> = 1.9, -CH<sub>2</sub>-, *Z*-isomer), 3.23 (2H, dd, <sup>3</sup>J<sub>HH</sub> = 7.1, <sup>4</sup>J<sub>HH</sub> = 1.6, -CH<sub>2</sub>-, *E*-isomer) ppm; **<sup>13</sup>C{<sup>1</sup>H}-NMR** (151 MHz, DMSO-*d*<sub>6</sub>): δ<sub>C</sub> = 171.9 (-CH<sub>2</sub>-CO<sub>2</sub>H, *Z*-isomer), 171.5 (-CH<sub>2</sub>-CO<sub>2</sub>H, *E*-isomer), 167.1 (HO<sub>2</sub>C-CH=, *Z*-isomer), 166.8 (HO<sub>2</sub>C-CH=, *E*-isomer), 141.1 (HO<sub>2</sub>C-CH=CH-, *E*-isomer), 137.3 (HO<sub>2</sub>C-CH=CH-, *Z*-isomer), 124.5 (HO<sub>2</sub>C-CH=CH-, *E*-isomer), 122.1 (HO<sub>2</sub>C-CH=CH-, *Z*-isomer), 36.7 (-CH<sub>2</sub>-, *E*-isomer), 33.8



(-CH<sub>2</sub>-, *Z*-isomer) ppm; **ATR-IR** (neat):  $\nu_{\max}$  = 2884 (C-H), 1680 (C=O), 1275 (C-O), 910 (C=C-H) cm<sup>-1</sup>; **HRMS** (ESI<sup>+</sup>): C<sub>5</sub>H<sub>7</sub>O<sub>4</sub> [M+H]<sup>+</sup> requires 131.0339, found 131.0338 ( $\Delta$  = -0.9 ppm). The spectroscopic data of the *E*-isomer are consistent with those available in the literature.<sup>20</sup>

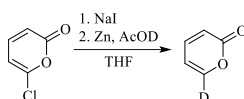
#### 6-Chloro-2-pyrone



The title compound was prepared following a modified literature procedure.<sup>17</sup> Neat glutaric acid (7.04 g, 54.1 mmol, 1 equiv.) was cooled to 0 °C. PCl<sub>5</sub> (22.6 g, 108.7 mmol, 2.0 equiv.) was added carefully, and the mixture was gradually heated to 100 °C. The HCl generated was captured in a gas washing bottle (1 M aq. NaOH). After full consumption of starting materials (no more gas evolution), the mixture was allowed to cool down to RT, quenched with ice, and extracted with CH<sub>2</sub>Cl<sub>2</sub> (3 × 100 mL). The combined organic layers were washed with cold satd. aq. NaHCO<sub>3</sub> (3 × 100 mL), treated with charcoal for 15 min, dried over MgSO<sub>4</sub> and concentrated *in vacuo* at RT. The residue was distilled *in vacuo* to give the title compound as a colorless solid (5.64 g, 43.2 mmol, 80 %). The product was stored at -30 °C to prevent decomposition.

**M.p.**: 27 °C {Lit.:<sup>18</sup> 27 °C (dist.)}; **<sup>1</sup>H-NMR** (600 MHz, CDCl<sub>3</sub>):  $\delta_{\text{H}}$  = 7.31 (1H, dd, <sup>3</sup>*J*<sub>HH</sub> = 9.4, <sup>3</sup>*J*<sub>HH</sub> = 7.0, O=C-CH=CH-), 6.24 (1H, d, <sup>3</sup>*J*<sub>HH</sub> = 9.4, -C=CH-), 6.22 (1H, d, <sup>3</sup>*J*<sub>HH</sub> = 7.0, O=C-CH=) ppm; **<sup>13</sup>C{<sup>1</sup>H}-NMR** (151 MHz, CDCl<sub>3</sub>):  $\delta_{\text{C}}$  = 160.5 (C=O), 150.3 (C=O), 144.3 (O=C-CH=CH-), 113.2 (O=C-CH=), 104.3 (-C=CH-) ppm. The spectroscopic data are consistent with those reported in the literature.<sup>17</sup>

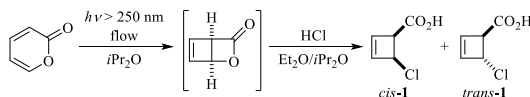
#### [6-<sup>2</sup>H]-2-Pyrone



The title compound was prepared following a modified literature procedure.<sup>18</sup> Prior to use, zinc dust (< 10  $\mu\text{m}$ ) was activated by treating with 2 % aq. HCl, successively washing with water, EtOH and freshly distilled anhydrous Et<sub>2</sub>O, and drying at 105 °C under high vacuum for at least 2 h. NaI was dried at 105 °C for at least 48 h. To a stirred solution of 6-chloro-2-pyrone (13.00 g, 99.6 mmol, 1 equiv.) in anhydrous THF (70 mL) were added molecular sieves 3 Å (0.5 g) and the mixture was stirred at RT overnight (16 h). After addition of NaI (25.38 g, 169.5 mmol, 1.7 equiv.), the mixture was stirred at RT for 4 h and then added dropwise to a suspension of activated zinc dust (65.12 g, 995.7 mmol, 10 equiv.) in AcOD ( $\geq$  99.5 %D, 47 mL, 820 mmol, 8.2 equiv.). The resulting reaction mixture was stirred at RT overnight (16 h), diluted with CH<sub>2</sub>Cl<sub>2</sub> (250 mL), and filtrated. The filtrate was washed with water (2 × 75 mL), satd. aq. Na<sub>2</sub>CO<sub>3</sub> (2 × 75 mL) and brine (80 mL), dried over MgSO<sub>4</sub> and concentrated *in vacuo* at RT. The residue was purified by flash column chromatography on silica gel (*n*-pentane:Et<sub>2</sub>O 25:75) to give the title compound as a colorless oil (2.79 g, 28.9 mmol, 29 %, 94 %D). The product was stored at -30 °C under light protection to prevent decomposition.

**R<sub>f</sub>** = 0.35 (*n*-pentane:Et<sub>2</sub>O 25:75); **<sup>1</sup>H-NMR** (600 MHz, CDCl<sub>3</sub>):  $\delta_{\text{H}}$  = 7.48 (0.06H, d, <sup>3</sup>*J*<sub>HH</sub> = 5.2, residual O-CH=), 7.32 (1H, dd, <sup>3</sup>*J*<sub>HH</sub> = 9.5, <sup>3</sup>*J*<sub>HH</sub> = 6.4, O=C-CH=CH-), 6.34 (1H, d, <sup>3</sup>*J*<sub>HH</sub> = 9.5, O=C-CH=), 6.21 (1H, br. d, <sup>3</sup>*J*<sub>HH</sub> = 6.4, =CH-CD-) ppm; **<sup>2</sup>H-NMR** (92 MHz, CHCl<sub>3</sub>):  $\delta_{\text{D}}$  = 7.53 (s) ppm; **<sup>13</sup>C{<sup>1</sup>H}-NMR** (151 MHz, CDCl<sub>3</sub>):  $\delta_{\text{C}}$  = 161.8 (C=O), 152.1 (residual O-CH=), 151.8 (1:1:1 t, <sup>1</sup>*J*<sub>CD</sub> = 30.4, O-CD=), 142.9 (O=C-CH=CH-), 117.1 (O=C-CH=), 106.1 (residual =CH-CH-O), 105.9 (=CH-CD-O) ppm; **HRMS** (ESI<sup>+</sup>): C<sub>5</sub>H<sub>4</sub>DO<sub>2</sub> [M+H]<sup>+</sup> requires 98.0347, found 98.0348 ( $\Delta$  = 1.0 ppm). The spectroscopic data are consistent with those reported in the literature.<sup>12,21</sup>

#### 4-Chlorocyclobutene-2-enecarboxylic acid (**1**)



*Cis*- and *trans*-4-chlorocyclobutene-2-enecarboxylic acid **1** were prepared following modified literature procedures.<sup>14,15</sup> The photoisomerization of 2-pyrone was performed in a circulating flow photoreactor equipped with a water-cooled 125 W mercury arc lamp (Photochemical Reactors Ltd), a 250 nm cut-off filter (1 M aq. Na<sub>2</sub>WO<sub>4</sub>), an fluorinated ethylene propylene (FEP) tubing coil (8.1 mL active volume), a Jasco PU-2080 Plus high-performance liquid chromatography (HPLC) pump with a 60 psi back-pressure valve, and an external compressed air cooling of the active reactor zone. Prior to use, 2-pyrone was distilled (b.p. 97 °C, 22 mbar), and the reactor was flushed with degassed anhydrous degassed *i*Pr<sub>2</sub>O.

A degassed solution of 2-pyrone (1.00 g, 10.1 mmol, 1 equiv.) in anhydrous *i*Pr<sub>2</sub>O (200 mL) was cooled to -20 °C and then circulated through the reactor at 5 mL min<sup>-1</sup> until <sup>1</sup>H-NMR analysis indicates quantitative conversion (ca. 21 h). The intermediate bicyclic lactone, which is only stable in diluted solution at low temperature, was directly used in the next step. The reactor coil was cleaned from fouling products by successively flushing with acetone, water, aq. NaOH (1 M) and water.

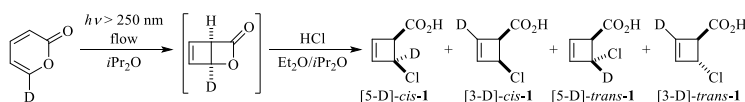
To the lactone solution were added activated molecular sieves 3 Å (10 g). At  $-20\text{ }^{\circ}\text{C}$ , anhydrous HCl (2 M in Et<sub>2</sub>O, 20 mL, 40 mmol, 4 equiv.) was added dropwise and the mixture was stirred intensively overnight (18 h). The mixture was filtrated over celite® and concentrated *in vacuo* at  $0\text{ }^{\circ}\text{C}$  to give a crude diastereomeric mixture of the title compounds **1** (*cis:trans* = 6.5:1). Purification by flash column chromatography on silica gel (*n*-heptane:EtOAc 95:5 with 2 % AcOH, wet load from CH<sub>2</sub>Cl<sub>2</sub>) afforded *trans*-**1** (97 mg, 0.73 mmol, 7.2 %) as a colorless oil, closely followed by *cis*-**1** (563 mg, 4.25 mmol, 42 %) as a colorless solid. The products were stored at  $-30\text{ }^{\circ}\text{C}$  to prevent decomposition.

*cis*-**1**:  $R_f = 0.72$  (*n*-hexane:EtOAc 3:7 with 2 % AcOH); **<sup>1</sup>H-NMR** (700 MHz, CDCl<sub>3</sub>, 273 K):  $\delta_H = 11.4$  (1H, br. s, CO<sub>2</sub>H), 6.32 (1H, dd,  $^3J_{HH} = 2.7$ ,  $^3J_{HH} = 0.9$ , =CH-CClH-), 6.29 (1H, dt,  $^3J_{HH} = 2.7$ ,  $^3J_{HH} \approx ^4J_{HH} \approx 0.9$ , =CH-CH-CO<sub>2</sub>H), 5.12 (1H, dt,  $^3J_{HH} = 4.4$ ,  $^3J_{HH} \approx ^4J_{HH} \approx 0.9$ , -CClH-), 4.14 (1H, dd,  $^3J_{HH} = 4.4$ ,  $^3J_{HH} = 0.9$ , -CH-CO<sub>2</sub>H) ppm; **<sup>13</sup>C{<sup>1</sup>H}-NMR** (176 MHz, CDCl<sub>3</sub>, 273 K):  $\delta_C = 176.9$  (CO<sub>2</sub>H), 141.3 (=CH-CClH-), 135.6 (=CH-CH-CO<sub>2</sub>H), 55.8 (-CClH-), 53.8 (-CH-CO<sub>2</sub>H) ppm; **HRMS** (ESI<sup>+</sup>): C<sub>5</sub>H<sub>6</sub>ClO<sub>2</sub> [M+H]<sup>+</sup> requires 133.0051, found 133.0048 ( $\Delta = -1.9$  ppm).

*trans*-**1**:  $R_f = 0.77$  (*n*-hexane:EtOAc 3:7 with 2 % AcOH); **<sup>1</sup>H-NMR** (700 MHz, CDCl<sub>3</sub>, 273 K):  $\delta_H = 12.1$  (1H, br. s, CO<sub>2</sub>H), 6.33 – 6.30 (1H, m, =CH-CClH-), 6.29 – 6.27 (1H, m, =CH-CH-CO<sub>2</sub>H), 5.00 (1H, dd,  $^3J_{HH} = 1.9$ ,  $^3J_{HH} = 1.2$ , -CClH-), 3.79 (1H, dd,  $^3J_{HH} = 2.6$ ,  $^3J_{HH} = 1.2$ , -CH-CO<sub>2</sub>H) ppm; **<sup>13</sup>C{<sup>1</sup>H}-NMR** (176 MHz, CDCl<sub>3</sub>, 273 K):  $\delta_C = 177.0$  (CO<sub>2</sub>H), 141.3 (=CH-CClH-), 135.6 (=CH-CH-CO<sub>2</sub>H), 57.0 (-CH-CO<sub>2</sub>H), 55.8 (-CClH-) ppm; **HRMS** (ESI<sup>+</sup>): C<sub>5</sub>H<sub>6</sub>ClO<sub>2</sub> [M+H]<sup>+</sup> requires 133.0051, found 133.0049 ( $\Delta = -1.5$  ppm).

The spectroscopic data of both diastereomers are consistent with those reported in the literature.<sup>22</sup>

#### [2-<sup>2</sup>H<sub>1,0</sub>,4-<sup>2</sup>H<sub>0,1</sub>]-4-chlorocyclobutene-2-enecarboxylic acid ([5-D]/[3-D]-**1**)



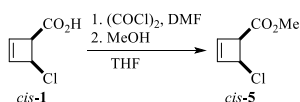
[2-<sup>2</sup>H<sub>1,0</sub>,4-<sup>2</sup>H<sub>0,1</sub>]-*cis*- and -*trans*-4-chlorocyclobutene-2-enecarboxylic acid [5-D]/[3-D]-**cis-1** and [5-D]/[3-D]-**trans-1** were prepared analogously to the unlabeled isotopologues (*vide supra*). Irradiation of [6-<sup>2</sup>H]-2-pyrone (2.00 g, 20.6 mmol, 1 equiv.) was stopped after 78 h at 93 % conversion. After treating with HCl, the crude diastereomeric product mixture (*cis:trans* = 5:1) was subjected to flash column chromatography to afford a 3.7:1 mixture of [5-D]- and [3-D]-**trans-1** (242 mg, 1.81 mmol, 8.8 %, 74 %D  $\alpha$  to Cl, 20 %D at olefinic position, overall 94 %D) as a colorless oil, followed by a 1:1.7 mixture of [5-D]- and [3-D]-**cis-1** (1.11 g, 8.31 mmol, 40 %, 35 %D  $\alpha$  to Cl, 59 %D at olefinic position, overall 94 %D) as a colorless solid. The products were stored at  $-30\text{ }^{\circ}\text{C}$  to prevent decomposition.

[5-D]- and [3-D]-**cis-1**:  $R_f = 0.72$  (*n*-hexane:EtOAc 3:7 with 2 % AcOH); **<sup>1</sup>H-NMR** (700 MHz, CDCl<sub>3</sub>, 273 K):  $\delta_H = 12.3$  (1H, br. s, CO<sub>2</sub>H), 6.31 – 6.30 (1H, m, =CH-CClH/D-), 6.29 (0.41H, dd,  $^3J_{HH} = 2.8$ ,  $^3J_{HH} = 0.9$ , residual =CH-CH-CO<sub>2</sub>H), 5.12 (0.65H, dd,  $^3J_{HH} = 4.4$ ,  $^3J_{HH} = 0.8$ , residual -CClH-), 4.15 – 4.13 (1H, m, -CH-CO<sub>2</sub>H) ppm; **<sup>2</sup>H-NMR** (92 MHz, CHCl<sub>3</sub>, 273 K):  $\delta_D = 6.33$  (1D, s, =CD-CH-CO<sub>2</sub>H), 5.13 (0.59D, s, -CClD-) ppm; **<sup>13</sup>C{<sup>1</sup>H}-NMR** (176 MHz, CDCl<sub>3</sub>, 273 K):  $\delta_C = 176.7$  (CO<sub>2</sub>H), 141.0 (residual -CH=CH-CClH-), 140.9 (-CH=CH-CClD-), 140.8 (-CD=CH-CClH-), 136.1 (-CH=CH-CClD-), 136.1 (residual -CH=CH-CClH-), 135.8 (1:1:1 t,  $^1J_{CD} = 27.6$ , -CD=CH-CClH-), 55.8 (m, -CD=CH-CClH- and residual -CH=CH-CClH-), 55.6 (1:1:1 t,  $^1J_{CD} = 26.0$ , -CClD-), 53.8 (residual =CH-CH(CO<sub>2</sub>H)-CClH-), 53.7 (=CD-CH(CO<sub>2</sub>H)-CClH-), 53.7 (=CH-CH(CO<sub>2</sub>H)-CClD-) ppm; **HRMS** (ESI<sup>+</sup>): C<sub>5</sub>H<sub>5</sub>DClO<sub>2</sub> [M+H]<sup>+</sup> requires 134.0114, found 134.0116 ( $\Delta = 1.5$  ppm).

[5-D]- and [3-D]-**trans-1**:  $R_f = 0.75$  (*n*-hexane:EtOAc 3:7 with 2 % AcOH); **<sup>1</sup>H-NMR** (700 MHz, CDCl<sub>3</sub>, 273 K):  $\delta_H = 11.9$  (1H, br. s, CO<sub>2</sub>H), 6.32 – 6.30 (1H, m, =CH-CClH/D-), 6.29 – 6.27 (0.80H, m, residual =CH-CH-CO<sub>2</sub>H), 5.01 – 4.99 (0.26H, m, residual -CClH-), 3.80 – 3.78 (1H, m, -CH-CO<sub>2</sub>H) ppm; **<sup>2</sup>H-NMR** (92 MHz, CHCl<sub>3</sub>, 273 K):  $\delta_D = 6.29$  (0.27D, s, =CD-CH-CO<sub>2</sub>H), 5.01 (1D, s, -CClD-) ppm; **<sup>13</sup>C{<sup>1</sup>H}-NMR** (176 MHz, CDCl<sub>3</sub>, 273 K):  $\delta_C = 176.7$  (CO<sub>2</sub>H), 141.3 (residual -CH=CH-CClH-), 141.2 (-CH=CH-CClD-), 141.1 (-CD=CH-CClH-), 135.7 (-CH=CH-CClD-), 135.6 (residual -CH=CH-CClH-), 135.4 (1:1:1 t,  $^1J_{CD} = 27.9$ , -CD=CH-CClH-), 57.0 (residual =CH-CH(CO<sub>2</sub>H)-CClH-), 56.9 (=CD-CH(CO<sub>2</sub>H)-CClH-), 56.9 (=CH-CH(CO<sub>2</sub>H)-CClD-), 55.8 (m, -CD=CH-CClH- and residual -CH=CH-CClH-), 55.5 (1:1:1 t,  $^1J_{CD} = 26.0$ , -CClD-) ppm; **HRMS** (ESI<sup>+</sup>): C<sub>5</sub>H<sub>5</sub>DClO<sub>2</sub> [M+H]<sup>+</sup> requires 134.0114, found 134.0116 ( $\Delta = 1.5$  ppm).

The spectroscopic data of both labeled diastereomers are consistent with those reported in the literature.<sup>22,23</sup>

#### *Cis*-methyl-4-chlorocyclobutene-2-enecarboxylic carboxylate (*cis*-**5**)

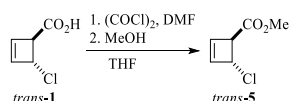


*Cis*-methyl-4-chlorocyclobutene-2-enecarboxylic carboxylate *cis*-**5** was prepared following a modified literature procedure.<sup>16</sup> To a stirred solution of *cis*-4-chlorocyclobutene-2-enecarboxylic acid *cis*-**1** (288 mg, 2.17 mmol, 1 equiv.) and DMF (34  $\mu$ L, 0.43 mmol, 20 mol%) in anhydrous CH<sub>2</sub>Cl<sub>2</sub> (25 mL) was added oxalyl chloride (0.37 mL, 3.80 mmol, 1.75 equiv.) dropwise at  $0\text{ }^{\circ}\text{C}$ . After stirring at  $0\text{ }^{\circ}\text{C}$  for 1 h, anhydrous MeOH (0.44 mL, 10.9 mmol, 5 equiv.) was added dropwise, and the reaction mixture was stirred at  $0\text{ }^{\circ}\text{C}$  overnight (19 h). The mixture was concentrated *in vacuo* at

0 °C and then subjected to flash column chromatography on silica gel (*n*-hexane:CH<sub>2</sub>Cl<sub>2</sub> 2:1) to give the title compound as a colorless oil (192 mg, 1.31 mmol, 60 %). The product was stored at -30 °C to prevent decomposition.

$R_f$  = 0.11 (*n*-hexane:CH<sub>2</sub>Cl<sub>2</sub> 2:1); **<sup>1</sup>H-NMR** (700 MHz, CDCl<sub>3</sub>):  $\delta_H$  = 6.29 (1H, dt,  $^3J_{HH}$  = 2.8,  $^3J_{HH} \approx ^4J_{HH} \approx 0.8$ , =CH-CH-CO<sub>2</sub>Me), 6.27 (1H, dd,  $^3J_{HH}$  = 2.8,  $^3J_{HH}$  = 0.8, =CH-CClH-), 5.09 (1H, dt,  $^3J_{HH}$  = 4.3,  $^3J_{HH} \approx ^4J_{HH} \approx 0.8$ , -CClH-), 4.09 (1H, dd,  $^3J_{HH}$  = 4.3,  $^3J_{HH}$  = 0.8, -CH-CO<sub>2</sub>Me), 3.77 (3H, s, -CH<sub>3</sub>) ppm; **<sup>13</sup>C{<sup>1</sup>H}-NMR** (176 MHz, CDCl<sub>3</sub>):  $\delta_C$  = 170.4 (CO<sub>2</sub>Me), 140.5 (=CH-CClH-), 136.6 (=CH-CH-CO<sub>2</sub>Me), 56.4 (-CClH-), 54.1 (-CH-CO<sub>2</sub>Me), 52.2 (-CH<sub>3</sub>) ppm; **HRMS** (ESI<sup>+</sup>): C<sub>6</sub>H<sub>8</sub>ClO<sub>2</sub> [M+H]<sup>+</sup> requires 147.0207, found 147.0207 ( $\Delta$  = 0). The spectroscopic data are consistent with those reported in the literature.<sup>24</sup>

#### **Trans-methyl-4-chlorocyclobutene-2-enecarboxylic carboxylate (*trans*-5)**

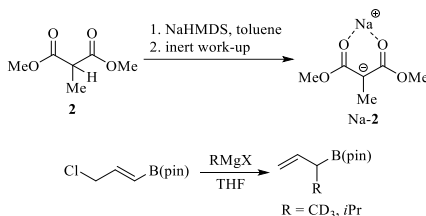


*Trans*-methyl-4-chlorocyclobutene-2-enecarboxylic carboxylate *trans*-5 was prepared following a modified literature procedure.<sup>16</sup> To a stirred solution of *trans*-4-chlorocyclobutene-2-enecarboxylic acid *trans*-1 (74.0 mg, 558  $\mu$ mol, 1 equiv.) and DMF (9  $\mu$ L, 112  $\mu$ mol, 20 mol%) in anhydrous CH<sub>2</sub>Cl<sub>2</sub> (6 mL) was added oxalyl chloride (95  $\mu$ L, 977  $\mu$ mol, 1.75 equiv.) dropwise at 0 °C. After stirring at 0 °C for 1 h, anhydrous MeOH (200  $\mu$ L, 5.0 mmol, 9 equiv.) was added dropwise, and the reaction mixture was allowed to gradually reach RT overnight (15 h). The mixture was concentrated *in vacuo* at 0 °C and then subjected to flash column chromatography on silica gel (*n*-hexane:CH<sub>2</sub>Cl<sub>2</sub> 2:1) to give the title compound as a colorless oil (192 mg, 1.31 mmol, 60 %). The product was stored at -30 °C to prevent decomposition.

$R_f$  = 0.23 (*n*-hexane:CH<sub>2</sub>Cl<sub>2</sub> 2:1); **<sup>1</sup>H-NMR** (700 MHz, CDCl<sub>3</sub>):  $\delta_H$  = 6.29 – 6.27 (1H, m, =CH-), 6.27 – 6.26 (1H, m, =CH-), 4.97 (1H, dd,  $^3J_{HH}$  = 2.0,  $^3J_{HH}$  = 1.1, -CClH-), 3.76 – 3.75 (1H, m, -CH-CO<sub>2</sub>Me), 3.74 (3H, s, -CH<sub>3</sub>) ppm; **<sup>13</sup>C{<sup>1</sup>H}-NMR** (176 MHz, CDCl<sub>3</sub>):  $\delta_C$  = 170.8 (CO<sub>2</sub>Me), 140.9 (=CH-), 136.2 (=CH-), 57.4 (-CH-CO<sub>2</sub>Me), 56.3 (-CClH-), 52.3 (-CH<sub>3</sub>) ppm; **HRMS** (ESI<sup>+</sup>): C<sub>6</sub>H<sub>8</sub>ClO<sub>2</sub> [M+H]<sup>+</sup> requires 147.0207, found 147.0207 ( $\Delta$  = 0.1 ppm).

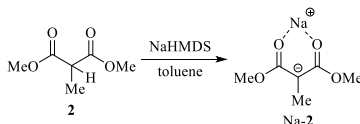
## Nucleophiles

Malonate nucleophile Na-2 and allyl boronates were synthesized as shown in Scheme S3. The precursors dimethyl methylmalonate **2**<sup>25</sup> and (*E*)-2-chloromethylvinylboronic acid pinacol ester<sup>26</sup> were prepared according to literature procedures.



**Scheme S3.** Synthesis of malonate and boronate nucleophiles.

#### **Sodium dimethyl methylmalonate (Na-2)**

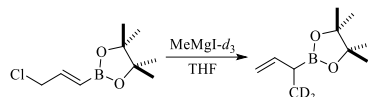


Prior to use, dimethyl methylmalonate **2** was distilled (b.p. 67 – 68 °C, 8 mbar) and dried over molecular sieves 4 Å under argon. To a filtered solution of NaHMDS (1.48 g, 7.51 mmol, 1.05 equiv.) in anhydrous toluene (25 mL) was added dimethyl methylmalonate **2** (1.00 mL, 7.51 mmol, 1 equiv.) dropwise at 0 °C. After stirring for 15 min, the colorless precipitate was filtered off inertly, washed with anhydrous toluene (3  $\times$  10 mL) followed by anhydrous *n*-hexane (3  $\times$  10 mL), and dried under high vacuum for 30 min. The crude product was dissolved in a minimum amount of anhydrous THF (8 mL), crystallized by slow addition of anhydrous *n*-hexane (80 mL), filtered off inertly and dried under high vacuum for 1 h. The title compound Na-2 was obtained as a colorless solid (993 mg, ca. 95 % purity, ca. 5.64 mmol, ca. 75 % yield), which was stored and handled under inert atmosphere to prevent decomposition.

Na-2 was found to be highly moisture sensitive, as it undergoes reprotonation and partial mono- and dihydrolysis upon contact with water. The compound exhibited high solubility in THF (>690 mM), with solutions being stable over months. In MeCN, on the other hand, slow decomposition upon formation of a colorless precipitate was observed.

**<sup>1</sup>H-NMR** (600 MHz, THF-*d*<sub>8</sub>): δ<sub>H</sub> = 3.41 (6H, s, O-CH<sub>3</sub>), 1.64 (3H, s, C<sub>q</sub>-CH<sub>3</sub>) ppm; **<sup>13</sup>C{<sup>1</sup>H}-NMR** (151 MHz, THF-*d*<sub>8</sub>): δ<sub>C</sub> = 172.3 (C=O), 67.9 (C<sub>q</sub>-CH<sub>3</sub>), 48.9 (O-CH<sub>3</sub>), 11.9 (C<sub>q</sub>-CH<sub>3</sub>) ppm; **<sup>23</sup>Na-NMR** (106 MHz, THF-*d*<sub>8</sub>): δ<sub>Na</sub> = 1.0 (br. s) ppm; **ATR-IR** (neat): ν<sub>max</sub> = 2948 (C-H), 1632 (C=O), 1503 (C=C), 1357 (CH<sub>3</sub>), 1095 (C-O-C) cm<sup>-1</sup>; **HRMS** (APCI<sup>-</sup>): C<sub>6</sub>H<sub>9</sub>O<sub>4</sub> [M-Na]<sup>-</sup> requires 145.0506, found 145.0502 (Δ = -2.8 ppm).

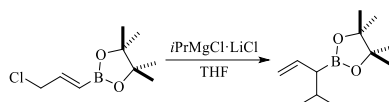
#### 2-(But-3-en-2-yl-1,1,1-*d*<sub>3</sub>)-4,4,5,5-tetramethyl-1,3,2-dioxaborolane



The title compound was prepared following a modified literature procedure.<sup>27</sup> To a stirred suspension of freshly crushed magnesium turnings (456 mg, 18.8 mmol, 3.75 equiv.) in anhydrous Et<sub>2</sub>O (5 mL) was carefully added iodomethane-*d*<sub>3</sub> (>99% D, 467 μL, 7.5 mmol, 1.5 equiv.) at 0 °C. The mixture was stirred at RT for 1 h, and then added dropwise to a vigorously stirred solution of (*E*)-2-chloromethylvinylboronic acid pinacol ester (1.01 g, 5.00 mmol, 1 equiv.) in anhydrous THF (10 mL) at -90 °C. The resulting mixture was allowed to gradually reach RT overnight (17 h), and then diluted with *n*-hexane (15 mL). The mixture was cooled to 0 °C, quenched with 1 M aq. NH<sub>4</sub>Cl (10 mL) and stirred for 10 min. The layers were separated and the aqueous layer was extracted with *n*-hexane (3 × 15 mL). The combined organic layers were dried over MgSO<sub>4</sub> and concentrated *in vacuo* at RT. The residue was purified by flash column chromatography on silica gel (*n*-hexane:EtOAc 99:1) to give the title compound as a colorless oil (312 mg, 1.69 mmol, 34 %, >99 %D). The product was stored in a sealed flask at 4 °C to prevent decomposition.

**R<sub>f</sub>** = 0.50 (*n*-hexane:EtOAc 90:10); **<sup>1</sup>H-NMR** (700 MHz, CDCl<sub>3</sub>): δ<sub>H</sub> = 5.94 (1H, ddd, <sup>3</sup>J<sub>HH</sub> = 17.3, <sup>3</sup>J<sub>HH</sub> = 10.3, <sup>3</sup>J<sub>HH</sub> = 7.1, =CH-), 4.97 (1H, dt, <sup>3</sup>J<sub>HH</sub> = 17.3, <sup>2</sup>J<sub>HH</sub> ≈ <sup>4</sup>J<sub>HH</sub> ≈ 1.6, =CHH<sub>cis</sub>), 4.92 (1H, dt, <sup>3</sup>J<sub>HH</sub> = 10.3, <sup>2</sup>J<sub>HH</sub> ≈ <sup>4</sup>J<sub>HH</sub> ≈ 1.6, =CHH<sub>trans</sub>), 1.88 (1H, br. d, <sup>3</sup>J<sub>HH</sub> = 7.1, CHB), 1.24 (12H, s, -CH<sub>3</sub>) ppm; **<sup>2</sup>H-NMR** (92 MHz, CHCl<sub>3</sub>): δ<sub>D</sub> = 1.08 (d, <sup>3</sup>J<sub>DH</sub> = 1.1) ppm; **<sup>11</sup>B-NMR** (193 MHz, CDCl<sub>3</sub>): δ<sub>B</sub> = 33.3 (br. s) ppm; **<sup>13</sup>C{<sup>1</sup>H}-NMR** (176 MHz, CDCl<sub>3</sub>): δ<sub>C</sub> = 144.1 (=CH-), 112.1 (=CH<sub>2</sub>), 83.3 (-C<sub>q</sub>(CH<sub>3</sub>)<sub>2</sub>), 24.8 (-C<sub>a</sub>H<sub>3</sub>), 24.8 (-C<sub>b</sub>H<sub>3</sub>), 22.8 (broad, CHB), 13.4 (sept, <sup>1</sup>J<sub>CD</sub> = 19.4, -CD<sub>3</sub>) ppm; **HRMS** (ESI<sup>+</sup>): C<sub>10</sub>H<sub>16</sub>D<sub>3</sub>BO<sub>2</sub> [M+H]<sup>+</sup> requires 186.1741, found 186.1739 (Δ = -1.1 ppm). The spectroscopic data are consistent with those reported in the literature.<sup>28</sup>

#### 4,4,5,5-Tetramethyl-2-(4-methylpent-1-en-3-yl)-1,3,2-dioxaborolane

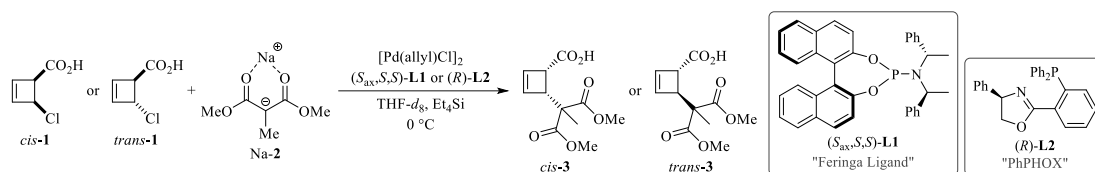


The title compound was prepared following a modified literature procedure.<sup>27</sup> *i*PrMgCl·LiCl (1.3 M in THF, 10.2 mL, 13.3 mmol, 1.8 equiv.) was added dropwise to a vigorously stirred solution of (*E*)-2-chloromethylvinylboronic acid pinacol ester (1.50 g, 7.40 mmol, 1 equiv.) in anhydrous THF (15 mL) at -90 °C. The resulting mixture was allowed to gradually reach RT overnight (18 h), and then diluted with *n*-hexane (15 mL). The mixture was cooled to 0 °C, quenched with 1 M aq. NH<sub>4</sub>Cl (10 mL) and stirred for 10 min. The layers were separated and the aqueous layer was extracted with *n*-hexane (3 × 15 mL). The combined organic layers were dried over MgSO<sub>4</sub> and concentrated *in vacuo* at RT. The residue was purified by flash column chromatography on silica gel (*n*-hexane:EtOAc 99:1) to give the title compound as a colorless oil (985 mg, 4.69 mmol, 63 %). The product was stored in a sealed flask at 4 °C to prevent decomposition.

**R<sub>f</sub>** = 0.51 (*n*-hexane:EtOAc 90:10); **<sup>1</sup>H-NMR** (600 MHz, CDCl<sub>3</sub>): δ<sub>H</sub> = 5.75 (1H, dt, <sup>3</sup>J<sub>HH</sub> = 17.1, <sup>3</sup>J<sub>HH</sub> ≈ 9.9, =CH-), 4.99 – 4.93 (2H, m, =CH<sub>2</sub>), 1.88 – 1.79 (1H, m, -CH(CH<sub>3</sub>)<sub>2</sub>), 1.60 (1H, br. t, <sup>3</sup>J<sub>HH</sub> ≈ 9.0, CHB), 1.24 (12H, s, C<sub>q</sub>-CH<sub>3</sub>), 0.93 (3H, d, <sup>3</sup>J<sub>HH</sub> = 6.7, -CH-CH<sub>3</sub>), 0.89 (3H, d, <sup>3</sup>J<sub>HH</sub> = 6.7, -CH-CH<sub>3</sub>) ppm; **<sup>11</sup>B-NMR** (193 MHz, CDCl<sub>3</sub>): δ<sub>B</sub> = 33.0 (br. s) ppm; **<sup>13</sup>C{<sup>1</sup>H}-NMR** (151 MHz, CDCl<sub>3</sub>): δ<sub>C</sub> = 138.8 (=CH-), 114.7 (=CH<sub>2</sub>), 83.2 (-C<sub>q</sub>(CH<sub>3</sub>)<sub>2</sub>), 39.4 (broad, CHB), 29.5 (-CH(CH<sub>3</sub>)<sub>2</sub>), 24.9 C<sub>q</sub>-C<sub>a</sub>H<sub>3</sub>), 24.8 (C<sub>q</sub>-C<sub>b</sub>H<sub>3</sub>), 22.6 (-CH-C<sub>a</sub>H<sub>3</sub>), 21.9 (-CH-C<sub>b</sub>H<sub>3</sub>) ppm; **ATR-IR** (neat): ν<sub>max</sub> = 2978 (C-H), 1352 (B-C), 1316 (B-O), 1141 (C-O), 971, 901 (=CH<sub>2</sub>), 851 cm<sup>-1</sup>; **HRMS** (ESI<sup>+</sup>): C<sub>12</sub>H<sub>24</sub>BO<sub>2</sub> [M+H]<sup>+</sup> requires 211.1864, found 211.1866 (Δ = 0.9 ppm).

### 3 Test Reactions Allylic Alkylation of Cyclobutenes

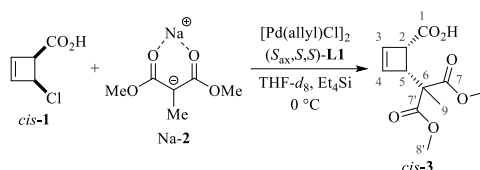
#### General Procedure



Catalytic allylic alkylation reactions with sodium dimethyl methylmalonate Na-2 as nucleophile were performed in an NMR tube sealed with a rubber septum and parafilm®, and monitored by <sup>1</sup>H-NMR. Reaction conditions were adopted from the literature,<sup>22</sup> with the total volume of the reaction mixture being 1.0 mL. To a solution of *cis*- or *trans*-4-chlorocyclobutene-2-enecarboxylic acid **1** (6.6 mg, 50 μmol, 1 equiv.) and Et<sub>4</sub>Si (7.2 mg, 50 μmol, 1 equiv.) in anhydrous THF-*d*<sub>8</sub> (400 μL) was carefully added a solution of nucleophile Na-2 (ca. 95 % purity, 26.5 mg, 150 μmol, 3 equiv.) in anhydrous THF-*d*<sub>8</sub> (400 – 500 μL) at 0 °C. The NMR tube was sealed and loaded into the NMR spectrometer set to 273 K. After wobbling on <sup>1</sup>H and shimming, a single-scan <sup>1</sup>H-NMR spectrum was recorded. The tube was ejected and a solution of [Pd(allyl)Cl]<sub>2</sub> and ligand (*S*<sub>ax</sub>,*S*<sub>ax</sub>,*S*<sub>ax</sub>,*S*<sub>ax</sub>)-L1 or (*R*)-L2 in anhydrous THF-*d*<sub>8</sub> (100 – 200 μL) was added rapidly upon shaking. After shaking vigorously for about 5 s and additionally inverting one time, the sample was loaded into the NMR spectrometer again, and a series of <sup>1</sup>H-NMR spectra was recorded with an interval of 60 s until reaching full conversion of substrate **1**.

The reaction was quenched with NaHCO<sub>3</sub> (12.6 mg, 150 μmol, 3 equiv.) at 0 °C followed by brine (2 mL). The aqueous layer was washed with Et<sub>2</sub>O (3 × 5 mL), carefully acidified with 1 N HCl (pH ≤ 2) and extracted with CH<sub>2</sub>Cl<sub>2</sub> (6 × 5 mL). The combined organic layers were dried over Na<sub>2</sub>SO<sub>4</sub> and concentrated *in vacuo* to give the crude product, which was investigated by NMR spectroscopy and ESI-HRMS. The e.e. was determined by <sup>1</sup>H-NMR after addition of (*S*)-PEA to the NMR sample. If required for complete characterization, a sample of the crude product was purified by flash column chromatography on silica gel (CH<sub>2</sub>Cl<sub>2</sub>:EtOAc 99:1, then CH<sub>2</sub>Cl<sub>2</sub>:EtOH 97:3).

#### (1*S*,4*R*)-4-(1,3-dimethoxy-2-methyl-1,3-dioxopropan-2-yl)cyclobut-2-ene-1-carboxylic acid (*cis*-3) from substrate *cis*-1



The title compound was obtained from *cis*-1 according to the general procedure, using 1.5 mol% [Pd(allyl)Cl]<sub>2</sub> and 6 mol% (*S*<sub>ax</sub>,*S*<sub>ax</sub>,*S*<sub>ax</sub>,*S*<sub>ax</sub>)-L1 (200 μL of a stock solution of 3.75 mM [Pd(allyl)Cl]<sub>2</sub> and 15 mM (*S*<sub>ax</sub>,*S*<sub>ax</sub>,*S*<sub>ax</sub>,*S*<sub>ax</sub>)-L1). A reaction time of 20 min was required to reach quantitative conversion, with an NMR yield of 68 %. Characterization of the crude product obtained after work-up gave a stereoselectivity of d.r. = 90:10 and e.e. = 83 %.

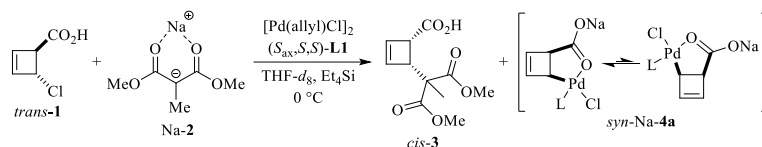
The absolute configuration of products obtained by Pd-catalyzed allylic alkylation of *cis*-1 with malonate nucleophiles and ligand (*R*<sub>ax</sub>,*R*<sub>ax</sub>,*R*<sub>ax</sub>,*R*<sub>ax</sub>)-L1 has been determined in the literature to be (1*R*,4*S*).<sup>22</sup> As we used the enantiomeric ligand (*S*<sub>ax</sub>,*S*<sub>ax</sub>,*S*<sub>ax</sub>,*S*<sub>ax</sub>)-L1, the absolute configuration of *cis*-3 is expected to be (1*S*,4*R*), accordingly.

<sup>1</sup>H-NMR (600 MHz, CDCl<sub>3</sub>, 273 K): δ<sub>H</sub> = 6.22 – 6.20 (1H, m, C(4)*H*), 6.18 – 6.16 (1H, m, C(3)*H*), 3.94 (1H, dt, <sup>3</sup>J<sub>HH</sub> = 4.9, <sup>3</sup>J<sub>HH</sub> ≈ <sup>4</sup>J<sub>HH</sub> ≈ 0.9, C(5)*H*), 3.85 (1H, dt, <sup>3</sup>J<sub>HH</sub> = 4.9, <sup>3</sup>J<sub>HH</sub> ≈ <sup>4</sup>J<sub>HH</sub> ≈ 1.0, C(2)*H*), 3.70 (3H, s, C(8/8')*H*s), 3.70 (3H, s, C(8/8')*H*s), 1.43 (3H, s, C(9)*H*s) ppm; <sup>13</sup>C{<sup>1</sup>H}-NMR (151 MHz, CDCl<sub>3</sub>, 273 K): δ<sub>C</sub> = 175.2 (C(1)), 172.0 (C(7/7')), 171.2 (C(7/7')), 139.2 (C(4)), 134.3 (C(3)), 54.5 (C(6)), 52.8 (C(8/8')), 52.7 (C(8/8')), 51.0 (C(5)), 48.3 (C(2)), 18.0 (C(9)) ppm; HRMS (ESI<sup>+</sup>): C<sub>11</sub>H<sub>14</sub>O<sub>6</sub> [M+H]<sup>+</sup> requires 243.0863, found 243.0863 (Δ = 0.1 ppm). The spectroscopic data are consistent with those reported in the literature.<sup>29</sup>

When performing the reaction in a Schlenk flask equipped with a magnetic stirrer bar rather than in an NMR tube, with dropwise addition of substrate to a solution of malonate Na-2, [Pd(allyl)Cl]<sub>2</sub> and (*S*<sub>ax</sub>,*S*<sub>ax</sub>,*S*<sub>ax</sub>,*S*<sub>ax</sub>)-L1 at 0 °C, the stereoselectivity was only slightly better (d.r. = 92:8, e.e. = 85 %), confirming that stereoselectivities obtained from reactions performed in NMR tubes are representative, despite decreased mass transport<sup>30</sup> compared to stirred reactions.

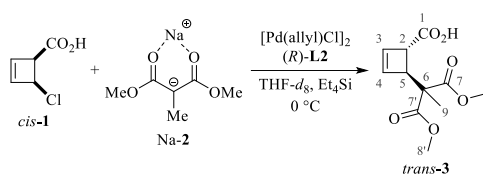
When performing the reaction in MeCN as reported in the literature<sup>22</sup> (Schlenk flask equipped with a magnetic stirrer, dropwise addition of substrate *cis*-1 to a solution of malonate Na-2, [Pd(allyl)Cl]<sub>2</sub> and (*S*<sub>ax</sub>,*S*<sub>ax</sub>,*S*<sub>ax</sub>,*S*<sub>ax</sub>)-L1 at 0 °C), the stereoselectivity was somewhat better (d.r. = 95:5, e.e. = 88 %). However, nucleophile Na-2 was found to slowly decompose in MeCN upon formation of voluminous precipitate, thus complicating reaction monitoring by NMR. Therefore, THF was used for all experiments, despite the slightly decreased stereoselectivity.

**(1*S*,4*R*)-4-(1,3-dimethoxy-2-methyl-1,3-dioxopropan-2-yl)cyclobut-2-ene-1-carboxylic acid (*cis*-3) from substrate *trans*-1**



The title compound was obtained from *trans*-1 according to the general procedure, using 2.5 mol% [Pd(allyl)Cl]<sub>2</sub> (0.5 mg, 1.3 μmol) and 10 mol% (*S,S,S,S*)-L1 (2.7 mg, 5.0 μmol). A reaction time of approximately 6 h was required to reach quantitative conversion, with an NMR yield of 64 %. Furthermore, small amounts of diastereomeric Pd-species *syn*-Na-4a were identified in the reaction mixture (ca. 3 % NMR yield, d.r. = 56:44, spectroscopic data *vide infra*), which were still detectable after 2 days. Characterization of the crude product obtained after work-up gave a stereoselectivity of d.r. = 92:8 and e.e. = 88 %. Comparison of the NMR spectra after addition of (*S*)-PEA showed that the major enantiomer was the same as with substrate *cis*-1. Furthermore, the crude product contained ca. 9 % of unconverted substrate *trans*-1 which was found to be racemic (e.e. ≤ 3 %).

**(1*S*,4*S*)-4-(1,3-dimethoxy-2-methyl-1,3-dioxopropan-2-yl)cyclobut-2-ene-1-carboxylic acid (*trans*-3) from substrate *cis*-1**



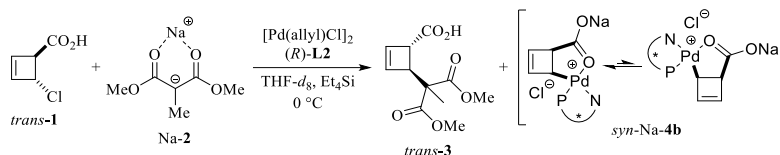
The title compound was obtained from *cis*-1 according to the general procedure, using 2.5 mol% [Pd(allyl)Cl]<sub>2</sub> and 15 mol% (*R*)-L2 (100 μL of a stock solution of 12.5 mM [Pd(allyl)Cl]<sub>2</sub> and 75 mM (*R*)-L2). A reaction time of 90 min was required to reach quantitative conversion, with an NMR yield of 84 %. Characterization of the crude product obtained after work-up gave a stereoselectivity of d.r. = 99:1 and e.e. = 99 %.

The absolute configuration of products obtained by Pd-catalyzed allylic alkylation of *cis*-1 with malonate nucleophiles and ligand (*S*)-L2 has been determined in the literature to be (1*R*,4*R*).<sup>22</sup> As we used the enantiomeric ligand (*R*)-L2, the absolute configuration of *trans*-3 is expected to be (1*S*,4*S*), accordingly.

<sup>1</sup>H-NMR (700 MHz, CDCl<sub>3</sub>, 273 K): δ<sub>H</sub> = 6.19 (1H, br. d, <sup>3</sup>J<sub>HH</sub> = 2.8, C(3)*H*), 6.17 (1H, br. d, <sup>3</sup>J<sub>HH</sub> = 2.8, C(4)*H*), 3.76 (3H, s, C(8/8')*H*<sub>3</sub>), 3.74 (3H, s, C(8/8')*H*<sub>3</sub>), 3.57 (1H, br. s, C(2)*H*), 3.56 (1H, br. s, C(5)*H*), 1.46 (3H, s, C(9)*H*<sub>3</sub>) ppm; <sup>13</sup>C{<sup>1</sup>H}-NMR (176 MHz, CDCl<sub>3</sub>, 273 K): δ<sub>C</sub> = 176.0 (C(1)), 172.4 (C(7/7')), 171.8 (C(7/7')), 138.8 (C(4)), 135.4 (C(3)), 54.8 (C(6)), 53.2 (C(8/8')), 53.1 (C(8/8')), 50.5 (C(5)), 47.4 (C(2)), 17.6 (C(9)) ppm; HRMS (ESI<sup>+</sup>): C<sub>11</sub>H<sub>14</sub>O<sub>6</sub> [M+H]<sup>+</sup> requires 243.0863, found 243.0862 (Δ = -0.5 ppm).

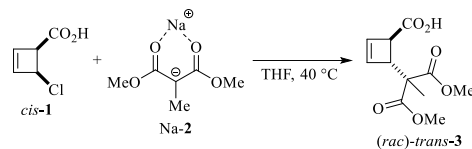
When performing the reaction in a Schlenk flask equipped with a magnetic stirrer bar rather than in an NMR tube, with slow addition of substrate *cis*-1 via a syringe pump to a solution of malonate Na-2, [Pd(allyl)Cl]<sub>2</sub> and (*R*)-L2 at 40 °C as described in the literature,<sup>22</sup> the stereoselectivity achieved was equally high (d.r. = 99:1, e.e. = 99 %), confirming that stereoselectivities obtained from reactions performed in NMR tubes are representative, despite decreased mass transport<sup>30</sup> compared to stirred reactions. This comparison furthermore showcases that it is not necessary to heat the reaction to 40 °C to reach full conversion.

**(1*S*,4*S*)-4-(1,3-dimethoxy-2-methyl-1,3-dioxopropan-2-yl)cyclobut-2-ene-1-carboxylic acid (*trans*-3) from substrate *trans*-1**



The title compound was obtained from *trans*-1 according to the general procedure, using 15 mol% [Pd(allyl)Cl]<sub>2</sub> (2.7 mg, 7.5 μmol) and 60 mol% (*R*)-L2 (12.2 mg, 30 μmol). A reaction time of approximately 30 min was required to reach quantitative conversion, with an NMR yield of 57 %. Furthermore, diastereomeric Pd-species *syn*-Na-4b were identified in the reaction mixture (26 % NMR yield, d.r. = 52:48, spectroscopic data *vide infra*), which were still detectable after 2 days. Characterization of the crude product obtained after work-up gave a stereoselectivity of d.r. = 99:1 and e.e. = 88 %. Comparison of the NMR spectra after addition of (*S*)-PEA showed that the major enantiomer was the same as with substrate *cis*-1.

**Background Reactivity:** (*rac*)-*Trans*-4-(1,3-dimethoxy-2-methyl-1,3-dioxopropan-2-yl)cyclobut-2-ene-1-carboxylic acid (*trans*-**3**) from substrate *cis*-**1**



To a solution of nucleophile **Na-2** (ca. 95 w% purity, 60.0 mg, 339  $\mu\text{mol}$ , 3 equiv.) in anhydrous THF (1 mL) was added dropwise a solution of *cis*-4-chlorocyclobutene-2-enecarboxylic acid *cis*-**1** (15.0 mg, 113  $\mu\text{mol}$ , 1 equiv.) in anhydrous THF (1 mL) at 0 °C. The temperature was gradually increased to 40 °C and the reaction mixture was stirred at this temperature for 17 h. As no product formation could be detected by TLC analysis, a second portion of dimethyl methylmalonate (ca. 95 w% purity, 60.0 mg, 339  $\mu\text{mol}$ , 3 equiv.) was added and stirring was continued for further 29 h.

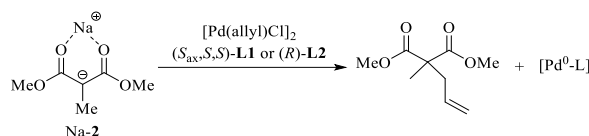
The reaction was quenched with  $\text{NaHCO}_3$  (57.0 mg, 678  $\mu\text{mol}$ , 6 equiv.) at 0 °C followed by brine (4 mL). The aqueous layer was washed with  $\text{Et}_2\text{O}$  ( $3 \times 7$  mL), carefully acidified with 1 N HCl ( $\text{pH} \leq 2$ ) and extracted with  $\text{CH}_2\text{Cl}_2$  ( $6 \times 7$  mL). The combined organic layers were dried over  $\text{Na}_2\text{SO}_4$  and concentrated *in vacuo* to give the crude product, which was investigated by NMR spectroscopy and ESI-HRMS.

The obtained crude product was found to be an approximately 4:1 mixture of substrate *cis*-**1** and product (*rac*)-*trans*-**3** (d.r.  $\approx$  96:4) along with various decomposition products. The same procedure performed at 0 °C did not give any detectable amount of product **3**.

#### Influence of Pd-Loading on Stereoselectivity

The influence of Pd-loading was investigated by performing the general procedure at five different Pd-ligand concentrations each. With ligand **L1**, 20 – 200  $\mu\text{L}$  of a stock solution of 3.75 mM  $[\text{Pd}(\text{allyl})\text{Cl}]_2$  and 15 mM ( $S_{\text{ax}},S,S$ )-**L1** were used, corresponding to 0.3 – 3.0 mol% Pd. With ligand **L2**, 20 – 200  $\mu\text{L}$  of a stock solution of 12.5 mM  $[\text{Pd}(\text{allyl})\text{Cl}]_2$  and 75 mM (*R*)-**L2** were used, corresponding to 1.0 – 10 mol% Pd.

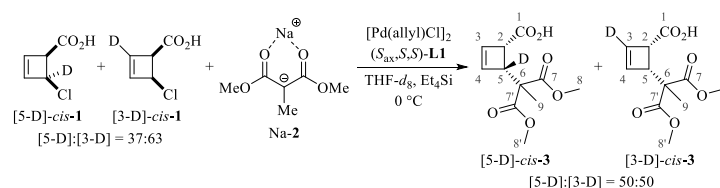
For quantifying the precise amount of active  $\text{Pd}^0$ , the stoichiometry of  $\text{Pd}^0$  generation from the  $\text{Pd}^{\text{II}}$  source  $[\text{Pd}(\text{allyl})\text{Cl}]_2$  was employed (Scheme S4). Accordingly, 1 equiv. (relative to generated  $\text{Pd}^0$ ) of the initiation by-product dimethyl 2-allyl-2-methylmalonate is formed, which can readily be quantified by  $^1\text{H-NMR}$  analysis of the reaction mixture after initiation. The resonance  $\delta_{\text{H}} = 2.55$  (2H, d,  $^3J_{\text{HH}} = 7.4$ ,  $-\text{CH}_2$ )<sup>31</sup> proved to be most suitable for integration, allowing for accurate determination of the Pd-loading.



**Scheme S4.** Generation of active  $\text{Pd}^0$  by nucleophilic attack of the malonate nucleophile on  $[\text{Pd}(\text{allyl})\text{Cl}]_2$ , forming the allylated nucleophile as by-product.

At the lowest Pd-loading, the reaction stalled at incomplete conversion with both ligand **L1** (ca. 84 %) and **L2** (ca. 38 %). In both cases, unconverted substrate *cis*-**1** was found to be racemic (e.e.  $\leq 3$  %).

#### Reaction with Deuterated Substrate ([5-D]/[3-D]-**1** and Ligand **L1**)



Labeled substrate [5-D]/[3-D]-*cis*-**1** ([5-D]:[3-D] = 37:63, overall 94 %D, preparation see section 2) was subjected to the general procedure, using 1.5 mol%  $[\text{Pd}(\text{allyl})\text{Cl}]_2$  and 6 mol% ( $S_{\text{ax}},S,S$ )-**L1** (200  $\mu\text{L}$  of a stock solution of 3.75 mM  $[\text{Pd}(\text{allyl})\text{Cl}]_2$  and 15 mM ( $S_{\text{ax}},S,S$ )-**L1**). Quantitative conversion was reached after 2 h. After work-up, the product was obtained as a 50:50 mixture of isotopomers [5-D]- and [3-D]-*cis*-**3**, as determined by  $^1\text{H-NMR}$  and confirmed by  $^2\text{H-NMR}$  (overall 94 %D, d.r. = 94:6, yield and e.e. n.d.). The absolute configuration of [5-D]/[3-D]-*cis*-**3** is assumed to be identical to the absolute configuration of the product obtained by the same reaction performed with unlabeled *cis*-**1**, i.e. (1*S*,4*R*) (vide supra).

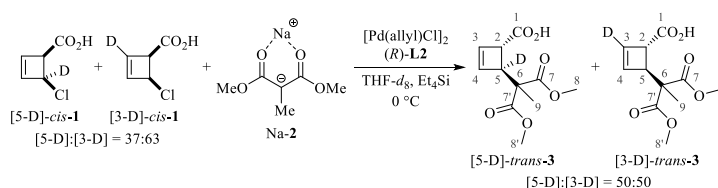
$^1\text{H-NMR}$  (700 MHz,  $\text{CDCl}_3$ , 273 K):  $\delta_{\text{H}} = 6.23 - 6.20$  (1H, m, C(4)*H*), 6.18 (0.53H, dd,  $^3J_{\text{HH}} = 2.8$ ,  $^3J_{\text{HH}} = 1.1$ , residual C(3)*H*), 3.95 (0.53H, dd,  $^3J_{\text{HH}} = 4.9$ ,  $^3J_{\text{HH}} = 1.0$ , residual C(5)*H*), 3.88 – 3.86 (1H, m, C(2)*H*), 3.73 (3H, s, C(8/8')*H*s), 3.72 (3H, s, C(8/8')*H*s), 1.45 (3H, br. s, C(9)*H*s) ppm;  $^2\text{H-NMR}$  (108 MHz,  $\text{CHCl}_3$ , 273 K):  $\delta_{\text{D}} = 6.24$  (1D, br. s, C(3)*D*), 3.95 (1D, br. s, C(5)*D*) ppm;  $^{13}\text{C}\{^1\text{H}\}\text{-NMR}$  (176 MHz,  $\text{CDCl}_3$ , 273 K):  $\delta_{\text{C}} = 177.0$  (C(1)), 172.1 (C(7/7')), 171.2 (C(7/7')), 139.1 (C(4)), 139.0 (C(4)), 134.4 (C(3)*H*), 54.3 (C(6)), 54.2 (C(6)), 53.0 (C(8/8')), 52.8 (C(8/8')),



50.8 (C(2)), 48.1 (C(5)H), 17.9 (C(9)), 17.9 (C(9)) ppm; C<sub>11</sub>H<sub>13</sub>DO<sub>6</sub> [M+H]<sup>+</sup> requires 244.0926, found 244.0924 ( $\Delta = -1.0$  ppm). The spectroscopic data are consistent with those reported for the unlabeled isotopologue. Due to limited sensitivity, the split <sup>13</sup>C-resonances of deuterated carbons were not detected.

The quantitative deuterium scrambling across the allylic termini, albeit not a highly significant result, indicates that no stereochemical memory effect is operative under these conditions, as this would lead to a (partial) conservation of the 37:63 ratio of substrate isotopomers. Consistent observations have been reported in the literature for a closely related allylic alkylation system with a cyclobutene substrate selectively deuterated at one of the allylic termini, giving a fully scrambled substitution product as well.<sup>29</sup>

#### Reaction with Deuterated Substrate ([5-D]/[3-D]-1 and Ligand L2



Labeled substrate [5-D]/[3-D]-*cis*-1 ([5-D]:[3-D] = 37:63, overall 94 %D, preparation see section 2) was subjected to the general procedure, using 2.5 mol% [Pd(allyl)Cl]<sub>2</sub> and 15 mol% (R)-L2 (100  $\mu$ L of a stock solution of 12.5 mM [Pd(allyl)Cl]<sub>2</sub> and 75 mM (R)-L2). Quantitative conversion was reached after 5 h. After work-up, the product was obtained as a 50:50 mixture of isotopomers [5-D]- and [3-D]-*trans*-3, as determined by <sup>1</sup>H-NMR and confirmed by <sup>2</sup>H-NMR (overall 94 %D, d.r. > 98:2, yield and e.e. n.d.). The absolute configuration of [5-D]/[3-D]-*trans*-3 is assumed to be identical to the absolute configuration of the product obtained by the same reaction performed with unlabeled *cis*-1, i.e. (1*R*,4*R*) (vide supra).

**<sup>1</sup>H-NMR** (700 MHz, CDCl<sub>3</sub>, 273 K):  $\delta_{\text{H}}$  = 6.22 (0.53H, dd, <sup>3</sup>*J*<sub>HH} = 2.9, <sup>3</sup>*J*<sub>HH} = 1.0, residual C(3)*H*), 6.14 – 6.13 (1H, m, C(4)*H*), 3.77 (3H, s, C(8/8')*H*<sub>3</sub>), 3.75 (3H, s, C(8/8')*H*<sub>3</sub>), 3.61 – 3.58 (1H, m, C(2)*H*), 3.55 – 3.53 (0.53H, m, residual C(5)*H*), 1.47 (3H, br. s, C(9)*H*<sub>3</sub>) ppm; **<sup>2</sup>H-NMR** (108 MHz, CHCl<sub>3</sub>, 273 K):  $\delta_{\text{D}}$  = 6.22 (1D, br. s, C(3)*D*), 3.59 (1D, br. s, C(5)*D*) ppm; **<sup>13</sup>C{<sup>1</sup>H}-NMR** (176 MHz, CDCl<sub>3</sub>, 273 K):  $\delta_{\text{C}}$  = 177.0 (C(1)), 172.2 (C(7/7')), 171.8 (C(7/7')), 139.2 (C(4)), 139.1 (C(4)), 135.3 (C(3)*H*), 135.0 (1:1:1 t, <sup>1</sup>*J* = 26.9, C(3)*D*), 54.8 (C(6)), 54.7 (C(6)), 53.1 (C(8/8')), 53.1 (C(8/8')), 50.5 (C(5)*H*), 50.2 (1:1:1 t, <sup>1</sup>*J* = 22.1, C(5)*D*), 47.3 (C(2)), 17.6 (C(9)), 17.5 (C(9)) ppm; **HRMS** (ESI<sup>+</sup>): C<sub>11</sub>H<sub>13</sub>DO<sub>6</sub> [M+H]<sup>+</sup> requires 244.0926, found 244.0924 ( $\Delta = -0.7$  ppm). The spectroscopic data are consistent with those reported for the unlabeled isotopologue.</sub></sub>

The quantitative deuterium scrambling across the allylic termini, albeit not a highly significant result, indicates that no stereochemical memory effect is operative under these conditions, as this would lead to a (partial) conservation of the 37:63 ratio of substrate isotopomers. Consistent observations have been reported in the literature for a closely related allylic alkylation system with a cyclobutene substrate selectively deuterated at one of the allylic termini, giving a fully scrambled substitution product as well.<sup>29</sup>

## 4 Preparation and Investigation of Pd-Cyclobutene Complexes

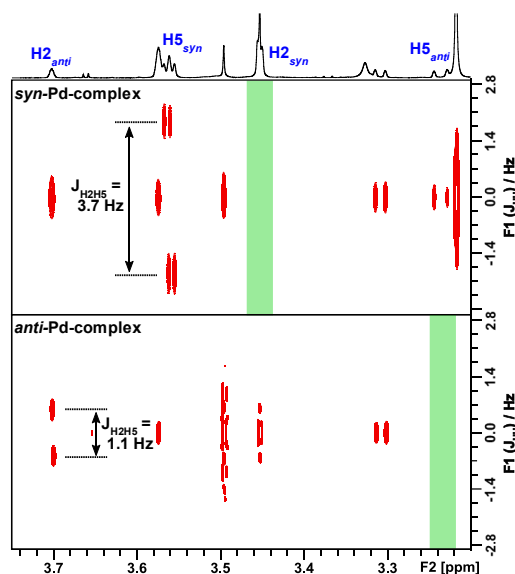


All Pd-cyclobutene complexes were prepared under inert atmosphere (glove box) and then directly analyzed by NMR spectroscopy at 273 K. The connectivity was determined by <sup>1</sup>H, <sup>13</sup>C and <sup>31</sup>P-NMR and suitable correlation experiments such as <sup>1</sup>H-<sup>1</sup>H-CLIP-COSY, <sup>1</sup>H-<sup>13</sup>C-HSQC, <sup>1</sup>H-<sup>13</sup>C-HMBC, <sup>1</sup>H-<sup>31</sup>P-HMBC and <sup>1</sup>H-<sup>15</sup>N-HMBC. Consistent with previous studies,<sup>32,33</sup> all oxidative addition products were found to be  $\eta^1$ - rather than  $\eta^3$ -allyl complexes, as indicated by the <sup>13</sup>C-chemical shift of C3 and C4 being consistent with a localized double bond.

The relative position of phosphorous ligands in the Pd-coordination sphere was established by means of experimental <sup>2</sup>*J*<sub>PP}, <sup>2</sup>*J*<sub>CP} and <sup>3</sup>*J*<sub>HP} coupling constants.<sup>34–36</sup> From the <sup>2</sup>*J*<sub>PP} coupling constants, the ligands were concluded to be in *cis*- (<sup>2</sup>*J*<sub>PP}  $\approx$  80 – 120 Hz) or *trans*-position (<sup>2</sup>*J*<sub>PP}  $\approx$  1100 – 1200 Hz) relative to each other.<sup>34</sup> Coupling constants between C(5) or C(5)*H* in the cyclobutene unit and the ligand's phosphorous site were indicative for a *cis*- (<sup>2</sup>*J*<sub>CP}  $\approx$  20 Hz, <sup>3</sup>*J*<sub>HP} < 12 Hz) or *trans*-relationship (<sup>2</sup>*J*<sub>CP}  $\approx$  130 – 170 Hz, <sup>3</sup>*J*<sub>HP}  $\approx$  8 – 18 Hz) across the Pd-center.<sup>35,36</sup></sub></sub></sub></sub></sub></sub></sub></sub></sub></sub>

The relative configuration at the cyclobutene ring was established by intramolecular distances *r*<sub>H2-H5} extracted from NOE/ROE mixing time series and – if ambiguous – confirmed by <sup>3</sup>*J*<sub>H2-H5} couplings extracted from PSYCHEDELIC experiments. A distance of *r*<sub>H2-H5} = 3.0 – 3.1 Å and a coupling constant of <sup>3</sup>*J*<sub>H2-H5} < 2 Hz are indicative for an *anti*-configuration, whereas a distance of *r*<sub>H2-H5} = 2.5 – 2.6 Å and a coupling constant of <sup>3</sup>*J*<sub>H2-H5} = 2 – 5 Hz correspond to a *syn*-configuration.<sup>32,33,37,38</sup> The extraction of <sup>3</sup>*J*<sub>H2-H5} coupling constants by PSYCHEDELIC experiments is demonstrated in Figure S1.</sub></sub></sub></sub></sub></sub></sub>





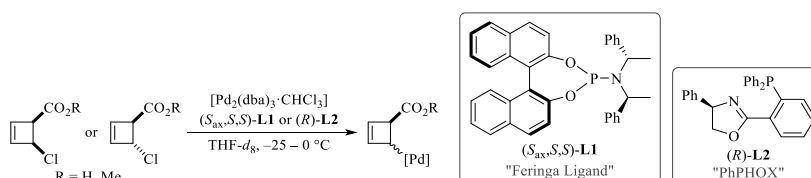
**Figure S1.** Example for the extraction of  $^3J_{\text{H2-H5}}$  coupling constants by PSYCHEDELIC experiments. The spectra were recorded on a mixture of complexes *syn*-**6b** and *anti*-**6b** (700 MHz, THF-*d*<sub>8</sub>, 253 K, *vide infra*), with the selectively excited spectral region marked in green.

Most of the *syn*-configured species were found to be stabilized by internal Pd–O chelation exerted by the cyclobutene unit, as indicated by a significant  $^{13}\text{C}$ -chemical deshielding of the cyclobutene's carboxy carbon C(1).<sup>33</sup> The proposed structures were confirmed by ESI-HRMS in positive and negative ion mode and by  $^1\text{H}$ -DOSY experiments, which also did not deliver any evidence for aggregation or oligomerization. Furthermore, for all Pd-complexes computational geometry optimization and frequency calculation was performed (cf. section 10).

For better clarity, the  $^1\text{H}$ - and  $^{13}\text{C}$ -NMR resonances are assigned to the respective Pd-species (major or minor), followed by the part of the molecule (CB = cyclobutene, L = **L1** or **L2**) and the atom number within the fragment. The most characteristic NMR spectroscopic data are further summarized in tabular form for each Pd-species prepared.

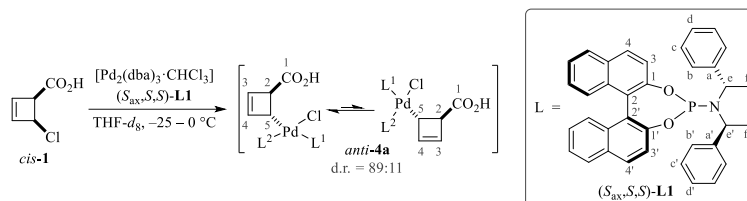
## Oxidative Addition of Acid and Ester Substrates

### General Procedure



$[\text{Pd}_2(\text{dba})_3 \cdot \text{CHCl}_3]$  (25.9 mg, 25  $\mu\text{mol}$ , 0.5 equiv.) and ligand ( $S_{\text{axx}},S_{\text{axx}}$ )-**L1** (54.0 mg, 100  $\mu\text{mol}$ , 2 equiv.) or (*R*)-**L2** (20.4 mg, 50  $\mu\text{mol}$ , 1 equiv.) were dissolved in anhydrous THF-*d*<sub>8</sub> (0.5 mL) and stirred at RT for 10 min. The solution was cooled to approximately  $-25\text{ }^\circ\text{C}$  and a solution of the cyclobutene substrate (50  $\mu\text{mol}$ , 1 equiv.) in anhydrous THF-*d*<sub>8</sub> (0.3 mL) was added dropwise upon stirring vigorously. After further 5 min of stirring, one drop of the reaction mixture was taken for subsequent MS analysis, and the residual solution was transferred into a precooled NMR tube. The tube was sealed and centrifuged (2000 rpm, 1 min) prior to NMR analysis.

## Oxidative Addition of Acid Substrate *cis*-1 with Ligand L1



Oxidative addition of *cis*-4-chlorocyclobutene-2-encarboxylic acid *cis*-1 with phosphoramidite ligand (*S*<sub>ax</sub>,*S*,*S*)-L1 according to the general procedure gave a diastereomeric mixture of Pd-complexes *anti*-4a. From the magnitude of the experimental <sup>2</sup>J<sub>PP</sub>, <sup>2</sup>J<sub>CP</sub> and <sup>3</sup>J<sub>HP</sub> coupling constants, the two ligands can be concluded to be in *cis*- and *trans*-position relative to the cyclobutene ring, respectively.<sup>34–36</sup> The relative configuration of the cyclobutene ring was derived from quantitative NOE data. Although the 2D EASY-ROESY and NOESY spectra do not exhibit exchange cross-peaks, complexes *anti*-4a are very likely to be in equilibrium, as the d.r. was found to be time-dependent (d.r. = 50:50 → 89:11 over ca. 17 min, see section 5).

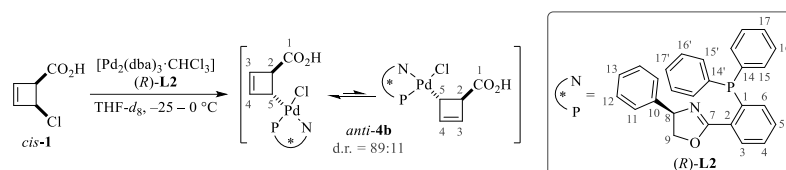
**<sup>1</sup>H-NMR** (700 MHz, THF-*d*<sub>8</sub>, 273 K): δ<sub>H</sub> = 10.9 (1.12H, br. s, major + minor CB C(1)O<sub>2</sub>H), 8.75 (0.12H, d, <sup>3</sup>J<sub>HH</sub> = 8.9, minor L<sup>1</sup> C(3)*H*), 8.59 (1H, d, <sup>3</sup>J<sub>HH</sub> = 8.9, major L<sup>1</sup> C(3)*H*), 8.29 (1H, d, <sup>3</sup>J<sub>HH</sub> = 8.9, major L<sup>2</sup> C(4')*H*), 8.24 (0.12H, d, <sup>3</sup>J<sub>HH</sub> = 8.9, minor L<sup>2</sup> C(4')*H*), 8.11 (1H, d, <sup>3</sup>J<sub>HH</sub> = 8.9, major L<sup>1</sup> C(4')*H*), 7.93 (1H, d, <sup>3</sup>J<sub>HH</sub> = 8.9, major L<sup>2</sup> C(4)*H*), 7.86 (1H, d, <sup>3</sup>J<sub>HH</sub> = 8.9, major L<sup>2</sup> C(3')*H*), 7.84 (1H, d, <sup>3</sup>J<sub>HH</sub> = 8.9, major L<sup>1</sup> C(4)*H*), 7.79 (0.12H, d, <sup>3</sup>J<sub>HH</sub> = 8.9, minor L<sup>2</sup> C(3')*H*), 7.70 (0.12H, d, <sup>3</sup>J<sub>HH</sub> = 8.9, minor L<sup>1</sup> C(4)*H*), 7.64 (1H, d, <sup>3</sup>J<sub>HH</sub> = 8.9, major L<sup>1</sup> C(3')*H*), 7.22 (1H, d, <sup>3</sup>J<sub>HH</sub> = 8.9, major L<sup>2</sup> C(3)*H*), 6.86–6.83 (6H, m, major L<sup>1</sup> C(b)*H*, C(b')*H*, C(d)*H*, C(d')*H*), 6.73 (4H, dd, <sup>3</sup>J<sub>HH</sub> = 8.3, <sup>3</sup>J<sub>HH</sub> = 7.4, major L<sup>1</sup> C(c)*H*, C(c')*H*), 6.08 (0.12H, br. s, minor CB C(3)*H*), 5.96 (0.12H, br. s, minor CB C(4)*H*), 5.58–5.56 (1H, m, major CB C(3)*H*), 4.90 (1H, br. s, major CB C(4)*H*), 4.70 (0.24H, dq, <sup>3</sup>J<sub>HP</sub> = 10.2, <sup>3</sup>J<sub>HH</sub> = 7.0, minor L<sup>1</sup> C(e)*H*, C(e')*H*), 4.66 (2H, dq, <sup>3</sup>J<sub>HP</sub> = 11.6, <sup>3</sup>J<sub>HH</sub> = 7.1, major L<sup>1</sup> C(e)*H*, C(e')*H*), 4.45 (0.12H, d, <sup>4</sup>J<sub>HP</sub> = 3.8, minor CB C(2)*H*), 4.26 (1H, d, <sup>4</sup>J<sub>HP</sub> = 4.6, major CB C(2)*H*), 4.23 (0.12H, dd, <sup>3</sup>J<sub>HP</sub> = 16.6, <sup>3</sup>J<sub>HP</sub> = 7.8, minor CB C(5)*H*), 4.08 (1H, d, <sup>3</sup>J<sub>HP</sub> = 10.5, major CB C(5)*H*), 0.84 (0.72H, d, <sup>3</sup>J<sub>HH</sub> = 7.0, minor L<sup>1</sup> C(f)*H*<sub>3</sub>, C(f')*H*<sub>3</sub>), 0.80 (6H, d, <sup>3</sup>J<sub>HH</sub> = 7.1, major L<sup>1</sup> C(f)*H*<sub>3</sub>, C(f')*H*<sub>3</sub>) ppm; **<sup>13</sup>C{<sup>1</sup>H}-NMR** (176 MHz, THF-*d*<sub>8</sub>, 273 K): δ<sub>C</sub> = 175.4 (major CB C(1)), 174.0 (minor CB C(1)), 150.9 (d, <sup>2</sup>J<sub>CP</sub> = 14.8, major L<sup>1</sup> C(1')), 150.4 (major L<sup>2</sup> C(1')), 150.0 (d, <sup>2</sup>J<sub>CP</sub> = 3.0, minor L<sup>1</sup> C(1)), 149.7 (d, <sup>2</sup>J<sub>CP</sub> = 2.7, major L<sup>1</sup> C(1)), 149.1 (minor CB C(4)), 148.3 (major CB C(4)), 148.1 (major L<sup>2</sup> C(1)), 142.4 (d, <sup>3</sup>J<sub>CP</sub> = 4.6, minor L<sup>1</sup> C(a), C(a')), 142.2 (d, <sup>3</sup>J<sub>CP</sub> = 4.0, major L<sup>1</sup> C(a), C(a')), 132.3 (major L<sup>2</sup> C(4)), 132.2 (major L<sup>1</sup> C(4)), 132.0 (minor L<sup>1</sup> C(4)), 131.8 (major L<sup>2</sup> C(4')), 131.5 (major CB C(3)), 131.4 (major L<sup>1</sup> C(4')), 131.0 (minor L<sup>2</sup> C(4')), 130.5 (minor L<sup>2</sup> C(3')), 130.3 (minor CB C(3)), 129.5 (major L<sup>1</sup> C(b), C(b')), 127.8 (major L<sup>1</sup> C(c), C(c')), 127.2 (major L<sup>1</sup> C(d), C(d')), 124.9 (minor L<sup>1</sup> C(3)), 124.7 (major L<sup>1</sup> C(3)), 122.6 (major L<sup>1</sup> + L<sup>2</sup> C(3')), 122.1 (major L<sup>2</sup> C(3)), 56.6 (d, <sup>3</sup>J<sub>CP</sub> = 8.8, major CB C(2)), 56.2 (d, <sup>2</sup>J<sub>CP</sub> ≈ 11, minor L<sup>1</sup> C(e), C(e')), 56.1 (d, <sup>2</sup>J<sub>CP</sub> = 10.2, major L<sup>1</sup> C(e), C(e')), 55.8 (br. s, minor CB C(2)), 50.6 (dd, <sup>2</sup>J<sub>CP</sub> = 151.7, <sup>2</sup>J<sub>CP</sub> = 11.2, major CB C(5)), 49.2 (d, <sup>2</sup>J<sub>CP</sub> ≈ 153, minor CB C(5)), 21.4 (br. s, major L<sup>1</sup> C(f), C(f')), 21.3 (br. s, minor L<sup>1</sup> C(f), C(f')) ppm; **<sup>31</sup>P{<sup>1</sup>H}-NMR** (283 MHz, THF-*d*<sub>8</sub>, 273 K): δ<sub>P</sub> = 146.8 (0.12P, d, <sup>2</sup>J<sub>PP</sub> = 92.0, minor L<sup>1</sup>), 144.0 (1P, d, <sup>2</sup>J<sub>PP</sub> = 109.4, major L<sup>1</sup>), 139.7 (1P, d, <sup>2</sup>J<sub>PP</sub> = 109.4, major L<sup>2</sup>), 139.3 (0.12P, d, <sup>2</sup>J<sub>PP</sub> = 92.0, minor L<sup>2</sup>) ppm; **ID NOE** (700 MHz, THF-*d*<sub>8</sub>, 273 K): *r*<sub>HH</sub> = 3.01 ± 0.05 (major CB H2-H5), 2.94 ± 0.05 (major CB H3-H4), 2.79 ± 0.08 (major CB H2-H3), 2.83 ± 0.05 (major CB H4-H5), 4.1 ± 0.2 (major CB H2-H4), 3.85 ± 0.05 (major CB H3-H5), 2.486 (major L<sup>1</sup> H3-H4, reference<sup>32</sup>), 3.06 ± 0.09 (minor CB H2-H5), 2.865 (minor CB H3-H4, reference<sup>32</sup>), 2.85 ± 0.07 (minor CB H2-H3), 2.84 ± 0.05 (minor CB H4-H5), 3.81 ± 0.08 (minor CB H2-H4) Å; **DOSY** (700 MHz, THF-*d*<sub>8</sub>, 273 K): *D* = (4.97 ± 0.02) · 10<sup>-10</sup> (major), (4.96 ± 0.03) · 10<sup>-10</sup> (minor) m<sup>2</sup> s<sup>-1</sup>; **HRMS** (ESI<sup>+</sup>): C<sub>77</sub>H<sub>65</sub>N<sub>2</sub>O<sub>6</sub>P<sub>2</sub>Pd [M-Cl]<sup>+</sup> requires 1281.3347, found 1281.3376 (Δ = 2.2 ppm), C<sub>41</sub>H<sub>35</sub>NO<sub>4</sub>PPd [M-L-Cl]<sup>+</sup> requires 742.1333, found 742.1346 (Δ = 1.7 ppm). Due to signal overlap and the presence of excess dba, not all signals in the aromatic region could be assigned. The most characteristic NMR spectroscopic data are summarized in Table S1.

**Table S1.** Characteristic NMR data for complexes major- (top) and minor- (bottom) *anti*-4a.

Position	δ <sub>H</sub> / ppm	δ <sub>C</sub> or δ <sub>P</sub> / ppm	Additional data
CB 1	–	175.4	
CB 2	4.25	56.6	<i>r</i> <sub>H2-H5</sub> = (3.01 ± 0.05) Å
CB 3	5.56	131.5	
CB 4	4.90	148.3	
CB 5	4.07	50.6	<sup>3</sup> J <sub>HP</sub> = 16.6, 7.8 Hz <sup>2</sup> J <sub>CP</sub> = 151.7, 11.2 Hz
L <sub>1</sub> P	–	144.0	
L <sub>2</sub> P	–	139.7	<sup>2</sup> J <sub>PP</sub> = 109.4 Hz
CB 1	–	174.0	

CB 2	4.45	55.8	$r_{H2-H5} = (3.06 \pm 0.09) \text{ \AA}$
CB 3	6.07	130.3	
CB 4	5.95	149.1	
CB 5	4.23	49.2	$^3J_{HP} = 10.5 \text{ Hz}$ $^2J_{CP} \approx 153 \text{ Hz}$
L <sub>1</sub> P	–	146.8	
L <sub>2</sub> P	–	139.3	$^2J_{PP} = 92.0 \text{ Hz}$

### Oxidative Addition of Acid Substrate *cis*-1 with Ligand L2



Oxidative addition of *cis*-4-chlorocyclobutene-2-enecarboxylic acid *cis*-1 with PHOX ligand (*R*)-L2 according to the general procedure gave a diastereomeric mixture of Pd-complexes *anti*-4b. From the magnitude of the experimental  $^2J_{CP}$  and  $^3J_{HP}$  coupling constants, the phosphine site can be concluded to be in *cis*-position relative to the cyclobutene ring.<sup>34-36</sup> The relative configuration of the cyclobutene ring was derived from quantitative ROE data and confirmed by  $^3J_{H2-H5}$  coupling constants extracted from PSYCHEDELIC experiments. The 2D EASY-ROESY and NOESY spectra exhibit exchange cross-peaks between the two Pd-species, and the d.r. was found to be time-dependent (d.r. = 50:50  $\rightarrow$  89:11 over ca. 4 min, see section 5), clearly indicating that complexes *anti*-4b are in equilibrium. Upon standing at 0 °C, slow irreversible ring-opening to the corresponding diene (*E,E*)-7<sup>32</sup> was observed.

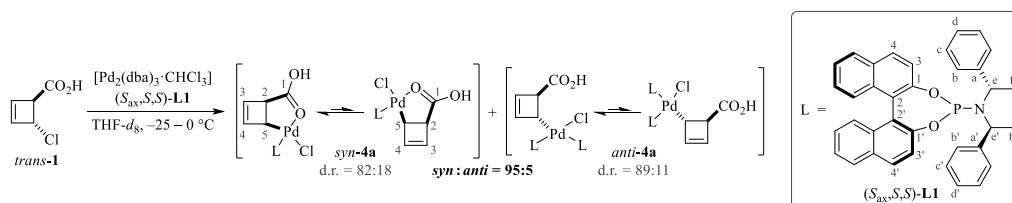
**<sup>1</sup>H-NMR** (700 MHz, THF-*d*<sub>8</sub>, 273 K):  $\delta_1 = 10.65$  (1.12H, br. s, major + minor CB C(1)O<sub>2</sub>H), 8.16 (1.12H, dd,  $^3J_{HH} = 7.8$ ,  $^4J_{HH} = 3.9$ , major + minor L C(3)H), 7.71 – 7.69 (1H, m, major L C(4)H), 7.60 – 7.57 (1H, m, major L C(5)H), 7.56 – 7.54 (1H, m, major L C(17)H), 7.54 – 7.52 (1H, m, major L C(17')H), 7.46 – 7.43 (2H, m, major L C(16')H), 7.36 – 7.33 (2H, m, major L C(16)H), 7.28 – 7.26 (2H, m, major L C(15')H), 7.25 – 7.22 (1H, m, major L C(13)H), 7.21 – 7.19 (2H, m, major L C(15)H), 7.13 – 7.10 (2H, m, major L C(12)H), 7.09 – 7.05 (2.24H, m, major + minor L C(11)H), 6.96 (1H, dd,  $^3J_{HP} = 10.3$ ,  $^3J_{HH} = 8.1$ , major L C(6)H), 6.54 – 6.50 (0.12H, m, minor L C(8)H), 6.24 (1H, dd,  $^3J_{HH} = 10.4$ ,  $^3J_{HH} = 5.5$ , major L C(8)H), 6.11 (0.12H, br. s, minor CB C(4)H), 5.58 (1H, d,  $^3J_{HH} = 2.5$ , major CB C(3)H), 5.49 (0.12H, d,  $^3J_{HH} = 1.6$ , minor CB C(3)H), 5.07 (1H, br. s, major CB C(4)H), 4.82 (1H, dd,  $^3J_{HH} = 10.4$ ,  $^2J_{HH} = 9.2$ , major L C(9)HH<sub>trans</sub>), 4.73 (0.12H, dd,  $^3J_{HH} = 10.0$ ,  $^2J_{HH} = 9.1$ , minor L C(9)HH<sub>trans</sub>), 4.52 (0.12H, dd,  $^2J_{HH} = 9.1$ ,  $^3J_{HH} = 4.6$ , minor L C(9)HH<sub>cis</sub>), 4.50 (1H, dd,  $^2J_{HH} = 9.2$ ,  $^3J_{HH} = 5.5$ , major L C(9)HH<sub>cis</sub>), 4.11 (1H, br. s, major CB C(2)H), 3.81 (0.12H, br. s, minor CB C(2)H), 3.37 (0.12H, d,  $^3J_{HP} = 10.0$ , minor CB C(5)H), 3.28 (1H, br. s, major CB C(5)H) ppm; **<sup>13</sup>C{<sup>1</sup>H}-NMR** (176 MHz, THF-*d*<sub>8</sub>, 273 K):  $\delta_c = 173.9$  (minor CB C(1)), 172.0 (major CB C(1)), 162.9 (d,  $^3J_{CP} = 3.3$ , major L C(7)), 162.4 (d,  $^3J_{CP} = 3.1$ , minor L C(7)), 148.9 (minor CB C(4)), 147.5 (d,  $^3J_{CP} = 6.4$ , major CB C(4)), 141.7 (minor L C(10)), 141.3 (major L C(10)), 135.2 (d,  $^2J_{CP} = 2.4$ , major L C(6)), 135.0 (br. s, major L C(15)), 133.9 (d,  $^2J_{CP} = 11.7$ , major L C(15')), 133.4 (d,  $^3J_{CP} = 2.0$ , major L C(5)), 132.6 (d,  $^3J_{CP} = 7.5$ , major + minor L C(3)), 132.1 (d,  $^4J_{CP} = 1.9$ , major L C(4), C(17)), 132.0 (d,  $^4J_{CP} = 4.3$ , major L C(17')), 131.3 (d,  $^1J_{CP} = 43.1$ , major L C(1)), 129.8 (d,  $^3J_{CP} = 5.5$ , major L C(16)), 129.8 (major L C(16')), 129.5 (d,  $^1J_{CP} = 59.4$ , major L C(14)), 129.2 (br. s, major L C(12)), 129.1 (minor L C(11)), 128.7 (br. s, major CB C(3)), 128.3 (major L C(13)), 128.1 (major L C(11)), 127.0 (d,  $^4J_{CP} = 4.3$ , minor CB C(3)), 75.5 (major L C(9)), 75.1 (minor L C(9)), 69.0 (major L C(8)), 68.5 (minor L C(8)), 55.9 (br. s, minor CB C(2)), 55.4 (d,  $^3J_{CP} = 2.1$ , major CB C(2)), 45.7 (d,  $^2J_{CP} = 4.3$ , major CB C(5)), 43.3 (br. s, minor CB C(5)) ppm; **<sup>15</sup>N-NMR** (71 MHz, THF-*d*<sub>8</sub>, 273 K):  $\delta_N = 195.8$  (minor), 194.1 (major) ppm; **<sup>31</sup>P{<sup>1</sup>H}-NMR** (283 MHz, THF-*d*<sub>8</sub>, 273 K):  $\delta_P = 32.7$  (0.12P, s, minor), 29.0 (1P, s, major) ppm; **ID ROE** (700 MHz, THF-*d*<sub>8</sub>, 253 K):  $r_{HH} \approx 2.9 \pm 0.2$  (major CB H2-H5),  $2.9 \pm 0.1$  (major CB H3-H4),  $2.8 \pm 0.1$  (major CB H2-H3),  $4.1 \pm 0.2$  (major CB H2-H4),  $3.9 \pm 0.2$  (major CB H3-H5), 1.783 (major L H9<sub>cis</sub>-H9<sub>trans</sub>, reference from DFT structure),  $3.0 \pm 0.2$  (minor CB H2-H5),  $3.0 \pm 0.2$  (minor CB H3-H4),  $2.8 \pm 0.1$  (minor CB H2-H3) Å (ROEs of minor species referenced externally to major L H9<sub>cis</sub>-H9<sub>trans</sub>); **PSYCHEDELICs** (700 MHz, THF-*d*<sub>8</sub>, 273 K):  $J_{HH} = 1.4 \pm 0.1$  (major CB H2-H5),  $1.4 \pm 0.1$  (minor CB H2-H5),  $1.5 \pm 0.1$  (minor CB H2-H3) Hz; **DOSY** (700 MHz, THF-*d*<sub>8</sub>, 273 K):  $D = (9.6 \pm 0.2) \cdot 10^{-10}$  (major),  $(9.5 \pm 0.3) \cdot 10^{-10}$  (minor) m<sup>2</sup> s<sup>-1</sup>; **HRMS** (ESI<sup>+</sup>): C<sub>32</sub>H<sub>27</sub>NO<sub>3</sub>PPd [M–Cl]<sup>+</sup> requires 610.0758, found 610.0772 ( $\Delta = 2.3$  ppm); **HRMS** (ESI<sup>+</sup>): C<sub>32</sub>H<sub>26</sub>ClNO<sub>3</sub>PPd [M–H]<sup>+</sup> requires 644.0379, found 644.0385 ( $\Delta = 0.9$  ppm). The spectroscopic data of major-*anti*-4b are consistent with those reported in the literature.<sup>32</sup> Due to signal overlap and the presence of excess dba, not all signals in the aromatic region could be assigned. ROE analysis was complicated by chemical exchange and did thus not allow for extracting accurate internuclear distances. The most characteristic NMR spectroscopic data are summarized in Table S2.

**Table S2.** Characteristic NMR data for complexes major- (top) and minor- (bottom) *anti*-4b.

Position	$\delta_1$ / ppm	$\delta_c$ or $\delta_p$ or $\delta_N$ / ppm	Additional data
CB 1	–	172.0	

CB 2	4.11	55.4	$r_{\text{H2-H5}} \approx (2.9 \pm 0.2) \text{ \AA}$ $^3J_{\text{H2-H5}} = (1.4 \pm 0.1) \text{ Hz}$
CB 3	5.58	128.7	
CB 4	5.07	147.5	
CB 5	3.28	45.7	$^2J_{\text{CP}} = 4.3 \text{ Hz}$
P	–	29.0	
N	–	194.1	
<hr/>			
CB 1	–	173.9	
CB 2	3.81	55.9	$r_{\text{H2-H5}} \approx (3.0 \pm 0.2) \text{ \AA}$ $^3J_{\text{H2-H5}} = (1.4 \pm 0.1) \text{ Hz}$
CB 3	5.49	127.0	
CB 4	6.11	148.9	
CB 5	3.37	43.3	$^3J_{\text{HP}} = 10.0 \text{ Hz}$
P	–	32.7	
N	–	195.8	

#### Oxidative Addition of Acid Substrate *trans*-1 with Ligand L1



Oxidative addition of *trans*-4-chlorocyclobutene-2-enecarboxylic acid *trans*-1 with phosphoramidite ligand  $(S_{\text{ax}}, S, S)\text{-L1}$  according to the general procedure gave a diastereomeric mixture of Pd-complexes *syn*-4a, along with small amounts of *anti*-4a (*syn:anti* = 95:5). *Syn*-4a was found to slowly equilibrate to d.r. = 82:18 over ca. 20 h, whereas *anti*-4a was obtained with a d.r. of 89:11, identical to the value obtained after its selective preparation from substrate *cis*-1 (*vide supra*). In contrast to its *anti*-analogue, *syn*-4a was found to have only one equivalent of ligand L1 coordinated, which is located in *cis*-position relative to the cyclobutene ring according to the magnitude of the experimental  $^2J_{\text{CP}}$  and  $^3J_{\text{HP}}$  coupling constants.<sup>34–36</sup> Variation of the stoichiometry of L1 (1 or 2 equiv.) was found not to affect the outcome of this reaction.

The relative configuration of *anti*-4a was derived from quantitative NOE data and confirmed by  $^3J_{\text{H2-H5}}$  coupling constants extracted from PSYCHEDELIC experiments. Since the carboxy group experiences significant deshielding upon complex formation ( $\Delta\delta = 17.4$  ppm for major-*syn*-4a,  $\Delta\delta = 17.2$  ppm for minor-*syn*-4a compared to free *trans*-1), *syn*-4a is likely to be stabilized by internal Pd–O coordination,<sup>33</sup> thus requiring only 1 equiv. of L1 for saturation of the coordination sphere. This effect was not observed for the corresponding *anti*-complexes *anti*-4a.

Although the 2D EASY-ROESY and NOESY spectra do not exhibit exchange cross-peaks, the time dependence observed for the d.r. (d.r. = 50:50  $\rightarrow$  82:18, see section 5) indicates complexes *syn*-4a to be in equilibrium. The drastically decreased equilibration rate compared to *anti*-4a is consistent with an internal Pd–O coordination which has to be broken prior to interconversion between the  $\eta^1$ -species, thus increasing the energy barrier.

Given below are the characterization data for *syn*-4a; for characterization of *anti*-4a see its selective preparation (oxidative addition of acid substrate *cis*-1 with ligand L1).

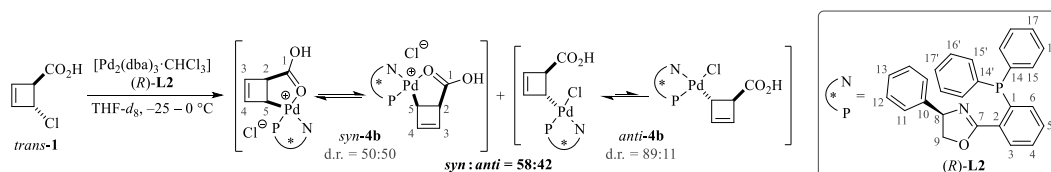
**<sup>1</sup>H-NMR** (700 MHz, THF-*d*<sub>8</sub>, 273 K):  $\delta_{\text{H}} = 11.3$  (1.22H, br. s, major + minor CB C(1)O<sub>2</sub>H), 8.58 (1H, d,  $^3J_{\text{HH}} = 8.9$ , major L C(3)H), 8.54 (0.22H, d,  $^3J_{\text{HH}} = 8.9$ , minor L C(3)H), 8.08 (1H, d,  $^3J_{\text{HH}} = 8.9$ , major L C(4)H), 8.06 (0.22H, d,  $^3J_{\text{HH}} = 8.9$ , minor L C(4)H), 7.98 (1H, d,  $^3J_{\text{HH}} = 8.9$ , major L C(4')H), 7.29 (4H, d,  $^3J_{\text{HH}} = 7.9$ , major L C(b)H, C(b')H), 7.16 – 7.12 (6H, m, major L C(c)H, C(c')H, C(d)H, C(d')H), 7.03 – 7.01 (1.32H, m, minor L C(b)H, C(b')H, C(d)H, C(d')H), 6.99 – 6.97 (0.88H, m, minor L C(c)H, C(c')H), 6.97 (1H, d,  $^3J_{\text{HH}} = 8.9$ , major L C(3')H), 6.74 (0.22H, br. s, minor CB C(4)H), 5.87 (0.22H, br. s, minor CB C(3)H), 5.52 – 5.45 (0.44H, m, minor L C(e)H, C(e')H), 5.36 (1H, br. s, major CB C(3)H), 5.09 (2H, dq,  $^3J_{\text{HP}} = 15.4$ ,  $^3J_{\text{HH}} = 7.1$ , major L C(e)H, C(e')H), 5.02 (1H, br. s, major CB C(4)H), 3.78 (0.22H, d,  $^3J_{\text{HH}} \approx 3.0$ , minor CB C(2)H), 3.73 (1H, d,  $^3J_{\text{HH}} \approx 2.9$ , major CB C(2)H), 3.54 (0.22H, dd,  $^3J_{\text{HP}} = 5.8$ ,  $^3J_{\text{HH}} \approx 3.0$ , minor CB C(5)H), 3.38 (1H, dd,  $^3J_{\text{HP}} = 6.7$ ,  $^3J_{\text{HH}} \approx 2.9$ , major CB C(5)H), 1.86 (6H, d,  $^3J_{\text{HH}} = 7.1$ , major L C(f)H<sub>3</sub>, C(f')H<sub>3</sub>), 1.38 (1.32H, d,  $^3J_{\text{HH}} = 7.0$ , minor L C(f)H<sub>3</sub>, C(f')H<sub>3</sub>) ppm; **<sup>13</sup>C{<sup>1</sup>H}-NMR** (176 MHz, THF-*d*<sub>8</sub>, 273 K):  $\delta_{\text{C}} = 189.1$  (major CB C(1)), 188.9 (minor CB C(1)), 151.3 (minor CB C(4)), 151.2 (d,  $^3J_{\text{CP}} = 2.9$ , major CB C(4)), 150.2 (br. s, major L

$C(1')$ ), 149.7 (d,  $^2J_{CP} = 4.4$ , major L  $C(1)$ ), 149.2 (d,  $^2J_{CP} = 4.5$ , minor L  $C(1)$ ), 142.2 (d,  $^3J_{CP} = 3.5$ , major L  $C(a)$ ,  $C(a')$ ), 141.0 (br. s, minor L  $C(a)$ ,  $C(a')$ ), 131.7 (major L  $C(4)$ ), 131.2 (major L  $C(4')$ ), 131.1 (minor L  $C(4)$ ), 129.9 (major L  $C(b)$ ,  $C(b')$ ), 129.6 (minor L  $C(d)$ ,  $C(d')$ ), 128.2 (major L  $C(c)$ ,  $C(c')$ ), 127.7 (major L  $C(d)$ ,  $C(d')$ ), 127.6 (minor L  $C(b)$ ,  $C(b')$ ), 127.1 (minor L  $C(c)$ ,  $C(c')$ ), 127.0 (minor CB  $C(3)$ ), 126.4 (d,  $^4J_{CP} = 8.1$ , major CB  $C(3)$ ), 125.2 (major L  $C(3)$ ), 123.1 (minor L  $C(3)$ ), 121.9 (major L  $C(3')$ ), 58.8 (br. s, minor CB  $C(2)$ ), 58.2 (d,  $^3J_{CP} = 2.7$ , major CB  $C(2)$ ), 56.7 (d,  $^2J_{CP} = 11.8$ , minor L  $C(e)$ ,  $C(e')$ ), 56.1 (d,  $^2J_{CP} = 7.6$ , major L  $C(e)$ ,  $C(e')$ ), 44.2 (d,  $^2J_{CP} = 15.2$ , minor CB  $C(5)$ ), 43.3 (d,  $^2J_{CP} = 15.3$ , major CB  $C(5)$ ), 21.7 (br. s, minor L  $C(f)$ ,  $C(f')$ ), 21.4 (br. s, major L  $C(f)$ ,  $C(f')$ ) ppm;  $^{31}\text{P}\{^1\text{H}\}$ -NMR (283 MHz, THF- $d_6$ , 273 K):  $\delta_{\text{P}} = 135.0$  (0.22P, s, minor), 133.3 (1P, s, major) ppm; **ID NOE** (700 MHz, THF- $d_6$ , 273 K):  $r_{\text{HH}} = 2.49 \pm 0.05$  (major CB H2-H5), 2.865 (major CB H3-H4, reference<sup>33</sup>),  $2.91 \pm 0.05$  (major CB H2-H3),  $2.87 \pm 0.05$  (major CB H4-H5),  $3.95 \pm 0.11$  (major CB H3-H5),  $2.53 \pm 0.09$  (minor CB H2-H5), 2.865 (minor CB H3-H4, reference<sup>33</sup>) Å; **PSYCHEDELICs** (700 MHz, THF- $d_6$ , 273 K):  $J_{\text{HH}} = 2.9 \pm 0.1$  (major CB H2-H5),  $3.0 \pm 0.1$  (minor CB H2-H5) Hz; **DOSY** (700 MHz, THF- $d_6$ , 273 K):  $D = (9.24 \pm 0.03) \cdot 10^{-10}$  (major-*syn*),  $(9.04 \pm 0.05) \cdot 10^{-10}$  (minor-*syn*),  $(8.4 \pm 0.2) \cdot 10^{-10}$  (major-*anti*)  $\text{m}^2 \text{s}^{-1}$ ; **HRMS** (ESI<sup>+</sup>):  $\text{C}_{41}\text{H}_{35}\text{NO}_4\text{PPd} [\text{M}-\text{Cl}]^+$  requires 742.1333, found 742.1346 ( $\Delta = 1.8$  ppm); **HRMS** (ESI<sup>-</sup>):  $\text{C}_{41}\text{H}_{34}\text{ClNO}_4\text{PPd} [\text{M}-\text{H}]^-$  requires 776.0954, found 776.0956 ( $\Delta = 0.3$  ppm). Due to signal overlap and the presence of excess dba, not all signals in the aromatic region could be assigned. The most characteristic NMR spectroscopic data are summarized in Table S3.

**Table S3.** Characteristic NMR data for complexes major- (top) and minor- (bottom) *syn-4a*.

Position	$\delta_{\text{H}} / \text{ppm}$	$\delta_{\text{C}}$ or $\delta_{\text{P}} / \text{ppm}$	Additional data
CB 1	–	189.1	
CB 2	3.73	58.2	$r_{\text{H2-H5}} \approx (2.49 \pm 0.05) \text{ \AA}$ $^3J_{\text{H2-H5}} = (2.9 \pm 0.1) \text{ Hz}$
CB 3	5.36	126.4	
CB 4	5.02	151.2	
CB 5	3.38	43.3	$^3J_{\text{HP}} = 6.7 \text{ Hz}$ $^2J_{\text{CP}} = 15.3 \text{ Hz}$
P	–	133.3	
CB 1	–	188.9	
CB 2	3.78	58.8	$r_{\text{H2-H5}} \approx (2.53 \pm 0.09) \text{ \AA}$ $^3J_{\text{H2-H5}} = (3.0 \pm 0.1) \text{ Hz}$
CB 3	5.87	127.0	
CB 4	6.74	151.3	
CB 5	3.54	44.2	$^3J_{\text{HP}} = 5.8 \text{ Hz}$ $^2J_{\text{CP}} = 15.2 \text{ Hz}$
P	–	135.0	

#### Oxidative Addition of Acid Substrate *trans-1* with Ligand **L2**



Oxidative addition of *trans*-4-chlorocyclobutene-2-enecarboxylic acid *trans-1* with PHOX ligand (*R*)-**L2** according to the general procedure gave a mixture of Pd-complexes *syn-4b* and *anti-4b* (*syn:anti* = 58:42). *Syn-4b* was formed with one species slightly enriched (d.r.  $\approx$  54:46) directly after preparation, and then equilibrated to d.r. = 50:50 over ca. 12 h. *Anti-4b*, on the other hand, was obtained with a d.r. of 89:11, identical to the value obtained after its selective preparation from substrate *cis-1* (*vide supra*). From the magnitude of the  $^2J_{\text{CP}}$  and  $^3J_{\text{HP}}$  coupling constants extracted for *syn-4b*, the phosphine site can be concluded to be in *cis*-position relative to the cyclobutene ring.<sup>34–36</sup>

The relative configuration of *syn-4b* was derived from quantitative NOE data and confirmed by  $^3J_{\text{H2-H5}}$  coupling constants extracted from PSYCHEDELIC experiments. The carboxy group experiences significant deshielding upon complex formation ( $\Delta\delta_{\text{C}} = 10.3$  ppm for major-*syn-4b*,  $\Delta\delta_{\text{C}} = 10.2$  ppm for minor-*syn-4b* compared to free *trans-1*),<sup>33</sup> an effect that was not observed for the corresponding *anti*-complexes *anti-4b*. Hence, *syn-4b* is likely to be stabilized by internal Pd–O coordination. Ligand **L2** was found to still be coordinated via both P- and N-ligation site, as confirmed by cross-peaks between cyclobutene and ligand detected by both  $^1\text{H}$ - $^{15}\text{N}$ -HMBC and  $^1\text{H}$ - $^{31}\text{P}$ -HMBC experiments. Thus, chloride seems

not to be coordinated to the Pd(II)-center. The resulting ionic nature of *syn-4b* is further indicated by its chemical shifts being significantly concentration- and temperature-dependent, as well as the lines being broader than for *anti-4b*.

Although the 2D EASY-ROESY and NOESY spectra do not exhibit exchange cross-peaks, the time dependence observed for the d.r. (d.r. = 54:46 → 50:50 over ca. 12 h, see section 5) indicates complexes *syn-4b* to be in equilibrium. The drastically decreased equilibration rate compared to *anti-4b* is consistent with an internal Pd-O coordination which has to be broken prior to interconversion between the  $\eta^1$ -species, thus increasing the energy barrier.

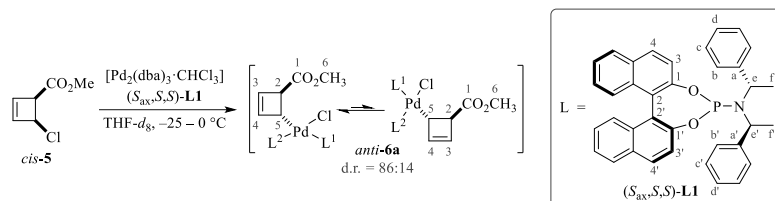
Given below are the characterization data for *syn-4b*; for characterization of *anti-4b* see its selective preparation (oxidative addition of acid substrate *cis-1* with ligand **L2**). Although both *syn*-species are populated equally in the end-point spectra, the diastereomer that is enriched before equilibration is termed “major” hereinafter.

**<sup>1</sup>H-NMR** (700 MHz, THF-*d*<sub>8</sub>, 273 K):  $\delta_{\text{H}}$  = 8.26 (1H, dd, <sup>3</sup>*J*<sub>HH</sub> = 7.9, <sup>4</sup>*J*<sub>HH</sub> = 4.3, major L C(3)*H*), 8.16 (1H, ddd, <sup>3</sup>*J*<sub>HH</sub> = 7.9, <sup>4</sup>*J*<sub>HH</sub> = 4.0, <sup>5</sup>*J*<sub>HH</sub> = 1.2, minor L C(3)*H*), 7.70 – 7.68 (2H, m, major + minor L C(4)*H*), 6.01 (1H, dd, <sup>3</sup>*J*<sub>HH</sub> = 10.1, <sup>3</sup>*J*<sub>HH</sub> = 4.6, major L C(8)*H*), 5.92 (1H, dd, <sup>3</sup>*J*<sub>HH</sub> = 10.0, <sup>3</sup>*J*<sub>HH</sub> = 4.4, minor L C(8)*H*), 5.85 (1H, br. s, minor CB C(4)*H*), 5.79 (1H, br. s, minor CB C(3)*H*), 5.78 (1H, br. s, major CB C(3)*H*), 5.34 (1H, d, <sup>3</sup>*J*<sub>HH</sub> = 2.3, major CB C(4)*H*), 4.78 – 4.75 (1H, m, major L C(9)*H**H*<sub>trans</sub>), 4.74 – 4.71 (1H, m, minor L C(9)*H**H*<sub>trans</sub>), 4.65 – 4.63 (1H, m, minor L C(9)*H**H*<sub>cis</sub>), 4.57 (1H, dd, <sup>2</sup>*J*<sub>HH</sub> = 9.1, <sup>3</sup>*J*<sub>HH</sub> = 4.5, major L C(9)*H**H*<sub>cis</sub>), 3.54 (1H, br. s, minor CB C(2)*H*), 3.49 (1H, br. s, major CB C(2)*H*), 2.63 (1H, br. d, <sup>3</sup>*J*<sub>HP</sub> = 9.8, major CB C(5)*H*), 2.30 (1H, br. d, <sup>3</sup>*J*<sub>HP</sub> = 9.9, minor CB C(5)*H*) ppm; **<sup>13</sup>C{<sup>1</sup>H}-NMR** (176 MHz, THF-*d*<sub>8</sub>, 273 K):  $\delta_{\text{C}}$  = 181.7 (br. s, major CB C(1)), 181.6 (br. s, minor CB C(1)), 162.7 (br. s, minor L C(7)), 162.3 (br. s, major L C(7)), 146.2 (br. s, minor CB C(4)), 145.6 (br. s, major CB C(4)), 141.6 (minor L C(10)), 141.4 (major L C(10)), 132.8 (br. s, major + minor L C(3), minor L C(4)), 131.2 (br. s, major CB C(3)), 130.6 (br. s, minor CB C(3)), 75.5 (major L C(9)), 75.1 (minor L C(9)), 68.7 (major L C(8)), 68.5 (minor L C(8)), 60.2 (br. s, major CB C(2)), 60.1 (br. s, minor CB C(2)), 41.8 (br. s, minor CB C(5)), 37.5 (br. s, major CB C(5)) ppm; **<sup>15</sup>N-NMR** (71 MHz, THF-*d*<sub>8</sub>, 273 K):  $\delta_{\text{N}}$  = 196.3 (minor), 194.3 (major) ppm; **<sup>31</sup>P{<sup>1</sup>H}-NMR** (283 MHz, THF-*d*<sub>8</sub>, 273 K):  $\delta_{\text{P}}$  = 32.3 (1P, br. s, major), 31.4 (1P, br. s, minor) ppm; **ID ROE** (700 MHz, THF-*d*<sub>8</sub>, 273 K): *r*<sub>HH</sub> ≈ 2.5 ± 0.1 (major CB H2-H5), 2.6 ± 0.2 (major CB H2-H3), 2.9 ± 0.1 (major CB H4-H5), 1.783 (major L H9<sub>cis</sub>-H9<sub>trans</sub>, reference from DFT structure), 2.4 ± 0.1 (minor CB H2-H5), 2.7 ± 0.2 (minor CB H4-H5), 3.6 ± 0.3 (minor CB H2-H4), 1.783 (minor L H9<sub>cis</sub>-H9<sub>trans</sub>, reference from DFT structure) Å; **PSYCHEDELICs** (700 MHz, THF-*d*<sub>8</sub>, 273 K): *J*<sub>HH</sub> = 3.0 ± 0.2 (major CB H2-H5), 1.4 ± 0.2 (major CB H2-H3), 3.0 ± 0.2 (minor CB H2-H5), 1.3 ± 0.1 (minor CB H2-H3) Hz; **DOSY** (700 MHz, THF-*d*<sub>8</sub>, 273 K): *D* = (6.9 ± 0.2) · 10<sup>-10</sup> (major-*syn*), (6.9 ± 0.2) · 10<sup>-10</sup> (minor-*syn*), (7.0 ± 0.2) · 10<sup>-10</sup> (major-*anti*), (7.0 ± 0.2) · 10<sup>-10</sup> (minor-*anti*) m<sup>2</sup> s<sup>-1</sup>; **HRMS** (ESI<sup>+</sup>): C<sub>32</sub>H<sub>27</sub>NO<sub>3</sub>PPd [M-Cl]<sup>+</sup> requires 610.0758, found 610.0767 ( $\Delta$  = 1.5 ppm); **HRMS** (ESI<sup>-</sup>): C<sub>32</sub>H<sub>26</sub>ClNO<sub>3</sub>PPd [M-H]<sup>-</sup> requires 644.0379, found 644.0388 ( $\Delta$  = 1.4 ppm). Due to signal overlap and the presence of excess dba, not all signals in the aromatic region could be assigned. ROE analysis was complicated by poor signal-to-noise ratio as well as resonances shifting during characterization, and did thus not allow for extracting accurate internuclear distances. The most characteristic NMR spectroscopic data are summarized in Table S4.

**Table S4.** Characteristic NMR data for complexes major- (top) and minor- (bottom) *syn-4b*.

Position	$\delta_{\text{H}}$ / ppm	$\delta_{\text{C}}$ or $\delta_{\text{P}}$ or $\delta_{\text{N}}$ / ppm	Additional data
CB 1	–	181.7	
CB 2	3.49	60.2	<i>r</i> <sub>H2-H5</sub> ≈ (2.5 ± 0.1) Å <sup>3</sup> <i>J</i> <sub>H2-H5</sub> = (3.0 ± 0.2) Hz
CB 3	5.78	131.2	
CB 4	5.34	145.6	
CB 5	2.63	37.5	<sup>3</sup> <i>J</i> <sub>HP</sub> = 9.8 Hz
P	–	32.3	
N	–	194.3	
CB 1	–	181.6	
CB 2	3.54	60.1	<i>r</i> <sub>H2-H5</sub> ≈ (2.4 ± 0.1) Å <sup>3</sup> <i>J</i> <sub>H2-H5</sub> = (3.0 ± 0.2) Hz
CB 3	5.79	130.6	
CB 4	5.85	146.2	
CB 5	2.30	41.8	<sup>3</sup> <i>J</i> <sub>HP</sub> = 9.9 Hz
P	–	31.4	
N	–	196.3	

## Oxidative Addition of Ester Substrate *cis*-5 with Ligand L1



Oxidative addition of *cis*-methyl-4-chlorocyclobutene-2-ene-1-carboxylate *cis*-5 with phosphoramidite ligand (*S,S,S,S*)-L1 according to the general procedure gave a diastereomeric mixture of Pd-complexes *anti*-6a, with one species being highly enriched (d.r. = 86:14). From the magnitude of the experimental  $^2J_{PP}$ ,  $^2J_{CP}$  and  $^3J_{HP}$  coupling constants, the two ligands can be concluded to be in *cis*- and *trans*-position relative to the cyclobutene ring, respectively.<sup>34-36</sup> As complexes *anti*-6a readily underwent decomposition during NMR characterization, ROEs could be extracted only for the major species, giving a distance  $r_{H2-H5}$  typical for *anti*-configured cyclobutenes. The configuration of the minor species can be concluded to be *anti* by comparison of the DOSY diffusion coefficients: Whilst almost identical values were obtained for major-*anti*-6a and minor-*anti*-6a, the corresponding *syn*-species *syn*-6a (*vide infra*) exhibit significantly higher diffusion coefficients, consistent with their lower molecular weight.

Although the 2D EASY-ROESY and NOESY spectra do not exhibit exchange cross-peaks, complexes *anti*-6a can be assumed to be in equilibrium due to their strong structural similarity to the corresponding acid complexes *anti*-6a for which equilibration could be evidenced (*vide supra*). Moreover, *anti*-6a was formed with an identical d.r. as side product by oxidative addition of ester substrate *anti*-6a with ligand L1 (*vide infra*), suggesting that its d.r. is determined by a given equilibrium constant.

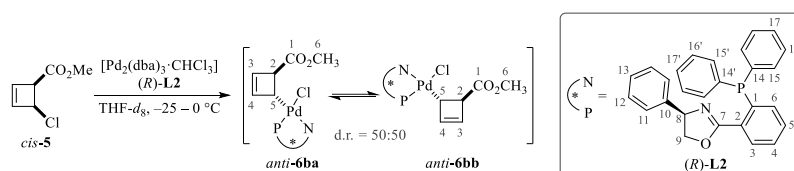
**<sup>1</sup>H-NMR** (700 MHz, THF-*d*<sub>8</sub>, 273 K):  $\delta_{\text{H}} = 8.74$  (0.16H, d,  $^3J_{\text{HH}} = 8.9$ , minor L<sup>1</sup> C(3)*H*), 8.71 (1H, d,  $^3J_{\text{HH}} = 8.9$ , major L<sup>1</sup> C(3)*H*), 8.28 (1H, d,  $^3J_{\text{HH}} = 8.8$ , major L<sup>2</sup> C(4')*H*), 8.23 (0.16H, d,  $^3J_{\text{HH}} = 8.9$ , minor L<sup>2</sup> C(4')*H*), 8.06 (1H, d,  $^3J_{\text{HH}} = 8.8$ , major L<sup>1</sup> C(4')*H*), 7.91 (1H, d,  $^3J_{\text{HH}} = 8.9$ , major L<sup>2</sup> C(4)*H*), 7.86 (1H, d,  $^3J_{\text{HH}} = 8.8$ , major L<sup>2</sup> C(3')*H*), 7.86 (1H, d,  $^3J_{\text{HH}} = 8.9$ , major L<sup>1</sup> C(4)*H*), 7.78 (0.16H, d,  $^3J_{\text{HH}} = 8.9$ , minor L<sup>2</sup> C(3')*H*), 7.70 (0.16H, d,  $^3J_{\text{HH}} = 8.9$ , minor L<sup>1</sup> C(4)*H*), 7.59 (1H, d,  $^3J_{\text{HH}} = 8.8$ , major L<sup>1</sup> C(3')*H*), 7.23 (1H, d,  $^3J_{\text{HH}} = 8.9$ , major L<sup>2</sup> C(3)*H*), 6.90 (4.64H, br. d,  $^3J_{\text{HH}} = 7.7$ , major + minor L<sup>1</sup> C(b)*H*, C(b')*H*), 6.86 – 6.83 (2.32H, m, major + minor L<sup>1</sup> C(d)*H*, C(d')*H*), 6.72 (4.64H, t,  $^3J_{\text{HH}} = 7.7$ , major + minor L<sup>1</sup> C(c)*H*, C(e')*H*), 6.05 (0.16H, br. s, minor CB C(4)*H*), 6.02 (0.16H, br. s, minor CB C(3)*H*), 5.55 (1H, br. s, major CB C(3)*H*), 5.06 (1H, br. s, major CB C(4)*H*), 4.74 – 4.66 (2.32H, m, major + minor L<sup>1</sup> C(e)*H*, C(e')*H*), 4.44 (0.16H, d,  $^4J_{\text{HP}} = 3.9$ , minor CB C(2)*H*), 4.28 (1H, d,  $^4J_{\text{HP}} = 3.6$ , major CB C(2)*H*), 4.25 (0.16H, dd,  $^3J_{\text{HP}} = 14.8$ ,  $^3J_{\text{HP}} = 8.4$ , minor CB C(5)*H*), 4.16 (1H, d,  $^3J_{\text{HP}} = 11.4$ , major CB C(5)*H*), 3.68 (3H, s, major CB C(6)*H*<sub>3</sub>), 3.61 (0.48H, s, major CB C(6)*H*<sub>3</sub>), 0.82 (0.96H, d,  $^3J_{\text{HH}} = 7.1$ , minor L<sup>1</sup> C(f)*H*<sub>3</sub>, C(f')*H*<sub>3</sub>), 0.71 (6H, d,  $^3J_{\text{HH}} = 7.0$ , major L<sup>1</sup> C(f)*H*<sub>3</sub>, C(f')*H*<sub>3</sub>) ppm; **<sup>13</sup>C{<sup>1</sup>H}-NMR** (176 MHz, THF-*d*<sub>8</sub>, 273 K):  $\delta_{\text{C}} = 174.9$  (major CB C(1)), 174.7 (minor CB C(1)), 150.8 (d,  $^2J_{\text{CP}} = 14.5$ , major L<sup>1</sup> C(1')), 150.3 (d,  $^2J_{\text{CP}} = 15.1$ , major L<sup>2</sup> C(1')), 150.3 (minor L<sup>2</sup> C(1')), 150.1 (dd,  $^4J_{\text{CP}} = 7.6$ ,  $^4J_{\text{CP}} = 6.5$ , major CB C(4)), 149.8 (minor L<sup>1</sup> C(1)), 149.7 (d,  $^2J_{\text{CP}} = 2.6$ , major L<sup>1</sup> C(1)), 149.7 (d,  $^4J_{\text{CP}} = 2.2$ , minor CB C(4)), 148.1 (d,  $^2J_{\text{CP}} = 4.1$ , major L<sup>2</sup> C(1)), 142.2 (d,  $^3J_{\text{CP}} = 4.2$ , major L<sup>1</sup> C(a), C(a')), 142.1 (d,  $^3J_{\text{CP}} = 4.5$ , minor L<sup>1</sup> C(a), C(a')), 132.0 (major L<sup>2</sup> C(4)), 131.8 (major L<sup>2</sup> C(3')), 131.7 (minor L<sup>1</sup> C(4)), 131.6 (major + minor L<sup>2</sup> C(4')), 131.0 (major L<sup>1</sup> C(4')), 130.7 (major CB C(3)), 129.7 (minor CB C(3)), 129.4 (major L<sup>1</sup> C(b), C(b')), 127.6 (major L<sup>1</sup> C(e), C(e')), 127.0 (major L<sup>1</sup> C(d), C(d')), 125.2 (br. s, major L<sup>1</sup> C(3)), 124.9 (d,  $^3J_{\text{CP}} = 5.6$ , minor L<sup>1</sup> C(3)), 122.5 (major L<sup>1</sup> C(4)), 122.4 (major L<sup>1</sup> C(3')), 122.4 (minor L<sup>2</sup> C(3')), 122.1 (major L<sup>2</sup> C(3)), 56.8 (br. d,  $^3J_{\text{CP}} = 7.2$ , major CB C(2)), 55.9 (d,  $^2J_{\text{CP}} = 10.5$ , minor L<sup>1</sup> C(e), C(e')), 55.7 (d,  $^2J_{\text{CP}} = 10.5$ , major L<sup>1</sup> C(e), C(e')), 55.2 (br. s, minor CB C(2)), 51.3 (major CB C(6)), 51.3 (minor CB C(6)), 50.7 (dd,  $^2J_{\text{CP}} = 152.6$ ,  $^2J_{\text{CP}} = 9.6$ , major CB C(5)), 49.2 (d,  $^2J_{\text{CP}} \approx 152$ , minor CB C(5)), 21.1 (br. s, minor L<sup>1</sup> C(f), C(f')), 21.0 (br. s, major L<sup>1</sup> C(f), C(f')) ppm; **<sup>31</sup>P{<sup>1</sup>H}-NMR** (283 MHz, THF-*d*<sub>8</sub>, 273 K):  $\delta_{\text{P}} = 146.7$  (0.16P, d,  $^2J_{\text{PP}} = 88.8$ , minor L<sup>1</sup>), 146.0 (1P, d,  $^2J_{\text{PP}} = 102.0$ , major L<sup>1</sup>), 141.3 (1P, d,  $^2J_{\text{PP}} = 102.0$ , major L<sup>2</sup>), 139.4 (0.16P, d,  $^2J_{\text{PP}} = 88.8$ , minor L<sup>2</sup>) ppm; **ID ROE** (700 MHz, THF-*d*<sub>8</sub>, 253 K):  $r_{\text{HH}} = 3.1 \pm 0.1$  (major CB H2-H5), 2.865 (major CB H3-H4, reference<sup>32</sup>),  $2.9 \pm 0.1$  (major CB H2-H3),  $2.9 \pm 0.1$  (major CB H4-H5),  $4.0 \pm 0.2$  (major CB H3-H5),  $4.2 \pm 0.2$  (major CB H5-H6) Å; **DOSY** (700 MHz, THF-*d*<sub>8</sub>, 273 K):  $D = (1.11 \pm 0.02) \cdot 10^{-10}$  (major),  $(1.12 \pm 0.02) \cdot 10^{-10}$  (minor) m<sup>2</sup> s<sup>-1</sup>; **HRMS** (ESI<sup>+</sup>): C<sub>78</sub>H<sub>67</sub>N<sub>2</sub>O<sub>6</sub>P<sub>2</sub>Pd [M–Cl]<sup>+</sup> requires 1295.3504, found 1295.3523 ( $\Delta = 1.5$  ppm), C<sub>42</sub>H<sub>37</sub>NO<sub>4</sub>PPd [M–L–Cl]<sup>+</sup> requires 756.1490, found 756.1515 ( $\Delta = 3.3$  ppm). Due to signal overlap and the presence of excess dba, not all signals in the aromatic region could be assigned. The most characteristic NMR spectroscopic data are summarized in Table S5.

**Table S5.** Characteristic NMR data for complexes major- (top) and minor- (bottom) *anti*-6a.

Position	$\delta_{\text{H}}$ / ppm	$\delta_{\text{C}}$ or $\delta_{\text{P}}$ / ppm	Additional data
CB 1	–	174.9	
CB 2	4.28	56.8	$r_{\text{H2-H5}} = (3.1 \pm 0.1)$ Å
CB 3	5.55	130.7	
CB 4	5.06	150.1	
CB 5	4.16	50.7	$^3J_{\text{HP}} = 11.4$ Hz $^2J_{\text{CP}} = 152.6, 9.6$ Hz

L <sub>1</sub> P	–	146.0	${}^2J_{PP} = 102.0$ Hz
L <sub>2</sub> P	–	141.3	
CB 1	–	174.7	
CB 2	4.44	55.2	
CB 3	6.02	129.7	
CB 4	6.05	149.7	
CB 5	4.25	49.2	${}^3J_{HP} = 8.4$ Hz ${}^2J_{CP} \approx 152$ Hz
L <sub>1</sub> P	–	146.7	${}^2J_{PP} = 88.8$ Hz
L <sub>2</sub> P	–	139.4	

### Oxidative Addition of Ester Substrate *cis*-5 with Ligand L2



Oxidative addition of *cis*-methyl-4-chlorocyclobutene-2-encarboxylic carboxylate *cis*-5 with PHOX ligand (*R*)-L2 according to the general procedure gave a diastereomeric 1:1 mixture of Pd-complexes *anti*-6b. From the magnitude of the experimental  ${}^2J_{CP}$  and  ${}^3J_{HP}$  coupling constants, the phosphine site can be concluded to be in *cis*-position relative to the cyclobutene ring.<sup>34–36</sup> The relative configuration of the cyclobutene ring was derived from quantitative ROE data and confirmed by  ${}^3J_{H2-H5}$  coupling constants extracted from PSYCHEDELIC experiments. The 2D EASY-ROESY and NOESY spectra exhibit exchange cross-peaks between the two Pd-species, indicating that complexes *anti*-6b are in equilibrium. Upon standing at 0 °C, slow irreversible ring-opening to the corresponding (*E,E*)-diene<sup>32</sup> was observed.

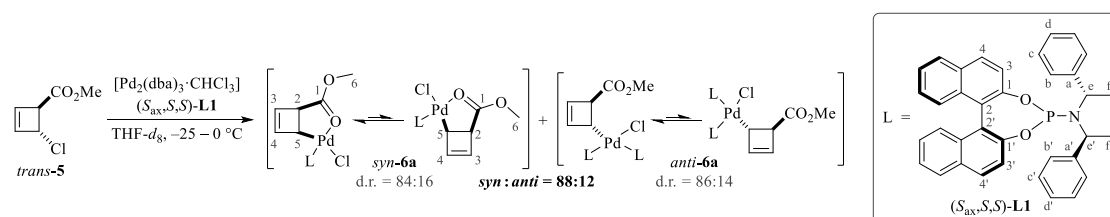
**<sup>1</sup>H-NMR** (700 MHz, THF-*d*<sub>6</sub>, 273 K):  $\delta_{\text{H}} = 8.14$  (2H, dd,  ${}^3J_{\text{HH}} = 7.8$ ,  ${}^4J_{\text{HH}} = 4.0$ , a + b L C(3)*H*), 7.69 – 7.66 (2H, m, a + b L C(4)*H*), 7.56 – 7.53 (2H, m, a + b L C(5)*H*), 7.50 – 7.47 (2H, m, a + b L C(17)*H*), 7.42 – 7.40 (2H, m, a + b L C(17')*H*), 7.29 – 7.27 (2H, m, a + b L C(16)*H*), 7.19 – 7.17 (2H, m, a + b L C(16')*H*), 7.09 – 7.06 (2H, m, a + b L C(15')*H*), 7.03 – 6.99 (2H, m, a + b L C(15)*H*), 6.98 – 6.93 (2H, m, a + b L C(6)*H*), 6.55 (1H, dd,  ${}^3J_{\text{HH}} = 10.1$ ,  ${}^3J_{\text{HH}} = 4.5$ , a L C(8)*H*), 6.52 (1H, dd,  ${}^3J_{\text{HH}} = 10.1$ ,  ${}^3J_{\text{HH}} = 4.7$ , b L C(8)*H*), 6.38 (1H, br. s, a CB C(4)*H*), 5.58 (1H, br. s, b CB C(4)*H*), 5.56 (1H, br. s, b CB C(3)*H*), 5.55 (1H, br. s, a CB C(3)*H*), 4.73 (1H, dd,  ${}^3J_{\text{HH}} = 10.1$ ,  ${}^2J_{\text{HH}} = 9.0$ , a L C(9)*HH*<sub>trans</sub>), 4.73 (1H, dd,  ${}^3J_{\text{HH}} = 10.1$ ,  ${}^2J_{\text{HH}} = 9.0$ , b L C(9)*HH*<sub>trans</sub>), 4.55 (1H, dd,  ${}^2J_{\text{HH}} = 9.0$ ,  ${}^3J_{\text{HH}} = 4.5$ , a L C(9)*HH*<sub>cis</sub>), 4.51 (1H, dd,  ${}^2J_{\text{HH}} = 9.0$ ,  ${}^3J_{\text{HH}} = 4.7$ , b L C(9)*HH*<sub>cis</sub>), 4.38 (1H, br. s, b CB C(2)*H*), 3.75 (1H, br. s, a CB C(2)*H*), 3.45 (3H, s, b CB C(6)*H*<sub>3</sub>), 3.31 (1H, d,  ${}^3J_{\text{HP}} = 8.8$ , b CB C(5)*H*), 3.23 (1H, d,  ${}^3J_{\text{HP}} = 11.5$ , a CB C(5)*H*), 3.20 (3H, s, a CB C(6)*H*<sub>3</sub>) ppm; **<sup>13</sup>C{<sup>1</sup>H}-NMR** (176 MHz, THF-*d*<sub>6</sub>, 273 K):  $\delta_{\text{C}} = 173.9$  (b CB C(1)), 173.4 (a CB C(1)), 162.4 (d,  ${}^3J_{\text{CP}} = 3.1$ , b L C(7)), 162.2 (d,  ${}^3J_{\text{CP}} = 3.3$ , a L C(7)), 150.6 (d,  ${}^4J_{\text{CP}} = 2.4$ , a CB C(4)), 149.0 (d,  ${}^4J_{\text{CP}} = 2.5$ , b CB C(4)), 141.8 (a + b L C(10)), 135.0 (d,  ${}^2J_{\text{CP}} = 13.8$ , a + b L C(6)), 134.8 (br. s, a + b L C(15)), 133.9 (d,  ${}^2J_{\text{CP}} = 11.6$ , a + b L C(15')), 133.1 (d,  ${}^3J_{\text{CP}} = 6.6$ , a/b L C(5)), 133.0 (d,  ${}^3J_{\text{CP}} = 6.6$ , a/b L C(5)), 132.5 (d,  ${}^3J_{\text{CP}} = 7.4$ , a/b L C(3)), 132.5 (d,  ${}^3J_{\text{CP}} = 7.2$ , a/b L C(3)), 132.0 (d,  ${}^1J_{\text{CP}} = 41.2$ , a/b L C(1)), 131.8 (d,  ${}^4J_{\text{CP}} = 2.0$ , a/b L C(4)), 131.8 (d,  ${}^4J_{\text{CP}} = 1.9$ , a/b L C(4)), 131.7 (d,  ${}^1J_{\text{CP}} = 41.2$ , a/b L C(1)), 131.6 (d,  ${}^4J_{\text{CP}} \approx 3$ , a/b L C(17)), 131.6 (d,  ${}^4J_{\text{CP}} \approx 3$ , a/b L C(17)), 131.4 (d,  ${}^4J_{\text{CP}} = 2.3$ , a + b L C(17')), 130.6 (br. s, a + b L C(16')), 129.5 (br. s, a/b L C(16)), 129.4 (br. s, a/b L C(16)), 127.9 (br. s, b CB C(3)), 126.1 (d,  ${}^3J_{\text{CP}} = 3.5$ , a CB C(3)), 75.2 (b L C(9)), 75.0 (a L C(9)), 68.9 (a L C(8)), 68.8 (b L C(8)), 56.1 (d,  ${}^3J_{\text{CP}} = 3.4$ , a CB C(2)), 55.8 (d,  ${}^3J_{\text{CP}} = 1.5$ , b CB C(2)), 50.5 (b CB C(6)), 50.2 (a CB C(6)), 44.6 (d,  ${}^2J_{\text{CP}} = 3.5$ , b CB C(5)), 44.1 (d,  ${}^2J_{\text{CP}} = 2.9$ , a CB C(5)) ppm; **<sup>15</sup>N-NMR** (71 MHz, THF-*d*<sub>6</sub>, 273 K):  $\delta_{\text{N}} = 196.9$  (b), 196.2 (a) ppm; **<sup>31</sup>P{<sup>1</sup>H}-NMR** (283 MHz, THF-*d*<sub>6</sub>, 273 K):  $\delta_{\text{P}} = 32.1$  (1P, s, a), 30.6 (1P, s, b) ppm; **ID ROE** (700 MHz, THF-*d*<sub>6</sub>, 253 K):  $r_{\text{HH}} = 3.02 \pm 0.05$  (a CB H2-H5),  $2.75 \pm 0.05$  (a CB H2-H3),  $2.81 \pm 0.05$  (a CB H4-H5),  $3.8 \pm 0.1$  (a CB H2-H4),  $3.9 \pm 0.2$  (a CB H3-H5), 1.783 (a L H9<sub>cis</sub>-H9<sub>trans</sub>, reference from DFT structure),  $3.01 \pm 0.05$  (b CB H2-H5),  $2.82 \pm 0.05$  (b CB H2-H3),  $2.82 \pm 0.05$  (b CB H4-H5),  $3.9 \pm 0.2$  (b CB H2-H4),  $3.7 \pm 0.2$  (b CB H3-H5), 1.783 (b L H9<sub>cis</sub>-H9<sub>trans</sub>, reference from DFT structure) Å; **PSYCHEDELICs** (700 MHz, THF-*d*<sub>6</sub>, 253 K):  $J_{\text{HH}} = 1.1 \pm 0.1$  (a CB H2-H5),  $1.0 \pm 0.2$  (a CB H2-H3),  $0.8 \pm 0.1$  (a CB H4-H5),  $1.2 \pm 0.1$  (a CB H2-H4),  $1.1 \pm 0.1$  (b CB H2-H5),  $1.4 \pm 0.1$  (b CB H2-H3),  $0.7 \pm 0.1$  (b CB H4-H5) Hz; **DOSY** (700 MHz, THF-*d*<sub>6</sub>, 273 K):  $D = (1.10 \pm 0.05) \cdot 10^{-9}$  (a),  $(1.1 \pm 0.1) \cdot 10^{-9}$  (b) m<sup>2</sup> s<sup>-1</sup>; **HRMS** (ESI<sup>+</sup>): C<sub>33</sub>H<sub>29</sub>NO<sub>3</sub>PPd [M-Cl]<sup>+</sup> requires 624.0914, found 624.0926 ( $\Delta = 1.9$  ppm); **HRMS** (ESI<sup>-</sup>): C<sub>33</sub>H<sub>29</sub>Cl<sub>2</sub>NO<sub>3</sub>PPd [M+Cl]<sup>-</sup> requires 694.0302, found 694.0312 ( $\Delta = 1.4$  ppm); C<sub>27</sub>H<sub>22</sub>CINOPPd [M-CB]<sup>-</sup> requires 548.0168, found 548.0178 ( $\Delta = 1.8$  ppm); C<sub>6</sub>H<sub>6</sub>CINO<sub>2</sub>PPd [M-L2-H]<sup>-</sup> requires 250.9097, found 250.9100 ( $\Delta = 1.3$  ppm). The spectroscopic data are consistent with those reported in the literature.<sup>32</sup> Due to signal overlap and the presence of excess dba, not all signals in the aromatic region could be assigned. The most characteristic NMR spectroscopic data are summarized in Table S6.



**Table S6.** Characteristic NMR data for *anti*-**6b**, species a (top) and b (bottom).

Position	$\delta_{\text{H}}$ / ppm	$\delta_{\text{C}}$ or $\delta_{\text{C}}$ or $\delta_{\text{C}}$ / ppm	Additional data
CB 1	–	173.4	
CB 2	3.75	56.1	$r_{\text{H2-H5}} \approx (3.02 \pm 0.05) \text{ \AA}$ ${}^3J_{\text{H2-H5}} = (1.1 \pm 0.1) \text{ Hz}$
CB 3	5.55	126.1	
CB 4	6.38	150.6	
CB 5	3.23	44.1	${}^3J_{\text{HP}} = 11.5 \text{ Hz}$ ${}^2J_{\text{CP}} = 2.9 \text{ Hz}$
P	–	32.1	
N	–	196.2	
CB 1	–	173.9	
CB 2	4.38	55.8	$r_{\text{H2-H5}} \approx (3.01 \pm 0.05) \text{ \AA}$ ${}^3J_{\text{H2-H5}} = (1.1 \pm 0.1) \text{ Hz}$
CB 3	5.56	127.9	
CB 4	5.58	149.0	
CB 5	3.31	44.6	${}^3J_{\text{HP}} = 8.8 \text{ Hz}$ ${}^2J_{\text{CP}} = 3.5 \text{ Hz}$
P	–	30.6	
N	–	196.9	

#### Oxidative Addition of Ester Substrate *trans*-**5** with Ligand **L1**



Oxidative addition of *trans*-methyl-4-chlorocyclobutene-2-carboxylic carboxylate *trans*-**5** with phosphoramidite ligand ( $S_{\text{ax}},S,S$ )-**L1** according to the general procedure gave a diastereomeric mixture of Pd-complexes *syn*-**6a**, with one species being highly enriched (d.r. = 84:16). Additionally, small amounts of *anti*-**6a** were formed (*syn:anti* = 88:12), featuring the same d.r. of 86:14 as after its selective preparation from substrate *cis*-**5** (*vide supra*). In contrast to its *anti*-analogue, *syn*-**6a** was found to have only one equivalent of ligand **L1** coordinated, which is located in *cis*-position relative to the cyclobutene ring according to the magnitude of the experimental  ${}^2J_{\text{CP}}$  and  ${}^3J_{\text{HP}}$  coupling constants.<sup>34-36</sup> Variation of the stoichiometry of **L1** (1 or 2 equiv.) was found not to affect the outcome of this reaction.

The relative configuration of *syn*-**6a** was derived from quantitative NOE data and confirmed by  ${}^3J_{\text{H2-H5}}$  coupling constants extracted from PSYCHEDELIC experiments. Since the carbonyl group experiences significant deshielding upon complex formation ( $\Delta\delta_{\text{C}} = 16.8$  ppm for major-*syn*-**6a**,  $\Delta\delta_{\text{C}} = 16.6$  ppm for minor-*syn*-**6a** compared to free *trans*-**1**), *syn*-**6a** is likely to be stabilized by internal Pd–O coordination,<sup>33</sup> thus requiring only 1 equiv. of **L1** for saturation of the coordination sphere. This effect was not observed for the corresponding *anti*-complexes *anti*-**6a**.

Although the 2D EASY-ROESY and NOESY spectra do not exhibit exchange cross-peaks, complexes *syn*-**6a** can be assumed to be in equilibrium due to their strong structural similarity to the corresponding acid complexes *syn*-**6a** for which equilibration could be evidenced (*vide supra*).

Given below are the characterization data for *syn*-**6a**; for characterization of *anti*-**6a** see its selective preparation (oxidative addition of ester substrate *cis*-**5** with ligand **L1**).

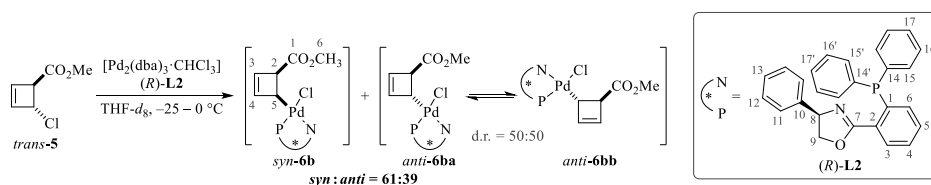
**<sup>1</sup>H-NMR** (700 MHz, THF-*d*<sub>8</sub>, 273 K):  $\delta_{\text{H}} = 8.60$  (1H, d,  ${}^3J_{\text{HH}} = 8.9$ , major L C(3)*H*), 8.56 (0.19H, d,  ${}^3J_{\text{HH}} = 8.9$ , minor L C(3)*H*), 8.13 (1H, d,  ${}^3J_{\text{HH}} = 8.9$ , major L C(4)*H*), 8.09 (0.19H, d,  ${}^3J_{\text{HH}} = 8.9$ , minor L C(4)*H*), 7.99 (1H, d,  ${}^3J_{\text{HH}} = 8.9$ , major L C(4')*H*), 6.92 (1H, d,  ${}^3J_{\text{HH}} = 8.9$ , major L C(3')*H*), 6.72 (0.19H, br. s, minor CB C(4)*H*), 5.80 (0.19H, br. s, minor CB C(3)*H*), 5.48 (0.38H, br. s, minor L C(e)*H*, C(e')*H*), 5.30 (1H, br. s, major CB C(3)*H*), 5.12–5.06 (2H, m, major L C(e)*H*, C(e')*H*), 4.96 (1H, d,  ${}^4J_{\text{HP}} = 2.2$ , major CB C(4)*H*), 3.83 (3H, s, major CB C(6)*H*s), 3.81 (0.57H, s, minor CB C(6)*H*s), 3.78 (0.19H, br. s, minor CB C(2)*H*), 3.74 (1H, d,  ${}^3J_{\text{HH}} \approx 3.0$ , major CB C(2)*H*), 3.54 (0.19H, br. s, minor CB C(5)*H*), 3.37 (1H,

d,  $^3J_{\text{HH}} \approx 3.0$ , major CB C(5)H), 1.87 (6H, d,  $^3J_{\text{HH}} = 7.1$ , major L C(f)H<sub>3</sub>, C(f')H<sub>3</sub>), 1.38 (1.14H, br. s, minor L C(f)H<sub>3</sub>, C(f')H<sub>3</sub>) ppm;  $^{13}\text{C}\{^1\text{H}\}$ -NMR (176 MHz, THF-*d*<sub>8</sub>, 273 K):  $\delta_{\text{C}} = 187.5$  (major CB C(1)), 187.3 (minor CB C(1)), 151.8 (minor CB C(4)), 151.6 (d,  $^3J_{\text{CP}} = 3.3$ , major CB C(4)), 150.3 (br. s, major L C(1')), 149.8 (d,  $^2J_{\text{CP}} = 4.5$ , major L C(1)), 142.3 (d,  $^3J_{\text{CP}} = 3.7$ , major L C(a), C(a')), 141.8 (br. s, minor L C(a), C(a')), 131.6 (major L C(4)), 131.0 (major L C(4')), 129.4 (minor L C(4)), 127.0 (minor CB C(3)), 126.3 (d,  $^4J_{\text{CP}} = 9.2$ , major CB C(3)), 125.3 (major L C(3)), 125.2 (minor L C(3)), 122.6 (major L C(3')), 58.7 (br. s, minor CB C(2)), 58.1 (d,  $^3J_{\text{CP}} = 3.8$ , major CB C(2)), 56.9 (br. s, minor L C(e), C(e')), 56.3 (d,  $^2J_{\text{CP}} = 7.6$ , major L C(e), C(e')), 55.3 (major + minor CB C(6)), 44.6 (br. s, minor CB C(5)), 43.8 (d,  $^2J_{\text{CP}} = 16.5$ , major CB C(5)), 21.9 (br. s, minor L C(f), C(f')), 21.5 (br. s, major L C(f), C(f')) ppm;  $^{31}\text{P}\{^1\text{H}\}$ -NMR (283 MHz, THF-*d*<sub>8</sub>, 273 K):  $\delta_{\text{P}} = 132.4$  (0.19P, s, minor), 130.6 (1P, s, major) ppm; **ID ROE** (700 MHz, THF-*d*<sub>8</sub>, 273 K):  $r_{\text{HH}} = 2.55 \pm 0.05$  (major CB H2-H5), 2.865 (major CB H3-H4, reference<sup>33</sup>),  $2.92 \pm 0.05$  (major CB H2-H3),  $2.92 \pm 0.05$  (major CB H4-H5),  $4.0 \pm 0.1$  (major CB H3-H5),  $2.6 \pm 0.1$  (minor CB H2-H5), 2.865 (minor CB H3-H4, reference<sup>33</sup>),  $2.8 \pm 0.1$  (minor CB H2-H3),  $4.2 \pm 0.2$  (minor CB H2-H4),  $4.4 \pm 0.2$  (minor CB H3-H6) Å; **PSYCHEDELICs** (700 MHz, THF-*d*<sub>8</sub>, 273 K):  $J_{\text{HH}} = 2.9 \pm 0.1$  (major CB H2-H5),  $0.6 \pm 0.2$  (major CB H4-H5),  $0.6 \pm 0.1$  (major CB H3-H5) Hz; **DOSY** (700 MHz, THF-*d*<sub>8</sub>, 273 K):  $D = (5.12 \pm 0.02) \cdot 10^{-10}$  (major-*syn*),  $(5.05 \pm 0.04) \cdot 10^{-10}$  (minor-*syn*),  $(4.40 \pm 0.05) \cdot 10^{-10}$  (major-*anti*) m<sup>2</sup> s<sup>-1</sup>; **HRMS** (ESI<sup>+</sup>): C<sub>42</sub>H<sub>37</sub>N<sub>4</sub>O<sub>4</sub>PPd [M-Cl]<sup>+</sup> requires 756.1490, found 756.1511 ( $\Delta = 2.8$  ppm). Due to signal overlap and the presence of excess dba, not all signals in the aromatic region could be assigned. The most characteristic NMR spectroscopic data are summarized in Table S7.

**Table S7.** Characteristic NMR data for complexes major- (top) and minor- (bottom) *syn*-6a.

Position	$\delta_{\text{C}} / \text{ppm}$	$\delta_{\text{C}}$ or $\delta_{\text{P}} / \text{ppm}$	Additional data
CB 1	–	187.5	
CB 2	3.74	58.1	$r_{\text{H2-H5}} \approx (2.55 \pm 0.05)$ Å $^3J_{\text{H2-H5}} = (2.9 \pm 0.1)$ Hz
CB 3	5.30	126.3	
CB 4	4.96	151.6	
CB 5	3.37	43.8	$^2J_{\text{CP}} = 16.5$ Hz
P	–	130.6	
CB 1	–	187.3	
CB 2	3.78	58.7	$r_{\text{H2-H5}} \approx (2.6 \pm 0.1)$ Å
CB 3	5.80	127.0	
CB 4	6.72	151.8	
CB 5	3.54	44.6	
P	–	132.4	

#### Oxidative Addition of Ester Substrate *trans*-5 with Ligand L2



Oxidative addition of *trans*-methyl-4-chlorocyclobutene-2-enecarboxylate *trans*-5 with PHOX ligand (*R*)-L2 according to the general procedure gave a mixture of Pd-complexes *syn*-6b and *anti*-6b (*syn:anti* = 61:39). *Syn*-6b was obtained as a single diastereomer, with no detectable amount of the corresponding minor species. *Anti*-6b, on the other hand, was obtained with a d.r. of 50:50, identical to the value obtained after its selective preparation from substrate *cis*-5 (*vide supra*). From the magnitude of the  $^2J_{\text{CP}}$  coupling constant extracted for *syn*-6b, the phosphine site can be concluded to be in *cis*-position relative to the cyclobutene ring.<sup>34–36</sup>

The relative configuration of *syn*-6b was derived from quantitative NOE data and confirmed by  $^3J_{\text{H2-H5}}$  coupling constants extracted from PSYCHEDELIC experiments. In contrast to the corresponding phosphoramidite complexes *syn*-6a, the carboxy group of *syn*-6b has a similar chemical shift as in the corresponding *anti*-complexes *anti*-6b ( $\delta_{\text{C}} = 174.8$  ppm for *syn*-6b, 173.4 ppm for *anti*-6ba, 173.9 ppm for *anti*-6bb), and does accordingly not experience significant deshielding upon complex formation ( $\Delta\delta_{\text{C}} = 4.0$  ppm compared to free *trans*-6b). Thus, there is no experimental evidence for *syn*-6b being stabilized by a significant contribution of internal Pd–O coordination.

Given below are the characterization data for *syn-6b*; for characterization of *anti-6b* see its selective preparation (oxidative addition of ester substrate *syn-6b* with ligand **L2**).

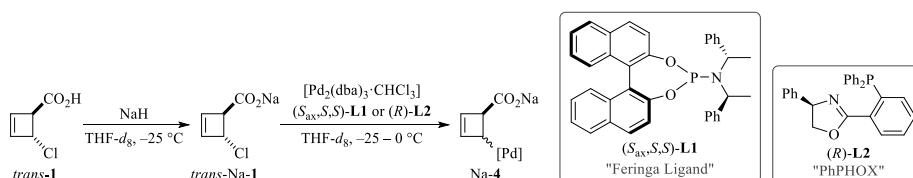
**<sup>1</sup>H-NMR** (700 MHz, THF-*d*<sub>8</sub>, 253 K): δ<sub>H</sub> = 8.16 (1H, dd, <sup>3</sup>J<sub>HH</sub> = 7.8, <sup>4</sup>J<sub>HH</sub> = 4.0, L C(3)*H*), 7.70 – 7.67 (1H, m, L C(4)*H*), 7.60 – 7.57 (1H, m, L C(5)*H*), 7.10 – 7.08 (1H, m, L C(6)*H*), 6.55 (1H, dd, <sup>3</sup>J<sub>HH</sub> = 10.0, <sup>3</sup>J<sub>HH</sub> = 4.5, L C(8)*H*), 5.51 (1H, d, <sup>3</sup>J<sub>HH</sub> = 2.6, CB C(3)*H*), 5.17 (1H, d, <sup>3</sup>J<sub>HH</sub> = 2.6, CB C(4)*H*), 4.69 (1H, dd, <sup>3</sup>J<sub>HH</sub> = 10.0, <sup>2</sup>J<sub>HH</sub> = 8.8, L C(9)*HH*<sub>trans</sub>), 4.33 (1H, dd, <sup>2</sup>J<sub>HH</sub> = 8.8, <sup>3</sup>J<sub>HH</sub> = 4.5, L C(9)*HH*<sub>cis</sub>), 3.57 – 3.55 (1H, m, CB C(5)*H*), 3.45 (1H, dd, <sup>3</sup>J<sub>HH</sub> = 3.7, <sup>3</sup>J<sub>HH</sub> = 0.9, CB C(2)*H*), 3.22 (3H, s, CB C(6)*H*<sub>5</sub>) ppm; **<sup>13</sup>C{<sup>1</sup>H}-NMR** (176 MHz, THF-*d*<sub>8</sub>, 253 K): δ<sub>C</sub> = 174.8 (CB C(1)), 162.8 (d, <sup>3</sup>J<sub>CP</sub> = 3.4, L C(7)), 150.0 (d, <sup>4</sup>J<sub>CP</sub> = 4.6, CB C(4)), 141.8 (L C(10)), 134.5 (br. s, L C(6)), 133.1 (br. s, L C(5)), 132.7 (d, <sup>3</sup>J<sub>CP</sub> = 7.2, L C(3)), 131.8 (br. s, L C(4)), 127.9 (br. s, CB C(3)), 75.5 (L C(9)), 68.8 (L C(8)), 50.6 (CB C(6)), 50.5 (br. s, CB C(2)), 42.3 (d, <sup>2</sup>J<sub>CP</sub> = 4.6, CB C(5)) ppm; **<sup>15</sup>N-NMR** (71 MHz, THF-*d*<sub>8</sub>, 253 K): δ<sub>N</sub> = 192.3 ppm; **<sup>31</sup>P{<sup>1</sup>H}-NMR** (283 MHz, THF-*d*<sub>8</sub>, 253 K): δ<sub>P</sub> = 28.8 (s) ppm; **1D ROE** (700 MHz, THF-*d*<sub>8</sub>, 253 K): *r*<sub>H2-H5</sub> = 2.63 ± 0.05 (CB H2-H5), 2.97 ± 0.05 (CB H4-H5), 4.1 ± 0.2 (CB H3-H5), 1.783 (L H9<sub>cis</sub>-H9<sub>trans</sub>, reference from DFT structure) Å; **PSYCHEDELICS** (700 MHz, THF-*d*<sub>8</sub>, 253 K): *J*<sub>HH</sub> = 3.7 ± 0.1 (CB H2-H5), 0.9 ± 0.1 (CB H2-H3) Hz; **DOSY** (700 MHz, THF-*d*<sub>8</sub>, 253 K): *D* = (5.0 ± 0.1) · 10<sup>-10</sup> (*syn*), (5.0 ± 0.1) · 10<sup>-10</sup> (*anti* a), (5.0 ± 0.1) · 10<sup>-10</sup> (*anti* b) m<sup>2</sup> s<sup>-1</sup>; **HRMS** (ESI<sup>+</sup>): C<sub>33</sub>H<sub>29</sub>NO<sub>3</sub>PPd [M-Cl]<sup>+</sup> requires 624.0914, found 624.0928 (Δ = 2.2 ppm); **HRMS** (ESI<sup>-</sup>): C<sub>27</sub>H<sub>22</sub>ClNO<sub>3</sub>PPd [M-Cl]<sup>-</sup> requires 548.0168, found 548.0168 (Δ = 0). Due to signal overlap and the presence of excess dba, not all signals in the aromatic region could be assigned. The most characteristic NMR spectroscopic data are summarized in Table S8.

**Table S8.** Characteristic NMR data for complex *syn-6b*.

Position	δ <sub>H</sub> / ppm	δ <sub>C</sub> or δ <sub>P</sub> or δ <sub>N</sub> / ppm	Additional data
CB 1	–	174.8	
CB 2	3.45	50.5	<i>r</i> <sub>H2-H5</sub> ≈ (2.63 ± 0.05) Å <sup>3</sup> <i>J</i> <sub>H2-H5</sub> = (3.7 ± 0.1) Hz
CB 3	5.51	127.9	
CB 4	5.17	150.0	
CB 5	3.56	42.3	<sup>2</sup> <i>J</i> <sub>CP</sub> = 4.6 Hz
P	–	28.8	
N	–	192.3	

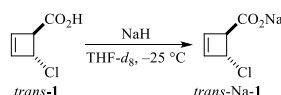
## Oxidative Addition of Carboxylate Substrates

### General Procedure



To a suspension of NaH (90 w%, 2.0 mg, 75 μmol, 1.5 equiv.) in anhydrous THF-*d*<sub>8</sub> (0.3 mL) was added dropwise a solution of *trans*-4-chlorocyclobutene-2-enecarboxylic acid *trans*-**1** (6.6 mg, 50 μmol, 1 equiv.) in anhydrous THF-*d*<sub>8</sub> (0.3 mL) at approximately –25 °C without stirring. The mixture was allowed to stand at –25 °C until no more gas evolution was observed. [Pd<sub>2</sub>(dba)<sub>3</sub>·CHCl<sub>3</sub>] (25.9 mg, 25 μmol, 0.5 equiv.) and ligand (*S*<sub>ax</sub>,*S*<sub>S</sub>)-**L1** (54.0 mg, 100 μmol, 2 equiv.) or (*R*)-**L2** (20.4 mg, 50 μmol, 1 equiv.) were dissolved in anhydrous THF-*d*<sub>8</sub> (0.5 mL) and stirred at RT for 10 min. The solution was cooled to approximately –25 °C and the freshly prepared solution of deprotonated *trans*-**1** was added dropwise upon stirring vigorously. After further 5 min of stirring, one drop of the reaction mixture was taken for subsequent MS analysis, and the residual solution was transferred into a precooled NMR tube. The tube was sealed and centrifuged (2000 rpm, 1 min) prior to NMR analysis.

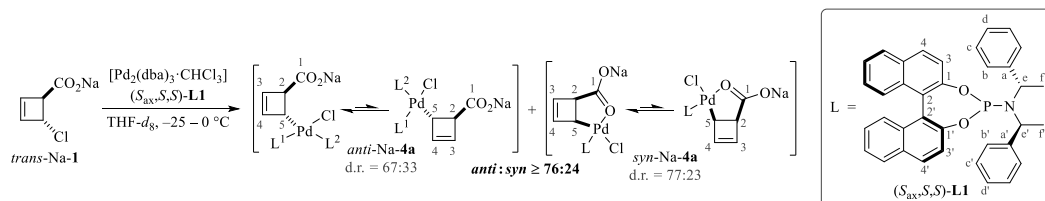
### Characterization of Carboxylate Substrate *trans*-Na-1



Carboxylate substrate *trans*-Na-**1** was prepared by deprotonation of acid *trans*-**1** according to the general procedure and characterized in solution. Attempts to isolate *trans*-Na-**1** were not successful, as it undergoes decomposition upon concentrating.

**<sup>1</sup>H-NMR** (400 MHz, THF-*d*<sub>8</sub>, 300 K):  $\delta_{\text{H}} = 6.35$  (1H, br. s, =CH-CClH-), 6.14 (1H, br. s, =CH-CH-CO<sub>2</sub><sup>-</sup>), 4.97 (1H, br. s, -CClH-), 3.51 (1H, br. s, -CH-CO<sub>2</sub><sup>-</sup>) ppm; **<sup>13</sup>C{<sup>1</sup>H}-NMR** (101 MHz, THF-*d*<sub>8</sub>, 300 K):  $\delta_{\text{C}} = 177.9$  (CO<sub>2</sub><sup>-</sup>), 141.0 (=CH-CClH-), 139.2 (=CH-CH-CO<sub>2</sub><sup>-</sup>), 63.0 (-CH-CO<sub>2</sub><sup>-</sup>), 59.1 (-CClH-) ppm; **HRMS** (ESI<sup>-</sup>): C<sub>5</sub>H<sub>4</sub>ClO<sub>2</sub> [M-Na]<sup>-</sup> requires 130.9905, found 130.9903 ( $\Delta = -1.5$  ppm).

#### Oxidative Addition of Carboxylate Substrate *trans*-Na-1 with Ligand L1



Deprotonation of *trans*-4-chlorocyclobutene-2-encarboxylic acid *trans*-1 and subsequent oxidative addition with phosphoramidite ligand (*S,S,S,S*)-L1 according to the general procedure gave a mixture of Pd-complexes *syn*-Na-4a and *anti*-Na-4a. *Anti*-Na-4a was found to be unstable and decomposed upon characterization, with a constant d.r. of 67:33 throughout its detectability. The concentration maximum of both *anti*-species was reached ca. 13 min after preparation of the reaction mixture (see also section 5), and a *anti:syn* ratio of ca. 76:24 was determined at this time. *Syn*-Na-4a, on the other hand, turned out to be stable, and slowly equilibrated to d.r. = 77:23 over ca. 6 h. The connectivity of all four Pd-species was found to be analogous to their protonated forms *anti*-4a and *syn*-4a. *Anti*-Na-4a has two equivalents of ligand L1 coordinated, located in *cis*- and *trans*-position relative to the cyclobutene ring, respectively, according to the magnitude of the experimental <sup>2</sup>J<sub>PP</sub>, <sup>2</sup>J<sub>CP</sub> and <sup>3</sup>J<sub>HP</sub> coupling constants. *Syn*-Na-4a, in contrast, has only one equivalent of ligand L1 coordinated, which is located in *cis*-position relative to the cyclobutene ring according to the magnitude of the experimental <sup>2</sup>J<sub>CP</sub> coupling constants.<sup>34-36</sup>

The relative configuration of *syn*-Na-4a was derived from its quantitative NOE data and confirmed by its <sup>3</sup>J<sub>H2-H5</sub> coupling constant extracted from PSYCHEDELIC experiments. For *anti*-Na-4a, neither internuclear distances nor <sup>3</sup>J<sub>H2-H5</sub> coupling constants could be obtained, but the 2D EASY-ROESY spectrum shows a significantly weaker cross-peak between H2 and H5 compared to H2-H3, H3-H4 and H4-H5, which is consistent with an *anti*-relationship.

For *anti*-Na-4a, the 2D EASY-ROESY spectrum exhibits exchange cross-peaks between the major- and the minor-species, indicating that complexes *anti*-Na-4a are in equilibrium. For *syn*-Na-4a, on the other hand, no exchange cross-peaks were observed. However, the time dependence observed for the d.r. (50:50 → 77:23 over ca. 6 h) indicates complexes *syn*-Na-4a to be in equilibrium.

Chemical shifts of Na-4a generally tend to vary strongly between different batches. Therefore, internal Pd-O coordination cannot be concluded reliably from the <sup>13</sup>C-shifts of the carboxylate moiety of *syn*-Na-4a, as done for complexes prepared from neutral substrates 1 and 5. However, internal coordination has clearly been evidenced for the corresponding protonated complexes *syn*-4a (*vide supra*). Since the donor strength of the carboxylate function is even higher after deprotonation, internal coordination should accordingly be present also under basic conditions. These considerations are in line with the drastically decreased equilibration rate of *syn*-Na-4a compared to *anti*-Na-4a, consistent with a strong internal Pd-O coordination which has to be broken prior to interconversion between the η<sup>1</sup>-species and thus increases the energy barrier.

**<sup>1</sup>H-NMR** (600 MHz, THF-*d*<sub>8</sub>, 273 K):  $\delta_{\text{H}} = 8.68$  (d, <sup>3</sup>J<sub>HH} = 8.8, \text{minor-anti L}^1 \text{C(3)H}), 8.63 (d, <sup>3</sup>J<sub>HH} = 8.9, \text{major-syn L C(3)H}), 8.63 (d, <sup>3</sup>J<sub>HH} = 8.9, \text{minor-syn L C(3)H}), 8.33 (d, <sup>3</sup>J<sub>HH} = 8.8, \text{major-anti L}^1 \text{C(3)H, L}^2 \text{C(4)H}), 8.25 (d, <sup>3</sup>J<sub>HH} = 8.8, \text{minor-anti L}^2 \text{C(4)H}), 8.11 (d, <sup>3</sup>J<sub>HH} = 8.9, \text{minor-anti L}^1 \text{C(4')H}), 8.10 (d, <sup>3</sup>J<sub>HH} = 8.9, \text{major-anti L}^1 \text{C(4')H}), 8.08 (d, <sup>3</sup>J<sub>HH} = 8.9, \text{minor-syn L C(4')H}), 8.05 (d, <sup>3</sup>J<sub>HH} = 8.9, \text{major-syn L C(4)H}), 8.05 (d, <sup>3</sup>J<sub>HH} = 8.9, \text{minor-syn L C(4)H}), 8.02 (d, <sup>3</sup>J<sub>HH} = 8.8, \text{major-anti L}^1 \text{C(4)H}), 7.97 (d, <sup>3</sup>J<sub>HH} = 8.8, \text{major-syn L C(4')H}), 7.90 (d, <sup>3</sup>J<sub>HH} = 8.8, \text{minor-anti L}^1 \text{C(4)H}), 7.88 (d, <sup>3</sup>J<sub>HH} = 8.8, \text{major-anti L}^2 \text{C(3)H}), 7.85 (d, <sup>3</sup>J<sub>HH} = 8.9, \text{major-anti L}^2 \text{C(3')H}), 7.78 (d, <sup>3</sup>J<sub>HH} = 8.9, \text{major-anti L}^1 \text{C(3')H}), 7.68 (d, <sup>3</sup>J<sub>HH} = 8.8, \text{minor-anti L}^2 \text{C(3)H}), 7.67 (d, <sup>3</sup>J<sub>HH} = 8.9, \text{minor-anti L}^2 \text{C(4')H}), 7.64 (d, <sup>3</sup>J<sub>HH} = 8.9, \text{minor-anti L}^1 \text{C(3')H}), 7.57 (d, <sup>3</sup>J<sub>HH} = 8.9, \text{minor-syn L C(3')H}), 7.21 (d, <sup>3</sup>J<sub>HH} = 8.9, \text{major-anti L}^2 \text{C(4')H}), 7.02 (d, <sup>3</sup>J<sub>HH} = 8.9, \text{minor-anti L}^2 \text{C(3')H}), 6.92 (d, <sup>3</sup>J<sub>HH} = 8.8, \text{major-syn L C(3')H}), 6.67 (br. d, <sup>3</sup>J<sub>HH} = 2.5, \text{minor-syn CB C(4)H}), 6.29 (br. d, <sup>3</sup>J<sub>HP} = 2.2, \text{minor-anti CB C(4)H}), 6.21 (br. s, \text{major-anti CB C(3)H}), 6.19 (br. d, <sup>3</sup>J<sub>HP} = 2.7, \text{minor-anti CB C(3)H}), 5.90 (br. s, \text{minor-syn CB C(3)H}), 5.75 (br. s, \text{major-anti CB C(4)H}), 5.59 (br. s, \text{minor-syn L C(e)H, C(e')H}), 5.39 (br. s, \text{major-syn CB C(3)H}), 5.24 (dq, <sup>3</sup>J<sub>HP} = 15.3, <sup>3</sup>J<sub>HH} = 7.0, \text{major-syn L C(e)H, C(e')H}), 4.94 (br. d, <sup>3</sup>J<sub>HH} = 1.9, \text{major-syn CB C(4)H}), 4.92 - 4.82 (m, \text{major- + minor-anti L C(e)H, C(e')H}), 3.80 (br. s, \text{minor-anti CB C(2)H}), 3.78 (br. s, \text{major-anti CB C(2)H}), 3.52 (br. d, <sup>3</sup>J<sub>HP} = 12.4, \text{major-anti CB C(5)H}), 3.47 (d, <sup>3</sup>J<sub>HH} ≈ 2.9, \text{major-syn CB C(2)H}), 3.45 (d, <sup>3</sup>J<sub>HH} ≈ 3.1, \text{minor-syn CB C(2)H}), 3.39 (br. d, <sup>3</sup>J<sub>HP} ≈ 12, \text{major-syn CB C(5)H}), 3.38 (br. d, <sup>3</sup>J<sub>HP} ≈ 11, \text{minor-syn CB C(5)H}), 3.04 (br. d, <sup>3</sup>J<sub>HP} = 16.6, \text{minor-anti CB C(5)H}), 1.76 (d, <sup>3</sup>J<sub>HH} = 7.0, \text{major-syn L C(f)H}\_3, \text{C(f')H}\_3}), 1.33 (d, <sup>3</sup>J<sub>HH} = 7.1, \text{minor-syn L C(f)H}\_3, \text{C(f')H}\_3}), 0.69 (d, <sup>3</sup>J<sub>HH} = 7.1, \text{minor-anti L C(f)H}\_3, \text{C(f')H}\_3}), 0.62 (d, <sup>3</sup>J<sub>HH} = 7.1, \text{major-anti L C(f)H}\_3, \text{C(f')H}\_3}) ppm (accurate integration of the 1H resonances was not possible); **<sup>13</sup>C{<sup>1</sup>H}-NMR** (151 MHz, THF-*d*<sub>8</sub>, 273 K):  $\delta_{\text{C}} = 185.0$  (major-syn CB C(1)), 184.4 (minor-syn CB C(1)), 183.0 (minor-anti CB C(1)), 182.6 (major-anti CB C(1)), 151.3 (br. s, \text{minor-syn L C(1')}), 150.8 (br. s, \text{major-anti L}^1 \text{C(1')}), 150.7 (br. s, \text{major-anti L}^2 \text{C(1')}), 150.7 (br. s, \text{major-syn L C(1')}), 150.0 (br. s, \text{major-anti L}^1 \text{C(1)}), 149.5 (br. s, \text{minor-syn L C(1)}), 148.9 (br. s, \text{major-anti CB C(4)}), 148.8 (br. s, \text{minor-anti CB C(4)}), 148.8 (br. s, \text{major-syn L C(1)}), 148.5 (minor-syn CB C(4)), 148.5 (br. s, \text{major-syn CB C(4)}), 141.6 (minor-anti L<sup>1</sup> C(a), C(a')), 141.5 (major-anti L<sup>1</sup> C(a), C(a')), 133.6 (br. s, \text{minor-anti CB C(3)}), 132.1 (br. s, \text{major-anti CB C(3)}), 132.0 (major-anti L<sup>2</sup></sub></sub></sub></sub></sub></sub></sub></sub></sub></sub></sub></sub></sub></sub></sub></sub></sub></sub></sub></sub></sub></sub></sub></sub></sub></sub></sub></sub></sub></sub></sub></sub></sub></sub></sub></sub></sub></sub></sub>

C(3')), 131.8 (minor-*anti* L<sup>2</sup> C(4)), 131.8 (major-*anti* L<sup>2</sup> C(4)), 131.4 (major-*anti* L<sup>1</sup> C(4')), 131.2 (major-*anti* L<sup>1</sup> C(4)), 131.2 (major-*syn* L C(4)), 131.2 (minor-*syn* L C(4)), 130.8 (major-*syn* L C(4')), 130.8 (minor-*syn* L C(4')), 130.5 (minor-*syn* CB C(3)), 129.4 (major-*syn* CB C(3)), 129.0 (minor-*anti* L<sup>1</sup> C(b), C(b')), 128.7 (major-*anti* L<sup>1</sup> C(b), C(b')), 127.0 (major-*anti* L<sup>2</sup> C(4')), 125.8 (major-*syn* L C(3)), 125.8 (minor-*syn* L C(3)), 125.0 (major-*anti* L<sup>1</sup> C(3)), 123.1 (major-*syn* L C(3')), 122.9 (minor-*syn* L C(3')), 122.2 (major-*anti* L<sup>2</sup> C(3)), 121.9 (major-*anti* L<sup>1</sup> C(3')), 60.4 (d, <sup>3</sup>J<sub>CP</sub> ≈ 2.8, minor-*syn* CB C(2)), 60.1 (d, <sup>3</sup>J<sub>CP</sub> ≈ 2.5, major-*syn* CB C(2)), 58.9 (br. s, minor-*anti* CB C(2)), 58.6 (br. s, major-*anti* CB C(2)), 56.4 (d, <sup>2</sup>J<sub>CP</sub> = 12.6, minor-*syn* L C(e), C(e')), 56.1 (br. s, minor-*anti* L<sup>1</sup> C(e), C(e')), 55.9 (d, <sup>2</sup>J<sub>CP</sub> = 9.7, major-*anti* L C(e), C(e')), 55.7 (br. s, major-*anti* L<sup>1</sup> C(e), C(e')), 45.0 (dd, <sup>2</sup>J<sub>CP</sub> ≈ 126, <sup>2</sup>J<sub>CP</sub> ≈ 14, minor-*anti* CB C(5)), 43.9 (dd, <sup>2</sup>J<sub>CP</sub> ≈ 125, <sup>2</sup>J<sub>CP</sub> ≈ 9, major-*anti* CB C(5)), 41.4 (d, <sup>2</sup>J<sub>CP</sub> ≈ 13.7, minor-*syn* CB C(5)), 41.2 (d, <sup>2</sup>J<sub>CP</sub> = 12.8, major-*syn* CB C(5)), 22.0 (br. s, minor-*syn* L C(f), C(f')), 21.9 (br. s, major-*syn* L C(f), C(f')), 20.9 (br. s, minor-*anti* L<sup>1</sup> C(f), C(f')), 20.6 (br. s, major-*anti* L<sup>1</sup> C(f), C(f')) ppm; <sup>31</sup>P{<sup>1</sup>H}-NMR (243 MHz, THF-*d*<sub>8</sub>, 273 K): δ<sub>P</sub> = 147.6 (1P, d, <sup>2</sup>J<sub>PP</sub> = 103.5, major-*anti* L<sup>1</sup>), 147.3 (0.49P, d, <sup>2</sup>J<sub>PP</sub> = 102.0, minor-*anti* L<sup>1</sup>), 144.1 (1P, d, <sup>2</sup>J<sub>PP</sub> = 103.5, major-*anti* L<sup>2</sup>), 143.4 (0.49P, d, <sup>2</sup>J<sub>PP</sub> = 102.0, minor-*anti* L<sup>2</sup>), 140.8 (0.11P, br. s, minor-*syn*), 139.1 (0.37P, br. s, major-*syn*) ppm; **ID NOE** (600 MHz, THF-*d*<sub>8</sub>, 273 K): r<sub>HH</sub> = 2.51 ± 0.05 (major-*syn* CB H2-H5), 2.90 ± 0.05 (major-*syn* CB H4-H5), 2.865 (major-*syn* CB H3-H4, reference<sup>33</sup>), 2.53 ± 0.05 (minor-*syn* CB H2-H5), 2.88 ± 0.05 (minor-*syn* CB H2-H3), 2.865 (minor-*syn* CB H3-H4, reference<sup>33</sup>) Å; **PSYCHEDELICs** (600 MHz, THF-*d*<sub>8</sub>, 273 K): J<sub>HH</sub> ≈ 2.9 ± 0.4 (major-*syn* CB H2-H5), 3.1 ± 0.3 (minor-*syn* CB H2-H5), 0.6 ± 0.2 (minor-*syn* CB H4-H5) Hz; **HRMS** (ESI<sup>+</sup>): C<sub>77</sub>H<sub>65</sub>N<sub>2</sub>O<sub>6</sub>P<sub>2</sub>Pd [M-NaCl+H]<sup>+</sup> of *anti* requires 1281.3347, found 1281.3407 (Δ = 4.7 ppm), C<sub>41</sub>H<sub>34</sub>ClNO<sub>4</sub>PPd [M-NaCl+H]<sup>+</sup> of *syn* or [M-L-NaCl+H]<sup>+</sup> of *anti* requires 776.0954, found 776.0954 (Δ = 0). Due to signal overlap and the presence of excess dba, not all signals in the aromatic region could be assigned. NMR analysis was generally complicated by the low spectral quality. The most characteristic NMR spectroscopic data are summarized in Table S9 (*anti*-Na-4a) and Table S10 (*syn*-Na-4a).

**Table S9.** Characteristic NMR data for complexes major- (top) and minor- (bottom) *anti*-Na-4a.

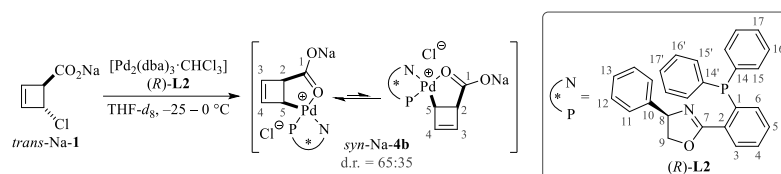
Position	δ <sub>H</sub> / ppm	δ <sub>C</sub> or δ <sub>C'</sub> / ppm	Additional data
CB 1	–	182.6	
CB 2	3.78	58.6	
CB 3	6.21	132.1	
CB 4	5.75	148.9	
CB 5	3.52	43.9	<sup>3</sup> J <sub>HP</sub> = 12.4 Hz <sup>2</sup> J <sub>CP</sub> = 125, 9 Hz
L <sub>1</sub> P	–	147.6	
L <sub>2</sub> P	–	144.1	<sup>2</sup> J <sub>PP</sub> = 103.5 Hz
CB 1	–	183.0	
CB 2	3.80	58.9	
CB 3	6.19	133.6	
CB 4	6.29	148.8	
CB 5	3.04	45.0	<sup>3</sup> J <sub>HP</sub> = 16.6 Hz <sup>2</sup> J <sub>CP</sub> ≈ 126, 14 Hz
L <sub>1</sub> P	–	147.3	
L <sub>2</sub> P	–	143.4	<sup>2</sup> J <sub>PP</sub> = 102.0 Hz

**Table S10.** Characteristic NMR data for complexes major- (top) and minor- (bottom) *syn*-Na-4a.

Position	δ <sub>H</sub> / ppm	δ <sub>C</sub> or δ <sub>C'</sub> / ppm	Additional data
CB 1	–	185.0	
CB 2	3.47	60.1	r <sub>H2-H5</sub> ≈ (2.51 ± 0.05) Å <sup>3</sup> J <sub>H2-H5</sub> = (2.9 ± 0.4) Hz
CB 3	5.39	129.4	
CB 4	4.95	148.5	
CB 5	3.39	41.2	<sup>3</sup> J <sub>HP</sub> ≈ 12 Hz <sup>2</sup> J <sub>CP</sub> = 12.8 Hz
P	–	139.1	

CB 1	–	184.4	
CB 2	3.45	60.4	$r_{H2-H5} \approx (2.53 \pm 0.05) \text{ \AA}$ $^3J_{H2-H5} = (3.1 \pm 0.3) \text{ Hz}$
CB 3	5.90	130.5	
CB 4	6.67	148.5	
CB 5	3.38	41.4	$^3J_{HP} \approx 11 \text{ Hz}$ $^3J_{CP} \approx 13.7 \text{ Hz}$
P	–	140.8	

### Oxidative Addition of Carboxylate Substrate *trans*-Na-1 with Ligand L2



Deprotonation of *trans*-4-chlorocyclobutene-2-enecarboxylic acid *trans*-1 and subsequent oxidative addition with PHOX ligand (*R*)-L2 according to the general procedure gave Pd-complexes *syn*-Na-4b, along with large amounts of unidentified impurities which are believed to originate from decomposition of the unstable corresponding *anti*-complex *anti*-Na-4b. Equilibration of *syn*-Na-4b was found to be sluggish, taking approximately 57 h to reach the end-point d.r. of 65:35. From the magnitude of the experimental  $^2J_{CP}$  and  $^3J_{HP}$  coupling constants, the phosphine site can be concluded to be in *cis*-position relative to the cyclobutene ring.<sup>34-36</sup> The relative configuration of the cyclobutene ring was derived from quantitative ROE data and confirmed by  $^3J_{H2-H5}$  coupling constants extracted from PSYCHEDELIC experiments.

Although the 2D EASY-ROESY and NOESY spectra do not exhibit exchange cross-peaks, the time dependence observed for the d.r. (d.r. = 50:50  $\rightarrow$  65:35 over ca. 57 h) indicates complexes *syn*-Na-4b to be in equilibrium.

Chemical shifts of *syn*-Na-4b generally tend to vary strongly between different batches. Therefore, internal Pd–O coordination cannot be concluded reliably from the  $^{13}C$ -shifts of the carboxylate moiety, as done for complexes prepared from neutral substrates 1 and 5. However, internal coordination has clearly been evidenced for the corresponding protonated complexes *syn*-4b (*vide supra*). Since the donor strength of the carboxylate function is even higher after deprotonation, internal coordination should accordingly be present also under basic conditions. These considerations are in line with the very low equilibration rate of *syn*-Na-4b, consistent with an internal Pd–O coordination which has to be broken prior to interconversion between the  $\eta^1$ -species and thus increases the energy barrier.

**$^1H$ -NMR** (700 MHz, THF-*d*<sub>8</sub>, 273 K):  $\delta_H = 8.24$  (1H, dd,  $^3J_{HH} = 7.6$ ,  $^4J_{HH} = 4.1$ , major L C(3)*H*), 8.19 (0.54H, dd,  $^3J_{HH} = 7.7$ ,  $^4J_{HH} = 4.1$ , minor L C(3)*H*), 7.72–7.70 (1H, m, major L C(4)*H*), 7.69–7.68 (0.54H, m, minor L C(4)*H*), 7.46–7.41 (1.54H, m, major + minor L C(13)*H*), 7.27–7.22 (3.08H, m, major + minor L C(12)*H*), 7.17–7.13 (3.08H, m, major + minor L C(11)*H*), 6.02 (1H, dd,  $^3J_{HH} = 9.8$ ,  $^3J_{HH} = 4.0$ , major L C(8)*H*), 5.93 (0.54H, dd,  $^3J_{HH} = 9.8$ ,  $^3J_{HH} = 4.1$ , minor L C(8)*H*), 5.84 (0.54H, d,  $^3J_{HH} = 2.3$ , minor CB C(4)*H*), 5.80 (0.54H, br. s, minor CB C(3)*H*), 5.79 (1H, br. s, major CB C(3)*H*), 5.32 (1H, d,  $^3J_{HH} = 2.3$ , major CB C(4)*H*), 4.75–4.69 (1.54H, m, major + minor L C(9)*HH*<sub>trans</sub>), 4.65 (0.54H, dd,  $^2J_{HH} = 9.0$ ,  $^3J_{HH} = 4.4$ , minor L C(9)*HH*<sub>cis</sub>), 4.57 (1H, dd,  $^2J_{HH} = 8.9$ ,  $^3J_{HH} = 4.3$ , major L C(9)*HH*<sub>cis</sub>), 3.51 (0.54H, dd,  $^3J_{HH} = 2.9$ ,  $^3J_{HH} = 1.2$ , minor CB C(2)*H*), 3.44 (1H, dd,  $^3J_{HH} = 2.9$ ,  $^3J_{HH} = 1.1$ , major CB C(2)*H*), 2.59 (1H, dd,  $^3J_{HP} = 9.8$ ,  $^3J_{HH} = 2.9$ , major CB C(5)*H*), 2.30 (0.54H, dd,  $^3J_{HP} = 10.0$ ,  $^3J_{HH} = 2.9$ , minor CB C(5)*H*) ppm;  **$^{13}C\{^1H\}$ -NMR** (176 MHz, THF-*d*<sub>8</sub>, 273 K):  $\delta_C = 181.8$  (br. s, minor CB C(1)), 181.6 (br. s, major CB C(1)), 163.1 (d,  $^3J_{CP} = 3.2$ , major L C(7)), 162.9 (d,  $^3J_{CP} = 3.1$ , minor L C(7)), 146.3 (br. s, minor CB C(4)), 145.8 (br. s, major CB C(4)), 142.3 (major L C(10)), 142.0 (minor L C(10)), 133.2 (d,  $^3J_{CP} \approx 7.7$ , minor L C(3)), 133.1 (d,  $^3J_{CP} \approx 7.6$ , major L C(3)), 132.5 (major L C(4)), 132.4 (minor L C(4)), 131.7 (d,  $^3J_{CP} = 2.3$ , major CB C(3)), 131.1 (d,  $^3J_{CP} = 2.6$ , minor CB C(3)), 129.4 (minor L C(13)), 129.4 (major L C(13)), 129.4 (minor L C(11)), 129.4 (major L C(11)), 75.8 (major L C(9)), 75.4 (minor L C(9)), 60.6 (br. s, major CB C(2)), 60.5 (br. s, minor CB C(2)), 41.9 (d,  $^2J_{CP} = 2.9$ , minor CB C(5)), 37.5 (d,  $^2J_{CP} = 2.9$ , major CB C(5)) ppm;  **$^{15}N$ -NMR** (71 MHz, THF-*d*<sub>8</sub>, 273 K):  $\delta_N = 196.5$  (minor), 194.6 (major) ppm;  **$^{31}P\{^1H\}$ -NMR** (283 MHz, THF-*d*<sub>8</sub>, 273 K):  $\delta_P = 32.1$  (1P, br. s, major), 31.3 (0.54P, br. s, minor) ppm; **ID ROE** (700 MHz, THF-*d*<sub>8</sub>, 273 K):  $r_{HH} = 2.56 \pm 0.05$  (major CB H2-H5), 2.865 (major CB H3-H4, reference<sup>33</sup>),  $3.0 \pm 0.1$  (major CB H2-H3),  $2.9 \pm 0.1$  (major CB H4-H5),  $4.1 \pm 0.2$  (major CB H2-H4),  $4.1 \pm 0.1$  (major CB H3-H5),  $2.58 \pm 0.05$  (minor CB H2-H5), 2.865 (minor CB H3-H4, reference<sup>33</sup>),  $3.0 \pm 0.1$  (minor CB H2-H3),  $2.9 \pm 0.1$  (minor CB H4-H5),  $4.2 \pm 0.2$  (minor CB H2-H4),  $4.1 \pm 0.1$  (minor CB H3-H5) Å (ROEs of minor species referenced externally to major CB H3-H4); **PSYCHEDELICs** (700 MHz, THF-*d*<sub>8</sub>, 273 K):  $J_{HH} = 2.9 \pm 0.1$  (major CB H2-H5),  $1.3 \pm 0.1$  (major CB H2-H3),  $0.7 \pm 0.1$  (major CB H4-H5),  $1.0 \pm 0.2$  (major CB H3-H5),  $2.9 \pm 0.1$  (minor CB H2-H5),  $1.3 \pm 0.1$  (minor CB H2-H3),  $0.6 \pm 0.1$  (minor CB H4-H5),  $0.5 \pm 0.2$  (minor CB H2-H4),  $1.4 \pm 0.2$  (minor CB H3-H5) Hz; **DOSY** (700 MHz, THF-*d*<sub>8</sub>, 273 K):  $D = (4.1 \pm 0.2) \cdot 10^{-10}$  (major),  $(4.1 \pm 0.2) \cdot 10^{-10}$  (minor) m<sup>2</sup> s<sup>-1</sup>; **HRMS** (ESI<sup>+</sup>): C<sub>32</sub>H<sub>27</sub>NO<sub>3</sub>PPd [M–NaCl+H]<sup>+</sup> requires 610.0758, found 610.0767 ( $\Delta = 1.6$  ppm). Due to signal overlap and the presence of excess dba, not all signals in the aromatic

region could be assigned. NMR analysis was generally complicated by the low spectral quality. The most characteristic NMR spectroscopic data are summarized in Table S11.

**Table S11.** Characteristic NMR data for complexes major- (top) and minor- (bottom) *anti*-Na-4b.

Position	$\delta_{\text{H}}$ / ppm	$\delta_{\text{C}}$ or $\delta_{\text{P}}$ or $\delta_{\text{N}}$ / ppm	Additional data
CB 1	–	181.6	
CB 2	3.44	60.6	$r_{\text{H2-H5}} \approx (2.56 \pm 0.05) \text{ \AA}$ ${}^3J_{\text{H2-H5}} = (2.9 \pm 0.1) \text{ Hz}$
CB 3	5.79	131.7	
CB 4	5.32	145.8	
CB 5	2.59	37.5	${}^3J_{\text{HP}} = 9.8 \text{ Hz}$ ${}^2J_{\text{CP}} = 2.9 \text{ Hz}$
P	–	32.1	
N	–	194.6	
CB 1	–	181.8	
CB 2	3.51	60.5	$r_{\text{H2-H5}} \approx (2.58 \pm 0.05) \text{ \AA}$ ${}^3J_{\text{H2-H5}} = (2.9 \pm 0.1) \text{ Hz}$
CB 3	5.80	131.1	
CB 4	5.84	146.3	
CB 5	2.30	41.9	${}^3J_{\text{HP}} = 10.0 \text{ Hz}$ ${}^2J_{\text{CP}} = 2.9 \text{ Hz}$
P	–	31.3	
N	–	196.5	

## 5 Reaction Monitoring and Kinetic Fitting of Oxidative Addition and $\eta^1$ - $\eta^3$ - $\eta^1$ Interconversion

In order to monitor the formation of Pd-cyclobutene complexes, NMR samples with stoichiometric amounts of a Pd<sup>0</sup> source and ligand **L1** or **L2** were treated with substrate **1**, and the subsequent oxidative addition and  $\eta^1$ - $\eta^3$ - $\eta^1$  isomerization were followed by <sup>1</sup>H-NMR and/or <sup>31</sup>P{<sup>1</sup>H}-NMR. With substrate *cis*-**1**, these processes were found to proceed on a timescale of just a few minutes, thus requiring a fast reaction monitoring approach. This was realized by using a rapid-injection set-up for addition of *cis*-**1** to the pre-complex solution, followed by either a <sup>1</sup>H-NMR series with spatially-selective and frequency-shifted excitation<sup>39</sup> or a <sup>31</sup>P{<sup>1</sup>H}-NMR series with small-angle excitation. The rapid injection set-up used is described in the literature.<sup>40-42</sup> The same set-up was employed for the preparation of unstable Pd-complex *anti*-Na-**4a** from deprotonated substrate *trans*-Na-**1**, and a <sup>31</sup>P{<sup>1</sup>H}-NMR series was recorded to monitor the formation and subsequent decomposition of the complexes.

With substrate *trans*-**1**, on the other hand, oxidative addition and  $\eta^1$ - $\eta^3$ - $\eta^1$  isomerization turned out to be much slower, requiring several hours until reaching a final state. Thus, a slow reaction monitoring approach with initiation outside the spectrometer and conventional pulse sequences was sufficient. Therefore, reactive samples of Pd<sup>0</sup> source, ligand **L1** or **L2** and *trans*-**1** were prepared under inert atmosphere (glove box), and then directly transferred to the NMR spectrometer and analyzed by an alternating <sup>1</sup>H- and <sup>31</sup>P{<sup>1</sup>H}-NMR series.

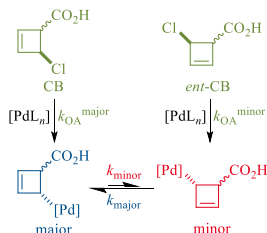
For all reactions involving acid substrate **1**, the d.r. of Pd-species formed was found to be highly time-dependent, clearly indicating formation of  $\eta^1$ -complexes to precede  $\eta^1$ - $\eta^3$ - $\eta^1$  isomerization, as direct formation of a  $\eta^3$ -species prior to isomerization to the  $\eta^1$ -species would imply the d.r. to be constant over time.

### Kinetic Model

#### Analytical Treatment

For analyzing the kinetics of the oxidative addition of substrate **1** and subsequent  $\eta^1$ - $\eta^3$ - $\eta^1$  isomerization between diastereomeric Pd-cyclobutene species, the model depicted in Scheme S5 was assumed. Accordingly, substrate enantiomers **CB** and *ent*-**CB** undergo second order oxidative addition with pre-complex [PdL<sub>n</sub>] (first order in both substrate and Pd<sup>0</sup>), described by rate constants  $k_{\text{OA}}^{\text{major}}$  and  $k_{\text{OA}}^{\text{minor}}$ , respectively. The resulting  $\eta^1$ -

Pd-species **major**, which is formed from **CB**, and **minor**, which is formed from *ent*-**CB**, subsequently interconvert via a first order equilibrium with rate constants  $k_{\text{major}}$  and  $k_{\text{minor}}$ .



**Scheme S5.** Kinetic model for second order oxidative addition of substrate enantiomers **CB** and *ent*-**CB** to Pd-complexes **major** and **minor**, followed by first order equilibration between both Pd-species. The configuration at the stereocenter adjacent to the carboxy group is not specified, i.e. the model includes both substrate *cis*- and *trans*-1, as well as *syn*- and *anti*-configured Pd-complexes.

In order to simulate the equilibrium between the diastereomeric  $\eta^1$ -Pd-species, the rate law of **major**

$$\frac{d[\text{major}]}{dt} = k_{\text{major}}[\text{minor}] - k_{\text{minor}}[\text{major}] + k_{\text{O}_A}^{\text{major}}[\text{CB}][\text{Pd}] \quad (1)$$

was taken as starting point. If the analysis is limited to equilibration after complete conversion of substrate (i.e.  $[\text{CB}] = [\text{ent-CB}] = 0$ ), the concentration of **minor** can be written as  $[\text{minor}] = [\text{S}]_0 - [\text{major}]$ , with  $[\text{S}]_0$  being the starting concentration of substrate. Thus, equation (1) simplifies to

$$\frac{d[\text{major}]}{dt} = k_{\text{major}}([\text{S}]_0 - [\text{major}]) - k_{\text{minor}}[\text{major}] \quad (2)$$

and can be solved to<sup>43</sup>

$$[\text{major}](t) = C'e^{-(k_{\text{major}}+k_{\text{minor}})t} + \frac{[\text{S}]_0 k_{\text{major}}}{k_{\text{major}}+k_{\text{minor}}} \quad (3)$$

using the time-independent factor  $C'$ . Dividing integrated rate law (3) by  $[\text{S}]_0$  gives the analogous expression for the mole fraction with respect to the total cyclobutene concentration  $x_{\text{major}} = \frac{[\text{major}]}{[\text{S}]_0}$

$$x_{\text{major}}(t) = Ce^{-(k_{\text{major}}+k_{\text{minor}})t} + \frac{k_{\text{major}}}{k_{\text{major}}+k_{\text{minor}}} \quad (4)$$

after introduction of modified constant  $C = \frac{C'}{[\text{S}]_0}$ . The mole fraction of **minor**  $x_{\text{minor}} = 1 - x_{\text{major}}$  thus follows the time-dependency

$$x_{\text{minor}}(t) = 1 - Ce^{-(k_{\text{major}}+k_{\text{minor}})t} - \frac{k_{\text{major}}}{k_{\text{major}}+k_{\text{minor}}} \quad (5)$$

Hence, both  $x_{\text{major}}(t)$  and  $x_{\text{minor}}(t)$  can be fitted as

$$x(t) = Ae^{kt} - x_0 \quad (6)$$

with constants  $A$ ,  $k$  and  $x_0$  as fitting parameters. Rate constants  $k_{\text{major}}$  and  $k_{\text{minor}}$  are readily obtained by comparison of the obtained fitting parameters  $k$  and  $x_0$  with equation (4) and (5). Equations (2) – (6) are valid only for experimental data recorded after full substrate consumption; for a numerical treatment over the full reaction time see below.

For fitting the consumption of substrate, we made use of the experimental observation that in all catalytic reactions which did not reach quantitative conversion, residual substrate was recovered as a racemate (cf. section 3 and 7). Thus, enantiomers **CB** and *ent*-**CB** can be assumed to be converted at approximately equal rate, i.e.  $k_{\text{O}_A}^{\text{major}} = k_{\text{O}_A}^{\text{minor}} \equiv k_{\text{O}_A}$ , and the decay of the total substrate concentration  $[\text{S}] = [\text{CB}] + [\text{ent-CB}]$  can be described as

$$\frac{d[\text{S}]}{dt} = -k_{\text{O}_A}[\text{S}][\text{Pd}] \quad (7)$$

The  $\text{Pd}^0$  concentration  $[\text{Pd}]$  can be substituted with

$$[\text{Pd}] = [\text{S}] + [\text{Pd}]_0 - [\text{S}]_0 \quad (8)$$

with the term  $[\text{Pd}]_0 - [\text{S}]_0$  correcting for potential experimental deviations from the attempted 1:1 (i.e.  $[\text{Pd}] = [\text{S}]$ ) stoichiometry. Combining equations (8) and (9) gives

$$\frac{d[\text{S}]}{dt} = -k_{\text{O}_A}[\text{S}]( [\text{S}] + [\text{Pd}]_0 - [\text{S}]_0 ). \quad (9)$$

This differential equation can be solved to<sup>43</sup>



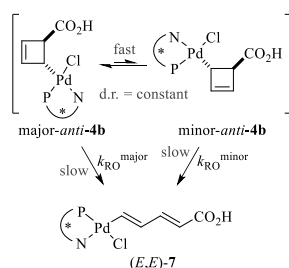
$$[S](t) = \frac{\left(1 - \frac{[S]_0}{[Pd]_0}\right)[S]_0 e^{([S]_0 - [Pd]_0)k_{OA}t}}{1 - \frac{[S]_0}{[Pd]_0} e^{([S]_0 - [Pd]_0)k_{OA}t}}, \quad (10)$$

and the substrate's mole fraction with respect to the total cyclobutene concentration  $x_S = \frac{[S]}{[S]_0}$  can be fitted as

$$x_S(t) = \frac{\left(1 - \frac{[S]_0}{[Pd]_0}\right)e^{([S]_0 - [Pd]_0)k_{OA}t}}{1 - \frac{[S]_0}{[Pd]_0} e^{([S]_0 - [Pd]_0)k_{OA}t}} \equiv \frac{(1-C)e^{Bt}}{1-Ce^{Bt}}, \quad (11)$$

with constants  $B$  and  $C$  as fitting parameters.

For complexes major-*anti*-**4b** and minor-*anti*-**4b**, slow  $4\pi$ -electrocyclic ring-opening to diene (*E,E*)-**7** was observed upon performing reaction monitoring over prolonged observation periods. This was treated with the kinetic model depicted in Scheme S6.



**Scheme S6.** Kinetic model for electrocyclic ring-opening of interconverting Pd-cyclobutene species major-*anti*-**4b** and minor-*anti*-**4b** to diene (*E,E*)-**7**.

Accordingly, major- and minor-*anti*-**4b** undergo ring-opening to the same product (*E,E*)-**7**, with the rate constants  $k_{RO}^{\text{major}}$  and  $k_{RO}^{\text{minor}}$ , respectively. As equilibration between major- and minor-*anti*-**4b** is fast compared to ring-opening (*vide infra*), the d.r. between both species is constant upon conversion, and only an averaged rate constant  $k_{RO}$  can be observed experimentally. Thus, major- and minor-*anti*-**4b** can be treated as one common species, hereinafter denoted as *anti*, with the rate law

$$\frac{d[anti]}{dt} = -k_{RO}[anti], \quad (12)$$

assuming formation of *anti* by oxidative addition to be completed during reaction monitoring of its conversion by ring-opening. Rate law (12) can be integrated to

$$[anti](t) = [anti]_0 e^{-k_{RO}t}. \quad (13)$$

Dividing by the reference concentration [total] gives the analogous expression for the mole fraction

$$x_{anti}(t) = x_{anti0} e^{-k_{RO}t}. \quad (14)$$

For the mole fractions of major- and minor-*anti*-**4b**,  $x_{\text{major-anti}} = \frac{d.r.}{1+d.r.} x_{anti}$  and  $x_{\text{minor-anti}} = \frac{1}{1+d.r.} x_{anti}$ , respectively, follows

$$x_{\text{major-anti}}(t) = Z e^{-k_{RO}t} \quad (15)$$

and

$$x_{\text{minor-anti}}(t) = Z' e^{-k_{RO}t}, \quad (16)$$

using constants  $Z$  and  $Z'$ . Hence, both  $x_{\text{major-anti}}(t)$  and  $x_{\text{minor-anti}}(t)$  can be fitted as

$$x(t) = A e^{-k_{RO}t}, \quad (17)$$

with constants  $A$  and  $k_{RO}$  as fitting parameters.

Analogously, the rate law of ring-opening product (*E,E*)-**7**, hereinafter denoted as *diene*, can be formulated as

$$\frac{d[diene]}{dt} = k_{RO}[anti] = k_{RO}([total] - [diene]) \quad (18)$$

which can be solved to

$$[diene](t) = Z'' e^{-k_{RO}t} + [total], \quad (19)$$

using constant  $Z''$ . Dividing by the reference concentration [total] gives the analogous expression for the mole fraction

$$x_{diene}(t) = P e^{-k_{RO}t} + 1 \quad (20)$$

after introduction of modified constant  $P = \frac{Z'}{[\text{total}]}$ . This expression can readily be used as regression function for  $x_{\text{diene}}(t)$ , using constants  $P$  and  $k_{\text{RO}}$  as fitting parameters.

### Numerical Treatment

For numerical fitting of the kinetic data covering the full reaction time of the oxidative addition of substrate **1** and subsequent  $\eta^1$ - $\eta^3$ - $\eta^1$  interconversion, the differential rate laws

$$\frac{dx}{dt} = x \cdot k \quad (21)$$

$$dx = x \cdot k \cdot dt \quad (22)$$

are transferred to

$$\Delta x = x \cdot k \cdot \Delta t, \quad (23)$$

assuming the time interval  $\Delta t$  to be sufficiently small (i.e.  $dt \approx \Delta t$ ). This equation can be used to obtain a numerical model, with the mole fraction  $x(t)$  of each species being calculated incrementally according to

$$x(t) = x(t-1) + \Delta x. \quad (24)$$

The model was fitted to the experimental temporal mole fraction profiles by minimization of the sum of residuals  $R_{\text{opt}}$  between calculated mole fractions  $x_{\text{model}}(t)$  and experimental values  $x_{\text{exp}}(t)$ .

$$R_{\text{opt}} = \sum_0^t R(t) \quad \text{with} \quad R(t) = |x_{\text{model}}(t) - x_{\text{exp}}(t)| \quad (25)$$

For the reaction of substrate *cis*-**1** to interconverting *anti*-complexes **major** and **minor** according to the model depicted in Scheme S5, the depletion of the mole fraction of substrate enantiomers **CB** and *ent*-**CB** depends on the concentration-independent rate constant analogues  $k_{\text{OA}}^{\text{major}}$  and  $k_{\text{OA}}^{\text{minor}}$ , their mole fractions  $x_{\text{cb}}$  and  $x_{\text{ent-CB}}$ , and the mole fraction of active palladium  $x_{\text{Pd}}$ .

$$x_{\text{cb}}(t) = x_{\text{cb}}(t-1) + \Delta x_{\text{cb}}(t) \quad (26)$$

$$\Delta x_{\text{cb}}(t) = -k_{\text{OA}}^{\text{major}} \cdot x_{\text{cb}}(t-1) \cdot x_{\text{Pd}}(t-1) \cdot \Delta t \quad (27)$$

$$x_{\text{ent-CB}}(t) = x_{\text{ent-CB}}(t-1) + \Delta x_{\text{ent-CB}}(t) \quad (28)$$

$$\Delta x_{\text{ent-CB}}(t) = -k_{\text{OA}}^{\text{minor}} \cdot x_{\text{ent-CB}}(t-1) \cdot x_{\text{Pd}}(t-1) \cdot \Delta t \quad (29)$$

The concurrent decrease of  $x_{\text{Pd}}$  can be described using the mole fractions  $x_{\text{major}}$  and  $x_{\text{minor}}$  of the Pd-cyclobutene species formed.

$$x_{\text{Pd}}(t) = x_{\text{Pd}}(t-1) + \Delta x_{\text{Pd}}(t) \quad (30)$$

$$\Delta x_{\text{Pd}}(t) = x_{\text{Pd}}(t-1) - \Delta x_{\text{major}}(t) - \Delta x_{\text{minor}}(t) \quad (31)$$

The time-dependent mole fraction of the two palladium *anti*-complexes **major** and **minor** depends on their formation via oxidative addition of **CB** and *ent*-**CB** with Pd as well as on the interconversion of **major** and **minor**. Hence, the time-dependent mole fractions of **major** and **minor** are described via

$$x_{\text{major}}(t) = x_{\text{major}}(t-1) + \Delta x_{\text{major}}(t) \quad (32)$$

$$\begin{aligned} \Delta x_{\text{major}}(t) &= (\Delta x_{\text{cb}}(t) - x_{\text{major}}(t-1) \cdot k_{\text{minor}} + x_{\text{minor}}(t-1) \cdot k_{\text{major}}) \cdot \Delta t \\ &= (x_{\text{cb}}(t-1) \cdot k_{\text{OA}}^{\text{major}} - x_{\text{major}}(t-1) \cdot k_{\text{minor}} + x_{\text{minor}}(t-1) \cdot k_{\text{major}}) \cdot \Delta t \end{aligned} \quad (33)$$

$$x_{\text{minor}}(t) = x_{\text{minor}}(t-1) + \Delta x_{\text{minor}}(t) \quad (34)$$

$$\begin{aligned} \Delta x_{\text{minor}}(t) &= (\Delta x_{\text{ent-CB}}(t) + x_{\text{major}}(t-1) \cdot k_{\text{minor}} - x_{\text{minor}}(t-1) \cdot k_{\text{major}}) \cdot \Delta t \\ &= (x_{\text{ent-CB}}(t-1) \cdot k_{\text{OA}}^{\text{minor}} + x_{\text{major}}(t-1) \cdot k_{\text{minor}} - x_{\text{minor}}(t-1) \cdot k_{\text{major}}) \cdot \Delta t \end{aligned} \quad (35)$$

For numeric treatment of kinetic data obtained with substrate *trans*-**1**, this model is extended in order to account for formation of both *anti*- and *syn*-complexes. The oxidative addition of substrate enantiomers **CB** and *ent*-**CB** is described by adding a second term for the formation of *syn*-complexes to equation (27) and (29), respectively.

$$x_{\text{CB}}(t) = x_{\text{CB}}(t-1) + \Delta x_{\text{CB}}(t) \quad (36)$$

$$\Delta x_{\text{CB}}(t) = -k_{\text{OA}}^{\text{major,anti}} \cdot x_{\text{CB}}(t-1) \cdot x_{\text{Pd}}(t-1) - k_{\text{OA}}^{\text{major,syn}} \cdot x_{\text{CB}}(t-1) \cdot x_{\text{Pd}}(t-1) \cdot \Delta t \quad (37)$$

$$x_{\text{ent-CB}}(t) = x_{\text{ent-CB}}(t-1) + \Delta x_{\text{ent-CB}}(t) \quad (38)$$

$$\Delta x_{\text{ent-CB}}(t) = -k_{\text{OA}}^{\text{minor,anti}} \cdot x_{\text{ent-CB}}(t-1) \cdot x_{\text{Pd}}(t-1) - k_{\text{OA}}^{\text{minor,syn}} \cdot x_{\text{ent-CB}}(t-1) \cdot x_{\text{Pd}}(t-1) \cdot \Delta t \quad (39)$$

In some cases, especially when *trans*-**1** is present in excess compared to the Pd<sup>0</sup> source, a significant extent of substrate decomposition is observed. This is taken into consideration by adding a term describing a first-order decay to equation (37) and (39), respectively, with the rate constant  $k_{\text{decomp}}$ .

$$\Delta x_{\text{CB}}(t) = -k_{\text{OA}}^{\text{major,anti}} \cdot x_{\text{CB}}(t-1) \cdot x_{\text{Pd}}(t-1) - k_{\text{OA}}^{\text{major,syn}} \cdot x_{\text{CB}}(t-1) \cdot x_{\text{Pd}}(t-1) - k_{\text{decomp}} \cdot x_{\text{CB}}(t-1) \cdot \Delta t \quad (40)$$

$$\Delta x_{\text{ent-CB}}(t) = -k_{\text{OA}}^{\text{minor,anti}} \cdot x_{\text{ent-CB}}(t-1) \cdot x_{\text{Pd}}(t-1) - k_{\text{OA}}^{\text{minor,syn}} \cdot x_{\text{ent-CB}}(t-1) \cdot x_{\text{Pd}}(t-1) - k_{\text{decomp}} \cdot x_{\text{ent-CB}}(t-1) \cdot \Delta t \quad (41)$$

The conversion of CB and *ent*-CB to *anti*- and *syn*-complexes, respectively, is also included into the decay of the Pd<sup>0</sup> source.

$$x_{\text{Pd}}(t) = x_{\text{Pd}}(t-1) + \Delta x_{\text{Pd}}(t) \quad (42)$$

$$\Delta x_{\text{Pd}}(t) = x_{\text{Pd}}(t-1) - \Delta x_{\text{major,anti}}(t) - \Delta x_{\text{minor,anti}}(t) - \Delta x_{\text{major,syn}}(t) - \Delta x_{\text{minor,syn}}(t) \quad (43)$$

As described in section 4, complexes *anti*-**4b** undergo slow electrocyclic ring-opening to the corresponding diene. This is considered by adding a first-order term to equation (33) and (35), respectively, using the rate constant  $k_{\text{RO}}$ .

$$x_{\text{major,anti}}(t) = x_{\text{major,anti}}(t-1) + \Delta x_{\text{major,anti}}(t) \quad (44)$$

$$\Delta x_{\text{major,anti}}(t) = (x_{\text{CB}}(t-1) \cdot k_{\text{OA}}^{\text{major,anti}} - x_{\text{major,anti}}(t-1) \cdot k_{\text{minor,anti}} + x_{\text{minor,anti}}(t-1) \cdot k_{\text{major,anti}} - x_{\text{major,anti}}(t-1) \cdot k_{\text{RO}}) \cdot \Delta t \quad (45)$$

$$\Delta x_{\text{major,anti}}(t) = (\Delta x_{\text{CB}}(t) - x_{\text{major,anti}}(t-1) \cdot k_{\text{minor,anti}} + x_{\text{minor,anti}}(t-1) \cdot k_{\text{major,anti}} - x_{\text{major,anti}}(t-1) \cdot k_{\text{RO}}) \cdot \Delta t \quad (46)$$

$$x_{\text{minor,anti}}(t) = x_{\text{minor,anti}}(t-1) + \Delta x_{\text{minor,anti}}(t) \quad (47)$$

$$\Delta x_{\text{minor,anti}}(t) = (x_{\text{ent-CB}}(t-1) \cdot k_{\text{OA}}^{\text{minor,anti}} + x_{\text{major,anti}}(t-1) \cdot k_{\text{minor,anti}} - x_{\text{minor,anti}}(t-1) \cdot k_{\text{major,anti}} - x_{\text{minor,anti}}(t-1) \cdot k_{\text{RO}}) \cdot \Delta t \quad (48)$$

$$\Delta x_{\text{minor,anti}}(t) = (\Delta x_{\text{ent-CB}}(t) + x_{\text{major,anti}}(t-1) \cdot k_{\text{minor,anti}} - x_{\text{minor,anti}}(t-1) \cdot k_{\text{major,anti}} - x_{\text{minor,anti}}(t-1) \cdot k_{\text{RO}}) \cdot \Delta t \quad (49)$$

Formation of the diene can be described via

$$x_{\text{diene}}(t) = x_{\text{diene}}(t-1) + \Delta x_{\text{diene}}(t) \quad (50)$$

$$\Delta x_{\text{diene}}(t) = (x_{\text{major,anti}}(t-1) \cdot k_{\text{RO}} + x_{\text{minor,anti}}(t-1) \cdot k_{\text{RO}}) \cdot \Delta t. \quad (51)$$

As the *syn*-complexes have been found not to undergo ring-opening, the time-dependent mole fraction can be sufficiently described by contributions from oxidative addition and first-order interconversion between *major*- and *minor*-*syn*.

$$x_{\text{major,syn}}(t) = x_{\text{major,syn}}(t-1) + \Delta x_{\text{major,syn}}(t) \quad (52)$$

$$\Delta x_{\text{major,syn}}(t) = (x_{\text{CB}}(t-1) \cdot k_{\text{OA}}^{\text{major,syn}} - x_{\text{major,syn}}(t-1) \cdot k_{\text{minor,syn}} + x_{\text{minor,syn}}(t-1) \cdot k_{\text{major,syn}}) \cdot \Delta t \quad (53)$$

$$\Delta x_{\text{major,syn}}(t) = (\Delta x_{\text{CB}}(t) - x_{\text{major,syn}}(t-1) \cdot k_{\text{minor,syn}} + x_{\text{minor,syn}}(t-1) \cdot k_{\text{major,syn}}) \cdot \Delta t \quad (54)$$

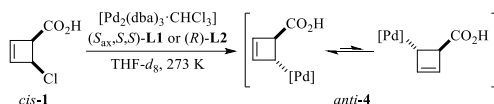
$$x_{\text{minor,syn}}(t) = x_{\text{minor,syn}}(t-1) + \Delta x_{\text{minor,syn}}(t) \quad (55)$$

$$\Delta x_{\text{minor,syn}}(t) = (x_{\text{ent-CB}}(t-1) \cdot k_{\text{OA}}^{\text{minor,syn}} + x_{\text{major,syn}}(t-1) \cdot k_{\text{minor,syn}} - x_{\text{minor,syn}}(t-1) \cdot k_{\text{major,syn}}) \cdot \Delta t \quad (56)$$

$$\Delta x_{\text{minor,syn}}(t) = (\Delta x_{\text{ent-CB}}(t) + x_{\text{major,syn}}(t-1) \cdot k_{\text{minor,syn}} - x_{\text{minor,syn}}(t-1) \cdot k_{\text{major,syn}}) \cdot \Delta t \quad (57)$$

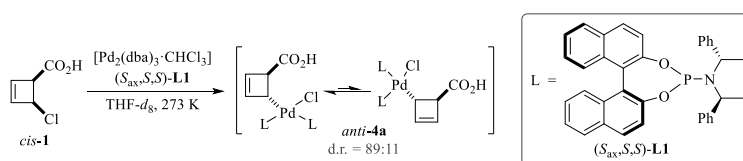
## Oxidative Addition of Substrate *cis*-1 and *trans*-Na-1 (fast Reaction Monitoring)

### General Procedure for Oxidative Addition of Substrate *cis*-1

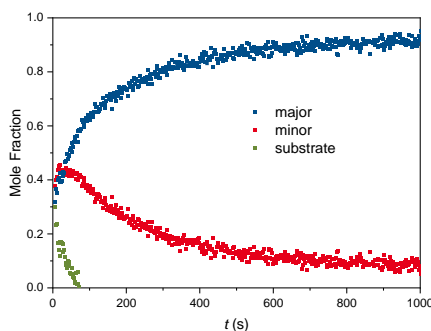


[Pd<sub>2</sub>(dba)<sub>3</sub>·CHCl<sub>3</sub>] (25.9 mg, 25 μmol, 0.5 equiv.) and ligand (*S*<sub>ax</sub>,*S*,*S*)-**L1** (54.0 mg, 100 μmol, 2 equiv.) or (*R*)-**L2** (20.4 mg, 50 μmol, 1 equiv.) were dissolved in anhydrous THF-*d*<sub>8</sub> (0.5 mL) and transferred into an NMR tube, which was capped, homogenized and loaded into the NMR spectrometer with the temperature set to 273 K. After wobbling and shimming, the sample was ejected. The rapid injection set-up was loaded with a solution of *cis*-4-chlorocyclobutene-2-enecarboxylic acid *cis*-1 (6.6 mg, 50 μmol, 1 equiv.) in anhydrous THF-*d*<sub>8</sub> (0.1 mL) and attached to the NMR tube, which was then loaded into the spectrometer again. The <sup>1</sup>H-NMR or <sup>31</sup>P{<sup>1</sup>H}-NMR series was started, and the substrate solution was added in one shot. <sup>1</sup>H-NMR monitoring was performed as a series of single-scan spectra with spatially-selective and frequency-shifted excitation using a linear, asymmetric frequency list with 32 values between -3000 and 12500 Hz relative to the offset, a 16.5 ms EBurp2<sup>44</sup> pulse and a rectangular gradient with a strength of 25 %. The spectra were recorded with a relaxation delay of 1530 ms (with **L1**) or 61 ms (with **L2**) and an acquisition time of 500 ms (with **L1**) or 993 ms (with **L2**), corresponding to an overall temporal resolution of 2047 ms (with **L1**) and 1070 ms (with **L2**), respectively. Monitoring by <sup>31</sup>P{<sup>1</sup>H}-NMR was performed as a series of single-scan spectra with a 20° pulse and inverse-gated decoupling. The relaxation delay was set to 500 ms, and the single-scan experiments were recorded with an acquisition time of 500 ms, corresponding to a final temporal resolution of 1003 ms. NMR reaction monitoring was continued until reaching complete consumption of substrate *cis*-1 and full equilibration between both diastereomeric Pd-cyclobutene species.

### Oxidative Addition of Acid Substrate *cis*-1 with Ligand **L1**

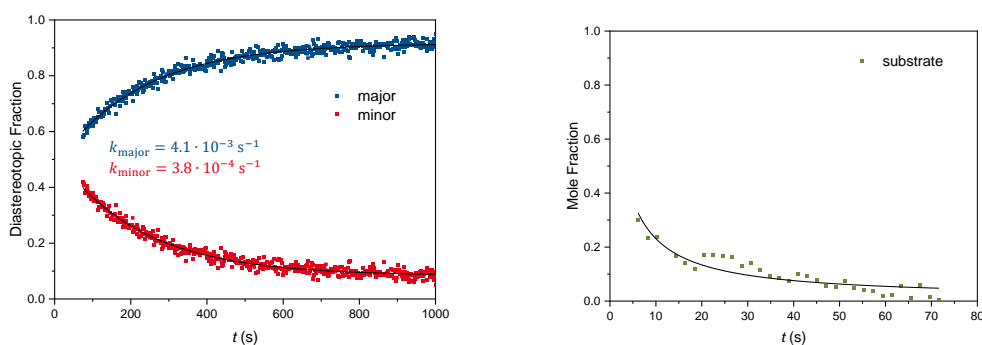


<sup>1</sup>H-NMR reaction monitoring of the oxidative addition of *cis*-4-chlorocyclobutene-2-enecarboxylic acid *cis*-1 with ligand (*S*<sub>ax</sub>,*S*,*S*)-**L1** gave the temporal mole fraction profile shown in Figure S2. Substrate *cis*-1 was fully converted within 74 s. Oxidative addition products major- and minor-*anti*-4a were found to be formed with an initial d.r. of approximately 50:50, and then equilibrated to d.r. = 89:11 over ca. 17 min.



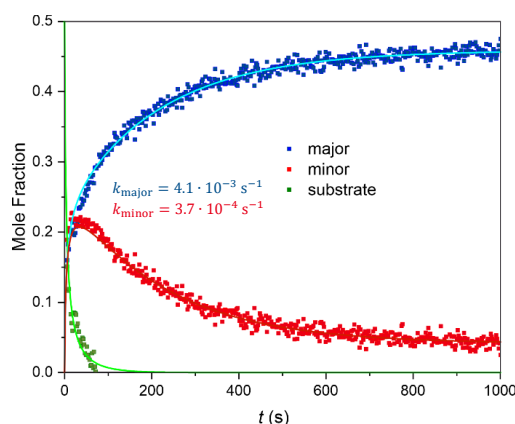
**Figure S2.** Temporal mole fraction profile for the oxidative addition of substrate *cis*-1 with ligand **L1** to interconverting Pd-cyclobutene species major- and minor-*anti*-4a, recorded by rapid-injection <sup>1</sup>H-NMR reaction monitoring with spatially-selective and frequency-shifted excitation. Mole fraction values refer to cyclobutene species only.

The rate constants  $k_{\text{major}}$  and  $k_{\text{minor}}$  for the  $\eta^1$ - $\eta^3$ - $\eta^1$  isomerization between major- and minor-*anti*-4a were extracted by fitting equation (6) to the experimental mole fraction profiles for  $t > 74$  s, i.e. after full consumption of substrate (Figure S3, left). The regression function was found to be in excellent agreement with the experimental data, giving rate constants of  $k_{\text{major}} = 4.1 \cdot 10^{-3} \text{ s}^{-1}$  and  $k_{\text{minor}} = 3.8 \cdot 10^{-4} \text{ s}^{-1}$ . The decay of substrate *cis*-1 could be fitted in reasonable quality with integrated second order kinetic rate law (11) (Figure S3, right).



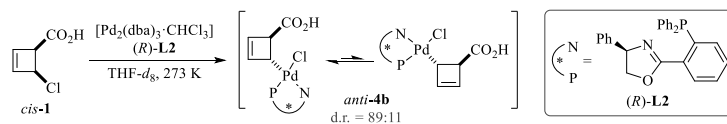
**Figure S3.** Analytical kinetic fitting of the oxidative addition of substrate *cis-1* with ligand **L1** to interconverting Pd-species *major-* and *minor-anti-4a*:  $\eta^1\text{-}\eta^3\text{-}\eta^1$  equilibration of *major-* and *minor-anti-4a* according to (6) (for  $t > 74$  s, left) and conversion of *cis-1* according to equation (11) (right).

Application of the numerical model with optimization as described above yielded the fitted mole fraction curves shown in Figure S4. The residual was minimized by varying  $k_{\text{OA}}^{\text{major}}$ ,  $k_{\text{OA}}^{\text{minor}}$ ,  $k_{\text{major}}$ ,  $k_{\text{minor}}$  and  $x_{\text{Pd}}(0)$ . Optimization was conducted by a different person than the analytical treatment, without prior knowledge of the analytical solution for the rate constants of interest. A minimal residual was found for the rate constants  $k_{\text{major}} = 4.1 \cdot 10^{-3} \text{ s}^{-1}$  and  $k_{\text{minor}} = 3.7 \cdot 10^{-4} \text{ s}^{-1}$ , the concentration-independent rate constant analogues  $k_{\text{OA}}^{\text{major}} = k_{\text{OA}}^{\text{minor}} = 0.34 \text{ s}^{-1}$  and an initial Pd<sup>0</sup> mole fraction of  $x_{\text{Pd}}(0) = 0.56$ . The rate constants  $k_{\text{major}}$  and  $k_{\text{minor}}$  are in excellent agreement with those obtained from the analytical solution.

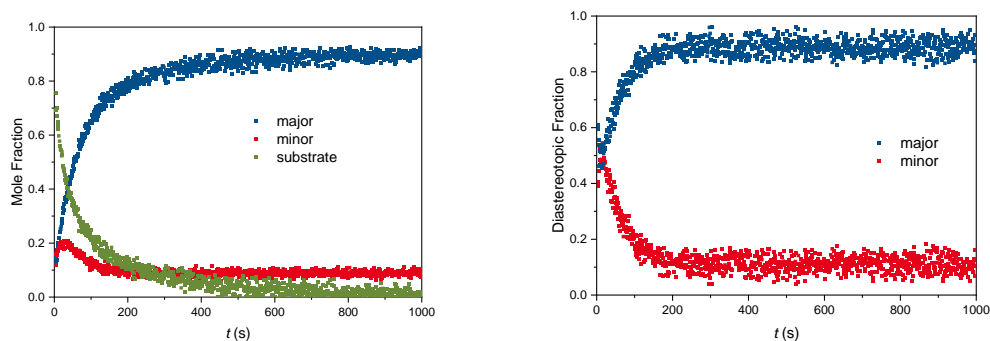


**Figure S4.** Numerical fitting of the <sup>1</sup>H-NMR reaction monitoring data for the oxidative addition of substrate *cis-1* with ligand **L1** to interconverting Pd-cyclobutene species *major-* and *minor-anti-4a*.

#### Oxidative Addition of Acid Substrate *cis-1* with Ligand **L2**



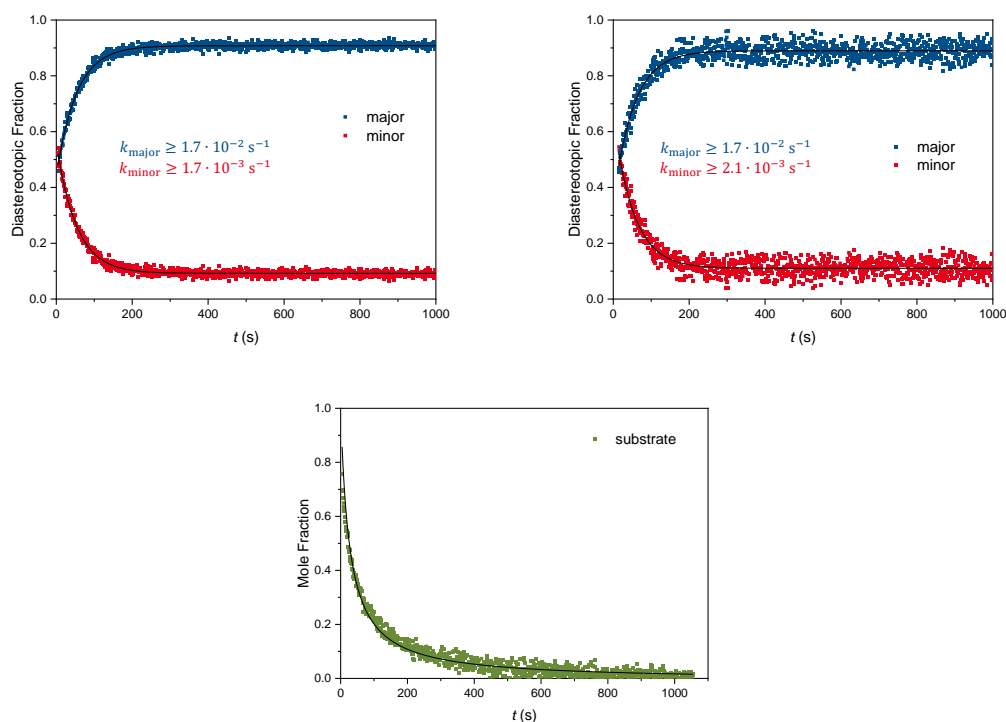
For real-time observation of the oxidative addition of *cis-4-chlorocyclobutene-2-enecarboxylic acid cis-1* with ligand *(R)-L2*, two runs were performed, using <sup>1</sup>H-NMR and <sup>31</sup>P{<sup>1</sup>H}-NMR monitoring, respectively. <sup>1</sup>H-NMR monitoring gave the temporal mole fraction profile with respect to all cyclobutene species (Figure S5, left), whilst the <sup>31</sup>P{<sup>1</sup>H}-NMR series did only allow for detection of Pd-complexes *major-* and *minor-anti-4b* (Figure S5, right), as the Pd-pre-complex of **L2** cannot be observed by <sup>31</sup>P-NMR.



**Figure S5.** Experimental reaction monitoring data for the oxidative addition of substrate *cis-1* with ligand **L2** to interconverting Pd-cyclobutene species **major-** and **minor-anti-4b**, recorded by rapid-injection  $^1\text{H}$ -NMR reaction monitoring with spatially-selective and frequency-shifted excitation (left) and  $^{31}\text{P}\{^1\text{H}\}$ -NMR reaction monitoring with small-angle excitation (right). Mole fraction values from  $^1\text{H}$ -NMR monitoring refer to cyclobutene species only, while diastereotopic fractions determined by  $^{31}\text{P}\{^1\text{H}\}$ -NMR refer to the ratio of **major-** and **minor-anti-4b**.

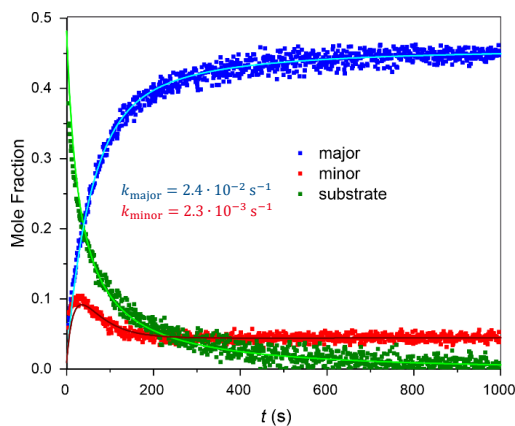
Again, oxidative addition products **major-** and **minor-anti-4b** were found to be formed with an initial d.r. of approximately 50:50, and then equilibrated to a constant d.r. of 89:11 within ca. 4 min. Other than in the analogous reaction with ligand **L1**, however, substrate consumption was rather slow compared to the subsequent  $\eta^1\text{-}\eta^3\text{-}\eta^1$  isomerization. Accordingly, the d.r. already plateaus before reaching quantitative substrate conversion, and rate constants  $k_{\text{major}}$  and  $k_{\text{minor}}$  cannot be extracted accurately by regression with analytically derived integrated rate law (6), which is only valid for  $x_s = 0$ . Accordingly, fitting equation (6) to the experimental temporal evolution of the diastereotopic fraction gives values for  $k_{\text{major}}$  and  $k_{\text{minor}}$  with a systematic downward deviation, as oxidative addition of *cis-1* still forms **major-** and **minor-anti-4b** in a 50:50 ratio, thus flattering the temporal d.r. profile. Hence, the rate constants extracted by analytical treatment can be understood as lower limits rather than accurate values. As shown in Figure S6, regression function (6) was found to excellently fit the experimental data from both  $^1\text{H}$ - and  $^{31}\text{P}\{^1\text{H}\}$ -NMR monitoring, giving rate constants of  $k_{\text{major}} \geq 1.7 \cdot 10^{-2} \text{ s}^{-1}$  and  $k_{\text{minor}} \geq 2 \cdot 10^{-3} \text{ s}^{-1}$ .

The decay of substrate *cis-1* could be fitted in good agreement with integrated second order kinetic rate law (11) (Figure S6, bottom).



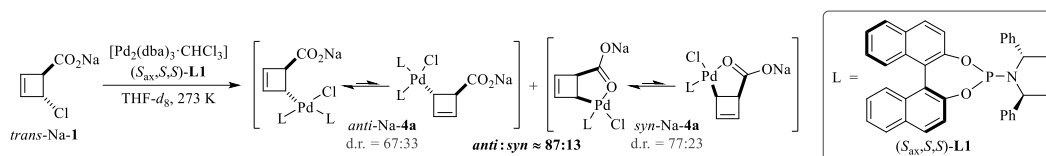
**Figure S6.** Analytical kinetic fitting of the oxidative addition of substrate *cis-1* with ligand **L2** to interconverting Pd-species *major*- and *minor-anti-4b*:  $\eta^1$ - $\eta^3$ - $\eta^1$  equilibration of *major*- and *minor-anti-4b* according to equation (6), using  $^1\text{H-NMR}$  (for  $t > 4$  s, top left) and  $^{31}\text{P}\{^1\text{H}\}$ -NMR data (for  $t > 3$  s, top right), and conversion of *cis-1* according to equation (11) (bottom).

Application of the numerical model to the  $^1\text{H-NMR}$  reaction monitoring data with optimization as described above yielded the fitted mole fraction curves shown in Figure S7. The residual was minimized by varying  $k_{\text{OA}}^{\text{major}}$ ,  $k_{\text{OA}}^{\text{minor}}$ ,  $k_{\text{major}}$ ,  $k_{\text{minor}}$  and  $x_{\text{Pd}}(0)$ . Optimization was conducted by a different person than the analytical treatment, without prior knowledge of the analytical solution for the rate constants of interest. A minimal residual was found for the rate constants  $k_{\text{major}} = 2.4 \cdot 10^{-2} \text{ s}^{-1}$  and  $k_{\text{minor}} = 2.3 \cdot 10^{-3} \text{ s}^{-1}$ , the concentration-independent rate constant analogues  $k_{\text{OA}}^{\text{major}} = k_{\text{OA}}^{\text{minor}} = 6.4 \cdot 10^{-2} \text{ s}^{-1}$  and an initial Pd<sup>0</sup> mole fraction of  $x_{\text{Pd}}(0) = 0.52$ . The rate constants  $k_{\text{major}}$  and  $k_{\text{minor}}$  are consistent with those obtained from the analytical solution.



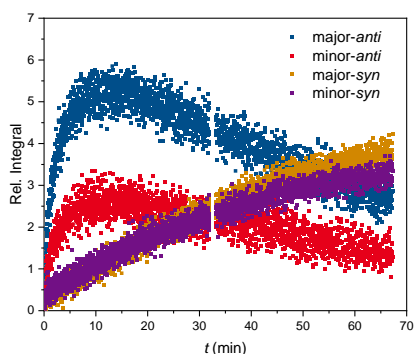
**Figure S7.** Numerical fitting of the experimental  $^1\text{H-NMR}$  reaction monitoring data for the oxidative addition of substrate *cis-1* with ligand **L2** to interconverting Pd-cyclobutene species *major*- and *minor-anti-4b*.

### Oxidative Addition of Carboxylate Substrate *trans*-Na-1 with Ligand L1



To a suspension of NaH (90 w%, 2.0 mg, 75  $\mu\text{mol}$ , 1.5 equiv.) in anhydrous THF- $d_8$  (0.3 mL) was added dropwise a solution of *trans*-4-chlorocyclobutene-2-enecarboxylic acid *trans*-1 (6.6 mg, 50  $\mu\text{mol}$ , 1 equiv.) in anhydrous THF- $d_8$  (0.3 mL) at 0 °C without stirring. The mixture was allowed to stand at 0 °C until no more gas evolution was observed.  $[\text{Pd}_2(\text{dba})_3 \cdot \text{CHCl}_3]$  (25.9 mg, 25  $\mu\text{mol}$ , 0.5 equiv.) and ligand  $(S_{ax},S,S)\text{-L1}$  (54.0 mg, 100  $\mu\text{mol}$ , 2 equiv.) were dissolved in anhydrous THF- $d_8$  (0.5 mL) and transferred into an NMR tube, which was capped, homogenized and loaded into the NMR spectrometer with the temperature set to 273 K. After wobbling and shimming, the sample was ejected. The rapid injection set-up was loaded with the solution of deprotonated *trans*-1 and attached to the NMR tube, which was then loaded into the spectrometer again. A  $^{31}\text{P}\{^1\text{H}\}$ -NMR series was started, and the substrate *trans* was added in one shot.  $^{31}\text{P}\{^1\text{H}\}$ -NMR monitoring was performed over 67 min as a series of single-scan spectra with a 30° pulse and broadband decoupling. The relaxation delay was set to 1.00 s, and the single-scan experiments were recorded with an acquisition time of 0.50 s, corresponding to a final temporal resolution of 1.50 s.

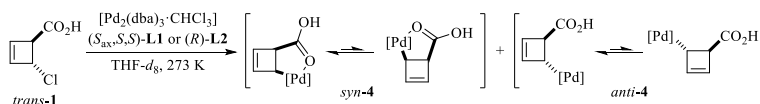
As shown in Figure S8, the integrals of major- and minor-*anti*-Na-4a reach a maximum ca. 13 min after addition of substrate *trans*-Na-1, and then gradually decrease. At the same time, the integrals of major- and minor-*syn*-Na-4a constantly increase. This suggests that complexes *anti*-Na-4a are unstable and readily decompose before oxidative addition reaches complete conversion, while the corresponding *syn*-species are stable. Initial rate analysis performed in the data range of 0.025 – 1.00 min furnished rates of 2.07  $\text{min}^{-1}$  (major-*anti*-Na-4a), 1.04  $\text{min}^{-1}$  (minor-*anti*-Na-4a), 0.225  $\text{min}^{-1}$  (major-*syn*-Na-4a), and 0.232  $\text{min}^{-1}$  (minor-*syn*-Na-4a), respectively. This corresponds to an initial *anti*:*syn* ratio of ca. 87:13 as a measure for the stereoselectivity of oxidative addition, which proceeds under both retention ( $\rightarrow$  *anti*-Na-4a) and inversion ( $\rightarrow$  *syn*-Na-4a). For *anti*-Na-4a, the initial rates determined for the major- and the minor-species translate to a d.r. of 67:33, consistent with the value determined by integration of  $^{31}\text{P}$ -NMR spectra recorded at higher concentrations of *anti*-Na-4a (e.g. after 13 min).



**Figure S8.** Temporal evolution of the relative integrals of complexes major- and minor-*anti*-Na-4a and major- and minor-*syn*-Na-4a after oxidative addition of deprotonated substrate *trans*-Na-1 with ligand L1, recorded by rapid-injection  $^{31}\text{P}\{^1\text{H}\}$ -NMR reaction monitoring.

### Oxidative Addition of Substrate *trans*-1 (slow Reaction Monitoring)

#### General Procedure for Oxidative Addition of Substrate *trans*-1

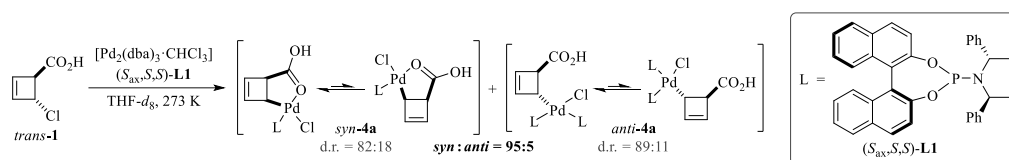


$[\text{Pd}_2(\text{dba})_3 \cdot \text{CHCl}_3]$  (25.9 mg, 25  $\mu\text{mol}$ , 0.5 equiv.) and ligand  $(S_{ax},S,S)\text{-L1}$  (54.0 mg, 100  $\mu\text{mol}$ , 2 equiv.) or  $(R)\text{-L2}$  (20.4 mg, 50  $\mu\text{mol}$ , 1 equiv.) were dissolved in anhydrous THF- $d_8$  (0.5 mL) and stirred at RT for 10 min. The solution was cooled to approximately  $-25$  °C and a solution of *trans*-4-chlorocyclobutene-2-enecarboxylic acid *trans*-1 (6.6 mg, 50  $\mu\text{mol}$ , 1 equiv.) in anhydrous THF- $d_8$  (0.3 mL) was added dropwise upon stirring vigorously. The resulting solution was directly transferred into a precooled NMR tube. The tube was sealed with a rubber septum and parafilm® and centrifuged (2000 rpm, 1 min), and then directly loaded into the NMR spectrometer with the temperature set to 273 K. After wobbling



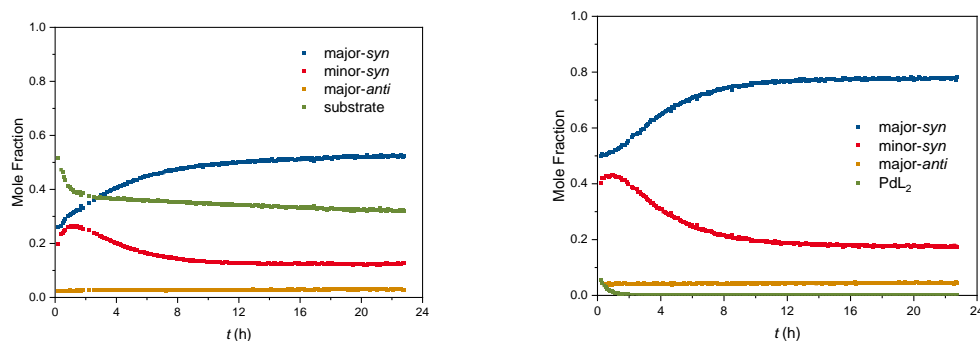
and shimming, an alternating  $^1\text{H}$ -NMR or  $^{31}\text{P}\{^1\text{H}\}$ -NMR series was started. The corresponding death time was 10 – 11 min for  $^1\text{H}$ -NMR monitoring and 11 – 12 min for the  $^{31}\text{P}\{^1\text{H}\}$ -NMR series. Monitoring by  $^1\text{H}$ -NMR was performed as a series of single-scan spectra with a  $90^\circ$  pulse.  $^{31}\text{P}\{^1\text{H}\}$ -NMR spectra were recorded with a  $90^\circ$  pulse, inverse-gated decoupling, 128 (with **L1**) or 32 scans (with **L2**), and a relaxation delay of 2 s (with **L1**) or 7 s (with **L2**). NMR reaction monitoring was continued until reaching complete consumption of substrate *trans*-**1** and full equilibration between both diastereomeric Pd-cyclobutene species.

#### Oxidative Addition of Acid Substrate *trans*-**1** with Ligand **L1**



Alternating  $^1\text{H}$ - and  $^{31}\text{P}\{^1\text{H}\}$ -NMR reaction monitoring of the oxidative addition of *trans*-4-chlorocyclobutene-2-enecarboxylic acid *trans*-**1** with ligand  $(\text{S}_{\text{ax}}, \text{S}_{\text{S}}, \text{S})\text{-L1}$  gave the temporal mole fraction profiles shown in Figure S9. In the  $^{31}\text{P}\{^1\text{H}\}$ -NMR series, all relevant Pd-P species could be quantified, including the pre-complex  $[\text{PdL}_2]$  ( $\text{L} = (\text{S}_{\text{ax}}, \text{S}_{\text{S}}, \text{S})\text{-L1}$ ) detected at  $\delta_{\text{P}} = 169.2$  ppm.<sup>45</sup> Only Pd-species minor-*anti*-**4a** was formed with a quantity too small for accurate integration in both the  $^1\text{H}$ - and the  $^{31}\text{P}\{^1\text{H}\}$ -NMR series (the reported d.r. was determined by a long end-point  $^{31}\text{P}\{^1\text{H}\}$ -NMR spectrum). As can be recognized from the  $^1\text{H}$ -NMR reaction monitoring data (Figure S9, left), substrate *trans*-**1** was not fully consumed, which might be attributed to a weighing error, as the physical state of *trans*-**1** (viscous oil) complicates accurate weighing in the glove box. The decay of  $[\text{PdL}_2]$  in the  $^{31}\text{P}\{^1\text{H}\}$ -NMR monitoring data (Figure S9, right), however, allows for determining oxidative addition to be completed after about 2.5 h. The subsequent slow substrate decay can most probably be attributed to decomposition.

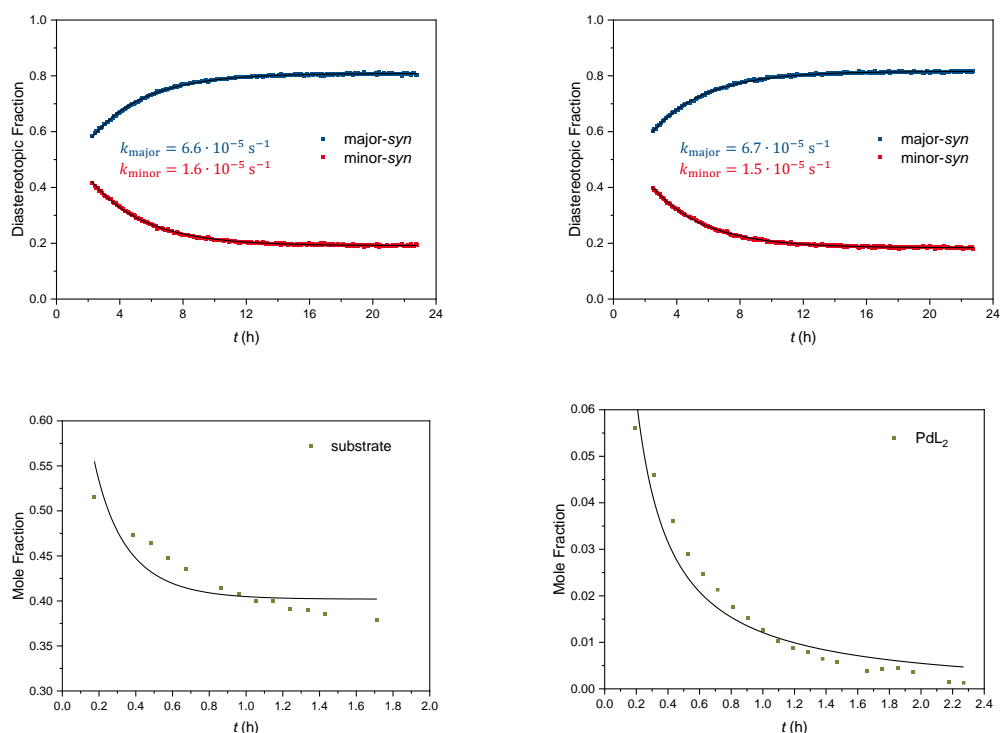
As already observed for the corresponding *anti*-species (*vide supra*), major- and minor-*syn*-**4a** were formed with an initial d.r. of approximately 50:50, and then equilibrated to d.r. = 82:18 over ca. 20 h, clearly indicating that the *syn*-species can undergo  $\eta^1\text{-}\eta^3\text{-}\eta^1$  interconversion as well.



**Figure S9.** Experimental reaction monitoring data for the oxidative addition of substrate *trans*-**1** with ligand **L1**, giving interconverting Pd-cyclobutene species major- and minor-*syn*-**4a** along with small amounts of major-*anti*-**4a** (amount of minor-*anti*-**4a** too small for accurate integration). Reaction monitoring was performed by an alternating  $^1\text{H}$ - and  $^{31}\text{P}\{^1\text{H}\}$ -NMR series after preparation outside the spectrometer. Mole fraction values extracted from  $^1\text{H}$ -NMR spectra (left) refer to cyclobutene species only, while mole fraction values extracted from  $^{31}\text{P}\{^1\text{H}\}$ -NMR spectra (right) refer to all Pd-P species.

The rate constants  $k_{\text{major}}$  and  $k_{\text{minor}}$  for the  $\eta^1\text{-}\eta^3\text{-}\eta^1$  isomerization between major- and minor-*syn*-**4a** were extracted by converting the reaction monitoring data from both  $^1\text{H}$ - and  $^{31}\text{P}\{^1\text{H}\}$ -NMR monitoring to temporal diastereotopic fraction profiles, which were subsequently fitted with equation (6) for  $t > 2.5$  h, i.e. after oxidative addition is completed (Figure S10, top). The regression function was found to be in excellent agreement with the experimental data, giving consistent rate constants of  $k_{\text{major}} = 6.6 \cdot 10^{-5} \text{ s}^{-1}$ ;  $k_{\text{minor}} = 1.6 \cdot 10^{-5} \text{ s}^{-1}$  ( $^1\text{H}$ -NMR) and  $k_{\text{major}} = 6.7 \cdot 10^{-5} \text{ s}^{-1}$ ;  $k_{\text{minor}} = 1.5 \cdot 10^{-5} \text{ s}^{-1}$  ( $^{31}\text{P}\{^1\text{H}\}$ -NMR), respectively.

Oxidative addition proceeded to > 90 % conversion during the death time (10 min for  $^1\text{H}$ -NMR monitoring, 11 min for  $^{31}\text{P}\{^1\text{H}\}$ -NMR monitoring) and could therefore not be modeled with high accuracy. Attempts to fit the decay of substrate *trans*-**1** with integrated second order kinetic rate law (11) resulted in a regression with poor quality (Figure S10, bottom left). This might be explained by competing first order decomposition of *trans*-**1**. However, the decay of pre-complex  $[\text{PdL}_2]$  could be fitted with reasonable quality as a second-order process (Figure S10, bottom right).

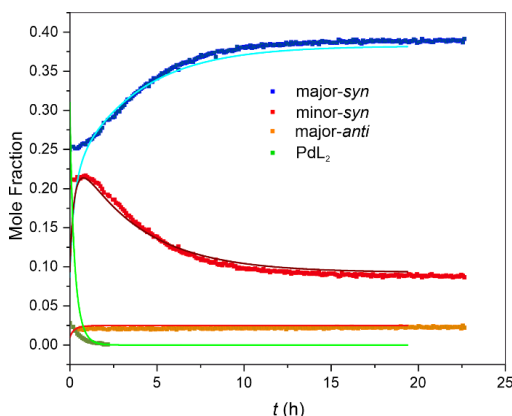


**Figure S10.** Analytical kinetic fitting of the oxidative addition of substrate *trans*-1 with ligand LI to interconverting Pd-cyclobutene species *major*- and *minor*-*syn*-4a:  $\eta^1$ - $\eta^3$ - $\eta^1$  equilibration of *major*- and *minor*-*syn*-4a according to equation (6), using data from  $^1\text{H}$ -NMR (top left) and  $^{31}\text{P}\{^1\text{H}\}$ -NMR monitoring (top right); and conversion of starting material, according to equation (11), using data from  $^1\text{H}$ -NMR (consumption of *trans*-1, bottom left) and  $^{31}\text{P}\{^1\text{H}\}$ -NMR monitoring (consumption of  $[\text{PdL}_2]$ , bottom right).

Numerical analysis was applied to the kinetic data obtained from  $^{31}\text{P}$ -NMR monitoring, as the  $^1\text{H}$ -NMR data are significantly overlaid by substrate decomposition (*vide supra*). Accurate modeling was found to be complicated, since more reaction steps have to be taken into consideration compared to reactions of substrate *cis*-1. As a result, there is a significantly larger space of possible solutions that exhibit comparable deviation from the experimental data.

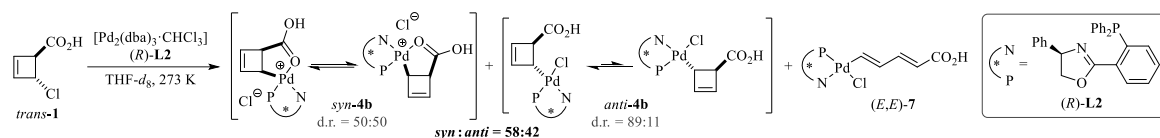
Optimization of the numerical model was performed as described above. The residual was minimized by varying  $k_{\text{OA}}^{\text{major},\text{syn}}$ ,  $k_{\text{OA}}^{\text{minor},\text{syn}}$ ,  $k_{\text{OA}}^{\text{major},\text{anti}}$ ,  $k_{\text{major},\text{syn}}$ ,  $k_{\text{minor},\text{syn}}$ ,  $k_{\text{major},\text{anti}}$ ,  $k_{\text{minor},\text{anti}}$  and  $k_{\text{decomp}}$  with pre-determined  $x_{\text{Pd}}(0) \equiv 0.5$  and  $k_{\text{OA}}^{\text{minor},\text{anti}} \equiv 0$ . Optimization was conducted by a different person than the analytical treatment, without knowledge of the analytical solution for the rate constants of interest. A consistent solution is shown in Figure S11, featuring rate constants of  $k_{\text{major},\text{syn}} = 5.9 \cdot 10^{-5} \text{ s}^{-1}$ ,  $k_{\text{minor},\text{syn}} = 1.4 \cdot 10^{-5} \text{ s}^{-1}$ ,  $k_{\text{major},\text{anti}} = 2.8 \cdot 10^{-7} \text{ s}^{-1}$ ,  $k_{\text{minor},\text{anti}} = 2.8 \cdot 10^{-8} \text{ s}^{-1}$  and  $k_{\text{decomp}} = 1.9 \cdot 10^{-6} \text{ s}^{-1}$ , along with concentration-independent rate constant analogues of  $k_{\text{OA}}^{\text{major},\text{syn}} = 1.4 \cdot 10^{-3} \text{ s}^{-1}$ ,  $k_{\text{OA}}^{\text{minor},\text{syn}} = 1.5 \cdot 10^{-3} \text{ s}^{-1}$  and  $k_{\text{OA}}^{\text{major},\text{anti}} = 1.5 \cdot 10^{-4} \text{ s}^{-1}$ .

The equilibration rate constants of interest  $k_{\text{major},\text{syn}}$  and  $k_{\text{minor},\text{syn}}$  are slightly smaller than the values obtained by analytical modeling. The extracted values for  $k_{\text{major},\text{anti}}$  and  $k_{\text{minor},\text{anti}}$  are of no relevance, as the experimental data do not allow for observation of the equilibration between *major*- and *minor*-*anti*-4a. The ratio  $\frac{k_{\text{OA}}^{\text{major},\text{syn}} + k_{\text{OA}}^{\text{minor},\text{syn}}}{k_{\text{OA}}^{\text{major},\text{anti}}} = 95:5$  is consistent with the *syn*:*anti* selectivity observed experimentally.



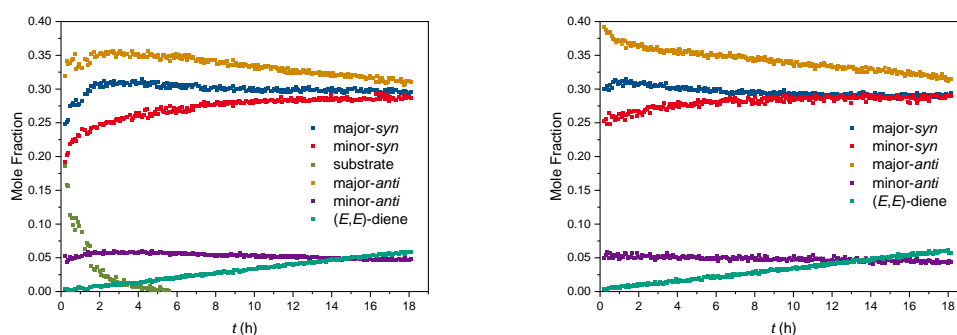
**Figure S11.** Numerical fitting of the experimental  $^{31}\text{P}$ -NMR reaction monitoring data for the oxidative addition of substrate *trans*-1 with ligand **L1** to interconverting Pd-cyclobutene species major- and minor-*syn*-**4a** along with small amounts of major-*anti*-**4a**.

#### Oxidative Addition of Acid Substrate *trans*-1 with Ligand **L2**



Alternating  $^1\text{H}$ - and  $^{31}\text{P}\{^1\text{H}\}$ -NMR reaction monitoring of the oxidative addition of *trans*-4-chlorocyclobutene-2-enecarboxylic acid *trans*-1 with ligand (*R*)-**L2** gave the temporal mole fraction profiles shown in Figure S12. In the  $^{31}\text{P}\{^1\text{H}\}$ -NMR series, only Pd-cyclobutene and Pd-diene species were quantified, as the Pd-pre-complex of **L2** cannot be observed by  $^{31}\text{P}$ -NMR. Consumption of substrate *trans*-1 was found to be slow, requiring ca. 5.6 h to reach full conversion.

In contrast to all other complexes investigated by NMR reaction monitoring, complexes major- and minor-*syn*-**4b** equilibrated to d.r. = 50:50 after being formed with an initial slight excess of major-*syn*-**4b** (d.r.  $\approx$  54:46). Complexes major- and minor-*anti*-**4b**, on the other hand, were detected with a constant d.r. of 89:11, confirming that equilibration between the *anti*-species involved is fast on the timescale of observation. Apart from the four Pd-cyclobutene species **4b**, small amounts of Pd-diene complex (*E,E*)-**7** were formed during reaction monitoring. According to the Woodward–Hoffmann rules,<sup>46</sup> (*E,E*)-**7** is the thermal electrocyclic ring-opening product of *anti*-**4b**. The corresponding (*E,Z*)- or (*Z,E*)-diene was not detected, indicating that *syn*-**4b** is stable against ring-opening at 273 K. In line with these observations, the overall mole fraction of major- and minor-*syn*-**4b** was approximately constant during the period of reaction monitoring, whilst the mole fractions of major- and minor-*anti*-**4b** slowly decreased.

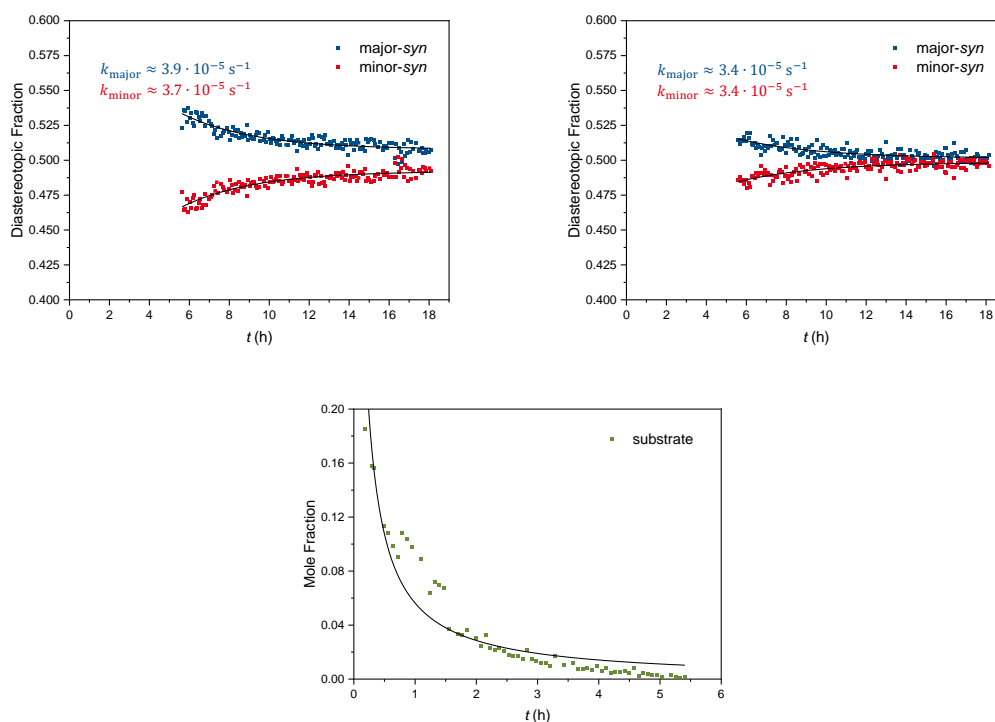


**Figure S12.** Experimental reaction monitoring data for the oxidative addition of substrate *trans*-1 with ligand **L2**, giving slowly interconverting Pd-cyclobutene species major- and minor-*syn*-**4b** along with rapidly equilibrating complexes major- and minor-*anti*-**4b**, as well as electrocyclic ring-opening product (*E,E*)-**7**. Reaction monitoring was performed by an alternating  $^1\text{H}$ - and  $^{31}\text{P}\{^1\text{H}\}$ -NMR series after preparation outside the spectrometer. Mole fraction values extracted from  $^1\text{H}$ -NMR spectra (left) refer to all cyclobutene and diene species involved, while mole fraction values extracted from  $^{31}\text{P}\{^1\text{H}\}$ -NMR spectra (right) refer to Pd-cyclobutene and Pd-diene species only.

The rate constants  $k_{\text{major}}$  and  $k_{\text{minor}}$  for the  $\eta^1\text{-}\eta^3\text{-}\eta^1$  isomerization between major- and minor-*syn*-**4b** were extracted by converting the reaction monitoring data from both  $^1\text{H}$ - and  $^{31}\text{P}\{^1\text{H}\}$ -NMR monitoring to temporal diastereotopic fraction profiles, which were subsequently fitted with equation (6) for  $t > 5.6$  h, i.e. after oxidative addition is completed (Figure S13, top). As the remaining part of the reaction monitoring data was not indicative enough for accurate regression, only approximate rate constants can be extracted by the analytical fitting approach. Still, the regression

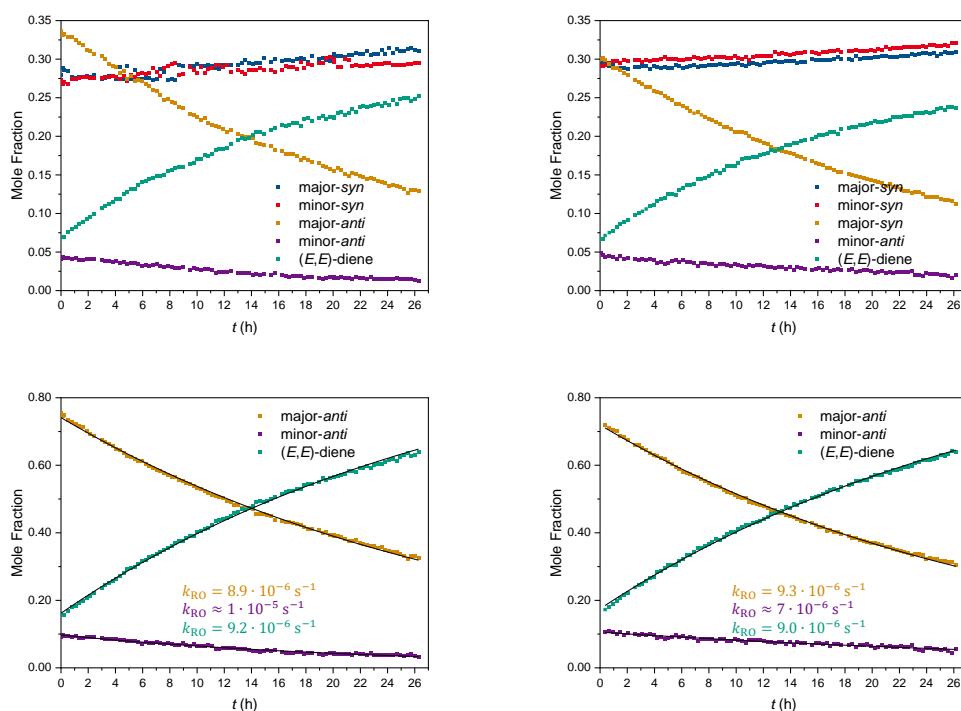
function was found to be in good agreement with the experimental data, giving consistent rate constants of  $k_{\text{major}} \approx 3.9 \cdot 10^{-5} \text{ s}^{-1}$ ;  $k_{\text{minor}} \approx 3.7 \cdot 10^{-5} \text{ s}^{-1}$  ( $^1\text{H}$ -NMR) and  $k_{\text{major}} \approx 3.4 \cdot 10^{-5} \text{ s}^{-1}$ ;  $k_{\text{minor}} \approx 3.4 \cdot 10^{-5} \text{ s}^{-1}$  ( $^{31}\text{P}\{^1\text{H}\}$ -NMR), respectively.

Oxidative addition proceeded to > 80 % conversion during the death time (11 min for  $^1\text{H}$ -NMR monitoring, 12 min for  $^{31}\text{P}\{^1\text{H}\}$ -NMR monitoring) and could therefore not be modeled with high accuracy. Attempts to fit the decay of substrate *trans*-**1** with integrated second order kinetic rate law (11) resulted in a regression with only moderate quality (Figure S13, bottom). A potential explanation is that the basic assumption  $k_{\text{O}_A}^{\text{major}} = k_{\text{O}_A}^{\text{minor}}$ , on which equation (11) is based on, is not valid for the formation of major- and minor-*syn*-**4b**, as major-*syn*-**4b** is slightly enriched prior to equilibration, and thus formed with a somewhat higher rate compared to minor-*syn*-**4b**. Furthermore, *trans*-**1** might undergo competing first order decomposition.



**Figure S13.** Analytical kinetic fitting of the oxidative addition of substrate *trans*-**1** with ligand **L2** to slowly interconverting Pd-cyclobutene species major- and minor-*syn*-**4b** and rapidly equilibrating complexes major- and minor-*anti*-**4b**:  $\eta^1\text{-}\eta^3\text{-}\eta^1$  equilibration of major- and minor-*syn*-**4b** according to equation (6), using data from  $^1\text{H}$ -NMR (top left) and  $^{31}\text{P}\{^1\text{H}\}$ -NMR monitoring (top right); and conversion of *trans*-**1** according to equation (11) (bottom).

In order to characterize the electrocyclic ring-opening of *anti*-**4b** to (*E,E*)-**7**, the temperature was increased to 283 K and the reaction was monitored by an alternating  $^1\text{H}$ - and  $^{31}\text{P}\{^1\text{H}\}$ -NMR series, giving the temporal mole fraction profiles shown in Figure S14. The decay of major-*anti*-**4b** and the formation of (*E,E*)-**7** extracted from both  $^1\text{H}$ - and  $^{31}\text{P}\{^1\text{H}\}$ -NMR reaction monitoring data could be accurately fitted using equation (17) and (20), respectively, giving experimental rate constants of  $k_{\text{R}0} = 8.9 - 9.3 \cdot 10^{-6} \text{ s}^{-1}$ . The decay of minor-*anti*-**4b** was found not to be indicative enough for accurate kinetic modeling.



**Figure S14.** Top: Experimental reaction monitoring data for the electrocyclic ring-opening of Pd-cyclobutene species **major-anti-4b** and **minor-syn-4b** to diene **(E,E)-7** in the presence of stable complexes **major-anti-4b** and **minor-syn-4b** along with rapidly equilibrating complexes **major-syn-4b** and **minor-anti-4b**. Reaction monitoring was performed by an alternating  $^1\text{H}$ - (left) and  $^{31}\text{P}\{^1\text{H}\}$ -NMR series (right) after increasing the temperature to 283 K, and mole fraction values were calculated with respect to all cyclobutene and diene species involved. Bottom: Analytical kinetic fitting of the ring-opening of **major-anti-4b** and **minor-syn-4b** to diene **(E,E)-7** according to equation (20), using data from  $^1\text{H}$ -NMR (left) and  $^{31}\text{P}\{^1\text{H}\}$ -NMR monitoring (right). Mole fraction values are given with respect to the reactive system considered, i.e. **major-anti-4b** and **minor-syn-4b** and **(E,E)-7** only.

Attempts to extract accurate values for rate constants  $k_{\text{major,syn}}$  and  $k_{\text{minor,syn}}$  by complementary numerical analysis were unproductive. The reason for this was the increased complexity of this system with ring-opening as additional path, resulting in a very large space of possible solutions that exhibit comparable deviation from the experimental data.

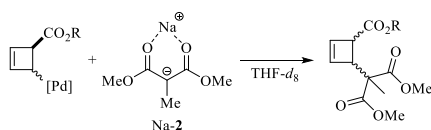
## Comparison

Table S12 gives an overview of the rate constants extracted for the four equilibria investigated, employing analytical and numerical analysis of  $^1\text{H}$ - and  $^{31}\text{P}$ -NMR reaction monitoring data. The values that are assumed to be the most accurate are highlighted in bold.

**Table S12.** Comparison of equilibrium rate constants  $k_{\text{major}}$  and  $k_{\text{minor}}$  extracted by analytical and numerical analysis of  $^1\text{H}$ - and  $^{31}\text{P}$ -NMR monitoring data, with the values that are considered to be the most accurate highlighted in bold.

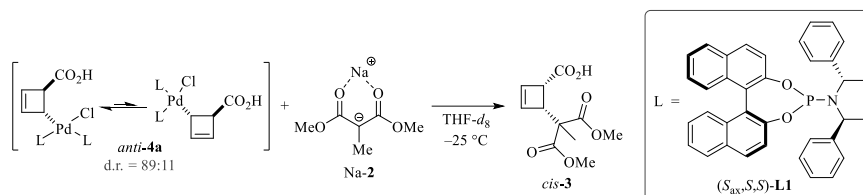
Equilibrium	Analytical Analysis $^1\text{H}$ -NMR		Analytical Analysis $^{31}\text{P}$ -NMR		Numerical Analysis $^1\text{H}$ -NMR		Numerical Analysis $^{31}\text{P}$ -NMR	
	$k_{\text{major}} / \text{s}^{-1}$	$k_{\text{minor}} / \text{s}^{-1}$	$k_{\text{major}} / \text{s}^{-1}$	$k_{\text{minor}} / \text{s}^{-1}$	$k_{\text{major}} / \text{s}^{-1}$	$k_{\text{minor}} / \text{s}^{-1}$	$k_{\text{major}} / \text{s}^{-1}$	$k_{\text{minor}} / \text{s}^{-1}$
<b>major-anti-4a</b> $\rightleftharpoons$ <b>minor-anti-4a</b>	<b><math>4.1 \cdot 10^{-3}</math></b>	<b><math>3.8 \cdot 10^{-4}</math></b>	n.d.	n.d.	<b><math>4.1 \cdot 10^{-3}</math></b>	<b><math>3.7 \cdot 10^{-4}</math></b>	n.d.	n.d.
<b>major-anti-4b</b> $\rightleftharpoons$ <b>minor-anti-4b</b>	$\geq 1.7 \cdot 10^{-2}$	$\geq 1.7 \cdot 10^{-3}$	$\geq 1.7 \cdot 10^{-2}$	$\geq 2.1 \cdot 10^{-3}$	<b><math>2.4 \cdot 10^{-2}</math></b>	<b><math>2.3 \cdot 10^{-3}</math></b>	n.d.	n.d.
<b>major-syn-4a</b> $\rightleftharpoons$ <b>minor-syn-4a</b>	$6.6 \cdot 10^{-5}$	$1.6 \cdot 10^{-5}$	<b><math>6.7 \cdot 10^{-5}</math></b>	<b><math>1.5 \cdot 10^{-5}</math></b>	n.d.	n.d.	$5.9 \cdot 10^{-5}$	$1.4 \cdot 10^{-5}$
<b>major-syn-4b</b> $\rightleftharpoons$ <b>minor-syn-4b</b>	$\approx 3.9 \cdot 10^{-5}$	$\approx 3.7 \cdot 10^{-5}$	$\approx 3.4 \cdot 10^{-5}$	$\approx 3.4 \cdot 10^{-5}$	n.d.	n.d.	n.d.	n.d.

## 6 Reactivity of Pd-Cyclobutene Complexes



The reactivity of Pd-cyclobutene complexes *anti*-**4a**, *anti*-**4b**, *syn*-Na-**4a**, *syn*-Na-**4b** and *syn*-**6a** (prepared according to section 4) as potential reaction intermediates was tested by treating with nucleophile Na-2 according to the subsequent procedures. All reactions were performed in anhydrous THF-*d*<sub>8</sub> under inert atmosphere upon cooling. The reaction mixture was directly investigated by <sup>1</sup>H-, <sup>13</sup>C and <sup>31</sup>P-NMR (if required supplemented by suitable 2D experiments such as <sup>1</sup>H-<sup>1</sup>H-COSY, <sup>1</sup>H-<sup>13</sup>C-HSQC, <sup>1</sup>H-<sup>13</sup>C/<sup>31</sup>P-HMBC, <sup>1</sup>H-<sup>1</sup>H-EASY-ROESY and <sup>1</sup>H-DOSY) and ESI-HRMS in positive and negative ion mode. If the Pd-cyclobutene complex was found to be completely converted, the reaction mixture was subjected to work-up, and the crude product was investigated by NMR spectroscopy and ESI-HRMS. The e.e. was determined by <sup>1</sup>H-NMR after addition of (*S*)-PEA (products *cis*- and *trans*-**4**) or Eu(hfc)<sub>3</sub> (product *trans*-**6**) to the NMR sample.

### Reactivity of Pd-Complex *anti*-**4a**



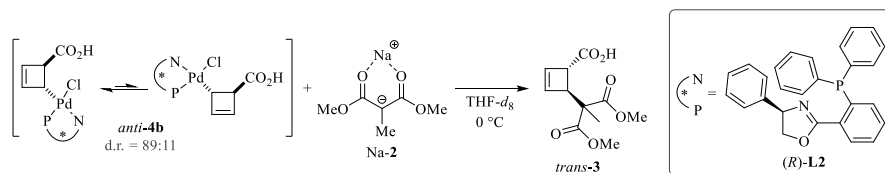
To a stirred solution of nucleophile Na-2 (ca. 95 w% purity, 26.5 mg, 150 μmol, 3 equiv.) in anhydrous THF-*d*<sub>8</sub> (1 mL) was carefully added a solution of Pd-complexes *anti*-**4a** (ca. 50 μmol, 1 equiv., prepared from *cis*-**1** according to section 4) in anhydrous THF-*d*<sub>8</sub> (1 mL) at -25 °C. After further 5 min of stirring, one drop of the reaction mixture was taken for subsequent MS analysis, and the residual solution was transferred into an NMR tube.

<sup>31</sup>P-NMR analysis indicated complete consumption of *anti*-**4a** upon regeneration of [PdL<sub>2</sub>] and free (*S*<sub>ax</sub>,*S*,*S*)-**L1**. Product *cis*-**3** was detected by <sup>1</sup>H-NMR, <sup>13</sup>C-NMR and ESI<sup>+</sup>-HRMS. Attempts to detect a potential η<sup>2</sup>-Pd-product complex by <sup>1</sup>H-, <sup>13</sup>C and <sup>31</sup>P-NMR, <sup>1</sup>H-<sup>1</sup>H-COSY, <sup>1</sup>H-<sup>13</sup>C-HSQC, <sup>1</sup>H-<sup>13</sup>C/<sup>31</sup>P-HMBC, <sup>1</sup>H-<sup>1</sup>H-ROESY, <sup>1</sup>H-DOSY and ESI<sup>+/−</sup>-HRMS were not successful.

The reaction mixture was then quenched with NaHCO<sub>3</sub> (12.6 mg, 150 μmol, 3 equiv.) at 0 °C followed by brine (2 mL). The aqueous layer was washed with Et<sub>2</sub>O (3 × 5 mL), carefully acidified with 1 N HCl (pH ≤ 2) and extracted with CH<sub>2</sub>Cl<sub>2</sub> (6 × 5 mL). The combined organic layers were dried over Na<sub>2</sub>SO<sub>4</sub> and concentrated *in vacuo*. The crude product *cis*-**3** was obtained with an NMR yield of approximately 25 % and a stereoselectivity of d.r. = 97:3 and e.e. = 83 %. Comparison of the NMR spectra after addition of (*S*)-PEA showed that the major enantiomer was the same as in the catalytic reactions (section 3).

When performing the reaction at 0 °C rather than -25 °C, product *cis*-**3** was obtained with lower yield (17 %) and significantly decreased stereoselectivity (d.r. = 68:32, e.e. = 44 %).

### Reactivity of Pd-Complex *anti*-**4b**

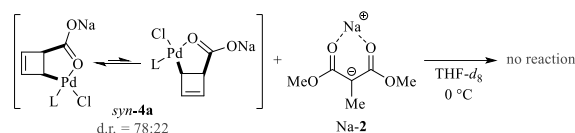


To a solution of nucleophile Na-2 (ca. 95 w% purity, 26.5 mg, 150 μmol, 3 equiv.) in anhydrous THF-*d*<sub>8</sub> (1 mL) sonicated in an ultrasonic bath at 0 °C was carefully added a solution of Pd-complexes *anti*-**4b** (ca. 50 μmol, 1 equiv., prepared from *cis*-**1** according to section 4) in anhydrous THF-*d*<sub>8</sub> (1 mL). After further 5 min of sonication, one drop of the reaction mixture was taken for subsequent MS analysis, and the residual solution was analyzed by NMR.

<sup>31</sup>P-NMR analysis indicated complete consumption of *anti*-**4b**. Product *trans*-**3** was detected by <sup>1</sup>H-NMR, <sup>13</sup>C-NMR and ESI<sup>+</sup>-HRMS. Attempts to detect a potential η<sup>2</sup>-Pd-product complex by <sup>1</sup>H-, <sup>13</sup>C and <sup>31</sup>P-NMR, <sup>1</sup>H-<sup>1</sup>H-COSY, <sup>1</sup>H-<sup>13</sup>C-HSQC, <sup>1</sup>H-<sup>13</sup>C/<sup>31</sup>P-HMBC, <sup>1</sup>H-<sup>1</sup>H-ROESY, and ESI<sup>+/−</sup>-HRMS were not successful.

The reaction mixture was then quenched with NaHCO<sub>3</sub> (12.6 mg, 150 μmol, 3 equiv.) at 0 °C followed by brine (2 mL). The aqueous layer was washed with Et<sub>2</sub>O (3 × 5 mL), carefully acidified with 1 N HCl (pH ≤ 2) and extracted with CH<sub>2</sub>Cl<sub>2</sub> (6 × 5 mL). The combined organic layers were dried over Na<sub>2</sub>SO<sub>4</sub> and concentrated *in vacuo*. The crude product *trans*-**3** was obtained with an NMR yield of approximately 41 % and a stereoselectivity of d.r. = 99:1 and e.e. = 99 %. Comparison of the NMR spectra after addition of (*S*)-PEA showed that the major enantiomer was the same as in the catalytic reactions (section 3).

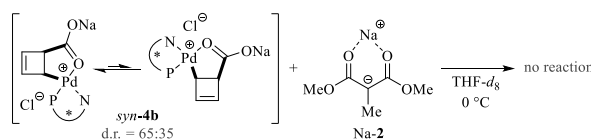
#### Reactivity of Pd-Complex *syn*-Na-4a



To a solution of Pd-complexes *syn*-Na-**4a** (ca. 50 μmol, 1 equiv., prepared from *trans*-**1** according to section 4) in anhydrous THF-*d*<sub>8</sub> (1 mL) sonicated in an ultrasonic bath at 0 °C was carefully added a solution of nucleophile Na-**2** (ca. 95 w% purity, 26.5 mg, 150 μmol, 3 equiv.) in anhydrous THF-*d*<sub>8</sub> (1 mL). After further 5 min of sonication, one drop of the reaction mixture was taken for subsequent MS analysis, and the residual solution was analyzed by NMR.

<sup>31</sup>P-NMR analysis indicated no consumption of *syn*-Na-**4a**, which was confirmed by <sup>1</sup>H-NMR, <sup>1</sup>H-<sup>31</sup>P-HMBC and ESI<sup>+</sup>-HRMS. <sup>1</sup>H-NMR and <sup>13</sup>C-NMR analysis furthermore indicated no detectable product formation and verified nucleophile Na-**2** to be present in excess. The mixture was allowed to stand at 4 °C for one week, which did not result in consumption of *syn*-Na-**4a** or any detectable product formation. Neither did treatment with additional [Pd<sub>2</sub>(dba)<sub>3</sub>·CHCl<sub>3</sub>] (25.9 mg, 25 μmol, 0.5 equiv.) and additional nucleophile Na-**2** (ca. 95 w% purity, 26.5 mg, 150 μmol, 3 equiv.).

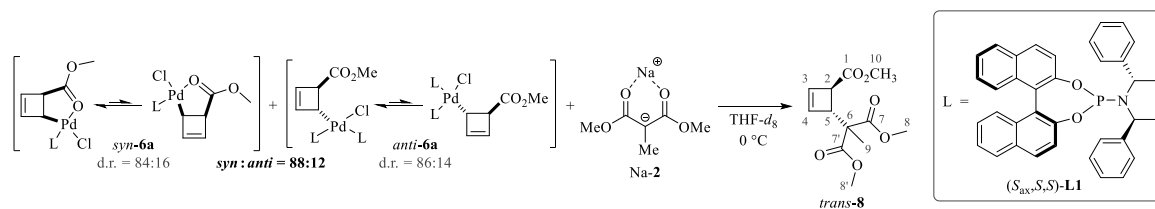
#### Reactivity of Pd-Complex *syn*-Na-4b



To a solution of Pd-complexes *syn*-Na-**4b** (ca. 50 μmol, 1 equiv., prepared from *trans*-**1** according to section 4) in anhydrous THF-*d*<sub>8</sub> (1 mL) sonicated in an ultrasonic bath at 0 °C was carefully added a solution of nucleophile Na-**2** (ca. 95 w% purity, 26.5 mg, 150 μmol, 3 equiv.) in anhydrous THF-*d*<sub>8</sub> (1 mL). After further 5 min of sonication, one drop of the reaction mixture was taken for subsequent MS analysis, and the residual solution was analyzed by NMR.

<sup>31</sup>P-NMR analysis indicated no consumption of *syn*-Na-**4b**, which was confirmed by <sup>1</sup>H-NMR, <sup>1</sup>H-<sup>31</sup>P-HMBC and ESI<sup>+</sup>-HRMS. <sup>1</sup>H-NMR and <sup>13</sup>C-NMR analysis furthermore indicated no detectable product formation and verified nucleophile Na-**2** to be present in excess. The mixture was allowed to stand at 4 °C for two weeks, which did not result in consumption of *syn*-Na-**4b** or any detectable product formation. Neither did treatment with additional [Pd<sub>2</sub>(dba)<sub>3</sub>·CHCl<sub>3</sub>] (25.9 mg, 25 μmol, 0.5 equiv.) and additional nucleophile Na-**2** (ca. 95 w% purity, 26.5 mg, 150 μmol, 3 equiv.).

#### Reactivity of Pd-Complex *syn*-6a – Preparation of Methyl-(1*R*,4*R*)-4-(1,3-dimethoxy-2-methyl-1,3-dioxopropan-2-yl)cyclobut-2-ene-1-carboxylate (*trans*-**8**)



To a solution of a 88:12 mixture of Pd-complexes *syn*- and *anti*-**6a** (ca. 50 μmol, 1 equiv., prepared from *trans*-**5** according to section 4) in anhydrous THF-*d*<sub>8</sub> (1 mL) sonicated in an ultrasonic bath at 0 °C was carefully added a solution of nucleophile Na-**2** (ca. 95 w% purity, 26.5 mg, 150 μmol, 3 equiv.) in anhydrous THF-*d*<sub>8</sub> (1 mL). After further 5 min of sonication, one drop of the reaction mixture was taken for subsequent MS analysis, and the residual solution was analyzed by NMR.

<sup>31</sup>P-NMR analysis indicated complete consumption of *syn*-**6a**. Product *trans*-**8** was detected by <sup>1</sup>H-NMR, <sup>13</sup>C-NMR and ESI<sup>+</sup>-HRMS. Attempts to detect a potential η<sup>2</sup>-Pd-product complex by <sup>1</sup>H, <sup>13</sup>C and <sup>31</sup>P-NMR, <sup>1</sup>H-<sup>1</sup>H-COSY, <sup>1</sup>H-<sup>13</sup>C-HSQC, <sup>1</sup>H-<sup>13</sup>C/<sup>31</sup>P-HMBC, <sup>1</sup>H-<sup>1</sup>H-ROESY, and ESI<sup>+</sup>-HRMS were not successful.

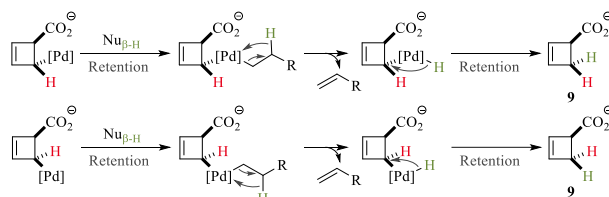
The reaction mixture was then quenched with NaHCO<sub>3</sub> (12.6 mg, 150 μmol, 3 equiv.) and directly subjected to flash column chromatography on silica gel (*n*-hexane:EtOAc 97:3 → 94:6) to give a crude sample of the title compound *trans*-**8**. The e.e. was determined to be 52 %. The absolute configuration of products obtained by Pd-catalyzed allylic alkylation of *trans*-configured cyclobutene ester substrates with chloride as leaving group, malonate nucleophiles and ligand (*R*<sub>ax</sub>,*R*,*R*)-**L1** has been determined in the literature to be (1*S*,4*S*).<sup>22,29</sup> As we used the enantiomeric ligand (*S*<sub>ax</sub>,*S*,*S*)-**L1**, the absolute configuration of *trans*-**8** should be (1*R*,4*R*), accordingly.

Product **8** was expected to be formed with a d.r. of 88:12, corresponding to the *syn:anti* ratio of complex mixture **6a** with the nucleophile attacking under inversion of configuration. However, the *cis*-diastereomer of **8** could be identified neither in the reaction mixture after nucleophile addition nor in the fractions obtained from flash column chromatography. Hence, the d.r. is assumed to be >95:5. The reason for the absence of *cis*-**8** might be decomposition of *anti*-**6a** rather than productive nucleophilic substitution.

<sup>1</sup>H-NMR (700 MHz, CDCl<sub>3</sub>, 273 K): δ<sub>H</sub> = 6.22 (1H, dt, <sup>3</sup>J<sub>HH</sub> = 2.8, <sup>3</sup>J<sub>HH</sub> ≈ <sup>4</sup>J<sub>HH</sub> ≈ 1.1, C(4)*H*), 6.13 (1H, br. d, <sup>3</sup>J<sub>HH</sub> = 2.8, C(3)*H*), 3.72 (3H, s, C(8/8')*H*<sub>3</sub>), 3.72 (3H, s, C(8/8')*H*<sub>3</sub>), 3.70 (3H, s, C(10)*H*<sub>3</sub>), 3.61 (1H, br. s, C(5)*H*), 3.45 (1H, br. s, C(2)*H*), 1.43 (3H, s, C(9)*H*<sub>3</sub>) ppm; <sup>13</sup>C{<sup>1</sup>H}-NMR (176 MHz, CDCl<sub>3</sub>, 273 K): δ<sub>C</sub> = 172.8 (C(1)), 171.8 (C(7/7')), 171.6 (C(7/7')), 140.0 (C(4)), 135.2 (C(3)), 54.6 (C(6)), 52.8 (C(8), C(8')), 52.2 (C(10)), 50.6 (C(5)), 47.3 (C(2)), 17.4 (C(9)) ppm; PSYCHEDELICs (700 MHz, CDCl<sub>3</sub>, 273 K): J<sub>HH</sub> = 1.9 ± 0.1 (H2-H5), 1.0 ± 0.1 (major CB H2-H3), 1.0 ± 0.1 (major CB H2-H4) Hz; HRMS (ESI<sup>+</sup>): C<sub>12</sub>H<sub>17</sub>O<sub>6</sub> [M+H]<sup>+</sup> requires 257.1020, found 257.1023 (Δ = 1.2 ppm).

## 7 Capture of Intermediates

In order to shine light on the relative configuration of the Pd-cyclobutene species involved under catalytic conditions, it was attempted to capture the Pd-complexes by stereoselective β-H elimination followed by reductive elimination of the intermediate palladium hydride species, which is a typical side reaction in catalytic allylic alkylation with unstabilized nucleophiles. Since both β-H elimination and reductive elimination proceed under retention of configuration,<sup>47,48</sup> the reduced cyclobutene **9** is obtained with overall retention with respect to the Pd-species captured (Scheme S7).



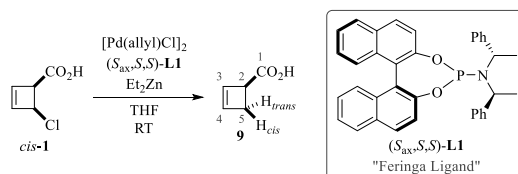
**Scheme S7.** β-H elimination of *anti*- (top) and *syn*-configured (bottom) Pd-cyclobutene complexes with unstabilized nucleophiles Nu<sub>β-H</sub>.

To make the hydrogen originating from β-H elimination (colored green in Scheme S7) distinguishable from the adjacent hydrogen in the final elimination product **9** (red), two strategies are conceivable. On the one hand, a substrate deuterated at one or both of the allylic termini, which are equivalent as η<sup>1</sup>-complexes readily interconvert by η<sup>1</sup>-η<sup>3</sup>-η<sup>1</sup> isomerization (*vide supra*), would furnish β-H elimination product **9** deuterated in the red position. If a nucleophile deuterated in β-position is used, on the other hand, the resulting β-D elimination product would be expected to be deuterated in the green position. In both cases, the relative position of deuteration in the elimination product **9** would allow for assigning the relative configuration of the Pd-species captured.

We followed both strategies, and the results obtained consistently revealed that under all reaction conditions investigated (*cis*- and *trans*-substrate, ligand **L1** and **L2**) *anti*-configured Pd-species are present, whereas *syn*-Pd-species are only present when substrate *trans*-**1** is used.

### Allylic Alkylation with Deuterated Substrates and Unstabilized Nucleophiles

#### Cyclobut-2-ene-1-carboxylic acid (**9**) (Reference Reaction)



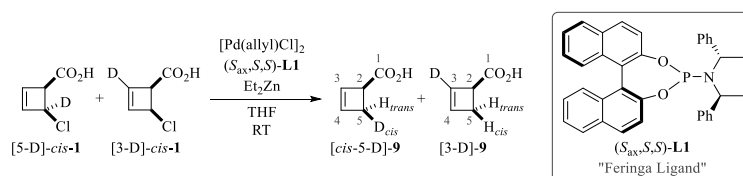
Cyclobut-2-ene-1-carboxylic acid **9** was prepared following a modified literature procedure.<sup>49</sup> To a stirred solution of [Pd(allyl)Cl]<sub>2</sub> (1.9 mg, 5.2 μmol, 5 mol%) and ligand (*S*<sub>ax</sub>,*S*,*S*)-**L1** (8.4 mg, 15.5 μmol, 15 mol%) in anhydrous THF (1 mL) was added one drop of Et<sub>2</sub>Zn (1.0 M in hexanes), followed by dropwise addition of a solution of *cis*-4-chlorocyclobutene-2-encarboxylic acid *cis*-**1** (13.7 mg, 103 μmol, 1 equiv.) in anhydrous THF (1 mL) and the remainder of Et<sub>2</sub>Zn (250 μL, 250 μmol, 2.4 equiv.). After stirring at RT for 2.5 h, the reaction mixture was cooled down to 0 °C and



quenched with satd. aq. NaHCO<sub>3</sub> (0.5 mL) followed by brine (3 mL). The aqueous layer was washed with Et<sub>2</sub>O (3 × 5 mL), carefully acidified with 1 N HCl (pH ≤ 2) and extracted with CH<sub>2</sub>Cl<sub>2</sub> (6 × 5 mL). The combined organic layers were dried over Na<sub>2</sub>SO<sub>4</sub> and concentrated *in vacuo* to give the crude product, which was found to be a 57:43 mixture of product **9** and substrate *cis*-**1**. Purification by flash column chromatography on silica gel (*n*-hexane:Et<sub>2</sub>O 70:30) gave the title compound as a colorless oil (3.2 mg, 33 μmol, 32 %).

<sup>1</sup>H-NMR (700 MHz, CDCl<sub>3</sub>, 273 K): δ<sub>H</sub> = 6.27 – 6.25 (1H, m, C(4)*H*), 6.05 (1H, dd, <sup>3</sup>J<sub>HH</sub> = 2.8, <sup>3</sup>J<sub>HH</sub> = 1.0, C(3)*H*), 3.72 – 3.70 (1H, m, C(2)*H*), 2.85 (1H, ddd, <sup>2</sup>J<sub>HH</sub> = 13.7, <sup>3</sup>J<sub>HH</sub> = 4.6, <sup>3</sup>J<sub>HH</sub> = 1.0, C(5)*HH*<sub>trans</sub>), 2.76 (1H, ddd, <sup>2</sup>J<sub>HH</sub> = 13.7, <sup>3</sup>J<sub>HH</sub> = 1.8, <sup>3</sup>J<sub>HH</sub> = 1.1, C(5)*HH*<sub>cis</sub>) ppm; <sup>13</sup>C{<sup>1</sup>H}-NMR (176 MHz, CDCl<sub>3</sub>, 273 K): δ<sub>C</sub> = 179.7 (C(1)), 139.9 (C(4)), 134.5 (C(3)), 45.6 (C(2)), 35.7 (C(5)) ppm; HRMS (ESI<sup>+</sup>): C<sub>5</sub>H<sub>7</sub>O<sub>2</sub> [M+H]<sup>+</sup> requires 99.0441, found 99.0441 (Δ = 0).

#### [2-<sup>2</sup>H<sub>1,0</sub>,*cis*-4-<sup>2</sup>H<sub>0,1</sub>]-Cyclobut-2-ene-1-carboxylic acid ([*cis*-5-D]/[3-D]-**9**) from Substrate [5-D]/[3-D]-*cis*-**1** with Ligand **L1**



The reaction was performed according to a modified literature procedure.<sup>49</sup> To a stirred solution of [Pd(allyl)Cl]<sub>2</sub> (1.9 mg, 5.1 μmol, 5 mol%) and ligand (S<sub>ax</sub>,S,S)-**L1** (8.3 mg, 15.3 μmol, 15 mol%) in anhydrous THF (1 mL) was added one drop of Et<sub>2</sub>Zn (1.0 M in hexanes), followed by dropwise addition of a solution of labeled substrate [5-D]/[3-D]-*cis*-**1** ([5-D]:[3-D] = 1:1.7, overall 94 %D, 13.6 mg, 102 μmol, 1 equiv., preparation see section 2) in anhydrous THF (1 mL) and the remainder of Et<sub>2</sub>Zn (250 μL, 250 μmol, 2.5 equiv.). After stirring at RT overnight (17.5 h), the reaction mixture was cooled down to 0 °C and quenched with satd. aq. NaHCO<sub>3</sub> (0.5 mL) followed by brine (3 mL). The aqueous layer was washed with Et<sub>2</sub>O (3 × 5 mL), carefully acidified with 1 N HCl (pH ≤ 2) and extracted with CH<sub>2</sub>Cl<sub>2</sub> (6 × 5 mL). The combined organic layers were dried over Na<sub>2</sub>SO<sub>4</sub> and concentrated *in vacuo* to give the crude product, which was investigated by NMR spectroscopy and ESI-HRMS.

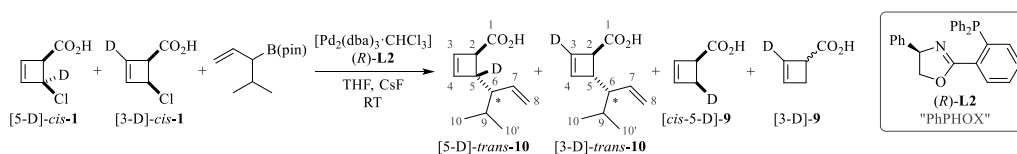
The crude product was found to be an isotopomeric 1:1 mixture of deuterated β-H elimination products [*cis*-5-D]- and [3-D]-**9**, obtained in 10 % NMR yield with an overall deuteration degree of 94 %D. The HRMS data are consistent with the product being only monodeuterated rather than 3,5-dideuterated. A <sup>1</sup>H-<sup>13</sup>C-HSQC experiment with increased resolution in the indirect dimension (TD(F1) = 744, SW = 60 ppm) confirmed that partial deuteration in 5-position was obtained exclusively *cis* to the carboxy group: The <sup>13</sup>C-resonance of C(5)DH (separated by Δδ = -0.3 ppm from C(5)H<sub>2</sub>) shows a correlation to the <sup>1</sup>H-resonance of C(5)*H*<sub>trans</sub>, but not to the <sup>1</sup>H-resonance of C(5)*H*<sub>cis</sub>.

The formation of [*cis*-5-D]-**9** shows that an *anti*-configured Pd-cyclobutene complex was captured (cf. Scheme S7). Furthermore, the 1:1 scrambling of the allylic termini rather than reproducing the 1:1.7 ratio of deuteration in the substrate indicates full η<sup>1</sup>-η<sup>3</sup>-η<sup>1</sup> equilibration to be operative under catalytic conditions.

<sup>1</sup>H-NMR (700 MHz, CDCl<sub>3</sub>, 273 K): δ<sub>H</sub> = 6.27 – 6.25 (1H, m, C(4)*H*), 6.05 (0.53H, dd, <sup>3</sup>J<sub>HH</sub> = 2.8, <sup>3</sup>J<sub>HH</sub> = 1.0, residual C(3)*H*), 3.72 – 3.70 (1H, m, C(2)*H*), 2.88 – 2.82 (1H, overlapping ddd and m, <sup>2</sup>J<sub>HH</sub> = 13.7, <sup>3</sup>J<sub>HH</sub> = 4.7, <sup>3</sup>J<sub>HH</sub> = 1.0, C(5)*HH*<sub>trans</sub> (ddd) and C(5)*DH*<sub>trans</sub> (m)), 2.76 (0.53H, ddd, <sup>2</sup>J<sub>HH</sub> = 13.7, <sup>3</sup>J<sub>HH</sub> = 1.8, <sup>3</sup>J<sub>HH</sub> = 1.0, residual C(5)*HH*<sub>cis</sub>) ppm; <sup>2</sup>H-NMR (108 MHz, CH<sub>2</sub>Cl<sub>2</sub>, 273 K): δ<sub>D</sub> = 6.07 (1D, s, C(3)*D*), 2.72 (1D, d, <sup>2</sup>J<sub>DH</sub> = 2.1, C(5)*HD*<sub>cis</sub>) ppm; <sup>13</sup>C{<sup>1</sup>H}-NMR (176 MHz, CDCl<sub>3</sub>, 273 K): δ<sub>C</sub> = 179.5 (C(1)), 139.8 (br. s, C(4)), 134.6 (C(3)*H*), 134.3 (1:1:1 t, <sup>1</sup>J<sub>CD</sub> = 27.0, C(3)*D*), 45.4 (C(2)), 45.4 (C(2)), 35.7 (C(5)H<sub>2</sub>), 35.4 (1:1:1 t, <sup>1</sup>J<sub>CD</sub> = 21.8, C(5)DH) ppm; HRMS (ESI<sup>+</sup>): C<sub>5</sub>H<sub>6</sub>DO<sub>2</sub> [M+H]<sup>+</sup> requires 100.0503, found 100.0506 (Δ = 2.7 ppm). In the <sup>13</sup>C-NMR spectrum, the two singlets observed for C(2) correspond to different product isotopomers (i.e. [*cis*-5-D]- and [3-D]-**9**) and could not be further assigned.

When performing this reaction with ligand (*R*)-**L2** (30 mol%) rather than (S<sub>ax</sub>,S,S)-**L1**, only unconverted substrate [5-D]/[3-D]-*cis*-**1** was obtained.

#### [2-<sup>2</sup>H<sub>1,0</sub>,4-<sup>2</sup>H<sub>0,1</sub>]-*trans*-4-(4-Methylpent-1-en-3-yl)cyclobut-2-ene-1-carboxylic acid ([5-D]/[3-D]-*trans*-**10**) and [2-<sup>2</sup>H<sub>1,0</sub>,*cis*-4-<sup>2</sup>H<sub>0,1</sub>]-Cyclobut-2-ene-1-carboxylic acid ([*cis*-5-D]/[3-D]-**9**) from Substrate [5-D]/[3-D]-*cis*-**1** with Ligand **L2**



The reaction was performed according to a modified literature procedure.<sup>27</sup> To a stirred mixture of [Pd<sub>2</sub>(dba)<sub>3</sub>·CHCl<sub>3</sub>] (5.2 mg, 5.0 μmol, 5 mol%), ligand (*R*)-**L2** (6.1 mg, 15.0 μmol, 15 mol%) and CsF (152 mg, 1.0 mmol, 10 equiv.) in anhydrous THF (1 mL) was added 4,4,5,5-tetramethyl-2-(4-methylpent-1-en-3-yl)-1,3,2-dioxaborolane (84.1 mg, 400 μmol, 4 equiv.), followed by dropwise addition of a solution of labeled substrate [5-D]/[3-D]-*cis*-**1** ([5-D]:[3-D] = 1:1.7, overall 94 %D, 13.6 mg, 102 μmol, 1 equiv., preparation see section 2) in anhydrous THF (1 mL). After

stirring at RT overnight (15 h), the reaction mixture was cooled down to 0 °C and quenched with satd. aq. Na<sub>2</sub>CO<sub>3</sub> (0.2 mL) followed by brine (3 mL). The aqueous layer was washed with Et<sub>2</sub>O (3 × 5 mL), carefully acidified with 1 N HCl (pH ≤ 2) and extracted with CH<sub>2</sub>Cl<sub>2</sub> (6 × 5 mL). The combined organic layers were dried over Na<sub>2</sub>SO<sub>4</sub> and concentrated *in vacuo* to give the crude product, which was investigated by NMR spectroscopy and ESI-HRMS.

The crude product was found to be a complex mixture of unconverted substrate [5-D]/[3-D]-*cis*-1 (40 % NMR yield), allylated product [5-D]/[3-D]-*trans*-10 (20 % NMR yield, overall 94 %D) and β-H elimination product [*cis*-5-D]/[3-D]-9 (4 % NMR yield, overall ca. 96 %D). Products [5-D]/[3-D]-*trans*-10 and [*cis*-5-D]/[3-D]-9 were obtained as 1:1 mixture of both isotopomers, and the HRMS data are consistent with all products being only monodeuterated rather than 3,5-dideuterated.

As the *cis*-isomer of [5-D]/[3-D]-*trans*-10 could not be detected (i.e. *trans:cis* > 95:5), productive allylic substitution is concluded to proceed stereoselectively with inversion of configuration. Substitution product [5-D]/[3-D]-*trans*-10 was obtained as an epimeric 74:26 mixture with respect to stereocenter C(6) (marked with an \*). For both the major and the minor epimer, an e.e. of 89 % was determined. Unconverted substrate [5-D]/[3-D]-*cis*-1 was found to be racemic (e.e. ≤ 2 %).

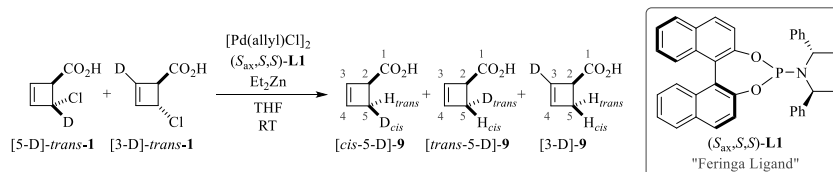
For elimination product [*cis*-5-D]/[3-D]-9, a <sup>1</sup>H-<sup>13</sup>C-HSQC experiment with increased resolution in the indirect dimension (TD(F1) = 744, SW = 60 ppm) confirmed that partial deuteration in 5-position was obtained exclusively *cis* to the carboxy group: The <sup>13</sup>C-resonance of C(5)DH (separated by Δδ = -0.3 ppm from C(5)H<sub>2</sub>) shows a correlation to the <sup>1</sup>H-resonance of C(5)H<sub>trans</sub>, but not to the <sup>1</sup>H-resonance of C(5)H<sub>cis</sub>.

The formation of [*cis*-5-D]-9 shows that an *anti*-configured Pd-cyclobutene complex was captured (cf. Scheme S7). Furthermore, the 1:1 scrambling of the allylic termini rather than reproducing the 1:1.7 ratio of deuteration in the substrate indicates full η<sup>1</sup>-η<sup>3</sup>-η<sup>1</sup> equilibration to be operative under catalytic conditions.

Given below are the characterization data for both epimers of allylated product isotopomers [5-D]/[3-D]-*trans*-10.

**<sup>1</sup>H-NMR** (700 MHz, CDCl<sub>3</sub>, 273 K): δ<sub>H</sub> = 6.39 (1H, br. s, major C(4)H), 6.27 (0.35H, br. s, minor C(4)H), 6.11 (0.53H, dd, <sup>3</sup>J<sub>HH</sub> = 2.8, <sup>3</sup>J<sub>HH</sub> = 1.0, major residual C(3)H), 6.07 (0.19H, dd, <sup>3</sup>J<sub>HH</sub> = 2.8, <sup>3</sup>J<sub>HH</sub> = 1.0, minor residual C(3)H), 5.65 (1H, dt, <sup>3</sup>J<sub>HH</sub> = 17.0, <sup>3</sup>J<sub>HH</sub> = 9.8, major C(7)H), 5.59 (0.35H, dt, <sup>3</sup>J<sub>HH</sub> = 17.1, <sup>3</sup>J<sub>HH</sub> = 9.9, minor C(7)H), 5.11 – 5.09 (1.35H, m, major + minor C(8)HH<sub>trans</sub>), 5.04 (1H, dd, <sup>3</sup>J<sub>HH</sub> = 17.0, <sup>2</sup>J<sub>HH</sub> = 1.6, major C(8)HH<sub>cis</sub>), 5.01 (0.35H, dd, <sup>3</sup>J<sub>HH</sub> = 17.1, <sup>2</sup>J<sub>HH</sub> = 1.9, minor C(8)HH<sub>cis</sub>), 3.27 (0.35H, dd, <sup>3</sup>J<sub>HH</sub> = 1.9, <sup>3</sup>J<sub>HH</sub> = 1.0, minor C(2)H), 3.24 (1H, dd, <sup>3</sup>J<sub>HH</sub> = 1.4, <sup>3</sup>J<sub>HH</sub> = 1.0, major C(2)H), 3.10 (0.19H, br. d, <sup>3</sup>J<sub>HH</sub> = 8.6, minor residual C(5)H), 3.08 (0.53H, br. d, <sup>3</sup>J<sub>HH</sub> = 10.1, major residual C(5)H), 1.96 – 1.93 (0.35H, m, minor C(6)H), 1.93 – 1.89 (1H, m, major C(6)H), 1.82 – 1.72 (1.35H, m, major + minor C(9)H), 0.90 (1.05H, d, <sup>3</sup>J<sub>HH</sub> = 6.9, minor C(10/10')H<sub>3</sub>), 0.89 (3H, d, <sup>3</sup>J<sub>HH</sub> = 6.9, major C(10/10')H<sub>3</sub>), 0.85 (1.05H, d, <sup>3</sup>J<sub>HH</sub> = 6.8, minor C(10/10')H<sub>3</sub>), 0.84 (3H, d, <sup>3</sup>J<sub>HH</sub> = 6.9, major C(10/10')H<sub>3</sub>) ppm; **<sup>2</sup>H-NMR** (108 MHz, CH<sub>2</sub>Cl<sub>2</sub>, 273 K): δ<sub>D</sub> = 6.12 (1D, br. s, major + minor C(3)D), 3.06 (1D, br. s, major + minor C(5)D) ppm; **<sup>13</sup>C{<sup>1</sup>H}-NMR** (176 MHz, CDCl<sub>3</sub>, 273 K): δ<sub>C</sub> = 179.8 (minor C(1)), 179.8 (major C(1)), 142.9 (major C(4)), 142.7 (major C(4)), 142.3 (minor C(4)), 142.1 (minor C(4)), 137.1 (major C(7)), 137.1 (major C(7)), 136.4 (minor C(7)), 133.7 (major C(3)H), 133.4 (1:1:1 t, <sup>1</sup>J<sub>CD</sub> ≈ 27.2, major C(3)D), 132.9 (minor C(3)H), 132.6 (1:1:1 t, <sup>1</sup>J<sub>CD</sub> ≈ 27.3, minor C(3)D), 117.6 (minor C(8)), 117.4 (major C(8)), 54.4 (major C(6)), 54.3 (major C(6)), 53.8 (minor C(6)), 49.9 (major C(2)), 49.9 (major C(2)), 49.8 (major C(5)H), 49.7 (minor C(5)H), 49.4 (1:1:1 t, <sup>1</sup>J<sub>CD</sub> ≈ 21.2, major + minor C(5)D), 30.2 (minor C(9)), 30.2 (minor C(9)), 29.7 (major C(9)), 29.7 (major C(9)), 21.6 (major C(10/10')), 21.6 (major C(10/10')), 21.5 (minor C(10/10')), 21.4 (minor C(10/10')), 18.5 (minor C(10/10')), 18.5 (minor C(10/10')), 17.9 (major C(10/10')), 17.9 (major C(10/10')) ppm; **HRMS** (ESI<sup>+</sup>): C<sub>11</sub>H<sub>16</sub>DO<sub>2</sub> [M+H]<sup>+</sup> requires 182.1286, found 182.1289 (Δ = 1.8 ppm). In the <sup>13</sup>C-NMR spectrum, the two singlets observed for major C(2), major + minor C(4), major C(7), major C(6), major + minor C(9) and major + minor C(10/10'), respectively, correspond to different product isotopomers (i.e. [*cis*-5-D]- and [3-D]-9) and could not be further assigned.

**[2-<sup>2</sup>H<sub>1,0,0</sub>,*cis*-4-<sup>2</sup>H<sub>0,1,0</sub>,*trans*-4-<sup>2</sup>H<sub>0,0,1</sub>]-Cyclobut-2-ene-1-carboxylic acid ([*cis*-5-D]/[*cis*-5-D]/[3-D]-9) from Substrate [5-D]/[3-D]-*trans*-1 with Ligand L1**



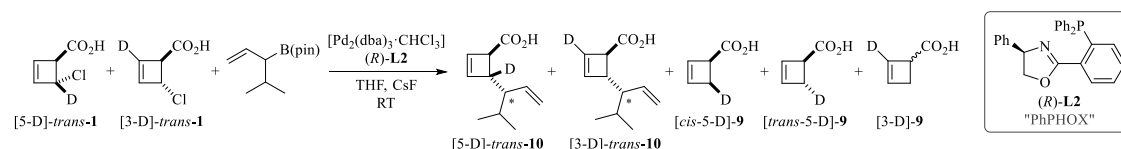
The reaction was performed according to a modified literature procedure.<sup>49</sup> To a stirred solution of [Pd(allyl)Cl]<sub>2</sub> (2.1 mg, 5.7 μmol, 5 mol%) and ligand (S<sub>ax</sub>,S,S)-L1 (9.3 mg, 17.2 μmol, 15 mol%) in anhydrous THF (1 mL) was added one drop of Et<sub>2</sub>Zn (1.0 M in hexanes), followed by dropwise addition of a solution of labeled substrate [5-D]/[3-D]-*trans*-1 ([5-D]:[3-D] = 3.6:1, overall 94 %D, 15.3 mg, 114 μmol, 1 equiv., preparation see section 2) in anhydrous THF (1 mL) and the remainder of Et<sub>2</sub>Zn (275 μL, 275 μmol, 2.5 equiv.). After stirring at RT overnight (16 h), the reaction mixture was cooled down to 0 °C and quenched with satd. aq. NaHCO<sub>3</sub> (0.5 mL) followed by brine (3 mL). The aqueous layer was washed with Et<sub>2</sub>O (3 × 5 mL), carefully acidified with 1 N HCl (pH ≤ 2) and extracted with CH<sub>2</sub>Cl<sub>2</sub> (6 × 5 mL). The combined organic layers were dried over Na<sub>2</sub>SO<sub>4</sub> and concentrated *in vacuo* to give the crude product, which was investigated by NMR spectroscopy and ESI-HRMS.

The crude product was found to be an isotopomeric ca. 43:8:49 mixture of deuterated  $\beta$ -H elimination products [*cis*-5-D]-, [*trans*-5-D]- and [3-D]-**9**, obtained in 7% NMR yield with an overall deuteration degree of ca. 95%**D**. The HRMS data are consistent with the product being only monodeuterated rather than di- or trideuterated. A  $^1\text{H}$ - $^{13}\text{C}$ -HSQC experiment with increased resolution in the indirect dimension (TD(F1) = 744, SW = 60 ppm) confirmed that partial deuteration was obtained in both *cis*- and *trans*-5-position with respect to the carboxy group: The  $^{13}\text{C}$ -resonance of C(5)DH (separated by  $\Delta\delta\text{c} = -0.3$  ppm from C(5)H<sub>2</sub>) shows a correlation to the  $^1\text{H}$ -resonance of C(5)H<sub>*trans*</sub> as well as to the  $^1\text{H}$ -resonance of C(5)H<sub>*cis*</sub>.

The formation of [*cis*-5-D]-**9** as well as [*trans*-5-D]-**9** shows that both an *anti*- and a *syn*-configured Pd-cyclobutene complex were captured (cf. Scheme S7).

**$^1\text{H}$ -NMR** (700 MHz, CDCl<sub>3</sub>, 273 K):  $\delta_{\text{H}} = 6.27 - 6.25$  (1H, m, C(4)H), 6.06 (0.53H, dd,  $^3J_{\text{HH}} = 2.8$ ,  $^3J_{\text{HH}} \approx 0.9$ , residual C(3)H), 3.72 - 3.69 (1H, m, C(2)H), 2.88 - 2.82 (0.92H, overlapping ddd and m,  $^2J_{\text{HH}} = 13.7$ ,  $^3J_{\text{HH}} = 4.7$ ,  $^3J_{\text{HH}} = 1.0$ , residual C(5)HH<sub>*trans*</sub> (ddd) and C(5)DH<sub>*trans*</sub> (m)), 2.78 - 2.72 (0.59H, overlapping ddd and m,  $^2J_{\text{HH}} = 13.7$ ,  $^3J_{\text{HH}} = 1.8$ ,  $^3J_{\text{HH}} = 1.0$ , residual C(5)HH<sub>*cis*</sub> (ddd) and C(5)DH<sub>*cis*</sub> (m)) ppm;  **$^2\text{H}$ -NMR** (108 MHz, CH<sub>2</sub>Cl<sub>2</sub>, 273 K):  $\delta_{\text{D}} = 6.07$  (1D, s, C(3)D), 2.83 (0.16D, d,  $^2J_{\text{DH}} = 2.0$ , C(5)HD<sub>*trans*</sub>), 2.72 (0.88D, d,  $^2J_{\text{DH}} = 2.1$ , C(5)HD<sub>*cis*</sub>) ppm;  **$^{13}\text{C}\{^1\text{H}\}$ -NMR** (176 MHz, CDCl<sub>3</sub>, 273 K):  $\delta_{\text{C}} = 179.7$  (C(1)), 139.8 (br. s, C(4)), 139.7 (C(4)), 134.6 (C(3)H), 134.3 (1:1:1 t,  $^1J_{\text{CD}} = 27.0$ , C(3)D), 45.5 (C(2)), 45.4 (C(2)), 35.7 (C(5)H<sub>2</sub>), 35.4 (1:1:1 t,  $^1J_{\text{CD}} = 21.8$ , C(5)DH) ppm; **HRMS** (ESI<sup>+</sup>): C<sub>3</sub>H<sub>6</sub>DO<sub>2</sub> [M+H]<sup>+</sup> requires 100.0503, found 100.0505 ( $\Delta = 2.0$  ppm). In the  $^{13}\text{C}$ -NMR spectrum, the two singlets observed for C(2) and C(4), respectively, correspond to different product isotopomers (i.e. [*cis*-5-D]- and [3-D]-**9**) and could not be further assigned.

**[2- $^2\text{H}_{1,0}$ ,4- $^2\text{H}_{0,1}$ ]-*trans*-4-(4-Methylpent-1-en-3-yl)cyclobut-2-ene-1-carboxylic acid ([5-D]/[3-D]-*trans*-**10**) and [2- $^2\text{H}_{1,0,0}$ ,*cis*-4- $^2\text{H}_{0,1,0}$ ]-*trans*-4- $^2\text{H}_{0,0,1}$ ]-Cyclobut-2-ene-1-carboxylic acid ([*cis*-5-D]/[3-D]-**9**) from Substrate [5-D]/[3-D]-*trans*-**1** with Ligand **L2****



The reaction was performed according to a modified literature procedure.<sup>27</sup> To a stirred mixture of [Pd<sub>2</sub>(dba)<sub>3</sub>·CHCl<sub>3</sub>] (10.9 mg, 10.5  $\mu\text{mol}$ , 10 mol%), ligand (*R*)-**L2** (12.8 mg, 31.5  $\mu\text{mol}$ , 30 mol%) and CsF (160 mg, 1.05 mmol, 10 equiv.) in anhydrous THF (1 mL) was added 4,4,5,5-tetramethyl-2-(4-methylpent-1-en-3-yl)-1,3,2-dioxaborolane (110.2 mg, 525  $\mu\text{mol}$ , 5 equiv.), followed by dropwise addition of a solution of labeled substrate [5-D]/[3-D]-*trans*-**1** ([5-D]:[3-D] = 3.6:1, overall 94%**D**, 14.0 mg, 105  $\mu\text{mol}$ , 1 equiv., preparation see section 2) in anhydrous THF (1 mL). After stirring at RT overnight (15 h), the reaction mixture was cooled down to 0  $^{\circ}\text{C}$  and quenched with satd. aq. Na<sub>2</sub>CO<sub>3</sub> (0.2 mL) followed by brine (3 mL). The aqueous layer was washed with Et<sub>2</sub>O (3  $\times$  5 mL), carefully acidified with 1 N HCl (pH  $\leq$  2) and extracted with CH<sub>2</sub>Cl<sub>2</sub> (6  $\times$  5 mL). The combined organic layers were dried over Na<sub>2</sub>SO<sub>4</sub> and concentrated *in vacuo* to give the crude product, which was investigated by NMR spectroscopy and ESI-HRMS.

The crude product was found to be a complex mixture of unconverted substrate [5-D]/[3-D]-*trans*-**1** (44% NMR yield), allylated product [5-D]/[3-D]-*trans*-**10** (13% NMR yield, overall 97%**D**) and  $\beta$ -H elimination product [*cis*-5-D]/[*trans*-5-D]/[3-D]-**9** (4% NMR yield, overall ca. 91%**D**).

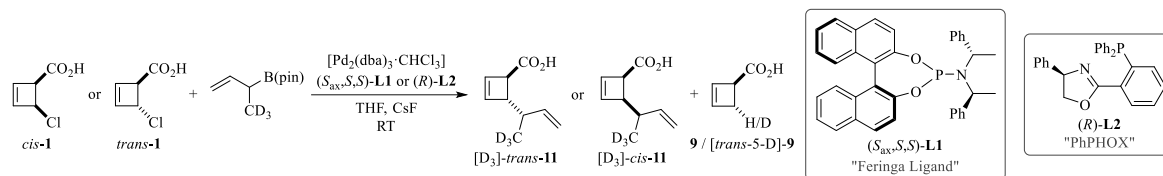
Substitution product [5-D]/[3-D]-*trans*-**10** was obtained as 1:1 mixture of both isotopomers, and the HRMS data are consistent with [5-D]/[3-D]-*trans*-**10** being only monodeuterated rather than 3,5-dideuterated. As the *cis*-isomer of [5-D]/[3-D]-*trans*-**10** could not be detected (i.e. *trans*:*cis* > 95:5), productive allylic substitution is concluded to proceed stereoselectively with retention of configuration. Substitution product [5-D]/[3-D]-*trans*-**10** was obtained as an epimeric 72:28 mixture with respect to stereocenter C(6) (marked with an \*), and the major epimer was the same as with substrate *cis*-**1**. For the major epimer, an e.e. of 94% was determined. Comparison of the NMR spectra after addition of (*S*)-PEA showed that the major enantiomer was the same as with substrate *cis*-**1**. The e.e. of the minor epimer could not be determined (no spectral separation of enantiomers). Unconverted substrate [5-D]/[3-D]-*trans*-**1** was found to be racemic (e.e.  $\leq$  2%).

For the isotopomers of deuterated  $\beta$ -H elimination product [*cis*-5-D]/[*trans*-5-D]/[3-D]-**9**, a ratio of 40:20:40 was determined. The HRMS data are consistent with [*cis*-5-D]/[*trans*-5-D]/[3-D]-**9** being only monodeuterated rather than di- or trideuterated. A  $^1\text{H}$ - $^{13}\text{C}$ -HSQC experiment with increased resolution in the indirect dimension (TD(F1) = 744, SW = 60 ppm) confirmed that partial deuteration was obtained in both *cis*- and *trans*-5-position with respect to the carboxy group: The  $^{13}\text{C}$ -resonance of C(5)DH (separated by  $\Delta\delta\text{c} = -0.3$  ppm from C(5)H<sub>2</sub>) shows a correlation to the  $^1\text{H}$ -resonance of C(5)H<sub>*trans*</sub> as well as to the  $^1\text{H}$ -resonance of C(5)H<sub>*cis*</sub>.

The formation of [*cis*-5-D]-**9** as well as [*trans*-5-D]-**9** shows that both an *anti*- and a *syn*-configured Pd-cyclobutene complex were captured (cf. Scheme S7).

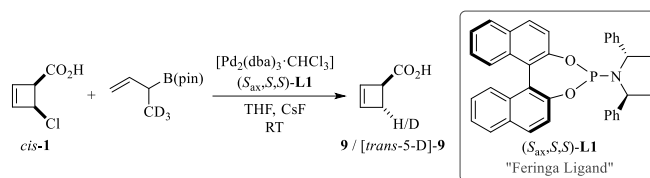
## Allylic Alkylation with Deuterated Unstabilized Nucleophiles

### General Procedure



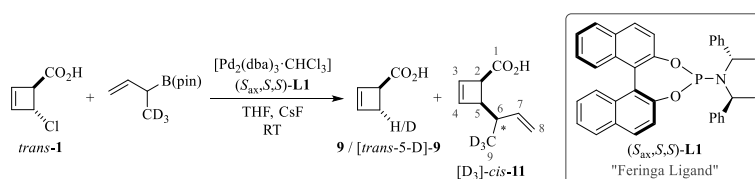
Allylic alkylation reactions with 2-(but-3-en-2-yl-1,1,1-*d*<sub>3</sub>)-4,4,5,5-tetramethyl-1,3,2-dioxaborolane as nucleophile were performed according to a modified literature procedure.<sup>27</sup> To a stirred mixture of [Pd<sub>2</sub>(dba)<sub>3</sub>·CHCl<sub>3</sub>] (3.6 mg, 3.5 μmol, 5 mol%), ligand (S<sub>ax</sub>,S,S)-L1 (7.6 mg, 14.0 μmol, 20 mol%) or (R)-L2 (4.2 mg, 10.5 μmol, 15 mol%) and CsF (106 mg, 700 μmol, 10 equiv.) in anhydrous THF (1 mL) was added 4,4,5,5-tetramethyl-2-(but-3-en-2-yl-1,1,1-*d*<sub>3</sub>)-4,4,5,5-tetramethyl-1,3,2-dioxaborolane (51.8 mg, 280 μmol, 4 equiv.), followed by dropwise addition of a solution of substrate *cis*-1 or *trans*-1 (9.3 mg, 70 μmol, 1 equiv.) in anhydrous THF (1 mL). After stirring at RT overnight (18 h), the reaction mixture was cooled down to 0 °C and quenched with satd. aq. NaHCO<sub>3</sub> (0.4 mL) followed by brine (3 mL). The aqueous layer was washed with Et<sub>2</sub>O (3 × 5 mL), carefully acidified with 1 N HCl (pH ≤ 2) and extracted with CH<sub>2</sub>Cl<sub>2</sub> (6 × 5 mL). The combined organic layers were dried over Na<sub>2</sub>SO<sub>4</sub> and concentrated *in vacuo* to give the crude product, which was investigated by NMR spectroscopy and ESI-HRMS. The e.e. was determined by <sup>1</sup>H-NMR after addition of (S)-PEA to the NMR sample. The absolute configuration of substitution products was not determined.

### [*trans*-4-<sup>1</sup>H<sub>1,30</sub>,*trans*-4-<sup>2</sup>H<sub>0,1</sub>]-Cyclobut-2-ene-1-carboxylic acid (9/[*trans*-5-D]-9) from Substrate *cis*-1



When substrate *cis*-1 was subjected to the general procedure using ligand (S<sub>ax</sub>,S,S)-L1, only small amounts of partially deuterated β-H/D elimination product [*trans*-5-D]-9 were obtained (ca. 4 % NMR yield, 49 %D), along with large amounts of unidentified decomposition products. Isotopomer [*cis*-5-D]-9 was not detected. The formation of [*trans*-5-D]-9 shows that an *anti*-configured Pd-cyclobutene complex was captured (cf. Scheme S7), consistent previous results (*vide supra*). The fact that no quantitative deuteration was obtained indicates that 9 can also be formed by other pathways such as protodepalladation.

### [*trans*-4-<sup>1</sup>H<sub>1,30</sub>,*trans*-4-<sup>2</sup>H<sub>0,1</sub>]-Cyclobut-2-ene-1-carboxylic acid (9/[*trans*-5-D]-9) and *cis*-4-(But-3-en-2-yl-1,1,1-*d*<sub>3</sub>)cyclobut-2-ene-1-carboxylic acid ([D<sub>3</sub>]-*cis*-11) from Substrate *trans*-1



When substrate *trans*-1 was subjected to the general procedure using ligand (S<sub>ax</sub>,S,S)-L1, only small amounts of partially deuterated β-H/D elimination product [*trans*-5-D]-9 (ca. 8 % NMR yield, ca. 8 %D) and allylated product [D<sub>3</sub>]-*cis*-11 (ca. 6 % NMR yield, >99 %D) were obtained, along with large amounts of unidentified decomposition products. Isotopomer [*cis*-5-D]-9 was not detected, and neither was *trans*-configured substitution product [D<sub>3</sub>]-*trans*-11. Allylated product [D<sub>3</sub>]-*cis*-11 was obtained as an epimeric 64:36 mixture with respect to stereocenter C(6) (marked with an \*). For both the major and the minor diastereomer, an e.e. of 5 % was determined.

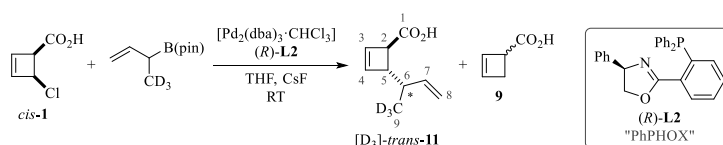
The formation of [*trans*-5-D]-9 indicates that an *anti*-configured Pd-cyclobutene complex was captured (cf. Scheme S7). Although this result is ambiguous due to the low degree of deuteration, the conclusion is consistent with previous findings (*vide supra*).

Given below are the characterization data for both epimers of allylated product [D<sub>3</sub>]-*cis*-11.

<sup>1</sup>H-NMR (700 MHz, CDCl<sub>3</sub>, 273 K): δ<sub>H</sub> = 6.36 (1H, dt, <sup>3</sup>J<sub>HH</sub> = 2.9, <sup>n</sup>J<sub>HH</sub> = 0.8, major C(4)*H*), 6.29 (0.56H, dt, <sup>3</sup>J<sub>HH</sub> = 2.9, <sup>n</sup>J<sub>HH</sub> = 0.8, minor C(4)*H*), 6.13 (1H, dt, <sup>3</sup>J<sub>HH</sub> = 2.9, <sup>n</sup>J<sub>HH</sub> = 0.8, major C(3)*H*), 6.11 (0.56H, dt, <sup>3</sup>J<sub>HH</sub> = 2.9, <sup>n</sup>J<sub>HH</sub> = 0.8, minor C(3)*H*), 5.71 – 5.65 (1.56H, m, major + minor C(7)*H*), 5.02 (0.56H, ddd, <sup>3</sup>J<sub>HH</sub> = 17.2, <sup>2</sup>J<sub>HH</sub> = 1.8, <sup>4</sup>J<sub>HH</sub> = 1.1, minor C(8)HH<sub>cis</sub>), 4.98 (0.56H, ddd, <sup>3</sup>J<sub>HH</sub> = 10.3, <sup>2</sup>J<sub>HH</sub> = 1.8, <sup>4</sup>J<sub>HH</sub> = 0.7, minor

C(8)HH<sub>trans</sub>), 4.97 (1H, ddd, <sup>3</sup>J<sub>HH</sub> = 17.2, <sup>2</sup>J<sub>HH</sub> = 1.7, <sup>4</sup>J<sub>HH</sub> = 1.2, major C(8)HH<sub>cis</sub>), 4.94 (1H, ddd, <sup>3</sup>J<sub>HH</sub> = 10.4, <sup>2</sup>J<sub>HH</sub> = 1.7, <sup>4</sup>J<sub>HH</sub> = 0.9, major C(8)HH<sub>trans</sub>), 3.76 (0.56H, d, <sup>3</sup>J<sub>HH</sub> = 4.6, minor C(2)H), 3.71 (1H, d, <sup>3</sup>J<sub>HH</sub> = 4.6, major C(2)H), 2.99 (1H, dd, <sup>3</sup>J<sub>HH</sub> = 10.5, <sup>3</sup>J<sub>HH</sub> = 4.6, major C(5)H), 2.95 (0.56H, dd, <sup>3</sup>J<sub>HH</sub> = 10.2, <sup>3</sup>J<sub>HH</sub> = 4.6, minor C(5)H), 2.45 (1H, dd, <sup>3</sup>J<sub>HH</sub> = 10.5, <sup>3</sup>J<sub>HH</sub> = 7.9, major C(6)H), 2.36 (0.56H, br. t, <sup>3</sup>J<sub>HH</sub> ≈ 9.0, minor C(6)H) ppm; <sup>2</sup>H-NMR (108 MHz, CH<sub>2</sub>Cl<sub>2</sub>, 273 K): δ<sub>D</sub> = 0.97 (3D, br. s, major), 0.94 (1.68D, br. s, minor) ppm; <sup>13</sup>C{<sup>1</sup>H}-NMR (176 MHz, CDCl<sub>3</sub>, 273 K): δ<sub>C</sub> = 178.9 (major C(1)), 178.7 (minor C(1)), 142.2 (minor C(4)), 141.9 (major C(4)), 141.4 (major C(7)), 141.3 (minor C(7)), 133.9 (major C(3)), 133.3 (minor C(3)), 114.6 (minor C(8)), 114.3 (major C(8)), 52.2 (minor C(5)), 51.3 (major C(5)), 48.5 (major + minor C(2)), 38.7 (minor C(6)), 38.0 (major C(6)), 17.7 – 17.0 (m, major + minor C(9)D<sub>3</sub>) ppm; HRMS (ESI<sup>+</sup>): C<sub>9</sub>H<sub>10</sub>D<sub>3</sub>O<sub>2</sub> [M+H]<sup>+</sup> requires 156.1098, found 156.1091 (Δ = -4.5 ppm).

**Trans-4-(but-3-en-2-yl-1,1,1-d<sub>3</sub>)cyclobut-2-ene-1-carboxylic acid ([D<sub>3</sub>]-trans-11) and Cyclobut-2-ene-1-carboxylic acid (9) from Substrate cis-1**

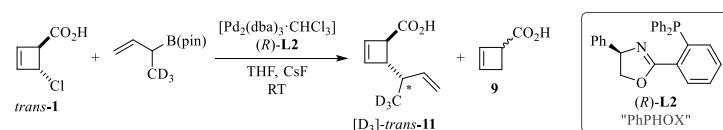


When substrate *cis*-1 was subjected to the general procedure using ligand (*R*)-L2, allylated product [D<sub>3</sub>]-*trans*-11 was obtained (75 % NMR yield, >99 %D), along with small amounts of undeuterated β-H elimination product 9 (ca. 4 % NMR yield). Substitution product [D<sub>3</sub>]-*trans*-11 was obtained as an epimeric 55:45 mixture with respect to stereocenter C(6) (marked with an \*). For the major epimer, an e.e. of approximately 99 % was determined (amount of minor enantiomer too small for accurate integration). The e.e. of the minor epimer was determined to be 84 %. Elimination product 9 was obtained without any detectable deuteration, i.e. assignment of the relative configuration of the Pd-species captured is not possible. 9 was found to be formed as a racemate (e.e. ≤ 3 %).

Given below are the characterization data for both epimers of allylated product [D<sub>3</sub>]-*trans*-11.

<sup>1</sup>H-NMR (700 MHz, CDCl<sub>3</sub>, 273 K): δ<sub>H</sub> = 6.35 (0.82H, d, <sup>3</sup>J<sub>HH</sub> = 2.8, minor C(4)H), 6.31 (1H, d, <sup>3</sup>J<sub>HH</sub> = 2.8, major C(4)H), 6.11 (0.82H, d, <sup>3</sup>J<sub>HH</sub> = 2.8, minor C(3)H), 6.10 (1H, d, <sup>3</sup>J<sub>HH</sub> = 2.8, major C(3)H), 5.80 (0.82H, ddd, <sup>3</sup>J<sub>HH</sub> = 17.3, <sup>3</sup>J<sub>HH</sub> = 10.3, <sup>3</sup>J<sub>HH</sub> = 7.2, minor C(7)H), 5.70 (1H, ddd, <sup>3</sup>J<sub>HH</sub> = 17.6, <sup>3</sup>J<sub>HH</sub> = 10.3, <sup>3</sup>J<sub>HH</sub> = 7.9, major C(7)H), 5.07 – 4.97 (3.64H, m, major + minor C(8)H<sub>2</sub>), 3.27 (0.82H, br. s, minor C(2)H), 3.26 (1H, br. s, major C(2)H), 2.88 (0.82H, br. d, <sup>3</sup>J<sub>HH</sub> = 8.7, minor C(5)H), 2.84 (1H, br. d, <sup>3</sup>J<sub>HH</sub> = 8.7, major C(5)H), 2.23 (1.82H, br. t, <sup>3</sup>J<sub>HH</sub> ≈ 8.1, major + minor C(6)H) ppm; <sup>2</sup>H-NMR (108 MHz, CH<sub>2</sub>Cl<sub>2</sub>, 273 K): δ<sub>D</sub> = 1.02 (3D, br. s, major), 0.99 (2.46D, br. s, minor) ppm; <sup>13</sup>C{<sup>1</sup>H}-NMR (176 MHz, CDCl<sub>3</sub>, 273 K): δ<sub>C</sub> = 179.5 (major C(1)), 179.5 (minor C(1)), 142.6 (minor C(4)), 142.1 (major C(4)), 141.2 (minor C(7)), 140.9 (major C(7)), 133.7 (minor C(3)), 133.3 (major C(3)), 114.5 (major C(8)), 114.4 (minor C(8)), 53.2 (major C(5)), 53.0 (minor C(5)), 49.3 (major C(2)), 49.1 (minor C(2)), 41.4 (major C(6)), 40.9 (minor C(6)), 17.2 (sept, <sup>1</sup>J<sub>CD</sub> = 19.2, major C(9)D<sub>3</sub>), 16.4 (sept, <sup>1</sup>J<sub>CD</sub> = 19.2, minor C(9)D<sub>3</sub>) ppm; HRMS (ESI<sup>+</sup>): C<sub>9</sub>H<sub>10</sub>D<sub>3</sub>O<sub>2</sub> [M+H]<sup>+</sup> requires 156.1098, found 156.1098 (Δ = 0). The spectroscopic data are consistent with those reported in the literature for the unlabeled isotopologue.<sup>27</sup>

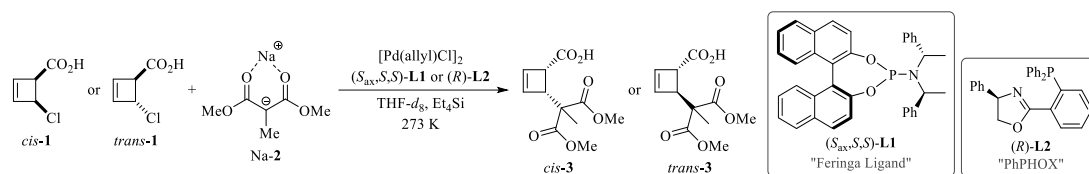
**Trans-4-(but-3-en-2-yl-1,1,1-d<sub>3</sub>)cyclobut-2-ene-1-carboxylic acid ([D<sub>3</sub>]-trans-11) and Cyclobut-2-ene-1-carboxylic acid (9) from Substrate trans-1**



When substrate *trans*-1 was subjected to the general procedure using ligand (*R*)-L2, allylated product [D<sub>3</sub>]-*trans*-11 was obtained (27 % NMR yield, >99 %D), along with unconverted substrate (44 % NMR yield) and trace amounts of undeuterated β-H elimination product 9 (ca. 1 % NMR yield). Substitution product [D<sub>3</sub>]-*trans*-11 was obtained as an epimeric 52:48 mixture with respect to stereocenter C(6) (marked with an \*), and the major epimer was the same as with substrate *cis*-1. For the minor epimer, an e.e. of 84 % was determined. The e.e. of the major epimer could not be determined (amount of minor enantiomer too small for detection). Comparison of the NMR spectra after addition of (*S*)-PEA showed that for both product epimers the major enantiomer was the same as with substrate *cis*-1. Hence, the absolute configuration of substitution product [D<sub>3</sub>]-*trans*-11 is independent of the substrate's configuration, showcasing that allylic alkylation of cyclobutenes with boronate nucleophiles acts as a de-epimerization as well. Unconverted substrate *trans*-1 was found to be racemic (e.e. ≤ 2 %). Elimination product 9 was obtained without any detectable deuteration, i.e. assignment of the relative configuration of the Pd-species captured is not possible.

## 8 $^{31}\text{P}\{^1\text{H}\}$ -NMR Reaction Monitoring

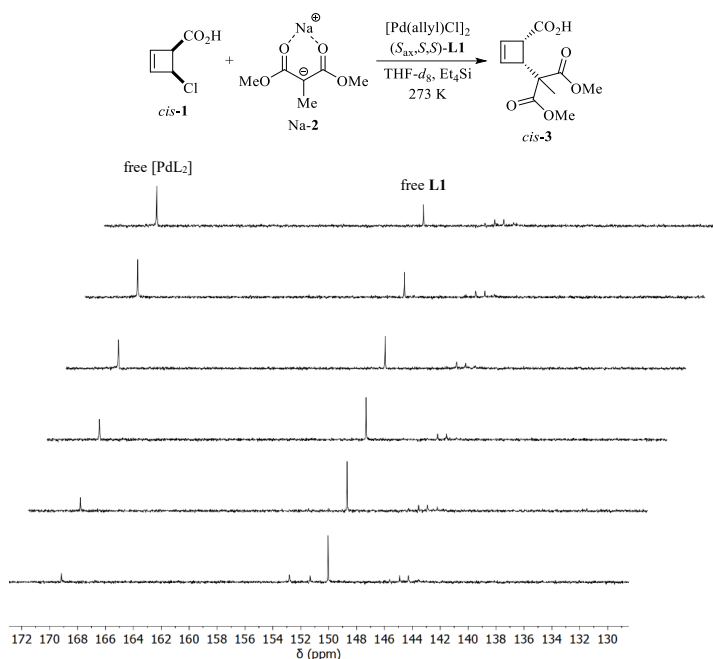
### General Procedure



$^{31}\text{P}\{^1\text{H}\}$ -NMR reaction monitoring was performed under similar conditions as described in section 3. In order to reach maximum intermediate concentrations, reactions were performed with Pd-loadings as high as possible. Prior to starting reaction monitoring, a reference sample of  $[\text{Pd}(\text{allyl})\text{Cl}]_2$  (0.5 equiv.) and ligand  $(S_{\text{ax}},S_{\text{ax}},S,S)\text{-L1}$  (2 equiv.) or  $(R)\text{-L2}$  (3 equiv.) in THF- $d_8$  was prepared and used for  $^{31}\text{P}$  wobbling, pulse calibration and estimation of the  $T_1$  relaxation time constant.

In an NMR tube, *cis*- or *trans*-4-chlorocyclobutene-2-encarboxylic acid **1** (1 equiv.) and Et $_4$ Si (1 equiv.) were dissolved in anhydrous THF- $d_8$  (ca. 400  $\mu\text{L}$ ), and a solution of nucleophile Na-2 (ca. 95 w% purity, 2.5 equiv. with **L1**, 3 equiv. with **L2**) in anhydrous THF- $d_8$  (ca. 400  $\mu\text{L}$ ) was carefully added at  $-25^\circ\text{C}$ . The NMR tube was sealed and loaded into the NMR spectrometer set to 273 K. After shimming, a single-scan  $^1\text{H}$ -NMR spectrum was recorded. The tube was ejected and a solution of  $[\text{Pd}(\text{allyl})\text{Cl}]_2$  and ligand  $(S_{\text{ax}},S_{\text{ax}},S,S)\text{-L1}$  or  $(R)\text{-L2}$  in anhydrous THF- $d_8$  (ca. 200  $\mu\text{L}$ ) was added rapidly upon shaking. After shaking vigorously for about 5 s and additionally inverting one time, the sample was loaded into the NMR spectrometer again, and a series of single-scan  $^{31}\text{P}\{^1\text{H}\}$ -NMR spectra with a  $90^\circ$  pulse, broadband decoupling and a relaxation delay of 0.5 – 3 s was recorded over 90 min. Full conversion of substrate **1** was verified by recording a  $^1\text{H}$ -NMR spectrum.

### $^{31}\text{P}\{^1\text{H}\}$ -NMR Reaction Monitoring with Substrate *cis*-1 and Ligand **L1**

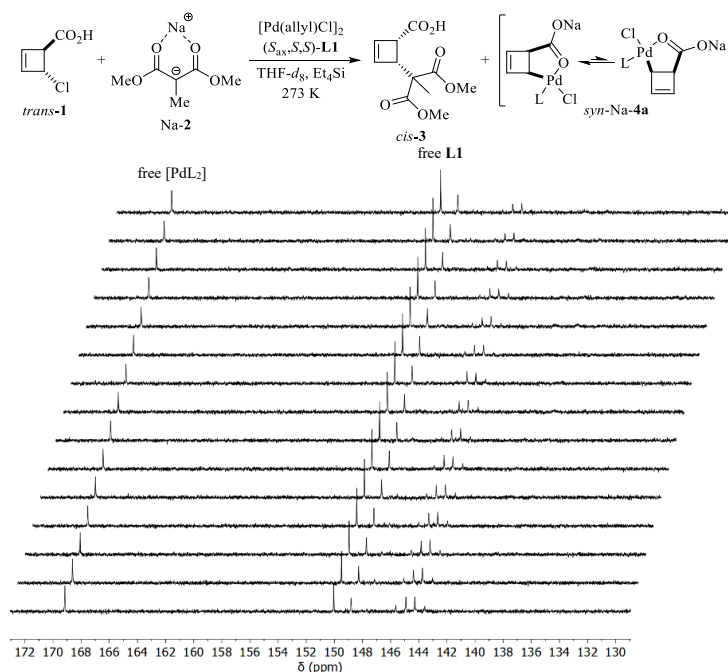


**Scheme S8.**  $^{31}\text{P}\{^1\text{H}\}$ -NMR monitoring of the allylic alkylation of substrate *cis*-1 with ligand  $(S_{\text{ax}},S_{\text{ax}},S,S)\text{-L1}$ , recorded with a spectral width of 200 ppm, an offset of 140 ppm, a single scan, and a relaxation delay of 0.5 s. For each spectrum shown, 320 individual spectra were summed up, and the stack covers an overall reaction time of 28 min.

Reaction monitoring of the allylic alkylation of substrate *cis*-1 (16.6 mg, 125  $\mu\text{mol}$ , 1 equiv.) and nucleophile Na-2 (ca. 95 w% purity, 55.3 mg, 312.5  $\mu\text{mol}$ , 2.5 equiv.) with  $[\text{Pd}(\text{allyl})\text{Cl}]_2$  (1.1 mg, 3.1  $\mu\text{mol}$ , 2.5 mol%) and ligand  $(S_{\text{ax}},S_{\text{ax}},S,S)\text{-L1}$  (6.7 mg, 12.5  $\mu\text{mol}$ , 10 mol%) according to the general procedure gave the  $^{31}\text{P}\{^1\text{H}\}$ -NMR series shown in Scheme S8. The spectra allowed for observation of free ligand **L1** ( $\delta = 150.0$  ppm)<sup>50</sup> and pre-complex  $[\text{PdL}_2]$  ( $L = (S_{\text{ax}},S_{\text{ax}},S,S)\text{-L1}$ ,  $\delta = 169.2$  ppm)<sup>45</sup> under reactive conditions. Furthermore, an additional species with two non-equivalent and strongly coupled *cis*-oriented phosphine sites was observed at  $\delta = 145.3$  (d,  $J_{\text{PP}} = 200$  Hz), 143.9 (d,  $J_{\text{PP}} = 200$  Hz) ppm, with spectroscopic data suggesting a  $[\text{PdL}_2\text{X}_n]$ -type structure. This unidentified species was present during turnover and was then slowly consumed, but did not disappear

completely. However, no transient species consistent with the Pd-cyclobutene intermediates expected could be observed, even after summing up all spectra recorded during the reaction.

### $^{31}\text{P}\{^1\text{H}\}$ -NMR Reaction Monitoring with Substrate *trans*-1 and Ligand L1

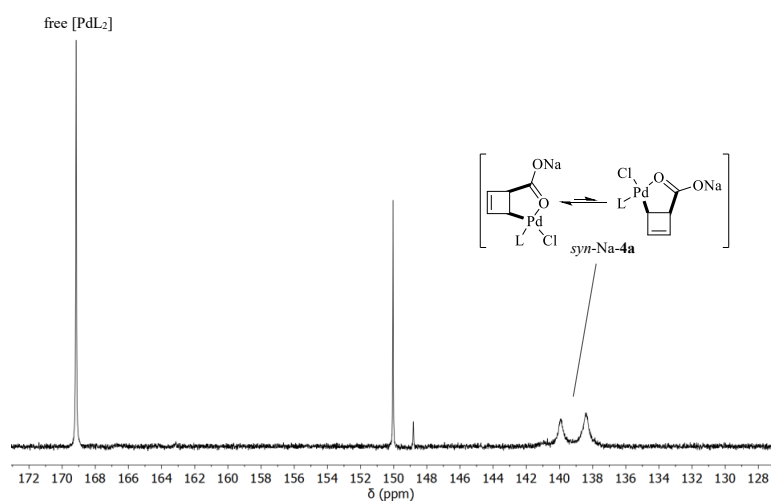


**Scheme S9.**  $^{31}\text{P}\{^1\text{H}\}$ -NMR monitoring of the allylic alkylation of substrate *trans*-1 with ligand ( $S_{\text{ax}},S,S$ )-L1, recorded with a spectral width of 200 ppm, an offset of 140 ppm, a single scan, and a relaxation delay of 1 s. For each spectrum shown, 160 individual spectra were summed up, and the stack covers an overall reaction time of 80 min.

Reaction monitoring of the allylic alkylation of substrate *trans*-1 (19.9 mg, 150  $\mu\text{mol}$ , 1 equiv.) and nucleophile Na-4a (ca. 95 w% purity, 66.4 mg, 375  $\mu\text{mol}$ , 2.5 equiv.) with  $[\text{Pd}(\text{allyl})\text{Cl}]_2$  (1.4 mg, 3.8  $\mu\text{mol}$ , 2.5 mol%) and ligand ( $S_{\text{ax}},S,S$ )-L1 (8.1 mg, 15  $\mu\text{mol}$ , 10 mol%) according to the general procedure gave the  $^{31}\text{P}\{^1\text{H}\}$ -NMR series shown in Scheme S9. The spectra allowed for observation of free ligand L1 ( $\delta_{\text{P}} = 150.0 \text{ ppm}$ )<sup>50</sup> and pre-complex  $[\text{PdL}_2]$  ( $L = (S_{\text{ax}},S,S)\text{-L1}$ ,  $\delta_{\text{P}} = 169.2 \text{ ppm}$ )<sup>35</sup> under reactive conditions. Furthermore, an additional species with two non-equivalent and strongly coupled *cis*-oriented phosphine sites was observed at  $\delta_{\text{P}} = 145.3 \text{ (d, } J_{\text{PP}} = 200 \text{ Hz)}$ ,  $143.9 \text{ (d, } J_{\text{PP}} = 200 \text{ Hz)}$  ppm, with spectroscopic data suggesting a  $[\text{PdL}_2\text{X}_n]$ -type structure. This unidentified species was present during turnover and then slowly disappeared (present over >6 h, not detected anymore after 24 h). However, no transient species consistent with the Pd-cyclobutene intermediates expected could be observed, even after summing up all spectra recorded during the reaction.

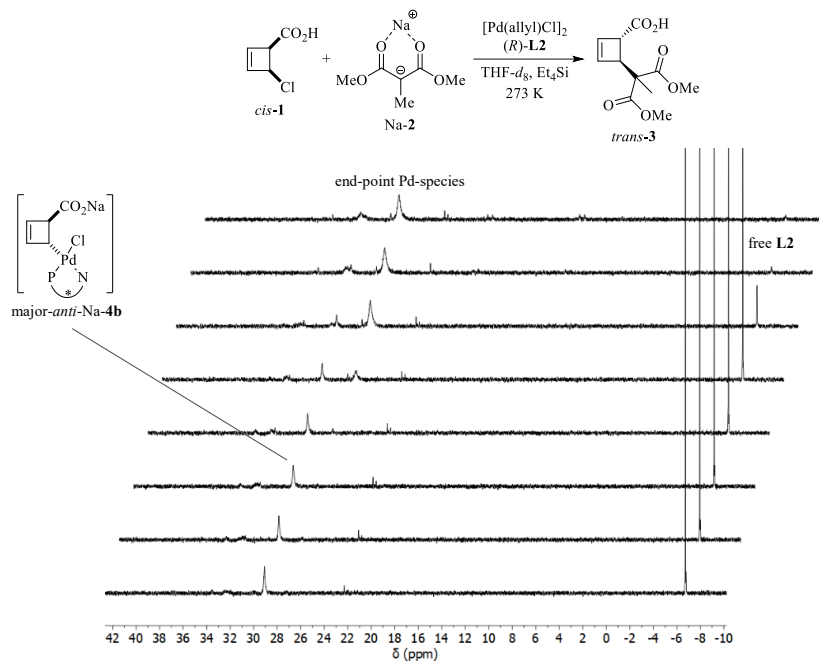
Unreactive *syn*-configured Pd-species *syn*-Na-4a, which are formed as side product when using substrate *trans*-1 (cf. section 3), could not be observed during the reaction, probably due to the amount of generated *syn*-Na-4a being too small. Both species could be detected by recording a long end-point  $^{31}\text{P}\{^1\text{H}\}$ -NMR spectrum (Scheme S10) as broad singlets at  $\delta_{\text{P}} = 138.1 \text{ ppm}$  (major-*syn*) and  $\delta_{\text{P}} = 139.7 \text{ ppm}$  (minor-*syn*), respectively (see section 4 for full characterization).





**Scheme S10.** End-point  $^{31}\text{P}\{^1\text{H}\}$ -NMR spectrum of the allylic alkylation of substrate *trans*-1 with ligand (*S,S,S,S*)-L1, recorded with a spectral width of 200 ppm, an offset of 140 ppm, 6000 scans and a relaxation delay of 1 s.

#### $^{31}\text{P}\{^1\text{H}\}$ -NMR Reaction Monitoring with Substrate *cis*-1 and Ligand L2

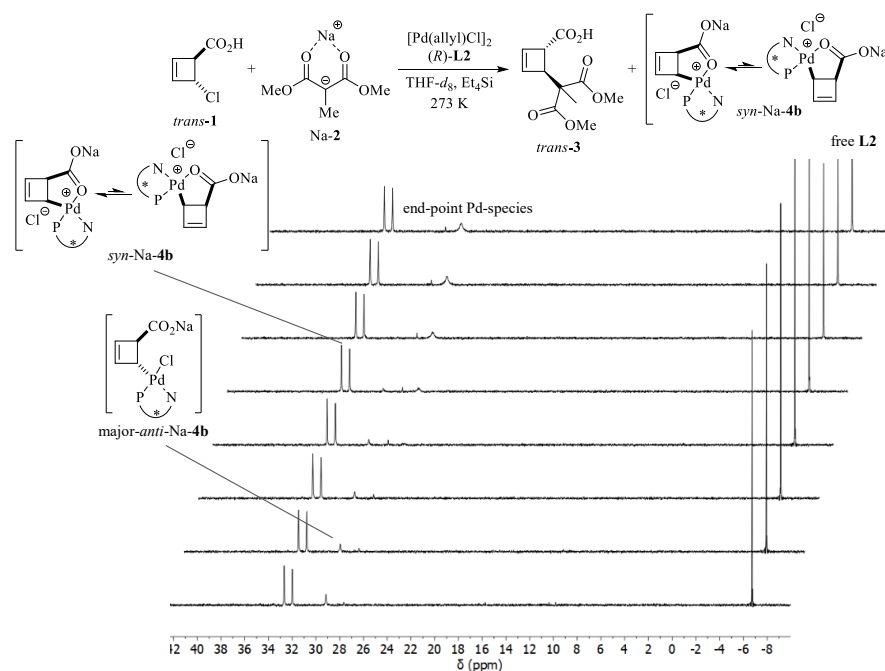


**Scheme S11.**  $^{31}\text{P}\{^1\text{H}\}$ -NMR monitoring of the allylic alkylation of substrate *cis*-1 with ligand (*R*)-L2, recorded with a spectral width of 200 ppm, an offset of 10 ppm, a single scan, and a relaxation delay of 3 s. For each spectrum shown, 100 individual spectra were summed up, and the stack covers an overall reaction time of 60 min.

Reaction monitoring of the allylic alkylation of substrate *cis*-1 (6.6 mg, 50  $\mu\text{mol}$ , 1 equiv.) and nucleophile Na-2 (ca. 95 w% purity, 26.5 mg, 150  $\mu\text{mol}$ , 3 equiv.) with  $[\text{Pd}(\text{allyl})\text{Cl}]_2$  (1.8 mg, 5.0  $\mu\text{mol}$ , 10 mol%) and ligand (*R*)-L2 (12.2 mg, 30  $\mu\text{mol}$ , 60 mol%) according to the general procedure gave the  $^{31}\text{P}\{^1\text{H}\}$ -NMR series shown in Scheme S11. A transient species with a chemical shift of  $\delta_{\text{P}} = 29.2$  ppm could be observed, consistent with the expected  $\eta^1$ -Pd-cyclobutene complex major-*anti*-Na-4b (corresponding protonated complex major-*anti*-4b:  $\delta_{\text{P}} = 29.0$  ppm, see section 4). The disappearance of this signal was accompanied by emergence of a new resonance at  $\delta_{\text{P}} = 26.2$  ppm, which could not be assigned, but seems to be the end-point Pd-species after reaching full conversion. Apart from that, the signal of free ligand L2 at  $\delta_{\text{P}} = -6.7$  ppm<sup>S1</sup> disappeared after reaching full conversion, presumably due to decomposition.



### $^{31}\text{P}\{^1\text{H}\}$ -NMR Reaction Monitoring with Substrate *trans*-1 and Ligand **L2**

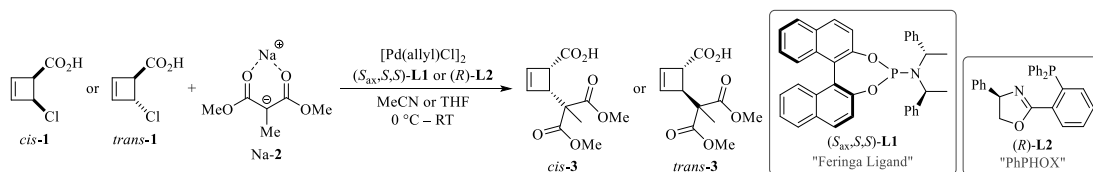


**Scheme S12.**  $^{31}\text{P}\{^1\text{H}\}$ -NMR monitoring of the allylic alkylation of substrate *trans*-1 with ligand (*R*)-**L2**, recorded with a spectral width of 200 ppm, an offset of 10 ppm, and a relaxation delay of 3 s. For each spectrum shown, 40 single-scan spectra were summed up, and the stack covers an overall reaction time of 30 min.

Reaction monitoring of the allylic alkylation of substrate *trans*-1 (6.6 mg, 50  $\mu\text{mol}$ , 1 equiv.) and nucleophile Na-2 (ca. 95 w% purity, 26.5 mg, 150  $\mu\text{mol}$ , 3 equiv.) with  $[\text{Pd}(\text{allyl})\text{Cl}]_2$  (2.7 mg, 7.5  $\mu\text{mol}$ , 15 mol%) and ligand (*R*)-**L2** (12.2 mg, 30  $\mu\text{mol}$ , 60 mol%) according to the general procedure gave the  $^{31}\text{P}\{^1\text{H}\}$ -NMR series shown in Scheme S12. A transient species with a chemical shift of  $\delta_{\text{P}} = 29.2$  ppm could be observed, consistent with the expected  $\eta^1$ -Pd-cyclobutene complex major-*anti*-Na-4b (corresponding protonated complex major-*anti*-4b:  $\delta_{\text{P}} = 29.0$  ppm, see section 4). The disappearance of this signal was accompanied by emergence of a new resonance at  $\delta_{\text{P}} = 26.2$  ppm, which could not be assigned, but seems to be the end-point Pd-species after reaching full conversion. Formation of unreactive Pd-complexes *syn*-Na-4b (major-*syn*:  $\delta_{\text{P}} = 32.7$  ppm, minor-*syn*:  $\delta_{\text{P}} = 32.0$  ppm, see section 4 for full characterization) was observed as well. Additionally, the signal of free ligand **L2** at  $\delta_{\text{P}} = -6.7$  ppm<sup>51</sup> decreased after reaching full conversion, but remained observable.

## 9 ESI-HRMS Analysis of Reactive Mixtures

### General Procedure



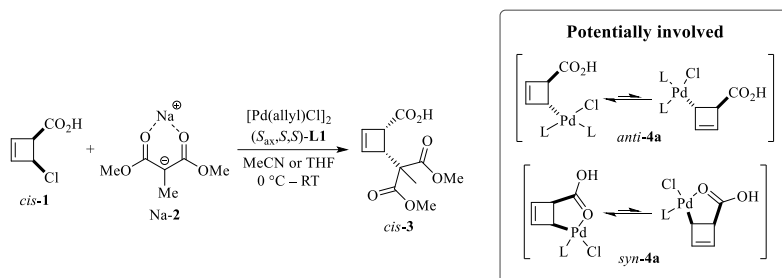
Reactions subjected to qualitative ESI-HRMS analysis in positive or negative ion mode were performed under similar conditions as described in section 3. With ligand **L1**, MeCN rather than THF was used as solvent, since slightly better stereoselectivities have been obtained in MeCN (see section 3). In order to reach maximum intermediate concentrations, reactions were performed with Pd-loadings as high as possible. The total volume was 500  $\mu\text{L}$  for all reactions.

In an HPLC vial equipped with a magnetic stirrer bar, *cis*- or *trans*-4-chlorocyclobutene-2-encarboxylic acid **1** (1.7 mg, 12.5  $\mu\text{mol}$ , 1 equiv.) was dissolved in anhydrous MeCN or THF (100  $\mu\text{L}$ ), and a solution of nucleophile Na-2 (ca. 95 w% purity, 4.4 mg, 25  $\mu\text{mol}$ , 2 equiv. with *cis*-1; 6.6 mg, 37.5  $\mu\text{mol}$ , 3 equiv. with *trans*-1) in anhydrous MeCN or THF (300 – 350  $\mu\text{L}$ ) was carefully added at  $-25$   $^{\circ}\text{C}$ . The vial was closed with a septum cap. The mixture was stirred vigorously at  $0$   $^{\circ}\text{C}$  and a solution of  $[\text{Pd}(\text{allyl})\text{Cl}]_2$  and ligand (*S*<sub>ax</sub>,*S*,*S*)-**L1** or (*R*)-**L2** in anhydrous MeCN or THF

(ca. 50 – 100  $\mu\text{L}$ ) was added in one shot. A sample was taken and directly subjected to ESI-HRMS analysis (< 1 min after initiation for all reactions). The reaction was allowed to reach full conversion at 4  $^{\circ}\text{C}$ , and then again analyzed by ESI-HRMS.

ESI-HRMS analysis was performed with an upstream HPLC  $\text{C}_{18}$  column equipped with a 254 nm UV detector. The sample was eluted with  $\text{H}_2\text{O}:\text{MeCN}$  95:5  $\rightarrow$  5:95 with 0.1 %  $\text{HCO}_2\text{H}$  and then ionized from this solvent mixture. Without HPLC separation (i.e. direct HRMS analysis of the reaction mixture), no Pd-species could be detected.

#### ESI-HRMS Analysis with Substrate *cis*-1 and Ligand L1

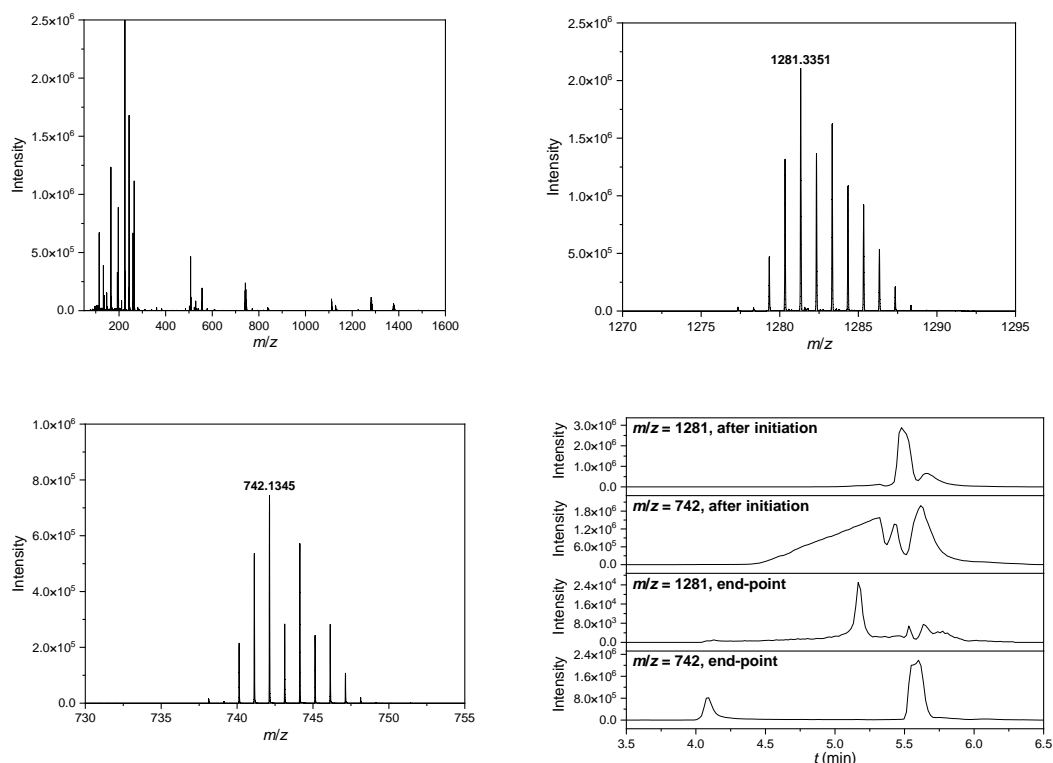


When a reaction mixture of substrate *cis*-1 and nucleophile Na-2 in MeCN was initiated with 1.0 mol%  $[\text{Pd}(\text{allyl})\text{Cl}]_2$  and 4.0 mol%  $(S_{\text{axx}},S_{\text{S}})\text{-L1}$  (50  $\mu\text{L}$  of a stock solution of 2.5 mM  $[\text{Pd}(\text{allyl})\text{Cl}]_2$  and 10 mM  $(S_{\text{axx}},S_{\text{S}})\text{-L1}$ ) and directly subjected to ESI-HRMS analysis in positive ion mode according to the general procedure, the mass fragments listed in Table S13 were obtained. Cations consistent with starting materials *cis*-1 ( $m/z = 133$  and 97) and Na-2 ( $m/z = 147$ ) as well as product 3 ( $m/z = 243$ ) were detected, confirming that a running reaction was analyzed. Fragments consistent with Pd-cyclobutene species were detected at  $m/z = 1281$  and  $m/z = 742$ , corresponding to complexes with two and one equivalents of ligand L1, respectively. The highly characteristic isotope patterns of these fragments (Figure S15, top) matched those calculated for the assigned sum formulas. As has been shown in section 4, *anti*-configured oxidative addition products *anti*-4a bear two equivalents of ligand L1, while the corresponding *syn*-configured species have only one equivalent of L1 attached. Thus, the species observed at  $m/z = 1281$  is likely to be the  $[\text{M}-\text{Cl}]^+$  fragment of *anti*-4a or its corresponding electrocyclic ring-opening product. On the other hand, assignment of the species detected at  $m/z = 742$  is ambiguous, as this mass is consistent with both  $[\text{M}-\text{L}-\text{Cl}]^+$  of *anti*-4a and  $[\text{M}-\text{Cl}]^+$  of *syn*-4a.

**Table S13.** ESI<sup>+</sup>-HRMS analysis of the Pd-catalyzed allylic alkylation of substrate *cis*-1 with nucleophile Na-2 and ligand L1 in MeCN (top, sample taken 35 s after initiation) and THF (bottom, sample taken 40 s after initiation): Assignment of ion formulas and possible structures to experimental mass numbers  $m/z$  and comparison with calculated values, with the corresponding deviation  $\Delta$  given.

Exp. $m/z$	Ion Formula	Possible Assignment	Calcd. $m/z$	$\Delta$ / ppm
1281.3351	$\text{C}_{77}\text{H}_{68}\text{N}_2\text{O}_6\text{P}_2\text{Pd}$	$[\text{M}-\text{Cl}]^+$ of <i>anti</i> -4a	1281.3347	0.3
742.1345	$\text{C}_{41}\text{H}_{35}\text{NO}_4\text{PPd}$	$[\text{M}-\text{L}-\text{Cl}]^+$ of <i>anti</i> -4a and/or $[\text{M}-\text{Cl}]^+$ of <i>syn</i> -4a	742.1333	1.6
243.0857	$\text{C}_{11}\text{H}_{14}\text{O}_6$	$[\text{M}+\text{H}]^+$ of 3	243.0863	-2.7
147.0646	$\text{C}_6\text{H}_{11}\text{O}_4$	$[\text{M}-\text{Na}+2\text{H}]^+$ of Na-2	147.0652	-4.3
133.0046	$\text{C}_3\text{H}_6\text{ClO}_2$	$[\text{M}+\text{H}]^+$ of <i>cis</i> -1	133.0051	-3.9
97.0282	$\text{C}_3\text{H}_6\text{O}_2$	$[\text{M}-\text{Cl}]^+$ of <i>cis</i> -1	97.0284	-2.6
1281.3363	$\text{C}_{77}\text{H}_{68}\text{N}_2\text{O}_6\text{P}_2\text{Pd}$	$[\text{M}-\text{Cl}]^+$ of <i>anti</i> -4a	1281.3347	1.2
742.1341	$\text{C}_{41}\text{H}_{35}\text{NO}_4\text{PPd}$	$[\text{M}-\text{L}-\text{Cl}]^+$ of <i>anti</i> -4a and/or $[\text{M}-\text{Cl}]^+$ of <i>syn</i> -4a	742.1333	1.1
243.0862	$\text{C}_{11}\text{H}_{14}\text{O}_6$	$[\text{M}+\text{H}]^+$ of 3	243.0863	-0.5
147.0651	$\text{C}_6\text{H}_{11}\text{O}_4$	$[\text{M}-\text{Na}+2\text{H}]^+$ of Na-2	147.0652	-0.7
133.0050	$\text{C}_3\text{H}_6\text{ClO}_2$	$[\text{M}+\text{H}]^+$ of <i>cis</i> -1	133.0051	-0.5
97.0286	$\text{C}_3\text{H}_6\text{O}_2$	$[\text{M}-\text{Cl}]^+$ of <i>cis</i> -1	97.0284	1.9

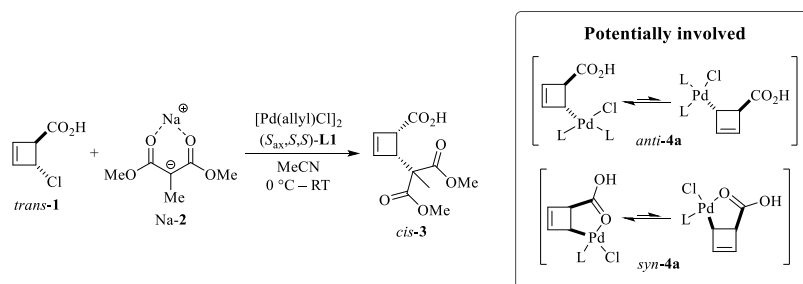
The mass-selective HPLC traces that were obtained for  $m/z = 1281$  and  $m/z = 742$ , respectively, are shown in Figure S15 (bottom right). In the HPLC trace of  $m/z = 1281$  ( $[\text{M}-\text{Cl}]^+$  of *anti*-4a) recorded directly after initiation, one large peak was observed, which is not present anymore in the HPLC trace obtained after reaching full conversion. This confirms that the species detected at  $m/z = 1281$  has a transient nature, i.e. that *anti*-4a is only present during turnover. The HPLC trace of  $m/z = 742$  ( $[\text{M}-\text{L}-\text{Cl}]^+$  of *anti*-4a and/or  $[\text{M}-\text{Cl}]^+$  of *syn*-4a), on the other hand, exhibits three large peaks, one of which is still present in the end-point trace. Thus, several transient and non-transient species with fragments  $m/z = 742$  appear to be involved.



**Figure S15.** ESI<sup>-</sup>-HRMS analysis of the Pd-catalyzed allylic alkylation of substrate *cis*-**1** with nucleophile Na-**2** and ligand **L1** in MeCN: Full mass range (sum over total HPLC run after initiation, top left), enlarged MS peaks of Pd-cyclobutene species (top right and bottom left) and respective mass-selective HPLC traces (bottom right).

Identical results were obtained when the same reaction was performed in THF rather than MeCN. Other expected Pd-intermediates along the catalytic cycle such as the zerovalent palladium species or a  $\eta^2$ -product complex could not be identified. Attempts to detect Pd-species in negative ion mode were not successful.

#### ESI-HRMS Analysis with Substrate *trans*-**1** and Ligand **L1**

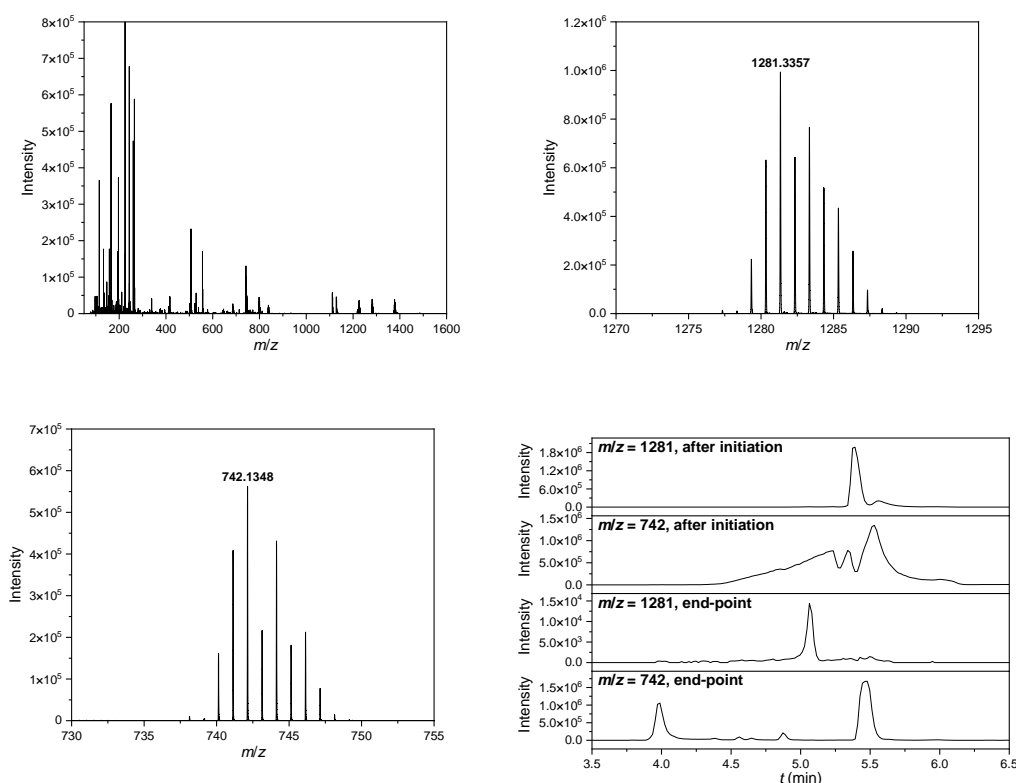


When a reaction mixture of substrate *trans*-**1** and nucleophile Na-**2** in MeCN was initiated with 2.0 mol% [Pd(allyl)Cl]<sub>2</sub> and 8.0 mol% (*S*<sub>ax</sub>,*S*<sub>x</sub>)-**L1** (100  $\mu$ L of a stock solution of 2.5 mM [Pd(allyl)Cl]<sub>2</sub> and 10 mM (*S*<sub>ax</sub>,*S*<sub>x</sub>)-**L1**) and directly subjected to ESI-HRMS analysis in positive ion mode according to the general procedure, the mass fragments listed in Table S14 were obtained. Cations consistent with starting materials *trans*-**1** ( $m/z = 97$ ) and Na-**2** ( $m/z = 147$ ) as well as product **3** ( $m/z = 243$ ) were detected, confirming that a running reaction was analyzed. Fragments consistent with Pd-cyclobutene species were detected at  $m/z = 1281$  and  $m/z = 742$ , corresponding to complexes with two and one equivalents of ligand **L1**, respectively. The highly characteristic isotope patterns of these fragments (Figure S16, top) matched those calculated for the assigned sum formulas. As has been shown in section 4, *anti*-configured oxidative addition products *anti*-**4a** bear two equivalents of ligand **L1**, while the corresponding *syn*-configured species have only one equivalent of **L1** attached. Thus, the species observed at  $m/z = 1281$  is likely to be the [M-Cl]<sup>+</sup> fragment of *anti*-**4a** or its corresponding electrocyclic ring-opening product. On the other hand, assignment of the species detected at  $m/z = 742$  is ambiguous, as this mass is consistent with both [M-L-Cl]<sup>+</sup> of *anti*-**4a** and [M-Cl]<sup>+</sup> of *syn*-**4a**.

**Table S14.** ESI<sup>+</sup>-HRMS analysis of the Pd-catalyzed allylic alkylation of substrate *trans*-1 with nucleophile Na-2 and ligand L1 in MeCN, sample taken 47 s after initiation: Assignment of ion formulas and possible structures to experimental mass numbers *m/z* and comparison with calculated values, with the corresponding deviation Δ given.

Exp. <i>m/z</i>	Ion Formula	Possible Assignment	Calcd. <i>m/z</i>	Δ / ppm
1281.3357	C <sub>77</sub> H <sub>65</sub> N <sub>2</sub> O <sub>6</sub> Pd	[M-Cl] <sup>+</sup> of <i>anti</i> -4a	1281.3347	0.7
742.1348	C <sub>41</sub> H <sub>33</sub> NO <sub>4</sub> PPd	[M-L-Cl] <sup>+</sup> of <i>anti</i> -4a and/or [M-Cl] <sup>+</sup> of <i>syn</i> -4a	742.1333	2.0
243.0862	C <sub>11</sub> H <sub>14</sub> O <sub>6</sub>	[M+H] <sup>+</sup> of 3	243.0863	-0.5
147.0649	C <sub>6</sub> H <sub>11</sub> O <sub>4</sub>	[M-Na+2H] <sup>+</sup> of Na-2	147.0652	-2.0
97.0285	C <sub>5</sub> H <sub>6</sub> O <sub>2</sub>	[M-Cl] <sup>+</sup> of <i>trans</i> -1	97.0284	0.7

The mass-selective HPLC traces that were obtained for *m/z* = 1281 and *m/z* = 742, respectively, are shown in Figure S16 (bottom). In the HPLC trace of *m/z* = 1281 ([M-Cl]<sup>+</sup> of *anti*-4a) recorded directly after initiation, one large peak was observed, which is not present anymore in the HPLC trace obtained after reaching full conversion. This confirms that the species detected at *m/z* = 1281 has a transient nature, i.e. that *anti*-4a is only present during turnover. The HPLC trace of *m/z* = 742 ([M-L-Cl]<sup>+</sup> of *anti*-4a and/or [M-Cl]<sup>+</sup> of *syn*-4a), on the other hand, exhibits three large peaks, one of which is still present in the end-point trace. Thus, several transient and non-transient species with fragments *m/z* = 742 appear to be involved.

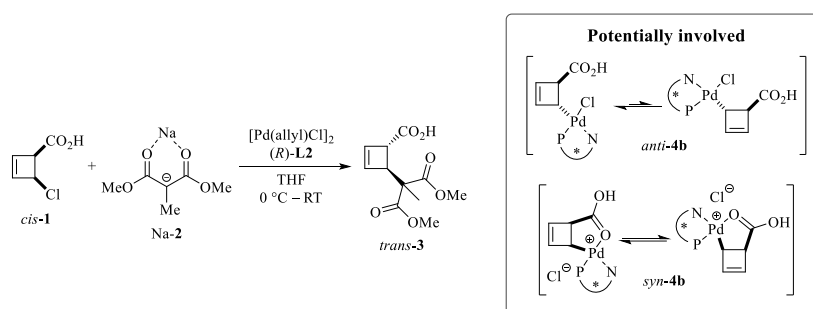


**Figure S16.** ESI<sup>+</sup>-HRMS analysis of the Pd-catalyzed allylic alkylation of substrate *trans*-1 with nucleophile Na-2 and ligand L1 in MeCN: Full mass range (sum over total HPLC run after initiation, top left), enlarged MS peaks of Pd-cyclobutene species (top right and bottom left) and respective mass-selective HPLC traces (bottom right).

The HPLC traces for *m/z* = 1281 and *m/z* = 742 are virtually identical to those obtained by analysis of the same reaction using substrate *cis*-1 (cf. Figure S15). This indicates that the same Pd-cyclobutene species are involved regardless which substrate diastereomer is used. These results suggest a convergent scenario for the oxidative addition, with *cis*-1 and *trans*-1 reacting via the same Pd-intermediate(s).

Other expected Pd-intermediates along the catalytic cycle such as the zerovalent palladium species or a  $\eta^2$ -product complex could not be identified.

## ESI-HRMS Analysis with Substrate *cis*-1 and Ligand L2

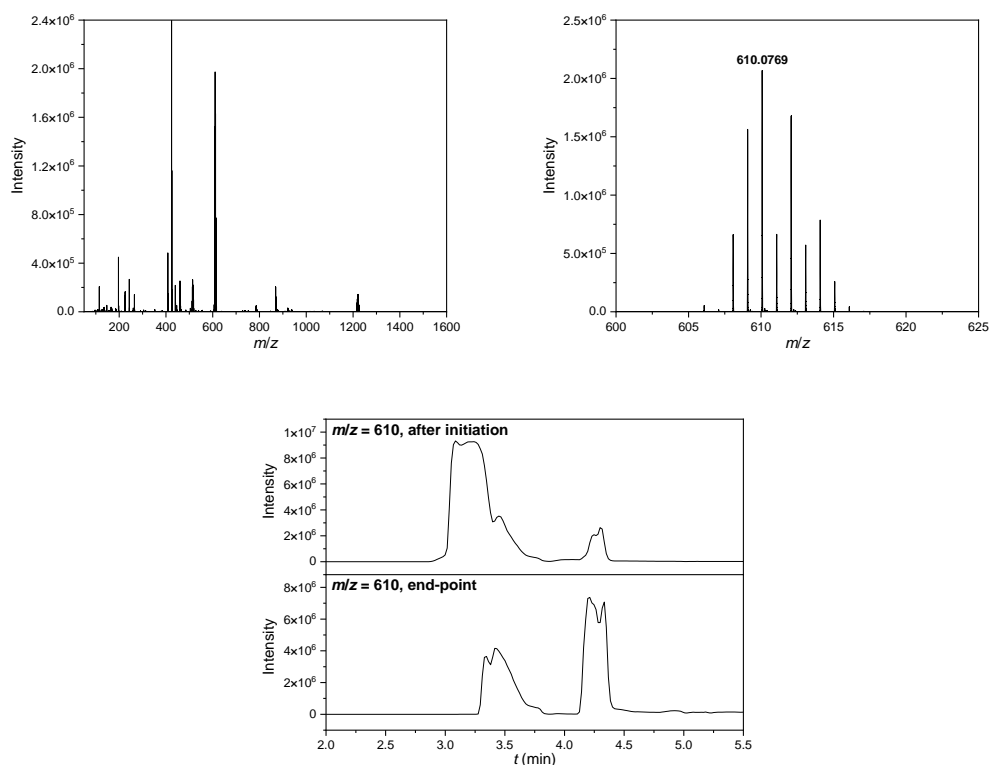


When a reaction mixture of substrate *cis*-1 and nucleophile Na-2 in THF was initiated with 2.0 mol% [Pd(allyl)Cl]<sub>2</sub> and 12 mol% (*R*)-L2 (50  $\mu$ L of a stock solution of 5 mM [Pd(allyl)Cl]<sub>2</sub> and 30 mM (*R*)-L2) and directly subjected to ESI-HRMS analysis in positive ion mode according to the general procedure, the mass fragments listed in Table S15 were obtained. Cations consistent with starting materials *cis*-1 ( $m/z = 133$  and 97) and Na-2 ( $m/z = 147$ ) as well as product **3** ( $m/z = 243$ ) were detected, confirming that a running reaction was analyzed. At  $m/z = 610$ , a Pd-containing species was detected which is consistent with the [M-Cl]<sup>+</sup> fragment of Pd-cyclobutene species *anti*- and *syn*-4b characterized as oxidative addition products in section 4. Also, assignment to the corresponding electrocyclic ring-opening products, which are isomeric to the Pd-cyclobutene complexes, is possible. The highly characteristic isotope pattern (Figure S17, left side) matched the calculated pattern for the assigned sum formula. In contrast to the analogous species with ligand L1, *anti*- and *syn*-configured Pd-cyclobutene species with ligand L2 do not differ in their molecular weight and can therefore not be differentiated by mass spectrometry.

**Table S15.** ESI<sup>+</sup>- (top) and ESI<sup>-</sup>- (bottom) HRMS analysis of the Pd-catalyzed allylic alkylation of substrate *trans*-1 with nucleophile Na-2 and ligand L2 in THF, sample taken 27 s and 10 min after initiation, respectively: Assignment of ion formulas and possible structures to experimental mass numbers  $m/z$  and comparison with calculated values, with the corresponding deviation  $\Delta$  given.

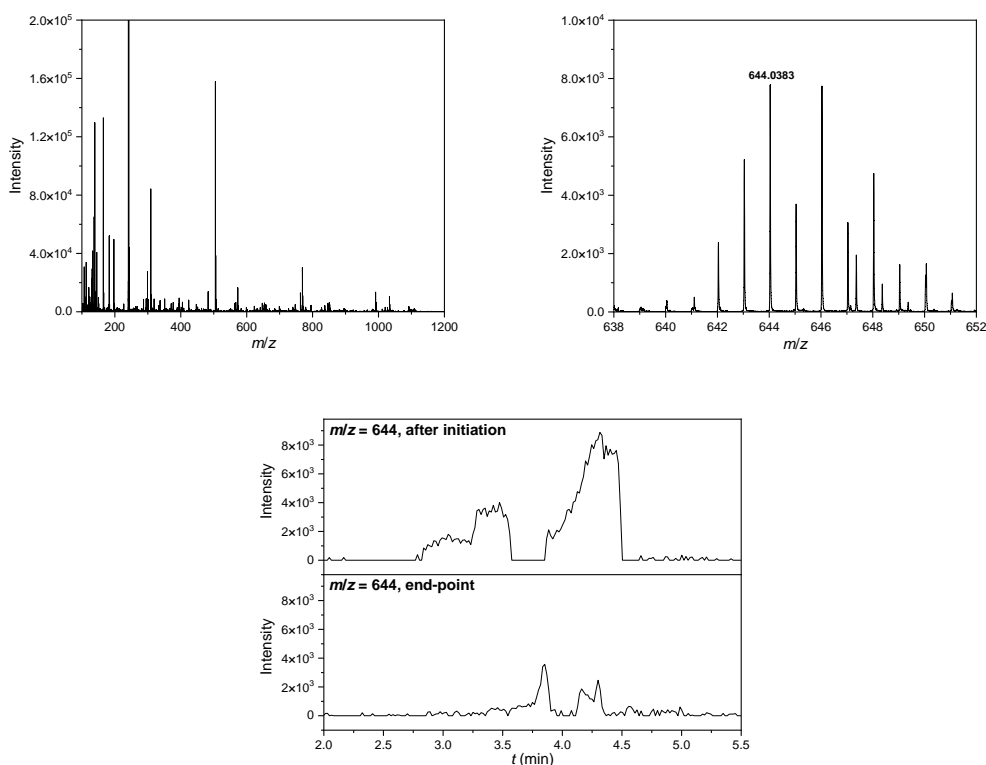
Exp. $m/z$	Ion Formula	Possible Assignment	Calcd. $m/z$	$\Delta$ / ppm
1219.1498	C <sub>66</sub> H <sub>53</sub> N <sub>2</sub> O <sub>6</sub> P <sub>2</sub> Pd <sub>2</sub>	[2M-2Cl+H] <sup>+</sup> of <i>anti</i> - and/or <i>syn</i> -4b	1219.1443	4.5
610.0769	C <sub>32</sub> H <sub>27</sub> NO <sub>3</sub> PPd	[M-Cl] <sup>+</sup> of <i>anti</i> - or <i>syn</i> -4b	610.0758	1.8
243.0861	C <sub>11</sub> H <sub>14</sub> O <sub>6</sub>	[M+H] <sup>+</sup> of <b>3</b>	243.0863	-0.9
147.0648	C <sub>6</sub> H <sub>11</sub> O <sub>6</sub>	[M-Na+2H] <sup>+</sup> of Na-2	147.0652	-2.7
133.0047	C <sub>5</sub> H <sub>6</sub> ClO <sub>2</sub>	[M+H] <sup>+</sup> of <i>cis</i> -1	133.0051	-2.9
97.0283	C <sub>5</sub> H <sub>6</sub> O <sub>2</sub>	[M-Cl] <sup>+</sup> of <i>cis</i> -1	97.0284	-0.7
644.0383	C <sub>32</sub> H <sub>26</sub> ClNO <sub>3</sub> PPd	[M-H] <sup>-</sup> of <i>anti</i> - or <i>syn</i> -4b	644.0379	0.8
241.0720	C <sub>11</sub> H <sub>13</sub> O <sub>6</sub>	[M-H] <sup>-</sup> of <b>3</b>	241.0718	0.8
145.0505	C <sub>6</sub> H <sub>9</sub> O <sub>4</sub>	[M-Na] <sup>-</sup> of Na-2	145.0506	-0.7
130.9904	C <sub>5</sub> H <sub>4</sub> ClO <sub>2</sub>	[M-H] <sup>-</sup> of <i>cis</i> -1	130.9905	-0.8

As shown in Figure S17 (right side), the mass-selective HPLC trace obtained for  $m/z = 610$  ([M-Cl]<sup>+</sup> of *anti*- or *syn*-4b) directly after initiation exhibits one dominant peak (cut due to detector saturation) along with several small signals. In the HPLC trace recorded after reaching full conversion, only the small peaks are still detectable. Thus, the dominant HPLC peak belongs to a transient species, which is likely to be *anti*-4b, as *syn*-4b has been shown not to be catalytically competent (cf. section 6).



**Figure S17.** ESI<sup>-</sup>-HRMS analysis of the Pd-catalyzed allylic alkylation of substrate *cis*-**1** with nucleophile Na-**2** and ligand L**2** in THF: Full mass range (sum over total HPLC run after initiation, top left), enlarged [M-CI]<sup>-</sup> peak of Pd-cyclobutene species (top right) and respective mass-selective HPLC traces (bottom).

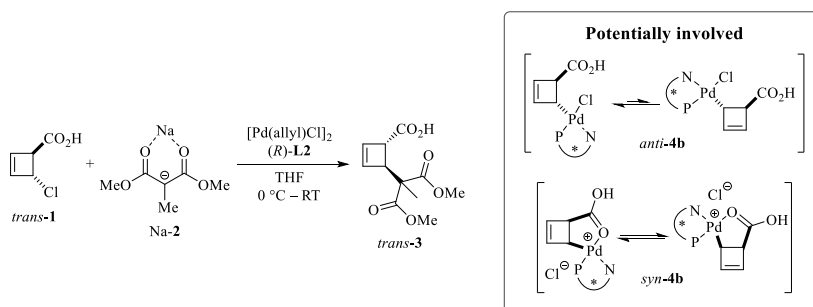
ESI-HRMS analysis in negative ion mode of a reaction performed under the same conditions gave consistent results, but was generally plagued by a low signal-to-noise ratio and large amounts of impurities complicating spectral analysis. As listed in Table S15, anions consistent with starting materials *cis*-**1** ( $m/z = 131$ ) and Na-**2** ( $m/z = 145$ ) as well as product **3** ( $m/z = 241$ ) were detected, confirming that a running reaction was analyzed. At  $m/z = 644$ , a species consistent with the [M-H]<sup>-</sup> fragment of Pd-cyclobutene species *anti*- or *syn*-**4b** (or the corresponding dienes) was observed. The experimental isotope pattern (Figure S18, left side) matched the calculated pattern for the assigned sum formula. The mass-selective HPLC traces (Figure S18, right side), albeit exhibiting poor-signal-to-noise ratio and resolution, were consistent with those obtained in positive ion mode.



**Figure S18.** ESI-HRMS analysis of the Pd-catalyzed allylic alkylation of substrate *cis*-**1** with nucleophile Na-**2** and ligand **L2** in THF: Full mass range (sum over total HPLC run after initiation, top left), enlarged [M-H]<sup>+</sup> peak of Pd-cyclobutene species (top right, overlapping with an impurity with higher *m/z*) and respective mass-selective HPLC traces (bottom).

Other expected Pd-intermediates along the catalytic cycle such as the zerovalent palladium species or a  $\eta^2$ -product complex could not be identified, neither in positive nor in negative ion mode.

#### ESI-HRMS Analysis with Substrate *trans*-**1** and Ligand **L2**

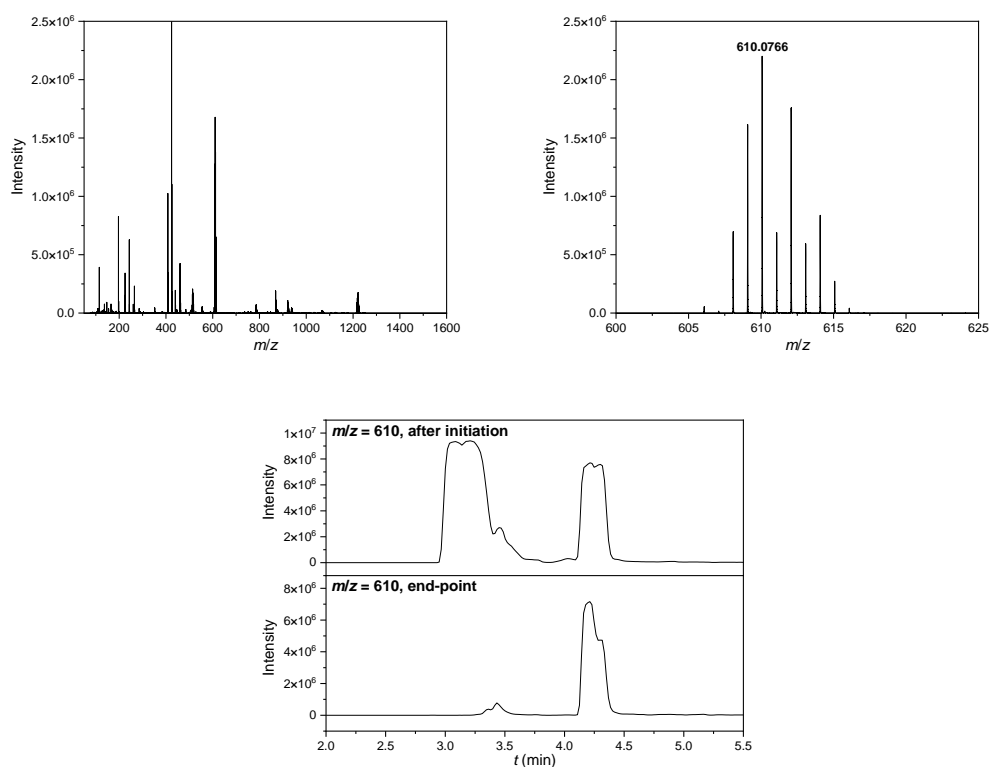


When a reaction mixture of substrate *trans*-**1** and nucleophile Na-**2** in THF was initiated with 4.0 mol% [Pd(allyl)Cl]<sub>2</sub> and 24 mol% (*R*)-**L2** (100  $\mu$ L of a stock solution of 5 mM [Pd(allyl)Cl]<sub>2</sub> and 30 mM (*R*)-**L2**) and directly subjected to ESI-HRMS analysis in positive ion mode according to the general procedure, the mass fragments listed in Table S16 were obtained. Cations consistent with starting materials *trans*-**1** (*m/z* = 97) and Na-**2** (*m/z* = 147) as well as product **3** (*m/z* = 243) were detected, confirming that a running reaction was analyzed. At *m/z* = 610, a Pd-containing species was detected which is consistent with the [M-Cl]<sup>+</sup> fragment of Pd-cyclobutene species *anti*- and *syn*-**4b** characterized as oxidative addition products in section 4. Also, assignment to the corresponding electrocyclic ring-opening products, which are isomeric to the Pd-cyclobutene complexes, is possible. The highly characteristic isotope pattern (Figure S19, left side) matched the calculated pattern for the assigned sum formula. In contrast to the analogous species with ligand **L1**, *anti*- and *syn*-configured Pd-cyclobutene species with ligand **L2** do not differ in their molecular weight and can therefore not be differentiated by mass spectrometry.

**Table S16.** ESI<sup>+</sup>-HRMS analysis of the Pd-catalyzed allylic alkylation of substrate *trans*-**1** with nucleophile Na-**2** and ligand **L2** in THF, sample taken 35 s after initiation: Assignment of ion formulas and possible structures to experimental mass numbers *m/z* and comparison with calculated values, with the corresponding deviation Δ given.

Exp. <i>m/z</i>	Ion Formula	Possible Assignment	Calcd. <i>m/z</i>	Δ / ppm
1219.1437	C <sub>64</sub> H <sub>53</sub> N <sub>2</sub> O <sub>6</sub> P <sub>2</sub> Pd <sub>2</sub>	[2M-2Cl+H] <sup>+</sup> of <i>anti</i> - and/or <i>syn</i> - <b>4b</b>	1219.1443	-0.5
610.0766	C <sub>32</sub> H <sub>27</sub> NO <sub>3</sub> PPd	[M-Cl] <sup>+</sup> of <i>anti</i> - or <i>syn</i> - <b>4b</b>	610.0758	1.4
243.0863	C <sub>11</sub> H <sub>14</sub> O <sub>6</sub>	[M+H] <sup>+</sup> of <b>3</b>	243.0863	0.1
147.0651	C <sub>6</sub> H <sub>11</sub> O <sub>4</sub>	[M-Na+2H] <sup>+</sup> of Na- <b>2</b>	147.0652	-0.7
97.0286	C <sub>5</sub> H <sub>6</sub> O <sub>2</sub>	[M-Cl] <sup>+</sup> of <i>trans</i> - <b>1</b>	97.0284	1.5

As shown in Figure S19 (right side), the mass-selective HPLC trace obtained for *m/z* = 610 ([M-Cl]<sup>+</sup> of *anti*- or *syn*-**4b**) directly after initiation exhibits one dominant peak (cut due to detector saturation) along with several small signals. In the HPLC trace recorded after reaching full conversion, only the small peaks are still detectable. Thus, the dominant HPLC peak belongs to a transient species, which is likely to be *anti*-**4b**, as *syn*-**4b** has been shown not to be catalytically competent (cf. section 6).



**Figure S19.** ESI<sup>+</sup>-HRMS analysis of the Pd-catalyzed allylic alkylation of substrate *trans*-**1** with nucleophile Na-**2** and ligand **L2** in THF: Full mass range (sum over total HPLC run after initiation, top left), enlarged [M-Cl]<sup>+</sup> peak of Pd-cyclobutene species (top right) and respective mass-selective HPLC traces (bottom).

The HPLC traces for *m/z* = 610 are virtually identical to those obtained by analysis of the same reaction using substrate *cis*-**1** (cf. Figure S17). This indicates that the same Pd-cyclobutene species are involved regardless which substrate diastereomer is used. These results suggest a convergent scenario for the oxidative addition, with *cis*-**1** and *trans*-**1** reacting via the same Pd-intermediate(s).

Other expected Pd-intermediates along the catalytic cycle such as the zerovalent palladium species or a η<sup>2</sup>-product complex could not be identified. Attempts to detect Pd-species in negative ion mode were not successful.



## 10 Computational Details

The conformer space of the Pd-cyclobutene complexes investigated was sampled using CREST (Conformer–Rotamer Ensemble Sampling Tool, version 2.11.2)<sup>52</sup> and the iMTD-sMTD (iterative MeTaDynamics-static MeTaDynamics) workflow. The GFN2-xTB (Geometry, Frequency, Noncovalent 2, Extended TightBinding)<sup>53</sup> method and the ALPB (Analytical Linearized Poisson-Boltzmann)<sup>54</sup> solvent model with the parameters for THF were employed. All conformers obtained from the CREST runs were further refined and sorted using CENSO at a higher level of theory (Commandline ENergetic SORTing of Conformer Rotamer Ensembles, version 1.2.0).<sup>55</sup> ORCA 5.0.3<sup>56</sup> was used as external quantum chemistry program for CENSO. After a prescreening at the B97-D3<sup>57</sup> def2-SV(P) (Split valence basis set with polarization functions on heavy atoms)<sup>58</sup> level of theory, the resulting ensemble was optimized using the r<sup>2</sup>SCAN-3c method<sup>59</sup> and the SMD (Solvation Model Based on Density) solvent model<sup>60</sup> with parameters for THF.

Following the CENSO run, the reduced conformer ensemble was subjected to a geometry optimization and frequency calculation using ORCA 5.0.3 at the BP86<sup>61</sup> def2-SVP (def2-TZVP was used for Palladium)<sup>58</sup> D3BJ<sup>57</sup> CPCM (Conductor-like Polarizable Continuum Model) (THF)<sup>62</sup> level. The obtained Gibbs free energy (minus the electronic energy) for each conformer was enhanced by relativistic ZORA (zero-order regular approximation)<sup>63</sup> single point energy calculations at the  $\omega$ B97M-V<sup>64</sup> ZORA-TZVPP (SARC-ZORA-TZVPP for Palladium)<sup>65</sup> CPCM (THF)<sup>62</sup> level on the previously optimized geometries to obtain the final Gibbs energies. Gibbs energies are listed in Table S17 and Table S18 while the corresponding structures (over 5 % Boltzmann weight according to the Gibbs energies) can be found in the xyz file attached. Van der Waals radii were visualized using UCSF (University of California, San Francisco) Chimera 1.15.<sup>66</sup>

For all obtained conformers (over 5 % Boltzmann weight according to the Gibbs energies), <sup>1</sup>H- and <sup>13</sup>C-chemical shieldings were computed with the gauge invariant atomic orbital (GIAO) approach<sup>67,68</sup> considering relativistic effects with the Zero-Order Regular Approximation<sup>69</sup> using the mPW1LYP<sup>70</sup> functional and the ZORA-TZVPP (SARC-ZORA-TZVPP for Palladium)<sup>65</sup> basis set while solvent effects were taken into account implicitly using CPCM (THF).<sup>62</sup> The chemical shieldings  $\sigma^{\text{calc}}(i)$  of Pd-cyclobutene complexes were converted to chemical shifts  $\delta^{\text{calc}}(i)$  according to

$$\delta^{\text{calc}}(i) = \sigma^{\text{calc}}(\text{TMS}) - \sigma^{\text{calc}}(i) \quad (58)$$

using the shielding of tetramethylsilane  $\sigma^{\text{calc}}(\text{TMS})$  as a reference which was calculated at the same level of theory. Comparison with experimental data showed that calculated <sup>13</sup>C-chemical shifts  $\delta^{\text{calc}}$  are in good reasonable agreement with experimental <sup>13</sup>C-chemical shifts  $\delta^{\text{exp}}$ , whilst calculated <sup>1</sup>H-chemical shifts  $\delta^{\text{calc}}$  turned out not to be accurate enough for reliable chemical shift analysis. Therefore, only <sup>13</sup>C-chemical shifts were used for correlating calculated with experimental structures.

**Table S17.** Conformers of Pd-cyclobutene species with ligand **L1** calculated at the  $\omega$ B97M-V/ZORA-TZVPP level of theory at 273.15 K: Difference of Gibbs and electronic energy  $G - E_{\text{el}}$  obtained at the BP86/def2-SVP (def2-TZVP on Pd) level, electronic energy  $E_{\text{el}}$  obtained at the  $\omega$ B97M-V/ZORA-TZVPP level, Gibbs energy  $G$  calculated from these values, relative Gibbs energy  $\Delta G$  to compare between interconverting diastereomeric species, and coefficient of determination  $R^2$  for the correlation between Boltzmann weighted calculated <sup>13</sup>C-chemical shifts  $\delta^{\text{calc}}$  and experimental shifts  $\delta^{\text{exp}}$ .

Species	Conformer	$G - E_{\text{el}} / \text{kcal mol}^{-1}$	$E_{\text{el}} / \text{kcal mol}^{-1}$	$G / \text{kcal mol}^{-1}$	$\Delta G / \text{kcal mol}^{-1}$	$R^2$ of $\delta^{\text{calc}}$ vs $\delta^{\text{exp}}$
FER 1 (minor-anti-4a)	CONF87	696.46	-6142370.61	-6141674.15	2.69	0.9873
FER 1_1 (major-anti-4a)	CONF45	697.35	-6142372.69	-6141675.34	1.50	
FER 1_1 (major-anti-4a)	CONF217	696.50	-6142373.34	-6141676.84	0	0.9843
FER 1_1 (major-anti-4a)	CONF253	697.24	-6142373.85	-6141676.61	0.23	
FER 13 (minor-syn-4a)	CONF1	366.31	-4925618.71	-4925252.40	10.77	0.9786
FER 13_1 (major-syn-4a)	CONF9	365.77	-4925628.94	-4925263.17	0	0.9942
FER 14 (minor-anti-Na-4a)	CONF30	689.82	-6244079.34	-6243389.53	3.96	0.9112
FER 14_1 (major-anti-Na-4a)	CONF16	688.89	-6244082.38	-6243393.49	0	0.9795
FER 15 (minor-anti-6a)	CONF53	713.16	-6167038.49	-6166325.33	3.26	
FER 15 (minor-anti-6a)	CONF105	712.25	-6167038.21	-6166325.96	2.63	
FER 15 (minor-anti-6a)	CONF360	713.33	-6167039.60	-6166326.26	2.32	0.9905
FER 15 (minor-anti-6a)	CONF648	712.61	-6167038.13	-6166325.52	3.07	
FER 15 (minor-anti-6a)	CONF725	713.27	-6167038.96	-6166325.69	2.90	
FER 15 (minor-anti-6a)	CONF795	712.43	-6167037.51	-6166325.08	3.50	
FER 15_1 (major-anti-6a)	CONF191	713.13	-6167041.72	-6166328.59	0	0.9683

FER 15_1 (major- <i>anti</i> - <b>6a</b> )	CONF200	712.63	-6167040.88	-6166328.24	0.34	
FER 15_1 (major- <i>anti</i> - <b>6a</b> )	CONF539	713.13	-6167041.11	-6166327.99	0.60	
FER 16 (major- <i>syn</i> - <b>6a</b> )	CONF4	381.54	-4950288.33	-4949906.80	0	0.9887
FER 16_1 (minor- <i>syn</i> - <b>6a</b> )	CONF21	381.82	-4950285.40	-4949903.58	3.22	0.9926
FER 17 (minor- <i>syn</i> -Na- <b>4a</b> )	CONF1	357.81	-5027333.98	-5026976.168	6.94	
FER 17 (minor- <i>syn</i> -Na- <b>4a</b> )	CONF2	357.87	-5027337.26	-5026979.39	4.34	
FER 17 (minor- <i>syn</i> -Na- <b>4a</b> )	CONF3	357.43	-5027337.15	-5026979.73	4.00	0.9903
FER 17 (minor- <i>syn</i> -Na- <b>4a</b> )	CONF4	357.98	-5027340.64	-5026982.66	1.07	
FER 17_1 (major- <i>syn</i> -Na- <b>4a</b> )	CONF1	358.05	-5027341.16	-5026983.11	0	
FER 17_1 (major- <i>syn</i> -Na- <b>4a</b> )	CONF2	357.68	-5027333.57	-5026975.89	7.83	0.9834
FER 17_1 (major- <i>syn</i> -Na- <b>4a</b> )	CONF4	357.91	-5027326.16	-5026968.25	15.48	

**Table S18.** Conformers of Pd-cyclobutene species with ligand **L2** calculated at the  $\omega$ B97M-V/ZORA-TZVPP level of theory at 273.15 K: Difference of Gibbs and electronic energy  $G - E_{el}$  obtained at the BP86/def2-SVP (def2-TZVP on Pd) level, electronic energy  $E_{el}$  obtained at the  $\omega$ B97M-V/ZORA-TZVPP level, Gibbs energy  $G$  calculated from these values, relative Gibbs energy  $\Delta G$  to compare between interconverting diastereomeric species, and coefficient of determination  $R^2$  for the correlation between Boltzmann weighted calculated  $^{13}\text{C}$ -chemical shifts  $\delta_{\text{C}}^{\text{calc}}$  and experimental shifts  $\delta_{\text{C}}^{\text{exp}}$ .

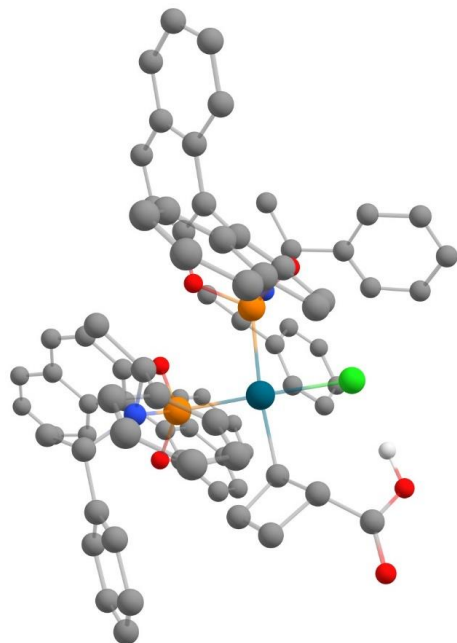
Species	Conformer	$G - E_{el} / \text{kcal mol}^{-1}$	$E_{el} / \text{kcal mol}^{-1}$	$G / \text{kcal mol}^{-1}$	$\Delta G / \text{kcal mol}^{-1}$	$R^2$ of $\delta_{\text{C}}^{\text{calc}}$ vs $\delta_{\text{C}}^{\text{exp}}$
PHOX 1 (major- <i>anti</i> - <b>4b</b> )	CONF41	278.44	-4659947.84	-4659669.40	0	0.9865
PHOX 1_1 (minor- <i>anti</i> - <b>4b</b> )	CONF3	278.13	-4659945.95	-4659667.82	1.59	
PHOX 1_1 (minor- <i>anti</i> - <b>4b</b> )	CONF58	278.68	-4659945.71	-4659667.02	2.38	0.9971
PHOX 13 (major- or minor- <i>syn</i> - <b>4b</b> )	CONF5	276.63	-4659941.37	-4659664.74	0	0.9789
PHOX 13_1 (major- or minor- <i>syn</i> - <b>4b</b> )	CONF5	276.92	-4659941.18	-4659664.26	0.48	0.9947
PHOX 17 ( <i>anti</i> - <b>6ba</b> or - <b>6bb</b> )	CONF55	294.72	-4684613.13	-4684318.40	2.45	
PHOX 17 ( <i>anti</i> - <b>6ba</b> or - <b>6bb</b> )	CONF66	294.21	-4684613.00	-4684318.79	2.06	0.9173
PHOX 17 ( <i>anti</i> - <b>6ba</b> or - <b>6bb</b> )	CONF80	294.65	-4684613.71	-4684319.06	1.80	
PHOX 17_1 ( <i>anti</i> - <b>6ba</b> or - <b>6bb</b> )	CONF65	294.52	-4684615.38	-4684320.85	0	0.9119
PHOX 18 (major- <i>syn</i> - <b>6b</b> )	CONF1	294.53	-4684614.45	-4684319.91	0	
PHOX 18 (major- <i>syn</i> - <b>6b</b> )	CONF17	294.29	-4684613.79	-4684319.50	0.42	0.9455
PHOX 18 (major- <i>syn</i> - <b>6b</b> )	CONF22	295.20	-4684613.40	-4684318.21	1.71	
PHOX 18_1 (minor- <i>syn</i> - <b>6b</b> )	CONF7	294.95	-4684610.68	-4684315.73	4.19	
PHOX 18_1 (minor- <i>syn</i> - <b>6b</b> )	CONF23	293.68	-4684609.11	-4684315.42	4.49	0.9153
PHOX 18_1 (minor- <i>syn</i> - <b>6b</b> )	CONF37	294.59	-4684612.47	-4684317.88	2.03	
PHOX 20 (major- <i>syn</i> -Na- <b>4b</b> )	CONF1	271.11	-4761674.66	-4761403.56	0.44	
PHOX 20 (major- <i>syn</i> -Na- <b>4b</b> )	CONF5	270.25	-4761674.25	-4761404.00	0	0.9773
PHOX 20_1 (minor- <i>syn</i> -Na- <b>4b</b> )	CONF1	270.55	-4761673.99	-4761403.43	0.56	
PHOX 20_1 (minor- <i>syn</i> -Na- <b>4b</b> )	CONF3	270.37	-4761673.03	-4761402.67	1.33	0.9916

Structural models of all conformers calculated with >5 % Boltzmann weight according to the Gibbs energies as well as the correlations between calculated, Boltzmann averaged  $^{13}\text{C}$ -chemical shifts  $\delta_{\text{C}}^{\text{calc}}$  and experimental shifts  $\delta_{\text{C}}^{\text{exp}}$  are shown below. For exceptionally large molecules, hydrogen atoms bonded to carbons were omitted for clarity. For each pair of interconverting Pd-species (i.e. diastereomeric Pd-cyclobutene species with identical relative configuration at the cyclobutene ring), the species with a lower Gibbs energy was assumed to be the major species, and consequently the calculated  $^{13}\text{C}$ -chemical shifts were correlated with the experimental shifts detected for the major species. Accordingly, the species with a higher Gibbs energy was assumed to be the minor species, and calculated  $^{13}\text{C}$ -chemical shifts were thus correlated with the experimental shifts detected for

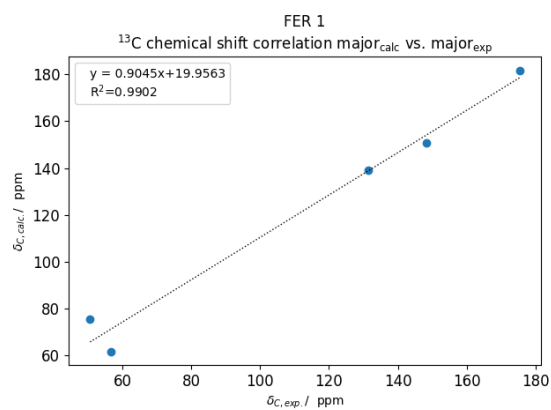
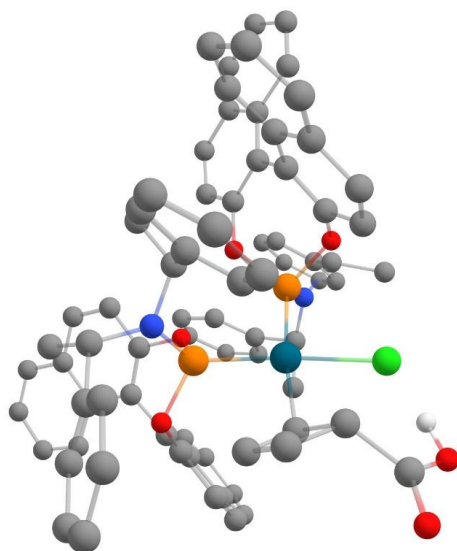
the minor species. If no species is favored experimentally, the best fit is shown. Fits of only  $^1\text{H}$ - as well as combined  $^1\text{H}/^{13}\text{C}$ -chemical shift comparisons can be found in the file attachment.

**FER 1\_1 (major-*anti*-4a)**

CONF217

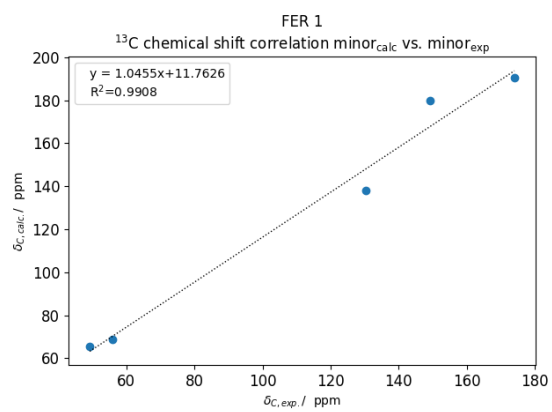
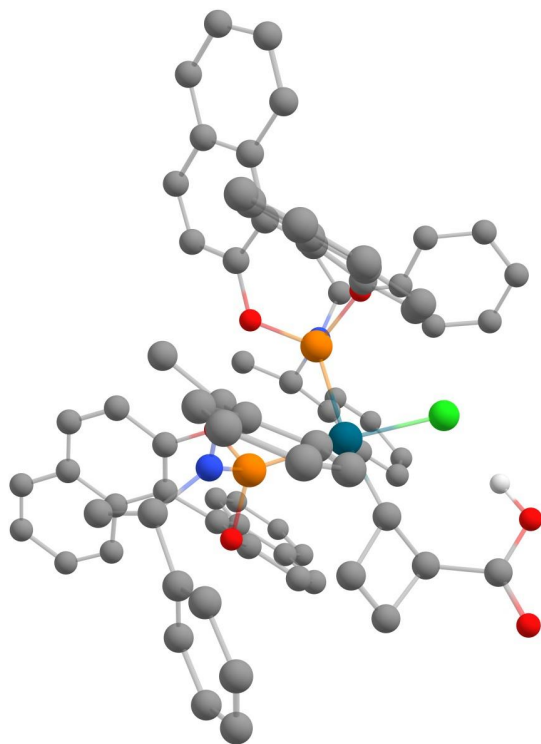


CONF253



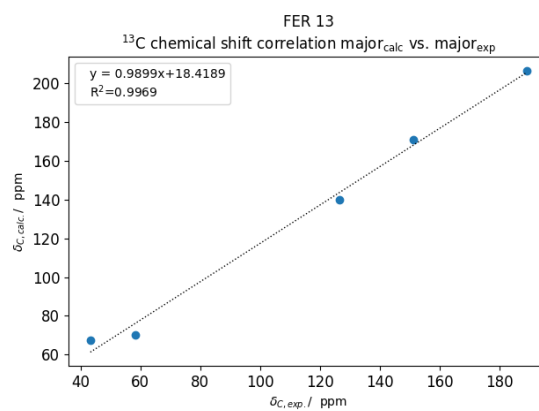
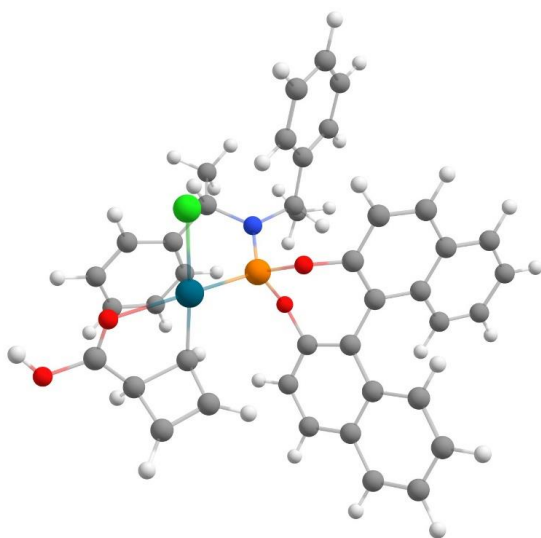
FER 1 (minor-*anti*-4a)

CONF87



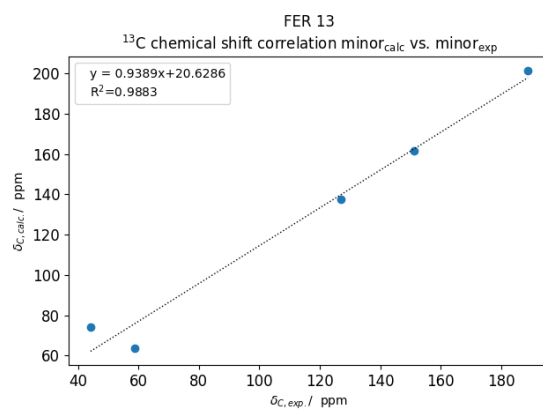
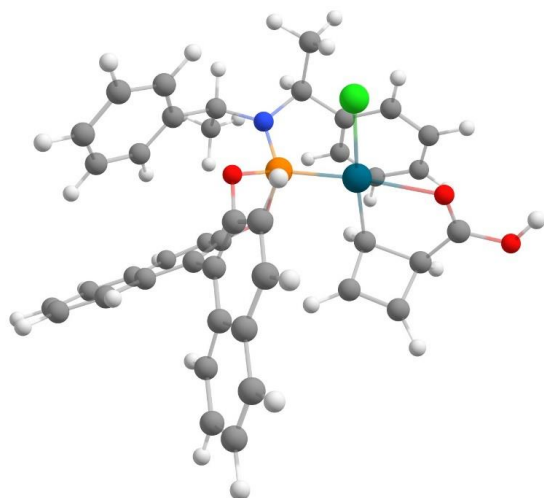
FER 13\_1 (major-*syn*-4a)

CONF9



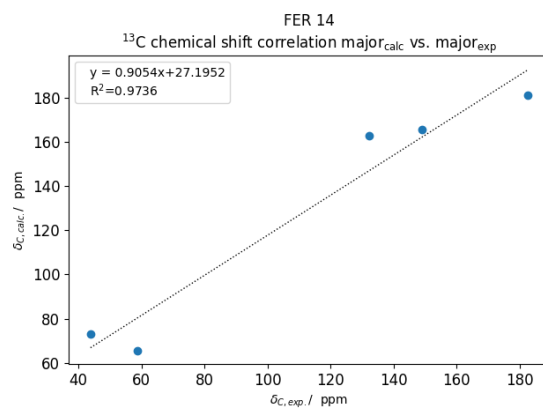
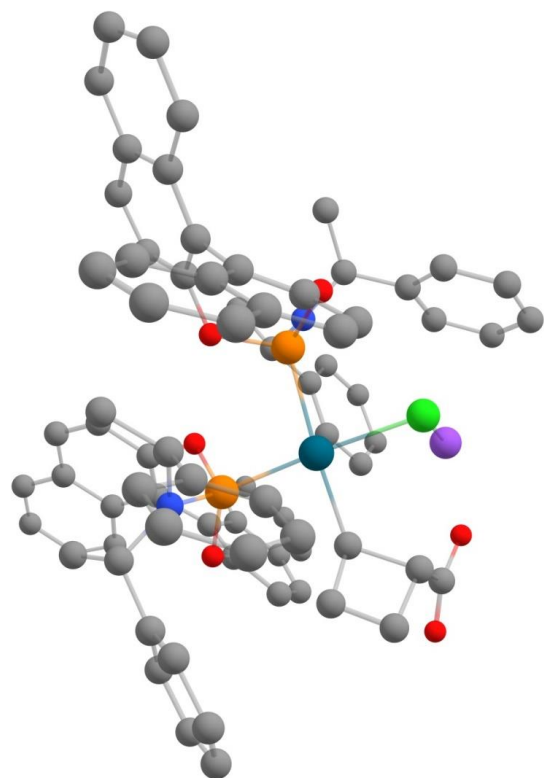
FER 13 (minor-*syn*-4a)

CONF1



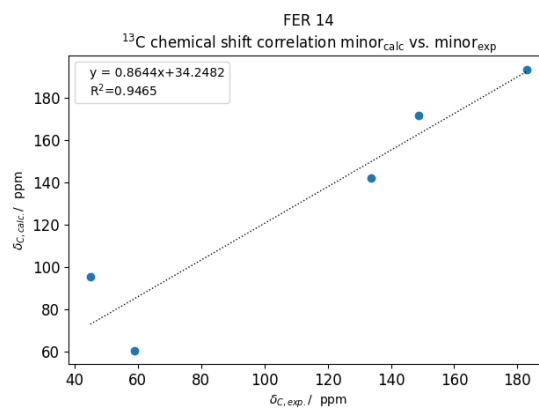
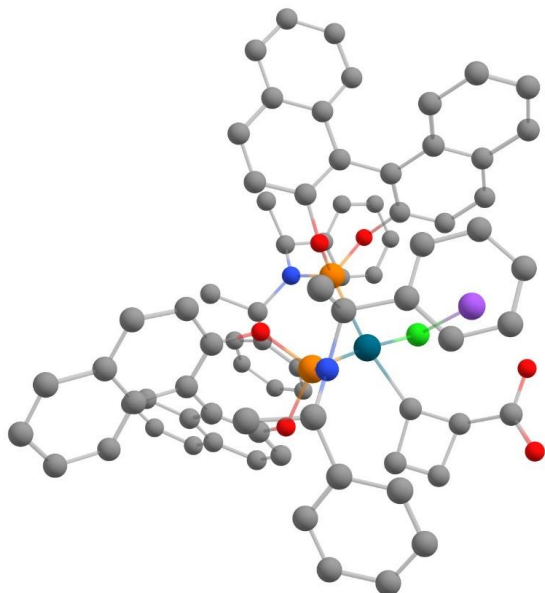
FER 14\_1 (major-*anti*-Na-4a)

CONF16



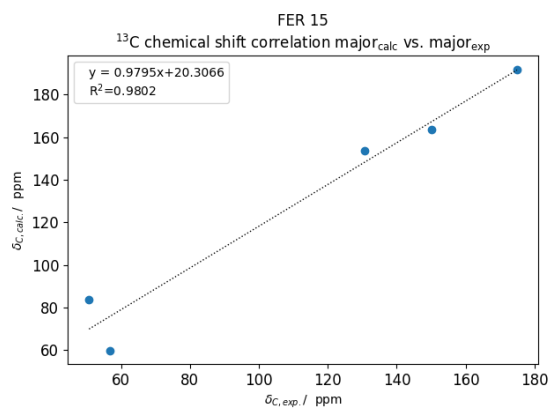
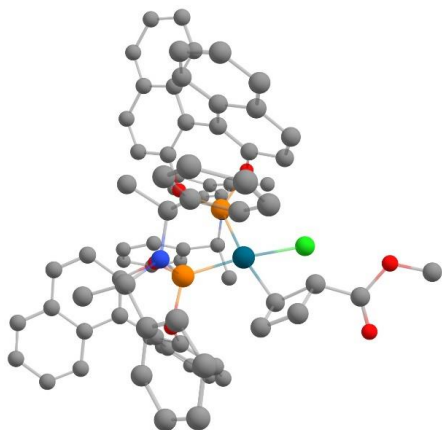
FER 14 (minor-*anti*-Na-4a)

CONF30



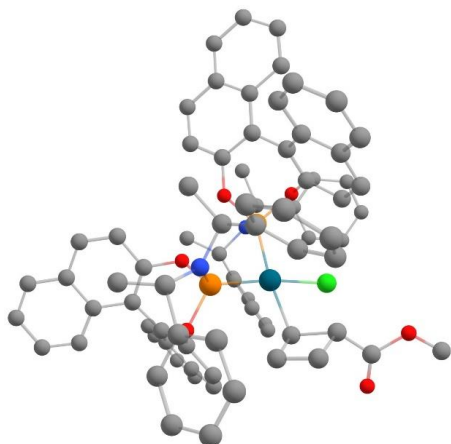
FER 15\_1 (major-*anti*-6a)

CONF191

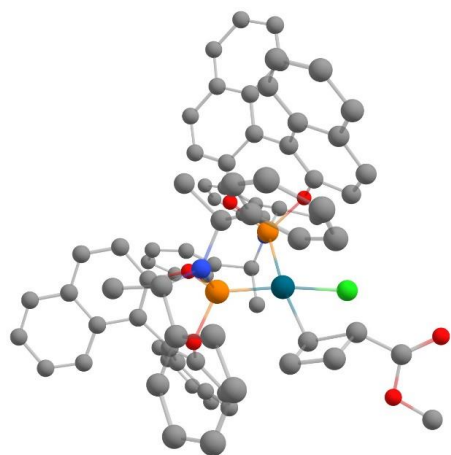


---

CONF200

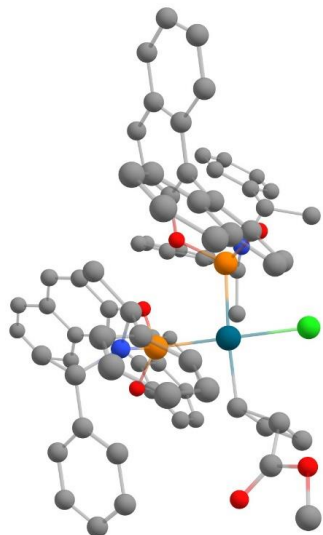


CONF539

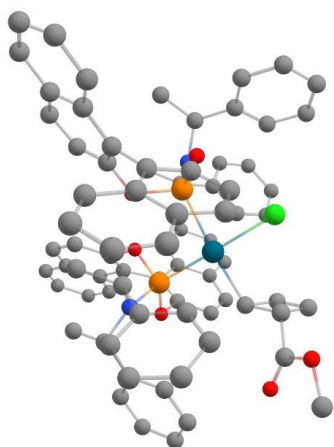


FER 15 (minor-*anti*-6a)

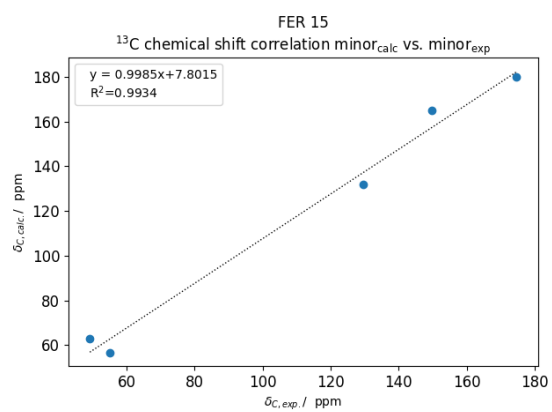
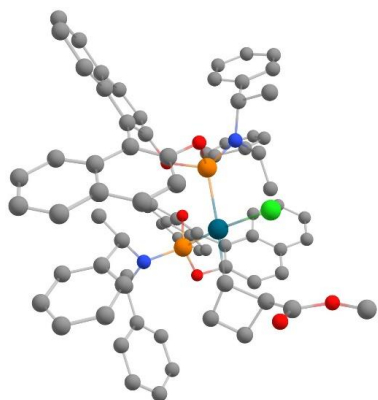
CONF53



CONF105

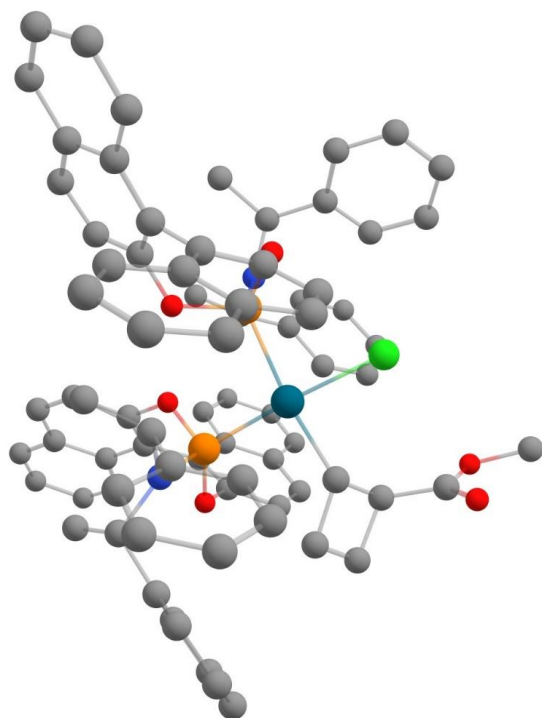


CONF360

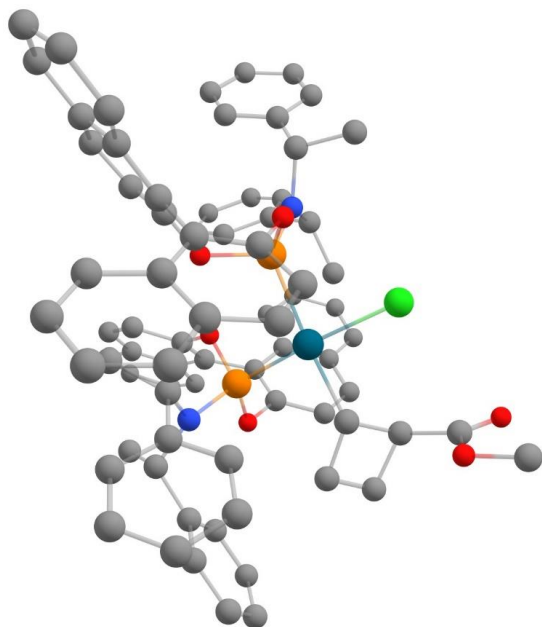




CONF648



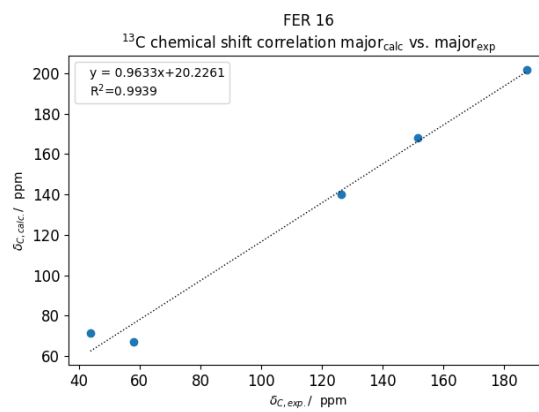
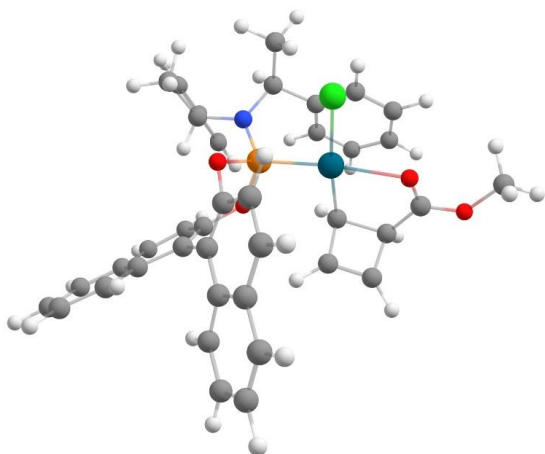
CONF725



S70

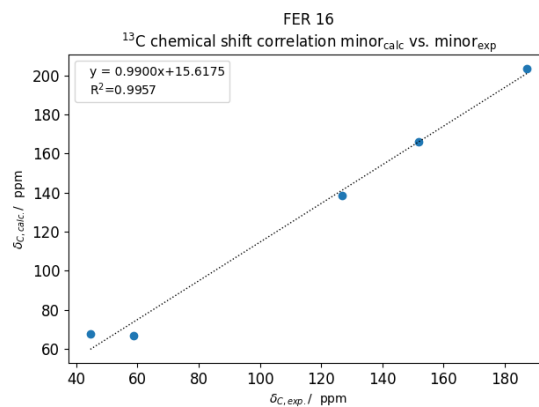
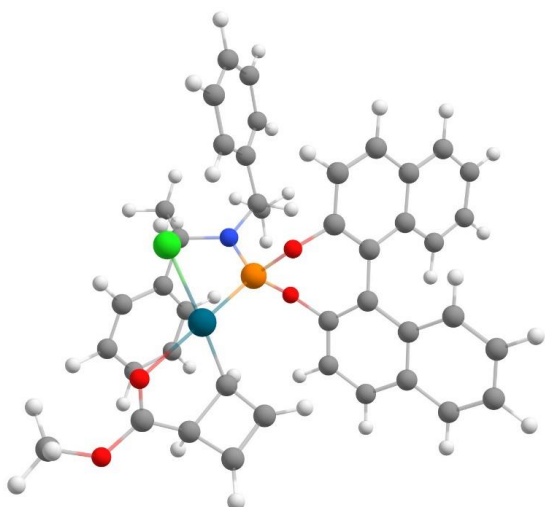
FER 16 (major-syn-6a)

CONF4



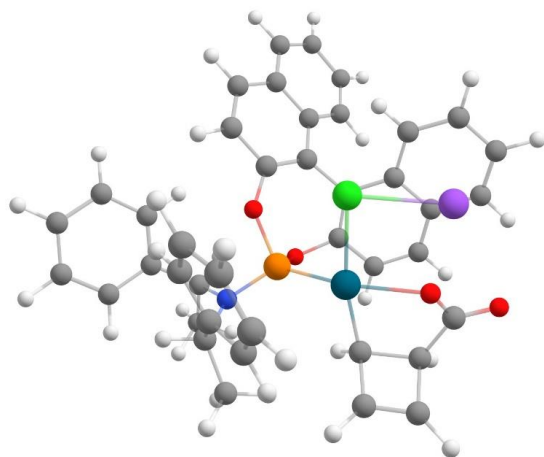
FER 16\_1 (minor-syn-6a)

CONF21

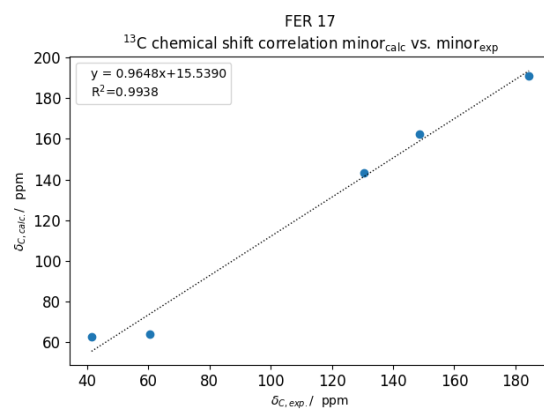
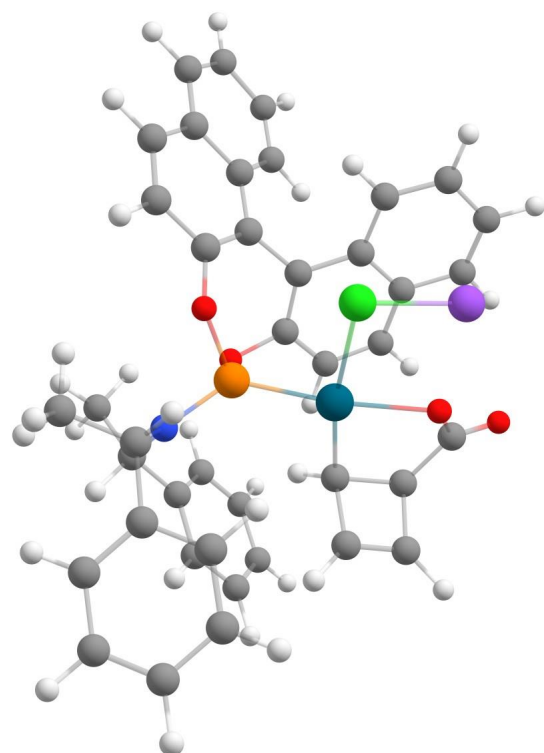


FER 17 (minor-*syn*-Na-4a)

CONF1

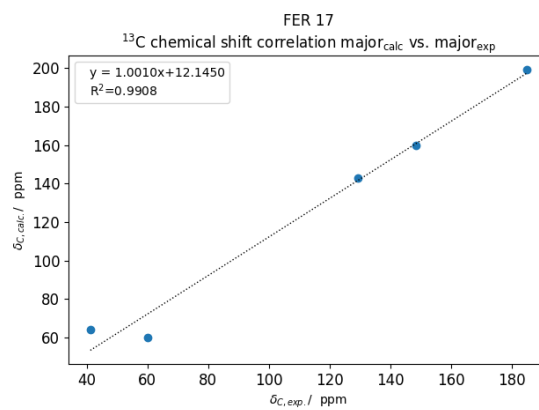
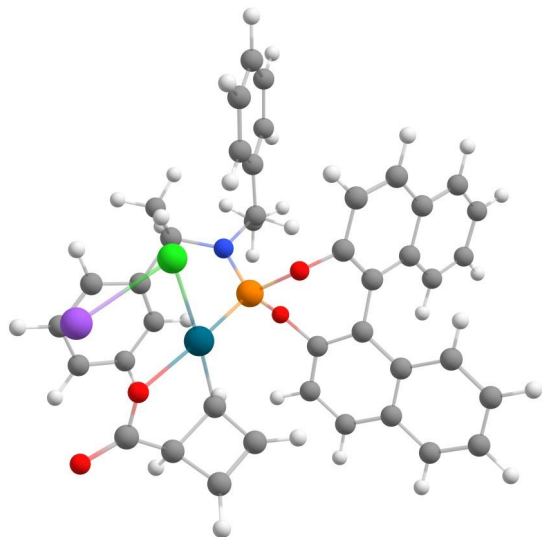


CONF4



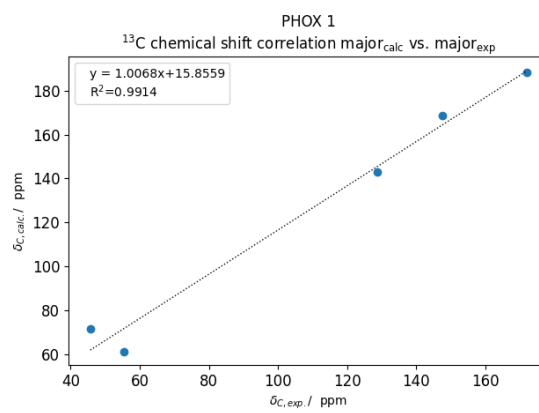
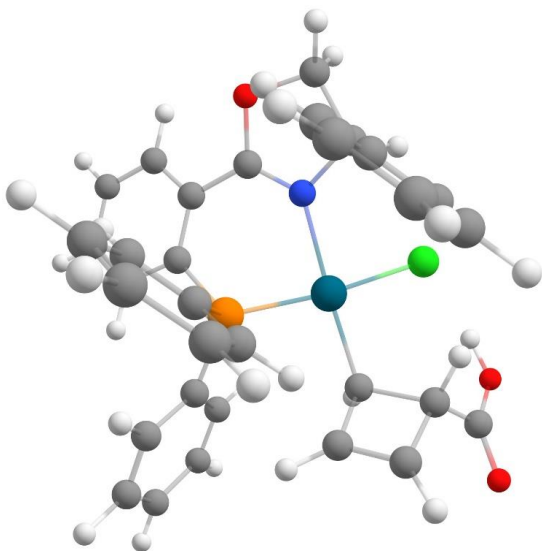
**FER 17\_1 (major-syn-Na-4a)**

CONF1



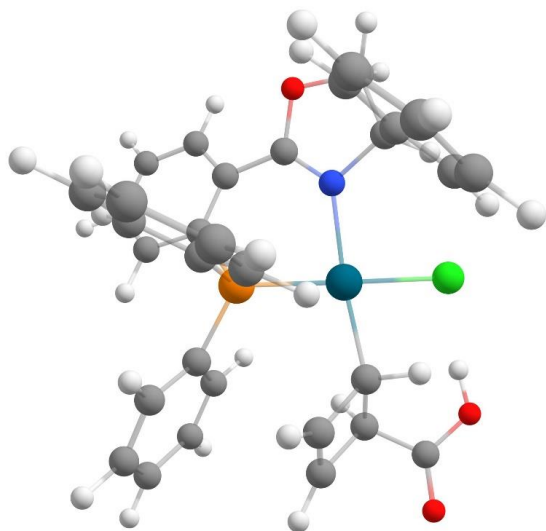
**PHOX 1 (major-anti-4b)**

CONF41

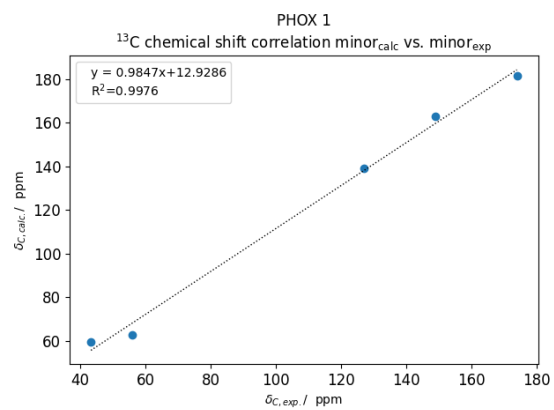
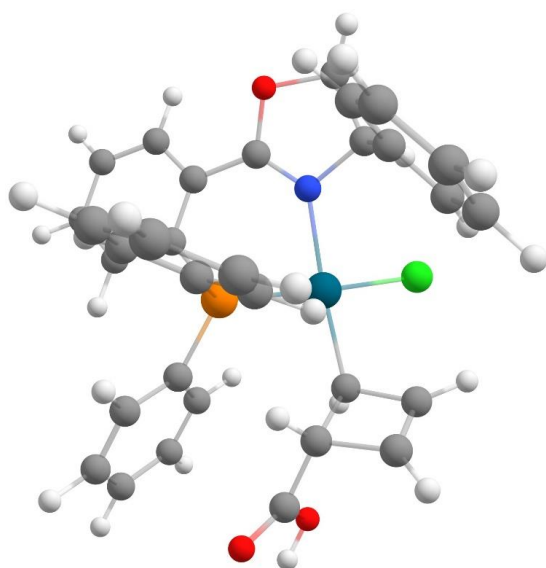


PHOX 1\_1 (minor-*anti*-4b)

CONF3

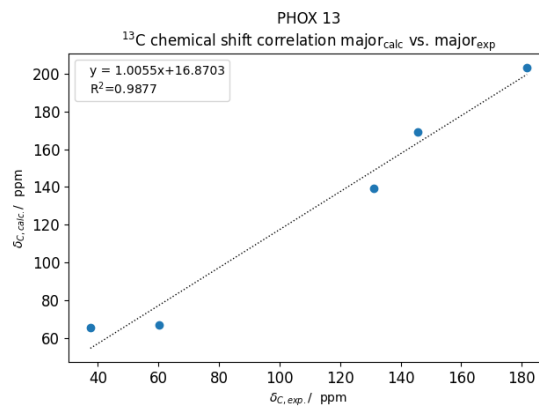
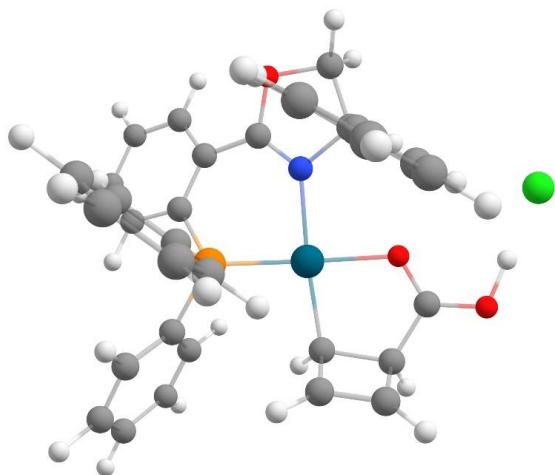


CONF58



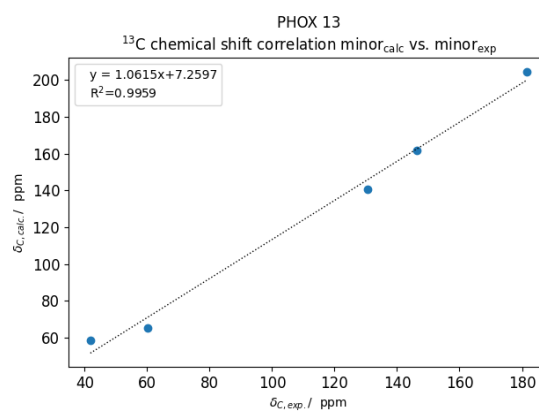
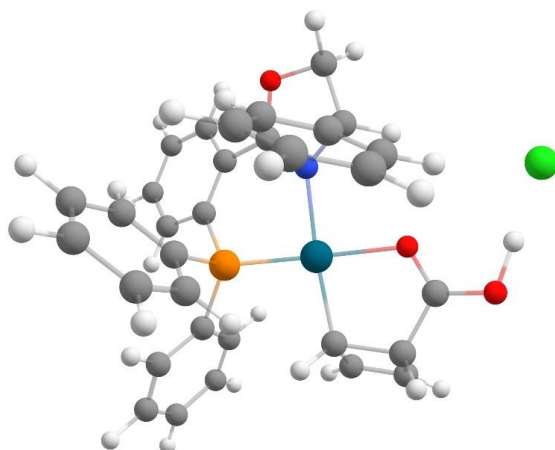
PHOX 13 (major- or minor-syn-4b)

CONF5



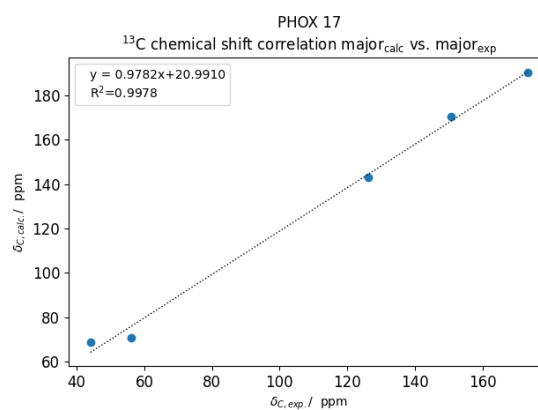
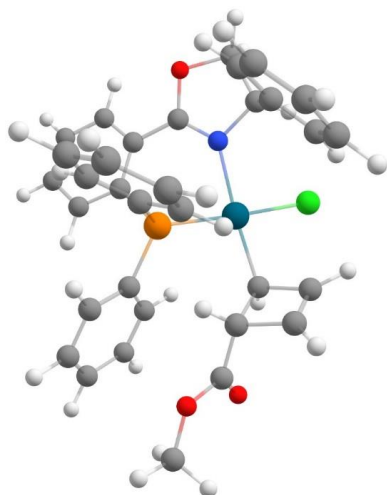
PHOX 13\_1 (major- or minor-syn-4b)

CONF5



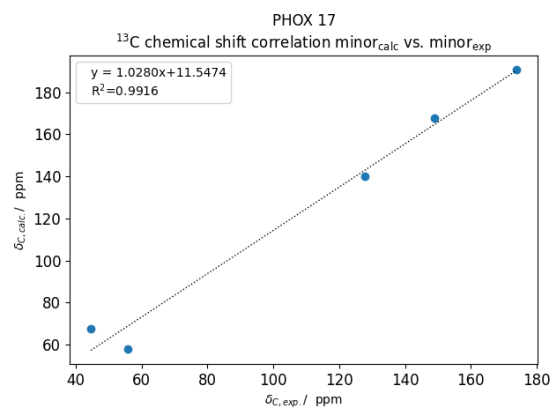
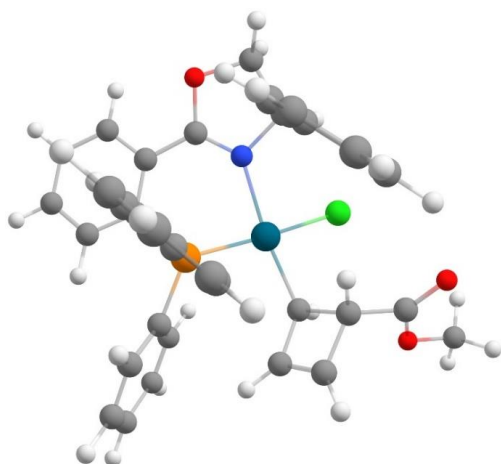
PHOX 17\_1 (*anti*-6ba or -6bb)

CONF65

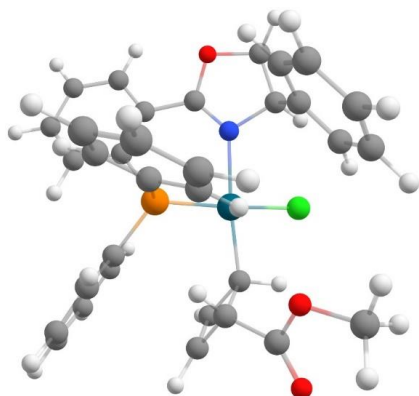


PHOX 17 (*anti*-6ba or -6bb)

CONF55

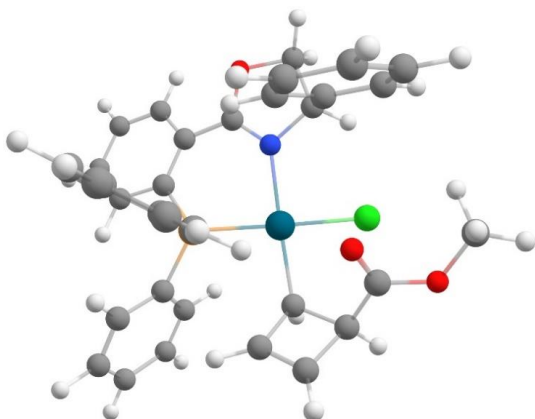


CONF66

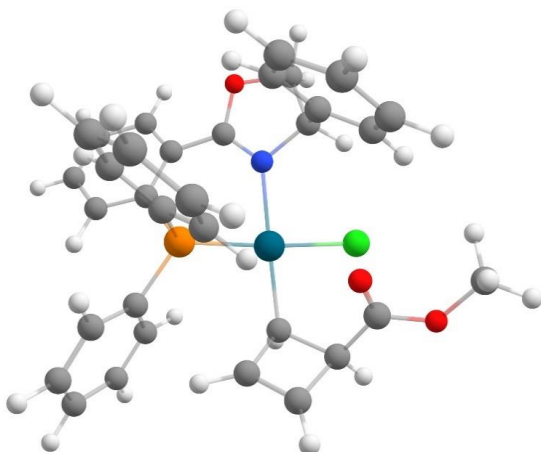


PHOX 18 (major-*syn*-6b)

CONF1

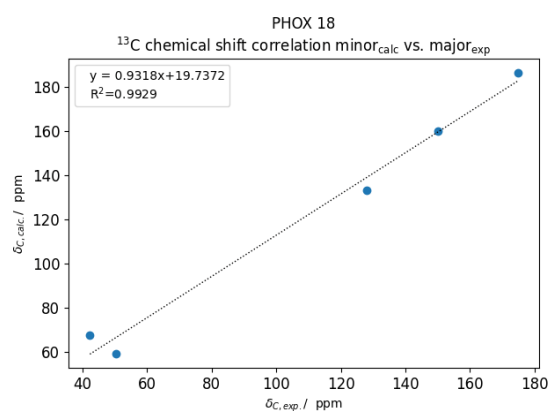
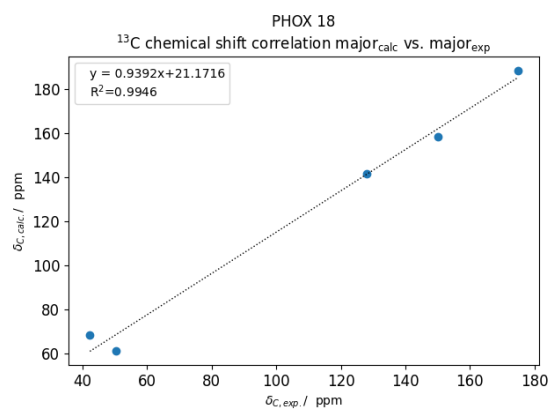
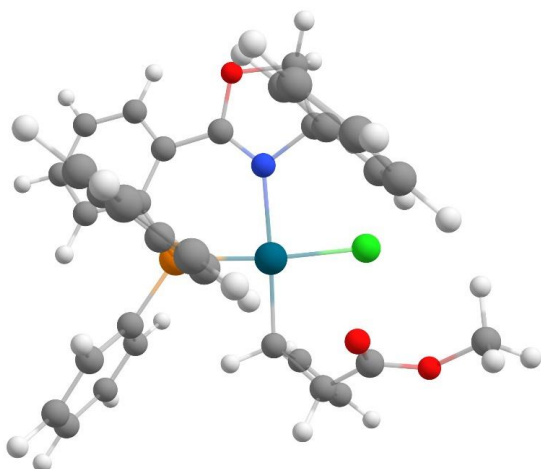


CONF17



PHOX 18\_1 (minor-*syn*-6b)

CONF37

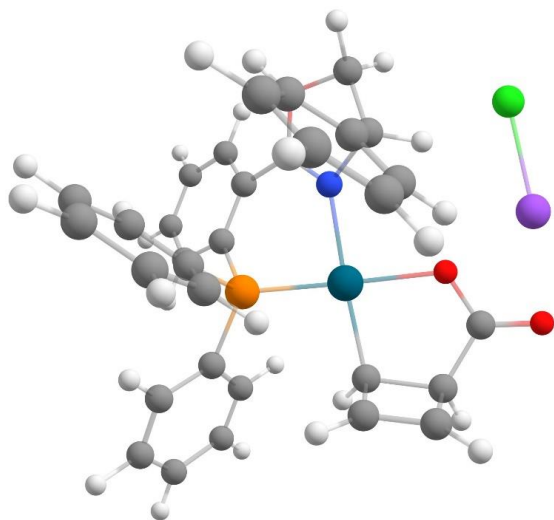


As experimental shifts could not be obtained for minor-*syn*-6b, the calculated shifts were correlated with the experimental shifts of major-*syn*-6b instead.

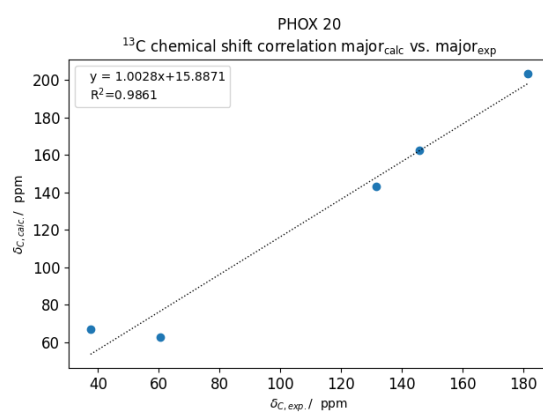
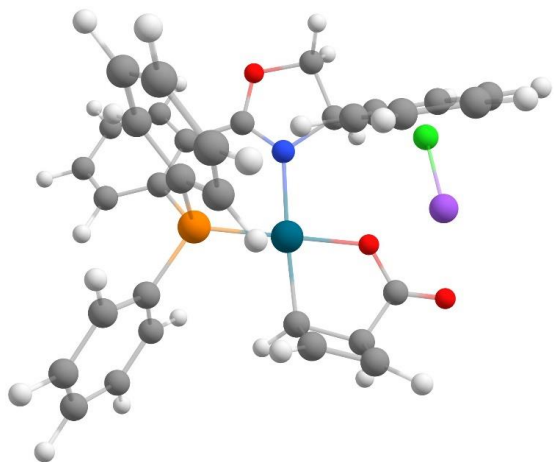


PHOX 20 (major-*syn*-Na-4b)

CONF1

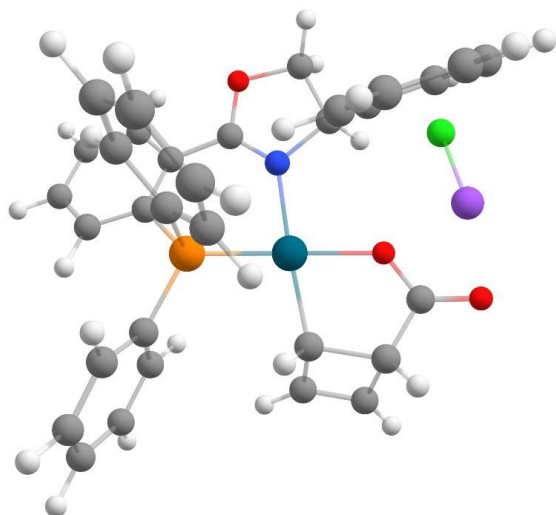


CONF5

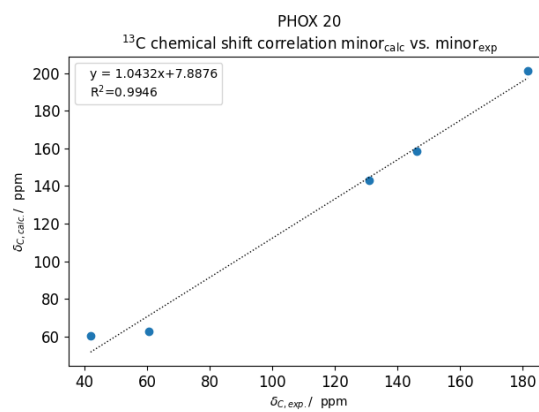
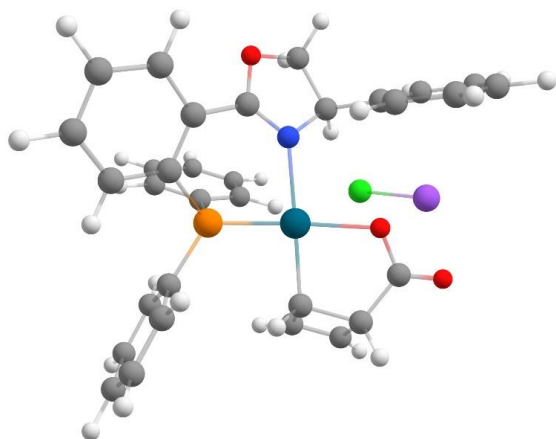


PHOX 20\_1 (minor-syn-Na-4b)

CONF1



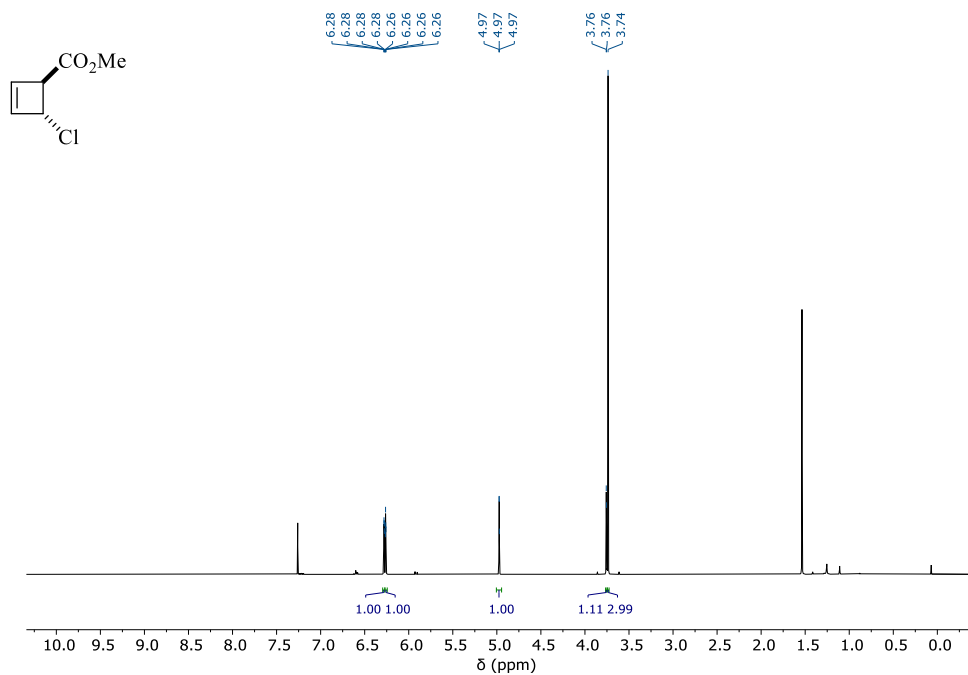
CONF3



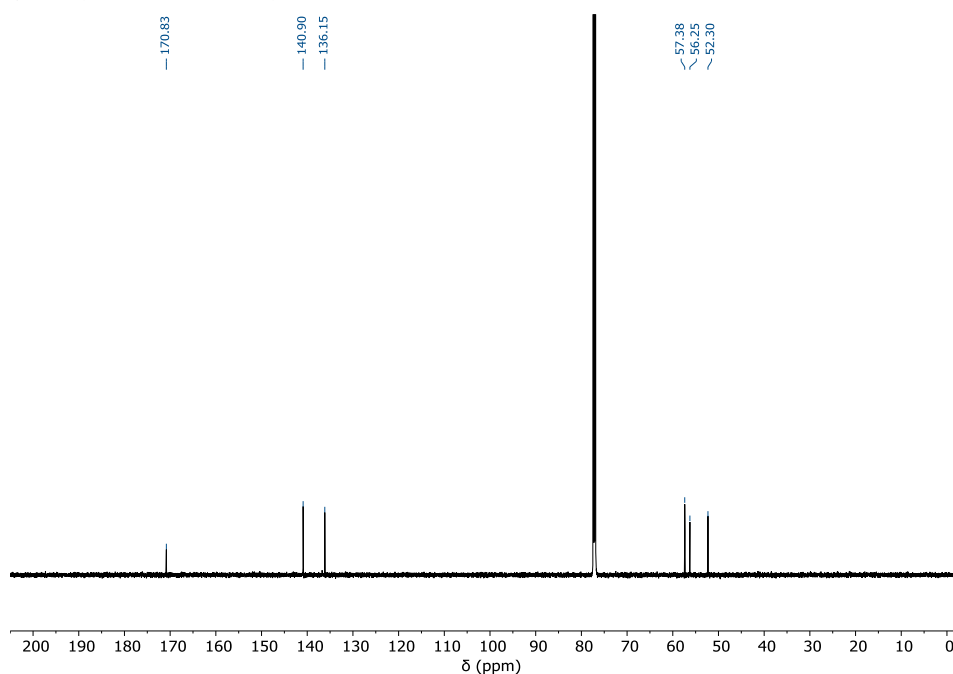
## 11 NMR Spectra of New Compounds

### *Trans*-methyl-4-chlorocyclobutene-2-enecarboxylate (*trans*-5)

$^1\text{H-NMR}$  (700 MHz,  $\text{CDCl}_3$ , 300 K)

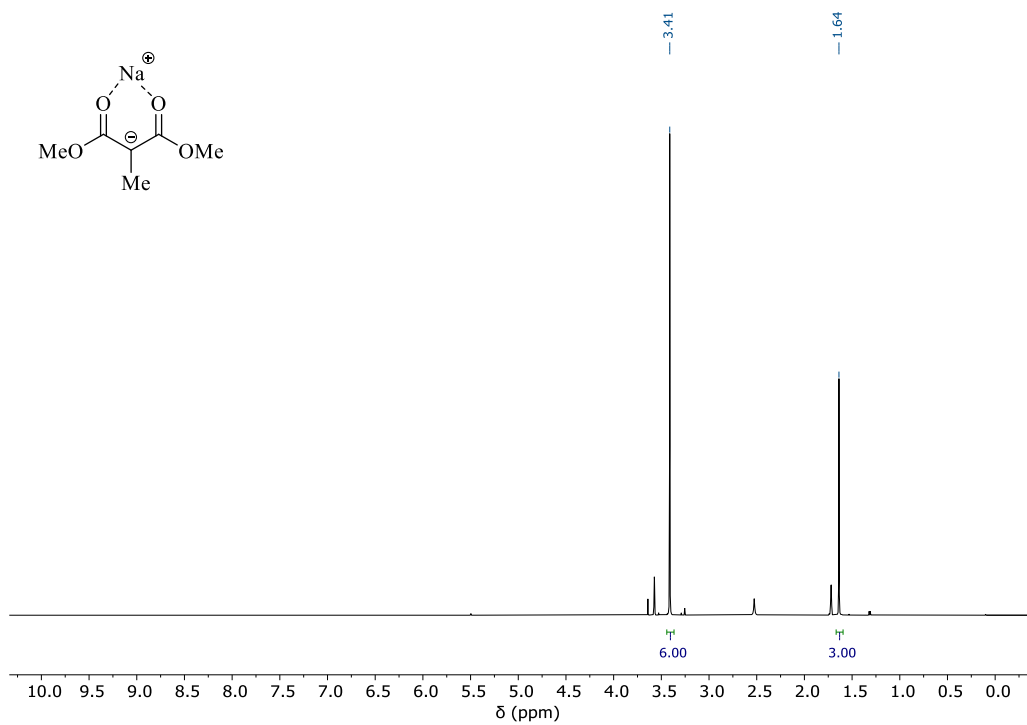
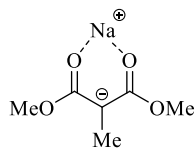


$^{13}\text{C}\{^1\text{H}\}$ -NMR (176 MHz,  $\text{CDCl}_3$ , 300 K)

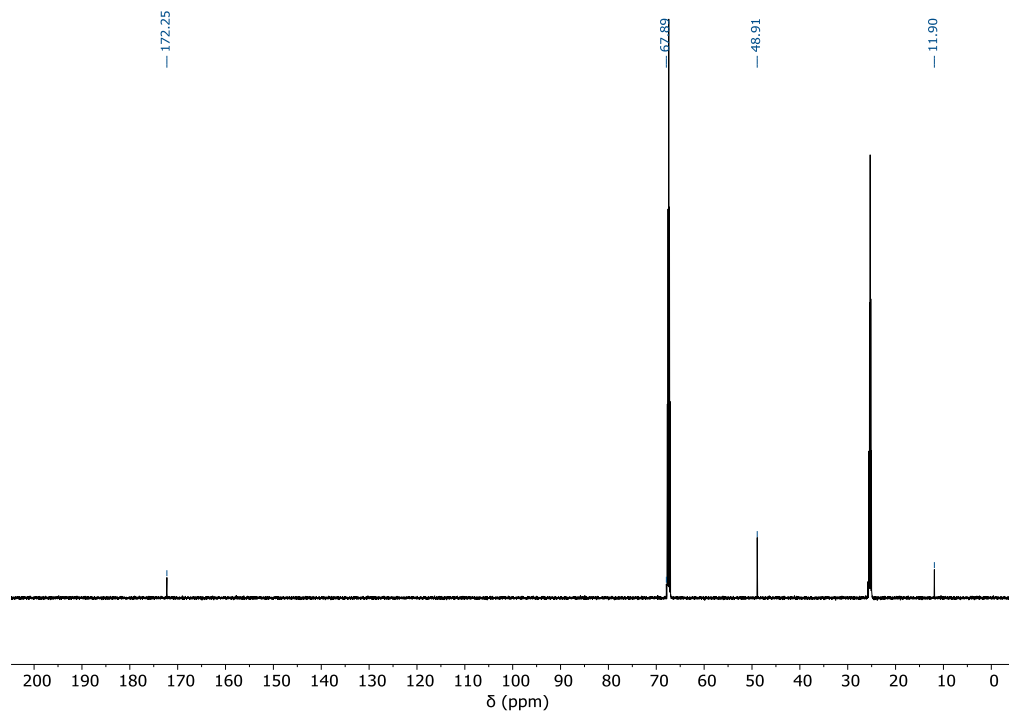


Sodium dimethyl methylmalonate (Na-2)

$^1\text{H-NMR}$  (600 MHz,  $\text{THF-}d_6$ , 300 K)

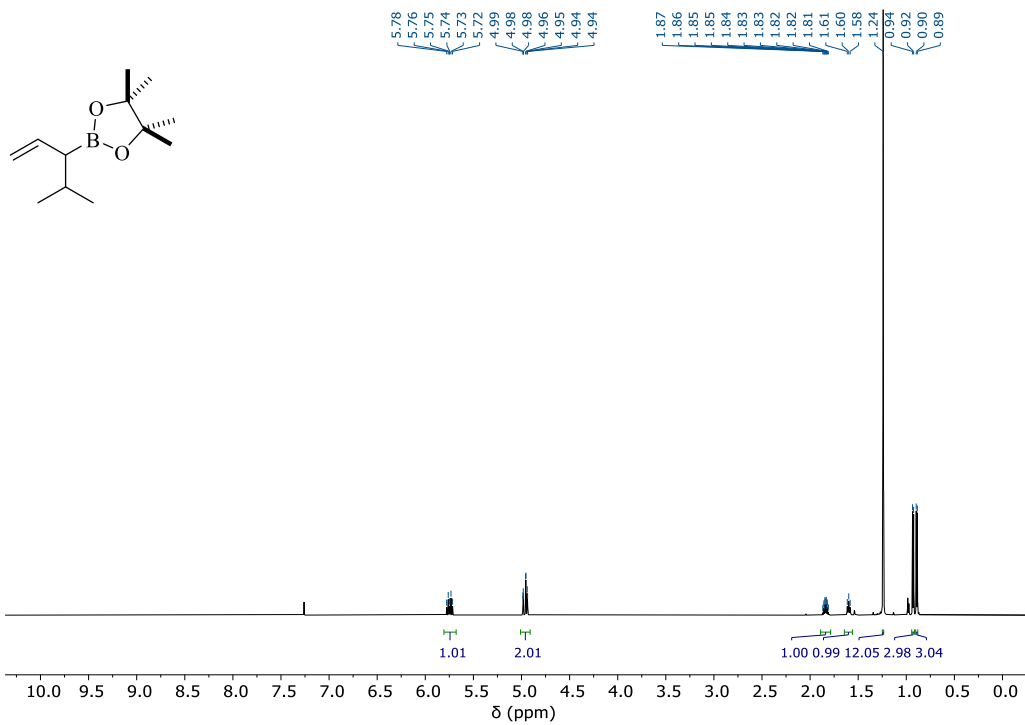


$^{13}\text{C}\{^1\text{H}\}$ -NMR (151 MHz,  $\text{THF-}d_6$ , 300 K)

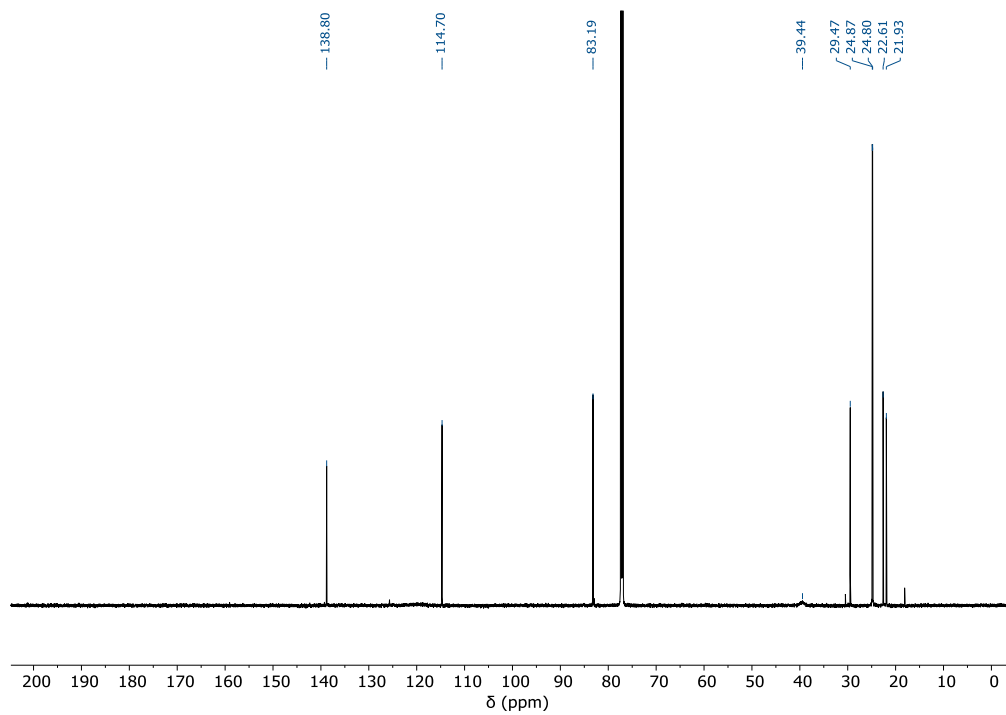


4,4,5,5-Tetramethyl-2-(4-methylpent-1-en-3-yl)-1,3,2-dioxaborolane

$^1\text{H-NMR}$  (600 MHz,  $\text{CDCl}_3$ , 300 K)

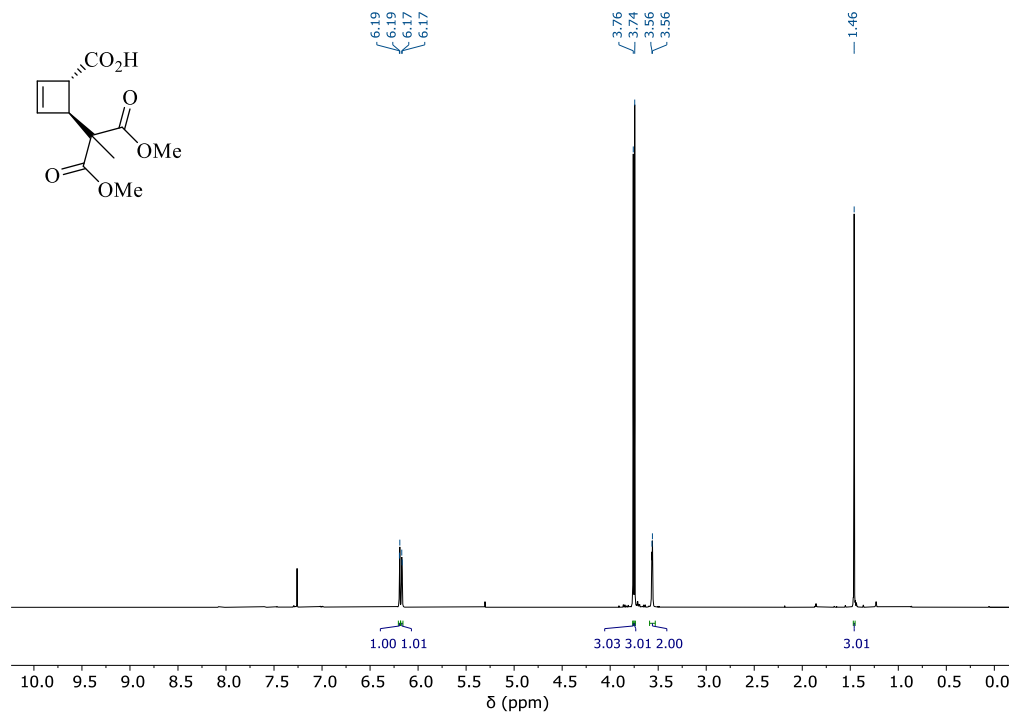


$^{13}\text{C}\{^1\text{H}\}$ -NMR (151 MHz,  $\text{CDCl}_3$ , 300 K)

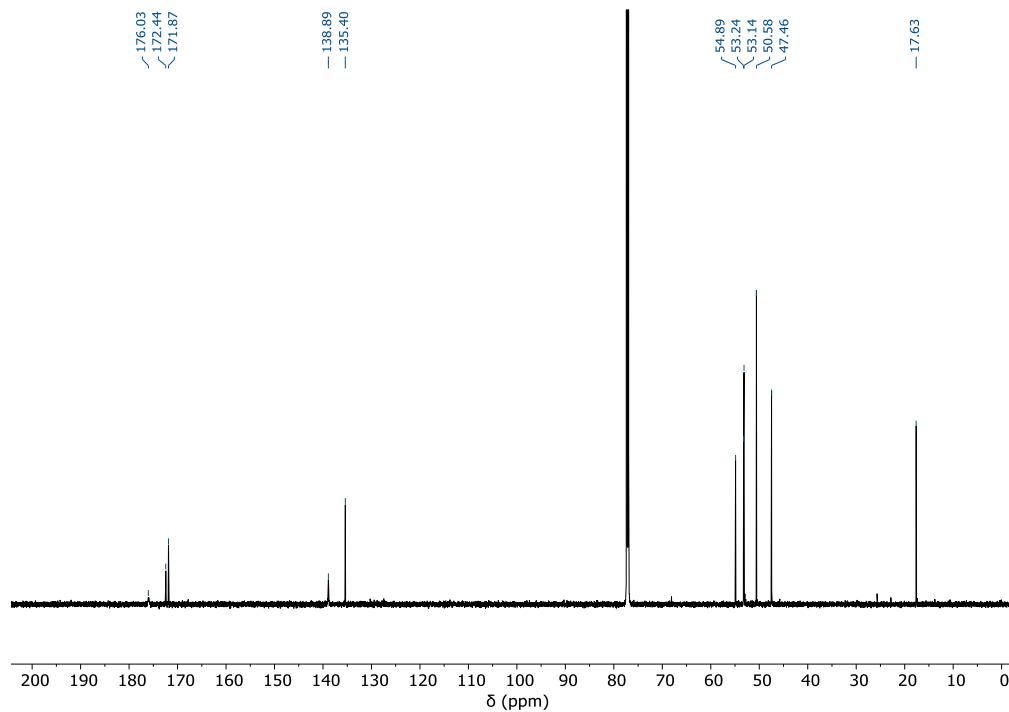


(1*S*,4*S*)-4-(1,3-dimethoxy-2-methyl-1,3-dioxopropan-2-yl)cyclobut-2-ene-1-carboxylic acid (*trans*-3)

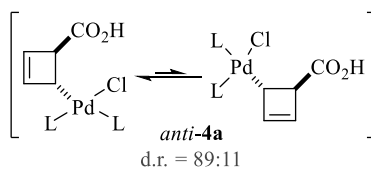
<sup>1</sup>H-NMR (700 MHz, CDCl<sub>3</sub>, 273 K)



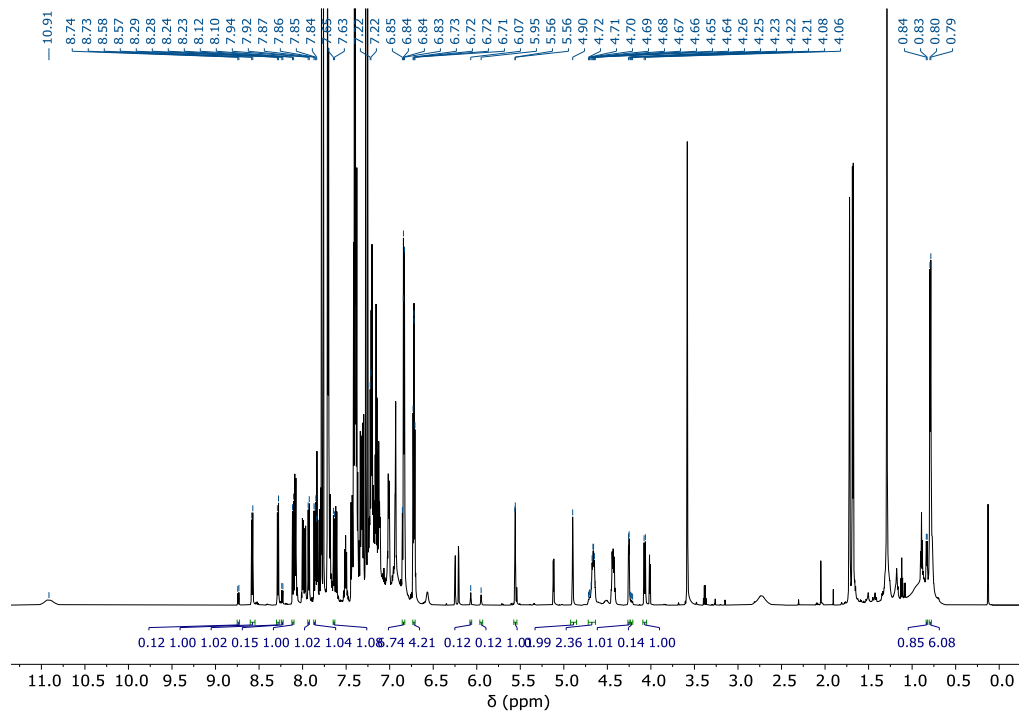
<sup>13</sup>C{<sup>1</sup>H}-NMR (176 MHz, CDCl<sub>3</sub>, 273 K)



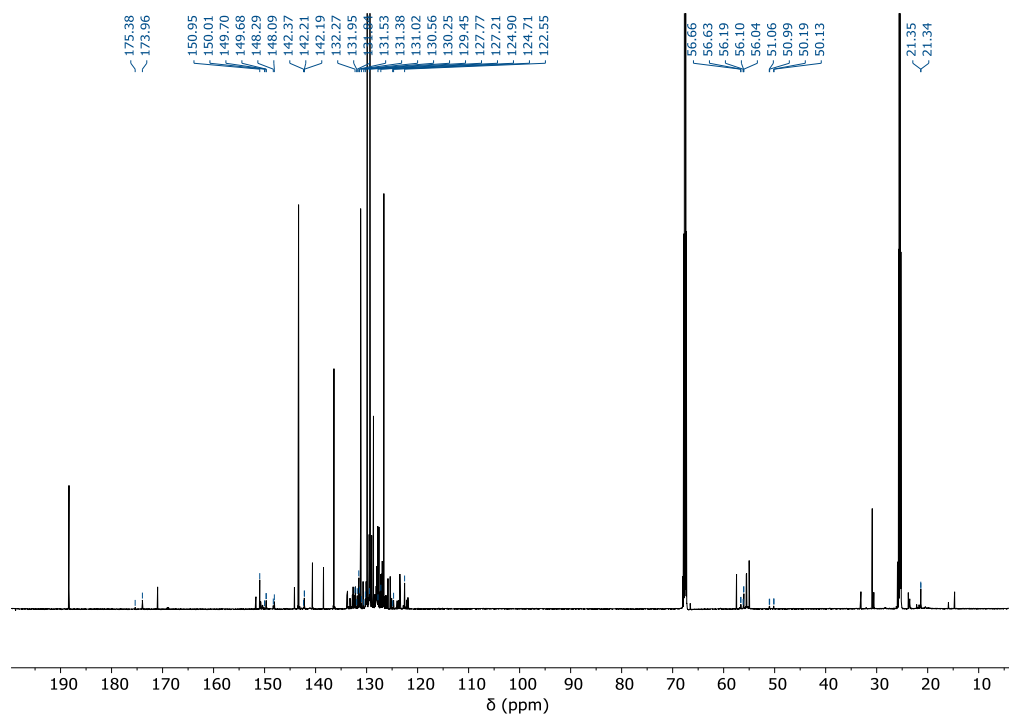
Pd-Complexes from Acid Substrate *cis*-1 with Ligand L1



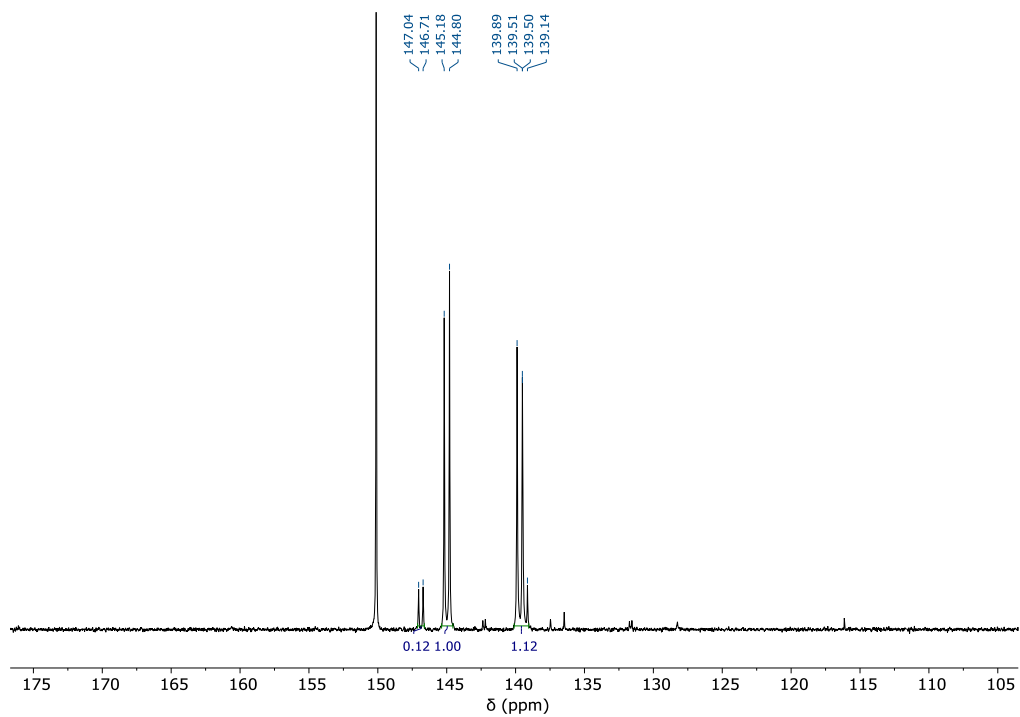
<sup>1</sup>H-NMR (700 MHz, THF-*d*<sub>8</sub>, 273 K)



$^{13}\text{C}\{^1\text{H}\}$ -NMR (176 MHz, THF-*d*<sub>8</sub>, 273 K)

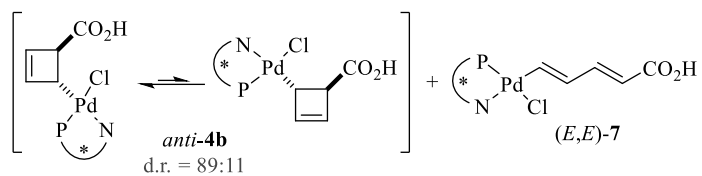


$^{31}\text{P}\{^1\text{H}\}$ -NMR (283 MHz, THF-*d*<sub>8</sub>, 273 K)

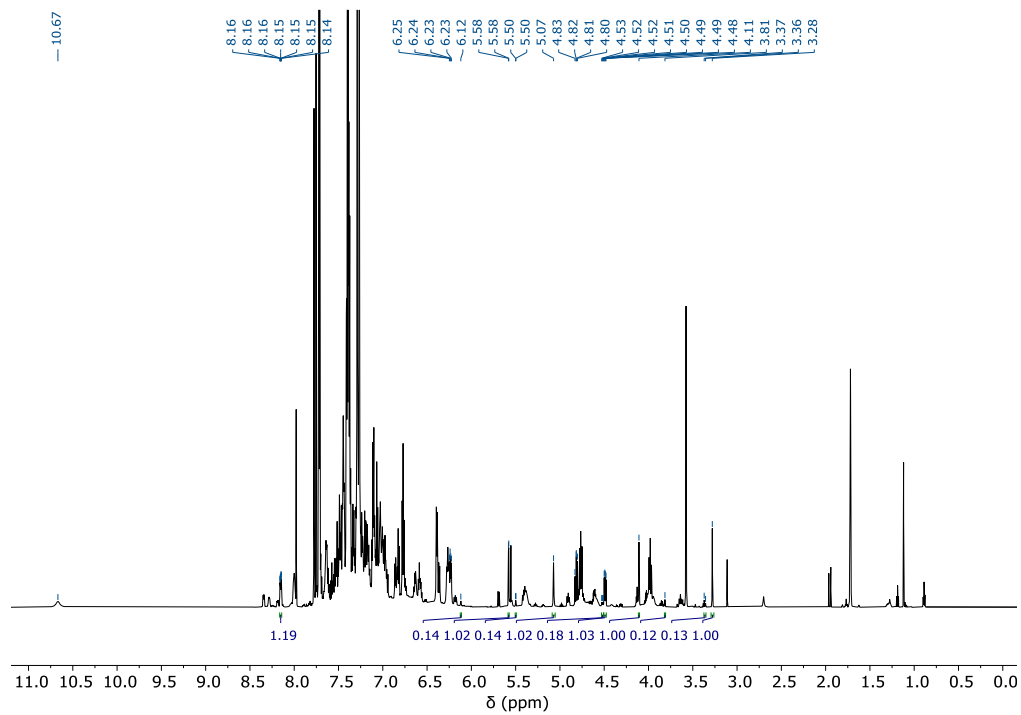




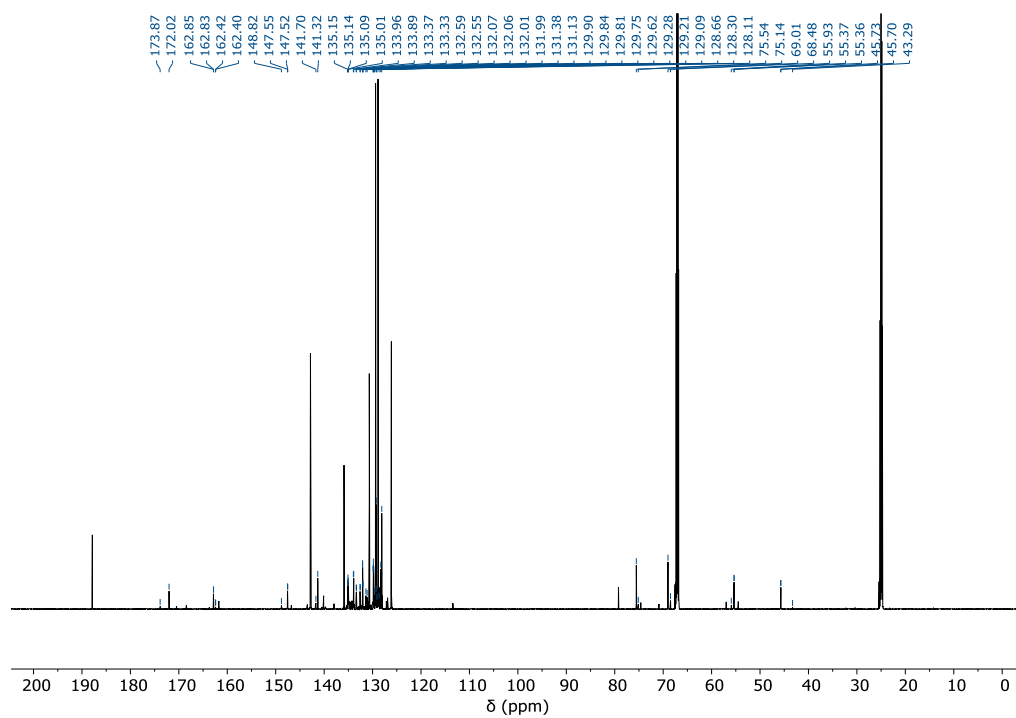
Pd-Complexes from Acid Substrate *cis*-1 with Ligand L2



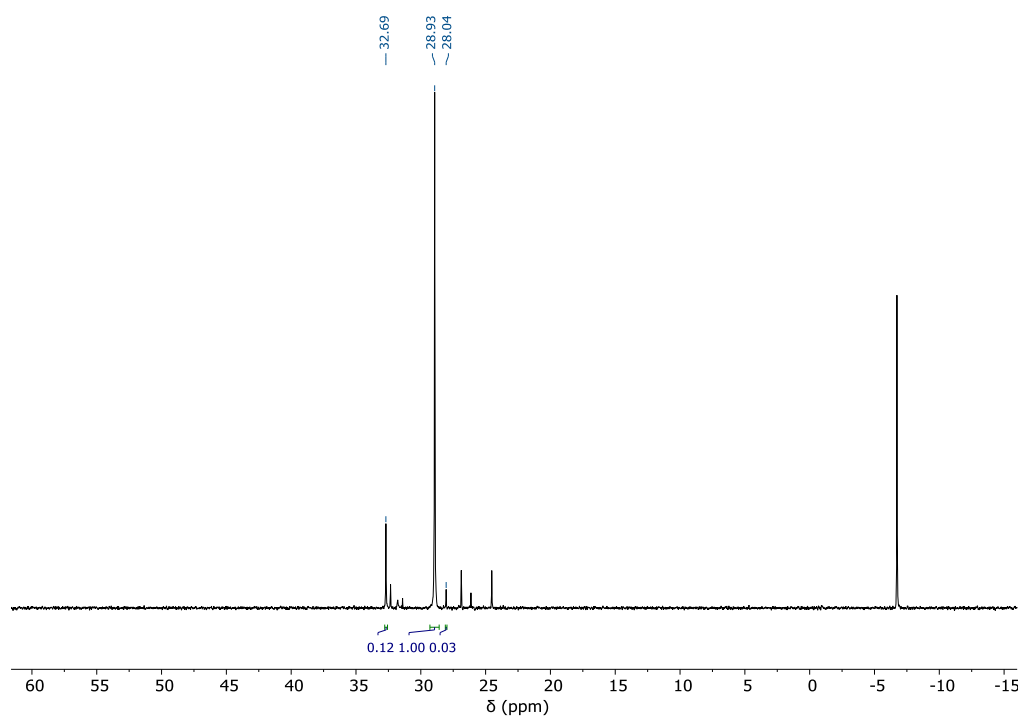
<sup>1</sup>H-NMR (700 MHz, THF-*d*<sub>8</sub>, 273 K)



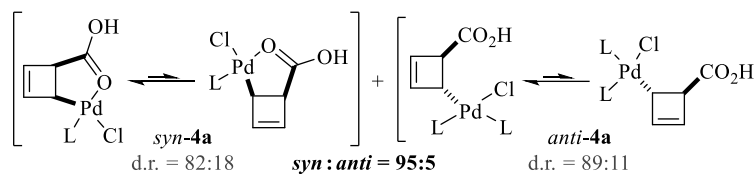
$^{13}\text{C}\{^1\text{H}\}$ -NMR (176 MHz, THF-*d*<sub>8</sub>, 273 K)



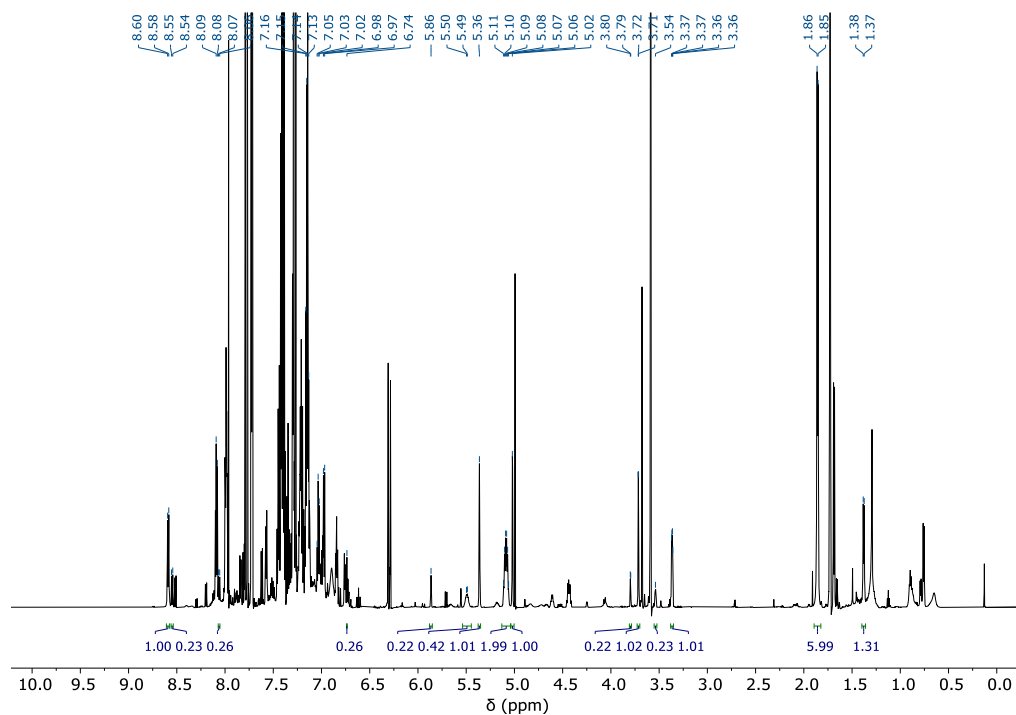
$^{31}\text{P}\{^1\text{H}\}$ -NMR (283 MHz, THF-*d*<sub>8</sub>, 273 K)



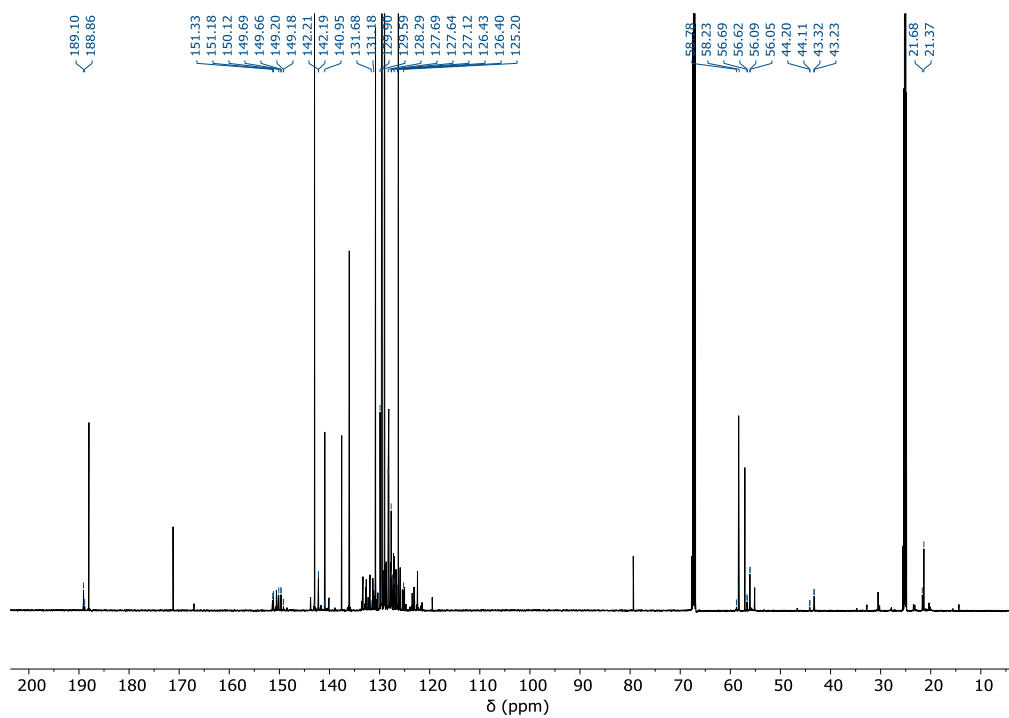
Pd-Complexes from Acid Substrate *trans*-1 with Ligand L1



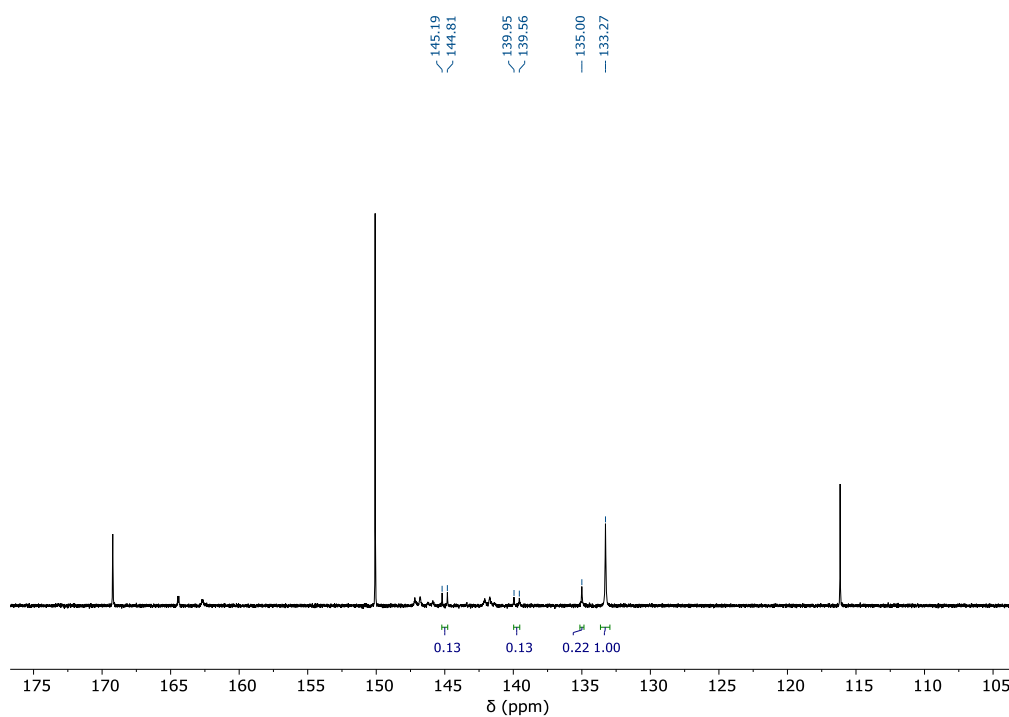
<sup>1</sup>H-NMR (700 MHz, THF-*d*<sub>6</sub>, 273 K)



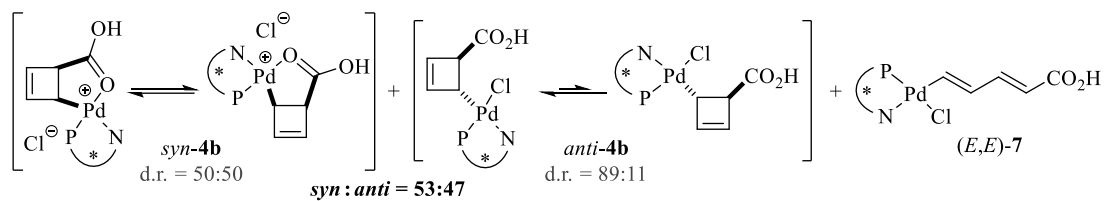
$^{13}\text{C}\{^1\text{H}\}$ -NMR (176 MHz, THF-*d*<sub>8</sub>, 273 K)



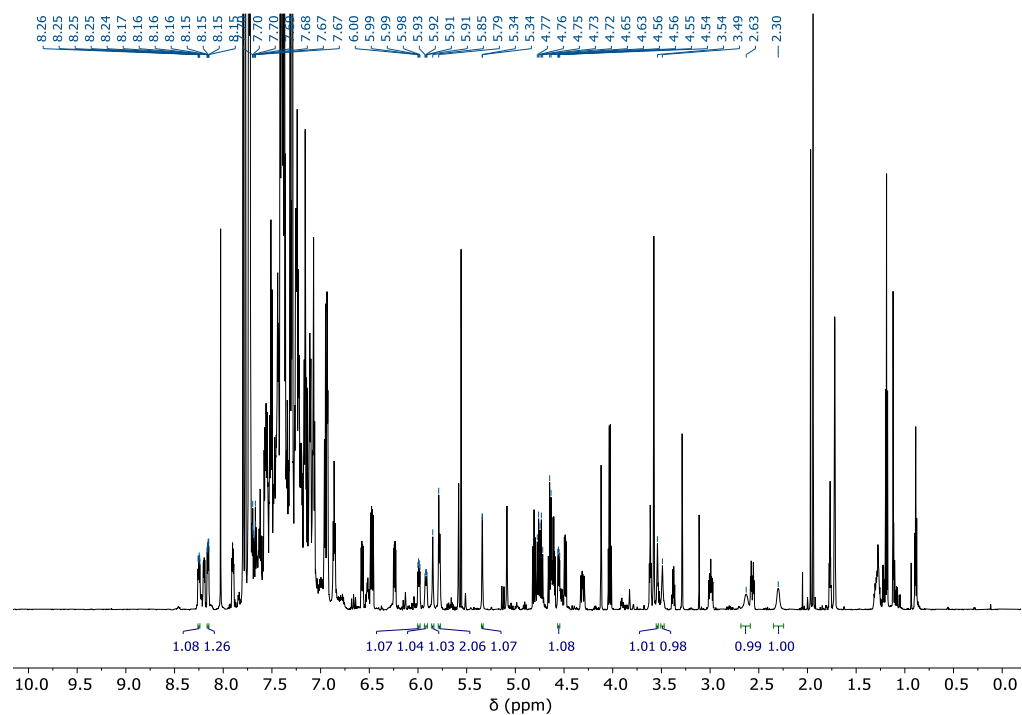
$^{31}\text{P}\{^1\text{H}\}$ -NMR (283 MHz, THF-*d*<sub>8</sub>, 273 K)



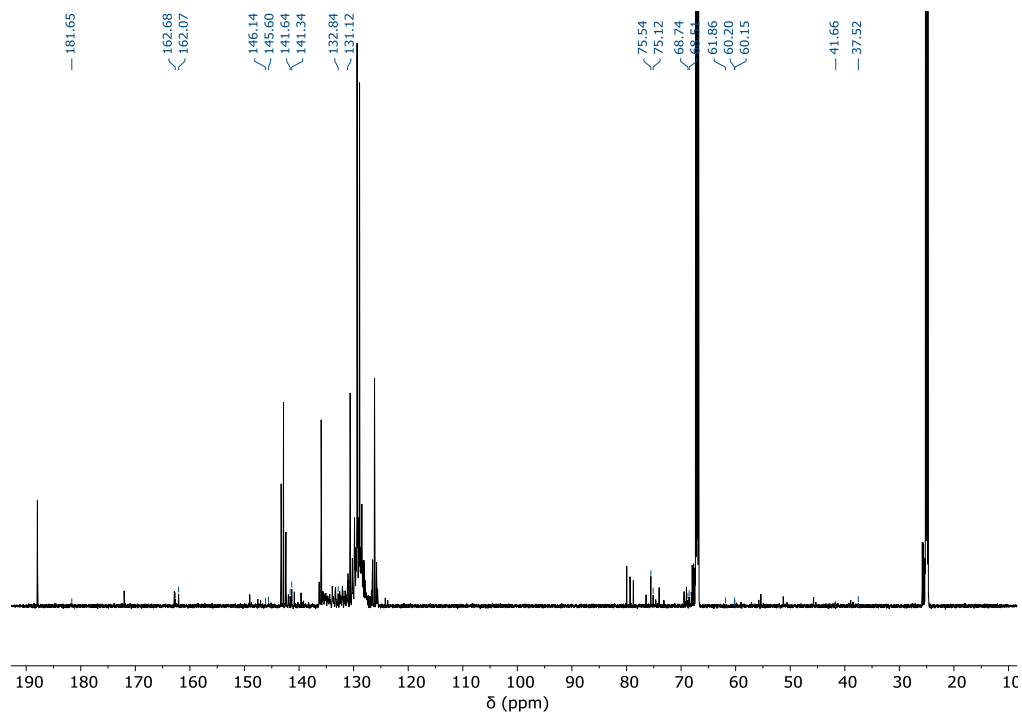
Pd-Complexes from Acid Substrate *trans*-1 with Ligand L2



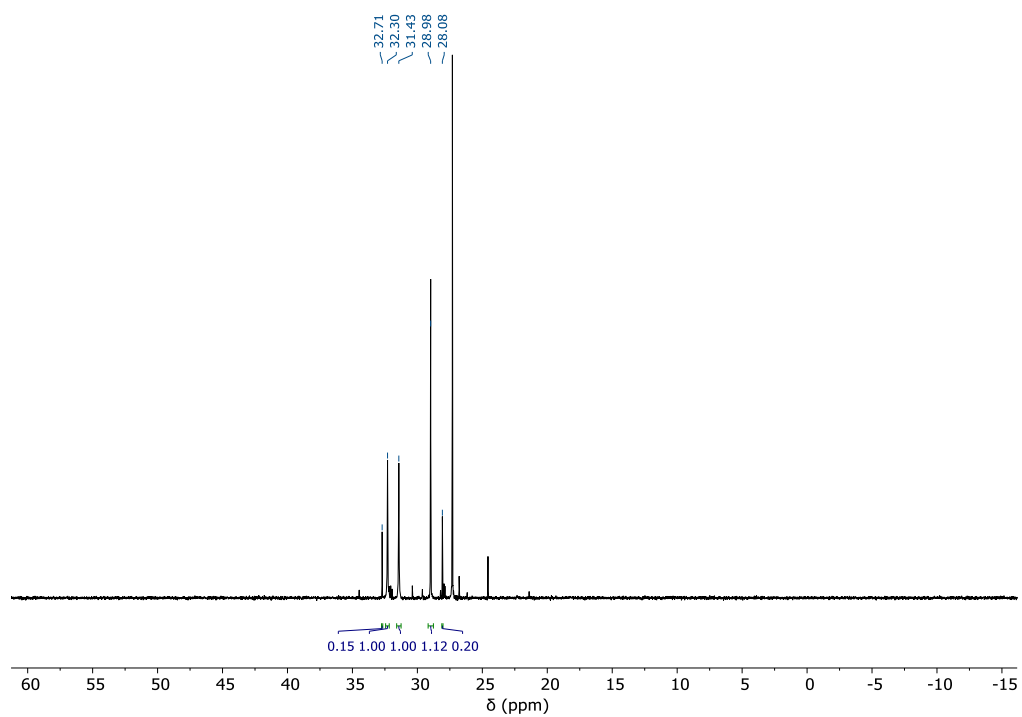
<sup>1</sup>H-NMR (700 MHz, THF-*d*<sub>8</sub>, 273 K)



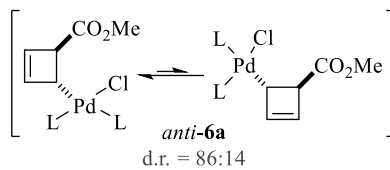
$^{13}\text{C}\{^1\text{H}\}$ -NMR (176 MHz, THF-*d*<sub>8</sub>, 273 K)



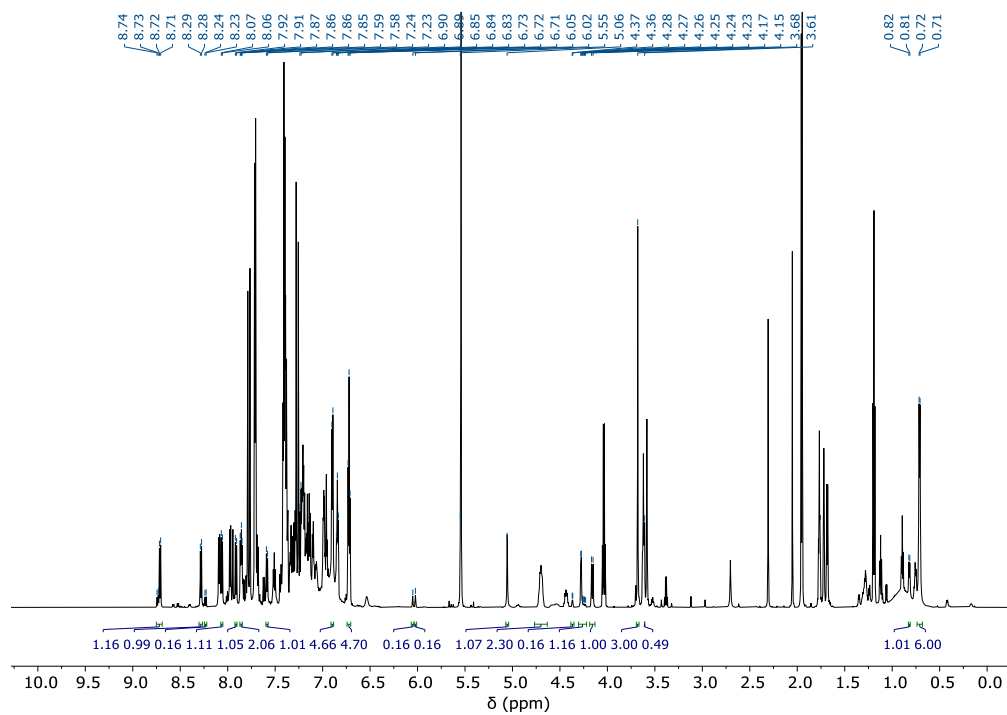
$^{31}\text{P}\{^1\text{H}\}$ -NMR (283 MHz, THF-*d*<sub>8</sub>, 273 K)



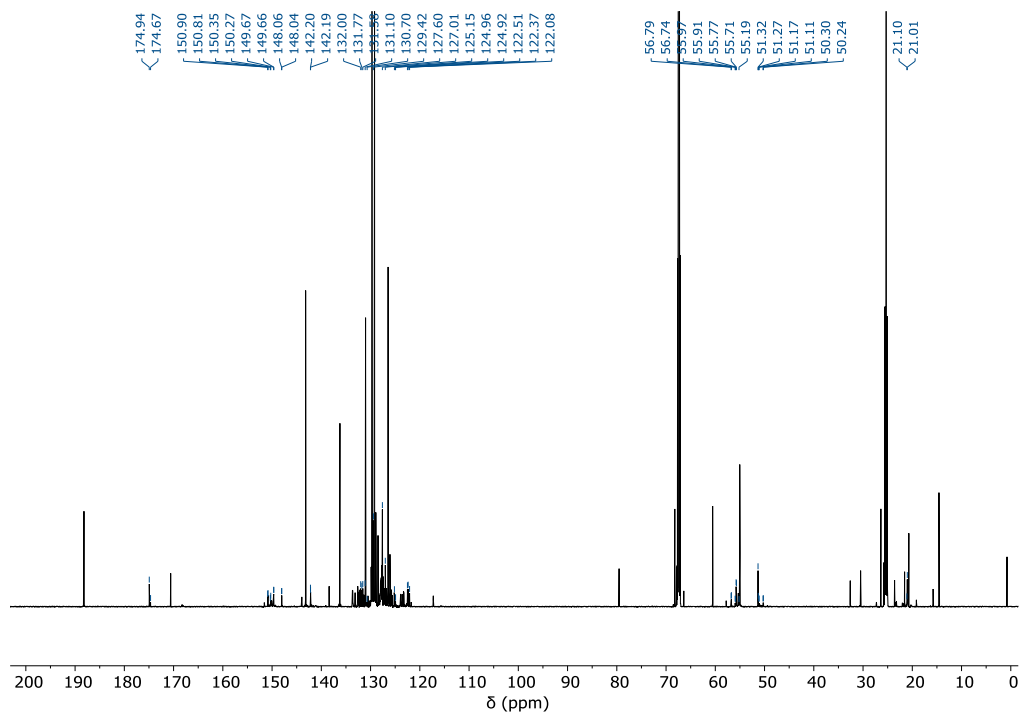
Pd-Complexes from Ester Substrate *cis*-5 with Ligand L1



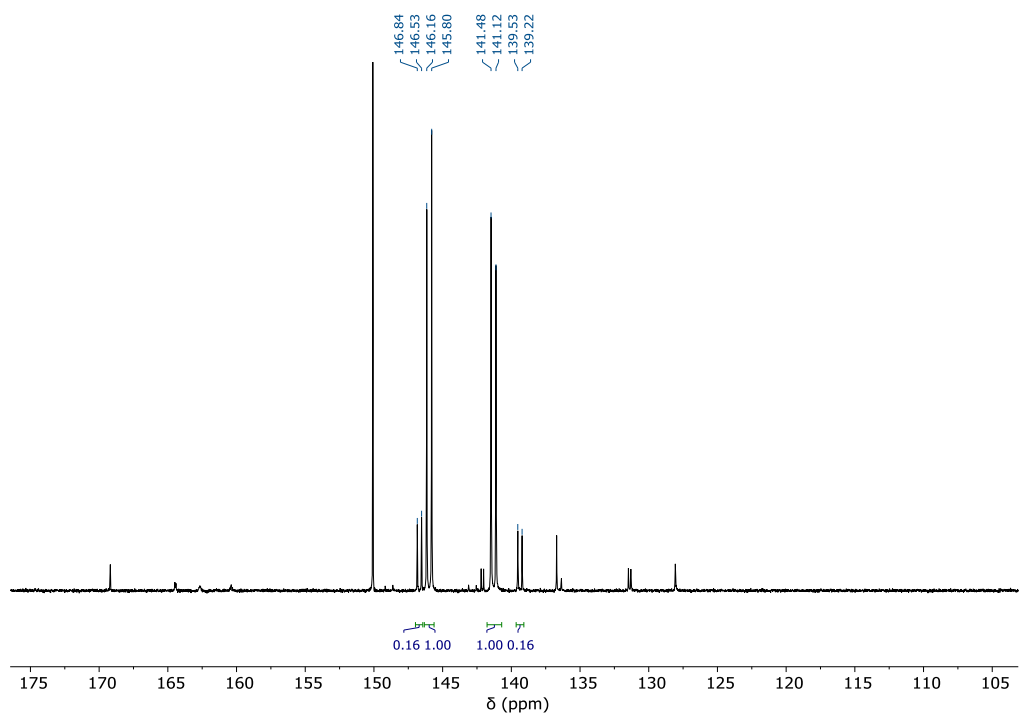
<sup>1</sup>H-NMR (700 MHz, THF-*d*<sub>8</sub>, 273 K)



$^{13}\text{C}\{^1\text{H}\}$ -NMR (176 MHz, THF- $d_6$ , 273 K)

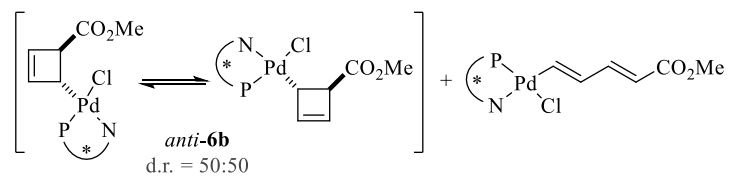


$^{31}\text{P}\{^1\text{H}\}$ -NMR (283 MHz, THF- $d_6$ , 273 K)

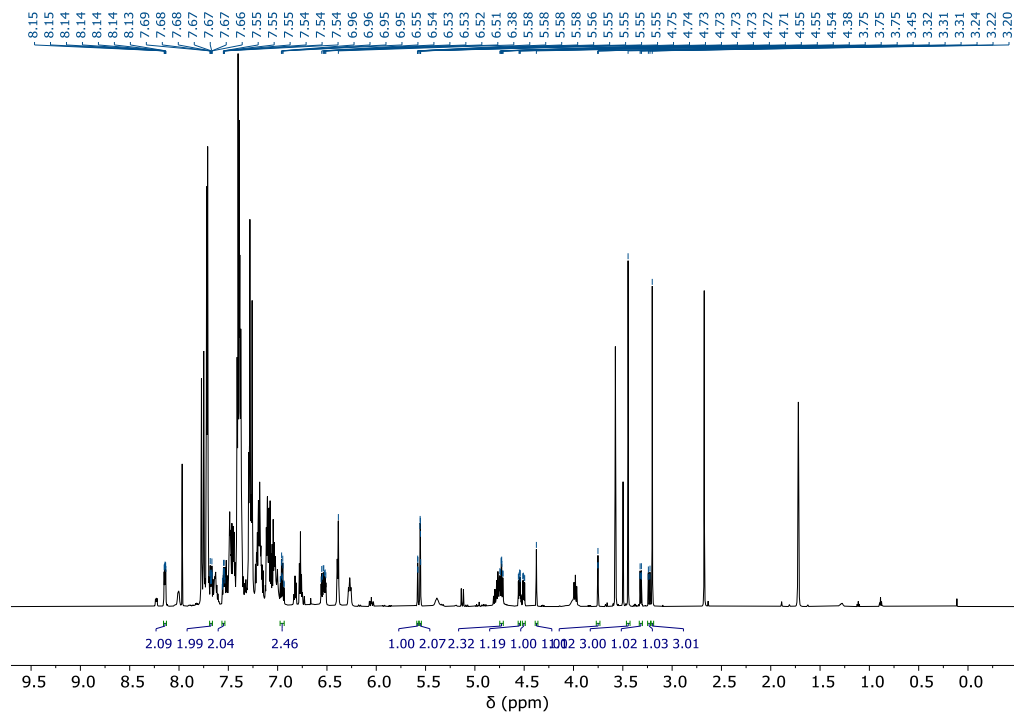




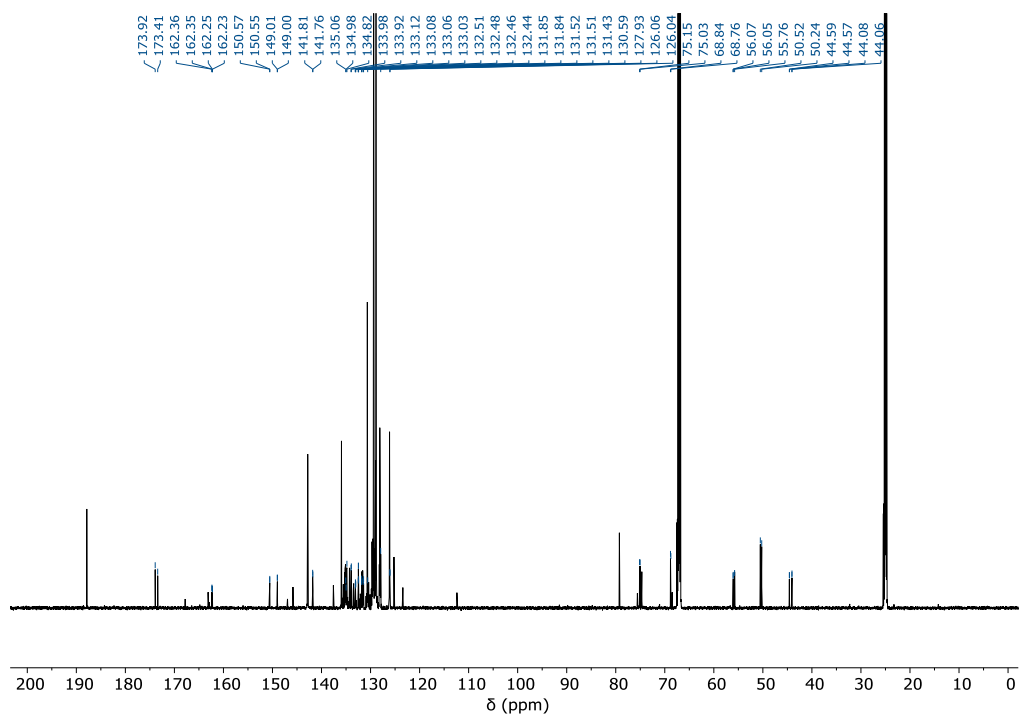
Pd-Complexes from Ester Substrate *cis*-5 with Ligand L2



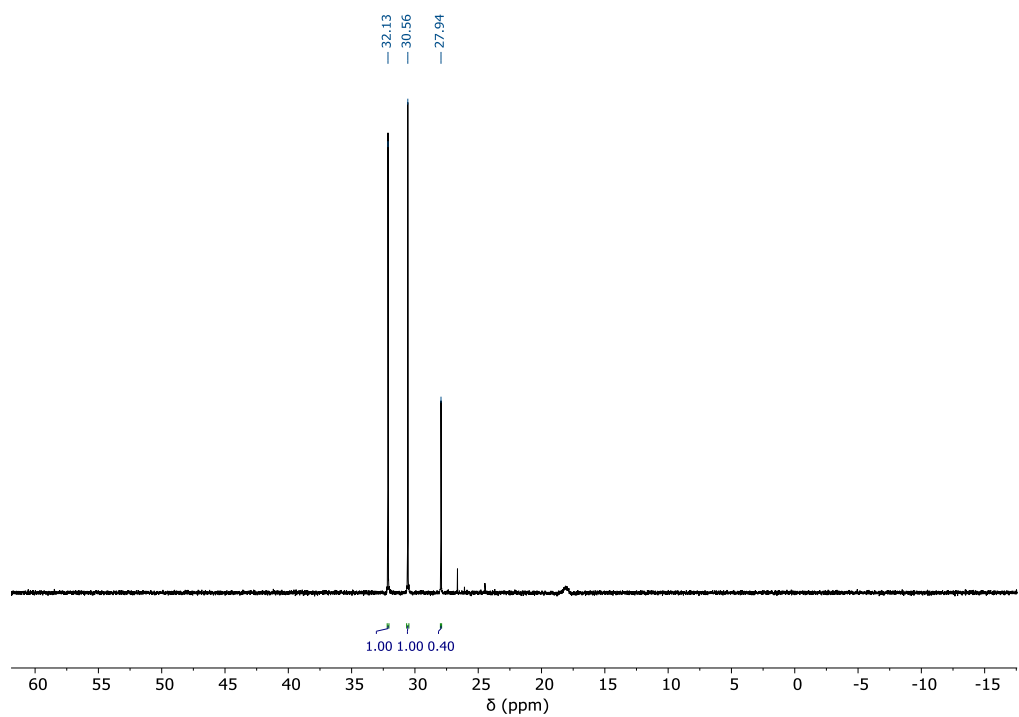
<sup>1</sup>H-NMR (700 MHz, THF-*d*<sub>6</sub>, 273 K)



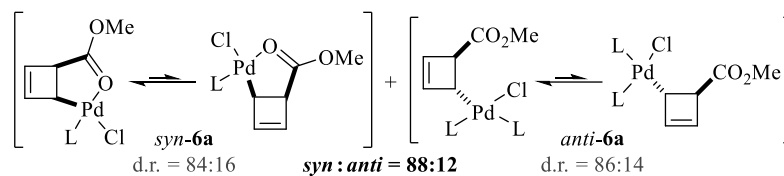
$^{13}\text{C}\{^1\text{H}\}$ -NMR (176 MHz, THF-*d*<sub>8</sub>, 273 K)



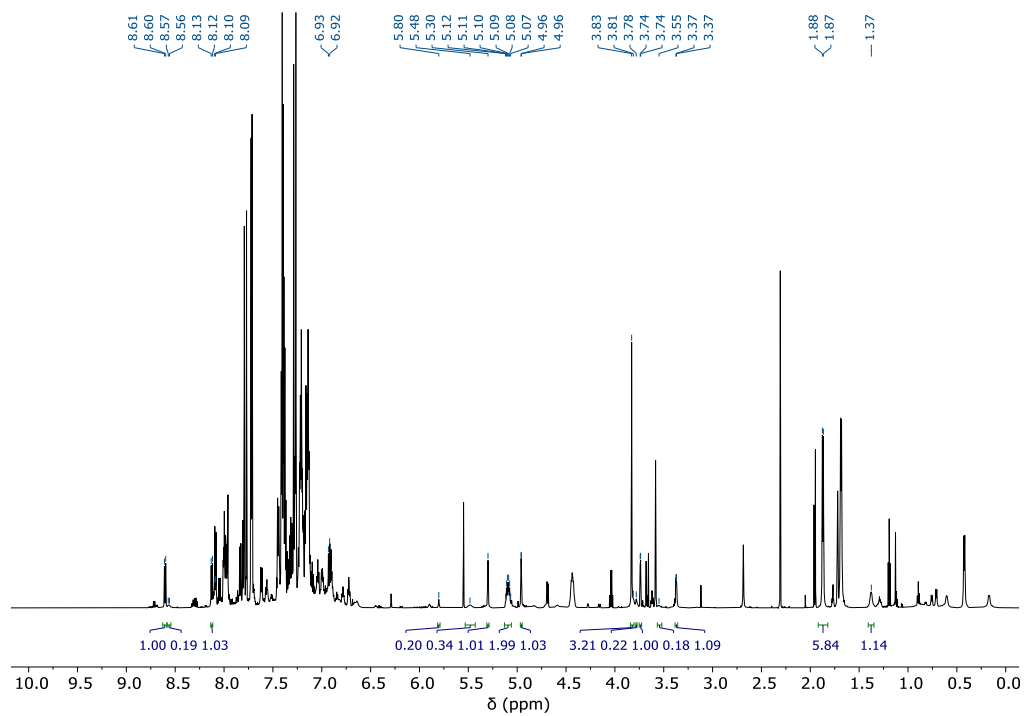
$^{31}\text{P}\{^1\text{H}\}$ -NMR (283 MHz, THF-*d*<sub>8</sub>, 273 K)



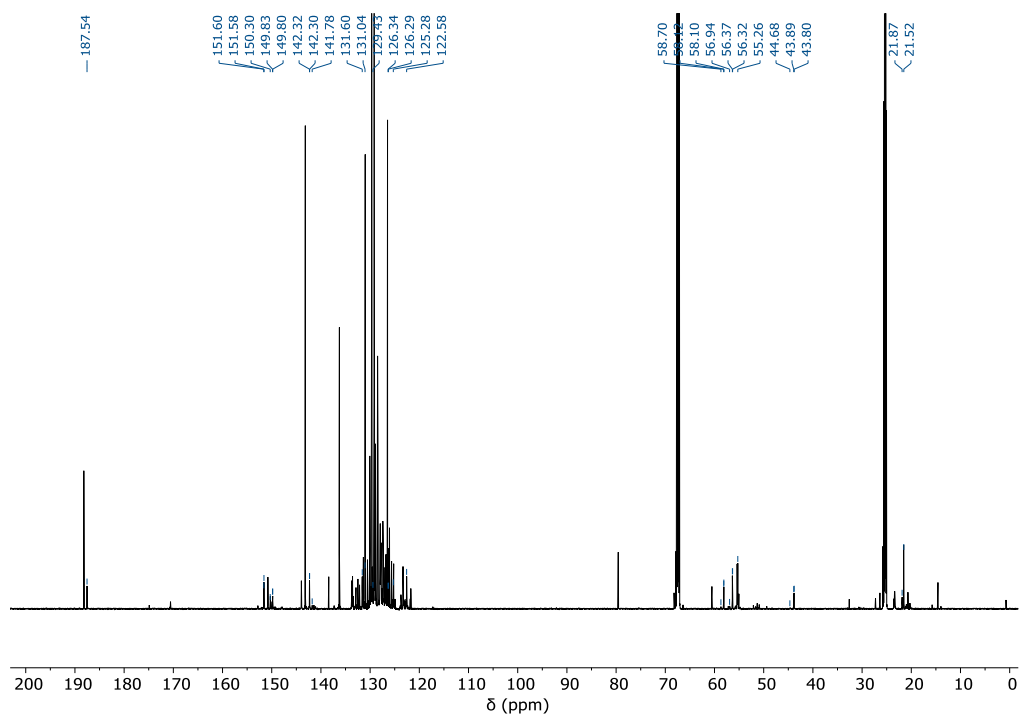
Pd-Complexes from Ester Substrate *trans*-5 with Ligand L1



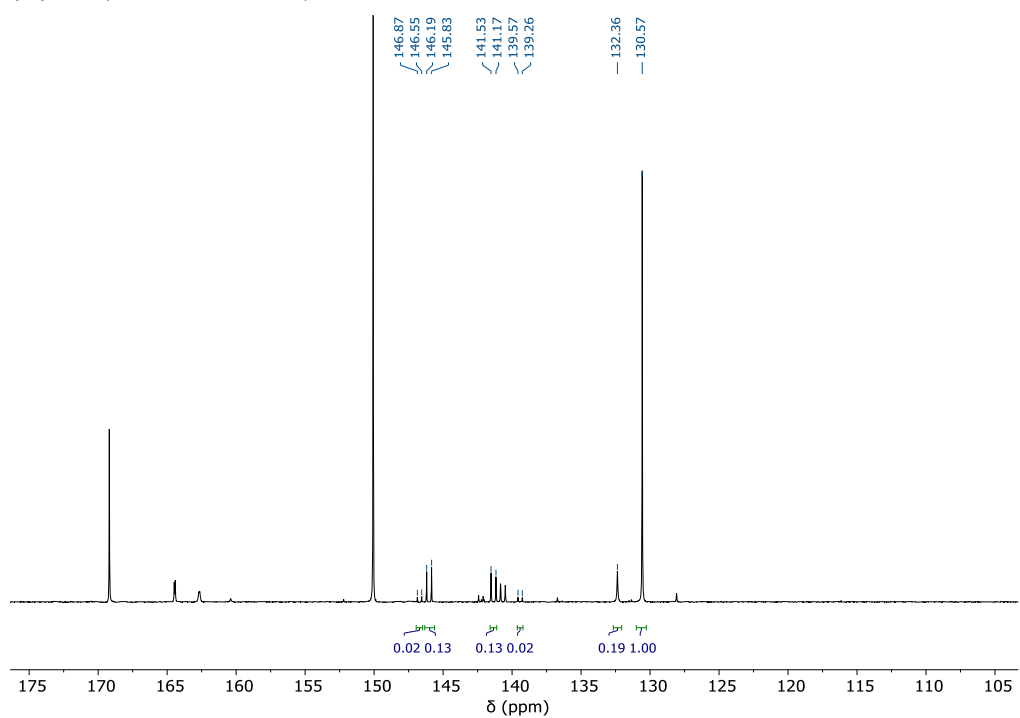
<sup>1</sup>H-NMR (700 MHz, THF-*d*<sub>8</sub>, 273 K)



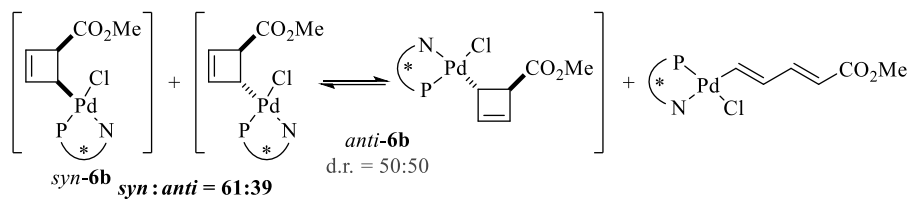
$^{13}\text{C}\{^1\text{H}\}$ -NMR (176 MHz, THF-*d*<sub>8</sub>, 273 K)



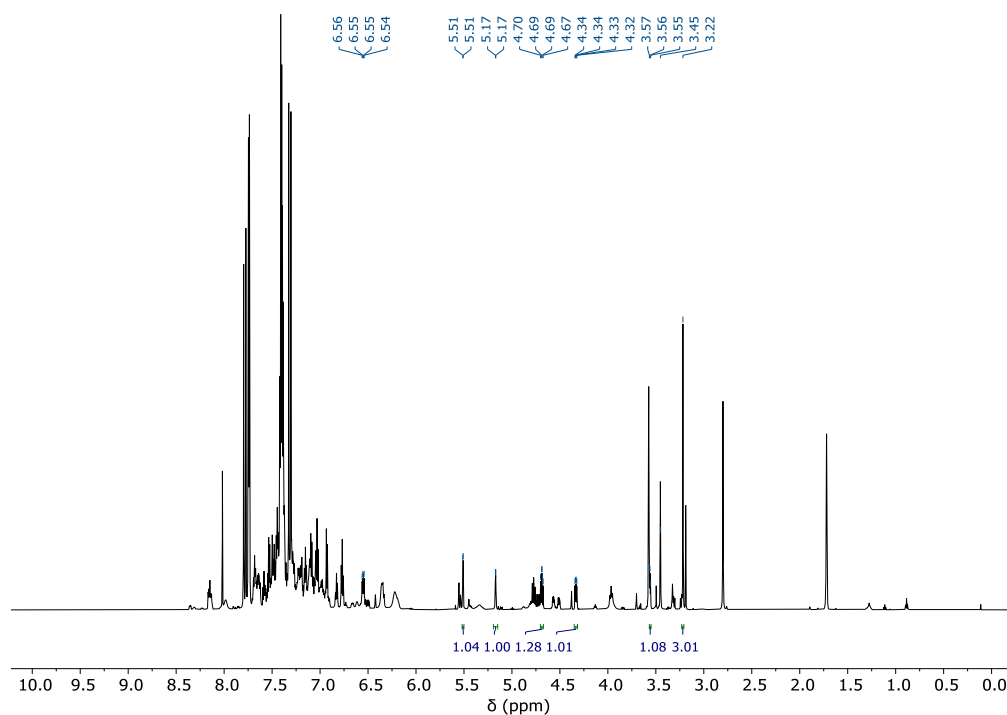
$^{31}\text{P}\{^1\text{H}\}$ -NMR (283 MHz, THF-*d*<sub>8</sub>, 273 K)



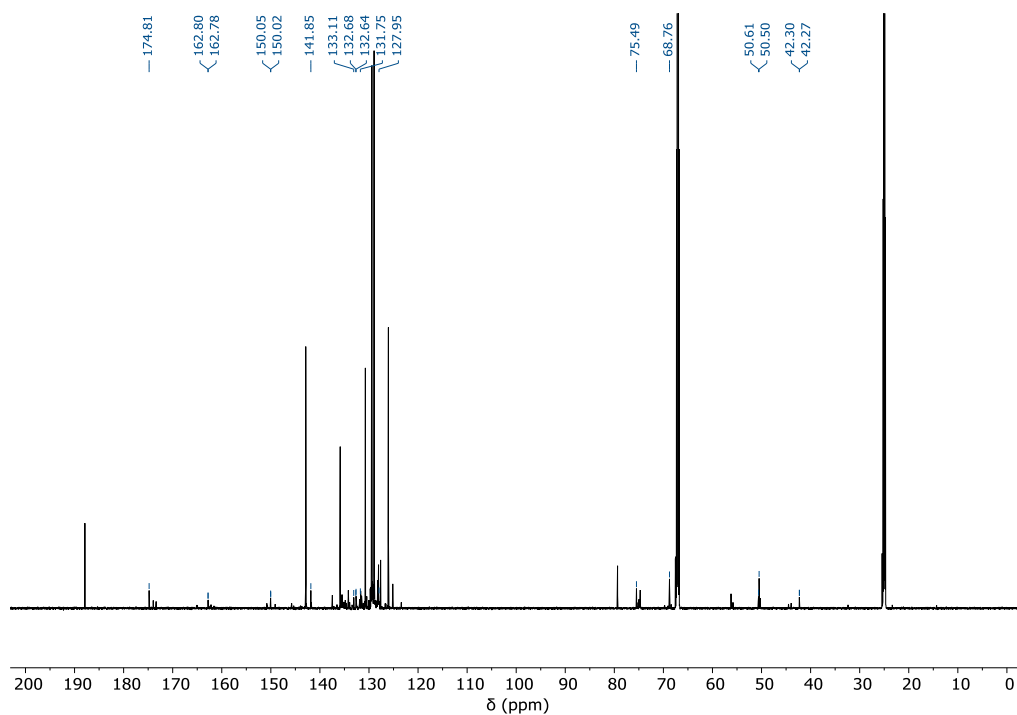
Pd-Complexes from Ester Substrate *trans*-5 with Ligand L2



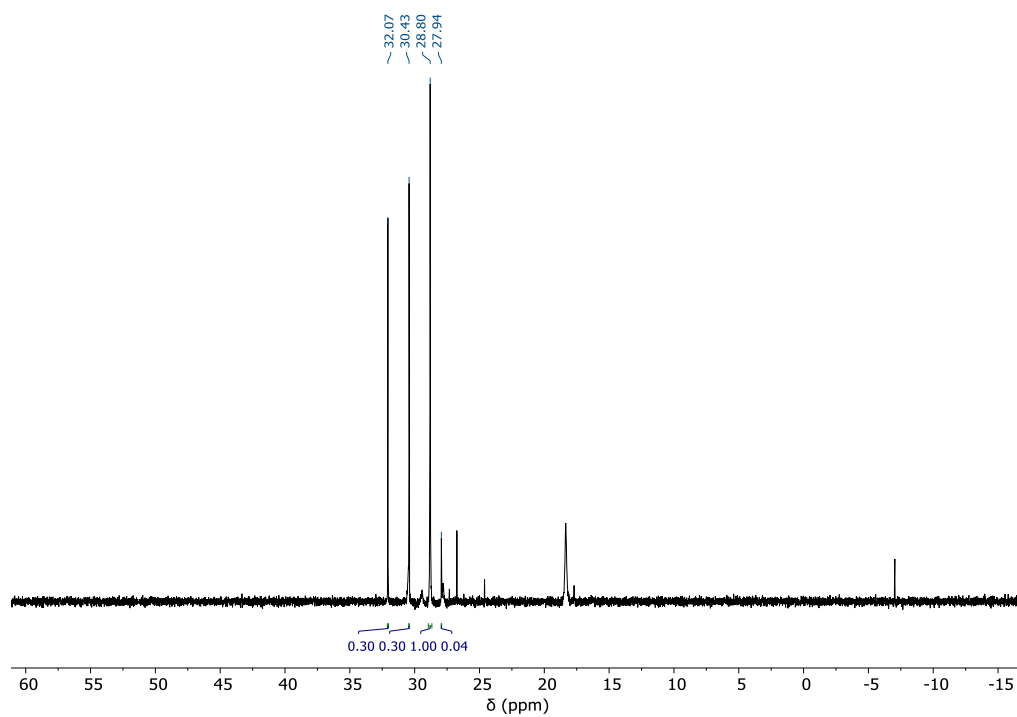
<sup>1</sup>H-NMR (700 MHz, THF-*d*<sub>8</sub>, 253 K)



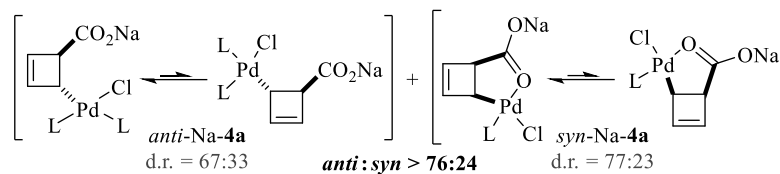
$^{13}\text{C}\{^1\text{H}\}$ -NMR (176 MHz, THF-*d*<sub>8</sub>, 253 K)



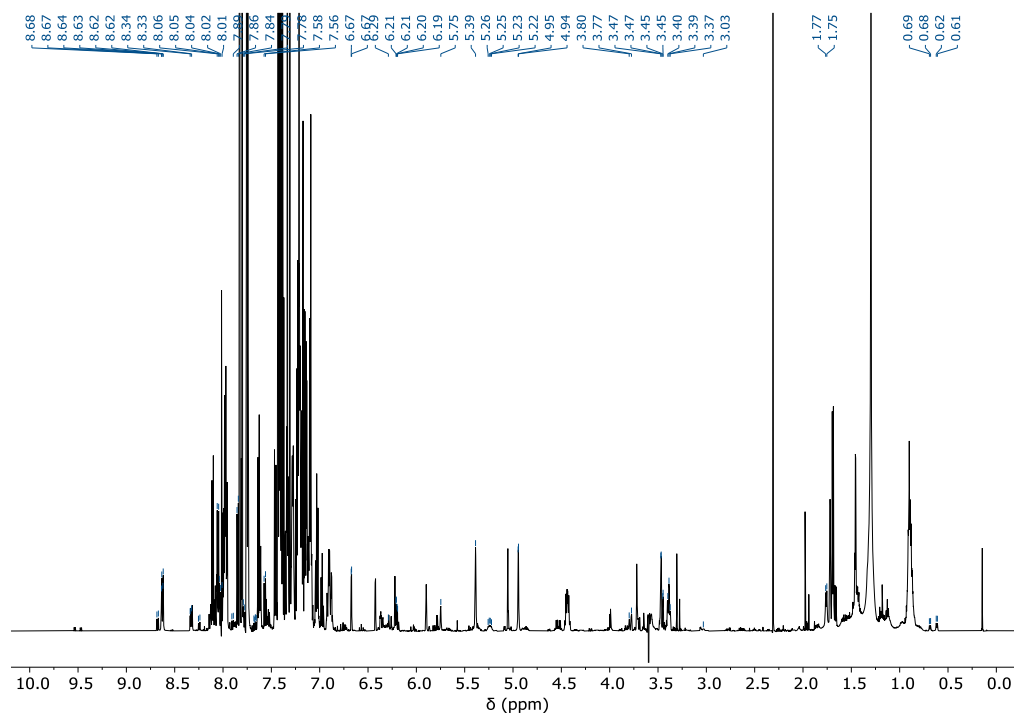
$^{31}\text{P}\{^1\text{H}\}$ -NMR (283 MHz, THF-*d*<sub>8</sub>, 253 K)



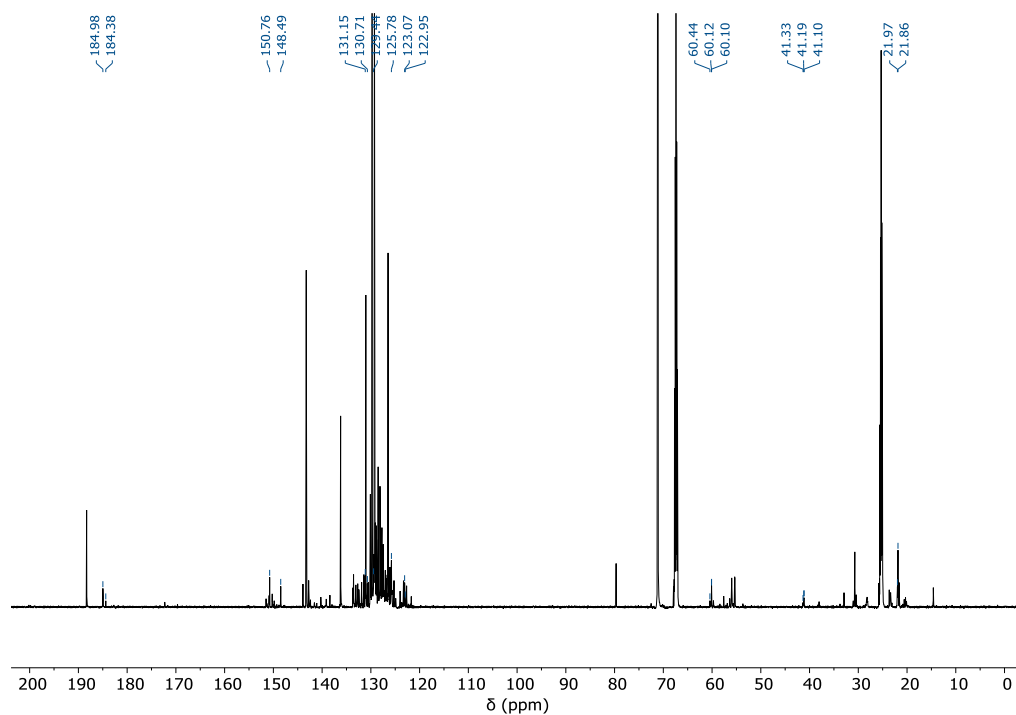
Pd-Complexes from Deprotonated Acid Substrate *trans*-Na-1 with Ligand L1



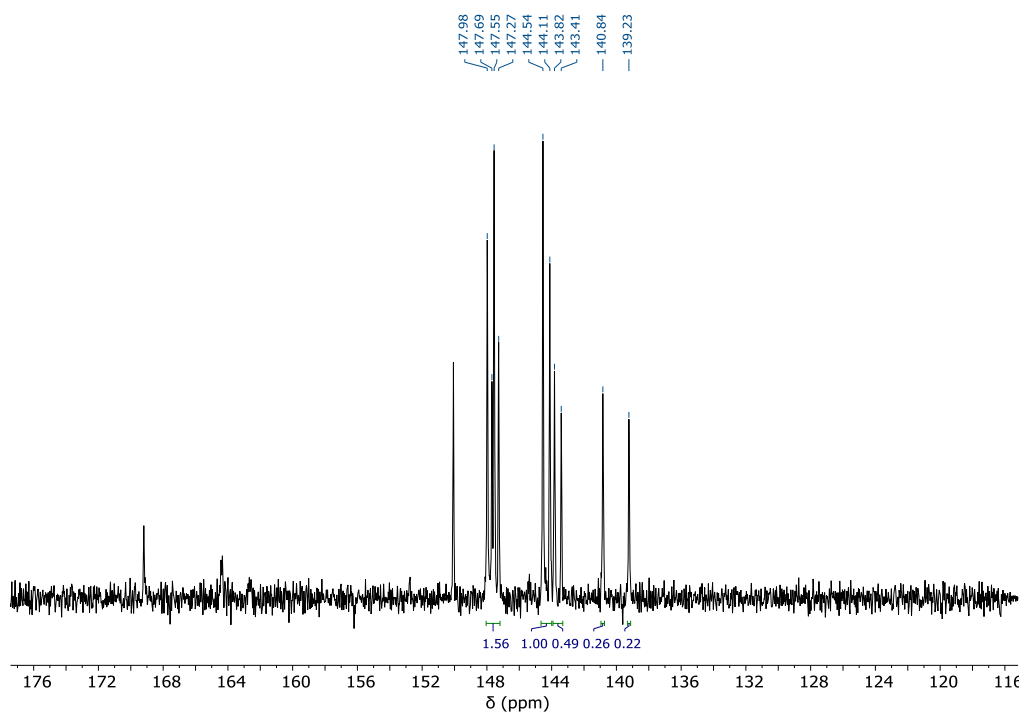
<sup>1</sup>H-NMR (600 MHz, THF-*d*<sub>8</sub>, 273 K) (accurate integration not possible due to low spectral quality)



$^{13}\text{C}\{^1\text{H}\}$ -NMR (151 MHz,  $\text{THF-}d_6$ , 273 K) (*anti*-Na-**4a** already largely decomposed)



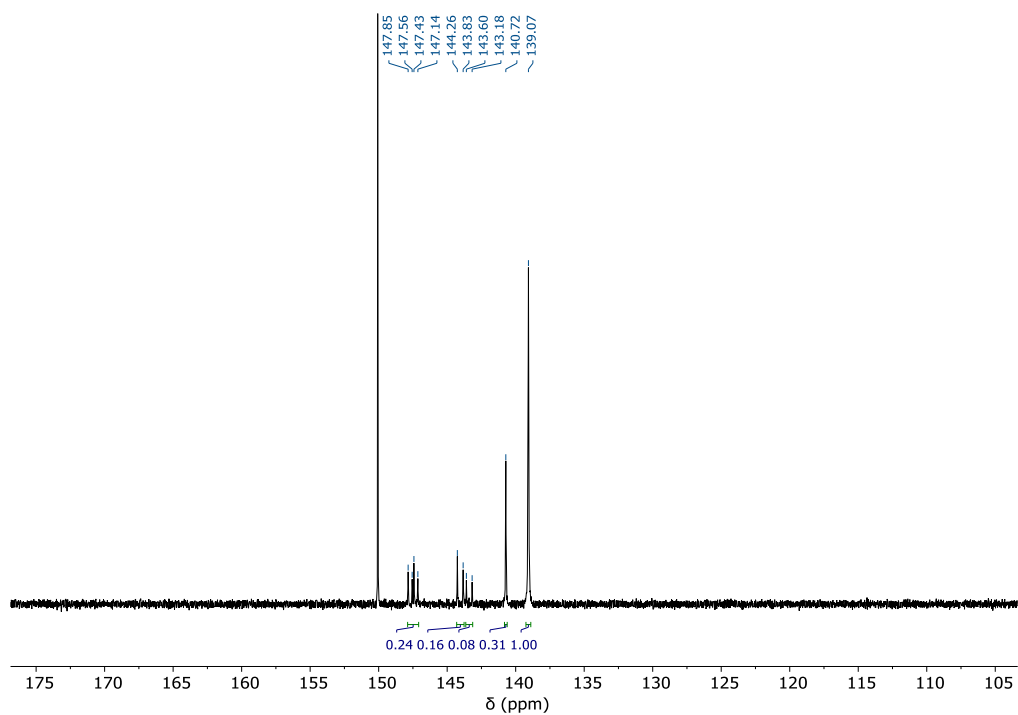
$^{31}\text{P}\{^1\text{H}\}$ -NMR (243 MHz,  $\text{THF-}d_6$ , 273 K), 13 min after preparation



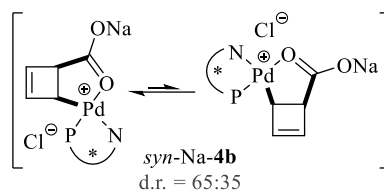
S101



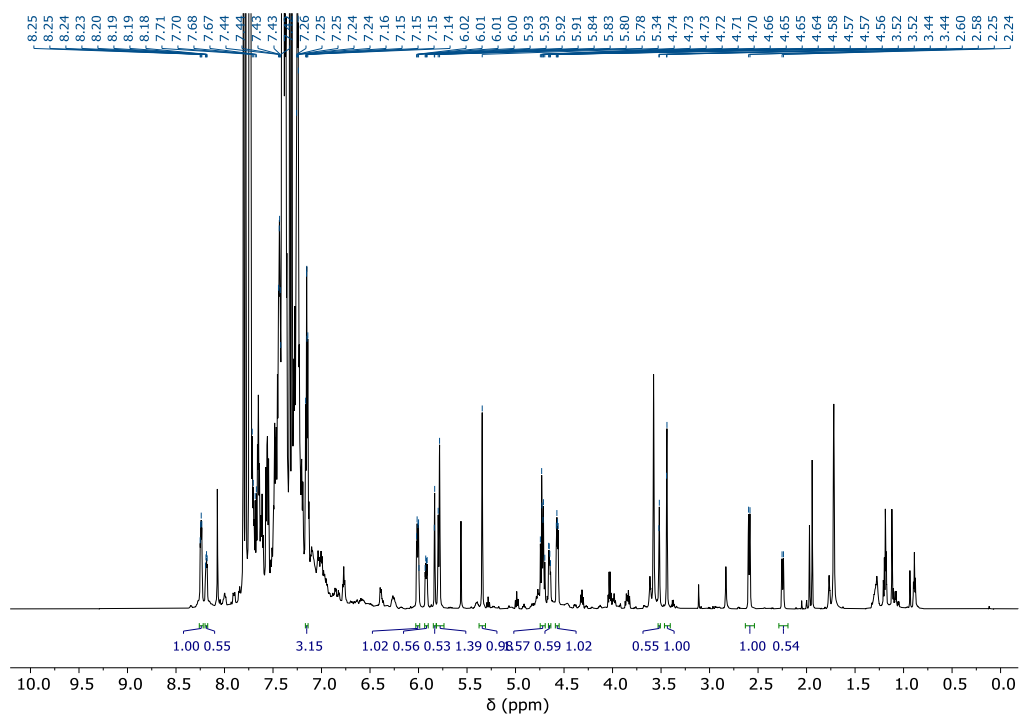
$^{31}\text{P}\{^1\text{H}\}$ -NMR (243 MHz, THF- $d_8$ , 273 K), 9.5 h after preparation



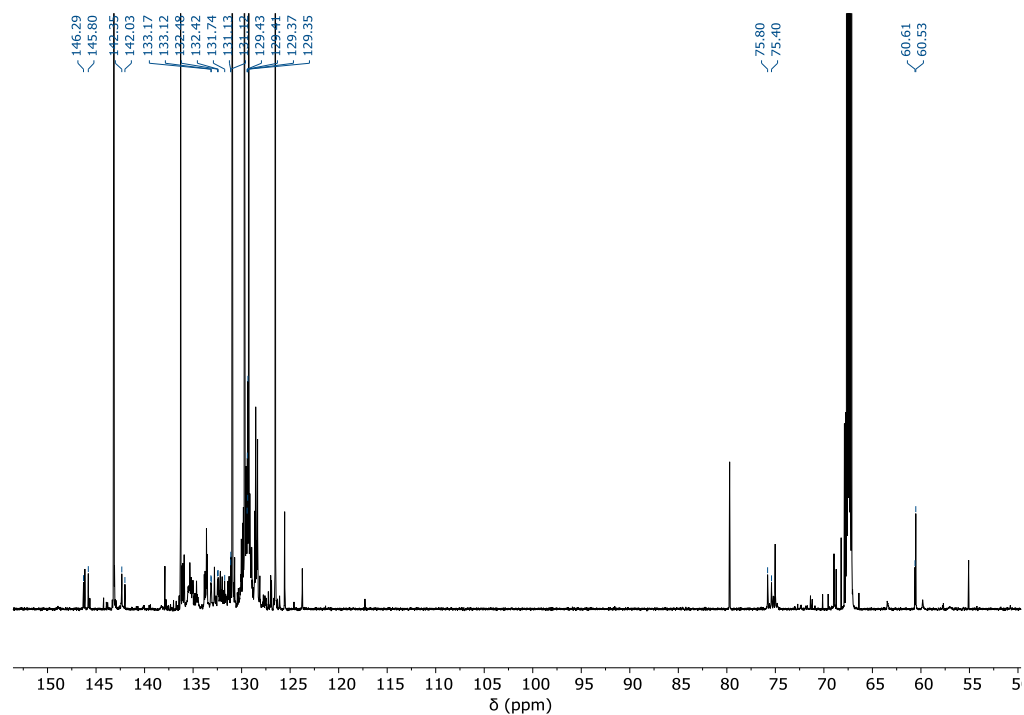
Pd-Complexes from Deprotonated Acid Substrate *trans*-Na-1 with Ligand L2



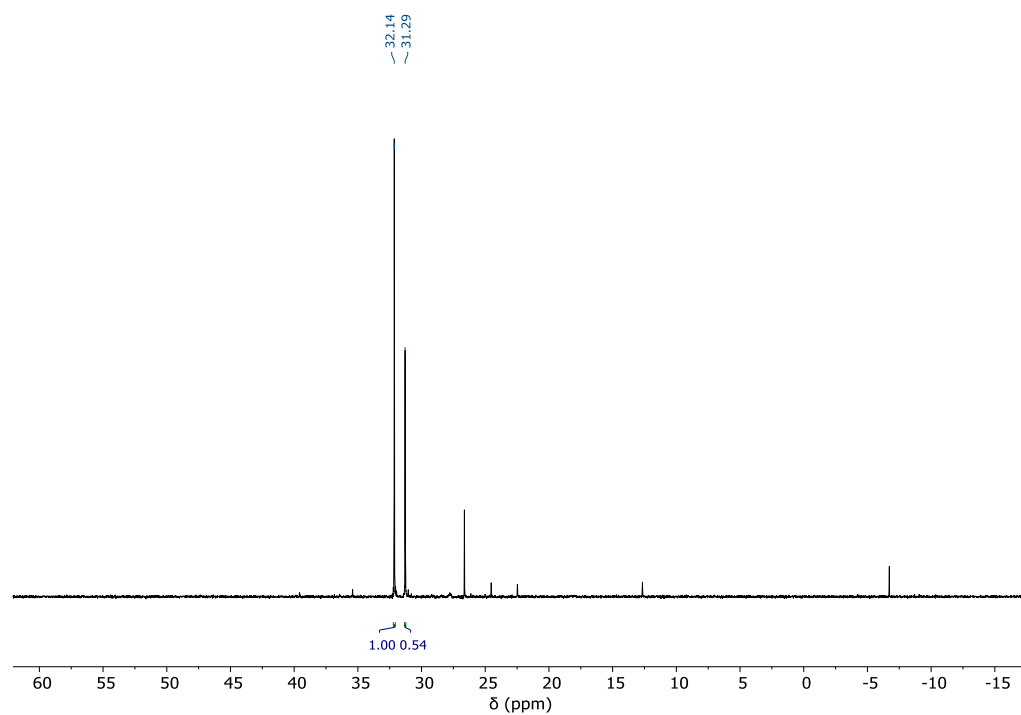
<sup>1</sup>H-NMR (700 MHz, THF-*d*<sub>8</sub>, 273 K)



$^{13}\text{C}\{^1\text{H}\}$ -NMR (176 MHz, THF-*d*<sub>8</sub>, 273 K)



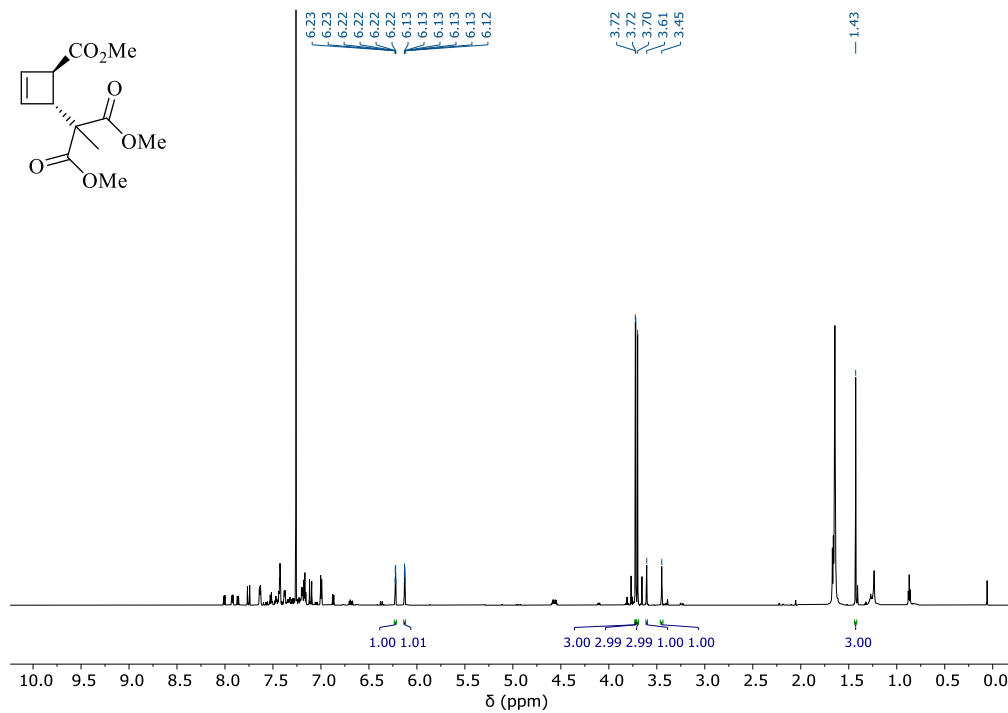
$^{31}\text{P}\{^1\text{H}\}$ -NMR (283 MHz, THF-*d*<sub>8</sub>, 273 K)



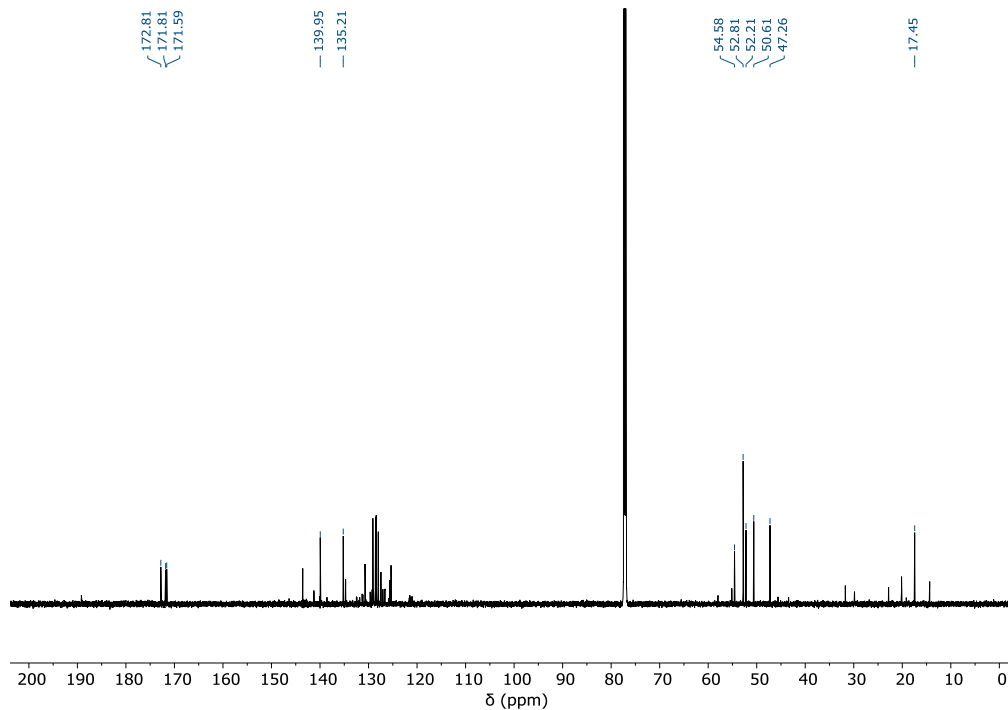
S104

Methyl-(1*R*,4*R*)-4-(1,3-dimethoxy-2-methyl-1,3-dioxopropan-2-yl)cyclobut-2-ene-1-carboxylate (*trans*-8)

<sup>1</sup>H-NMR (700 MHz, CDCl<sub>3</sub>, 273 K)

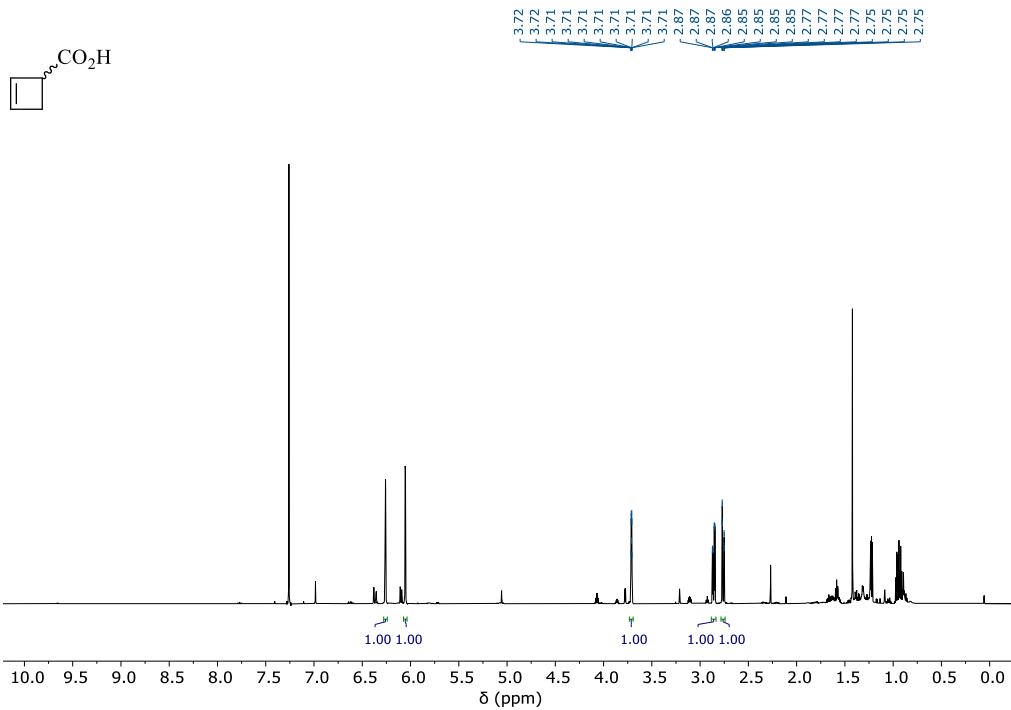


<sup>13</sup>C{<sup>1</sup>H}-NMR (176 MHz, CDCl<sub>3</sub>, 273 K)

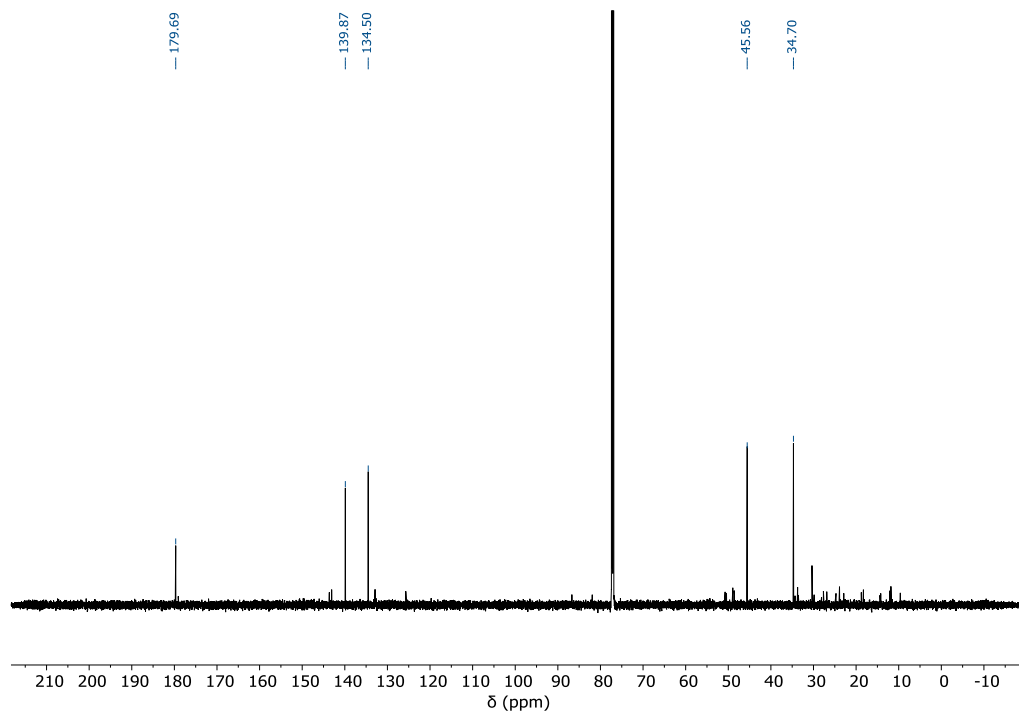


Cyclobut-2-ene-1-carboxylic acid (9)

$^1\text{H-NMR}$  (700 MHz,  $\text{CDCl}_3$ , 273 K)

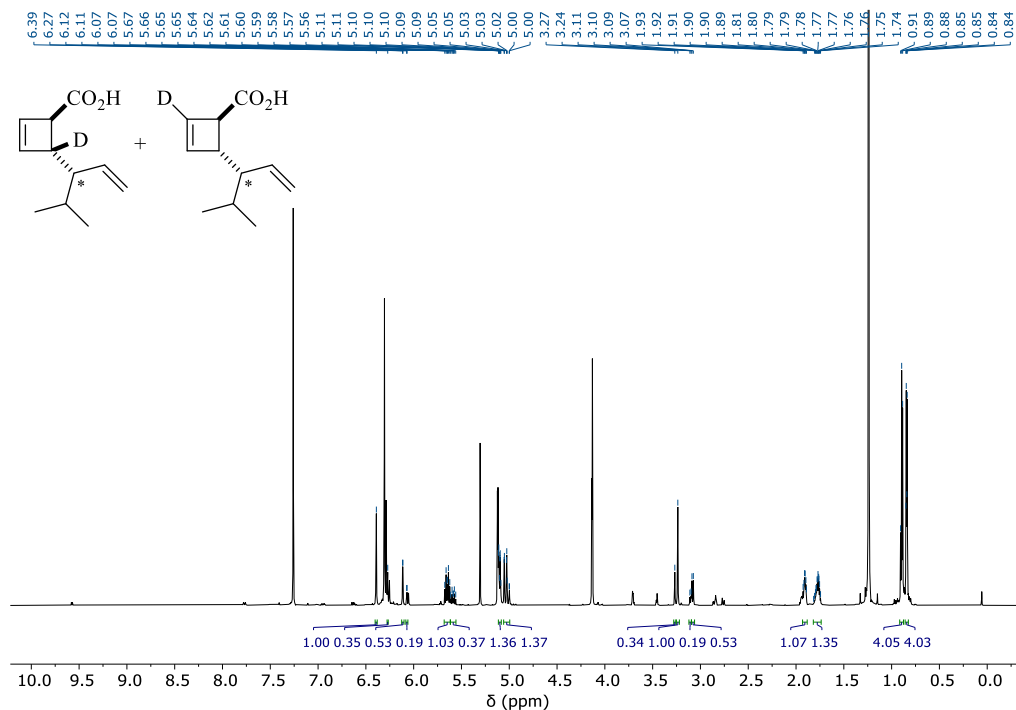


$^{13}\text{C}\{^1\text{H}\}$ -NMR (176 MHz,  $\text{CDCl}_3$ , 273 K)

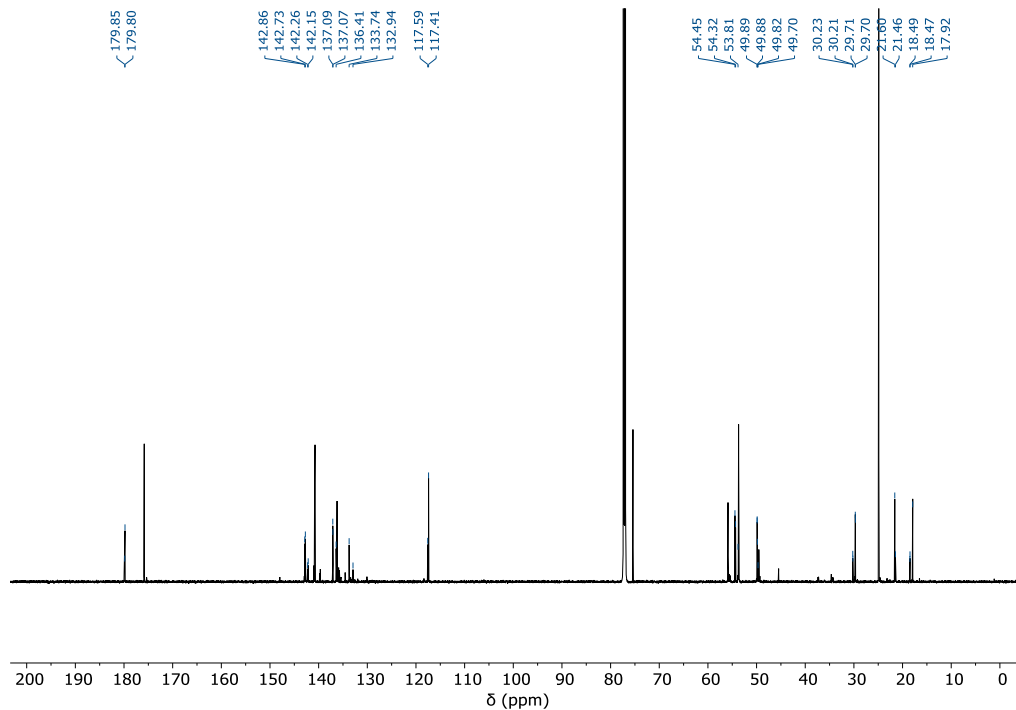


[2-<sup>2</sup>H<sub>1,0</sub>,4-<sup>2</sup>H<sub>0,1</sub>]-*trans*-4-(4-Methylpent-1-en-3-yl)cyclobut-2-ene-1-carboxylic acid ([5-D]/[3-D]-*trans*-10)

<sup>1</sup>H-NMR (700 MHz, CDCl<sub>3</sub>, 273 K)

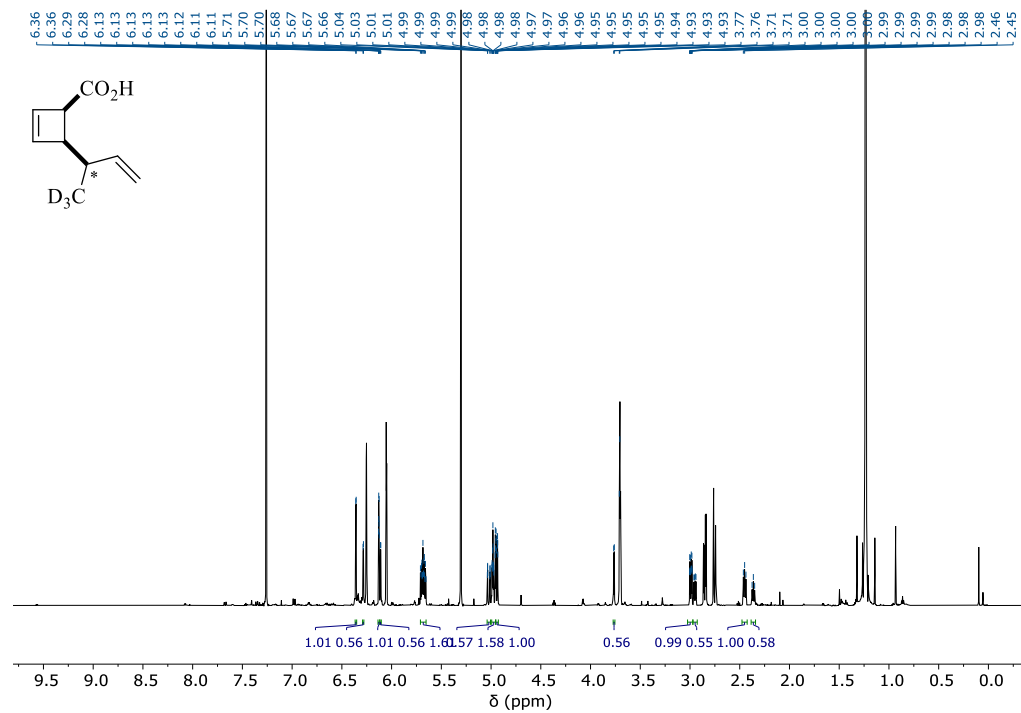


<sup>13</sup>C{<sup>1</sup>H}-NMR (176 MHz, CDCl<sub>3</sub>, 273 K)

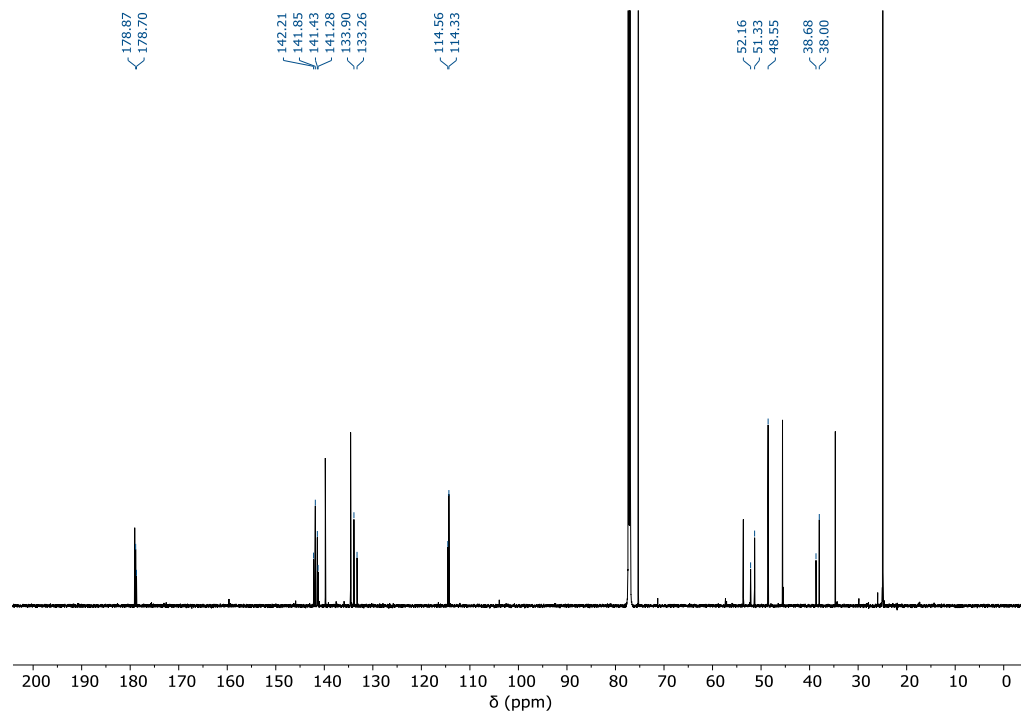


**Cis-4-(but-3-en-2-yl-1,1,1-*d*<sub>3</sub>)cyclobut-2-ene-1-carboxylic acid ([D<sub>3</sub>]-*cis*-11)**

<sup>1</sup>H-NMR (700 MHz, CDCl<sub>3</sub>, 273 K)



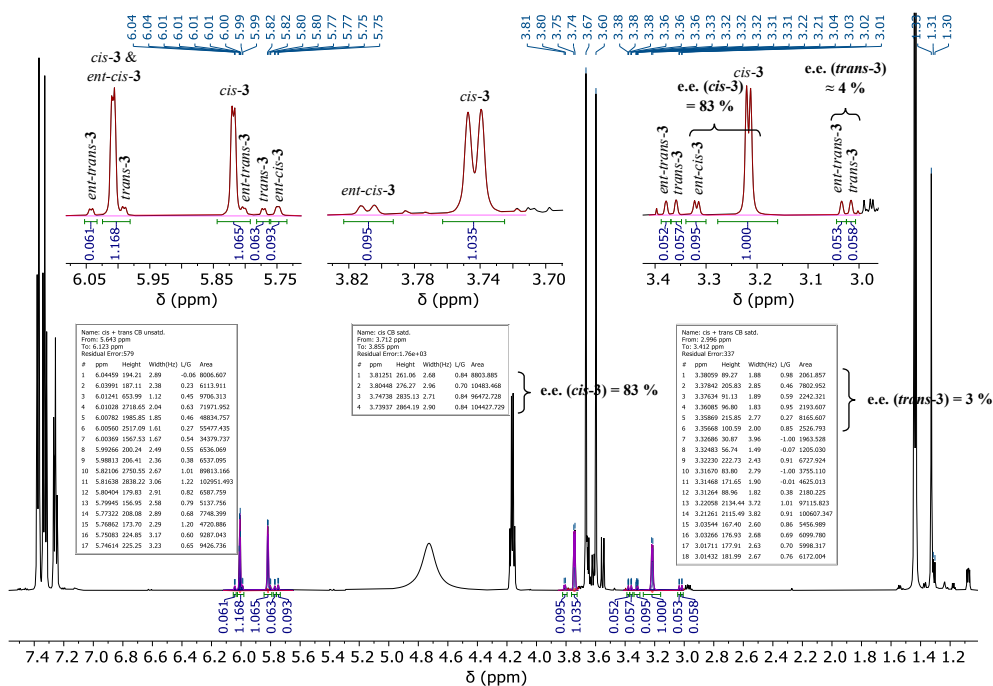
<sup>13</sup>C{<sup>1</sup>H}-NMR (176 MHz, CDCl<sub>3</sub>, 273 K)



## 12 NMR Spectra with Chiral Solvating Agent

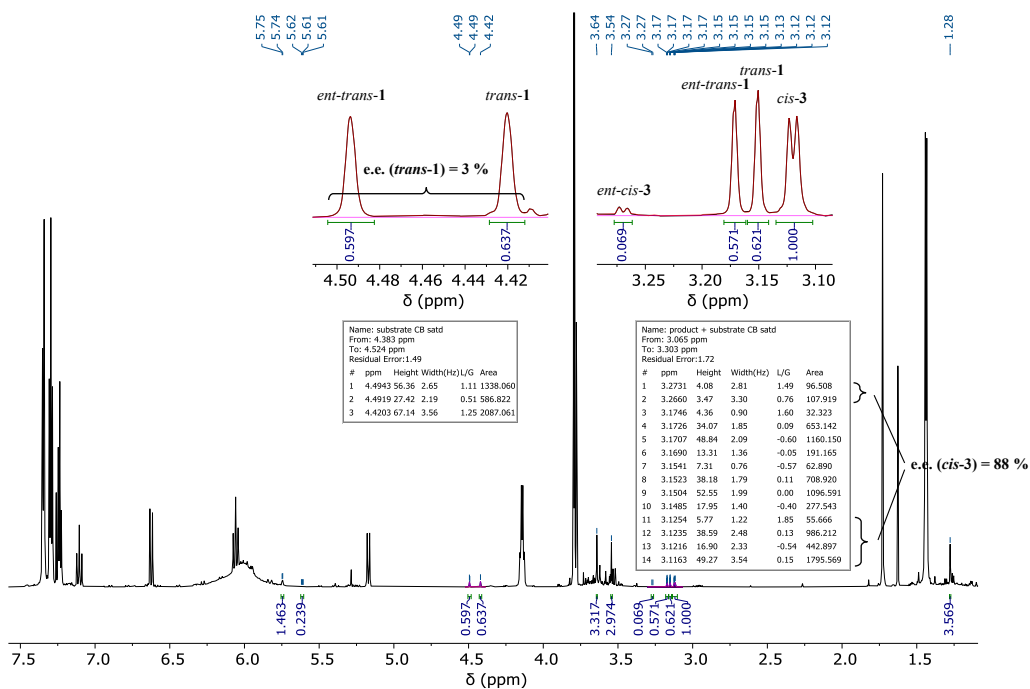
### (1*S*,4*R*)-4-(1,3-dimethoxy-2-methyl-1,3-dioxopropan-2-yl)cyclobut-2-ene-1-carboxylic acid *cis*-3 from Substrate *cis*-1

<sup>1</sup>H-NMR (700 MHz, CDCl<sub>3</sub>, 273 K) after addition of (*S*)-PEA, analyzed by manual integration and signal deconvolution



### (1*S*,4*R*)-4-(1,3-dimethoxy-2-methyl-1,3-dioxopropan-2-yl)cyclobut-2-ene-1-carboxylic acid *cis*-3 from Substrate *trans*-1

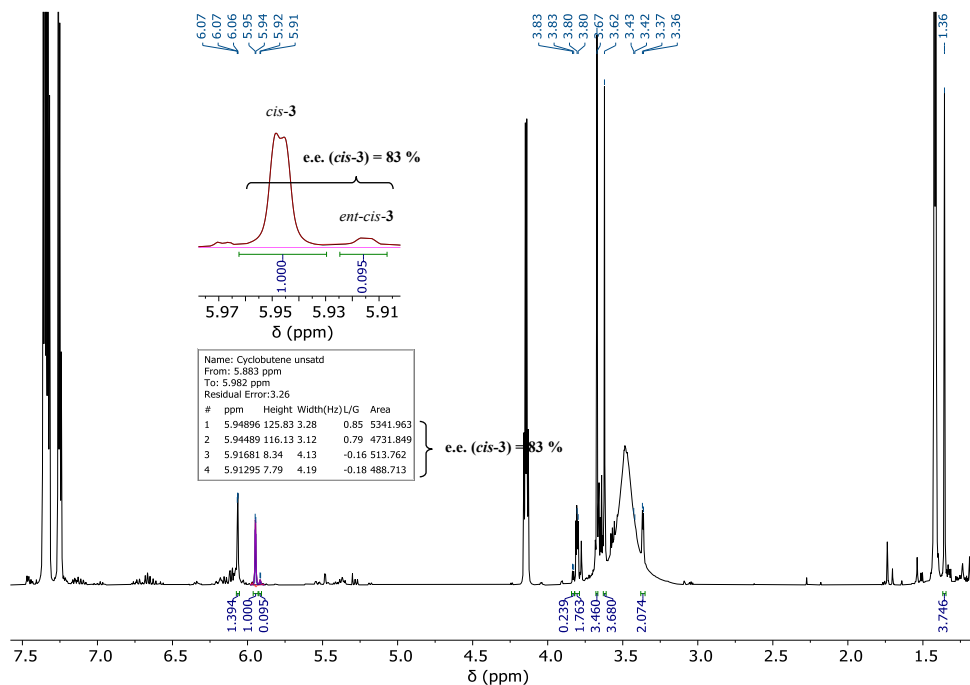
<sup>1</sup>H-NMR (700 MHz, CDCl<sub>3</sub>, 273 K) after addition of (*S*)-PEA, analyzed by manual integration and signal deconvolution





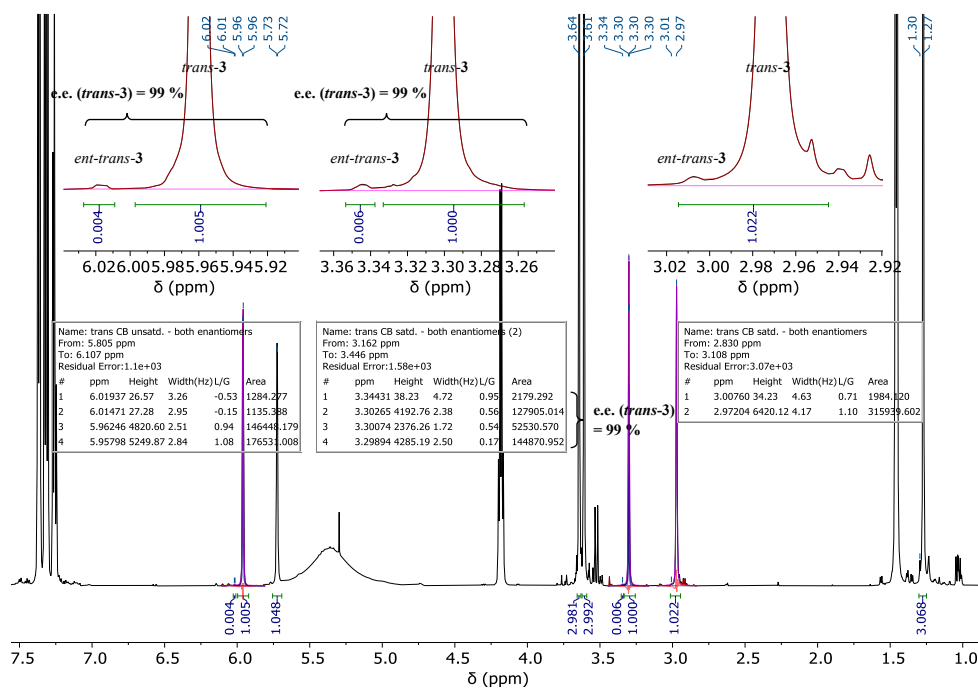
(1*S*,4*R*)-4-(1,3-dimethoxy-2-methyl-1,3-dioxopropan-2-yl)cyclobut-2-ene-1-carboxylic acid *cis*-3 from Pd-Complex *anti*-4a

<sup>1</sup>H-NMR (700 MHz, CDCl<sub>3</sub>, 273 K) after addition of (*S*)-PEA, analyzed by manual integration and signal deconvolution



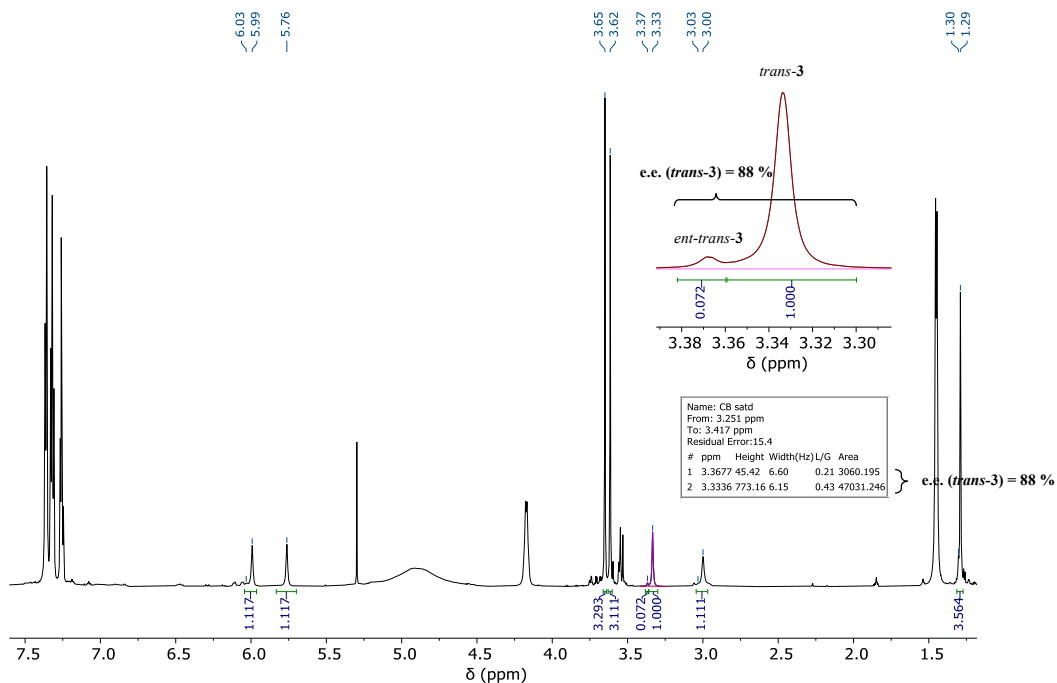
(1*S*,4*S*)-4-(1,3-dimethoxy-2-methyl-1,3-dioxopropan-2-yl)cyclobut-2-ene-1-carboxylic acid *trans*-3 from Substrate *cis*-1

<sup>1</sup>H-NMR (700 MHz, CDCl<sub>3</sub>, 273 K) after addition of (*S*)-PEA, analyzed by manual integration and signal deconvolution



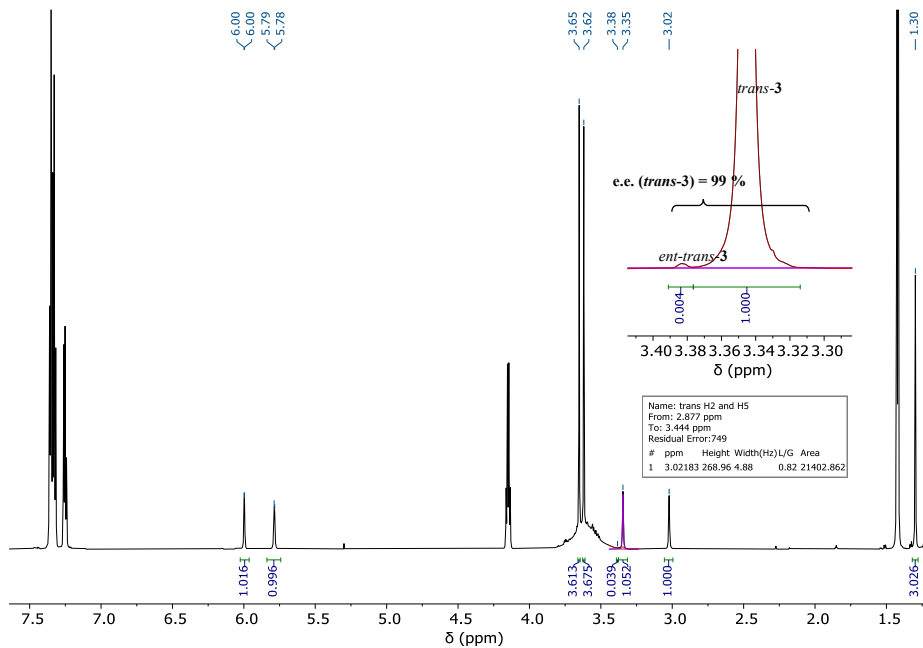
(1*S*,4*S*)-4-(1,3-dimethoxy-2-methyl-1,3-dioxopropan-2-yl)cyclobut-2-ene-1-carboxylic acid *trans*-3 from Substrate *trans*-1

<sup>1</sup>H-NMR (700 MHz, CDCl<sub>3</sub>, 273 K) after addition of (*S*)-PEA, analyzed by signal deconvolution



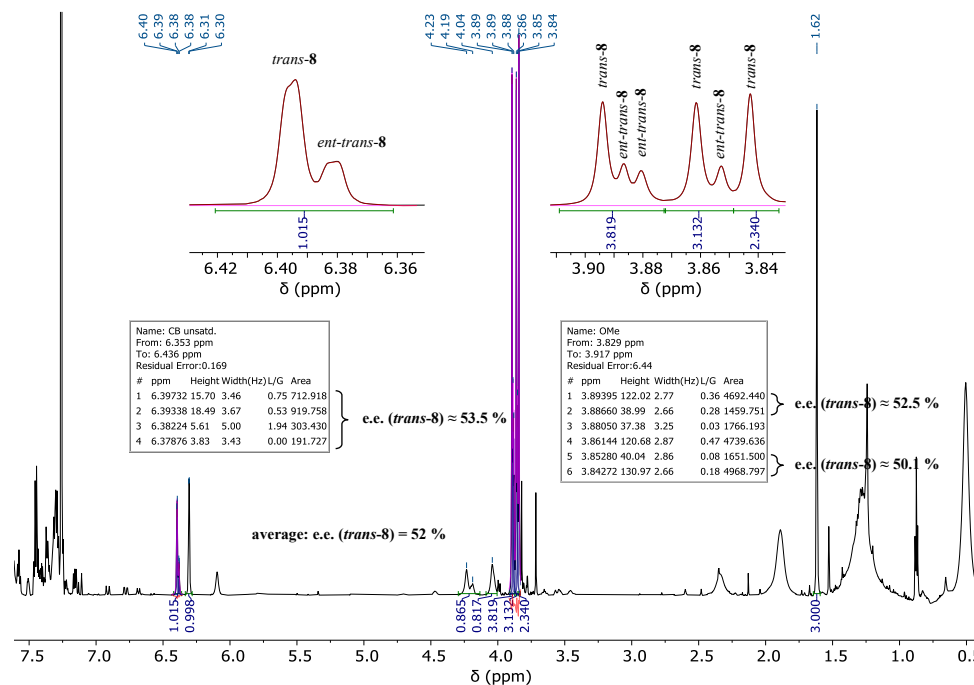
(1*S*,4*S*)-4-(1,3-dimethoxy-2-methyl-1,3-dioxopropan-2-yl)cyclobut-2-ene-1-carboxylic acid *trans*-3 from Pd-Complex *anti*-4b

<sup>1</sup>H-NMR (700 MHz, CDCl<sub>3</sub>, 273 K) after addition of (*S*)-PEA, analyzed by manual integration (signal deconvolution not successful as the signal of the minor enantiomer could not be fitted), manual integrals in the expanded region were extracted after baseline correction applied only to the region  $\delta_1 = 3.97 - 2.89$  ppm

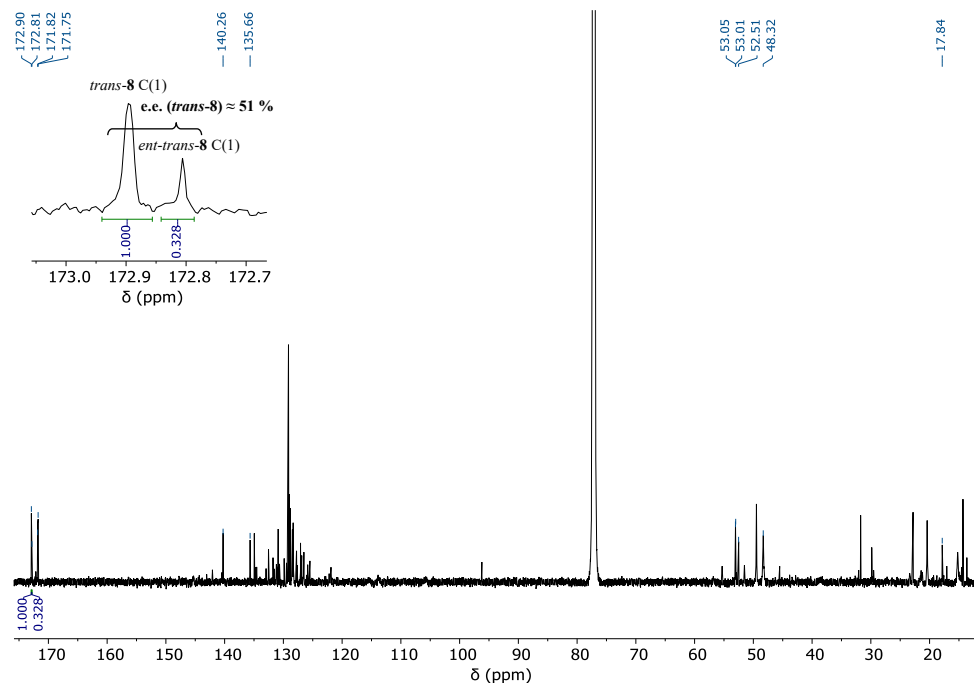


Methyl-(1*R*,4*R*)-4-(1,3-dimethoxy-2-methyl-1,3-dioxopropan-2-yl)cyclobut-2-ene-1-carboxylate (*trans*-8)

<sup>1</sup>H-NMR (700 MHz, CDCl<sub>3</sub>, 283 K) after addition of Eu(hfc)<sub>3</sub>, analyzed by signal deconvolution

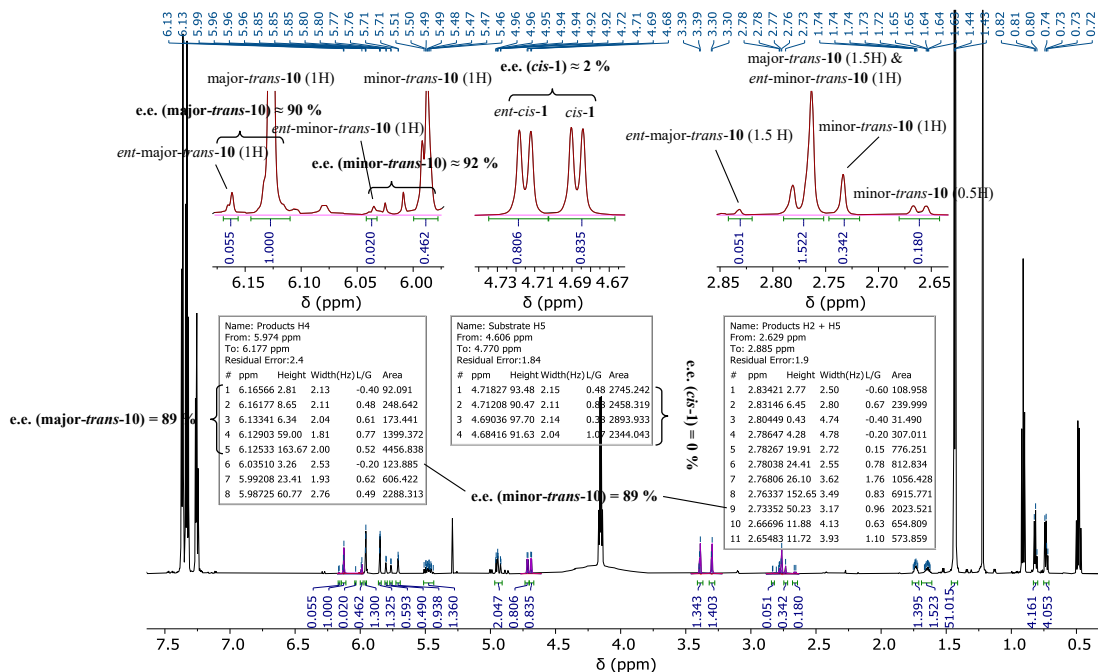


Semi-quantitative <sup>13</sup>C-NMR (176 MHz, CDCl<sub>3</sub>, 283 K, inverse-gated decoupling, 30° excitation, 2 s relaxation delay) after addition of Eu(hfc)<sub>3</sub>, recorded for verifying the e.e. extracted from the <sup>1</sup>H-NMR spectrum, analyzed by manual integration of the C(1) resonance of both enantiomers



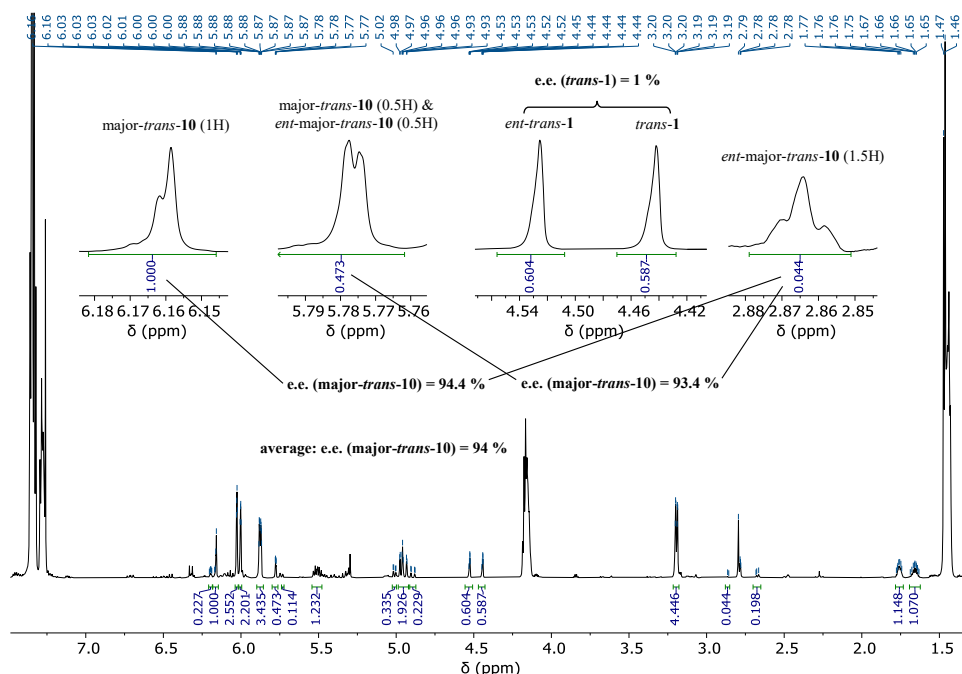
[2-<sup>2</sup>H<sub>1,0</sub>,4-<sup>2</sup>H<sub>0,1</sub>]-*trans*-4-(4-Methylpent-1-en-3-yl)cyclobut-2-ene-1-carboxylic acid ([5-D]/[3-D]-*trans*-10) from Substrate [5-D]/[3-D]-*cis*-1

<sup>1</sup>H-NMR (700 MHz, CDCl<sub>3</sub>, 273 K) after addition of (*S*)-PEA, analyzed by manual integration and signal deconvolution



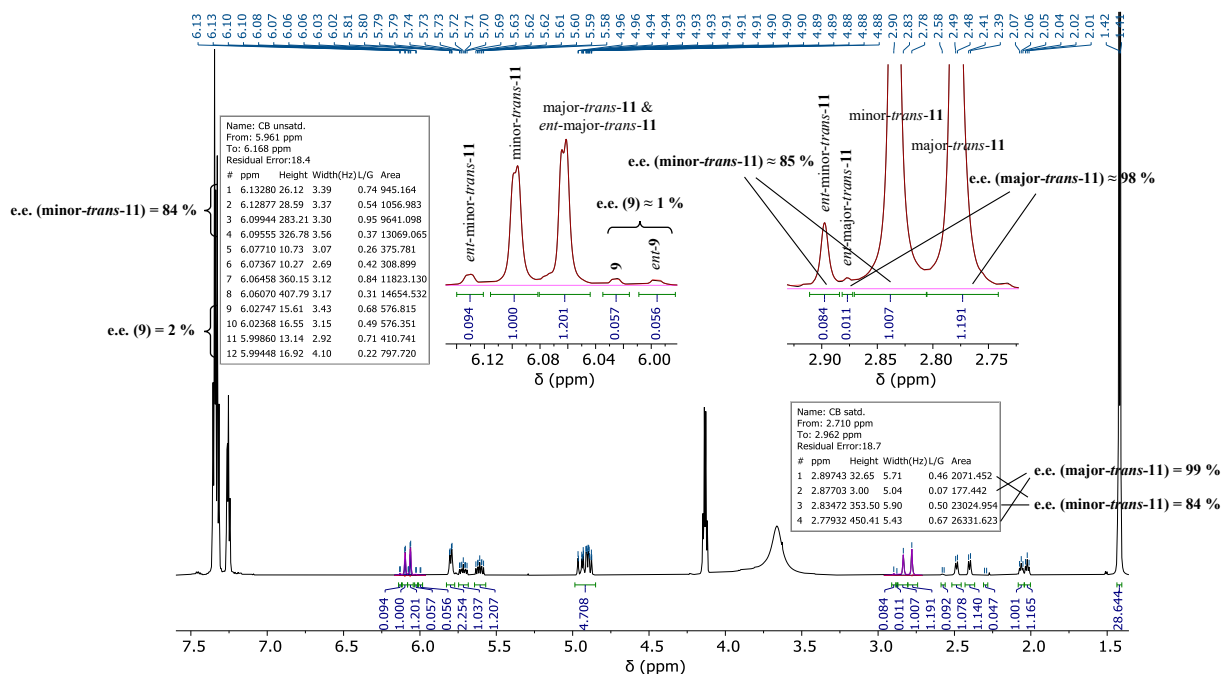
[2-<sup>2</sup>H<sub>1,0</sub>,4-<sup>2</sup>H<sub>0,1</sub>]-*trans*-4-(4-Methylpent-1-en-3-yl)cyclobut-2-ene-1-carboxylic acid ([5-D]/[3-D]-*trans*-10) from Substrate [5-D]/[3-D]-*trans*-1

<sup>1</sup>H-NMR (700 MHz, CDCl<sub>3</sub>, 273 K) after addition of (*S*)-PEA, analyzed by manual integration



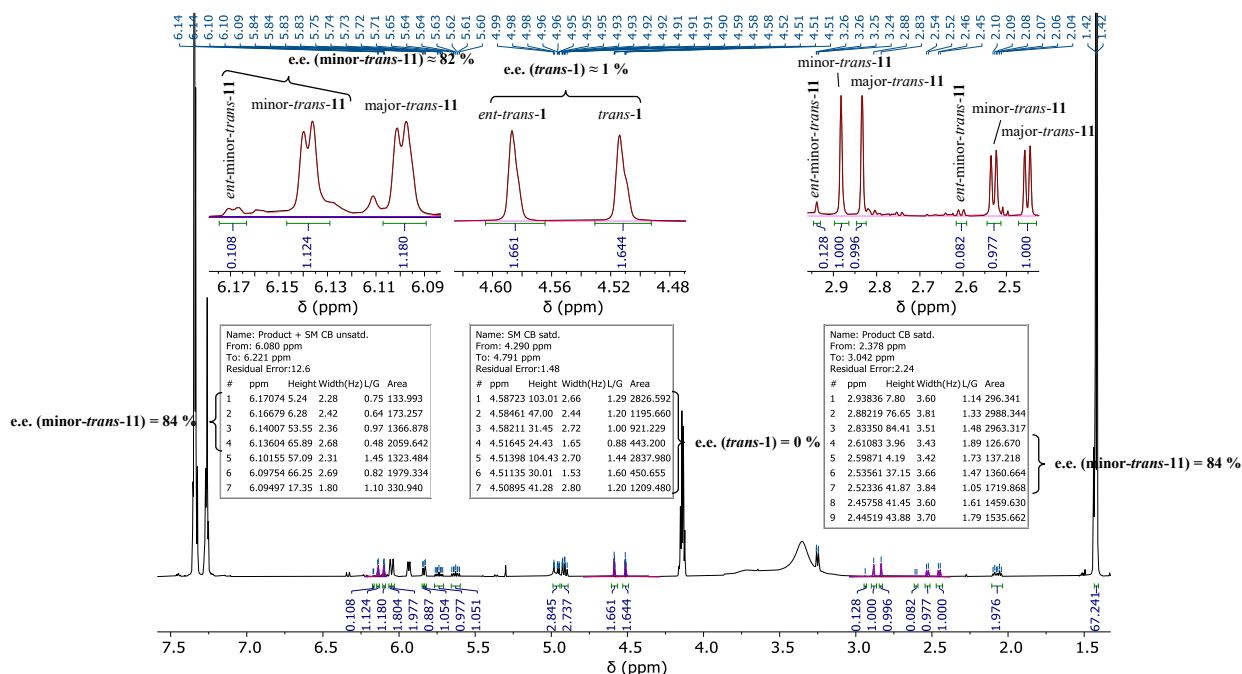
**Trans-4-(but-3-en-2-yl-1,1,1-*d*<sub>3</sub>)cyclobut-2-ene-1-carboxylic acid (*[D*<sub>3</sub>]-*trans*-11) from Substrate *cis*-1**

<sup>1</sup>H-NMR (700 MHz, CDCl<sub>3</sub>, 273 K) after addition of (*S*)-PEA, analyzed by manual integration and signal deconvolution



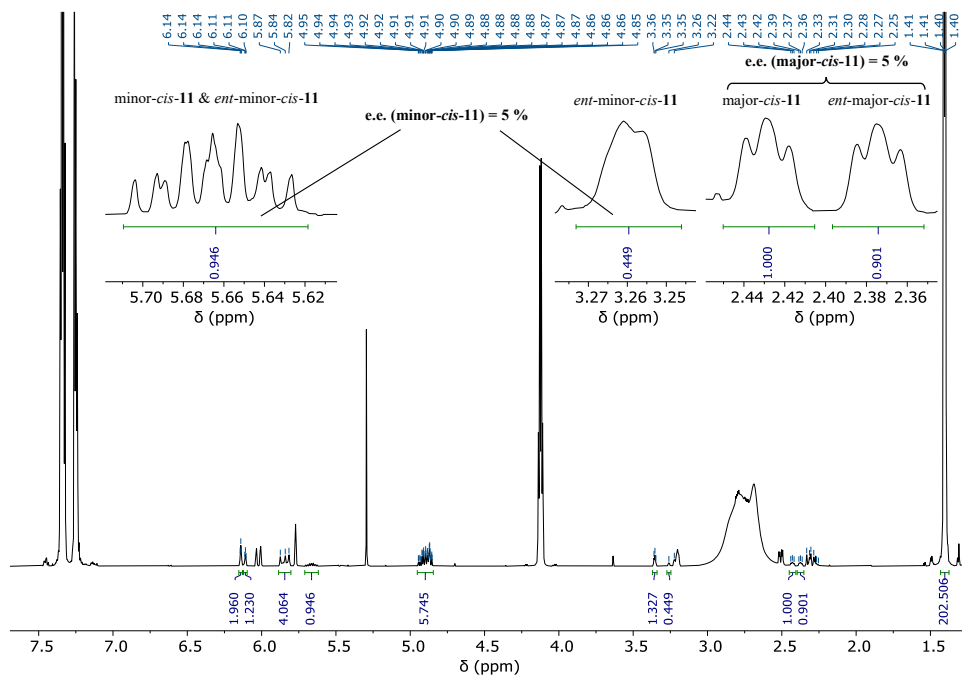
**Trans-4-(but-3-en-2-yl-1,1,1-*d*<sub>3</sub>)cyclobut-2-ene-1-carboxylic acid (*[D*<sub>3</sub>]-*trans*-11) from Substrate *trans*-1**

<sup>1</sup>H-NMR (700 MHz, CDCl<sub>3</sub>, 273 K) after addition of (*S*)-PEA, analyzed by manual integration and signal deconvolution



*Cis*-4-(but-3-en-2-yl-1,1,1-*d*<sub>3</sub>)cyclobut-2-ene-1-carboxylic acid (*[D*<sub>3</sub>*]-cis*-11)

<sup>1</sup>H-NMR (700 MHz, CDCl<sub>3</sub>, 273 K) after addition of (*S*)-PEA, analyzed by manual integration



### 13 References

- (1) Thiele, C. M.; Petzold, K.; Schleucher, J. EASY ROESY: Reliable Cross-Peak Integration in Adiabatic Symmetrized ROESY. *Chem. Eur. J.* **2009**, *15* (3), 585–588. <https://doi.org/10.1002/chem.200802027>.
- (2) Thruppelton, M. J.; Keeler, J. Elimination of Zero-Quantum Interference in Two-Dimensional NMR Spectra. *Angew. Chem. Int. Ed.* **2003**, *42* (33), 3938–3941. <https://doi.org/10.1002/anie.200351947>.
- (3) Wu, D. H.; Chen, A. D.; Johnson, C. S. An Improved Diffusion-Ordered Spectroscopy Experiment Incorporating Bipolar-Gradient Pulses. *J. Magn. Reson. A* **1995**, *115* (2), 260–264. <https://doi.org/10.1006/jmra.1995.1176>.
- (4) Koos, M. R. M.; Kummerlöwe, G.; Kaltschnee, L.; Thiele, C. M.; Luy, B. CLIP-COSY: A Clean In-Phase Experiment for the Rapid Acquisition of COSY-Type Correlations. *Angew. Chem. Int. Ed.* **2016**, *55* (27), 7655–7659. <https://doi.org/10.1002/anie.201510938>.
- (5) Sinnaeve, D.; Forozaandeh, M.; Nilsson, M.; Morris, G. A. A General Method for Extracting Individual Coupling Constants from Crowded <sup>1</sup>H NMR Spectra. *Angew. Chem. Int. Ed.* **2016**, *55* (3), 1102–1105. <https://doi.org/10.1002/anie.201508691>.
- (6) Fulmer, G. R.; Miller, A. J. M.; Sherden, N. H.; Gottlieb, H. E.; Nudelman, A.; Stoltz, B. M.; Bercaw, J. E.; Goldberg, K. I. NMR Chemical Shifts of Trace Impurities: Common Laboratory Solvents, Organics, and Gases in Deuterated Solvents Relevant to the Organometallic Chemist. *Organometallics* **2010**, *29* (9), 2176–2179. <https://doi.org/10.1021/om100106e>.
- (7) Ilgen, J.; Nowag, J.; Kaltschnee, L.; Schmidts, V.; Thiele, C. M. Gradient Selected Pure Shift EASY-ROESY Techniques Facilitate the Quantitative Measurement of <sup>1</sup>H,<sup>1</sup>H-Distance Restraints in Congested Spectral Regions. *J. Magn. Reson.* **2021**, *324*, 106900.
- (8) Stonehouse, J.; Adell, P.; Keeler, J.; Shaka, A. J. Ultrahigh-Quality NOE Spectra. *J. Am. Chem. Soc.* **1994**, *116* (13), 6037–6038.
- (9) Stott, K.; Keeler, J.; Van, Q. N.; Shaka, A. J. One-Dimensional NOE Experiments Using Pulsed Field Gradients. *J. Magn. Reson.* **1997**, *125* (2), 302–324.
- (10) Hu, H.; Krishnamurthy, K. Revisiting the Initial Rate Approximation in Kinetic NOE Measurements. *J. Magn. Reson.* **2006**, *182* (1), 173–177. <https://doi.org/10.1016/j.jmr.2006.06.009>.
- (11) Krout, M. R.; Mohr, J. T.; Stoltz, B. M. Preparation of (S)-Tert-ButylPHOX (Oxazole, 4-(1,1-Dimethylethyl)-2-(2-(Diphenylphosphino)Phenyl)-4,5-Dihydro-(4S)-). *Org. Synth.* **2009**, *86*, 181–193. <https://doi.org/10.15227/orgsyn.086.0181>.
- (12) Einziger, C. Beiträge Zur Stereoselektiven Synthese von Kohlenhydrat-Derivaten. PhD Thesis, Technische Universität Wien, 2007.
- (13) Nakagawa, M.; Saegusa, J.; Tonozuka, M.; Obi, M.; Kiuchi, M.; Hino, T.; Ban, Y. 5,6-Dihydro-2H-Pyran-2-One and 2H-Pyran-2-One. *Org. Synth.* **1977**, *56*, 49. <https://doi.org/10.15227/orgsyn.056.0049>.
- (14) Williams, J. D.; Otake, Y.; Coussanes, G.; Saridakis, I.; Maulide, N.; Kappe, C. O. Towards a Scalable Synthesis of 2-Oxabicyclo[2.2.0]Hex-5-En-3-One Using Flow Photochemistry. *ChemPhotoChem* **2019**, *3* (5), 229–232. <https://doi.org/10.1002/cptc.201900017>.
- (15) Chen, Y.; Coussanes, G.; Souris, C.; Aillard, P.; Kaldre, D.; Runggatscher, K.; Kubicek, S.; Mauro, G. D.; Maryasin, B.; Maulide, N. A Domino 10-Step Total Synthesis of FR252921 and Its Analogues, Complex Macrocylic Immunosuppressants. *J. Am. Chem. Soc.* **2019**, *141* (35), 13772–13777. <https://doi.org/10.1021/jacs.9b07185>.
- (16) Souris, C.; Frébault, F.; Patel, A.; Audisio, D.; Houk, K. N.; Maulide, N. Stereoselective Synthesis of Dienyl-Carboxylate Building Blocks: Formal Synthesis of Inthomycin C. *Org. Lett.* **2013**, *15* (13), 3242–3245. <https://doi.org/10.1021/ol401226y>.
- (17) Bellina, F.; Carpita, A.; Mannocci, L.; Rossi, R. First Total Synthesis of Naturally Occurring (–)-Nitidon and Its Enantiomer. *Eur. J. Org. Chem.* **2004**, *2004* (12), 2610–2619. <https://doi.org/10.1002/ejoc.200400101>.
- (18) Pirkle, W. H.; Dines, M. Structure of Electron Impact Fragments. The C<sub>4</sub>H<sub>4</sub>O Radical Cation from 2-Pyrone. *J. Am. Chem. Soc.* **1968**, *90* (9), 2318–2323. <https://doi.org/10.1021/ja01011a020>.
- (19) Malachowski, R. Stereochemie Der Glutaconsäuren (I. Mitteil.). *Chem. Ber.* **1929**, *62* (5), 1323–1326. <https://doi.org/10.1002/cber.19290620535>.
- (20) Kanoo, P.; Haldar, R.; Cyriac, S. T.; Maji, T. K. Coordination Driven Axial Chirality in a Microporous Solid Assembled from an Achiral Linker via in Situ C–N Coupling. *Chem. Commun.* **2011**, *47* (39), 11038–11040. <https://doi.org/10.1039/C1CC13877D>.
- (21) Pirkle, W. H.; Dines, M. NMR Spectra of 2-Pyrone and 2-Pyrone Derivatives. *J. Heterocycl. Chem.* **1969**, *6* (1), 1–3. <https://doi.org/10.1002/jhet.5570060101>.
- (22) Audisio, D.; Luparia, M.; Oliveira, M. T.; Klütt, D.; Maulide, N. Diastereodivergent De-Epimerization in Catalytic Asymmetric Allylic Alkylation. *Angew. Chem. Int. Ed.* **2012**, *51* (29), 7314–7317. <https://doi.org/10.1002/anie.201202853>.
- (23) Pirkle, W. H.; McKendry, L. H. Photochemical Reactions of 2-Pyrone and Thermal Reactions of the 2-Pyrone Photoproducts. *J. Am. Chem. Soc.* **1969**, *91* (5), 1179–1186. <https://doi.org/10.1021/ja01033a025>.
- (24) Seo, J.; Lee, S. Y.; Bielawski, C. W. Dewar Lactone as a Modular Platform to a New Class of Substituted Poly(Acetylene)s. *Polym. Chem.* **2019**, *10* (47), 6401–6412. <https://doi.org/10.1039/C9PY01282F>.
- (25) Jiang, B.; Liang, Q.-J.; Han, Y.; Zhao, M.; Xu, Y.-H.; Loh, T.-P. Copper-Catalyzed Dehydrogenative Diels–Alder Reaction. *Org. Lett.* **2018**, *20* (11), 3215–3219. <https://doi.org/10.1021/acs.orglett.8b01067>.
- (26) Carosi, L.; Hall, D. G. Catalytic Enantioselective Preparation of  $\alpha$ -Substituted Allylboronates: One-Pot Addition to Functionalized Aldehydes and a Route to Chiral Allylic Trifluoroborate Reagents. *Angew. Chem. Int. Ed.* **2007**, *46* (31), 5913–5915. <https://doi.org/10.1002/anie.200700975>.
- (27) Niyomchon, S.; Audisio, D.; Luparia, M.; Maulide, N. Regio- and Enantioselective Cyclobutene Allylations. *Org. Lett.* **2013**, *15* (9), 2318–2321. <https://doi.org/10.1021/ol401033g>.
- (28) Hoffmann, R. W.; Wolff, J. J. Stereoselective Synthesis of Alcohols, XXXVII. Origins of Stereoselectivity in Reactions of  $\alpha$ -Substituted Allylboronates with Aldehydes. *Chem. Ber.* **1991**, *124* (3), 563–569. <https://doi.org/10.1002/cber.19911240323>.
- (29) Luparia, M.; Oliveira, M. T.; Audisio, D.; Frébault, F.; Goddard, R.; Maulide, N. Catalytic Asymmetric Diastereodivergent Deracemization. *Angew. Chem. Int. Ed.* **2011**, *50* (52), 12631–12635. <https://doi.org/10.1002/anie.201106321>.
- (30) Foley, D. A.; Dunn, A. L.; Zell, M. T. Reaction Monitoring Using Online vs Tube NMR Spectroscopy: Seriously Different Results. *Magn. Reson. Chem.* **2016**, *54* (6), 451–456. <https://doi.org/10.1002/mrc.4259>.
- (31) Tan, E. H. P.; Lloyd-Jones, G. C.; Harvey, J. N.; Lennox, A. J. J.; Mills, B. M. [(RCN)<sub>2</sub>PdCl<sub>2</sub>]-Catalyzed E/Z Isomerization of Alkenes: A Non-Hydride Binuclear Addition–Elimination Pathway. *Angew. Chem. Int. Ed.* **2011**, *50* (41), 9602–9606. <https://doi.org/10.1002/anie.201103947>.
- (32) Audisio, D.; Gopakumar, G.; Xie, L.-G.; Alves, L. G.; Wirtz, C.; Martins, A. M.; Thiel, W.; Farès, C.; Maulide, N. Palladium-Catalyzed Allylic Substitution at Four-Membered-Ring Systems: Formation of H<sup>1</sup>-Allyl Complexes and Electrocyclic Ring Opening. *Angew. Chem. Int. Ed.* **2013**, *52* (24), 6313–6316. <https://doi.org/10.1002/anie.201301034>.
- (33) Xie, L.-G.; Bagutski, V.; Audisio, D.; Wolf, L. M.; Schmidts, V.; Hofmann, K.; Wirtz, C.; Thiel, W.; Thiele, C. M.; Maulide, N. Dynamic Behaviour of Monohaptoallylpalladium Species: Internal Coordination as a Driving Force in Allylic Alkylation Chemistry. *Chem. Sci.* **2015**, *6* (10), 5734–5739. <https://doi.org/10.1039/C5SC01867F>.

- (34) Hartmann, E.; Hammer, M.; Gschwind, R. M. Structures and Interligand Interaction Pattern of Phosphoramidite Pd Complexes by NMR Spectroscopy: Modulations in Extended Interaction Surfaces as Stereoselection Mode of a Privileged Class of Ligands. *Chem. Eur. J.* **2013**, *19* (32), 10551–10562. <https://doi.org/10.1002/chem.201300095>.
- (35) Viviente, E. M.; Pregosin, P. S.; Schott, D. NMR Spectroscopy and Homogeneous Catalysis. In *Mechanisms in Homogeneous Catalysis: A Spectroscopic Approach*; Heaton, B., Ed.; Wiley-VCH: Weinheim, 2005; pp 1–80.
- (36) Verkade, J. G. Spectroscopic Studies of Metal-Phosphorus Bonding in Coordination Complexes. *Coord. Chem. Rev.* **1972**, *9* (1–2), 1–106. [https://doi.org/10.1016/S0010-8545\(00\)80224-6](https://doi.org/10.1016/S0010-8545(00)80224-6).
- (37) Hill, E. A.; Roberts, J. D. A Reinterpretation of the Nuclear Magnetic Resonance Spectrum of Cyclobutene. *J. Am. Chem. Soc.* **1967**, *89* (9), 2047–2049. <https://doi.org/10.1021/ja00985a013>.
- (38) Hansen, P. E.; Led, J. J. CH, CD, CC and HH Coupling Constants in Isotopically Enriched Cyclobutene. *Org. Magn. Reson.* **1981**, *15* (3), 288–293. <https://doi.org/10.1002/mrc.1270150316>.
- (39) Wagner, G. E.; Sakhaei, P.; Bernmel, W.; Zangger, K. Monitoring Fast Reactions by Spatially-Selective and Frequency-Shifted Continuous NMR Spectroscopy: Application to Rapid-Injection Protein Unfolding. *Chem. Commun.* **2013**, *49* (30), 3155–3157. <https://doi.org/10.1039/C3CC39107H>.
- (40) Kind, J.; Thiele, C. M. Still Shimming or Already Measuring? – Quantitative Reaction Monitoring for Small Molecules on the Sub Minute Timescale by NMR. *J. Magn. Reson.* **2015**, *260*, 109–115. <https://doi.org/10.1016/j.jmr.2015.09.008>.
- (41) Hun Mok, K.; Nagashima, T.; Day, I. J.; Jones, J. A.; Jones, C. J. V.; Dobson, C. M.; Hore, P. J. Rapid Sample-Mixing Technique for Transient NMR and Photo-CIDNP Spectroscopy: Applications to Real-Time Protein Folding. *J. Am. Chem. Soc.* **2003**, *125* (41), 12484–12492. <https://doi.org/10.1021/ja036357v>.
- (42) Pardo, Z. D.; Olsen, G. L.; Fernández-Valle, M. E.; Frydman, L.; Martínez-Álvarez, R.; Herrera, A. Monitoring Mechanistic Details in the Synthesis of Pyrimidines via Real-Time, Ultrafast Multidimensional NMR Spectroscopy. *J. Am. Chem. Soc.* **2012**, *134* (5), 2706–2715. <https://doi.org/10.1021/ja210154g>.
- (43) Laidler, K. J. *Chemical Kinetics*, 3rd ed.; Pearson: London, 1987.
- (44) Geen, H.; Freeman, R. Band-Selective Radiofrequency Pulses. *J. Magn. Reson.* **1969**, *93* (1), 93–141. [https://doi.org/10.1016/0022-2364\(91\)90034-Q](https://doi.org/10.1016/0022-2364(91)90034-Q).
- (45) Hartmann, E. NMR Spectroscopic Studies on Phosphoramidite Palladium Complexes: Structures, Intermediates and Interaction Patterns. PhD Thesis, Universität Regensburg, 2012.
- (46) Woodward, R. B.; Hoffmann, R. The Conservation of Orbital Symmetry. *Angew. Chem. Int. Ed.* **1969**, *8* (11), 781–853. <https://doi.org/10.1002/anie.196907811>.
- (47) Crabtree, R. H. *The Organometallic Chemistry of the Transition Metals*, 6th ed.; John Wiley & Sons: Hoboken, 2014.
- (48) Bates, R. *Organic Synthesis Using Transition Metals*, 2nd ed.; John Wiley & Sons: Hoboken, 2012.
- (49) Misale, A.; Niyomchon, S.; Luparia, M.; Maulide, N. Asymmetric Palladium-Catalyzed Allylic Alkylation Using Dialkylzinc Reagents: A Remarkable Ligand Effect. *Angew. Chem. Int. Ed.* **2014**, *53* (27), 7068–7073. <https://doi.org/10.1002/anie.201309074>.
- (50) Smith, C. R.; RajanBabu, T. V. Efficient, Selective, and Green: Catalyst Tuning for Highly Enantioselective Reactions of Ethylene. *Org. Lett.* **2008**, *10* (8), 1657–1659. <https://doi.org/10.1021/ol800395m>.
- (51) Peer, M.; Jong, J. C. de; Kiefer, M.; Langer, T.; Rieck, H.; Schell, H.; Sennhenn, P.; Sprinz, J.; Steinhagen, H.; Wiese, B.; Helmchen, G. Preparation of Chiral Phosphorus, Sulfur and Selenium Containing 2-Aryloxazolines. *Tetrahedron* **1996**, *52* (21), 7547–7583. [https://doi.org/10.1016/0040-4020\(96\)00267-0](https://doi.org/10.1016/0040-4020(96)00267-0).
- (52) Grimme, S. Exploration of Chemical Compound, Conformer, and Reaction Space with Meta-Dynamics Simulations Based on Tight-Binding Quantum Chemical Calculations. *J. Chem. Theory Comput.* **2019**, *15* (5), 2847–2862. <https://doi.org/10.1021/acs.jctc.9b00143>.
- (53) Bannwarth, C.; Ehlert, S.; Grimme, S. GFN2-XTB – An Accurate and Broadly Parametrized Self-Consistent Tight-Binding Quantum Chemical Method with Multipole Electrostatics and Density-Dependent Dispersion Contributions. *J. Chem. Theory Comput.* **2019**, *15* (3), 1652–1671. <https://doi.org/10.1021/acs.jctc.8b01176>.
- (54) Ehlert, S.; Stahn, M.; Spicher, S.; Grimme, S. Robust and Efficient Implicit Solvation Model for Fast Semiempirical Methods. *J. Chem. Theory Comput.* **2021**, *17* (7), 4250–4261. <https://doi.org/10.1021/acs.jctc.1c00471>.
- (55) Grimme, S.; Bohle, F.; Hansen, A.; Pracht, P.; Spicher, S.; Stahn, M. Efficient Quantum Chemical Calculation of Structure Ensembles and Free Energies for Nonrigid Molecules. *J. Phys. Chem. A* **2021**, *125* (19), 4039–4054. <https://doi.org/10.1021/acs.jpca.1c00971>.
- (56) Neese, F. Software Update: The ORCA Program System – Version 5.0. *WIREs Comput. Mol. Sci.* **2022**, *12* (5), e1606. <https://doi.org/10.1002/wcms.1606>.
- (57) Grimme, S.; Antony, J.; Ehrlich, S.; Krieg, H. A Consistent and Accurate Ab Initio Parametrization of Density Functional Dispersion Correction (DFT-D) for the 94 Elements H–Pu. *J. Chem. Phys.* **2010**, *132* (15), 154104. <https://doi.org/10.1063/1.3382344>.
- (58) Weigend, F.; Ahlrichs, R. Balanced Basis Sets of Split Valence, Triple Zeta Valence and Quadruple Zeta Valence Quality for H to Rn: Design and Assessment of Accuracy. *Phys. Chem. Chem. Phys.* **2005**, *7* (18), 3297–3305. <https://doi.org/10.1039/B508541A>.
- (59) Grimme, S.; Hansen, A.; Ehlert, S.; Mewes, J.-M. R2SCAN-3c: A “Swiss Army Knife” Composite Electronic-Structure Method. *J. Chem. Phys.* **2021**, *154* (6), 064103. <https://doi.org/10.1063/5.0040021>.
- (60) Marenich, A. V.; Cramer, C. J.; Truhlar, D. G. Universal Solvation Model Based on Solute Electron Density and on a Continuum Model of the Solvent Defined by the Bulk Dielectric Constant and Atomic Surface Tensions. *J. Phys. Chem. B* **2009**, *113* (18), 6378–6396. <https://doi.org/10.1021/jp810292n>.
- (61) Becke, A. D. Density-Functional Exchange-Energy Approximation with Correct Asymptotic Behavior. *Phys. Rev. A* **1988**, *38* (6), 3098–3100. <https://doi.org/10.1103/PhysRevA.38.3098>.
- (62) Barone, V.; Cossi, M. Quantum Calculation of Molecular Energies and Energy Gradients in Solution by a Conductor Solvent Model. *J. Phys. Chem. A* **1998**, *102* (11), 1995–2001. <https://doi.org/10.1021/jp9716997>.
- (63) Lenthe, E. van; Snijders, J. G.; Baerends, E. J. The Zero-order Regular Approximation for Relativistic Effects: The Effect of Spin-Orbit Coupling in Closed Shell Molecules. *J. Chem. Phys.* **1996**, *105* (15), 6505. <https://doi.org/10.1063/1.472460>.
- (64) Mardirossian, N.; Head-Gordon, M.  $\omega$ B97M-V: A Combinatorially Optimized, Range-Separated Hybrid, Meta-GGA Density Functional with VV10 Nonlocal Correlation. *J. Chem. Phys.* **2016**, *144* (21), 214110. <https://doi.org/10.1063/1.4952647>.
- (65) Rolles, J. D.; Neese, F.; Pantazis, D. A. All-Electron Scalar Relativistic Basis Sets for the Elements Rb–Xe. *J. Comput. Chem.* **2020**, *41* (20), 1842–1849. <https://doi.org/10.1002/jcc.26355>.
- (66) Pettersen, E. F.; Goddard, T. D.; Huang, C. C.; Couch, G. S.; Greenblatt, D. M.; Meng, E. C.; Ferrin, T. E. UCSF Chimera – A Visualization System for Exploratory Research and Analysis. *J. Comput. Chem.* **2004**, *25* (13), 1605–1612. <https://doi.org/10.1002/jcc.20084>.
- (67) Ditchfield, R. Self-Consistent Perturbation Theory of Diamagnetism. *Mol. Phys.* **1974**, *27* (4), 789–807. <https://doi.org/10.1080/00268977400100711>.

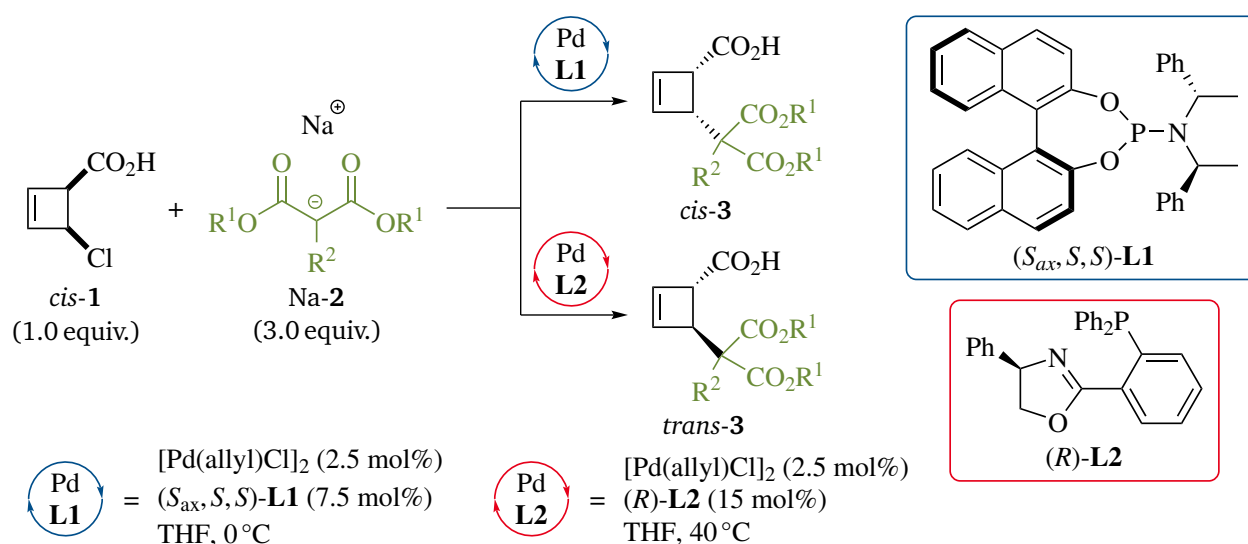


- 
- (68) Stoychev, G. L.; Auer, A. A.; Izsák, R.; Neese, F. Self-Consistent Field Calculation of Nuclear Magnetic Resonance Chemical Shielding Constants Using Gauge-Including Atomic Orbitals and Approximate Two-Electron Integrals. *J. Chem. Theory Comput.* **2018**, *14* (2), 619–637. <https://doi.org/10.1021/acs.jctc.7b01006>.
- (69) Bouten, R.; Baerends, E. J.; Lenthe, E. van; Visscher, L.; Schreckenbach, G.; Ziegler, T. Relativistic Effects for NMR Shielding Constants in Transition Metal Oxides Using the Zeroth-Order Regular Approximation. *J. Phys. Chem. A* **2000**, *104* (23), 5600–5611. <https://doi.org/10.1021/jp994480w>.
- (70) Adamo, C.; Barone, V. Exchange Functionals with Improved Long-Range Behavior and Adiabatic Connection Methods without Adjustable Parameters: The MPW and MPW1PW Models. *J. Chem. Phys.* **1998**, *108* (2), 664–675. <https://doi.org/10.1063/1.475428>.

### 4.3 Steric Influence of Nucleophile

If the selectivity determining step is governed by steric interactions between ligand and nucleophile, the selectivity is expected to be affected by the bulkiness of nucleophile. For instance, the regio- and diastereoselectivity of Mo-catalyzed allylic alkylations with prochiral oxindole nucleophiles has been reported to be sensitive towards variation of the steric demand of nucleophile.<sup>[419,420]</sup> In order to test whether the stereoselectivity of the reaction of interest exhibits such a dependency, five different malonate pronucleophiles **2a–e**, prepared by one-step proce-

**Table 4.1:** Pd-catalyzed asymmetric allylic alkylation of substrate *cis*-**1** in the presence of ligand (*S*<sub>ax</sub>, *S*, *S*)-**L1** (entries 1–5) or (*R*)-**L2** (entries 6–10), using different malonate nucleophiles Na-**2a–e**.



Entry	Ligand	Nucleophile <sup>[a]</sup>	R <sup>1</sup>	R <sup>2</sup>	Main product	d.r. of <b>3</b>	e.e. of <b>3</b> <sup>[b]</sup>
1	( <i>S</i> <sub>ax</sub> , <i>S</i> , <i>S</i> )- <b>L1</b>	Na- <b>2a</b>	Me	Me	<i>cis</i> - <b>3a</b>	92:8	85 %
2	( <i>S</i> <sub>ax</sub> , <i>S</i> , <i>S</i> )- <b>L1</b>	Na- <b>2b</b>	Et	Me	<i>cis</i> - <b>3b</b>	83:17	78 %
3	( <i>S</i> <sub>ax</sub> , <i>S</i> , <i>S</i> )- <b>L1</b>	Na- <b>2c</b>	<i>i</i> Pr	Me	<i>cis</i> - <b>3c</b>	95:5	80 %
4	( <i>S</i> <sub>ax</sub> , <i>S</i> , <i>S</i> )- <b>L1</b>	Na- <b>2d</b>	<i>t</i> Bu	Me	<i>cis</i> - <b>3d</b>	88:12	78 %
5	( <i>S</i> <sub>ax</sub> , <i>S</i> , <i>S</i> )- <b>L1</b>	Na- <b>2e</b>	<i>t</i> Bu	<i>i</i> Pr	no reaction		
6	( <i>R</i> )- <b>L2</b>	Na- <b>2a</b>	Me	Me	<i>trans</i> - <b>3a</b>	99:1	99 %
7	( <i>R</i> )- <b>L2</b>	Na- <b>2b</b>	Et	Me	<i>trans</i> - <b>3b</b>	93:7	91 %
8	( <i>R</i> )- <b>L2</b>	Na- <b>2c</b>	<i>i</i> Pr	Me	<i>trans</i> - <b>3c</b>	96:4	96 %
9	( <i>R</i> )- <b>L2</b>	Na- <b>2d</b>	<i>t</i> Bu	Me	( <i>trans</i> - <b>3d</b> ) <sup>[c]</sup>	(95:5)	(66 %)
10	( <i>R</i> )- <b>L2</b>	Na- <b>2e</b>	<i>t</i> Bu	<i>i</i> Pr	no reaction		

[a] Prepared by *in situ* deprotonation of the corresponding pronucleophile **2** with NaH prior to addition of precatalyst solution ([Pd(allyl)Cl]<sub>2</sub> and (*S*<sub>ax</sub>, *S*, *S*)-**L1** or (*R*)-**L2**) followed by substrate *cis*-**1**

[b] Determined by <sup>1</sup>H-NMR using (*S*)-1-phenylethylamine ((*S*)-PEA) as chiral solvating agent, value given for main diastereomer of product **3**

[c] ≤ 15 % yield

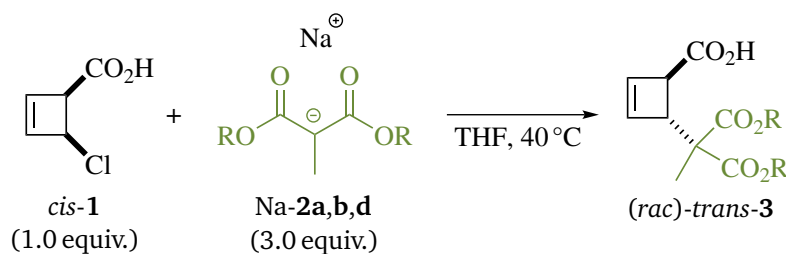
dures (**2a,c-e**)<sup>[421–423]</sup> or commercially obtained (**2b**), were subjected to the reaction conditions investigated,<sup>[56]</sup> with the reactive nucleophile Na-**2** generated by *in situ* deprotonation prior to sequential addition of catalyst and substrate *cis*-**1**. The diastereo- and enantioselectivities obtained with both **L1** and **L2** as ligand are compiled in Table 4.1.

With phosphoramidite ligand **L1**, nucleophiles Na-**2a–d** were found to be competent alkylating agents, furnishing enantioenriched substitution products *cis*-**3a–d**. The stereoselectivities observed ranged from 83:17 to 95:5 d.r. and from 78% to 85% e.e. (Table 4.1, entries 1–4), however without unambiguous correlation with the steric bulk of nucleophile. Sterically congested nucleophile Na-**2e**, on the other hand, was found to be unreactive under the reaction conditions investigated, giving only unconverted starting material along with unidentified decomposition products (4.1, entry 5).

When PHOX ligand **L2** was employed, reactions with nucleophiles Na-**2a–c** afforded deracemized products *trans*-**3a–c** with high d.r. (93:7–99:1) and e.e. values (91–99%, entries 6–8). As for reactions with ligand **L1**, the stereoselectivity of products *trans*-**3** does not display a clear dependence on the steric demand of nucleophile. Malonate salt Na-**2d** was found to react sluggish (ca. 15% conversion after 17 h), giving product *trans*-**3d** with high diastereoselectivity (95:5 d.r.), but only moderate e.e. (66%, entry 9), which can likely be attributed to an increased influence of racemic background reactivity. Nucleophile Na-**2e** again turned out not to give any substitution product (entry 10).

The extent of uncatalyzed background reaction was tested with nucleophiles Na-**2a**, Na-**2b** and Na-**2d** (Table 4.2). In all cases, reactions were found to be slow (incomplete conversion after 24 h at 40 °C), giving products (*rac*)-*trans*-**3** with inversion of configuration (93:7–99:1 d.r.).

**Table 4.2:** Slow background reactivity in the allylic alkylation of substrate *cis*-**1** with malonate nucleophiles Na-**2a,b,d**. All reactions were quenched at incomplete conversion after 24–46 h.



Entry	Nucleophile <sup>[a]</sup>	R	Main product	d.r. of <b>3</b>
1	Na- <b>2a</b>	Me	<i>trans</i> - <b>3a</b>	96:4
2	Na- <b>2b</b>	Et	<i>trans</i> - <b>3b</b>	99:1
3	Na- <b>2d</b>	<i>t</i> Bu	<i>trans</i> - <b>3d</b>	93:7

[a] Prepared by *in situ* deprotonation of the corresponding pronucleophile **2** with NaH prior to addition of *cis*-**1**

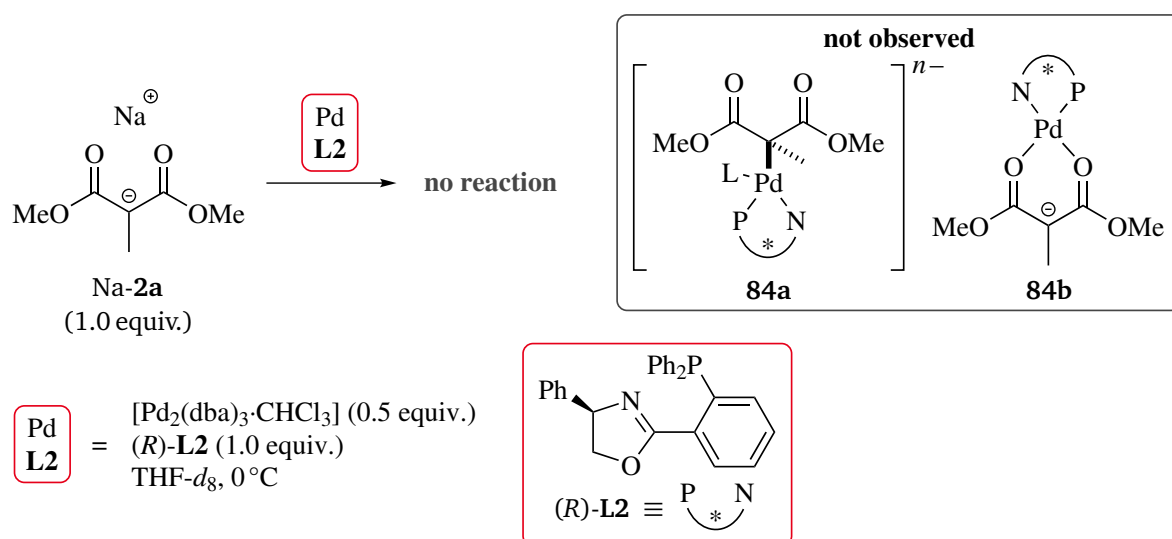
Summing up, the stereoselectivity of the reaction investigated has been shown to be independent of the bulkiness of nucleophile with ligand **L1** as well as with **L2**. Only if the catalyzed reaction is slow as a consequence of low Pd loading (see section 4.2) or a nucleophile of low reactivity, stereoselectivity might erode due to increased influence of racemic background reactivity. Overall, these results suggest that nucleophilic attack does not involve a pronounced steric interplay between ligand and nucleophile.

#### 4.4 Towards the Possibility of an Inner-Sphere Mechanism for Nucleophilic Attack

As potential explanation for the retention–inversion dichotomy observed in the nucleophilic displacement step, one might consider the malonate anion to react via an outer-sphere mechanism (i.e. as stabilized nucleophile) with ligand **L1** and via an inner-sphere path (i.e. as non-stabilized nucleophile) with **L2** (cf. Scheme 2.10). The latter scenario has been suggested for Mo-catalyzed allylic alkylations with malonate nucleophiles,<sup>[211]</sup> for which nucleophilic attack has been shown to proceed under retention.<sup>[210–213]</sup>

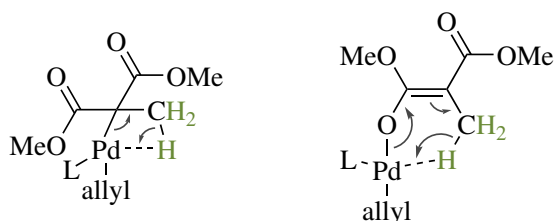
For undergoing inner-sphere nucleophilic attack, the nucleophile needs to be capable of coordinating to the Pd-center. Various Pd–malonate complexes have been reported in the literature, with the malonate anion acting either as monodentate *C* ligand<sup>[424–427]</sup> or as bidentate *O,O* chelator.<sup>[428–431]</sup> However, when model nucleophile Na-**2a** was treated with stoichiometric amounts of [Pd<sub>2</sub>(dba)<sub>3</sub>·CHCl<sub>3</sub>] and (*R*)-**L2**, neither C-coordinated complex **84a** nor O,O-chelated Pd species **84b** could be detected by NMR and HRMS analysis (Scheme 4.7).

It should be noted, though, that this experiment has limited significance, given that a zero-valent Pd source was used, whereas the catalytic Pd–allyl intermediate has an oxidation state of +II. Therefore, a further attempt to obtain evidence for a potential inner-sphere path was undertaken



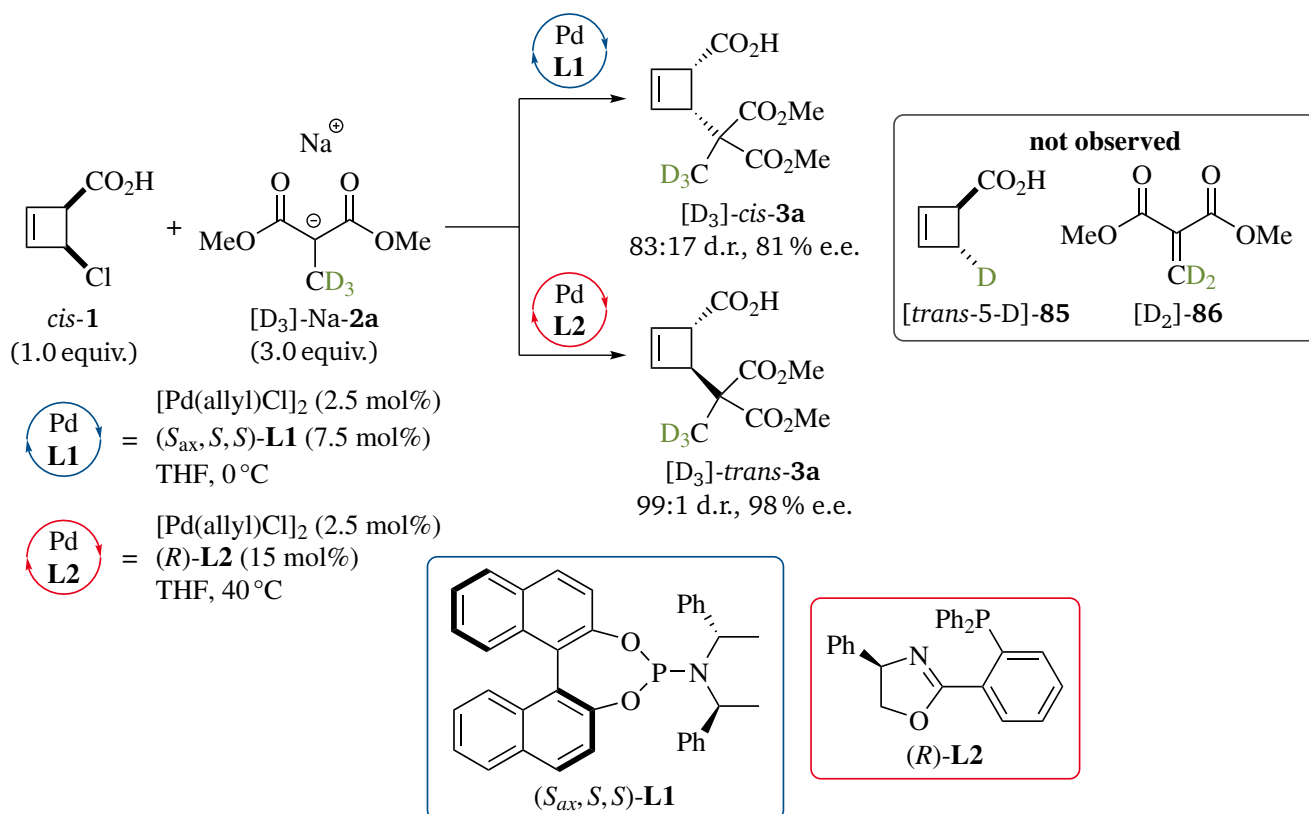
**Scheme 4.7:** Unsuccessful attempt to prepare a Pd–malonate complex **84**, with L being a variable ligand such as dba, a solvent molecule or an additional malonate anion.

under catalytic conditions. If the malonate undergoes transient Pd–C coordination with the Pd-center, a  $\beta$ -hydride elimination would be expected as side reaction.<sup>[120–122]</sup> Similarly, an inner-sphere intermediate with the malonate anion coordinating in a Pd–O fashion bond might give rise to a detectable extent of  $\delta$ -hydride elimination, leading to the same side products. The latter process, which is less prominent than the well-known  $\beta$ -hydride elimination, has been proposed to be operative in other Pd-catalyzed transformations.<sup>[432–434]</sup> Both side reactions are illustrated in Scheme 4.8



**Scheme 4.8:**  $\beta$ - (Left) and  $\delta$ -hydride elimination (right) as potential side reactions in allylic alkylations with malonate nucleophile Na-**2a**, provided an inner-sphere mechanism is operative.

In order to track these potential side reactions and distinguish them from other formal hydrodehalogenation paths such as protodepalladation,<sup>[435]</sup> deuterated malonate salt  $[D_3]$ -Na-**2a** was employed as nucleophile in the allylic alkylation of *cis*-**1**. However, only substitution products



**Scheme 4.9:** Labeling studies on the allylic alkylation of substrate *cis*-**1**, using deuterated nucleophile  $[D_3]$ -Na-**2a**.

---

[D<sub>3</sub>]-**3a** were obtained with both ligand **L1** and **L2**, and no detectable amounts of β/δ-deuteride elimination products [*trans*-5-D]-**85** and [D<sub>2</sub>]-**86** were identified by <sup>2</sup>H-NMR and ESI-HRMS analysis (Scheme 4.9).

Hence, no evidence could be obtained supporting that an inner-sphere mechanism was responsible for the unusual stereospecificity of nucleophilic attack with PHOX ligand **L2**. Given that, furthermore, inner-sphere attack has under Pd catalysis only been proposed for the somewhat less stabilized enolate anions,<sup>[136,436–439]</sup> but is – to the best of the author’s knowledge – unprecedented for malonate anions, this path seems improbable and was therefore not further pursued.

---

## 4.5 Kinetic Analysis

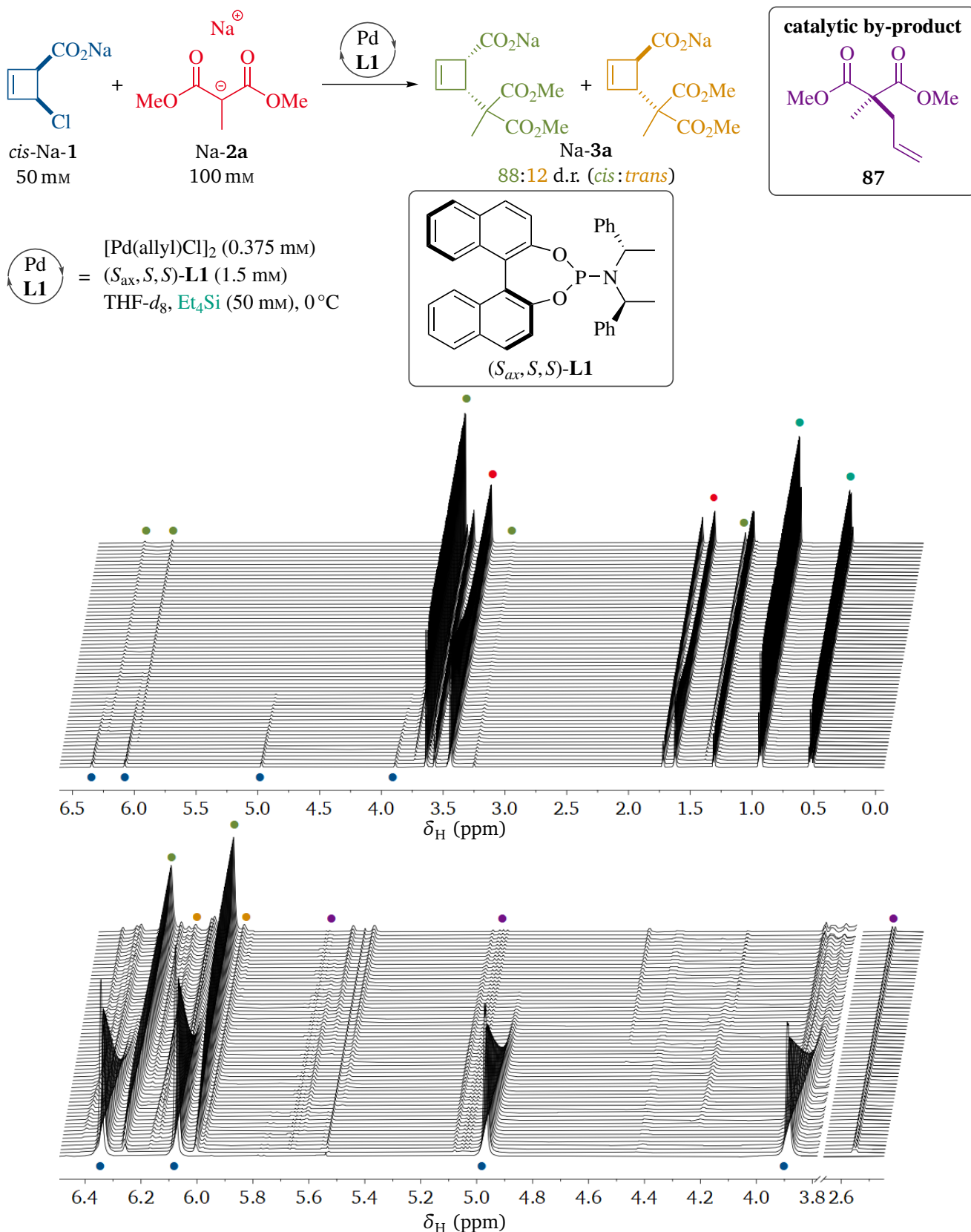
---

In order to gain deeper insight into the role of the different reaction components, the allylic alkylation of cyclobutenes was further investigated by a kinetic analysis. The aim was to extract apparent rate orders in substrate, nucleophile and catalyst, allowing for determination of the turnover-limiting step. To this end, experimental conditions for reproducible quantitative <sup>1</sup>H-NMR reaction monitoring were established, as described in subsection 4.5.1. Kinetic characterization was subsequently achieved by complementary use of the initial rate method<sup>[440]</sup> and reaction progress kinetic analysis (RPKA),<sup>[441]</sup> the results of which are presented in parts 4.5.2 and 4.5.3, respectively. The rate orders obtained are eventually discussed in subsection 4.5.4.

### 4.5.1 Model Reaction and Quantitative Reaction Monitoring

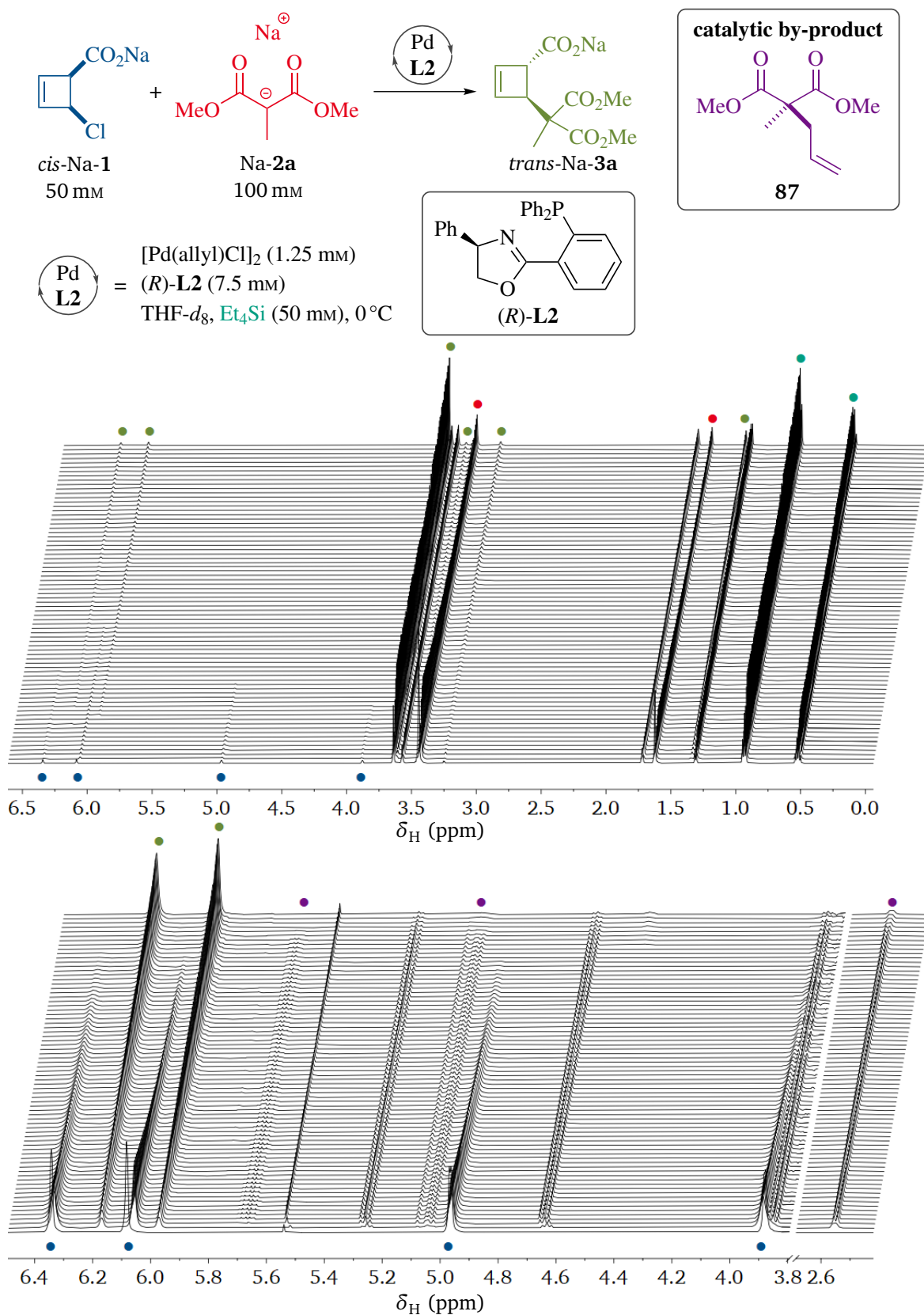
Kinetic analysis was performed on the catalytic reaction of substrate *cis*-**1** with malonate nucleophile Na-**2a**, which has already been employed as model reaction in section 4.2. Et<sub>4</sub>Si<sup>[442,443]</sup> was chosen as internal standard for <sup>1</sup>H-NMR reaction monitoring, enabling calculation of absolute concentrations. Mixing of starting materials *cis*-**1** and Na-**2a** resulted in immediate deprotonation of *cis*-**1** to give its sodium salt *cis*-Na-**1**, consuming 1 equiv. of Na-**2a**. This step tended to be accompanied by a low extent of decomposition and was therefore performed carefully upon cooling.

With ligand **L1**, starting concentrations of 50 mM *cis*-Na-**1**, 100 mM Na-**2a**, 50 mM Et<sub>4</sub>Si, 0.375 mM [Pd(allyl)Cl]<sub>2</sub> and 1.5 mM **L1** were found to allow for convenient <sup>1</sup>H-NMR reaction monitoring, giving the spectral series shown in Figure 4.1. Upon addition of Pd source and ligand, the formation of both major product *cis*-Na-**3a** and minor diastereomer *trans*-Na-**3a** could be observed. Furthermore, the spectra showed that dimethyl 2-allyl-2-methylmalonate **87** is formed as initiation by-product, consistent with a precatalyst activation by nucleophilic displacement of [Pd(allyl)Cl]<sub>2</sub> with Na-**2a** to give the reactive zerovalent Pd species along with an equimolar amount of **87**. Thus, integration of the resonances of **87** allowed for calculating the concentration of active Pd<sup>0</sup> (see also section 4.2, Scheme S4 in the supporting information).



**Figure 4.1:** <sup>1</sup>H-NMR monitoring of the model reaction investigated, using ligand (*S*<sub>ax</sub>, *S*, *S*)-L1: Spectral region of interest (top) and enlarged view (bottom), with resonances of substrate *cis*-Na-1, nucleophile Na-2a, substitution products *cis*-3a (major) and *trans*-3a (minor), catalytic by-product **87** and internal standard Et<sub>4</sub>Si assigned. The reaction was monitored over 60 min, with the time course in the spectral series running from bottom to top.



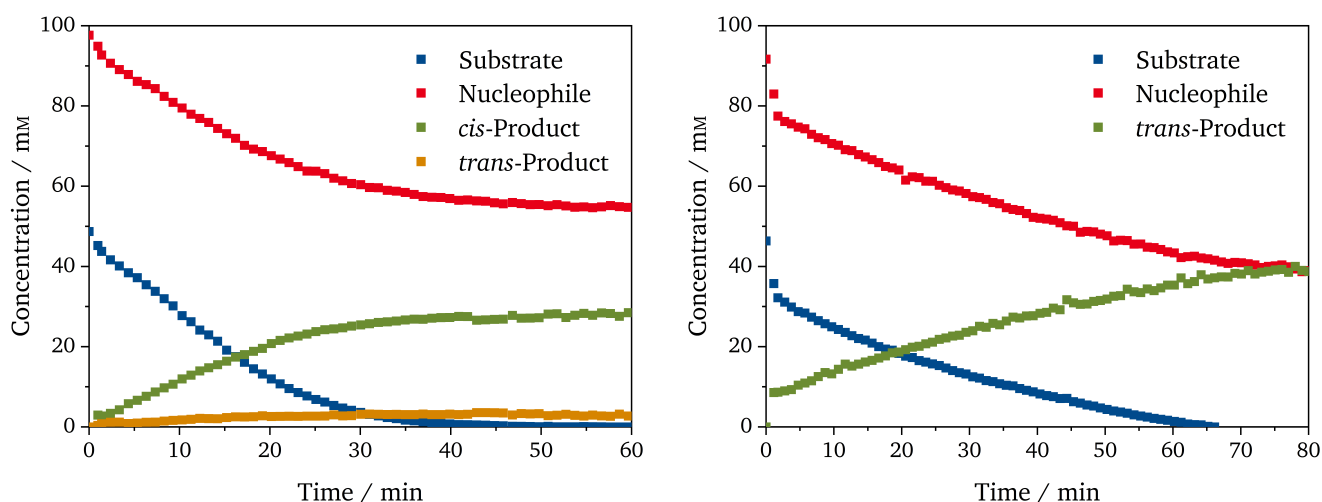


**Figure 4.2:** <sup>1</sup>H-NMR monitoring of the model reaction investigated, using ligand (*R*)-L2: Spectral region of interest (top) and enlarged view (bottom), with resonances of substrate *cis*-Na-1, nucleophile Na-2a, substitution product *trans*-3a, catalytic by-product 87 and internal standard Et<sub>4</sub>Si assigned. The reaction was monitored over 80 min, with the time course in the spectral series running from bottom to top.



The analogous reaction with ligand **L2** was monitored under similar conditions, albeit requiring a significantly higher precatalyst concentration of 1.25 mM [Pd(allyl)Cl]<sub>2</sub> and 7.5 mM **L2** for proceeding to completion within a comparable reaction time (Figure 4.2). Other than with **L1**, only the main product diastereomer *trans*-Na-**3a** could be detected in the spectral series.

Quantification of the reaction monitoring data obtained gave the temporal concentration profiles shown in Figure 4.3. Strikingly, the reaction catalyzed by [Pd-**L2**] exhibited an initial boost giving 23 % conversion within the dead time of 68 s, followed by strongly attenuated turnover. With **L1**, on the other hand, no such drop of turnover rate in the initial phase of the reaction was observed.



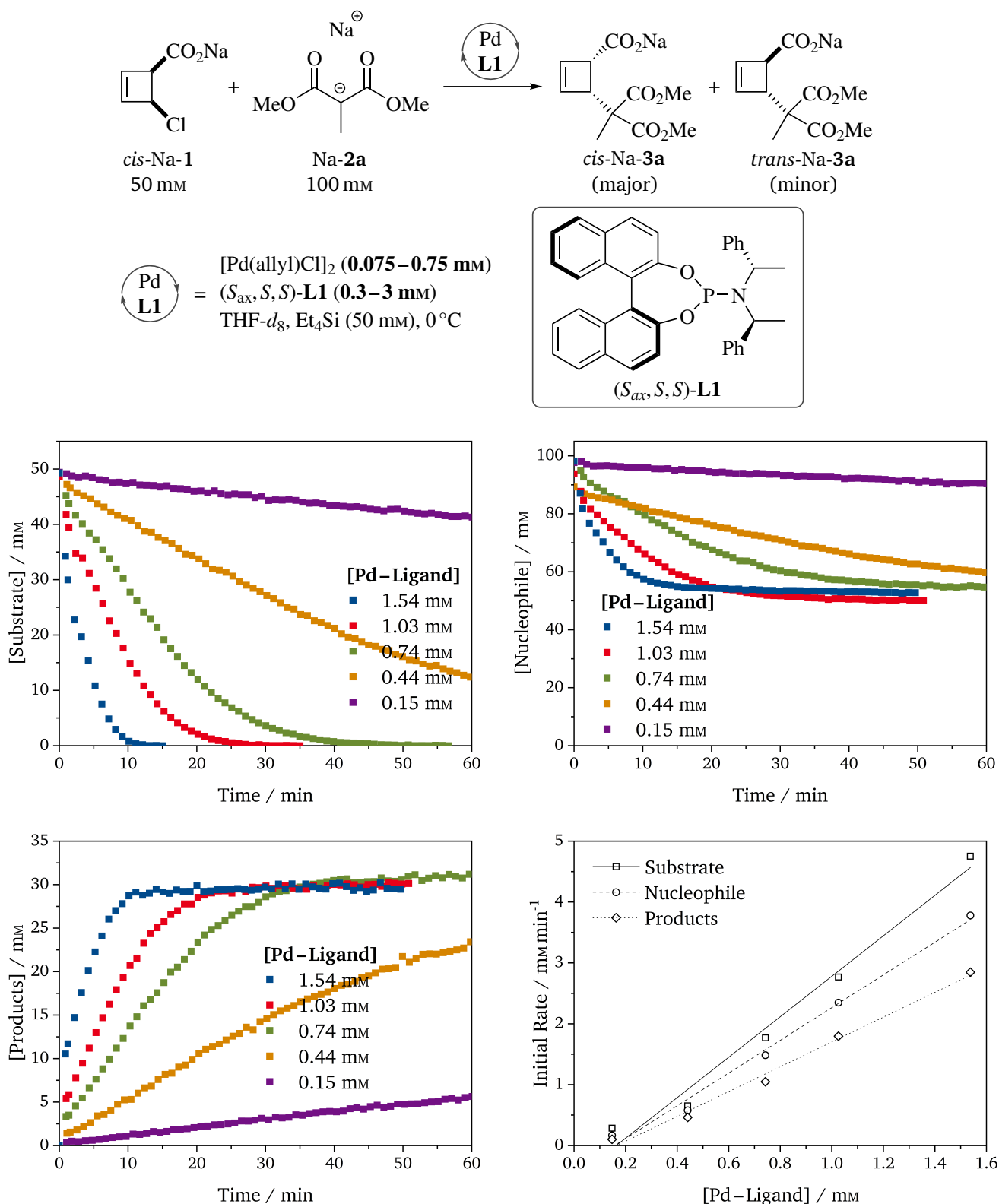
**Figure 4.3:** Typical temporal concentration profiles for the model reaction investigated, using ligand (*S*<sub>ax</sub>,*S,S*)-**L1** (left) and (*R*)-**L2** (right), respectively. Concentrations extracted from the <sup>1</sup>H-NMR reaction monitoring data shown in Figures 4.1 and 4.2 by integration against internal standard Et<sub>4</sub>Si.

With optimized conditions for facile reaction monitoring in hand, the kinetic behavior of the reaction investigated was explored. The results obtained are disclosed in the following.

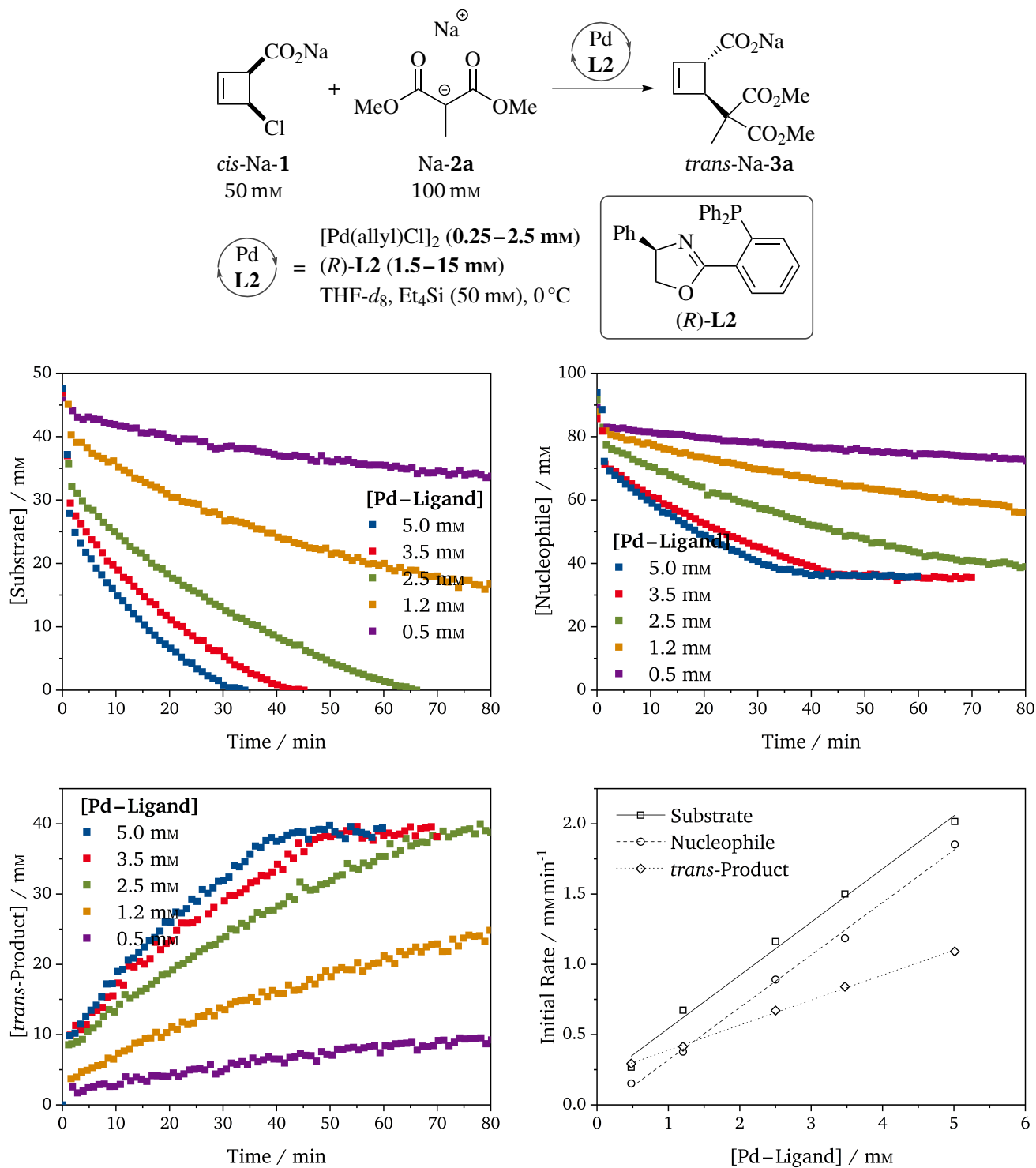
#### 4.5.2 Initial Rate Analysis

Initial rate analysis has been shown to be a robust tool for extraction of apparent rate orders, without the need for making simplifying assumptions upon mathematical treatment.<sup>[444–449]</sup> In order to extract rate orders in substrate, nucleophile and catalyst by means of the initial rate approach, the concentration of these components was varied systematically.

With both ligand **L1** and **L2**, the turnover rate was found to react highly sensitive upon variation of catalyst concentration (Figures 4.4 and 4.5). Initial rates extracted from the temporal concentration profiles of substrate *cis*-Na-**1**, nucleophile Na-**2a** and products Na-**3a** (both diastereomers for **L1**, only *trans* for **L2**) consistently displayed a proportional dependence on the concentration of active Pd<sup>0</sup>, showing that the reaction is first order in catalyst under both conditions investigated.



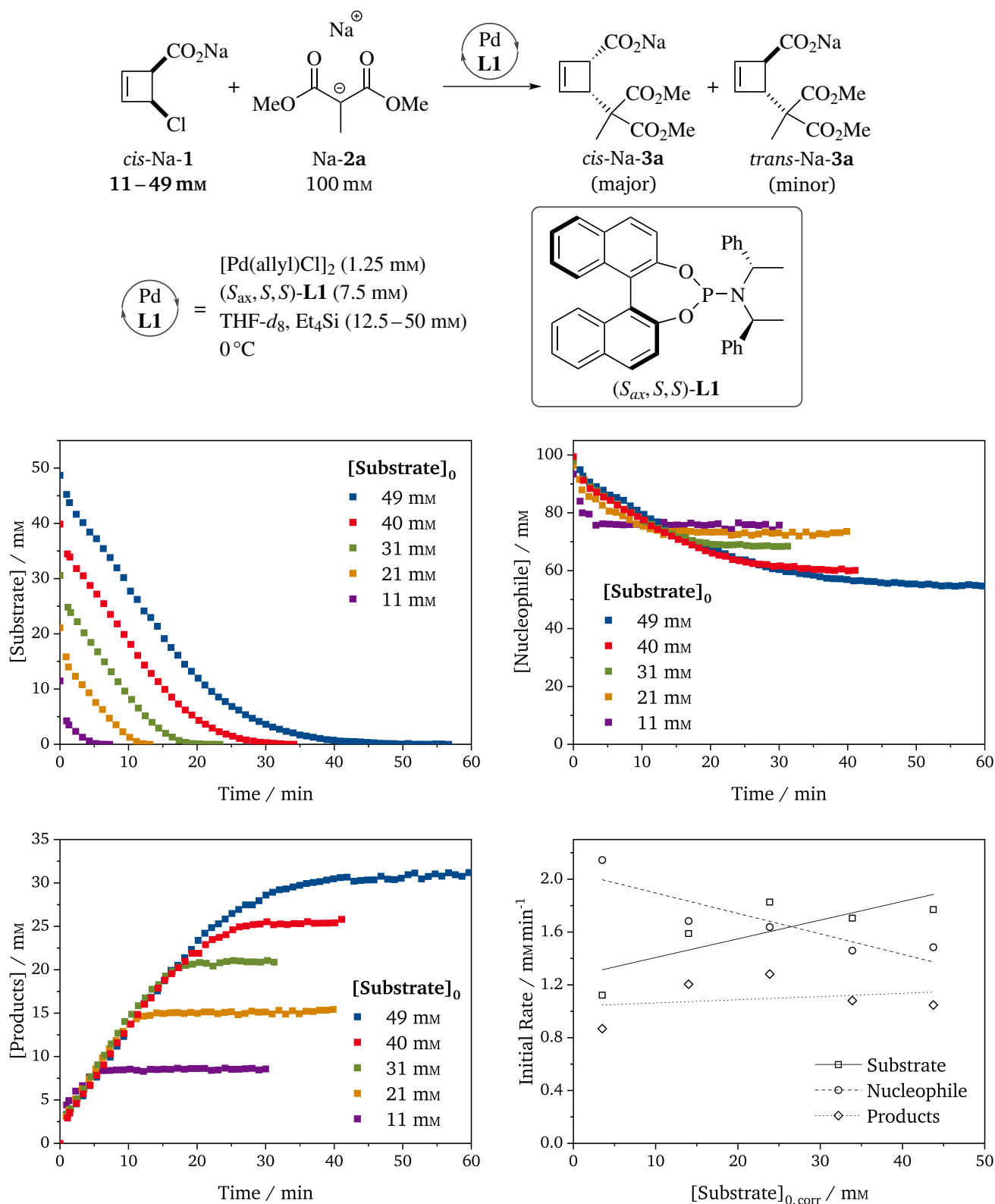
**Figure 4.4:** Temporal concentration profiles of substrate *cis*-Na-1, nucleophile Na-2a and products Na-3a (both diastereomers) at different Pd–ligand concentrations with (*S*<sub>ax</sub>, *S*, *S*)-L1 as ligand, and resulting initial rate plot indicating a first-order dependence. The concentration of active Pd catalyst [Pd–Ligand] was determined from the relative integral of the initiation by-product **87**.



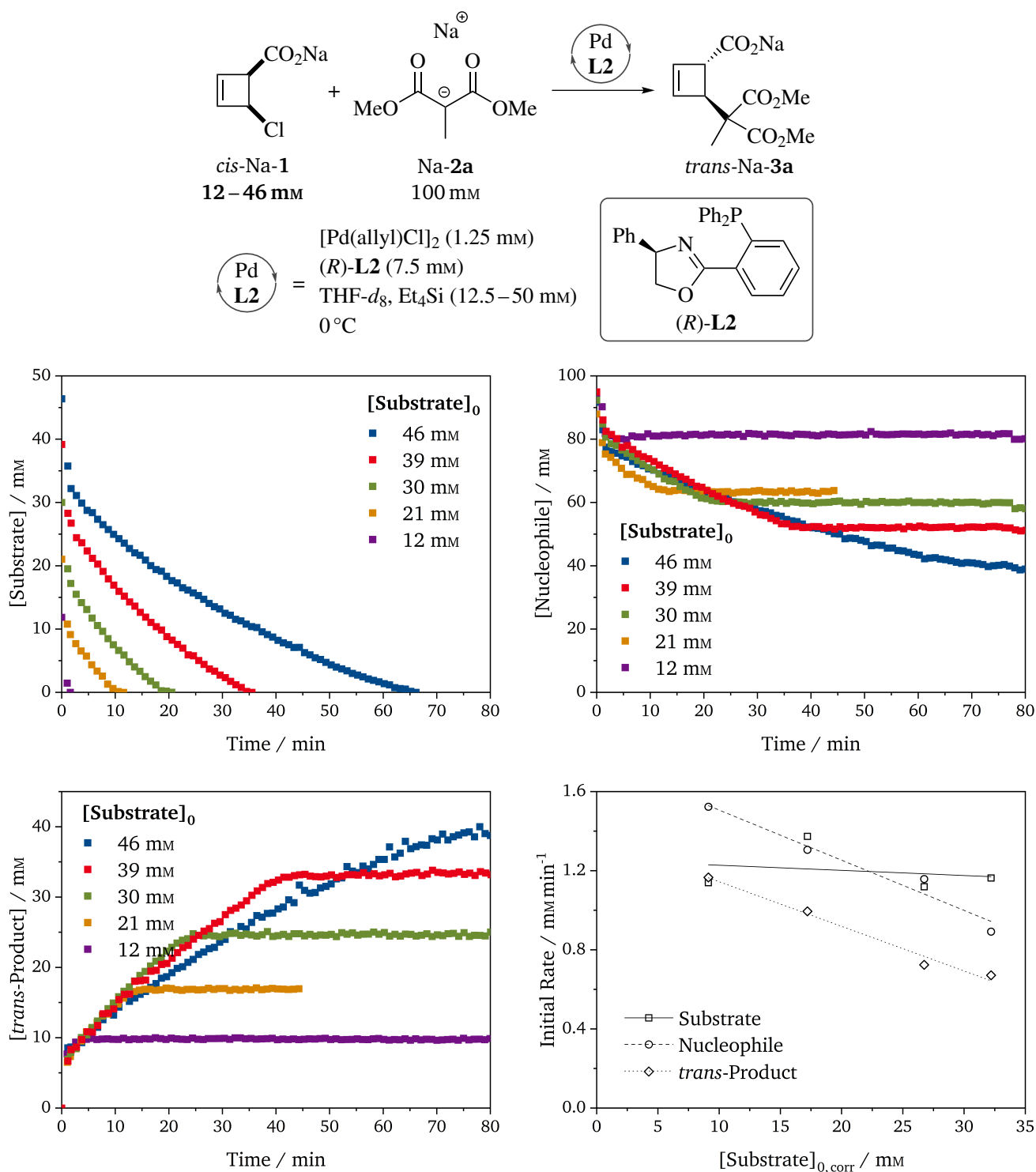
**Figure 4.5:** Temporal concentration profiles of substrate *cis*-Na-1, nucleophile Na-2a and product *trans*-Na-3a at different Pd–ligand concentrations with (*R*)-L2 as ligand, and resulting initial rate plot indicating a first-order dependence. The concentration of active Pd catalyst [Pd–Ligand] was determined from the relative integral of the initiation by-product **87**.

---

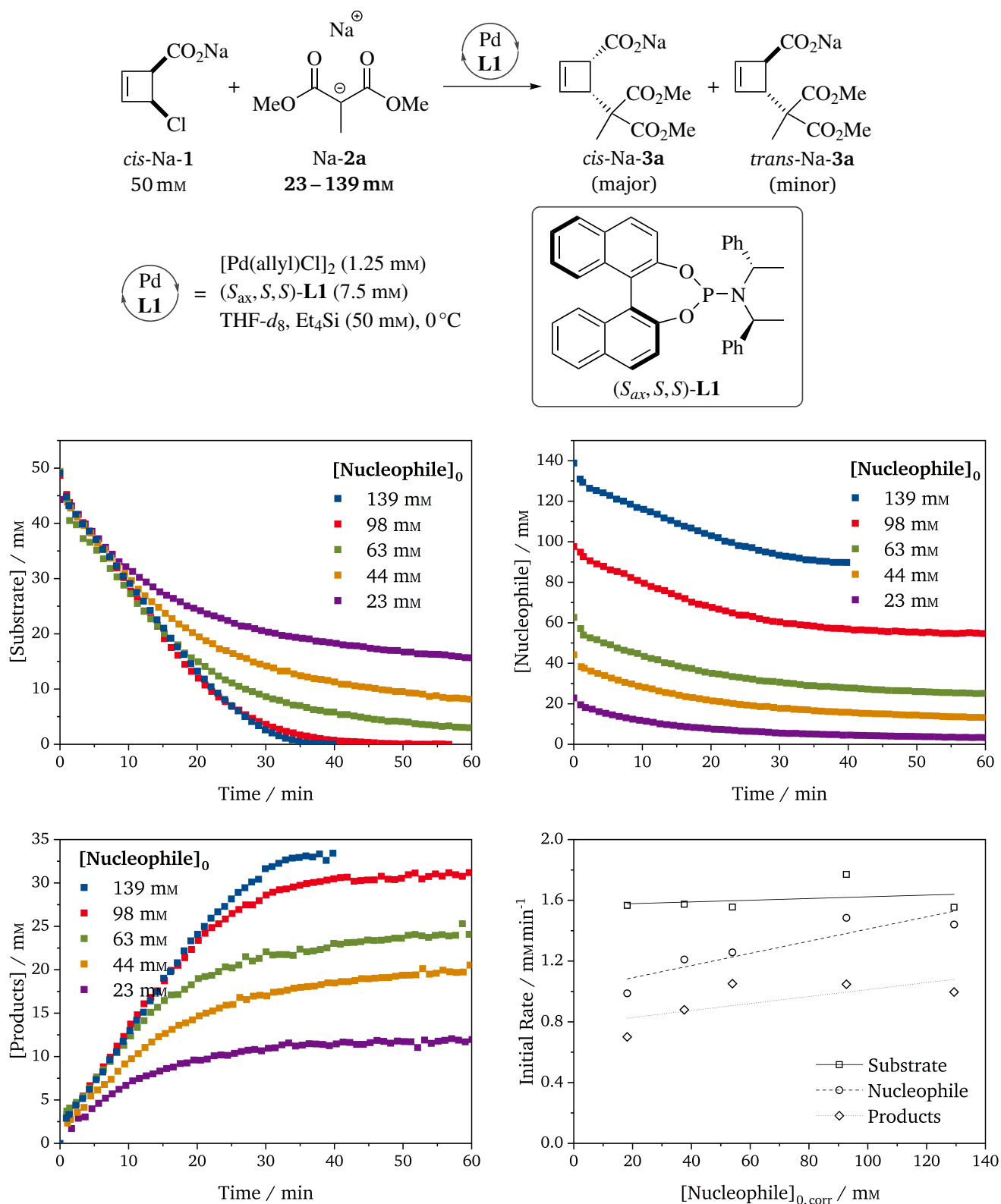
Conversely, variation of substrate concentration turned out not to have a strong influence on the reaction rate (Figures 4.6 and 4.7). The temporal product concentration profiles recorded at different initial substrate concentrations are approximately superimposable over a large part of the reaction, which is characteristic for a zero-order dependence. The initial rates extracted are not perfectly independent of substrate concentration, especially with ligand **L2**. This can, however, likely be attributed to experimental errors of catalyst and nucleophile concentration. When the concentration of nucleophile Na-**3a** was screened, strikingly different effects were observed for **L1** and **L2**. With ligand **L1**, initial rate analysis reveals a zero-order behavior, as evident from the product concentration profiles overlaying for the initial phase of the reaction and the experimental initial rates being nearly independent of the starting concentration of nucleophile (Figure 4.8). In the presence of **L2**, on the other hand, the initial rates extracted turned out to increase proportionally with the starting concentration of Na-**3a**, disclosing that the reaction is first order in nucleophile under these conditions (Figure 4.9).



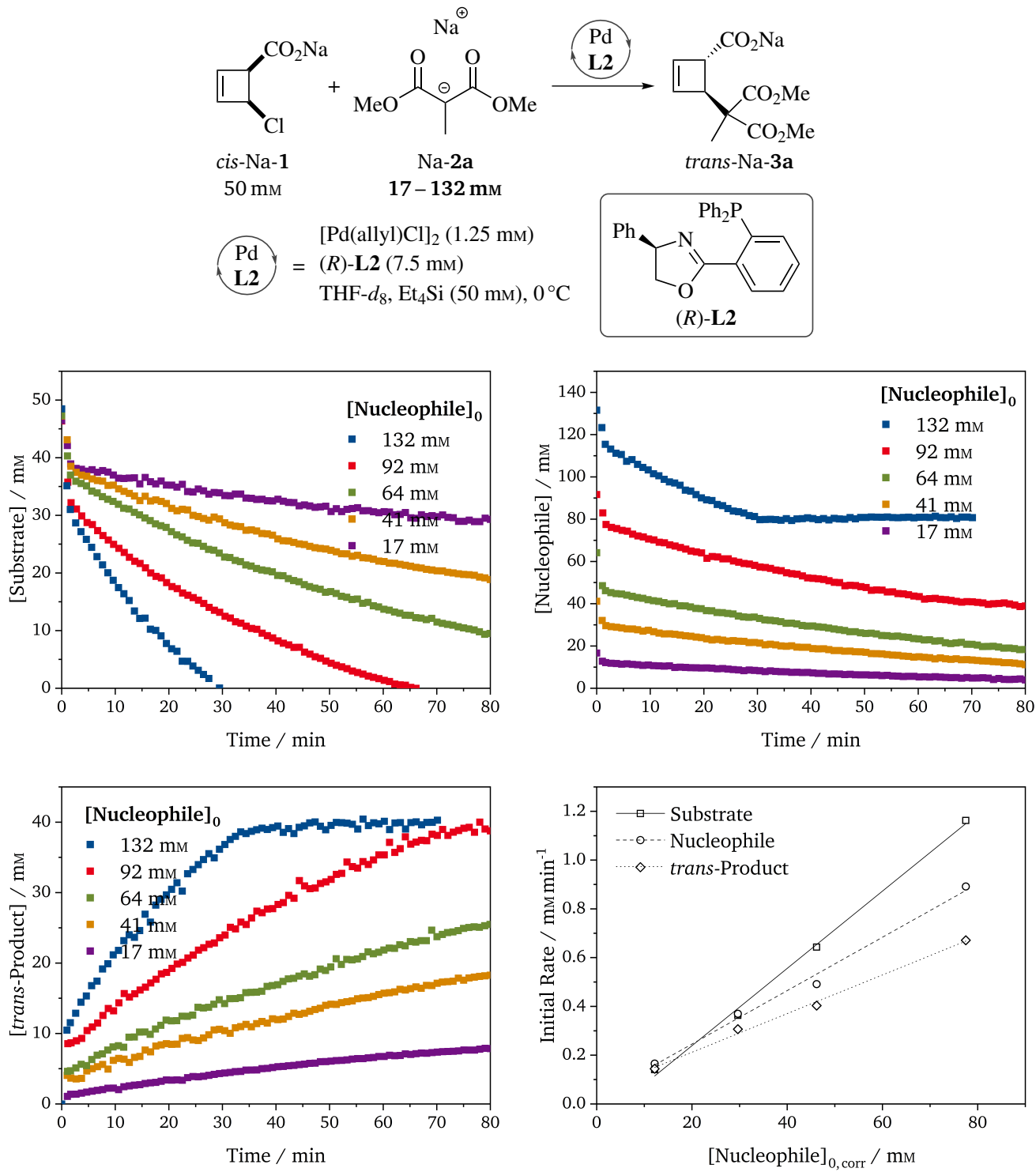
**Figure 4.6:** Temporal concentration profiles of substrate *cis*-Na-1, nucleophile Na-2a and products Na-3a (both diastereomers) at different initial concentrations of *cis*-Na-1 with (*S*<sub>ax</sub>, *S*, *S*)-L1 as ligand, and resulting initial rate plot suggesting a zero-order dependence. The initial concentrations [Substrate]<sub>0</sub> given were determined by <sup>1</sup>H-NMR after mixing *cis*-1 and Na-2a, resulting in deprotonation of *cis*-1 with 1 equiv. of Na-2a. For the initial rate plot, the concentrations [Substrate]<sub>0,corr</sub> plotted were determined from the first spectrum after catalyst addition, in order to correct for conversion during dead time.



**Figure 4.7:** Temporal concentration profiles of substrate *cis*-Na-1, nucleophile Na-2a and product *trans*-Na-3a at different initial concentrations of *cis*-Na-1 with (*R*)-L2 as ligand, and resulting initial rate plot suggesting a zero-order dependence. The initial concentrations [Substrate]<sub>0</sub> given were determined by <sup>1</sup>H-NMR after mixing *cis*-1 and Na-2a, resulting in deprotonation of *cis*-1 with 1 equiv. of Na-2a. For the initial rate plot, the concentrations [Substrate]<sub>0,corr</sub> plotted were determined from the first spectrum after catalyst addition, in order to correct for conversion during dead time. For the run with the lowest concentration of *cis*-Na-1 (12 mM), accurate initial rates could not be extracted.



**Figure 4.8:** Temporal concentration profiles of substrate *cis*-Na-1, nucleophile Na-2a and products Na-3a (both diastereomers) at different initial concentrations of Na-2a with (*S*<sub>ax</sub>, *S*, *S*)-L1 as ligand, and resulting initial rate plot indicating a zero-order dependence. The initial concentrations [Nucleophile]<sub>0</sub> given were determined by <sup>1</sup>H-NMR after mixing *cis*-1 and Na-2a, resulting in deprotonation of *cis*-1 with 1 equiv. of Na-2a. For the initial rate plot, the concentrations [Nucleophile]<sub>0,corr</sub> plotted were determined from the first spectrum after catalyst addition, in order to correct for conversion during dead time.

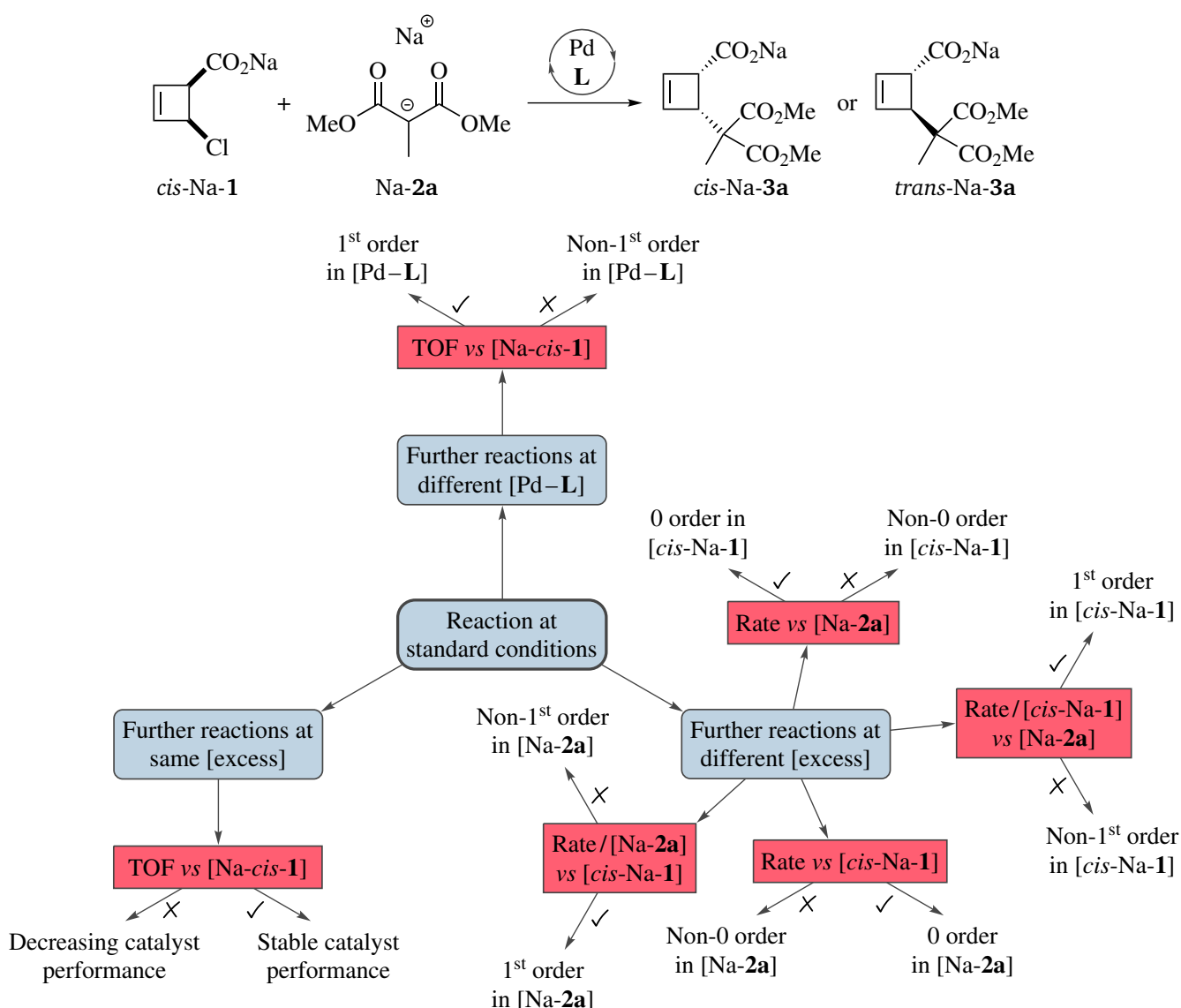


**Figure 4.9:** Temporal concentration profiles of substrate *cis*-Na-1, nucleophile Na-2a and product *trans*-Na-3a at different initial concentrations of Na-2a with (R)-L2 as ligand, and resulting initial rate plot indicating a first-order dependence. The initial concentrations [Nucleophile]<sub>0</sub> given were determined by <sup>1</sup>H-NMR after mixing *cis*-1 and Na-2a, resulting in deprotonation of *cis*-1 with 1 equiv. of Na-2a. For the initial rate plot, the concentrations [Nucleophile]<sub>0,corr</sub> plotted were determined from the first spectrum after catalyst addition, in order to correct for conversion during dead time. The run with the highest starting concentration of Na-2a (132 mM) was not used for initial rate analysis, as it was carried out with different stock solutions than the other reactions.



### 4.5.3 Reaction Progress Kinetic Analysis (RPKA)

In order to confirm the rate orders extracted by the initial rate method, the reaction monitoring data recorded were reanalyzed by means of RPKA as a complementary tool. This approach additionally offers the advantage of visualizing potential changes during turnover, as it considers the total course of the reaction rather than being limited to its initial period.<sup>[441,450,451]</sup> The analysis was carried out following the workflow for a catalytic two-substrates reaction developed by BLACKMOND<sup>[441]</sup> (Scheme 4.10). For detailed deviation of the mathematical manipulations on which the graphical analyses are based on, the reader is referred to references [441] and [450]. Importantly, rate order determination by RPKA is generally based on the assumption that no side reactions occur.<sup>[441,450,451]</sup>



**Scheme 4.10:** Workflow for RPKA performed in this work, following the procedure reported by BLACKMOND.<sup>[441]</sup> Boxes highlighted in blue indicate reaction monitoring experiments to be carried out. Boxes colored in red correspond to plots to be constructed. Check marks (✓) indicate superimposing graphs, whereas X marks (X) mark curves which are not overlaying.

For performing an RPKA, experimental data for the turnover rate  $\nu$  as a function of substrate concentration are required. To this end, the concentrations of *cis*-Na-1 determined at different reaction times  $t$  were transformed into approximated turnover rates using slope triangles, i.e.

$$\nu = -\frac{d[\text{Substrate}]}{dt} \approx -\frac{\Delta[\text{Substrate}](t)}{\Delta t}, \quad (4.1)$$

where  $\Delta t$  and  $\Delta[\text{Substrate}](t)$  are the changes in reaction time and substrate concentration between two data points, respectively.

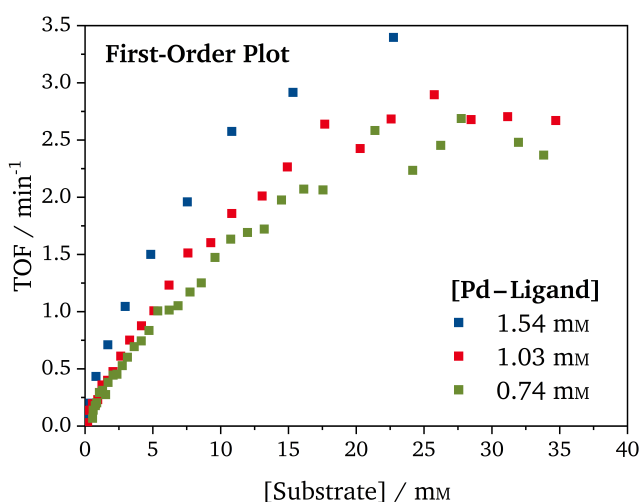
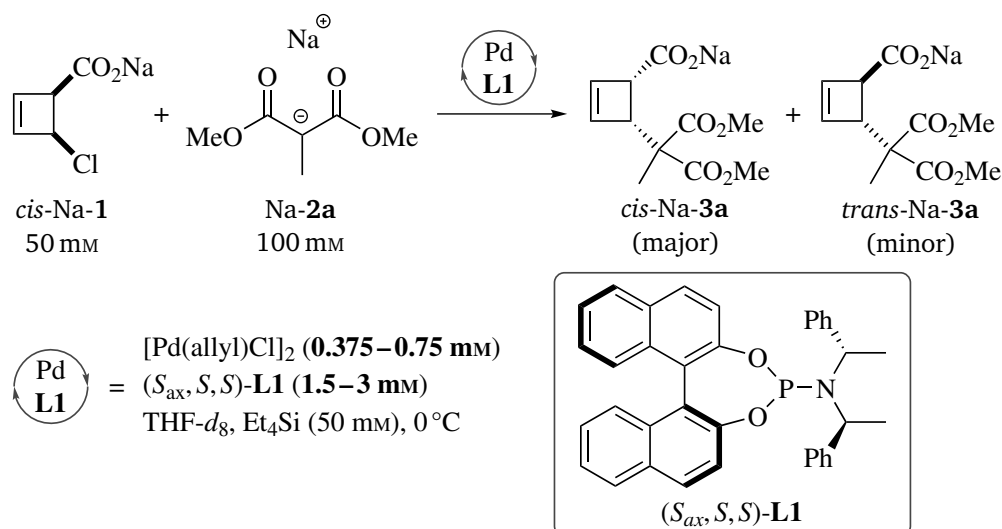
The rate order in catalyst was probed by plotting the turnover frequency (TOF) =  $\frac{\nu}{[\text{Pd-Ligand}]}$  [452] against the concentration of substrate *cis*-Na-1 for different catalyst concentrations  $[\text{Pd-Ligand}]$ . In case of a first-order dependence on  $[\text{Pd-Ligand}]$ , as extracted by initial rate analysis (subsection 4.5.2), the curves are expected to overlay. [441,450,451] When the kinetic data of the model reaction performed in the presence of ligand **L1** at three different catalyst concentrations were treated in this way, moderately overlaying graphs were obtained (Figure 4.10), which – albeit not unambiguous – verifies the first-order behavior determined in subsection 4.5.2. A better superimposition was obtained in the analogous plot for ligand **L2**, confirming that the reaction is first order in catalyst (Figure 4.11).

The deviation from exact overlays in the case of ligand **L1** can likely be explained by a significant contribution of unidentified side reactions, violating a basic assumption of RPKA (*vide supra*). In fact, the reaction investigated typically reaches NMR yields of about 68% with **L1** (both diastereomers of product Na-3a) and 84% with **L2** upon full conversion of substrate *cis*-Na-1, i.e. 32% and 16% side reactions, respectively. Hence, the RPKA plots obtained are generally expected to be distorted by side reactions, especially when ligand **L1** is employed.

The rate orders in substrate and nucleophile were examined by comparing mathematically manipulated kinetic profiles of reactions performed at different excess concentrations

$$[\text{excess}] = [\text{Nucleophile}]_0 - [\text{Substrate}]_0, \quad (4.2)$$

calculated from the initial concentrations of nucleophile and substrate  $[\text{Nucleophile}]_0$  and  $[\text{Substrate}]_0$ , respectively. In RPKA, the  $[\text{excess}]$  represents a central parameter to reduce complexity in rate order laws of two-substrates reactions and is assumed to be constant during turnover, based on the general neglect of side reactions. [441,450] With ligand **L1**, neither the zero-order plot for substrate *cis*-Na-1 (rate vs  $[\text{Nucleophile}]$ ) nor the corresponding first-order plot ( $\frac{\text{rate}}{[\text{Substrate}]}$  vs  $[\text{Nucleophile}]$ ) exhibit overlaying graphs (Figure 4.12, top). Hence, RPKA does not lead to a reasonable rate order in substrate under these conditions, which is again attributed to side reactions making the assumption of a constant  $[\text{excess}]$  inaccurate. Conversely, the zero-order plot with respect to nucleophile Na-2a (rate vs  $[\text{Substrate}]$ ) displays superimposing

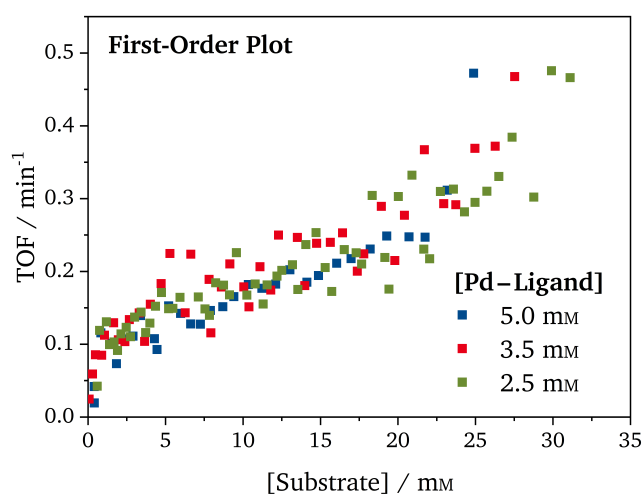
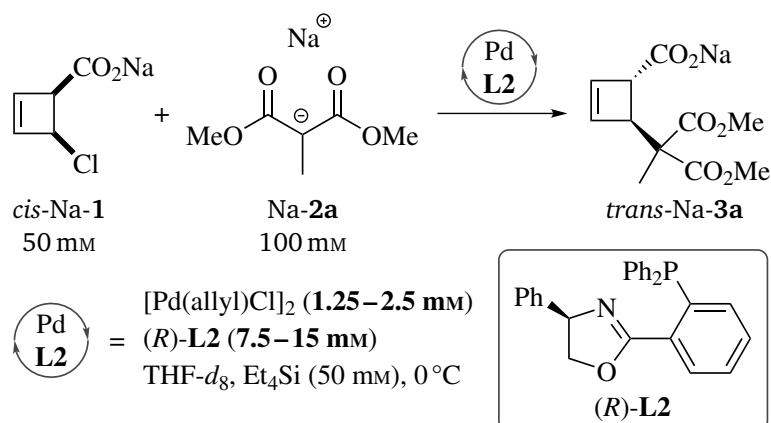


**Figure 4.10:** Examination of rate order in catalyst by RPKA, using  $(S_{ax}, S, S)\text{-L1}$  as ligand: TOF plotted against the concentration of substrate *cis*-Na-1 for different Pd–ligand concentrations, with the approximately overlaying curves suggesting a first-order dependence.

curves only at the beginning of the reactions (i.e. high substrate concentration), whereas in the respective first-order plot ( $\frac{\text{rate}}{[\text{Substrate}]}$  vs [Substrate]) the graphs approximately overlay at high conversion (low substrate concentrations). This suggests a change of rate order in nucleophile from zero to one with increasing conversion (Figure 4.12, bottom).

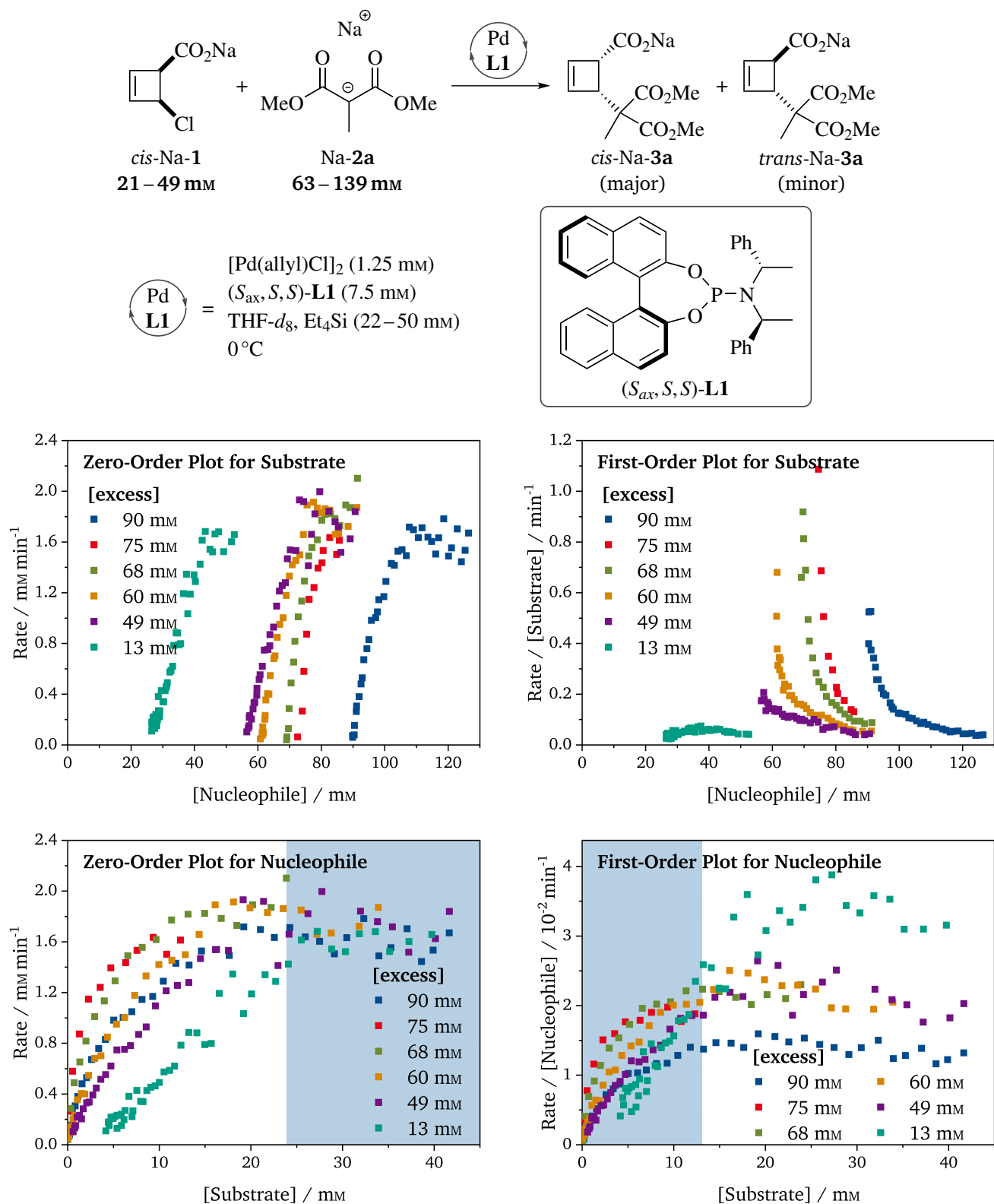
When ligand **L2** was employed, RPKA clearly indicates the reaction to be zero order in substrate, as shown by the kinetic profiles overlaying in the zero-order plot, but not in the first-order plot (Figure 4.13, top). This result is in line with the outcome of initial rate analysis. For nucleophile Na-2a, neither the zero-order nor the first-order plot exhibit superimposition (Figure 4.13, bottom). Thus, RPKA does not allow for determining a rate order in nucleophile with **L2** as ligand.

In order to probe if catalyst deactivation occurs during turnover, reaction monitoring experiments were performed at two different starting concentrations of substrate *cis*-Na-1 and nucleophile

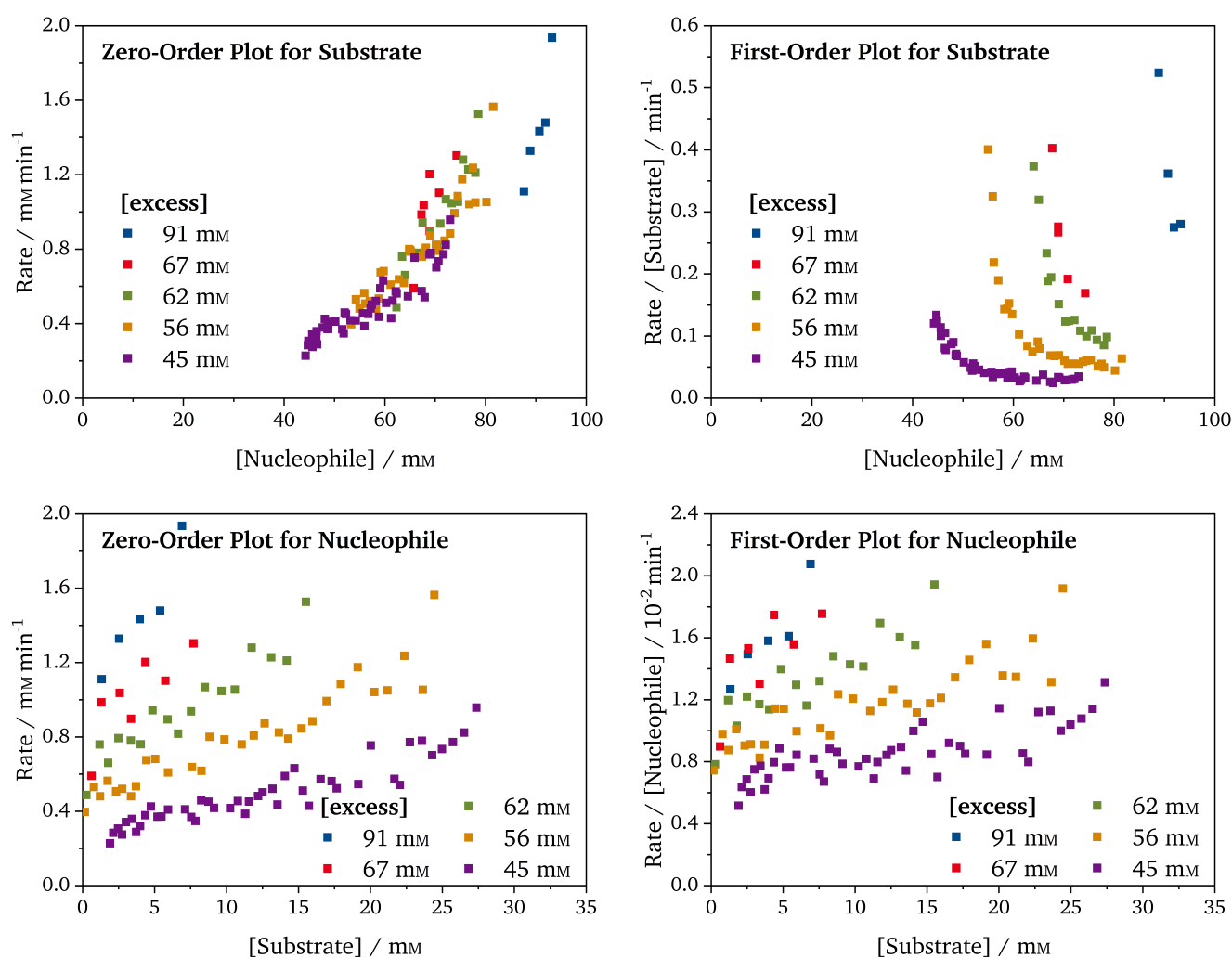
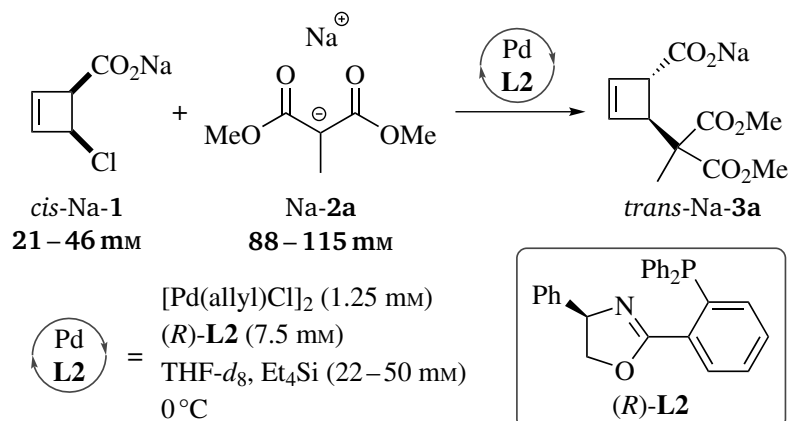


**Figure 4.11:** Examination of rate order in catalyst by RPKA, using  $(R)\text{-L2}$  as ligand: TOF plotted against the concentration of substrate  $\text{cis-Na-1}$  for different Pd–ligand concentrations, with the overlaying curves indicating first-order dependence.

$\text{Na-2a}$ , but approximately equal [excess] values. This simulates an identical reaction started from two different substrate concentrations, with the one carried out at higher  $[\text{Substrate}]_0$  having completed more turnovers at a given substrate concentration.<sup>[441,450,451]</sup> Realizing reactions with exactly identical [excess] was found to be challenging, since – due to initial protonation of 1 equiv. of nucleophile – experimental deviations of  $[\text{Substrate}]_0$  influence  $[\text{Nucleophile}]_0$  in the opposite direction. Nevertheless, evidence for catalyst deactivation could be obtained with both **L1** and **L2** as ligand, as shown by comparison of the TOFs determined at different initial starting material concentrations and plotted as a function of substrate concentration (Figures 4.14 and 4.15). Under both conditions studied, the reaction started at lower concentrations of  $\text{cis-Na-1}$  and  $\text{Na-2a}$  is faster, showcasing that the catalytic activity decreases as turnover advances. This is consistent with observations reported in section 4.2, where reactions performed at very low catalyst concentrations were found to come to a standstill at incomplete conversion, even at prolonged reaction times. It is noted that these results are no formal proof of catalyst deactivation, as product inhibition<sup>[441,450,451]</sup> would lead to the same observations. However, product inhibition

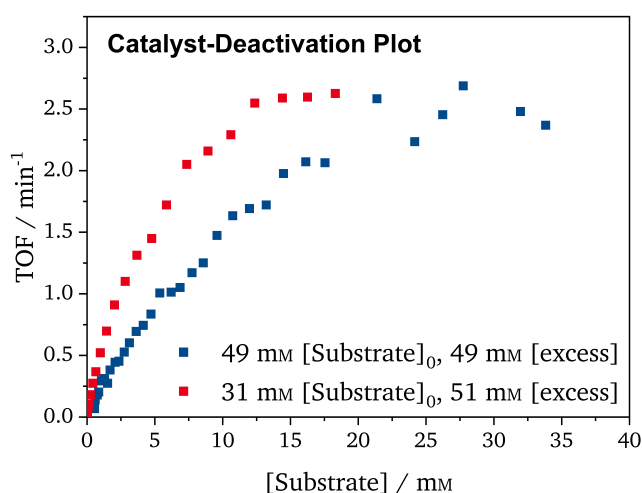
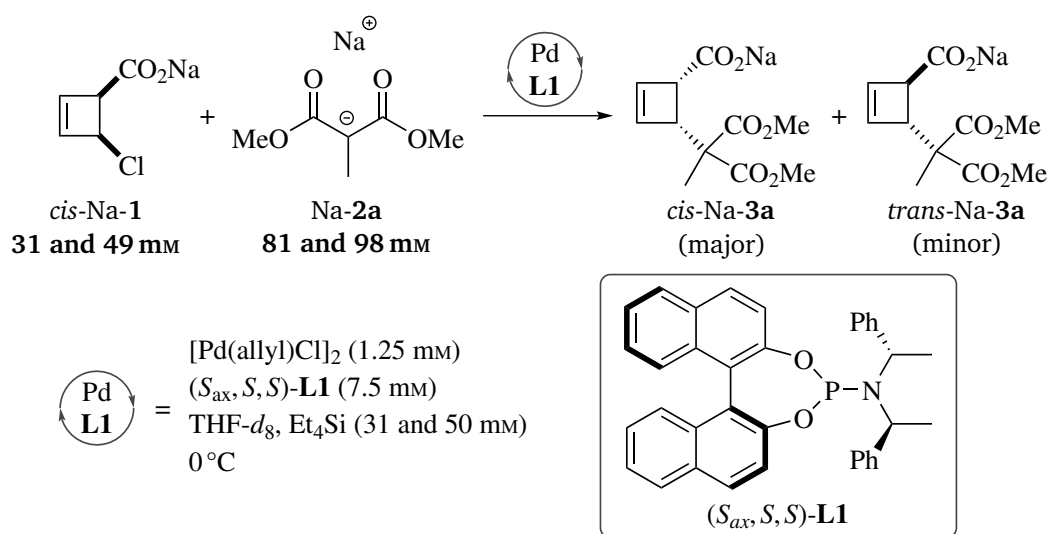


**Figure 4.12:** Examination of rate order in substrate *cis*-Na-1 and nucleophile Na-2a by RPKA with  $(S_{ax}, S, S)\text{-L1}$  as ligand, using kinetic data from six reactions with different [excess] values. The plots do not allow for extraction of an unambiguous rate order in *cis*-Na-1 (top). The rate order in Na-2a, on the other hand, appears to change from zero to one with decreasing substrate concentration (bottom), as concluded from the partially overlaying curves in the respective plots (superimposing regions highlighted with a colored background).

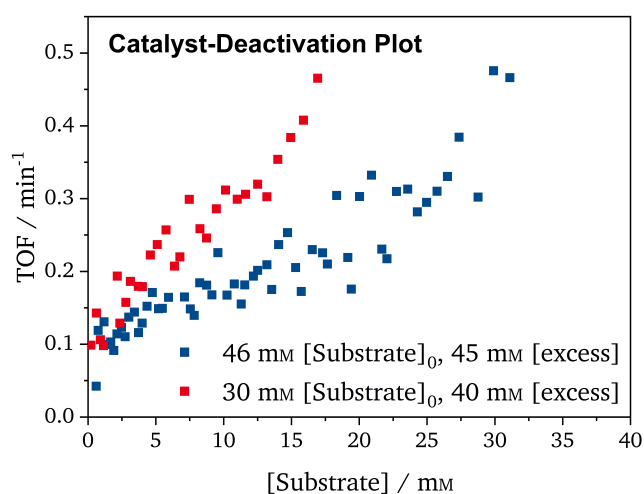
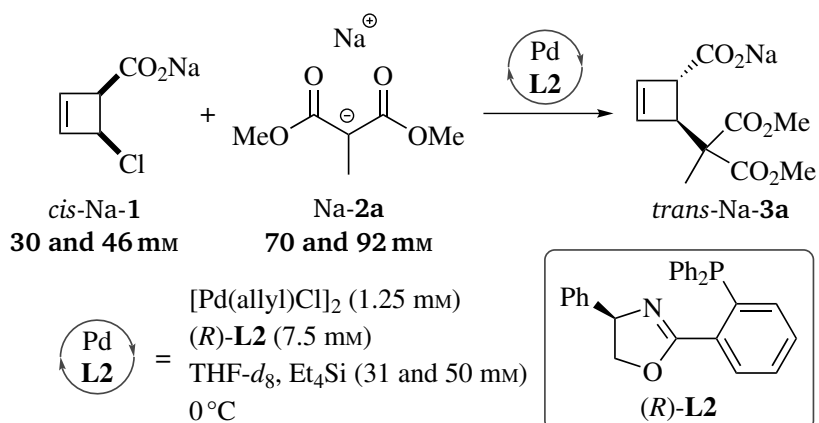


**Figure 4.13:** Examination of rate order in substrate *cis*-Na-1 and nucleophile Na-2a by RPKA with (*R*)-L2 as ligand, using kinetic data from five reactions with different [excess] values. The plots indicate a rate order of zero in *cis*-Na-1 (top), as concluded from the overlaying curves in the respective plot, but do not allow for extraction of an unambiguous rate order in Na-2a (bottom).

is anticipated to be very unlikely for the reaction investigated, as products Na-3 do not feature any functional group that is not present in either substrate or nucleophile, and thus there is no realistic reason why Na-3 should significantly interfere with the catalytic cycle.



**Figure 4.14:** Examination of catalyst deactivation by RPKA with (*S*<sub>ax</sub>, *S*, *S*)-L1 as ligand, using kinetic data from two reactions with approximately equal [excess] values (deviation due to experimental errors), but different initial concentrations of substrate *cis*-Na-1 and nucleophile Na-2a. The plots suggest catalyst deactivation to be operative during turnover, since the reaction with **lower starting concentrations** of *cis*-Na-1 and Na-2a is faster than the reaction with **higher initial concentrations**. As a slight modification compared to the literature,<sup>[441,450,451]</sup> TOFs rather than reaction rates were used for constructing the plot, in order to correct for experimental differences of catalyst concentration between both runs.



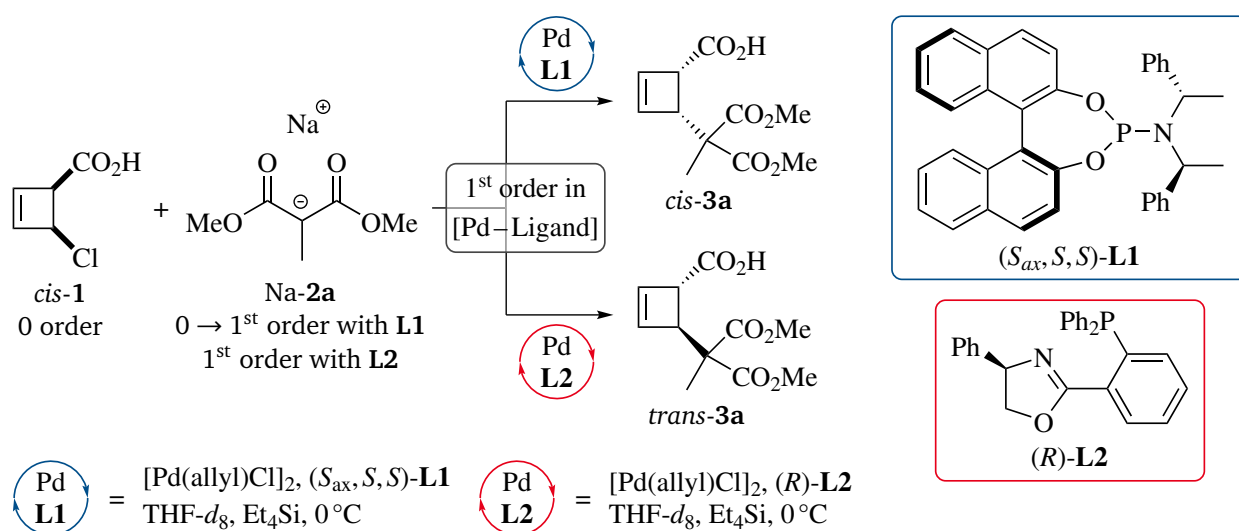
**Figure 4.15:** Examination of catalyst deactivation by RPKA with (R)-L2 as ligand, using kinetic data from two reactions with approximately equal [excess] values (deviation due to experimental errors), but different initial concentrations of substrate *cis*-Na-1 and nucleophile Na-2a. The plots suggest catalyst deactivation to be operative during turnover, since the reaction with **lower starting concentrations** of *cis*-Na-1 and Na-2a is faster than the reaction with **higher initial concentrations**. Note that, in the absence of catalyst deactivation, the reaction with lower starting concentrations would be expected to be slightly slower than the one with higher initial concentration, as the former run has been performed with somewhat lower [excess], which decreases its TOF due to the first-order dependence on nucleophile concentration. As a slight modification compared to the literature,<sup>[441,450,451]</sup> TOFs rather than reaction rates were used for constructing the plot, in order to correct for experimental differences of catalyst concentration between both runs.

#### 4.5.4 Summary of Kinetic Analysis

The reaction of interest has been characterized kinetically by complementary use of the initial rate approach and RPKA, giving apparent rate orders in catalyst, substrate and nucleophile (Figure 4.11). Under both conditions investigated, the reaction was found to be first order in the Pd<sup>0</sup> catalyst, as has also been reported for other allylic substitution systems.<sup>[453,454]</sup> In fact, a rate order of one in active catalyst is observed for the majority of catalytic reactions performed in homogeneous solution,<sup>[455–462]</sup> and exceptions have only been reported for rather uncommon mechanistic scenarios such as off-cycle oligomeric catalyst resting states<sup>[463–465]</sup> (rate order < 1)



or two catalytic species involved in the turnover-limiting step<sup>[466–468]</sup> (second order, see also [469] for detailed discussion of corresponding reaction kinetics). The apparent rate order in substrate has been determined to be zero with both ligands employed, showing that oxidative addition is not turnover-limiting. As for the nucleophile, the kinetic behavior differed between the two reaction conditions. With ligand **L2**, on the one hand, the reaction was ascertained to be apparent first order in nucleophile, and thus nucleophilic attack must be the turnover-limiting step. This is the most common kinetic scenario in allylic alkylation chemistry,<sup>[69,71,453,470,471]</sup> although systems where turnover is limited by oxidative addition have been reported as well.<sup>[70,454]</sup> On the other hand, an initial rate order of zero was extracted when **L1** was employed, and kinetic data suggest the rate order in nucleophile to gradually change to one during turnover. This reveals that under these conditions a monomolecular reaction step connecting two Pd intermediates is turnover-limiting at low conversion, whereas nucleophilic attack becomes turnover-limiting over the course of the reaction.



**Scheme 4.11:** Apparent rate orders extracted by complementary use of initial rate analysis and RPKA.

In general, reactions catalyzed by [Pd–**L1**] reached about 12 times higher TOFs than those performed in the presence of [Pd–**L2**], indicating that Pd–allyl complexes of **L1** are much more electrophilic. This can be ascribed to the electronic properties of the ‘hard’ N-ligation site of **L2** displaying an exclusively  $\sigma$ -donating character in contrast to the ‘soft’ P-ligation sites additionally acting as  $\pi$ -acceptors,<sup>[106,299]</sup> resulting in a lower electron density in the allylic system of **L1**-coordinated Pd–allyl species compared to those ligated by **L2**.

In addition, evidence for catalyst deactivation has been obtained with both ligands. This is consistent with the instability of the intermediate *anti*-configured Pd–cyclobutene complexes, which have been shown to undergo decomposition in the absence of nucleophile (section 4.2).

To get a deeper insight into the transition state of oxidative addition and nucleophilic attack as key reaction steps, the extraction of KIEs was envisioned. The values determined will be presented in the following section, as will be preliminary interpretations of those.

## 4.6 Kinetic Isotope Effects (KIEs)

KIEs have been established as a valuable tool for characterizing transition states in complex organic reaction networks.<sup>[347,472–475]</sup> In combination with transition state computations, they allow for experimental corroboration of a calculated mechanism, thus providing a unique link between experiment and theory.<sup>[476]</sup>

The KIE is defined as the relative reaction rate of two isotopologic substrates with rate constants  $k$  (light) and  $k$  (heavy) for the lighter and the heavier isotopologue, respectively, i.e.

$$\text{KIE} = \frac{k(\text{light})}{k(\text{heavy})}. \quad (4.3)$$

If during the reaction a bond to the atom considered is formed or broken, the corresponding KIE is referred to as *primary*, whereas KIEs of isotopic sites that are not directly involved in the bond forming/breaking step are termed *secondary*. The value obtained might be normal (KIE > 1) or inverse (KIE < 1), and its magnitude is predominantly determined by the relative mass difference of the isotopes.<sup>[477]</sup> For the most widely used <sup>2</sup>H-KIEs  $\frac{k(^1\text{H})}{k(^2\text{H})}$ ,<sup>[478]</sup> large primary KIEs of 2–8 can be obtained,<sup>[479–483]</sup> whereas secondary <sup>2</sup>H-KIEs are typically in the range of 0.8–1.2.<sup>[484–489]</sup> Secondary <sup>2</sup>H-KIEs can, for instance, arise from a hybridization change at the adjacent carbon, with a decrease in p-character ( $\text{sp}^3 \rightarrow \text{sp}^2$  or  $\text{sp}^2 \rightarrow \text{sp}$ ) giving a normal KIE and a change in the opposite direction furnishing an inverse value.<sup>[490]</sup> Primary heavy-atom KIEs such as  $\frac{k(^{12}\text{C})}{k(^{13}\text{C})}$  (1.00–1.05),<sup>[489,491–496]</sup>  $\frac{k(^{14}\text{N})}{k(^{15}\text{N})}$  (1.00–1.04),<sup>[496–498]</sup>  $\frac{k(^{16}\text{O})}{k(^{18}\text{O})}$  (1.00–1.04)<sup>[499–501]</sup> and  $\frac{k(^{35}\text{Cl})}{k(^{37}\text{Cl})}$  (1.00–1.01)<sup>[502–504]</sup> have been established as well. Albeit being small in magnitude, their computational determination benefits from a high degree of systematic error cancellation, making them robust parameters for transition state analyses.<sup>[472]</sup>

For interpretation of an experimental KIE, it is important to consider that, for a multi-step reaction, the method used for KIE extraction determines which step controls the overall value. If the KIE of interest is measured by separate rate constant determinations for each isotopologue, the value detected reflects the turn-over limiting step. In contrast, a KIE determined by a competition experiment is indicative for the ‘substrate-committing transition state’, provided an *intermolecular* competition is carried out (i.e. using two isotopologic substrates), or the ‘product-determining transition state’, if the competition is performed in an *intramolecular* fashion (i.e. by employing a single substrate with two homotopic or enantiotopic sites differing in isotopic constitution).<sup>[472,505]</sup>

Examples for KIE studies are scarce in allylic alkylation chemistry. SINGLETON *et al.* reported a set of <sup>13</sup>C-KIEs for an archetypal Pd–PPh<sub>3</sub> catalyzed allylic alkylation performed with an acyclic substrate.<sup>[70]</sup> The experimental values, determined at natural abundance by reisolating

unconverted allylic substrate from a reaction quenched at high conversion and measuring its change in isotopic composition,<sup>[506]</sup> were interpreted as indicative for an irreversible oxidative addition as substrate-committing step featuring an early transition state, in agreement with complementary reaction path calculations. LLOYD-JONES and coworkers determined a secondary <sup>2</sup>H-KIE of  $0.91 \pm 0.01$  for the enantiotopic allylic termini of a symmetrically substituted five-membered ring substrate subjected to the action of palladium and DACH standard ligand (*R,R*)-**L18**. This value was obtained from an intramolecular competition experiment and therefore reflects the nucleophilic capture of a common  $\pi$ -intermediate as product-determining step. Based on the experimental KIE, this step was concluded to have a medium or late transition state.<sup>[507]</sup>

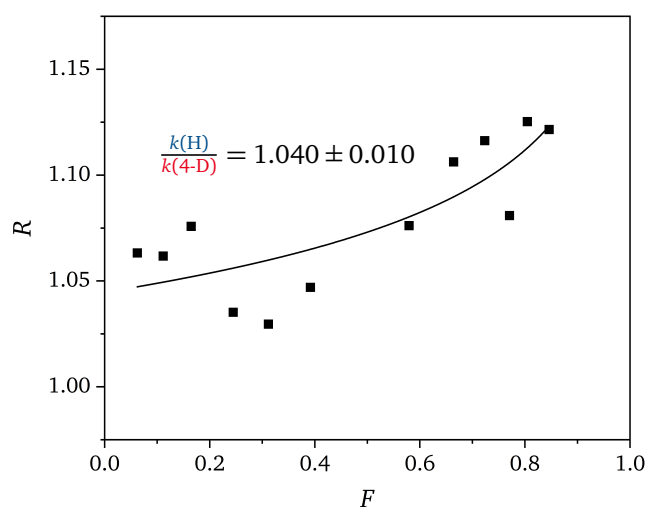
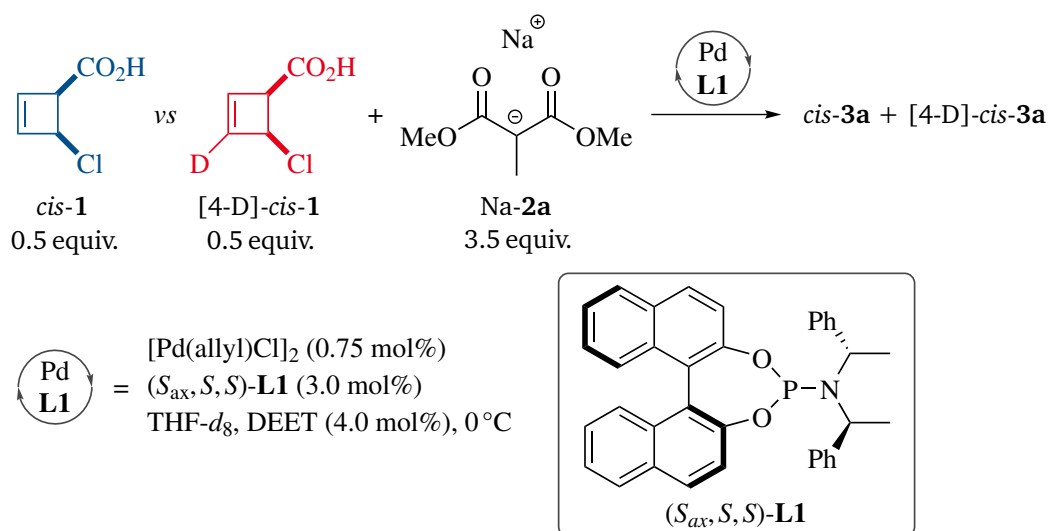
The KIE analysis reported in this chapter encompasses secondary <sup>2</sup>H-KIEs for the allylic system of substrate *cis-1* as well as primary <sup>13</sup>C-KIEs for model nucleophile Na-**2a**. The values of interest were presumed to be of small magnitude and were therefore determined by competition experiments, using isotopically labeled starting materials. As will be further discussed below, the KIEs obtained are expected to be controlled by different steps of the catalytic cycle. The applied procedures for KIE determination are outlined in subsections 4.6.1–4.6.3, organized by the different analytical methods employed. In part 4.6.4, the experimental values are summarized and discussed regarding potential mechanistic consequences.

#### 4.6.1 <sup>2</sup>H-KIEs for Allylic System by LC-MS Monitoring

Secondary <sup>2</sup>H-KIEs were determined by kinetic competition runs of deuterated substrates [4-D]-*cis-1* and [5-D]/[3-D]-*cis-1*,<sup>[378]</sup> respectively, against unlabeled *cis-1*. Preliminary experimentation showed that online <sup>1</sup>H-NMR monitoring, as applied for the kinetic analysis reported in section 4.5, is not competent to furnish isotopologue ratios  $R = \frac{[[D]-cis-1]}{[cis-1]}$  with the accuracy required for reliable KIE determination. As a more suitable reaction monitoring technique, offline liquid chromatography coupled with mass spectrometry (LC-MS) was employed. *N,N*-diethyl-*meta*-toluamide (DEET) was chosen as internal standard, featuring a high amenability for both liquid chromatography and mass spectrometry analysis.<sup>[508–511]</sup> To account for the limited stability of *cis-1*, ionization was performed by ESI in negative ion mode. Reaction monitoring of competition reactions was realized by taking samples at different conversions *F*, which were quenched with trifluoroacetic acid (TFA) and subsequently analyzed by LC-MS. The experimental substrate isotopologue ratios were then plotted against the conversion, and the KIE of interest was determined by regression analysis according to<sup>[512]</sup>

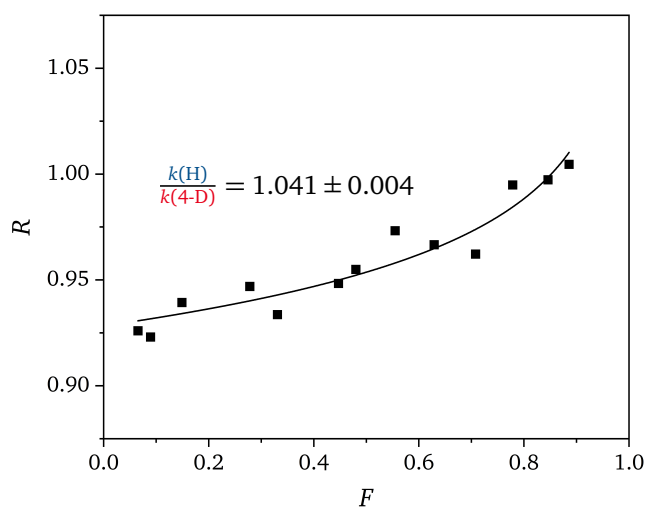
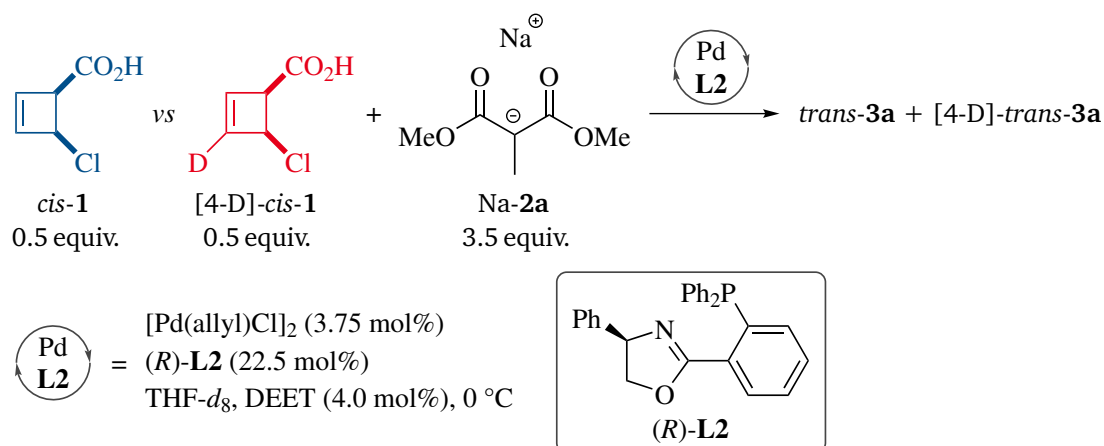
$$R = R_0 \cdot (1 - F)^{\frac{1}{KIE} - 1} \quad (4.4)$$

(hereinafter referred to as ‘substrate analysis’), where  $R_0$  is the initial ratio of deuterated and undeuterated substrate.

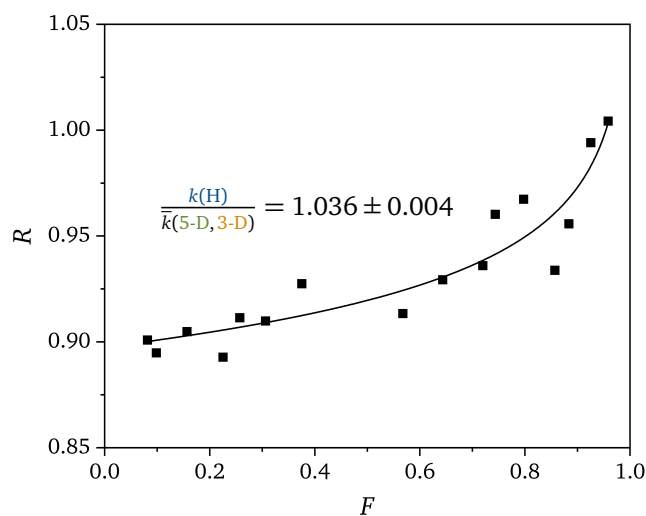
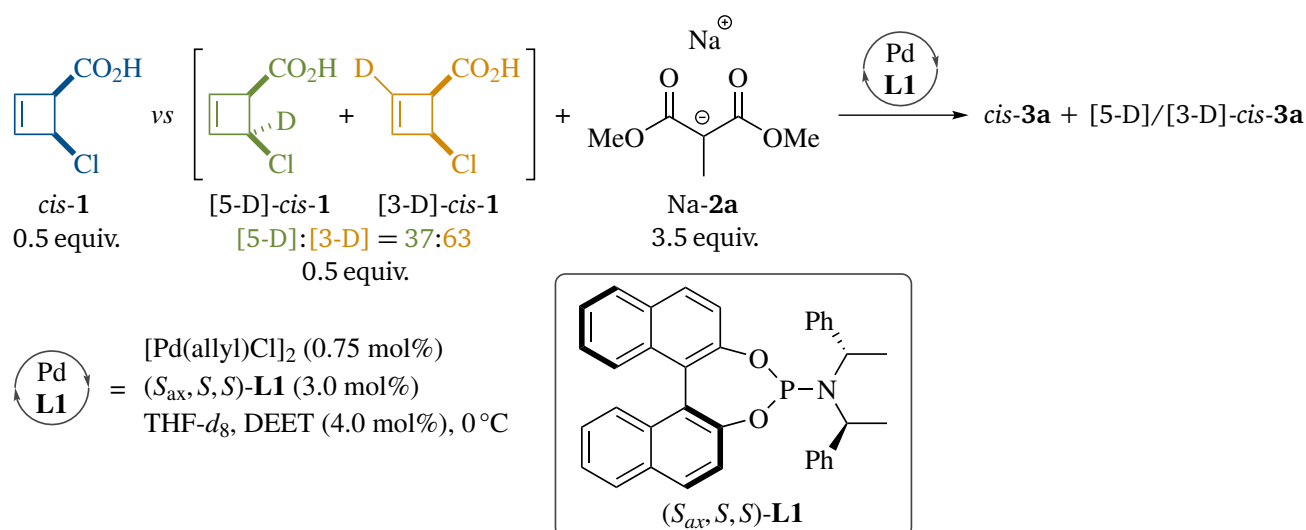


**Figure 4.16:** Extraction of  $^2\text{H}$ -KIE  $\frac{k(\text{H})}{k(4\text{-D})}$  by kinetic competition of labeled substrate  $[4\text{-D}]\text{-cis-1}$  against its unlabeled isotopologue  $\text{cis-1}$  with  $(S_{ax}, S, S)\text{-L1}$  as ligand, monitored by offline LC-MS. The experimental isotopologue ratios  $R = \frac{[4\text{-D}]\text{-cis-1}}{[\text{cis-1}]}$  determined at different conversions  $F$  were subjected to substrate analysis according to equation (4.4), giving the KIE as regression parameter.

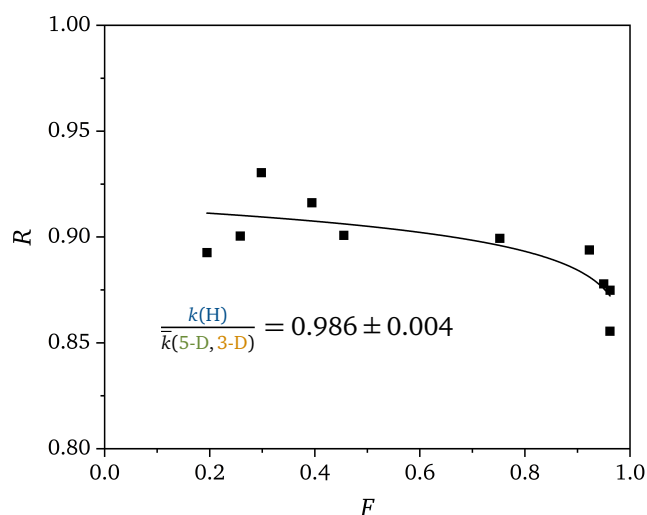
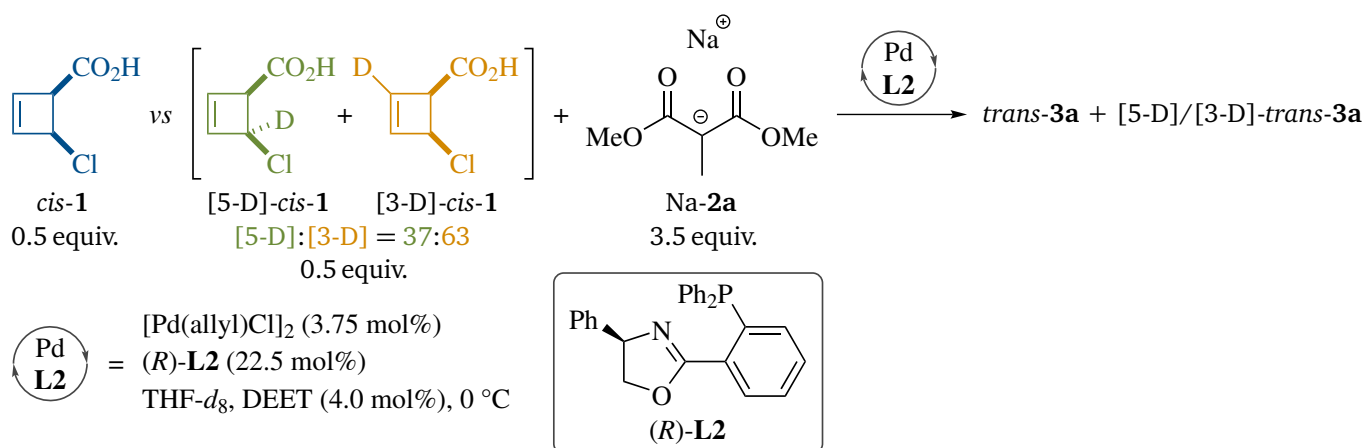
Under both reaction conditions investigated, reasonably accurate KIE plots were received, spanning a wide conversion range. Deuteration at the central allylic position C(4) gave virtually identical  $^2\text{H}$ -KIEs of  $1.040 \pm 0.010$  and  $1.041 \pm 0.004$  with ligand **L1** and **L2**, respectively (Figures 4.16 and 4.17). For the allylic termini C(3) and C(5), on the other hand, a normal  $^2\text{H}$ -KIE of  $1.036 \pm 0.004$  was determined with **L1**, whereas the same reaction performed in the presence of ligand **L2** afforded an inverse KIE of  $0.986 \pm 0.004$  (Figures 4.18 and 4.19). The latter values, measured by competition of  $[5\text{-D}]/[3\text{-D}]\text{-cis-1}$  against  $\text{cis-1}$ , are to be understood as weighted averaged KIEs  $\frac{k(\text{H})}{k(5\text{-D}, 3\text{-D})}$  for the allylic termini.



**Figure 4.17:** Extraction of <sup>2</sup>H-KIE  $\frac{k(\text{H})}{k(4\text{-D})}$  by kinetic competition of labeled substrate [4-D]-*cis*-1 against its unlabeled isotopologue *cis*-1 with (R)-L2 as ligand, monitored by offline LC-MS. The experimental isotopologue ratios  $R = \frac{[4\text{-D}]\text{-}i\text{-}1}{[i\text{-}1]}$  determined at different conversions  $F$  were subjected to substrate analysis according to equation (4.4), giving the KIE as regression parameter.



**Figure 4.18:** Extraction of  $^2\text{H-KIE}$   $\frac{k(\text{H})}{\bar{k}(5\text{-D}, 3\text{-D})}$  by kinetic competition of labeled substrates  $[\text{5-D}]\text{-cis-1}$  and  $[\text{3-D}]\text{-cis-1}$  (synthesized as inseparable 37:63 isotopomeric mixture,<sup>[378]</sup> cf. Scheme 4.3) against unlabeled isotopologue  $\text{cis-1}$  with  $(S_{\text{ax}}, S, S)\text{-L1}$  as ligand, monitored by offline LC-MS. The experimental isotopologue ratios  $R = \frac{[\text{5-D-cis-1}] + [\text{3-D-cis-1}]}{[\text{cis-1}]}$  determined at different conversions  $F$  were subjected to substrate analysis according to equation (4.4), giving the KIE as regression parameter.



**Figure 4.19:** Extraction of  $^2\text{H}$ -KIE  $\frac{k(\text{H})}{k(5\text{-D},3\text{-D})}$  by kinetic competition of labeled substrates  $[\text{5-D}]\text{-cis-1}$  and  $[\text{3-D}]\text{-cis-1}$  (synthesized as inseparable 37:63 isotopomeric mixture,<sup>[378]</sup> cf. Scheme 4.3) against unlabeled isotopologue  $\text{cis-1}$  with  $(R)\text{-L2}$  as ligand, monitored by offline LC-MS. The experimental isotopologue ratios  $R = \frac{[\text{5-D-cis-1}] + [\text{3-D-cis-1}]}{[\text{cis-1}]}$  determined at different conversions  $F$  were subjected to substrate analysis according to equation (4.4), giving the KIE as regression parameter.

#### 4.6.2 Relative $^2\text{H}$ -KIEs for Allylic System by $^1\text{H}$ -NMR Monitoring

Since LC-MS monitoring of competition runs only gave averaged KIEs for the allylic termini, the relative reactivity

$$\frac{k(5\text{-D})}{k(3\text{-D})} = \frac{\frac{k(\text{H})}{k(3\text{-D})}}{\frac{k(\text{H})}{k(5\text{-D})}} = \frac{\text{KIE}(3\text{-D})}{\text{KIE}(5\text{-D})} \quad (4.5)$$

was to be determined. To this end, a competition experiment was carried out using deuterated substrates [5-D]- and [3-D]-*cis*-**1**, which can be conveniently differentiated by  $^1\text{H}$ -NMR. Again, online monitoring failed to yield sufficiently accurate isotopomer ratios, and the reaction was therefore monitored offline.  $^1\text{H}$ -NMR analysis of samples quenched with TFA allowed for determining the conversion  $F$  against internal standard  $\text{Et}_4\text{Si}$  with reasonable precision. However, the extraction of isotopomer ratios was hampered by spectral overlap due to the presence of various unidentified impurities. This issue could be overcome by subjecting all samples to a standard extractive work-up. The samples purified in this way contained only minor amounts of residual impurities, making them more amenable for quantitative analysis by  $^1\text{H}$ -NMR. All samples were analyzed both on a 700 MHz and on a 950 MHz spectrometer. From the spectra recorded, isotopomer ratios  $R$  and  $R_{\text{p}}$  were calculated for both substrate [5-D]/[3-D]-*cis*-**1** and products [5-D]/[3-D]-**3a**, respectively. These were subjected to substrate analysis according to equation (4.4) and complementary ‘product analysis’ according to<sup>[512]</sup>

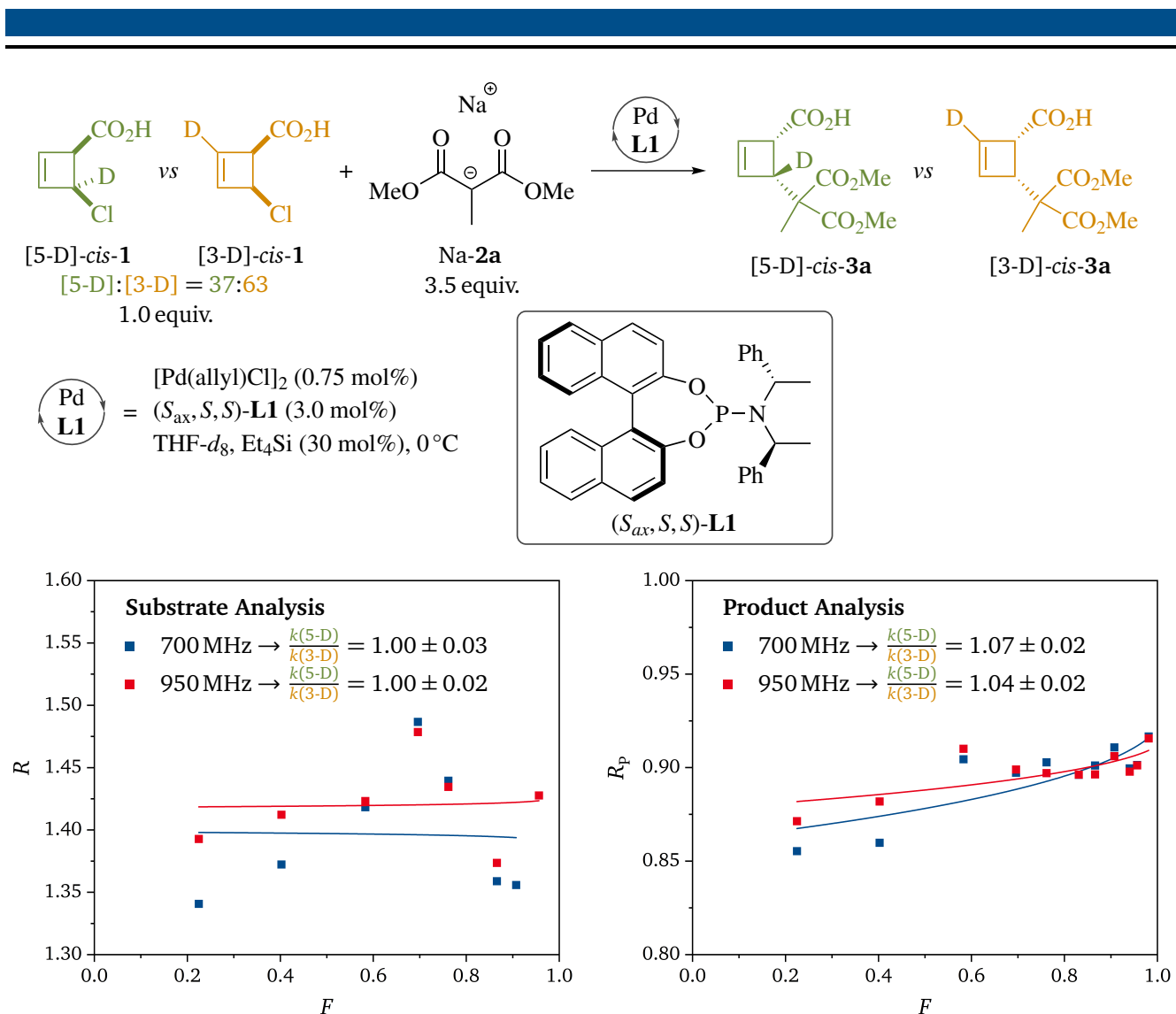
$$R_{\text{p}} = \frac{R_0}{F} \cdot \left( 1 - (1 - F)^{\frac{1}{\text{KIE}}} \right). \quad (4.6)$$

Noteworthy, the relative KIEs obtained from both methods were significantly different. As will be further discussed in part 4.6.4, this is consistent with a transient symmetrizing event which makes substrate and product analysis reflect different steps of the catalytic cycle.

With ligand **L1**, the KIE plots obtained by substrate analysis exhibit a relatively high extent of scattering, which is attributed to the poor spectral separation of the olefinic protons of *cis*-**1**. Nevertheless, the experimental data recorded at two different spectrometers consistently suggest that both substrate isotopomers are equally reactive, with an experimental value of  $\frac{k(5\text{-D})}{k(3\text{-D})} = 1.00 \pm 0.03$  (Figure 4.20, left). On the other hand, analysis of the competing formation of product isotopomers [5-D]-*cis*-**3a** and [3-D]-*cis*-**3a** gave fairly accurate KIE plots, furnishing a relative KIE of  $\frac{k(5\text{-D})}{k(3\text{-D})} = 1.05 \pm 0.02$  as average of the two values determined at different field strengths (Figure 4.20, right).

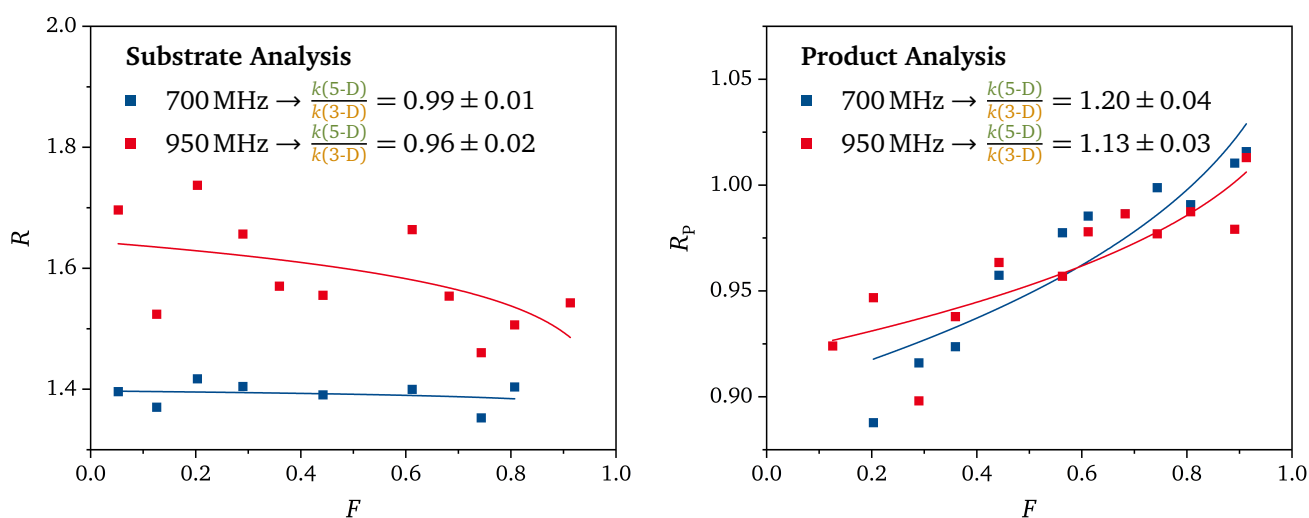
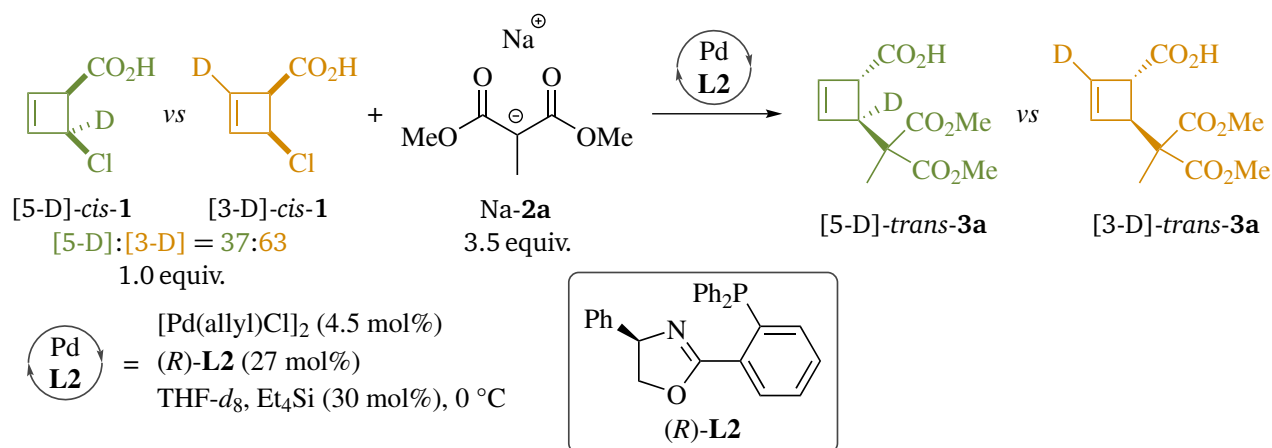
For the competition run performed with **L2** as ligand, substrate analysis again yielded a KIE close to unity. As the KIE plot obtained by  $^1\text{H}$ -NMR analysis at 700 MHz displays a clearly lower extent of scattering than the one prepared from experimental data recorded at 950 MHz, only the KIE





**Figure 4.20:** Extraction of relative  $^2\text{H}$ -KIE  $\frac{k(5-D)}{k(3-D)}$  by analyzing the competing consumption of labeled substrate isotopomers [5-D]-*cis*-1 and [3-D]-*cis*-1 and the competing formation of product isotopomers [5-D]-*trans*-3a and [3-D]-*trans*-3a with ( $S_{ax}, S, S$ )-L1 as ligand, monitored by offline  $^1\text{H}$ -NMR at 700 MHz and 950 MHz. The experimental isotopomer ratios  $R = \frac{[3-D]\text{-}cis\text{-}1}{[5-D]\text{-}cis\text{-}1}$  and  $R_p = \frac{[3-D]\text{-}trans\text{-}3a}{[5-D]\text{-}trans\text{-}3a}$  determined at different conversions  $F$  were subjected to substrate analysis according to equation (4.4) (left) and product analysis according to equation (4.6) (right), respectively, giving the KIE as regression parameter. The striking difference in magnitude is due to an intermediate symmetrizing event (cf. Scheme 4.15).

$\frac{k(5-D)}{k(3-D)} = 0.99 \pm 0.01$  extracted from the former plot is deemed reliable (Figure 4.21, left). The reason for this discrepancy might be that at 950 MHz it was generally more difficult to achieve a reasonable shim, and consequently the spectra measured at this spectrometer were mostly not superior in spectral resolution compared to the data recorded at 700 MHz. Complementary product analysis, on the other hand, afforded KIE plots with comparable accuracy for both measurement series, giving an average relative rate of  $\frac{k(5-D)}{k(3-D)} = 1.16 \pm 0.04$  for the formation of product isotopomers [5-D]-*trans*-3a and [3-D]-*trans*-3a (Figure 4.21, right).



**Figure 4.21:** Extraction of relative  $^2\text{H}$ -KIE  $\frac{k(5\text{-D})}{k(3\text{-D})}$  by analyzing the competing consumption of labeled substrate isotopomers  $[5\text{-D}]\text{-cis-1}$  and  $[3\text{-D}]\text{-cis-1}$  and the competing formation of product isotopomers  $[5\text{-D}]\text{-trans-3a}$  and  $[3\text{-D}]\text{-trans-3a}$  with  $(R)\text{-L2}$  as ligand, monitored by offline  $^1\text{H}$ -NMR at **700 MHz** and **950 MHz**. The experimental isotopomer ratios  $R = \frac{[3\text{-D}]\text{-cis-1}}{[5\text{-D}]\text{-cis-1}}$  and  $R_p = \frac{[3\text{-D}]\text{-trans-3a}}{[5\text{-D}]\text{-trans-3a}}$  determined at different conversions  $F$  were subjected to substrate analysis according to equation (4.4) (left) and product analysis according to equation (4.6) (right), respectively, giving the KIE as regression parameter. The striking difference in magnitude is due to an intermediate symmetrizing event (cf. Scheme 4.15).

#### 4.6.3 $^{13}\text{C}$ -KIEs for Nucleophile by $^{13}\text{C}$ -NMR Monitoring

The determination of a primary  $^{13}\text{C}$ -KIE for model nucleophile  $\text{Na-2a}$  was found to be challenging. Reactions performed with  $\text{Na-2a}$  as limiting component, as required to reach high conversions in nucleophile, tended to come to a premature standstill, even at elevated catalyst loadings. This is likely a consequence of the decreased rate of nucleophilic attack at low nucleophile concentrations, leading to an increased extent of catalyst deactivation eventually outcompeting nucleophilic attack. In addition, quantitative differentiation of labeled nucleophile  $[\alpha\text{-}^{13}\text{C}]\text{-Na-2a}$  and its unlabeled isotopologue  $\text{Na-2a}$  turned out to be complicated, as the  $^1\text{H}$ -NMR resonances of both isotopologues are not baseline-separated. Mass spectrometric analysis of  $\text{Na-2a}$  and its

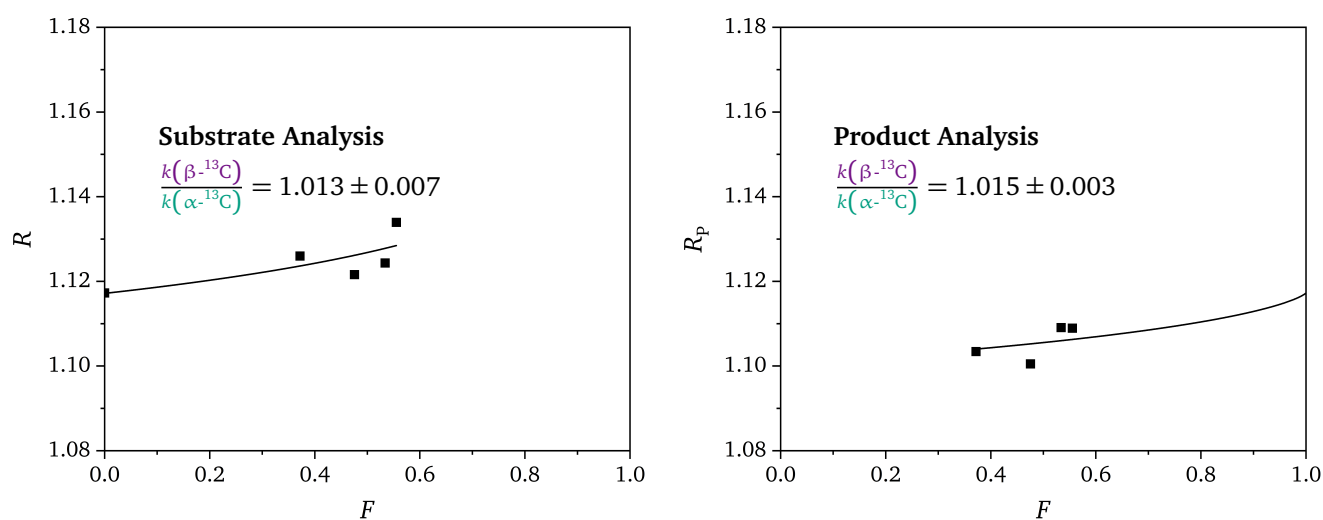
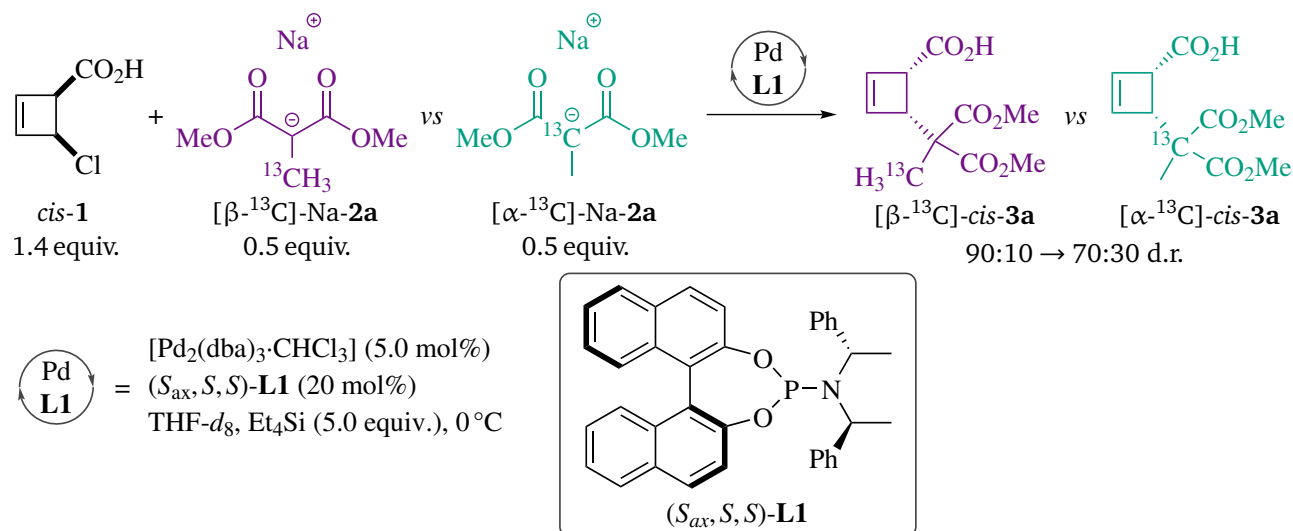
---

corresponding acid **2a** was furthermore plagued by decomposition upon ionization and was therefore anticipated not to be qualified for accurate determination of isotopologue ratios.

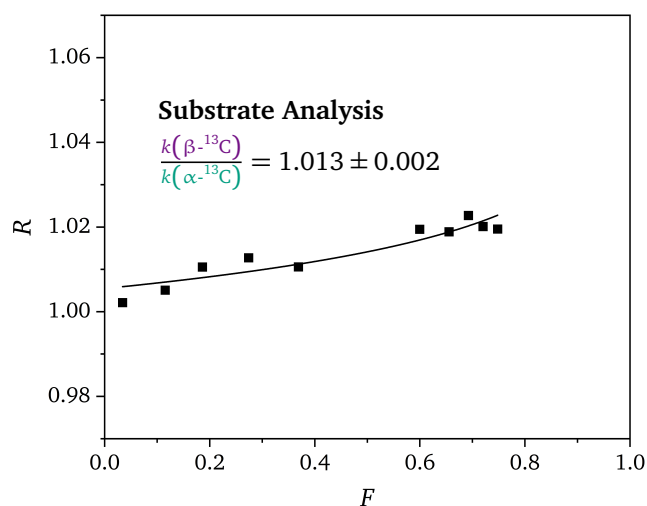
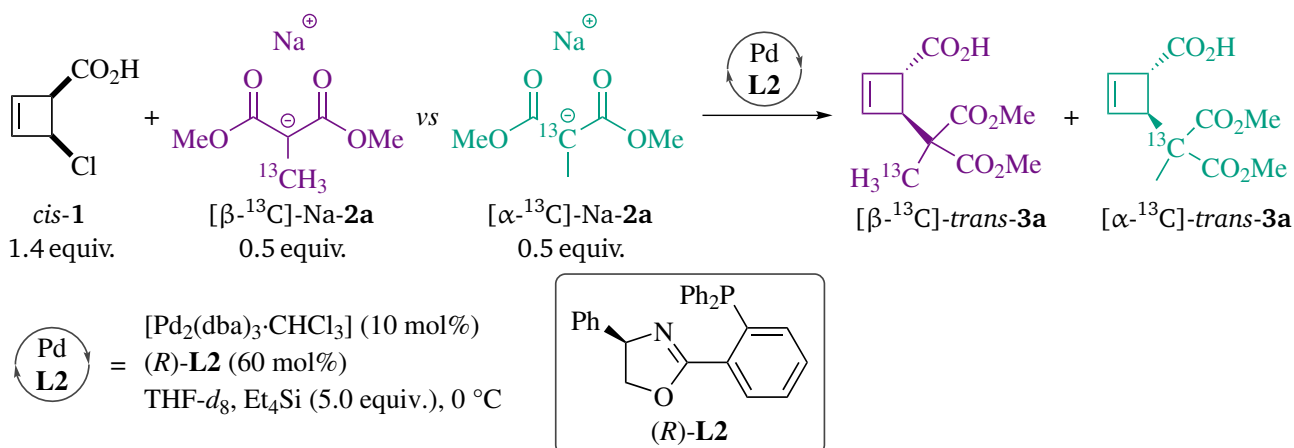
In spite of these obstacles, fairly accurate  $^{13}\text{C}$ -KIEs could be extracted by means of competition experiments using  $[\beta\text{-}^{13}\text{C}]\text{-Na-2a}$  rather than unlabeled **Na-2a** as reference isotopomer, similar to the double-labeling strategy established by LLOYD-JONES and coworkers.<sup>[496,513–515]</sup> This enabled the reaction to be monitored conveniently via quantitative  $^{13}\text{C}$ -NMR, which comes with a significantly higher spectral resolution compared to  $^1\text{H}$ -NMR preventing undesired overlap of resonances. However, the limited sensitivity of  $^{13}\text{C}$ -NMR as well as the long relaxation delays required made this method unsuitable for online monitoring. Therefore, competition runs were sampled in the same way as described before (subsection 4.6.2), which allowed for analyzing the quenched samples with an increased number of accumulated scans. The use of a superstoichiometric amount of natural abundance internal standard  $\text{Et}_4\text{Si}$  (5 equiv.) facilitated determination of conversion  $F$  from the  $^{13}\text{C}$ -NMR spectra. As  $\text{Pd}^0$  source,  $[\text{Pd}_2(\text{dba})_3 \cdot \text{CHCl}_3]$  was used rather than the previously employed precursor  $[\text{Pd}(\text{allyl})\text{Cl}]_2$ , since the latter gets activated *in situ* by nucleophilic displacement with the malonate nucleophile and would thus result in the experimental  $^{13}\text{C}$ -KIE being superimposed by this activation reaction. Labeled nucleophiles  $[\text{C}^{13}]\text{-Na-2a}$  were generated *in situ* prior to catalyst addition by deprotonation of parent acids  $[\text{C}^{13}]\text{-2a}$  with NaHMDS, as the isolated malonate salts could not be prepared in reasonably pure form (see section 4.1.2).

With ligand **L1**, the reaction stalled at 55% conversion, and attempts to obtain reaction monitoring data spanning a wider conversion range failed. Furthermore, the d.r. of product  $[\text{C}^{13}]\text{-cis-3a}$  was found to change from 90:10 in the first sample after initiation to 70:30 in the last sample, an issue that has not been observed in previous reaction monitoring experiments. Nevertheless, complementary substrate and product analysis gave consistent KIEs of  $\frac{k(\beta\text{-}^{13}\text{C})}{k(\alpha\text{-}^{13}\text{C})} = 1.013 \pm 0.007$  and  $\frac{k(\beta\text{-}^{13}\text{C})}{k(\alpha\text{-}^{13}\text{C})} = 1.015 \pm 0.003$ , respectively (Figure 4.22). The latter value is believed to be more reliable, since it reflects only the reaction path of interest, whereas substrate analysis is distorted by formation of undesired product diastereomer  $[\text{C}^{13}]\text{-trans-3a}$  as side path.

The corresponding competition experiment with **L2** as ligand turned out to be less problematic. The reaction could be brought to a conversion of up to 76%, featuring a constantly high d.r. of 99:1. Substrate analysis furnished a KIE of  $\frac{k(\beta\text{-}^{13}\text{C})}{k(\alpha\text{-}^{13}\text{C})} = 1.013 \pm 0.002$ . Verification of this value by product analysis was, however, not feasible due to  $[\text{C}^{13}]\text{-trans-3a}$  exhibiting problematic signal overlap with impurities.



**Figure 4.22:** Extraction of  $^{13}\text{C}$ -KIE  $\frac{k(\beta\text{-}^{13}\text{C})}{k(\alpha\text{-}^{13}\text{C})}$  by kinetic competition of labeled nucleophile  $[\alpha\text{-}^{13}\text{C}]\text{-Na-2a}$  against reference isotopomer  $[\beta\text{-}^{13}\text{C}]\text{-Na-2a}$  with  $(S_{\text{ax}}, S, S)\text{-L1}$  as ligand, monitored by offline  $^{13}\text{C}$ -NMR. Labeled nucleophiles  $[\text{C}^{13}]\text{-Na-2a}$  were generated *in situ* by deprotonation of parent acids  $[\text{C}^{13}]\text{-2a}$  with NaHMDS prior to initiation. The experimental isotopomer ratios  $R = \frac{[[\alpha\text{-}^{13}\text{C}]\text{-Na-2a}]}{[[\beta\text{-}^{13}\text{C}]\text{-Na-2a}]}$  and  $R_p = \frac{[[\alpha\text{-}^{13}\text{C}]\text{-cis-3a}]}{[[\beta\text{-}^{13}\text{C}]\text{-cis-3a}]}$  determined at different conversions  $F$  were subjected to substrate analysis according to equation (4.4) (left) and product analysis according to equation (4.6) (right, regression parameter  $R_0$  fixed to experimental value), respectively, giving the KIE as regression parameter.



**Figure 4.23:** Extraction of  $^{13}\text{C}$ -KIE  $\frac{k(\beta\text{-}^{13}\text{C})}{k(\alpha\text{-}^{13}\text{C})}$  by kinetic competition of labeled nucleophile  $[\alpha\text{-}^{13}\text{C}]\text{-Na-2a}$  against reference isotopomer  $[\beta\text{-}^{13}\text{C}]\text{-Na-2a}$  with  $(R)\text{-L2}$  as ligand, monitored by offline  $^{13}\text{C}$ -NMR. Labeled nucleophiles  $[\text{C}^{13}]\text{-Na-2a}$  were generated *in situ* by deprotonation of parent acids  $[\text{C}^{13}]\text{-2a}$  with NaHMDS prior to initiation. The experimental isotopomer ratios  $R = \frac{[\alpha\text{-}^{13}\text{C}]\text{-Na-2a}}{[\beta\text{-}^{13}\text{C}]\text{-Na-2a}}$  determined at different conversions  $F$  were subjected to substrate analysis according to equation (4.4), giving the KIE as regression parameter.

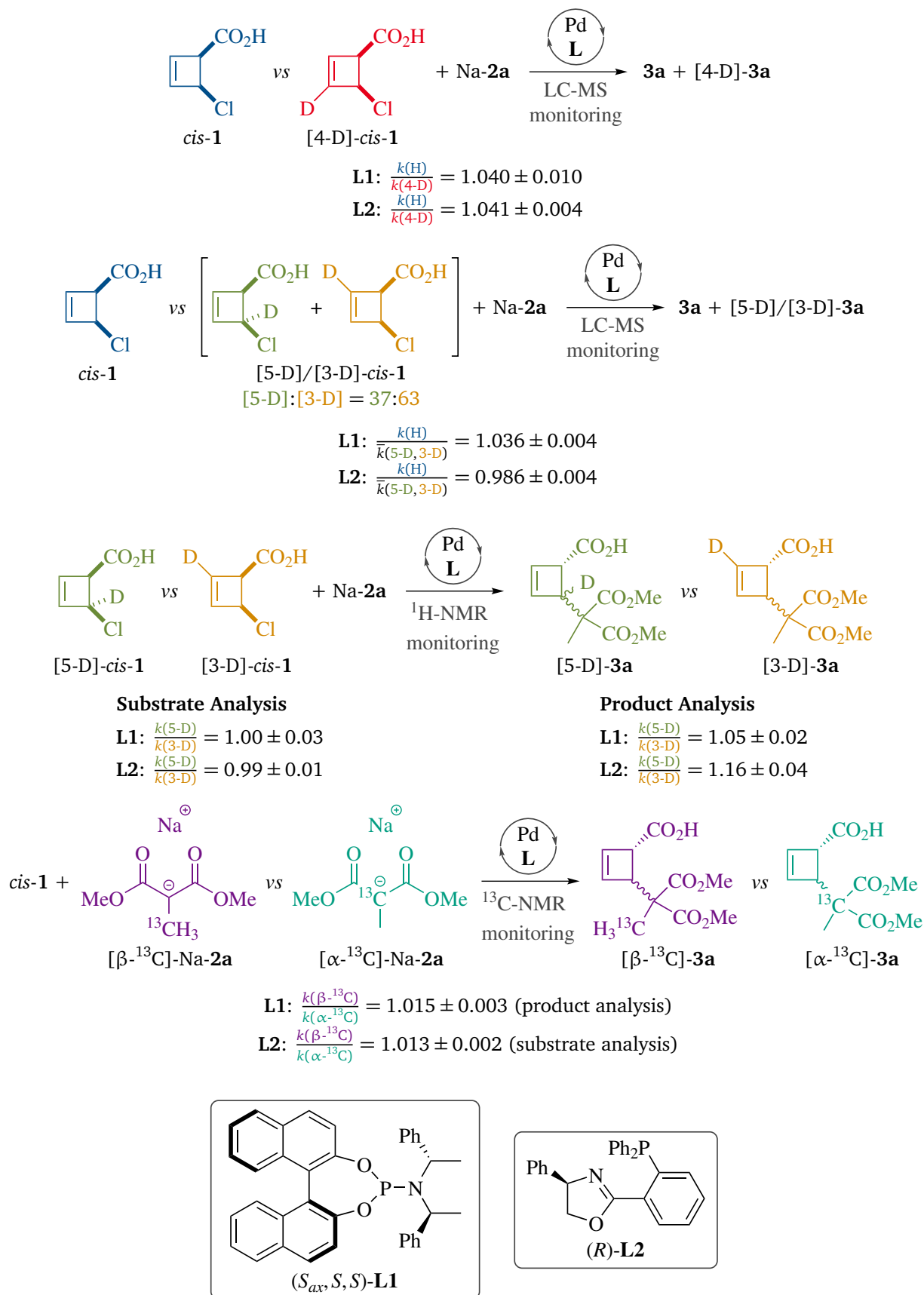
#### 4.6.4 Summary of Kinetic Isotope Effect Studies

A set of  $^2\text{H}$ - and  $^{13}\text{C}$ -KIEs has been determined by means of intermolecular competition experiments monitored by various analytical techniques (Scheme 4.12). With both ligands employed, LC-MS monitoring yielded nearly identical KIEs of  $\frac{k(\text{H})}{k(4\text{-D})} = 1.040 \pm 0.010$  (**L1**) and  $\frac{k(\text{H})}{k(4\text{-D})} = 1.041 \pm 0.004$  (**L2**) for the central allylic position C(4), but strikingly different values of  $\frac{k(\text{H})}{k(5\text{-D}, 3\text{-D})} = 1.036 \pm 0.004$  (**L1**) and  $\frac{k(\text{H})}{k(5\text{-D}, 3\text{-D})} = 0.986 \pm 0.004$  (**L2**) as averaged KIEs for the allylic termini C(3) and C(5). The relative reactivity  $\frac{k(5\text{-D})}{k(3\text{-D})}$  of substrate isotopomers [5-D]- and [3-D]-*cis*-**1** was found to be close to unity, as suggested by  $^1\text{H}$ -NMR monitoring. Product analysis of the same reaction furnished relative KIEs of  $\frac{k(5\text{-D})}{k(3\text{-D})} = 1.05 \pm 0.02$  (**L1**) and  $\frac{k(5\text{-D})}{k(3\text{-D})} = 1.16 \pm 0.04$  (**L2**). For nucleophile Na-**2a**, primary  $^{13}\text{C}$ -KIEs of  $\frac{k(\beta\text{-}^{13}\text{C})}{k(\alpha\text{-}^{13}\text{C})} = 1.015 \pm 0.003$  (**L1**) and  $\frac{k(\beta\text{-}^{13}\text{C})}{k(\alpha\text{-}^{13}\text{C})} = 1.013 \pm 0.002$  (**L2**) were determined by means of a double-labeling approach, using quantitative  $^{13}\text{C}$ -NMR monitoring.

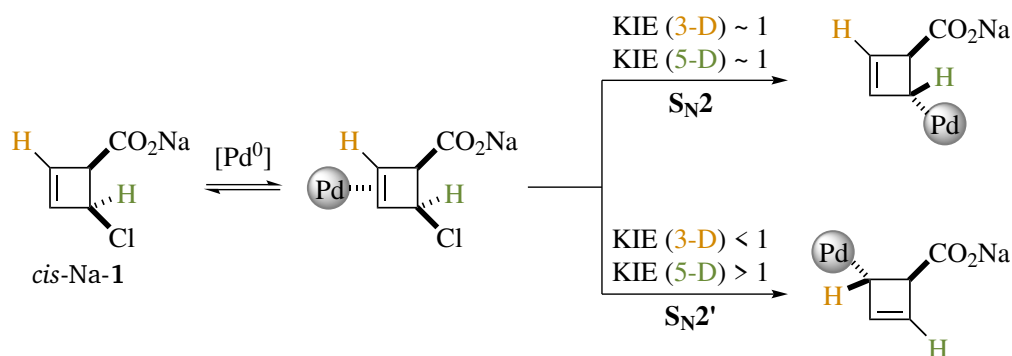
It is known that KIEs determined by intermolecular competition experiments, as done in this work, reflect the first irreversible step of the reaction consuming the substrate ('substrate-committing transition state'), unless preceded by a slow equilibrium with lower rate constants.<sup>[472,505]</sup> Based on literature precedence, initial  $\eta^2$ -complexation of the allylic substrate can be assumed to be faster than oxidative addition,<sup>[506,516–518]</sup> and accordingly the  $^2\text{H}$ -KIEs determined for *cis*-**1** are expected to be controlled by oxidative addition, which has been shown to be irreversible for the system studied (section 4.2). As outlined in Scheme 4.13, this step might proceed via either  $\text{S}_{\text{N}}2$ - or  $\text{S}_{\text{N}}2'$ -type displacement of the leaving group. The latter has been proposed for Fe- and Rh-catalyzed allylic substitutions,<sup>[97,100,173]</sup> which have been shown to include  $\eta^1$ -allyl complexes as reactive intermediates.<sup>[141–144]</sup> Whilst for an  $\text{S}_{\text{N}}2$  path the allylic termini are expected not to exhibit significant  $^2\text{H}$ -KIEs,  $\text{S}_{\text{N}}2'$ -type oxidative addition would be accompanied by a hybridization change at both positions. Thus, the allylic termini would display a normal and an inverse  $^2\text{H}$ -KIE, respectively, and the relative reactivity determined by substrate analysis would consequently be  $\frac{k(5\text{-D})}{k(3\text{-D})} = \frac{\text{KIE}(3\text{-D})}{\text{KIE}(5\text{-D})} \ll 1$ . However,  $\frac{k(5\text{-D})}{k(3\text{-D})}$  has been ascertained to be close to 1 under both reaction conditions investigated, which points towards an  $\text{S}_{\text{N}}2$ -like mechanism.

The origin of the other secondary  $^2\text{H}$ -KIEs obtained is speculative and demands complementary computational investigations of oxidative addition. For the central allylic position C(4), the normal KIEs of  $\frac{k(\text{H})}{k(4\text{-D})} = 1.040 \pm 0.010$  (**L1**) and  $\frac{k(\text{H})}{k(4\text{-D})} = 1.041 \pm 0.004$  (**L2**) might be a consequence of different abilities of C–H and C–D bonds to undergo hyperconjugation as a stabilizing interaction in the transition state, and the values determined are consistent with the normal  $\beta$ - $^2\text{H}$ -KIE usually observed for this effect.<sup>[490]</sup> Regarding the allylic termini C(3) and C(5), the clearly different weighted averaged  $^2\text{H}$ -KIEs of  $\frac{k(\text{H})}{k(5\text{-D}, 3\text{-D})} = 1.036 \pm 0.004$  (**L1**) and  $\frac{k(\text{H})}{k(5\text{-D}, 3\text{-D})} = 0.986 \pm 0.004$  (**L2**) indicate that the ligand has a profound impact on the mechanism of oxidative addition.

In contrast to the relative reactivity  $\frac{k(5\text{-D})}{k(3\text{-D})}$  determined by substrate analysis, the corresponding value obtained by product analysis reflects the attack of nucleophile, as the reaction includes

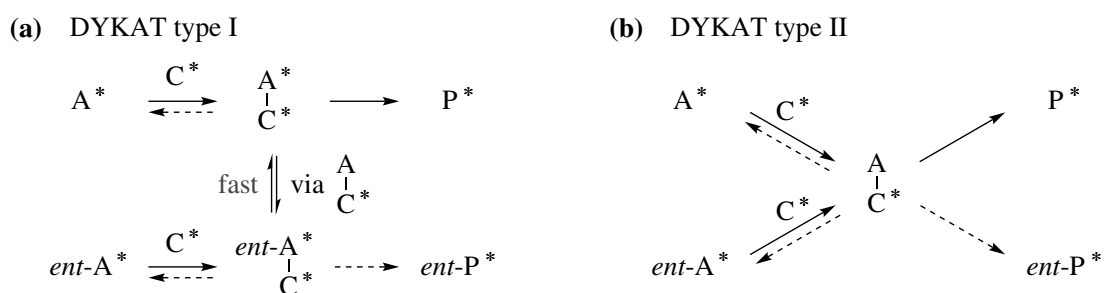


**Scheme 4.12:** Experimental  $^2\text{H}$ - and  $^{13}\text{C}$ -KIEs determined by kinetic competition runs with different reaction monitoring techniques.



**Scheme 4.13:**  $\text{S}_{\text{N}}2$ - and  $\text{S}_{\text{N}}2'$ -type oxidative addition on cyclobutene substrate *cis*-Na-1 and corresponding  $^2\text{H}$ -KIEs expected for the allylic termini as a consequence of adjacent hybridization changes.

a transient symmetrizing event (*vide infra*). Early labeling studies disclosed by MAULIDE and coworkers have shown that no memory effect is operative (cf. Scheme 2.28b),<sup>[55]</sup> i.e. the underlying equilibrium between Pd-allyl complexes is significantly faster than subsequent nucleophilic capture. As a corollary, the deuterated allylic termini of all intermediate Pd species get fully scrambled, regardless of the isotopic composition of substrate [5-D]/[3-D]-Na-1. The conversion dependence observed for the product's isotopomer ratio  $R_{\text{p}} = \frac{[\text{3-D}]\text{-3a}}{[\text{5-D}]\text{-3a}}$  is indicative for enantioselectivity being based on nucleophilic attack on two rapidly equilibrating upstream intermediates (DYKAT type I) rather than competing nucleophilic attack on the enantiotopic termini of one common intermediate (DYKAT type II, Scheme 4.14).<sup>[28–30]</sup> For the latter scenario, i.e. an *intramolecular* competition,  $R_{\text{p}}$  would be expected to be independent of conversion.<sup>[472,507]</sup> Hence, the relative KIE  $\frac{k(5\text{-D})}{k(3\text{-D})}$  observed for product formation arises from an *intermolecular* competition between the [5-D]- and the [3-D]-isotopomer of the reactive intermediate, with  $R_0 = 1$  due to complete isotopic scrambling. As will be further discussed in section 4.7, the Pd intermediate which undergoes nucleophilic displacement to the major enantiomer of product **3a** might be

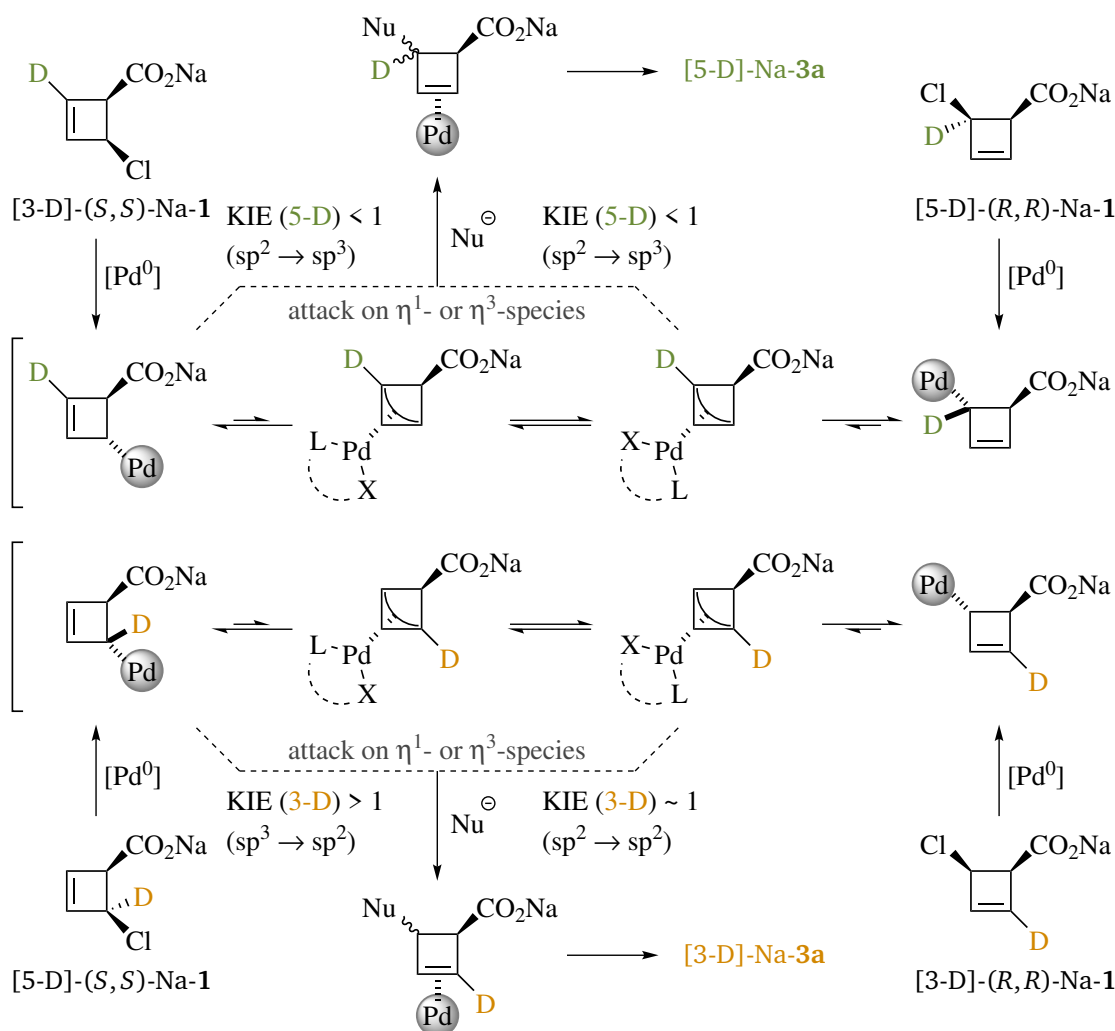


**Scheme 4.14:** General scenarios for the resolution of a racemic mixture of enantiomers  $A^*$  and *ent*- $A^*$  by means of a DYKAT, using a chiral, non-racemic catalyst or reagent  $C^*$ : **(a)** Enantioselectivity based on a fast upstream equilibrium between diastereomeric intermediates  $A^*C^*$  and *ent*- $A^*C^*$ , which can react to product enantiomers  $P^*$  and *ent*- $P^*$ , respectively (type I); **(b)** Competing formation of  $P^*$  and *ent*- $P^*$  from one common intermediate  $A-C^*$  (type II). In both scenarios, formation of these intermediates from  $A^*$  and *ent*- $A^*$  might be reversible or irreversible.



either one of the two diastereomeric  $\eta^1$ -species or one of the two possible electronically unsymmetric  $\eta^3$ -intermediates exhibiting a *trans*-effect that renders only one of the allylic termini reactive.

Regardless of whether the reactive Pd-allyl species is  $\eta^1$ - or  $\eta^3$ -coordinated, an inverse KIE is expected for the [5-D]-position ( $sp^2 \rightarrow sp^3$ ), whereas KIE (3-D) is supposed to be either normal ( $sp^3 \rightarrow sp^2$  for attack on  $\eta^1$ -complex) or close to unity (no hybridization change for attack on  $\eta^3$ -species, Scheme 4.15). Accordingly, the experimentally determined relative reactivities  $\frac{k(5-D)}{k(3-D)} = \frac{KIE(3-D)}{KIE(5-D)}$  are expected to be  $> 1$ , which is in agreement with the values  $\frac{k(5-D)}{k(3-D)} = 1.05 \pm 0.02$  (**L1**) and  $\frac{k(5-D)}{k(3-D)} = 1.16 \pm 0.04$  (**L2**) obtained by product analysis. The clearly larger value measured with ligand **L2** indicates a stronger relative hybridization change upon nucleophilic attack compared to the reaction performed with **L1**.



**Scheme 4.15:** Scrambling of the allylic termini upon  $\eta^1$ - $\eta^3$ - $\eta^1$  isomerization and expected magnitudes of the relative KIE  $\frac{k(5-D)}{k(3-D)} = \frac{KIE(3-D)}{KIE(5-D)}$  observed in the reaction with malonate nucleophile Na-2a (denoted as Nu<sup>⊖</sup>). L and X are two electronically distinct ligation sites, with L having a stronger *trans*-effect than X.

---

The  $^{13}\text{C}$ -KIEs determined for nucleophile Na-**2a** are informative on nucleophilic attack as well, since from the nucleophile's perspective this step denotes the substrate-committing transition state. The relatively small values of  $\frac{k(\beta\text{-}^{13}\text{C})}{k(\alpha\text{-}^{13}\text{C})} = 1.015 \pm 0.003$  (**L1**) and  $\frac{k(\beta\text{-}^{13}\text{C})}{k(\alpha\text{-}^{13}\text{C})} = 1.013 \pm 0.002$  (**L2**) are consistent with a late transition state for nucleophilic attack, as has been postulated for Pd-<sup>[306,507,519–521]</sup> and Mo-catalyzed<sup>[522]</sup> allylic alkylations using stabilized nucleophiles.

In order to allow for concluding if nucleophilic attack proceeds on a  $\eta^1$ - or on a  $\eta^3$ -intermediate, both paths were investigated computationally by MATTHIAS BRAUSER, giving calculated KIEs as comparative values for the experimental ones. In the following subchapter, the conclusions derived from these computational studies in conjunction with the experimental results disclosed in sections 4.2–4.6 will be discussed.

---

## 4.7 Discussion of the Mode of Nucleophilic Attack

---

Based on the experimental data presented in this work, two mechanistic scenarios can be conceived for nucleophilic attack. On the one hand, the malonate nucleophile might react directly with the spectroscopically characterized *anti*-configured  $\eta^1$ -complexes. These have been shown to rapidly interconvert between two diastereomeric species, with one of them being significantly enriched (section 4.2). Enantioselectivity may thus arise from the statistical advantage of the major species and/or from a difference in reactivity between both complexes. For  $\eta^1$ -coordinated Pd-allyl species ligated by chloride, experimental evidence has been reported for a direct  $\text{S}_{\text{N}}2'$ -type displacement with amines as nucleophiles,<sup>[137,138]</sup> albeit with an approximately 100 times lower rate constant than the corresponding  $\eta^3$ -complexes.<sup>[137]</sup> However, no such precedence exists – to the best of my knowledge – for malonate nucleophiles.

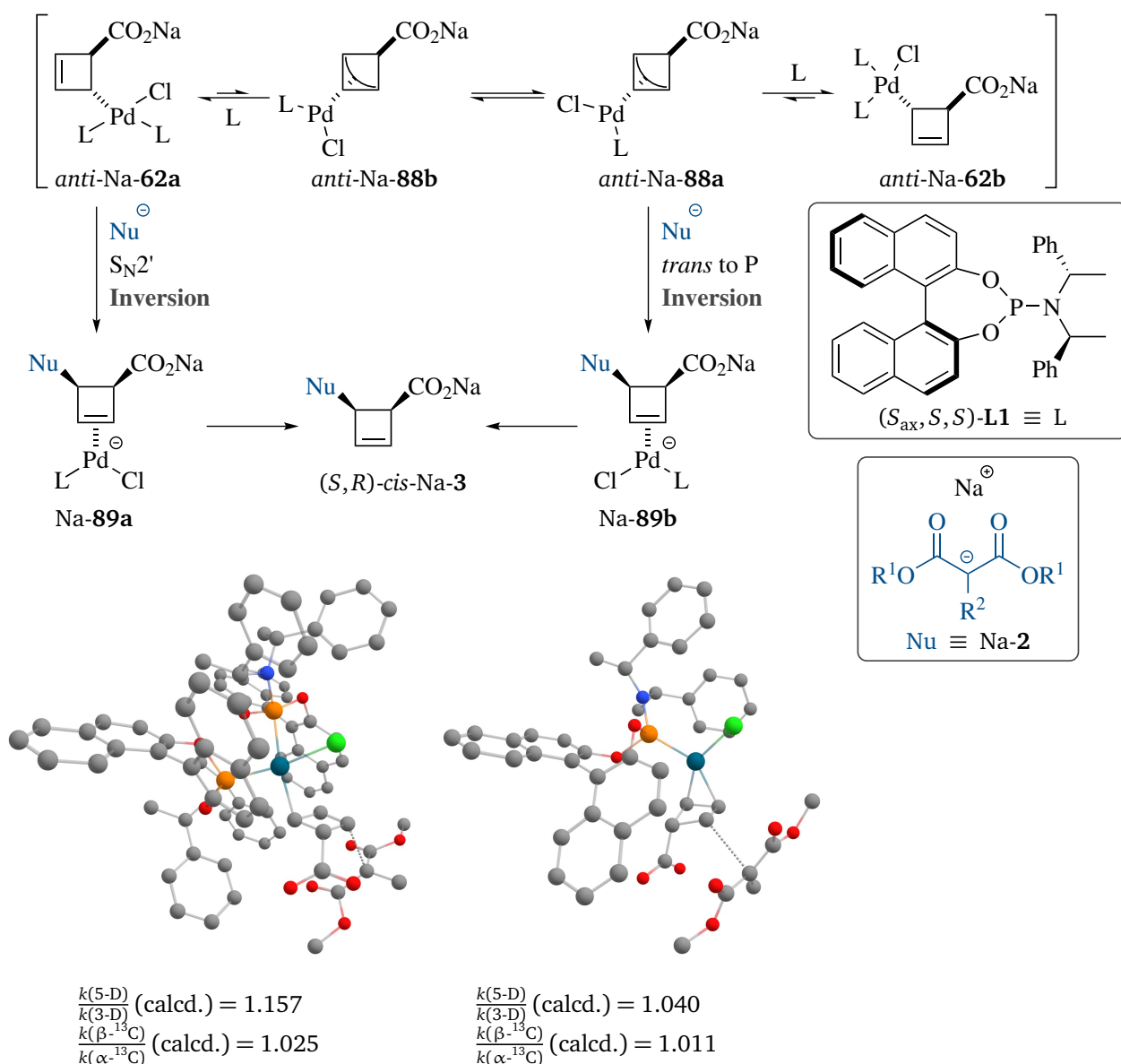
On the other hand, nucleophilic attack might proceed on the undetected  $\eta^3$ -coordinated Pd-cyclobutene species. As part of previous studies, DFT calculations have shown that these are transient intermediates in the suprafacial interconversion between diastereomeric  $\eta^1$ -complexes.<sup>[57,58]</sup> With both ligand **L1** and **L2**, two diastereomeric, electronically unsymmetric  $\eta^3$ -complexes are possible (*vide infra*), which might again be populated differently and/or differ in reactivity towards nucleophile, giving rise to enantioselectivity.

For all four scenarios, i.e. nucleophilic attack on a  $\eta^1$ - or a  $\eta^3$ -intermediate ligated by either **L1** or **L2**, the path leading to the major enantiomer of substitution product **3a** was explored computationally by MATTHIAS BRAUSER at the  $\omega\text{B97M-V}$ <sup>[523]</sup> ZORA-TZVPP (SARC-ZORA-TZVPP for palladium)<sup>[524]</sup> CPCM (THF)<sup>[525]</sup> level of theory, using implicit solvation at 273 K (part of ongoing Ph.D. work, unpublished results). From the transition states obtained, KIEs were calculated and refined by means of the WIGNER tunneling correction,<sup>[526]</sup> thus complementing the experimental values referring to the nucleophilic displacement step (section 4.6).

As a starting point for transition state calculations, the structure of reacting Pd species and the position of nucleophilic attack had to be decided. The structure of  $\eta^1$ -configured Pd-cyclobutene

species has been elucidated experimentally (section 4.2), whereas no characterization data are available for their  $\eta^3$ -analogues. Upon formation of  $\eta^3$ -species from the corresponding  $\eta^1$ -complexes, the weakest bound ligand is expected to dissociate to accommodate the increase in allyl hapticity. As has been shown in section 4.2, internally chelated Pd–cyclobutene species of monodentate ligand **L1** are coordinated by only one equivalent of **L1**, whereas the corresponding complexes without internal coordination contain two equivalents of **L1**. Hence,  $\eta^1$ -complexes *anti*-Na-**62** are anticipated to expel one equivalent of **L1** upon allyl slippage rather than losing chloride, giving chloride-coordinated  $\eta^3$ -intermediates *anti*-Na-**88** (Scheme 4.16). *P, Cl*-ligated Pd–allyl complexes have been reported to be more electrophilic than the corresponding *P, P* species, and nucleophilic attack on these has been shown to proceed *trans* with respect to the phosphine ligand (cf. section 2.2.3).<sup>[66,180,181]</sup> Thus, provided the predominantly reacting electrophile is  $\eta^3$ -coordinated, enantioselectivity is expected to be based on selective nucleophilic capture of diastereomeric *P, Cl*-ligated  $\eta^3$ -complexes *anti*-Na-**88a** and *anti*-Na-**88b**, which rapidly interconvert and are anticipated to differ in population and reactivity towards nucleophile Na-**2**. As for the alternative path, i.e. the selective nucleophilic displacement of  $\eta^1$ -intermediate *anti*-Na-**62a**, an  $S_N2'$ -like displacement is expected based on literature precedence invoking the direct reaction of  $\eta^1$ -coordinated Pd-,<sup>[137,138]</sup> Rh-<sup>[141,142]</sup> and Fe-complexes<sup>[143,144]</sup> with soft nucleophiles.

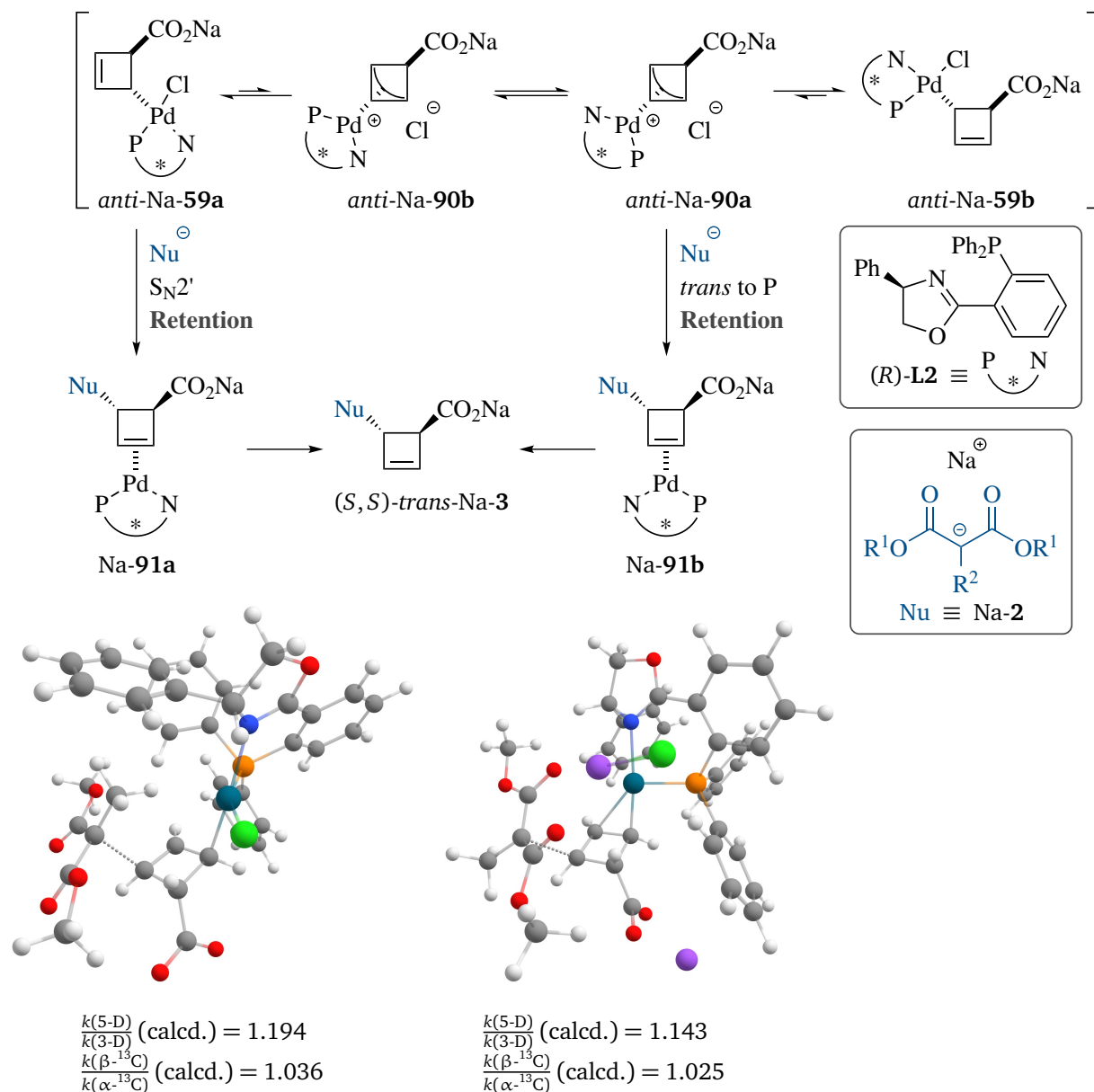
The transition states calculated for both scenarios with ligand **L1** are shown in Scheme 4.16. The energetic barrier for nucleophilic attack on  $\eta^3$ -species *anti*-Na-**88a** ( $\Delta^\ddagger G$  (calcd.)  $\approx 27$  kcal mol<sup>-1</sup>) was found to be significantly lower than for the corresponding path on  $\eta^1$ -complex *anti*-Na-**62a** ( $\Delta^\ddagger G$  (calcd.)  $\approx 37$  kcal mol<sup>-1</sup>). Furthermore, the KIEs calculated for the former scenario ( $\frac{k(5-D)}{k(3-D)}$  (calcd.) = 1.040,  $\frac{k(\beta-^{13}C)}{k(\alpha-^{13}C)}$  (calcd.) = 1.011) are in reasonable agreement with the experimentally determined values ( $\frac{k(5-D)}{k(3-D)}$  = 1.05  $\pm$  0.02 (product analysis),  $\frac{k(\beta-^{13}C)}{k(\alpha-^{13}C)}$  = 1.015  $\pm$  0.003), whereas the KIEs predicted for nucleophilic displacement on  $\eta^1$ -complex *anti*-Na-**62a** ( $\frac{k(5-D)}{k(3-D)}$  (calcd.) = 1.157,  $\frac{k(\beta-^{13}C)}{k(\alpha-^{13}C)}$  (calcd.) = 1.025) are clearly not consistent with those. Additional support for nucleophilic attack on a  $\eta^3$ -species as main path can be found in the kinetic rate orders extracted in section 4.5. With ligand **L1**, an initial zero-order dependence on both substrate and nucleophile concentration has been determined, which indicates that a monomolecular reaction step connecting two Pd intermediates is initially turnover-limiting. In case of nucleophilic attack on a  $\eta^1$ -species as the predominant scenario, this can only be the dissociation of product from Pd–product complex Na-**89**, which seems, however, improbable, as  $\eta^2$ -complexation/decomplexation processes are usually characterized as rapid equilibria.<sup>[527,528]</sup> If, on the other hand, nucleophilic capture proceeds on a  $\eta^3$ -coordinated species, the  $\eta^1$ – $\eta^3$  interconversion becomes on-cycle for both enantiomers of substrate **1**, thus coming into consideration as turnover-limiting step as well. This appears plausible, given the relatively high calculated barriers of  $\Delta G^\ddagger = 9$ –14 kcal mol<sup>-1</sup> that have been reported for  $\eta^1$ – $\eta^3$  processes of Pd–cyclobutene complexes.<sup>[57,58]</sup>



**Scheme 4.16:** Mechanistic scenarios considered for the C–C bond forming step with ligand ( $S_{ax}, S, S$ )-L1:  $S_N2'$ -type attack on  $\eta^1$ -complex *anti*-Na-62a (left) and outer-sphere attack on  $\eta^3$ -species *anti*-Na-88a *trans* to P (right), with calculated transition states and predicted relative KIEs  $\frac{k(5-D)}{k(3-D)}$  (calcd.) and  $\frac{k(\beta-^{13}C)}{k(\alpha-^{13}C)}$  (calcd.) for both paths (MATTHIAS BRAUSER, part of ongoing Ph.D. work, unpublished results).

For the reaction system involving PHOX ligand L2, allylic isomerization of  $\eta^1$ -species *anti*-Na-59 is expected to be accompanied by dissociation of chloride as weakest ligand, since internally coordinated Pd–cyclobutene complexes have been found still to be *P,N*-chelated, indicating that expulsion of chloride occurs rather than dissociation of one of the two ligating sites of L2 (section 4.2). The resulting  $\eta^3$ -complexes *anti*-Na-90 are again proposed to exist in two interconverting diastereomeric forms (Scheme 4.17). For related PHOX-ligated systems, this equilibrium has been reported to strongly favor one of these diastereomers,<sup>[300]</sup> and the major

species has been disclosed to be more reactive towards outer-sphere nucleophilic attack due to a stronger *trans*-effect exerted by the P-donor site compared to the minor species.<sup>[271,307]</sup>



**Scheme 4.17:** Mechanistic scenarios considered for the C–C bond forming step with ligand (R)-L2: S<sub>N</sub>2'-type attack on η<sup>1</sup>-complex *anti*-Na-59a (left) and outer-sphere attack on η<sup>3</sup>-species *anti*-Na-90a *trans* to P (right), with calculated transition states and predicted relative KIEs  $\frac{k(5-D)}{k(3-D)}$  (calcd.) and  $\frac{k(\beta-^{13}C)}{k(\alpha-^{13}C)}$  (calcd.) for both paths (MATTHIAS BRAUSER, part of ongoing Ph.D. work, unpublished results).

In section 4.2, nucleophilic displacement of L2-ligated Pd–cyclobutene complexes has been shown to proceed under retention, seemingly suggesting an inner-sphere mechanism. However, no experimental evidence has been obtained supporting this scenario (section 4.4), which is also – to the best of the author’s knowledge – unprecedented for malonates nucleophiles under Pd catalysis. Thus, it appears more probable that nucleophilic attack follows an outer-sphere

---

path with anomalous retentive stereospecificity, potentially as a consequence of electrostatic repulsion between the anionic carboxylate group and the incoming anionic nucleophile.

Computational analysis of nucleophilic attack on both  $\eta^1$ -intermediate *anti*-Na-**59a** and  $\eta^3$ -coordinated isomer *anti*-Na-**90a** furnished the transition states depicted in Scheme 4.17. The latter path was found to be clearly lower in activation energy ( $\Delta G^\ddagger$  (calcd.)  $\approx$  31 kcal mol<sup>-1</sup>) compared to nucleophilic capture of the corresponding  $\eta^1$ -complex ( $\Delta G^\ddagger$  (calcd.)  $\approx$  39 kcal mol<sup>-1</sup>), analogous to the computational results obtained with ligand **L1**. However, the calculated KIEs for nucleophilic displacement of both  $\eta^1$ -species *anti*-Na-**59a** ( $\frac{k(5-D)}{k(3-D)}$  (calcd.) = 1.194,  $\frac{k(\beta-^{13}C)}{k(\alpha-^{13}C)}$  (calcd.) = 1.036) and  $\eta^3$ -complex *anti*-Na-**90a** ( $\frac{k(5-D)}{k(3-D)}$  (calcd.) = 1.143,  $\frac{k(\beta-^{13}C)}{k(\alpha-^{13}C)}$  (calcd.) = 1.025) are not in agreement with the experimental values ( $\frac{k(5-D)}{k(3-D)}$  = 1.16  $\pm$  0.04 (product analysis),  $\frac{k(\beta-^{13}C)}{k(\alpha-^{13}C)}$  = 1.013  $\pm$  0.002), albeit the KIEs predicted for attack on the  $\eta^3$ -intermediate are somewhat closer. Hence, the reaction step considered might include additional interactions that have not been taken into account adequately by the transition state calculations performed.

In summary, combined interrogation of experimental and computational data clearly suggests nucleophilic capture of **L1**-ligated Pd-allyl species to proceed via outer-sphere attack on a short-living *P, Cl*  $\eta^3$ -intermediate under inversion of configuration. With ligand **L2**, on the other hand, the underlying mechanism of retentive nucleophilic displacement can not be concluded unambiguously, as the experimental data are not fully consistent with either of the two scenarios investigated computationally. Presently, outer-sphere attack on a transient *P, N*  $\eta^3$ -intermediate appears to be more likely, potentially involving more complex interactions such as tight ion-pair binding<sup>[68,69,418]</sup> that are difficult to model computationally.

---

## 5 Conclusion and Outlook

Due to its wide array of opportunities for controlling regio- and stereoselectivity, asymmetric allylic substitution has been established both as a valuable synthetic tool for the enantioselective construction of chiral building blocks and as a model reaction for chiral ligand design. The high levels of selectivity typically observed are based on a combination of delicate mechanistic interactions, which is individual for every system.<sup>[43,48]</sup> The Pd-catalyzed allylic alkylation of racemic cyclobutene substrates **1** with malonate nucleophiles Na-**2** represents an especially remarkable variant. This system has been showcased to exhibit the characteristics of a diastereodivergent deracemization and de-epimerization with the overall stereoselectivity mediated by the ligand, thus contrasting the commonly accepted ‘double inversion rule’.<sup>[55,56]</sup> Previous mechanistic work has revealed that oxidative addition furnishes stable  $\eta^1$ -coordinated Pd-allyl species, which can interconvert via a suprafacial  $\eta^1$ - $\eta^3$ - $\eta^1$  path.<sup>[57,58]</sup> However, the key interactions responsible for the unexpected stereoselectivity have remained elusive, which has prompted the THIELE group to perform a comprehensive mechanistic study aiming to elucidate those. Herein, the findings of this study are presented and an overarching reaction mechanism is proposed, which rationalizes the stereoselectivity observed.

As shown by a systematic screening of oxidative addition, *cis*-configured cyclobutene substrates react to a rapidly interconverting mixture of two diastereomeric *anti*-configured  $\eta^1$ -species, whereas *trans*-substrates afford both *anti*- and *syn*-configured complexes, the latter stabilized by internal Pd–O chelation through the substrate’s carboxy group. NMR reaction monitoring experiments, conducted in collaboration with JULIAN ILGEN,<sup>[345]</sup> have revealed the  $\eta^1$ -complexes to be the primary oxidative addition products, which subsequently equilibrate via the short living  $\eta^3$ -species. This  $\eta^1$ - $\eta^3$ - $\eta^1$  exchange has been found to be significantly faster for *anti*-configured complexes compared to their *syn*-analogues, which is likely a consequence of internal coordination stabilizing the *syn*-configured  $\eta^1$ -species towards allyl slippage. When the *anti*- and *syn*-configured Pd–cyclobutene species prepared were treated with model nucleophile Na-**2a**, only the former reacted to substitution products **3a**, whereas the *syn*-complexes turned out to be entirely unreactive. Further insight has been obtained by intermediate capture experiments, disclosing that under catalytic conditions *anti*-configured Pd–cyclobutene species are generally present regardless of the relative configuration of substrate **1**, whilst *syn*-complexes are only generated if *trans*-**1** is used. The general intermediacy of *anti*-configured Pd species was ultimately confirmed by means of ESI-HRMS and <sup>31</sup>P-NMR analyses under catalytic conditions, which were capable of detecting these complexes as transient species during turnover. Based on the findings described, a preliminary mechanism has been proposed, featuring a convergent



---

behavior for oxidative addition and a divergent behavior for nucleophilic attack (published in *J. Am. Chem. Soc.* **2023**, *145*, 15912–15923).

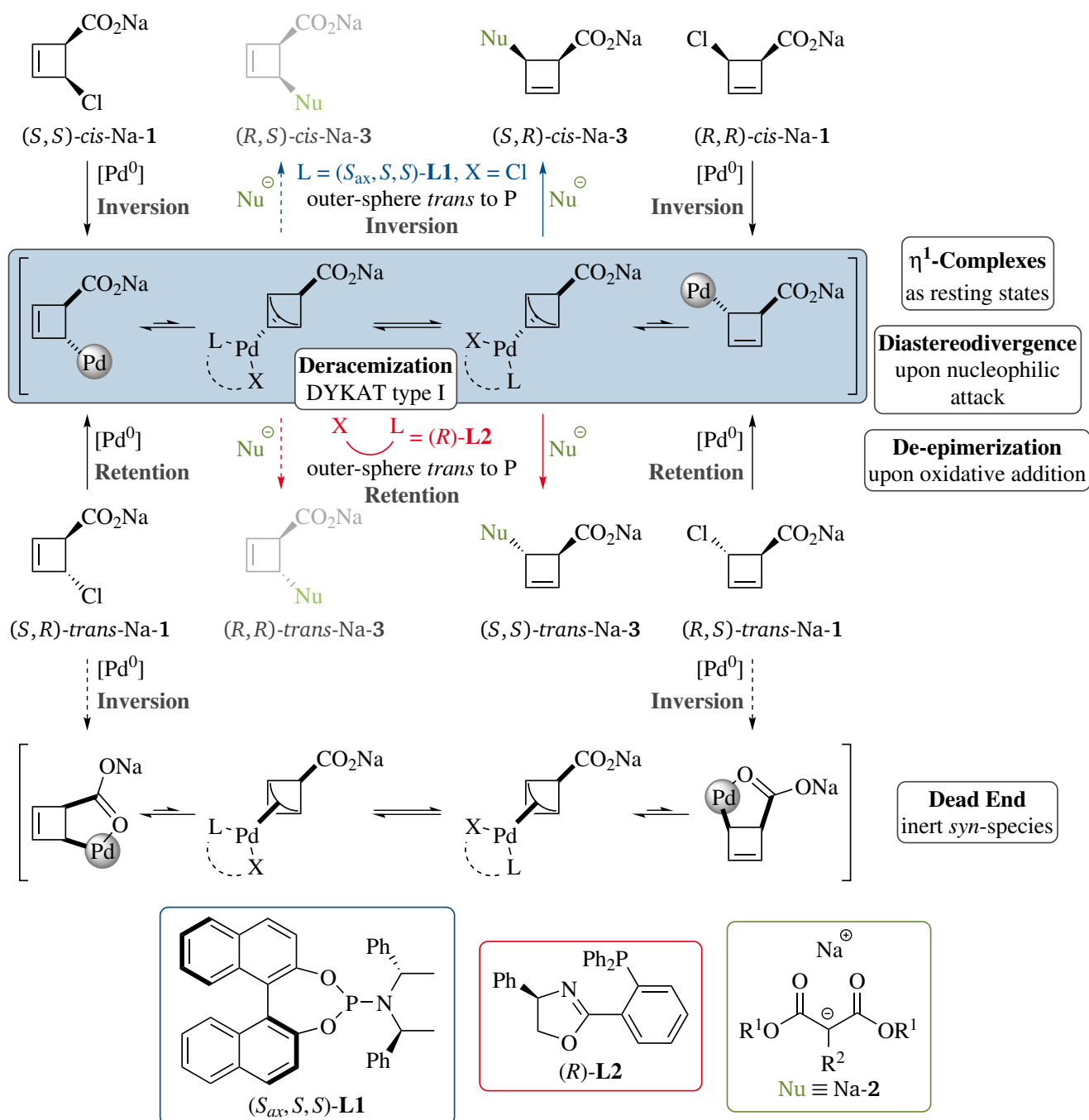
Further studies have been undertaken to gain deeper insight into the mechanism of key steps, with a special focus on nucleophilic attack, which has been shown to proceed under inversion with ligand **L1** and under retention in the presence of **L2**. Systematic variation of the bulkiness of nucleophile Na-**2** in the catalytic reaction displayed no significant influence on enantio- and diastereoselectivity, indicating that nucleophilic attack does not involve a pronounced steric interplay between Pd–allyl intermediate and incoming nucleophile. Experiments have been conducted designed to evidence a potential inner-sphere mechanism for nucleophilic attack with ligand **L2**, which has previously been proposed for the somewhat less stabilized enolate anions<sup>[136,436–439]</sup> and would rationalize the unconventional retentive stereospecificity observed with this ligand. However, catalytic reactions performed with a  $\beta$ -deuterated nucleophile did not yield any detectable amount of the  $\beta$ -deuteride elimination products expected as side products in the event of an inner-sphere mechanism, and complexation experiments exhibited no detectable affinity between [Pd–**L2**] and the malonate anion.

Kinetic rate order analysis has revealed that in the presence of **L2** the attack of nucleophile is the turnover-limiting step. For the reaction performed with **L1**, on the other hand, the experimental data suggest a monomolecular step connecting two Pd intermediates to be turnover-determining in the low-conversion regime, with nucleophilic attack becoming turnover-limiting at high conversion. In addition, reactions catalyzed by [Pd–**L1**] have been found to achieve significantly higher turnover rates compared to those promoted by [Pd–**L2**].

The reaction has further been studied by means of <sup>2</sup>H- and <sup>13</sup>C-KIEs, determined by intermolecular competition experiments for both substrate *cis*-**1** (deuterated isotopologues prepared by PATRICK MAIBACH<sup>[378]</sup>) and model nucleophile Na-**2a**. The different experimental values can be categorized into KIEs reflecting the transition state of oxidative addition and KIEs characterizing the nucleophilic displacement step, depending on which of these two steps irreversibly consumes the starting material considered. The former are in qualitative agreement with oxidative addition following an S<sub>N</sub>2- rather than an S<sub>N</sub>2'-type path. The values reflecting the nucleophilic displacement step could be used to appraise transition state calculations for nucleophilic attack on both  $\eta^1$ - and  $\eta^3$ -coordinated Pd–allyl intermediates (MATTHIAS BRAUSER, part of ongoing Ph.D. work, unpublished results). Under both conditions investigated, the latter scenario has been computed to be energetically favored. The KIEs determined in the presence of **L1** are in reasonable agreement with the values predicted for attack on a  $\eta^3$ -species, consistent with the energetic preference for this path. The KIEs extracted under catalysis of **L2**, on the other hand, do hitherto not match the values predicted for either of the two scenarios considered. A better match between experimental and calculated KIEs might be achieved either by further refinement of the transition state structures computed or by considering more possible scenarios for this step such as the involvement of tight ion-pair binding.<sup>[68,69,418]</sup>



The data reported in this work can be summarized to an overarching mechanistic proposal (Scheme 5.1). Accordingly, de-epimerization is anchored in oxidative addition, which proceeds under inversion with substrate *cis*-**1** and under retention with *trans*-**1** to give two diastereomeric *anti*-configured  $\eta^1$ -species as catalyst resting states. These rapidly interconvert via at least two short-living  $\eta^3$ -intermediates and thus enable deracemization via a DYKAT type I process, i.e.



**Scheme 5.1:** Overarching mechanism proposed for the Pd-catalyzed asymmetric allylic alkylation of cyclobutene substrates **1** with malonate nucleophiles Na-2. L and X are two electronically distinct ligation sites, with L having a stronger *trans*-effect than X. Dashed arrows indicate minor reaction paths.

---

enantioselective product formation based on a rapid upstream equilibrium.<sup>[28–30]</sup> For *trans*-**1**, oxidative addition under inversion constitutes a side reaction and catalyst deactivation path, giving slowly interconverting *syn*-configured Pd–cyclobutene complexes that are rendered inert towards nucleophile by strong internal Pd–O chelation. Nucleophilic attack on equilibrating *anti*-complexes can proceed under either inversion with ligand **L1** or retention in the presence of **L2**, which empowers the reaction to display diastereodivergence. For **L1**, experimental and computational data consistently suggest that the transient  $\eta^3$ -species are the reactive electrophiles for the nucleophilic displacement step. In the case of ligand **L2**, on the other hand, the mechanism of nucleophilic capture could not be elucidated unambiguously; however, computational investigations tentatively suggest the  $\eta^3$ -species to be the reactive electrophilic intermediates as well. The divergent nature of nucleophilic attack is believed to be based on a competition between steric hindrance by the ligand backbone ( $\rightarrow$  inversion) and electrostatic repulsion by the anionic carboxylate group ( $\rightarrow$  retention), with the ligand governing which interaction dominates. The results of the present work demand further computational analysis<sup>[529]</sup> of the entire reaction coordinate, with a special focus on oxidative addition, for which calculated transition states would complement the experimental KIEs reflecting this step. Also, the nucleophilic capture of **L2**-ligated Pd–allyl species should be explored in more detail, in order to refine the scenario proposed for this step.

In summary, this work has disclosed a highly unusual and unprecedented mechanistic rationale in the area of allylic substitution chemistry, going far beyond the commonly accepted mechanism for this class of transformations. The scenario proposed encompasses a stereochemical dichotomy for both oxidative addition and nucleophilic attack, allowing both steps to proceed under either inversion or retention. The findings presented represent a notable contribution to the mechanistic knowledge available in the field of asymmetric transition metal catalysis, which is indispensable for the rational design of new variants with innovative stereoselectivity.

---

## 6 Zusammenfassung und Ausblick

Aufgrund der vielfältigen Möglichkeit zur Kontrolle der Regio- und Stereoselektivität stellt die allylische Substitution sowohl eine wertvolle Methode für die enantioselektive Synthese chiraler Verbindungen als auch ein gutes Modellsystem zum Screening neuer chiraler Liganden dar. Die hohen Selektivitäten, wie sie üblicherweise bei dieser Reaktion beobachtet werden, basieren auf einer für jedes Reaktionssystem individuellen Kombination subtiler mechanistischer Wechselwirkungen.<sup>[43,48]</sup> Eine besonders bemerkenswerte Variante ist die Pd-katalysierte allylische Alkylierung racemischer Cyclobutensubstrate **1** mit Malonatnukleophilen Na-**2**. Dieses System weist die Charakteristika einer diastereodivergenten Deracemisierung und Deepimerisierung auf, wobei die Nettostereoselektivität durch den Liganden bestimmt wird und damit die allgemein anerkannte *double inversion* Regel verletzt.<sup>[55,56]</sup> Vorangegangene mechanistische Studien zeigten, dass bei der oxidativen Addition stabile  $\eta^1$ -koordinierte Pd-Allylspezies gebildet werden, welche über einen suprafacialen  $\eta^1-\eta^3-\eta^1$  Pfad miteinander im Gleichgewicht stehen.<sup>[57,58]</sup> Die für die ungewöhnliche Stereoselektivität verantwortlichen Schlüsselwechselwirkungen blieben jedoch spekulativ, was den Arbeitskreis THIELE zu einer umfangreichen mechanistischen Studie veranlasste. In der vorliegenden Arbeit werden die Ergebnisse dieses Projekts vorgestellt und ein allgemeiner Reaktionsmechanismus vorgeschlagen, welcher die beobachtete Selektivität hinreichend erklärt.

Wie durch ein systematisches Screening der oxidativen Addition gezeigt wurde, reagieren *cis*-konfigurierte Cyclobutensubstrate zu einer schnell äquilibrierenden Mischung zweier diastereomerer, *anti*-konfigurierter  $\eta^1$ -Spezies, wohingegen *trans*-Substrate sowohl *anti*- als auch *syn*-konfigurierte Komplexe bilden, letztere stabilisiert durch interne Pd–O Chelatisierung über die Carboxygruppe des Substrats. NMR-Reaktionsverfolgung, durchgeführt in Zusammenarbeit mit JULIAN ILGEN,<sup>[345]</sup> offenbarte, dass die  $\eta^1$ -Komplexe die primären Produkte der oxidativen Addition sind und daraufhin über die kurzlebigen  $\eta^3$ -Spezies miteinander im Gleichgewicht stehen. Dieser  $\eta^1-\eta^3-\eta^1$  Austausch verlief im Falle der *anti*-konfigurierten Komplexe wesentlich schneller als mit den entsprechenden *syn*-Spezies, was wahrscheinlich auf die interne Koordination der *syn*-koordinierten Komplexe und eine damit einhergehende Stabilisierung gegen allylische Isomerisierung zurückgeht. Durch Zugabe des Modellnukleophils Na-**2a** zu *anti*-konfigurierten Pd-Cyclobutenkomplexen wurden die entsprechenden Substitutionsprodukte **3a** erhalten, wohingegen sich die *syn*-Komplexe unter gleichen Bedingungen gänzlich unreaktiv verhielten. Weitere Einblicke wurden durch Intermediat-Abfangexperimente gewonnen. Diese förderten zu Tage, dass *anti*-konfigurierte Pd-Cyclobutenspezies unter katalytischen Bedingungen immer involviert sind, unabhängig von der Relativkonfiguration des Substrats **1**, wohingegen

---

*syn*-Komplexe nur dann gebildet werden, wenn *trans*-**1** verwendet wird. Die Rolle der *anti*-konfigurierten Pd-Spezies als generelle Intermediate wurde schließlich durch ESI-HRMS- und <sup>31</sup>P-NMR-Experimente unter katalytischen Bedingungen bestätigt. Dabei wurden diese Komplexe als transiente Spezies bei laufendem *turnover* beobachtet. Auf Basis der beschriebenen Ergebnisse wurde ein vorläufiger Mechanismus vorgeschlagen, wonach die oxidative Addition ein konvergentes und der nukleophile Angriff ein divergentes Verhalten aufweist (publiziert in *J. Am. Chem. Soc.* **2023**, *145*, 15912–15923).

Weitere Untersuchungen hatten zum Ziel, die Schlüsselschritte der Reaktion näher zu beleuchten. Dabei war vor allem der Mechanismus des nukleophilen Angriffs von Interesse, welcher – wie zuvor gezeigt worden war – mit Ligand **L1** unter Inversion und mit Ligand **L2** unter Retention verläuft. Durch Variation des sterischen Anspruchs von Nukleophil Na-**2** unter katalytischen Bedingungen wurde kein signifikanter Einfluss auf die Enantio- und Diastereoselektivität festgestellt. Daher kann davon ausgegangen werden, dass während des nukleophilen Angriffs keine ausgeprägten sterischen Wechselwirkungen zwischen intermediärem Pd-Allylkomplex und Nukleophil vorliegen. Weiterhin wurden Experimente durchgeführt, welche einen möglichen *inner sphere* Mechanismus für den nukleophilen Angriff mit Ligand **L2** belegen sollten. Dieser wurde in der Literatur für die etwas weniger stabilisierten Enolatanionen vorgeschlagen<sup>[136,436–439]</sup> und würde eine valide Erklärung für die mit **L2** beobachtete unkonventionelle retentive Stereospezifität darstellen. Allerdings lieferten katalytische Reaktionen, bei denen ein  $\beta$ -deuteriertes Nukleophil eingesetzt wurde, keine nachweisbare Menge der im Falle eines *inner sphere* Mechanismus durch eine konkurrierende  $\beta$ -Deuterideliminierung erwarteten Nebenprodukte, und Komplexierungsexperimente zeigten keine detektierbare Affinität zwischen [Pd–**L2**] und dem Malonatanion.

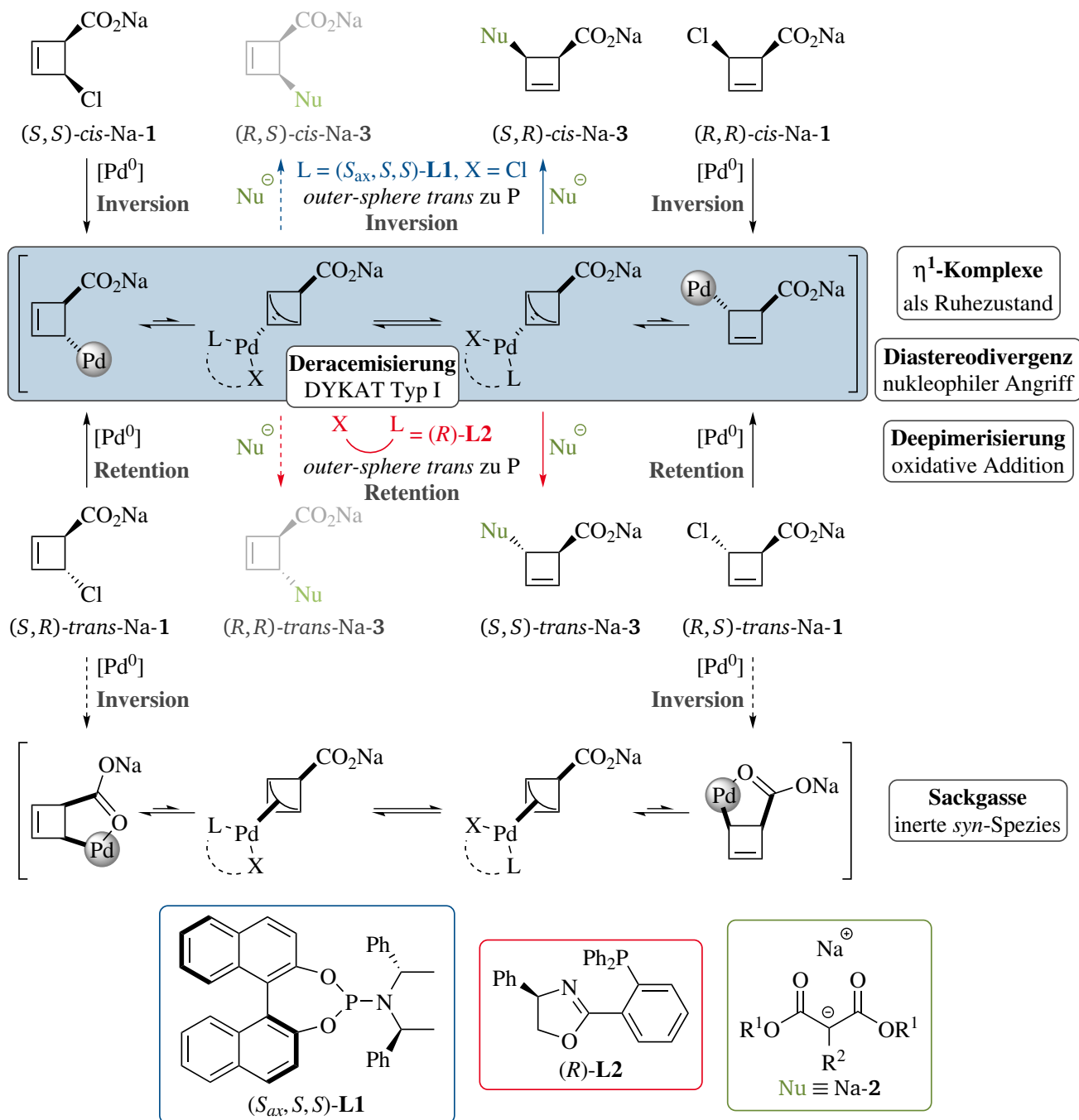
Durch Bestimmung der kinetischen Reaktionsordnungen wurde ermittelt, dass mit Ligand **L2** der Angriff des Nukleophils geschwindigkeitsbestimmend ist. Mit Ligand **L1** lassen die experimentellen Daten dagegen darauf schließen, dass bei niedrigem Umsatz eine monomolekulare Pd-Intermediatumwandlung der limitierende Schritt ist, wohingegen bei hohem Umsatz der Angriff des Nukleophils geschwindigkeitsbestimmend wird. Des Weiteren erreichten die durch [Pd–**L1**] katalysierten Reaktionen deutlich höhere Reaktionsraten als jene, die in Gegenwart von [Pd–**L2**] durchgeführt wurden.

Zur weiteren Untersuchung wurden <sup>2</sup>H- und <sup>13</sup>C-KIEs sowohl für das Substrat *cis*-**1** als auch für das Modellnukleophil Na-**2a** extrahiert. Die experimentelle Bestimmung erfolgte durch intermolekulare Konkurrenzexperimente (deuterierte Isotopologe von *cis*-**1** synthetisiert durch PATRICK MAIBACH<sup>[378]</sup>). Die verschiedenen experimentellen Werte können unterteilt werden in solche, die den Übergangszustand der oxidativen Addition widerspiegeln, und KIEs, welche den nukleophilen Substitutionsschritt charakterisieren, abhängig davon, in welchem dieser beiden Schritte das betrachtete Edukt irreversibel verbraucht wird. Erstere Werte stimmen qualitativ mit den Erwartungswerten für eine S<sub>N</sub>2-artige oxidative Addition überein und weichen klar von

---

den für einen  $S_N2'$ -artigen Mechanismus erwarteten KIEs ab. Jene Werte, die den nukleophilen Substitutionsschritt widerspiegeln, konnten zur Evaluierung berechneter Übergangszustände für einen nukleophilen Angriff an  $\eta^1$ - und an  $\eta^3$ -koordinierte Pd-Allylintermediate verwendet werden (MATTHIAS BRAUSER, Teil der in Arbeit befindlichen Dissertation, unveröffentlichte Ergebnisse). Unter beiden untersuchten Reaktionsbedingungen wurde für letzteres Szenario eine niedrigere Energiebarriere berechnet. Die mit Ligand **L1** ermittelten KIEs stimmen im Rahmen der experimentellen Abweichung mit den für einen Angriff an einer  $\eta^3$ -Spezies berechneten KIEs überein, konsistent damit, dass dieser Pfad energetisch bevorzugt ist. Die mit **L2** extrahierten KIEs passen dagegen nach bisherigem Stand zu keinem der beiden simulierten Szenarien. Eine bessere Übereinstimmung zwischen experimentellen und berechneten KIEs könnte entweder durch weitere Verfeinerung der simulierten Übergangszustände oder durch die Betrachtung weiterer möglicher Szenarien für diesen Reaktionsschritt, z.B. das Auftreten von Kontaktionenpaaren,<sup>[68,69,418]</sup> erreicht werden.

Die in der vorliegenden Arbeit dargelegten experimentellen Daten können zu dem in Schema 6.1 gezeigten allgemeinen Mechanismus zusammengefasst werden. Demnach ist die Deepimerisierung in der oxidativen Addition verankert, welche mit Substrat *cis-1* unter Inversion und mit *trans-1* unter Retention verläuft. Dabei werden zwei diastereomere *anti*-konfigurierte  $\eta^1$ -Spezies gebildet, welche den Ruhezustand des Katalysezyklus bilden. Diese wandeln sich über mindestens zwei kurzlebige  $\eta^3$ -Intermediate schnell ineinander um und ermöglichen so die Deracemisierung über eine DYKAT Typ I, d.h. die enantioselektive Produktbildung basiert auf einem schnellen vorgelagerten Gleichgewicht.<sup>[28–30]</sup> Im Falle von *trans-1* stellt die oxidative Addition unter Inversion gleichsam eine Nebenreaktion und einen Katalysatordeaktivierungspfad dar, wobei langsam äquilibrierende, *syn*-konfigurierte Pd-Cyclobutenkomplexe entstehen, die aufgrund einer starken internen Pd–O Chelatisierung inert gegenüber dem Nukleophil sind. Der nukleophile Angriff auf die miteinander im Gleichgewicht stehenden *anti*-Komplexe kann entweder unter Inversion mit Ligand **L1** oder unter Retention mit **L2** erfolgen, was sich makroskopisch in der experimentell beobachteten Diastereodivergenz äußert. Für **L1** legen experimentelle und theoretische Daten übereinstimmend nahe, dass die transienten  $\eta^3$ -Spezies die reaktiven Elektrophile für den nukleophilen Substitutionsschritt sind. Im Falle von Ligand **L2** konnte der Mechanismus des nukleophilen Angriffs dagegen nicht eindeutig geklärt werden; jedoch lassen die durchgeführten Rechnungen vorsichtig darauf schließen, dass auch unter diesen Bedingungen die  $\eta^3$ -Spezies die reaktiven elektrophilen Intermediate darstellen. Als Ursache für die divergente Natur des nukleophilen Angriffs werden eine sterische Hinderung durch den Liganden ( $\rightarrow$  Inversion) und eine elektrostatische Abstoßung durch die anionische Carboxylatgruppe ( $\rightarrow$  Retention) als konkurrierende Wechselwirkungen vermutet, wobei der Ligand bestimmt, welche von diesen dominiert. Zur Komplementierung und Absicherung der Daten dieser Arbeit sind weitergehende computergestützte Untersuchungen<sup>[529]</sup> der gesamten Reaktionskoordinate erforderlich, mit einem besonderen Fokus auf die oxidative Addition. Für diese würden die



**Scheme 6.1:** Allgemeiner mechanistischer Vorschlag für die Pd-katalysierte asymmetrische allylische Alkylierung von Cyclobutensubstraten **1** mit Malonatnukleophilen **Na-2**. L und X bezeichnen zwei elektronisch verschiedene, besetzte Koordinationsstellen, wobei L einen stärkeren *trans*-Effekt ausübt als X. Gestrichelte Pfeile kennzeichnen Nebenreaktionspfade.

simulierten Übergangszustände als komplementäre Daten zu den experimentellen KIEs dienen, welche die oxidative Addition abbilden. Auch der nukleophile Angriff an die **L2**-koordinierten Pd-Allylspezies sollte detaillierter untersucht werden, um das für diesen Schritt vorgeschlagene Szenario besser zu belegen oder gegebenenfalls nachzubessern.

---

Zusammenfassend wurde im Rahmen der vorliegenden Arbeit ein auf dem Gebiet der allylischen Substitution beispielloser Mechanismus aufgeklärt, der weit über die allgemein anerkannte *double inversion* Regel hinausgeht. Das vorgeschlagene Szenario beinhaltet eine stereochemische Dichotomie sowohl für die oxidative Addition als auch für den nukleophilen Angriff, wobei beide Schritte entweder unter Inversion oder unter Retention ablaufen können. Die vorgestellten Ergebnisse bilden einen bedeutenden Betrag zum verfügbaren mechanistischen Wissen auf dem Gebiet der asymmetrischen Metallkatalyse, welches für das rationale Design neuer Varianten mit innovativer Stereoselektivität unentbehrlich ist.



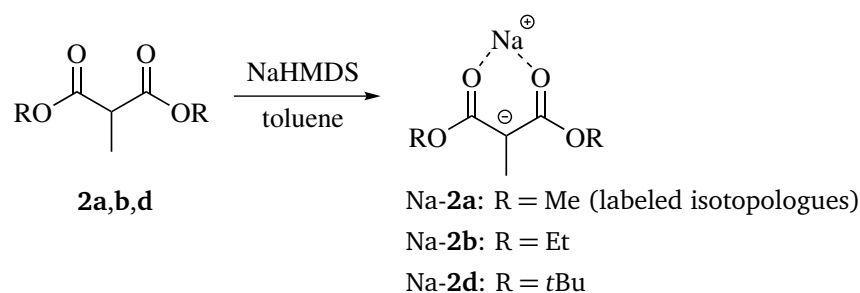


## 7 Experimental Part

The general experimental conditions as well as the synthetic procedures for *cis*- and *trans*-4-chlorocyclobut-2-ene-1-carboxylic acid *cis/trans*-**1**, sodium dimethyl methylmalonate Na-**2a**, *cis*- and *trans*-methyl-4-chlorocyclobutene-2-enecarboxylic carboxylate, 2-(but-3-en-2-yl-1,1,1-*d*<sub>3</sub>)-4,4,5,5-tetramethyl-1,3,2-dioxaborolane, and 4,4,5,5-tetramethyl-2-(4-methylpent-1-en-3-yl)-1,3,2-dioxaborolane can be found in section 4.2 (supporting information, chapters 1 and 2). In addition to the spectrometers reported therein, further measurements were performed on a Bruker AVANCE III 950 MHz spectrometer equipped with a 5 mm <sup>1</sup>H [<sup>13</sup>C, <sup>15</sup>N] TCI cryo probe (located at the Center for Biomolecular Magnetic Resonance (BMRZ), Goethe University Frankfurt). Di-*tert*-butyl methylmalonate **2d** was prepared according to a literature procedure<sup>[422]</sup> (JOP01-11, 19.5 mmol scale, 47 % yield). The synthesis of *cis*-4-chlorocyclobut-2-ene-1-carboxylic-3-*d* acid [4-D]-*cis*-**1** and *cis*-4-chlorocyclobut-2-ene-1-carboxylic-2-*d*<sub>1;0</sub>-4-*d*<sub>0;1</sub> acid [5-D]/[3-D]-*cis*-**1** is described in a related thesis.<sup>[378]</sup> The yields reported in this chapter are generally unoptimized.

### 7.1 Synthesis of Malonates

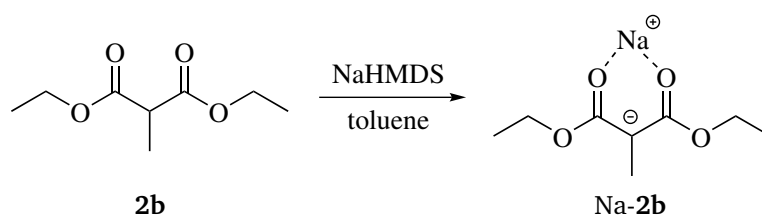
#### General Procedure A: Sodium dialkyl methylmalonates (Na-**2a,b,d**)



To a filtrated solution of NaHMDS (1.00 – 1.05 equiv.) in anhydrous toluene (10 mL) was added malonate **2** (1.0 equiv.) dropwise at 0 °C. After stirring for 15 min, the colorless precipitate was filtered off inertly, washed with anhydrous toluene (3 × 5 mL) followed by anhydrous *n*-hexane (3 × 5 mL), and dried under high vacuum for 30 min to afford crude malonate salts Na-**2a,b,d**, which were stored and handled under inert atmosphere to prevent decomposition.

The isotopologues of sodium dimethyl methylmalonate Na-**2a** were additionally purified by recrystallization from THF/*n*-hexane, realized by dissolving the crude product in a minimum amount of anhydrous THF, followed by slow addition of anhydrous *n*-hexane (tenfold volume of THF). The crystallized product was filtered off inertly and dried under high vacuum for 1 h.

## Sodium diethyl methylmalonate (Na-2b)

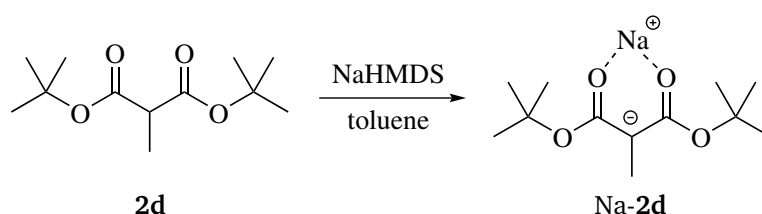


### JOP01-16

Deprotonation of diethyl methylmalonate **2b** (commercially obtained from Fisher Scientific, distilled from CaCl<sub>2</sub> prior to use, 400  $\mu$ L, 2.34 mmol, 1.0 equiv.) with NaHMDS (430 mg, 2.34 mmol, 1.0 equiv.) according to general procedure A afforded the title compound as a colorless solid (ca. 97 w% purity, 287 mg, 1.42 mmol, ca. 61 % yield). As the crude product was found to be sufficiently pure by NMR, further purification by recrystallization was not required.

<sup>1</sup>H-NMR (700 MHz, THF-*d*<sub>8</sub>):  $\delta_{\text{H}}$  = 3.91 (4H, q, <sup>3</sup>J<sub>HH</sub> = 7.1 Hz, OCH<sub>2</sub>), 1.66 (3H, s, C<sub>q</sub>CH<sub>3</sub>), 1.29 (6H, t, <sup>3</sup>J<sub>HH</sub> = 7.1 Hz, OCH<sub>2</sub>CH<sub>3</sub>) ppm; <sup>13</sup>C{<sup>1</sup>H}-NMR (176 MHz, THF-*d*<sub>8</sub>):  $\delta_{\text{C}}$  = 172.3 (C=O), 68.2 (C<sub>q</sub>CH<sub>3</sub>), 57.1 (OCH<sub>2</sub>), 15.7 (OC<sub>2</sub>CH<sub>3</sub>), 11.9 (C<sub>q</sub>CH<sub>3</sub>) ppm; <sup>23</sup>Na-NMR (106 MHz, THF-*d*<sub>8</sub>):  $\delta_{\text{Na}}$  = 0.9 (br. s) ppm; ATR-IR (neat):  $\nu_{\text{max}}$  = 2978 (C–H stretching), 1633 (C=O stretching), 1495 (C=C stretching), 1080 (C–O–C deformation), 784 (H–C–H deformation) cm<sup>-1</sup>; HRMS (APCI<sup>-</sup>): C<sub>8</sub>H<sub>13</sub>O<sub>4</sub> [M–Na]<sup>+</sup> requires 173.0819, found 173.0822 ( $\Delta$  = 1.7 ppm).

## Sodium di-*tert*-butyl methylmalonate (Na-2d)

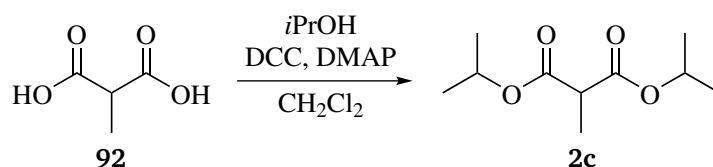


### JOP01-14

Deprotonation of di-*tert*-butyl methylmalonate **2d** (540 mg, 2.34 mmol, 1.0 equiv.) with NaHMDS (430 mg, 2.34 mmol, 1.0 equiv.) according to general procedure A afforded the title compound as a colorless solid (ca. 95 w% purity, 500 mg, 1.88 mmol, ca. 81 % yield). As the crude product was found to be sufficiently pure by NMR, further purification by recrystallization was not required.

<sup>1</sup>H-NMR (700 MHz, THF-*d*<sub>8</sub>):  $\delta_{\text{H}}$  = 1.60 (3H, s, CCH<sub>3</sub>), 1.38 (18H, s, OC(CH<sub>3</sub>)<sub>3</sub>) ppm; <sup>13</sup>C{<sup>1</sup>H}-NMR (176 MHz, THF-*d*<sub>8</sub>):  $\delta_{\text{C}}$  = 172.9 (C=O), 74.0 (OC(CH<sub>3</sub>)<sub>3</sub>), 70.4 (CCH<sub>3</sub>), 29.8 (OC(CH<sub>3</sub>)<sub>3</sub>), 13.4 (CCH<sub>3</sub>) ppm; <sup>23</sup>Na-NMR (159 MHz, THF-*d*<sub>8</sub>):  $\delta_{\text{Na}}$  = 1.4 (br. s) ppm; ATR-IR (neat):  $\nu_{\text{max}}$  = 2972 (C–H stretching), 1663 (C=O stretching), 1531 (C=C stretching), 1375 (C(CH<sub>3</sub>)<sub>3</sub> deformation), 1042 (C–O–C deformation) cm<sup>-1</sup>; HRMS (APCI<sup>-</sup>): C<sub>12</sub>H<sub>21</sub>O<sub>4</sub> [M–Na]<sup>+</sup> requires 229.1445, found 229.1447 ( $\Delta$  = 0.9 ppm).

## Diisopropyl methylmalonate (2c)

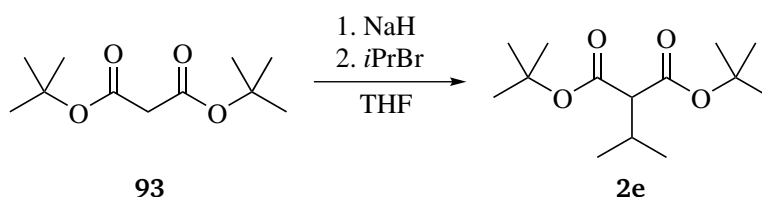


### JOP01-182

The title compound was prepared following a modified literature procedure.<sup>[421]</sup> To a stirred solution of methylmalonic acid (10.0 g, 83.0 mmol, 1.0 equiv.) in anhydrous  $\text{CH}_2\text{Cl}_2$  (60 mL) were added 4-dimethylaminopyridine (DMAP, 1.02 g, 8.3 mmol, 10 mol%) and anhydrous *i*PrOH (16 mL, 208 mmol, 2.5 equiv.). The solution was cooled to 0 °C and *N,N'*-dicyclohexylcarbodiimide (DCC, 38.1 g, 183 mmol, 2.2 equiv.) was added carefully. The reaction mixture was allowed to gradually reach RT over 3 h and then quenched with TFA (0.74 mL, 10.0 mmol, 12 mol%), followed by filtration over silica. The filtrate was concentrated *in vacuo* at 40 °C, and the residue was distilled under reduced pressure (b.p. 48 °C,  $3.1 \cdot 10^{-1}$  mbar) to give the title compound as a colorless oil (14.7 g, 72.2 mmol, 87 %).

<sup>1</sup>H-NMR (600 MHz,  $\text{CDCl}_3$ ):  $\delta_{\text{H}} = 5.04$  (2H, sept,  $^3J_{\text{HH}} = 6.3$  Hz, OCH), 3.34 (1H, q,  $^3J_{\text{HH}} = 7.3$  Hz, O=C-CH), 1.38 (3H, d,  $^3J_{\text{HH}} = 7.3$  Hz, O=C-CH- $\text{CH}_3$ ), 1.24 (6H, d,  $^3J_{\text{HH}} = 6.3$  Hz, OCH(C(a)H<sub>3</sub>)<sub>2</sub>), 1.24 (6H, d,  $^3J_{\text{HH}} = 6.3$  Hz, OC(b)H(CH<sub>3</sub>)<sub>2</sub>) ppm; <sup>13</sup>C{<sup>1</sup>H}-NMR (151 MHz,  $\text{CDCl}_3$ ):  $\delta_{\text{C}} = 169.9$  (C=O), 68.9 (OCH), 45.7 (O=C-CH), 21.8 (OCH(C(a)H<sub>3</sub>)<sub>2</sub>), 21.7 (OCH(C(b)H<sub>3</sub>)<sub>2</sub>), 13.5 (O=C-CH- $\text{CH}_3$ ) ppm; HRMS (APCI<sup>+</sup>): C<sub>10</sub>H<sub>19</sub>O<sub>4</sub> [M+H]<sup>+</sup> requires 203.1278, found 203.1279 ( $\Delta = 0.6$  ppm). The spectroscopic data are consistent with those reported in the literature.<sup>[421]</sup>

## Di-*tert*-butyl isopropylmalonate (2e)

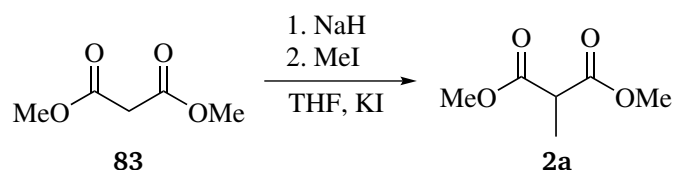


### JOP01-96

The title compound was prepared following a modified literature procedure.<sup>[423]</sup> To a stirred suspension of NaH (60 w%, 1.0 g, 25.0 mmol, 1.0 equiv.) in anhydrous THF (100 mL) was added dropwise di-*tert*-butyl malonate **93** (5.41 g, 25.0 mmol, 1.0 equiv.). When gas evolution was observed to be complete, *i*PrBr (5.4 mL, 57.5 mmol, 2.3 equiv.) was added, and the mixture was warmed to 40 °C and stirred at this temperature overnight. The reaction mixture was quenched with satd.  $\text{NH}_4\text{Cl}$  (50 mL) and extracted with EtOAc (2 × 60 mL). The combined organic layers were dried over  $\text{Na}_2\text{SO}_4$  and concentrated *in vacuo* at 40 °C. The residue was purified by flash column chromatography on silica gel (*n*-hexane: $\text{CH}_2\text{Cl}_2$  40:60) to give the title compound as a colorless oil (4.01 g, 15.5 mmol, 62 %).

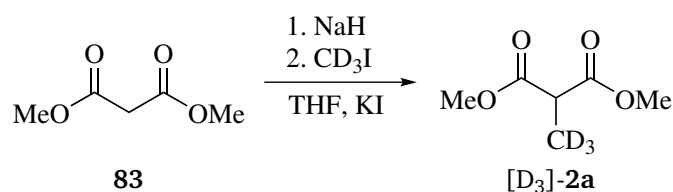
$R_f = 0.45$  (*n*-hexane:CH<sub>2</sub>Cl<sub>2</sub> 3:7); <sup>1</sup>H-NMR (600 MHz, CDCl<sub>3</sub>):  $\delta_H = 2.89$  (1H, d, <sup>3</sup>J<sub>HH</sub> = 8.6 Hz, CHiPr), 2.28 (1H, dsept, <sup>3</sup>J<sub>HH</sub> = 8.6 Hz, <sup>3</sup>J<sub>HH</sub> = 6.7 Hz, CH(CH<sub>3</sub>)<sub>2</sub>), 1.45 (18H, s, C(CH<sub>3</sub>)<sub>3</sub>), 0.99 (6H, d, <sup>3</sup>J<sub>HH</sub> = 6.7 Hz, CH(CH<sub>3</sub>)<sub>2</sub>) ppm; <sup>13</sup>C{<sup>1</sup>H}-NMR (151 MHz, CDCl<sub>3</sub>):  $\delta_C = 168.4$  (C=O), 81.3 (C(CH<sub>3</sub>)<sub>3</sub>), 61.2 (CHiPr), 28.5 (CH(CH<sub>3</sub>)<sub>2</sub>), 28.1 (C(CH<sub>3</sub>)<sub>3</sub>), 20.5 (CH(CH<sub>3</sub>)<sub>2</sub>) ppm; ATR-IR (neat):  $\nu_{\max} = 2977$  (C–H stretching), 1726 (C=O stretching), 1367 (C(CH<sub>3</sub>)<sub>3</sub> deformation), 1125 (C–O–C deformation) cm<sup>-1</sup>; HRMS (APCI<sup>+</sup>): C<sub>14</sub>H<sub>27</sub>O<sub>4</sub> [M+H]<sup>+</sup> requires 259.1904, found 259.1903 ( $\Delta = -0.3$  ppm).

### General Procedure B: Dimethyl methylmalonate isotopologues (**2a**)



Labeled isotopologues of dimethyl methylmalonate **2a** were prepared following modified literature procedures.<sup>[409,530]</sup> To a stirred suspension of NaH (60 w%, 1–1.05 equiv.) and KI (10 mol%) in anhydrous THF (15 mL) was added dropwise the required isotopologue of dimethyl methylmalonate **83** (for synthesis of <sup>13</sup>C-labeled isotopologue see below, 1–1.1 equiv.). When gas evolution was observed to be complete, the mixture was cooled to 0 °C and the required MeI isotopologue (1–1.2 equiv.) was added dropwise. Stirring was continued at RT for 4 h, after which 10 mM HCl (5 mL) was added. The mixture was extracted with Et<sub>2</sub>O (3 × 10 mL). The combined organic layers were washed with brine (8 mL), dried over Na<sub>2</sub>SO<sub>4</sub> and concentrated *in vacuo* at RT. The residue was purified by flash column chromatography on silica gel (*n*-hexane:Et<sub>2</sub>O 90:10 → 80:20) to afford the desired labeled isotopologue of dimethyl methylmalonate **2a**. The products were stored in sealed flasks at 4 °C to prevent decomposition.

### Dimethyl (methyl-*d*<sub>3</sub>)malonate ([D<sub>3</sub>]-**2a**)



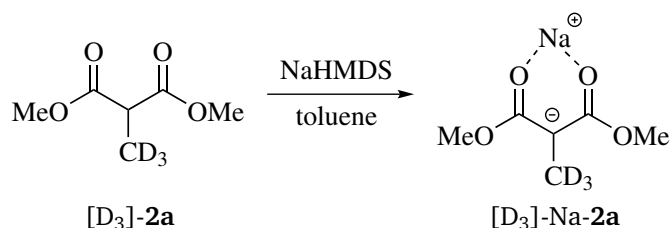
#### JOP01-141

Deprotonation of dimethyl malonate **83** (860 mg, 6.5 mmol, 1.05 equiv.) with NaH (60 w%, 248 mg, 6.2 mmol, 1.0 equiv.) and subsequent methylation with CD<sub>3</sub>I (commercially obtained from Fisher Scientific, ≥ 99% D, 1.00 g, 6.8 mmol, 1.1 equiv.) according to general procedure B afforded the title compound as a colorless oil (574 mg, 3.8 mmol, 62 %, > 99% D).

$R_f = 0.58$  (*n*-hexane:Et<sub>2</sub>O 3:7); <sup>1</sup>H-NMR (700 MHz, CDCl<sub>3</sub>):  $\delta_H = 3.73$  (6H, s, OCH<sub>3</sub>), 3.44 (1H, br. s, CHCD<sub>3</sub>) ppm; <sup>2</sup>H-NMR (92 MHz, CHCl<sub>3</sub>):  $\delta_D = 1.41$  (d, <sup>2</sup>J<sub>DH</sub> = 1.1 Hz) ppm; <sup>13</sup>C{<sup>1</sup>H}-NMR (176 MHz, CDCl<sub>3</sub>):  $\delta_C = 170.7$  (C=O), 52.6 (OCH<sub>3</sub>), 45.8 (CHCD<sub>3</sub>), 13.0

(sept,  $^1J_{CD} = 20.0$  Hz,  $CD_3$ ) ppm; HRMS (APCI<sup>+</sup>):  $C_6H_8D_3O_4$  [M+H]<sup>+</sup> requires 150.0840, found 150.0842 ( $\Delta = 1.0$  ppm). The spectroscopic data are consistent with those reported in the literature.<sup>[408,531]</sup>

### Sodium dimethyl (methyl- $d_3$ )malonate ([D<sub>3</sub>]-Na-2a)

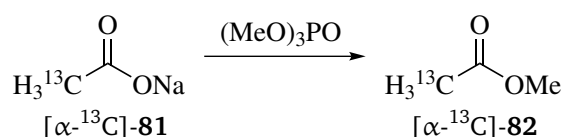


### JOP01-178

Deprotonation of dimethyl (methyl- $d_3$ )malonate **[D<sub>3</sub>]-2a** (537 mg, 3.60 mmol, 1.0 equiv.) with NaHMDS (693 mg, 3.78 mmol, 1.05 equiv.) according to general procedure A afforded the title compound as a colorless solid. The product contained various unidentified impurities that could not be removed by recrystallization (ca. 90 w% estimated purity, 312 mg, ca. 1.64 mmol, ca. 46 % yield).

$^1H$ -NMR (700 MHz, THF- $d_8$ ):  $\delta_H = 3.41$  (6H, s,  $OCH_3$ ) ppm;  $^2H$ -NMR (61 MHz, THF):  $\delta_D = 1.60$  (s) ppm;  $^{13}C\{^1H\}$ -NMR (176 MHz, THF- $d_8$ ):  $\delta_C = 172.3$  (C=O), 67.9 ( $CCD_3$ ), 48.9 ( $OCH_3$ ), 11.1 (sept,  $^1J_{CD} = 19.1$  Hz,  $CD_3$ ) ppm;  $^{23}Na$ -NMR (159 MHz, THF- $d_8$ ):  $\delta_{Na} = 0.8$  (br. s) ppm.

### Methyl acetate-2- $^{13}C$ ([ $\alpha$ - $^{13}C$ ]-82)

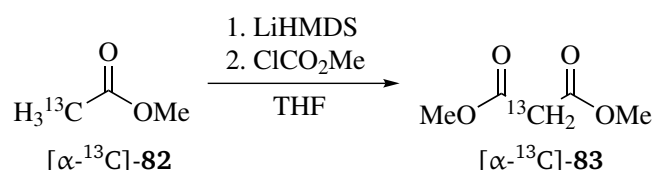


### JOP01-170

The title compound was prepared following a modified literature procedure.<sup>[410]</sup> A suspension of sodium acetate-2- $^{13}C$  [ $\alpha$ - $^{13}C$ ]-**81** (commercially obtained from Sigma Aldrich, dried under high vacuum prior to use, > 99 %  $^{13}C$ , 2.00 g, 24.0 mmol, 1.0 equiv.) in anhydrous ( $MeO$ )<sub>3</sub>PO (10 mL, 85 mmol, 3.6 equiv., distilled from CaH prior to use) was gradually heated to 175 °C, while the product was distilled into a trap cooled at -90 °C. Heating was continued for 2 h. The title compound was obtained as a colorless liquid (1.29 g, 17.2 mmol, 71 %, > 99 %  $^{13}C$ ), which was directly used in the next step in order to prevent yield loss due to its volatile nature.

$^1H$ -NMR (600 MHz,  $CDCl_3$ ):  $\delta_H = 3.66$  (3H, s,  $OCH_3$ ), 2.05 (3H, d,  $^1J_{HC} = 129.4$  Hz,  $^{13}CH_3$ ) ppm;  $^{13}C\{^1H\}$ -NMR (151 MHz,  $CDCl_3$ ):  $\delta_C = 171.7$  (d,  $^1J_{CC} = 59.5$  Hz, C=O), 51.7 (d,  $^3J_{CC} = 1.3$  Hz,  $OCH_3$ ), 20.8 (enriched,  $^{13}CH_3$ ) ppm. The spectroscopic data are consistent with those reported in the literature.<sup>[414]</sup>

## Dimethyl malonate-2-<sup>13</sup>C ([α-<sup>13</sup>C]-83)

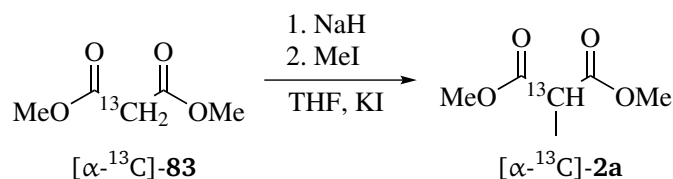


### JOP01-171

The title compound was prepared following a modified literature procedure.<sup>[411]</sup> To a stirred solution of LiHMDS (6.04 g, 36.1 mmol, 2.1 equiv.) in anhydrous THF (20 mL) was carefully added methyl acetate-2-<sup>13</sup>C [α-<sup>13</sup>C]-82 (> 99% <sup>13</sup>C, 1.29 g, 17.2 mmol, 1.0 equiv.) in anhydrous THF (2 mL) at -90 °C. After stirring for 15 min, methyl chloroformate (1.33 mL, 17.2 mmol, 1.0 equiv.) was added dropwise. Stirring was continued for 1 h, after which 6 M HCl (8 mL) was added at -90 °C in one portion. The mixture was allowed to warm to RT, diluted with water (20 mL), acidified with conc. HCl (pH ≤ 2) and extracted with Et<sub>2</sub>O (3 × 50 mL). The combined organic layers were washed with brine (30 mL), dried over Na<sub>2</sub>SO<sub>4</sub> and concentrated *in vacuo* at RT. The residue was purified by flash column chromatography on silica gel (*n*-hexane:Et<sub>2</sub>O 80:20 → 65:35) to give the title compound as a colorless oil (1.13 g, 8.5 mmol, 49%, > 99% <sup>13</sup>C). The product was stored in a sealed flask at 4 °C to prevent decomposition.

$R_f = 0.51$  (*n*-hexane:Et<sub>2</sub>O 3:7); <sup>1</sup>H-NMR (600 MHz, CDCl<sub>3</sub>): δ<sub>H</sub> = 3.75 (6H, s, OCH<sub>3</sub>), 3.40 (2H, d, <sup>1</sup>J<sub>HC</sub> = 132.1 Hz, <sup>13</sup>CH<sub>2</sub>) ppm; <sup>13</sup>C{<sup>1</sup>H}-NMR (151 MHz, CDCl<sub>3</sub>): δ<sub>C</sub> = 167.1 (d, <sup>1</sup>J<sub>CC</sub> = 59.6 Hz, C=O), 52.7 (d, <sup>3</sup>J<sub>CC</sub> = 1.3 Hz, OCH<sub>3</sub>), 41.3 (enriched, <sup>13</sup>CH<sub>2</sub>) ppm; HRMS (APCI<sup>+</sup>): C<sub>4</sub><sup>13</sup>CH<sub>9</sub>O<sub>4</sub> [M+H]<sup>+</sup> requires 133.0529, found 133.0535 (Δ = 4.5 ppm).

## Dimethyl methylmalonate-2-<sup>13</sup>C ([α-<sup>13</sup>C]-2a)



### JOP01-174

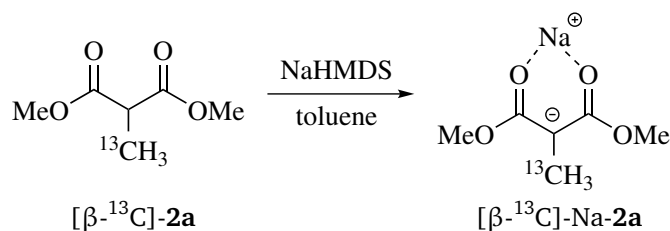
Deprotonation of dimethyl malonate-2-<sup>13</sup>C [α-<sup>13</sup>C]-83 (> 99% <sup>13</sup>C, 1.13 g, 8.5 mmol, 1.0 equiv.) with NaH (60 w%, 338 mg, 8.5 mmol, 1.0 equiv.) and subsequent methylation with MeI (0.63 mL, 10.2 mmol, 1.2 equiv.) according to general procedure B afforded the title compound as a colorless oil (700 mg, 4.8 mmol, 56%, > 99% <sup>13</sup>C).

$R_f = 0.58$  (*n*-hexane:Et<sub>2</sub>O 3:7); <sup>1</sup>H-NMR (600 MHz, CDCl<sub>3</sub>): δ<sub>H</sub> = 3.75 (6H, s, OCH<sub>3</sub>), 3.46 (1H, dq, <sup>1</sup>J<sub>HC</sub> = 132.0 Hz, <sup>3</sup>J<sub>HH</sub> = 7.3 Hz, <sup>13</sup>CH), 1.43 (3H, dd, <sup>3</sup>J<sub>HH</sub> = 7.3 Hz, <sup>2</sup>J<sub>HC</sub> = 4.4 Hz, <sup>13</sup>CCH<sub>3</sub>) ppm; <sup>13</sup>C{<sup>1</sup>H}-NMR (151 MHz, CDCl<sub>3</sub>): δ<sub>C</sub> = 170.7 (d, <sup>1</sup>J<sub>CC</sub> = 58.1 Hz, C=O), 52.7 (d, <sup>3</sup>J<sub>CC</sub> = 1.2 Hz, OCH<sub>3</sub>), 46.0 (enriched, <sup>13</sup>CH), 13.8 (d, <sup>1</sup>J<sub>CC</sub> = 34.2 Hz, <sup>13</sup>CCH<sub>3</sub>) ppm; HRMS (APCI<sup>+</sup>): C<sub>5</sub><sup>13</sup>CH<sub>11</sub>O<sub>4</sub> [M+H]<sup>+</sup> requires 148.0685, found 148.0691 (Δ = 4.0 ppm). The spectroscopic data are consistent with those reported in the literature.<sup>[531]</sup>





## Sodium dimethyl (methyl-<sup>13</sup>C)malonate ([β-<sup>13</sup>C]-Na-2a)



### JOP01-218

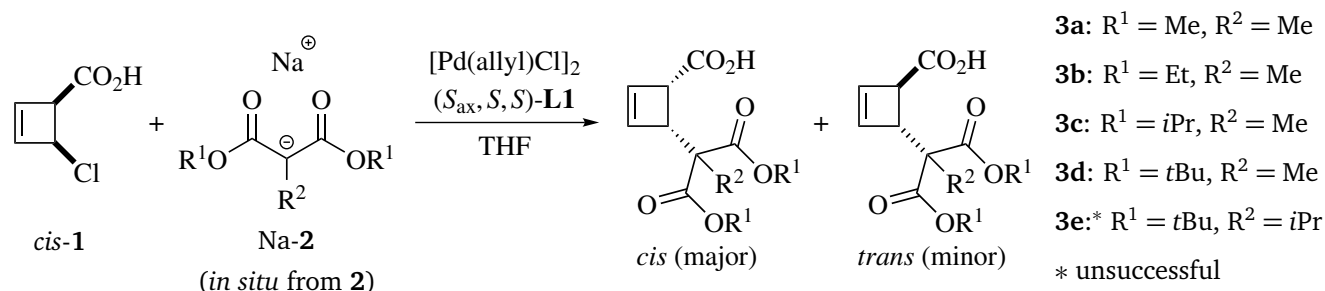
Deprotonation of dimethyl (methyl-<sup>13</sup>C)malonate [β-<sup>13</sup>C]-Na-2a (dried over MS 4 Å prior to use, 296 mg, 2.01 mmol, 1.0 equiv.) with NaHMDS (387 mg, 2.11 mmol, 1.05 equiv.) according to general procedure A afforded the title compound as a colorless solid. The product contained various unidentified impurities that could not be removed by recrystallization (ca. 85 w% estimated purity, 248 mg, ca. 1.25 mmol, ca. 62 % yield).

<sup>1</sup>H-NMR (700 MHz, THF-*d*<sub>8</sub>): δ<sub>H</sub> = 3.41 (6H, s, OCH<sub>3</sub>), 1.64 (3H, d, <sup>1</sup>J<sub>HC</sub> = 125.2 Hz, <sup>13</sup>CCH<sub>3</sub>) ppm; <sup>13</sup>C{<sup>1</sup>H}-NMR (176 MHz, THF-*d*<sub>8</sub>): δ<sub>C</sub> = 172.2 (d, <sup>2</sup>J<sub>CC</sub> = 1.8 Hz, C=O), 67.8 (d, <sup>1</sup>J<sub>CC</sub> = 22.2 Hz, C<sup>13</sup>CH<sub>3</sub>), 48.9 (s, OCH<sub>3</sub>), 11.9 (enriched, C<sup>13</sup>CH<sub>3</sub>) ppm; <sup>23</sup>Na-NMR (106 MHz, THF-*d*<sub>8</sub>): δ<sub>Na</sub> = 1.4 (br. s) ppm.

## 7.2 Allylic Alkylation Reactions

Catalytic allylic alkylation reactions with cyclobutene substrate *cis*-1 and ligand L1 or L2 were performed under the reaction conditions reported in the literature,<sup>[56]</sup> with the work-up slightly modified.

### General Procedure C: Allylic alkylation of substrate *cis*-1 with ligand L1



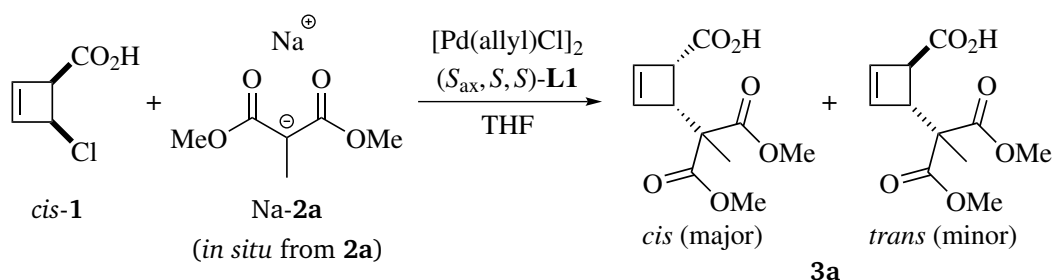
To a stirred suspension of NaH (60 w%, 12 mg, 300 μmol, 3.0 equiv.) in anhydrous THF (0.5 mL) was added dropwise the required malonate **2** (320 μmol, 3.2 equiv.). When gas evolution, which indicated the conversion of **2** to Na-2, was observed to be complete, the resulting solution was cooled to 0 °C, and a solution of [Pd(allyl)Cl]<sub>2</sub> (0.9 mg, 2.5 μmol, 2.5 mol%) and ligand (S<sub>ax</sub>,S,S)-L1 (4.1 mg, 7.5 μmol, 7.5 mol%) in anhydrous THF (0.5 mL) was added dropwise. Subsequently, a solution of *cis*-4-chlorocyclobutene-2-enecarboxylic acid *cis*-1 (13.3 mg, 100 μmol,



1.0 equiv.) in anhydrous THF (1 mL) was added dropwise, and stirring was continued at 0 °C until TLC analysis (CH<sub>2</sub>Cl<sub>2</sub>:EtOAc 3:1 with ca. 2 % AcOH) indicated quantitative conversion.

The reaction was quenched with NaHCO<sub>3</sub> (25.2 mg, 300 μmol, 3.0 equiv.) at 0 °C followed by brine (2 mL). The aqueous layer was washed with Et<sub>2</sub>O (3 × 5 mL), carefully acidified with 1 M HCl (pH ≤ 2) and extracted with CH<sub>2</sub>Cl<sub>2</sub> (6 × 5 mL). The combined organic layers were dried over Na<sub>2</sub>SO<sub>4</sub> and concentrated *in vacuo* to give the crude product, which was investigated by NMR spectroscopy and ESI-HRMS. The e.e. was determined by <sup>1</sup>H-NMR after addition of (*S*)-PEA to the NMR sample. The absolute configuration of products *cis*-**3** obtained by Pd-catalyzed allylic alkylation of *cis*-**1** with malonate nucleophiles Na-**2** and ligand (*R*<sub>ax</sub>, *R*, *R*)-**L1** has been determined in the literature to be (1*R*,4*S*).<sup>[56]</sup> As in this work the enantiomeric ligand (*S*<sub>ax</sub>, *S*, *S*)-**L1** was used, the absolute configuration of *cis*-**3** is expected to be (1*S*,4*R*), accordingly.

**(1*S*,4*R*)-4-(1,3-dimethoxy-2-methyl-1,3-dioxopropan-2-yl)cyclobut-2-ene-1-carboxylic acid**  
**(*cis*-**3a**)**

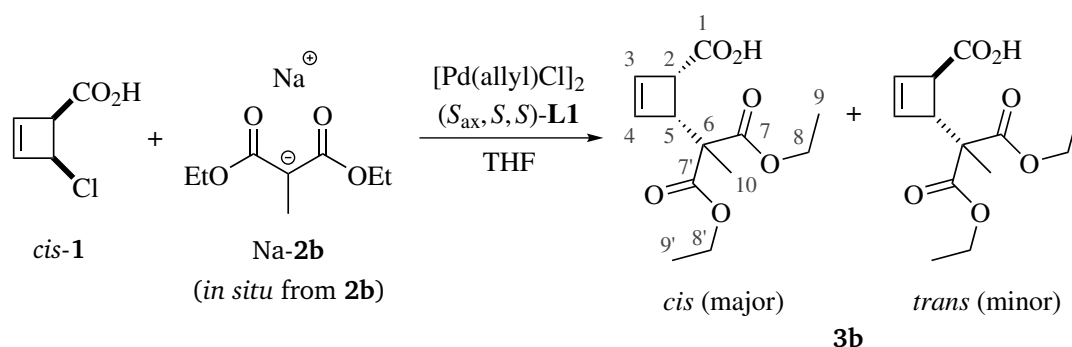


**JOP01-83**

The title compound was obtained according to general procedure C, using dimethyl methylmalonate **2a** (distilled from CaCl<sub>2</sub> prior to use) as pronucleophile. The reaction was quenched after 2 h. Characterization of the crude product obtained after work-up gave a d.r. of 92:8. The e.e. of the main product *cis*-**3a** was found to be 85 %. For the minor diastereomer *trans*-**3a**, an e.e. of 2 % was determined.

The characterization data of both *cis*- and *trans*-**3a** are reported in section 4.2 (supporting information, chapter 3).

**(1*S*,4*R*)-4-(1,3-diethoxy-2-methyl-1,3-dioxopropan-2-yl)cyclobut-2-ene-1-carboxylic acid**  
**(*cis*-3b)**

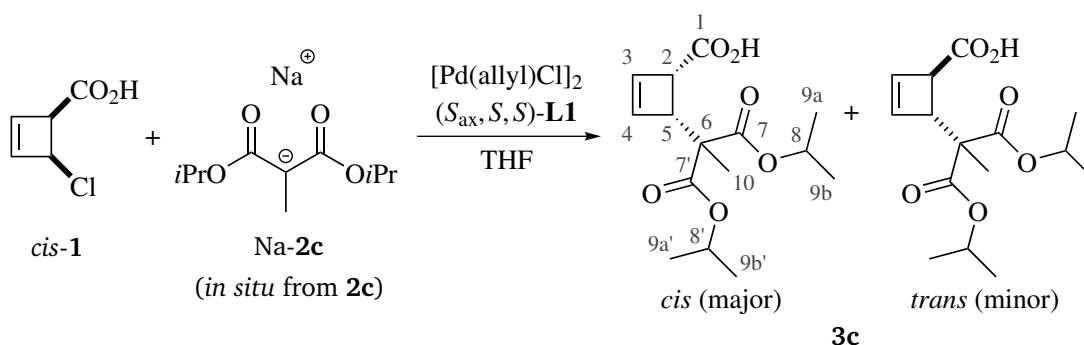


**JOP01-105**

The title compound was obtained according to general procedure C, using diethyl methylmalonate **2b** (distilled from  $\text{CaCl}_2$  prior to use) as pronucleophile. The reaction was quenched after 3.5 h. Characterization of the crude product obtained after work-up gave a d.r. of 83:17. The e.e. of the main product *cis*-**3b** was found to be 78%. For the minor diastereomer *trans*-**3b**, an e.e. of 50% was determined. The crude product contained approximately 38% unconverted substrate *cis*-**1**, for which an e.e. of 2% was determined.

*cis*-**3b**:  $^1\text{H-NMR}$  (600 MHz,  $\text{CDCl}_3$ , 273 K):  $\delta_{\text{H}} = 6.22 - 6.20$  (1H, m, C(3/4)*H*), 6.15 (1H, d,  $^3J_{\text{HH}} = 2.8$  Hz, C(3/4)*H*), 4.24 – 4.14 (4H, m, C(8)*H*, C(8')*H*), 3.95 (1H, d,  $^3J_{\text{HH}} = 4.9$  Hz, C(5)*H*), 3.86 (1H, dpt,  $^3J_{\text{HH}} = 4.9$  Hz,  $^3J_{\text{HH}} \approx ^4J_{\text{HH}} \approx 0.9$  Hz, C(2)*H*), 1.42 (3H, s, C(10) $\text{H}_3$ ), 1.24 (3H, t,  $^3J_{\text{HH}} = 7.0$  Hz, C(9/9') $\text{H}_3$ ), 1.23 (3H, t,  $^3J_{\text{HH}} = 7.1$  Hz, C(9/9') $\text{H}_3$ ) ppm;  $^{13}\text{C}\{^1\text{H}\}$ -NMR (151 MHz,  $\text{CDCl}_3$ , 273 K):  $\delta_{\text{C}} = 177.7$  (C(1)), 171.7 (C(7/7')), 170.8 (C(7/7')), 139.4 (C(3/4)), 134.0 (C(3/4)), 61.8 (C(8/8')), 61.7 (C(8/8')), 54.2 (C(6)), 50.7 (C(5)), 48.2 (C(2)), 17.6 (C(10)), 14.1 (C(9/9')), 14.0 (C(9/9')) ppm; HRMS (ESI<sup>+</sup>):  $\text{C}_{13}\text{H}_{19}\text{O}_6$  [M+H]<sup>+</sup> requires 271.1176, found 271.1178 ( $\Delta = 0.5$  ppm). The spectroscopic data are consistent with those reported in the literature.<sup>[55]</sup> For characterization of *trans*-**3b**, see its selective preparation according to general procedure D.

**(1*S*,4*R*)-4-(1,3-diisopropoxy-2-methyl-1,3-dioxopropan-2-yl)cyclobut-2-ene-1-carboxylic acid**  
**(*cis*-3c)**

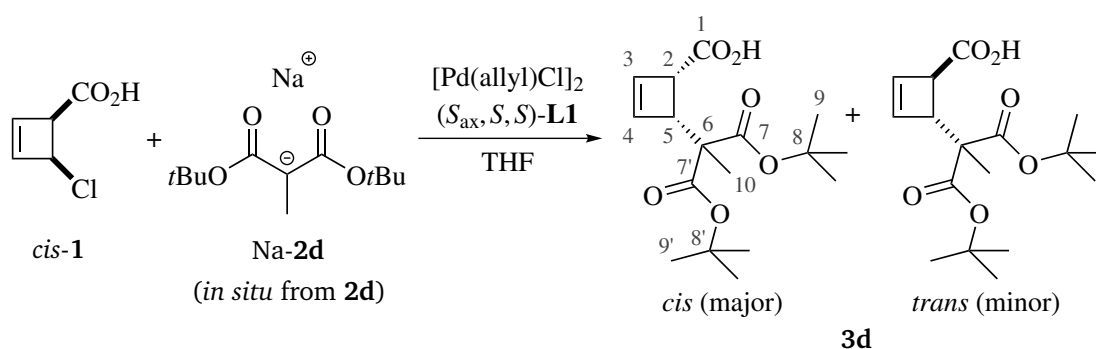


**JOP01-185**

The title compound was obtained according to general procedure C, using diisopropyl methylmalonate **2c** (dried over MS 4 Å prior to use) as pronucleophile. The reaction was quenched after 4 h. Characterization of the crude product obtained after work-up gave a d.r. of 95:5. The e.e. of the main product *cis*-**3c** was found to be 80%. For the minor diastereomer *trans*-**3c**, an e.e. of 39% was determined. The crude product contained trace amounts of unconverted substrate *cis*-**1**.

*cis*-**3c**: <sup>1</sup>H-NMR (600 MHz, CDCl<sub>3</sub>, 273 K): δ<sub>H</sub> = 6.20 (1H, br. s, C(3/4)H), 6.15 (1H, br. s, C(3/4)H), 5.09 – 4.96 (2H, m, C(8)H, C(8')H), 3.94 (1H, d, <sup>3</sup>J<sub>HH</sub> = 4.6 Hz, C(5)H), 3.85 (1H, d, <sup>3</sup>J<sub>HH</sub> = 4.6 Hz, C(2)H), 1.39 (3H, s, C(10)H<sub>3</sub>), 1.26 – 1.18 (12H, m, C(9a)H<sub>3</sub>, C(9b)H<sub>3</sub>, C(9a')H<sub>3</sub>, C(9b')H<sub>3</sub>) ppm; <sup>13</sup>C{<sup>1</sup>H}-NMR (151 MHz, CDCl<sub>3</sub>, 273 K): δ<sub>C</sub> = 177.1 (C(1)), 171.1 (C(7/7')), 170.4 (C(7/7')), 139.4 (C(3/4)), 134.0 (C(3/4)), 69.3 (C(8/8')), 69.2 (C(8/8')), 54.2 (C(6)), 50.5 (C(5)), 48.2 (C(2)), 21.6 (C(9a/9b/9a'/9b')), 21.6 (C(9a/9b/9a'/9b')), 21.6 (C(9a/9b/9a'/9b')), 17.1 (C(10)) ppm; HRMS (ESI<sup>+</sup>): C<sub>15</sub>H<sub>23</sub>O<sub>6</sub> [M+H]<sup>+</sup> requires 299.1489, found 299.1488 (Δ = -0.3 ppm). For characterization of *trans*-**3c**, see its selective preparation according to general procedure D.

### (1*S*,4*R*)-4-(1,3-di-*tert*-butoxy-2-methyl-1,3-dioxopropan-2-yl)cyclobut-2-ene-1-carboxylic acid (*cis*-**3d**)

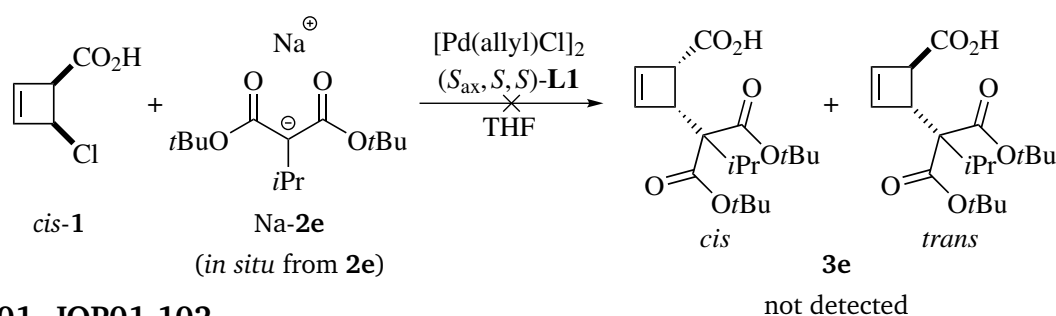


### JOP01-78

The title compound was obtained according to general procedure C, using di-*tert*-butyl methylmalonate **2d** (dried over MS 4 Å prior to use) as pronucleophile. The reaction was quenched after 12 h. Characterization of the crude product obtained after work-up gave a d.r. of 88:12. The e.e. of the main product *cis*-**3d** was found to be 78%. For the minor diastereomer *trans*-**3d**, an e.e. of 76% was determined.

*cis*-**3d**: <sup>1</sup>H-NMR (700 MHz, CDCl<sub>3</sub>, 273 K): δ<sub>H</sub> = 6.17 – 6.14 (2H, m, C(3)H, C(4)H), 3.88 (1H, d, <sup>3</sup>J<sub>HH</sub> = 5.0 Hz, C(2/5)H), 3.87 (1H, d, <sup>3</sup>J<sub>HH</sub> = 5.0 Hz, C(2/5)H), 1.44 (9H, s, C(9/9')H<sub>3</sub>), 1.43 (9H, s, C(9/9')H<sub>3</sub>), 1.34 (3H, s, C(10)H<sub>3</sub>) ppm; <sup>13</sup>C{<sup>1</sup>H}-NMR (176 MHz, CDCl<sub>3</sub>, 273 K): δ<sub>C</sub> = 176.9 (C(1)), 170.7 (C(7), C(7')), 139.3 (C(3/4)), 134.0 (C(3/4)), 82.5 (C(8/8')), 82.2 (C(8/8')), 55.6 (C(6)), 50.8 (C(5)), 48.3 (C(2)), 27.9 (C(9/9')), 27.8 (C(9/9')), 16.6 (C(10)) ppm; HRMS (ESI<sup>+</sup>): C<sub>17</sub>H<sub>27</sub>O<sub>6</sub> [M+H]<sup>+</sup> requires 327.1802, found 327.1802 (Δ = -0.1 ppm). For characterization of *trans*-**3d**, see its selective preparation according to general procedure D.

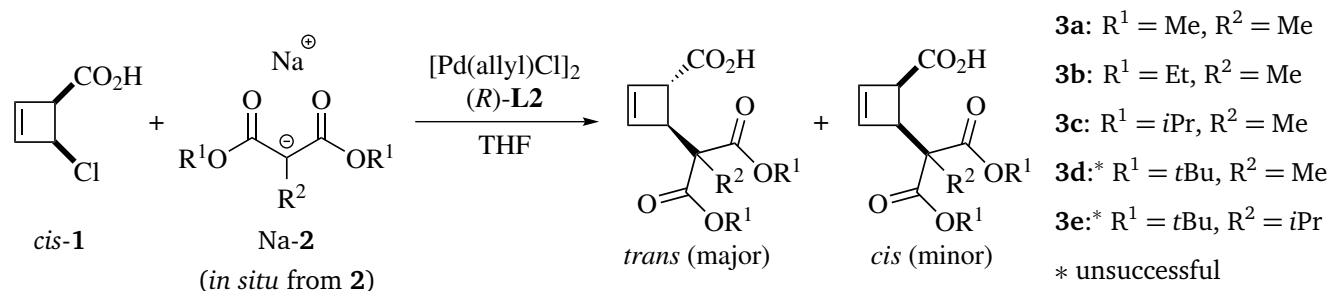
## Unsuccessful allylic alkylation with sodium di-*tert*-butyl isopropylmalonate (Na-2e) in the presence of [Pd-L1]



### JOP01-101, JOP01-102

When substrate *cis*-1 and pronucleophile di-*tert*-butyl isopropylmalonate **2e** (dried over MS 4 Å prior to use) were subjected to general procedure C for 3 days, only unconverted starting material *cis*-1 and unidentified dienes were detected in the crude product. Change of the solvent to MeCN did not afford any substitution product **3e** as well.

### General Procedure D: Allylic alkylation of substrate *cis*-1 with ligand L2

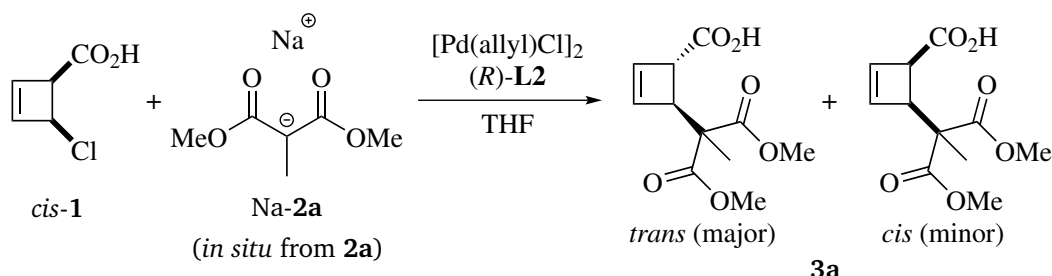


To a stirred suspension of NaH (60 w%, 12 mg, 300 μmol, 3.0 equiv.) in anhydrous THF (0.5 mL) was added dropwise the required malonate **2** (320 μmol, 3.2 equiv.). When gas evolution was observed to be complete, the resulting solution was heated to 40 °C, and a solution of [Pd(allyl)Cl]<sub>2</sub> (0.9 mg, 2.5 μmol, 2.5 mol%) and ligand (R)-L2 (6.1 mg, 15 μmol, 15 mol%) in anhydrous THF (0.5 mL) was added dropwise. Subsequently, a solution of *cis*-4-chlorocyclobutene-2-enecarboxylic acid *cis*-1 (13.3 mg, 100 μmol, 1.0 equiv.) in anhydrous THF (1 mL) was added with a syringe pump over 30 min, and stirring was continued at 40 °C overnight.

The reaction was cooled to 0 °C and then quenched with NaHCO<sub>3</sub> (25.2 mg, 300 μmol, 3.0 equiv.) followed by brine (2 mL). The aqueous layer was washed with Et<sub>2</sub>O (3 × 5 mL), carefully acidified with 1 M HCl (pH ≤ 2) and extracted with CH<sub>2</sub>Cl<sub>2</sub> (6 × 5 mL). The combined organic layers were dried over Na<sub>2</sub>SO<sub>4</sub> and concentrated *in vacuo* to give the crude product, which was investigated by NMR spectroscopy and ESI-HRMS. The e.e. was determined by <sup>1</sup>H-NMR after addition of (S)-PEA to the NMR sample. The absolute configuration of products *trans*-3 obtained by Pd-catalyzed allylic alkylation of *cis*-1 with malonate nucleophiles Na-2 and ligand (S)-L2 has been

determined in the literature to be (1*R*,4*R*).<sup>[56]</sup> As in this work the enantiomeric ligand (*R*)-**L1** was used, the absolute configuration of *trans*-**3** is expected to be (1*S*,4*S*), accordingly.

**(1*S*,4*S*)-4-(1,3-dimethoxy-2-methyl-1,3-dioxopropan-2-yl)cyclobut-2-ene-1-carboxylic acid (*trans*-**3a**)**

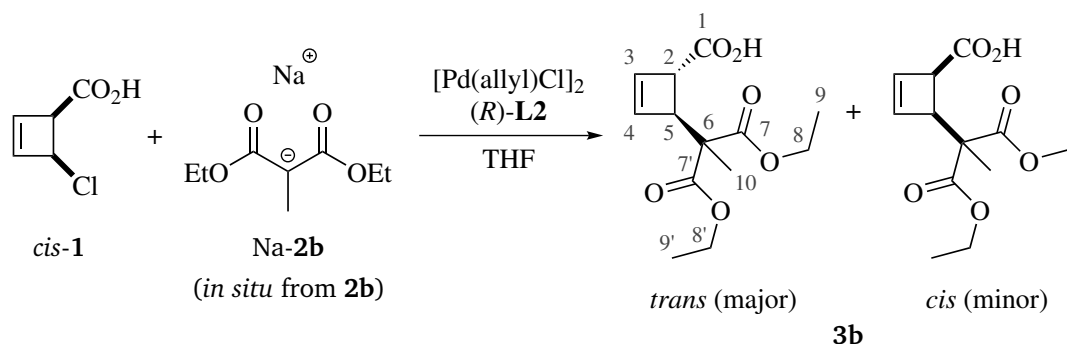


**JOP01-64**

The title compound was obtained according to general procedure D, using dimethyl methylmalonate **2a** (distilled from  $\text{CaCl}_2$  prior to use) as pronucleophile. The reaction was quenched at incomplete conversion after 11 h. Characterization of the crude product obtained after work-up gave a d.r. of 99:1. The e.e. of the main product *trans*-**3a** was found to be 96%. The crude product contained approximately 35% unconverted substrate *cis*-**1**, for which an e.e. of 3% was determined.

The characterization data of both *trans*- and *cis*-**3a** are reported in section 4.2 (supporting information, chapter 3).

**(1*S*,4*S*)-4-(1,3-diethoxy-2-methyl-1,3-dioxopropan-2-yl)cyclobut-2-ene-1-carboxylic acid (*trans*-**3b**)**

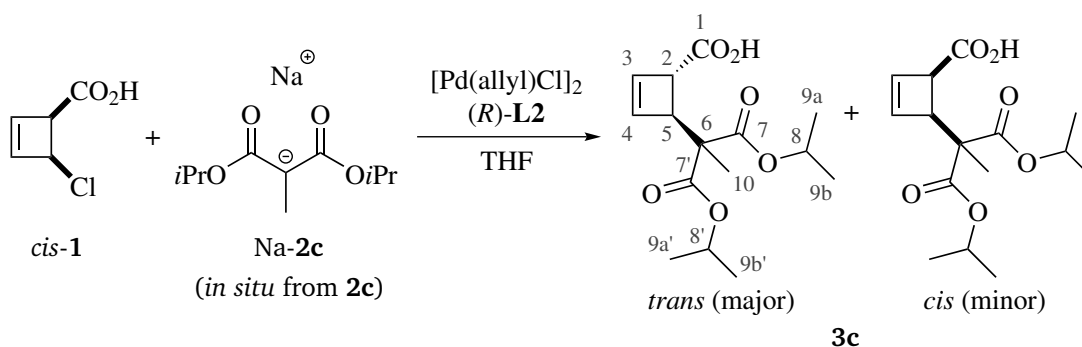


**JOP01-65**

The title compound was obtained according to general procedure D, using diethyl methylmalonate **2b** (distilled from  $\text{CaCl}_2$  prior to use) as pronucleophile. The reaction was quenched at incomplete conversion after 8 h. Characterization of the crude product obtained after work-up gave a d.r. of 93:7. The e.e. of the main product *trans*-**3b** was found to be 91%. For the minor diastereomer *cis*-**3b**, an e.e. of 9% was determined. The crude product contained approximately 57% unconverted substrate *cis*-**1**, for which an e.e. of 1% was determined.

*trans*-**3b**:  $^1\text{H-NMR}$  (600 MHz,  $\text{CDCl}_3$ , 273 K):  $\delta_{\text{H}} = 6.19$  (1H, d,  $^3J_{\text{HH}} = 2.7$  Hz, C(3/4)*H*), 6.18 (1H, d,  $^3J_{\text{HH}} = 2.7$  Hz, C(3/4)*H*), 4.23 – 4.17 (4H, m, C(8)*H*, C(8')*H*), 3.58 (1H, d,  $^3J_{\text{HH}} = 1.5$  Hz, C(2)*H*), 3.55 (1H, d,  $^3J_{\text{HH}} = 1.5$  Hz, C(5)*H*), 1.44 (3H, s, C(10) $\text{H}_3$ ), 1.25 (3H, t,  $^3J_{\text{HH}} = 7.1$  Hz, C(9/9') $\text{H}_3$ ), 1.24 (3H, t,  $^3J_{\text{HH}} = 7.1$  Hz, C(9/9') $\text{H}_3$ ) ppm;  $^{13}\text{C}\{^1\text{H}\}\text{-NMR}$  (151 MHz,  $\text{CDCl}_3$ , 273 K):  $\delta_{\text{C}} = 176.0$  (C(1)), 171.9 (C(7/7')), 171.4 (C(7/7')), 139.1 (C(3/4)), 135.2 (C(3/4)), 61.1 (C(8/8')), 61.0 (C(8/8')), 54.8 (C(6)), 50.5 (C(5)), 47.6 (C(2)), 17.6 (C(10)), 14.2 (C(9/9')), 14.1 (C(9/9')) ppm; **HRMS** ( $\text{ESI}^+$ ):  $\text{C}_{13}\text{H}_{19}\text{O}_6$  [ $\text{M}+\text{H}$ ] $^+$  requires 271.1176, found 271.1175 ( $\Delta = -0.3$  ppm). The spectroscopic data are consistent with those reported in the literature.<sup>[55]</sup> For characterization of *cis*-**3b**, see its selective preparation according to general procedure C.

### (1*S*,4*S*)-4-(1,3-diisopropoxy-2-methyl-1,3-dioxopropan-2-yl)cyclobut-2-ene-1-carboxylic acid (*trans*-**3c**)

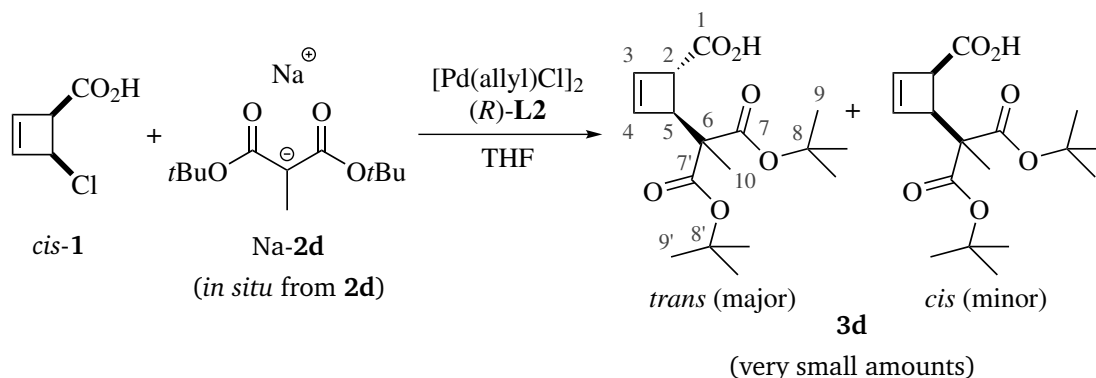


#### JOP01-184

The title compound was obtained according to general procedure D, using diisopropyl methylmalonate **2c** (dried over MS 4 Å prior to use) as pronucleophile. The reaction was quenched at incomplete conversion after 14 h. Characterization of the crude product obtained after work-up gave a d.r. of 96:4. The e.e. of the main product *cis*-**3c** was found to be 96%. The crude product contained approximately 42% unconverted substrate *cis*-**1**, for which an e.e. of < 1% was determined.

*trans*-**3c**:  $^1\text{H-NMR}$  (700 MHz,  $\text{CDCl}_3$ , 273 K):  $\delta_{\text{H}} = 6.18$  (1H, d,  $^3J_{\text{HH}} = 2.8$  Hz, C(3/4)*H*), 6.17 – 6.15 (1H, m, C(3/4)*H*), 5.06 (2H, sept,  $^3J_{\text{HH}} = 6.2$  Hz, C(8)*H*, C(8')*H*), 3.61 (1H, br. s, C(2)*H*), 3.51 (1H, br. s, C(5)*H*), 1.42 (3H, s, C(10) $\text{H}_3$ ), 1.24 – 1.20 (12H, m, C(9a) $\text{H}_3$ , C(9b) $\text{H}_3$ , C(9a') $\text{H}_3$ , C(9b') $\text{H}_3$ ) ppm;  $^{13}\text{C}\{^1\text{H}\}\text{-NMR}$  (176 MHz,  $\text{CDCl}_3$ , 273 K):  $\delta_{\text{C}} = 177.1$  (C(1)), 171.6 (C(7/7')), 171.0 (C(7/7')), 139.0 (C(3/4)), 135.2 (C(3/4)), 69.8 (C(8), C(8')), 54.7 (C(6)), 50.5 (C(5)), 47.7 (C(2)), 21.6 (C(9a/9b/9a'/9b')), 21.6 (C(9a/9b/9a'/9b')), 21.6 (C(9a/9b/9a'/9b')), 21.6 (C(9a/9b/9a'/9b')), 17.8 (C(10)) ppm; **HRMS** ( $\text{ESI}^+$ ):  $\text{C}_{15}\text{H}_{23}\text{O}_6$  [ $\text{M}+\text{H}$ ] $^+$  requires 299.1489, found 299.1493 ( $\Delta = 1.3$  ppm). For characterization of *cis*-**3c**, see its selective preparation according to general procedure C.

**(1S,4S)-4-(1,3-di-tert-butoxy-2-methyl-1,3-dioxopropan-2-yl)cyclobut-2-ene-1-carboxylic acid (*trans*-3d)**

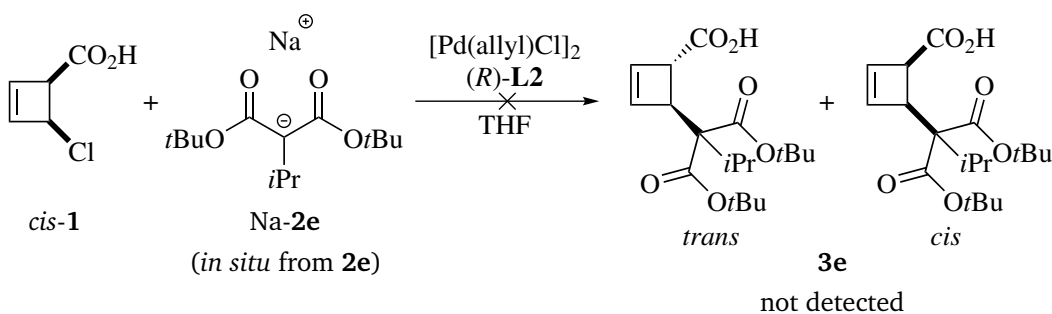


**JOP01-190**

The title compound was obtained in very low yield according to general procedure D, using di-*tert*-butyl methylmalonate **2d** (dried over MS 4 Å prior to use) as pronucleophile. The reaction was quenched at incomplete conversion after 17 h. Characterization of the crude product obtained after work-up gave a d.r. of 95:5. The e.e. of the main product *trans*-**3d** was found to be 66%. The crude product contained approximately 85% unconverted substrate *cis*-**1**, for which an e.e. of < 1% was determined.

*trans*-**3d**:  $^1\text{H-NMR}$  (700 MHz,  $\text{CDCl}_3$ , 273 K):  $\delta_{\text{H}}$  = 6.22 (1H, d,  $^3J_{\text{HH}}$  = 2.5 Hz, C(3/4)H), 6.12 (1H, br. s, C(3/4)H), 3.67 (1H, br. s, C(2)H), 3.43 (1H, br. s, C(5)H), 1.45 (18H, s, C(9)H<sub>3</sub>, C(9')H<sub>3</sub>), 1.37 (3H, s, C(10)H<sub>3</sub>) ppm;  $^{13}\text{C}\{^1\text{H}\}\text{-NMR}$  (176 MHz,  $\text{CDCl}_3$ , 273 K):  $\delta_{\text{C}}$  = 171.8 (C(7/7')), 170.9 (C(7/7')), 138.5 (C(3/4)), 135.4 (C(3/4)), 83.0 (C(8/8')), 83.0 (C(8/8')), 55.9 (C(6)), 50.6 (C(5)), 47.8 (C(2)), 28.0 (C(9/9')), 27.8 (C(9/9')), 18.0 (C(10)) ppm; HRMS (ESI<sup>+</sup>): C<sub>17</sub>H<sub>27</sub>O<sub>6</sub> [M+H]<sup>+</sup> requires 327.1802, found 327.1802 ( $\Delta$  = -0.1 ppm). Due to the very small amount of *trans*-**3d** obtained, characterization by one-dimensional  $^{13}\text{C}\{^1\text{H}\}\text{-NMR}$  was not successful, and the shifts were extracted by HSQC and HMBC experiments instead. However, no characteristic cross-peak and thus no  $^{13}\text{C-NMR}$  shift could be detected for C(1). For characterization of *cis*-**3d**, see its selective preparation according to general procedure C.

**Unsuccessful allylic alkylation with sodium di-*tert*-butyl isopropylmalonate (Na-2e) in the presence of [Pd-L2]**

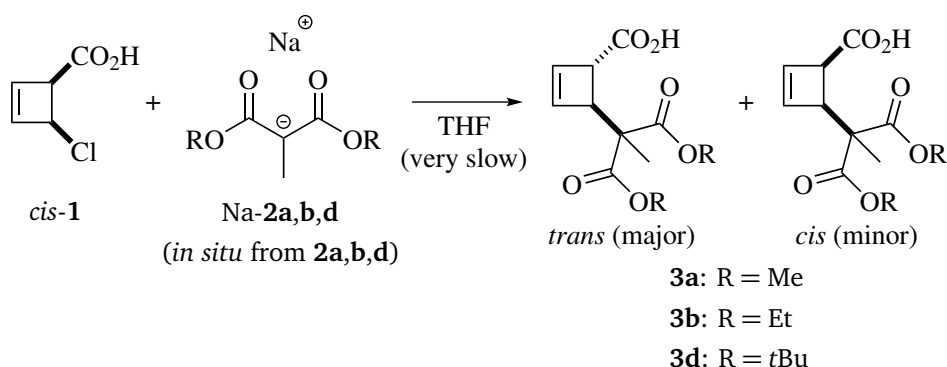


**JOP01-100, JOP01-103**



When substrate *cis*-**1** and pronucleophile di-*tert*-butyl isopropylmalonate **2e** (dried over MS 4 Å prior to use) were subjected to general procedure D for 20 h, only unconverted starting material *cis*-**1** and unidentified dienes were detected in the crude product. Change of the temperature to 30 °C did not afford any substitution product **3e** as well.

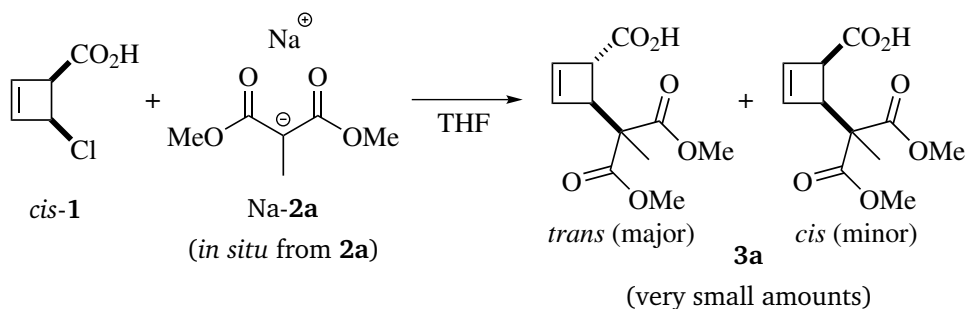
### General Procedure E: Uncatalyzed allylic alkylation of cyclobutene *cis*-**1**



To a stirred suspension of NaH (60 w%, 12 mg, 300  $\mu\text{mol}$ , 3.0 equiv.) in anhydrous THF (0.5 mL) was added dropwise the required malonate **2** (320  $\mu\text{mol}$ , 3.2 equiv.). When gas evolution was observed to be complete, the resulting solution was cooled to 0 °C, and a solution of *cis*-4-chlorocyclobutene-2-enecarboxylic acid *cis*-**1** (13.3 mg, 100  $\mu\text{mol}$ , 1.0 equiv.) in anhydrous THF (0.5 mL) was added dropwise. The reaction mixture was heated to 40 °C, and stirring was continued at this temperature for the indicated time.

The reaction was cooled to 0 °C and then quenched with NaHCO<sub>3</sub> (25.2 mg, 300  $\mu\text{mol}$ , 3.0 equiv.) followed by brine (2 mL). The aqueous layer was washed with Et<sub>2</sub>O (3  $\times$  5 mL), carefully acidified with 1 M HCl (pH  $\leq$  2) and extracted with CH<sub>2</sub>Cl<sub>2</sub> (6  $\times$  5 mL). The combined organic layers were dried over Na<sub>2</sub>SO<sub>4</sub> and concentrated *in vacuo* to give the crude product, which was investigated by NMR spectroscopy and ESI-HRMS.

### *rac-trans*-4-(1,3-dimethoxy-2-methyl-1,3-dioxopropan-2-yl)cyclobut-2-ene-1-carboxylic acid (*trans*-**3a**)



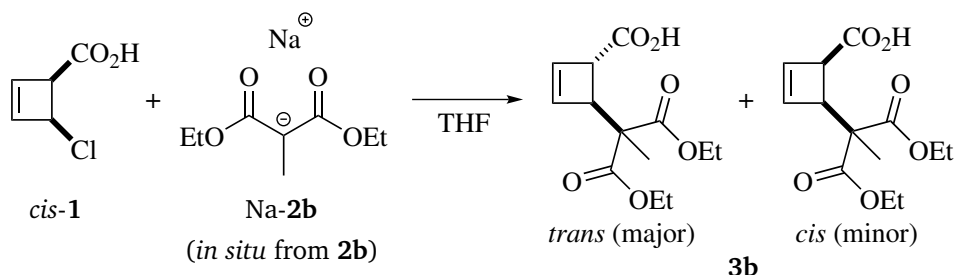
### JOP01-87

The title compound was obtained according to general procedure E, using dimethyl methylmalonate **2a** (distilled from CaCl<sub>2</sub> prior to use) as pronucleophile. The reaction was quenched at



incomplete conversion after 46 h. Characterization of the crude product obtained after work-up gave a d.r. of 96:4. The crude product contained approximately 79 % unconverted substrate *cis*-1.

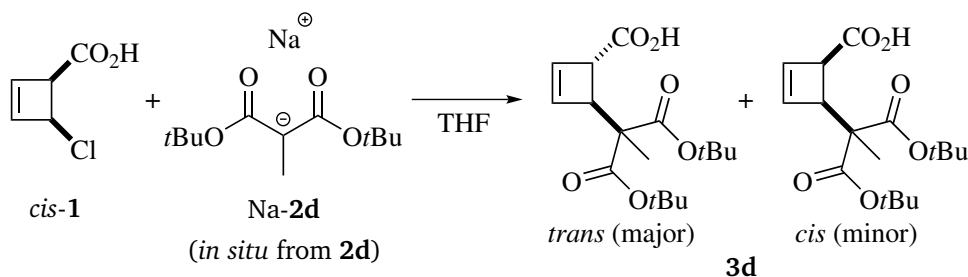
***rac*-trans-4-(1,3-diethoxy-2-methyl-1,3-dioxopropan-2-yl)cyclobut-2-ene-1-carboxylic acid (*trans*-3b)**



**JOP01-81**

The title compound was obtained according to general procedure E, using diethyl methylmalonate 2b (distilled from CaCl<sub>2</sub> prior to use) as pronucleophile. The reaction was quenched at incomplete conversion after 24 h. Characterization of the crude product obtained after work-up gave a d.r. of 99:1. The crude product contained approximately 29 % unconverted substrate *cis*-1.

***rac*-trans-4-(1,3-di-*tert*-butoxy-2-methyl-1,3-dioxopropan-2-yl)cyclobut-2-ene-1-carboxylic acid (*trans*-3d)**

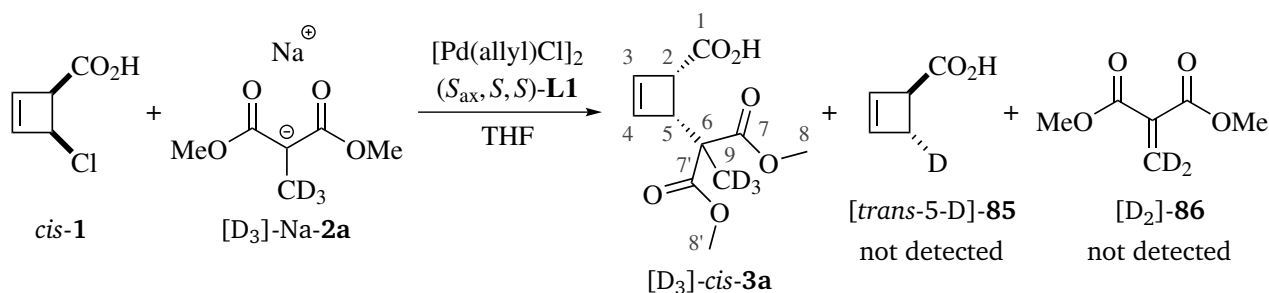


**JOP01-79**

The title compound was obtained according to general procedure E, using di-*tert*-butyl methylmalonate 2d (dried over MS 4 Å prior to use) as pronucleophile. The reaction was quenched at incomplete conversion after 39 h. Characterization of the crude product obtained after work-up gave a d.r. of 93:7. The crude product contained approximately 89 % unconverted substrate *cis*-1.

### 7.3 Investigation of the Nucleophilic Nature of Malonate Nucleophiles

#### (1*S*,4*R*)-4-(1,3-dimethoxy-2-methyl-1,3-dioxopropan-2-yl-3,3,3-*d*<sub>3</sub>)cyclobut-2-ene-1-carboxylic acid ([D<sub>3</sub>]-*cis*-3a)



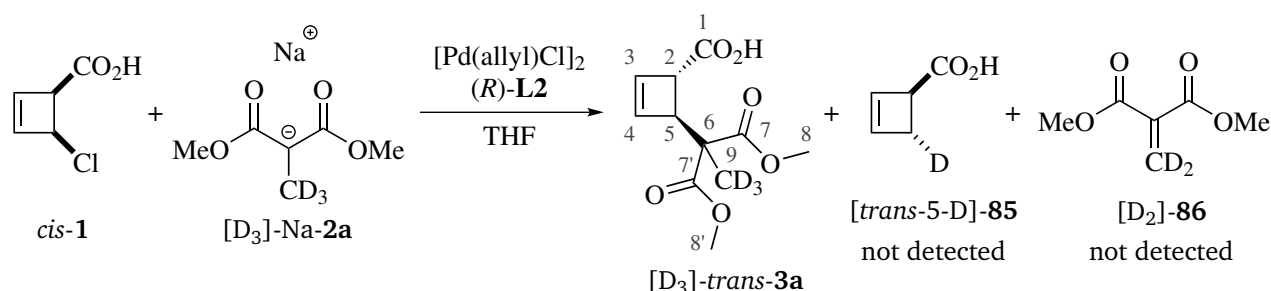
#### JOP01-183

The title compound was obtained according to general procedure C, using dimethyl (methyl-*d*<sub>3</sub>)malonate ([D<sub>3</sub>]-**2a**) as pronucleophile. The reaction was quenched after 2 h. Characterization of the crude product obtained after work-up gave a d.r. of 83:17 and quantitative deuteration at C(9) (> 99% D) for both diastereomers. The e.e. of the main product [D<sub>3</sub>]-*cis*-**3a** was found to be 81%. For the minor diastereomer [D<sub>3</sub>]-*trans*-**3a**, an e.e. of 31% was determined.

End-point analysis of the reaction mixture by <sup>1</sup>H-, <sup>2</sup>H- and <sup>13</sup>C-NMR as well as ESI-HRMS before quenching did not provide any evidence for the formation of β-deuteride elimination products [*trans*-5-D]-**85** and [D<sub>2</sub>]-**86**. Neither did analysis of the crude products using the same methods.

[D<sub>3</sub>]-*cis*-**3a**: <sup>1</sup>H-NMR (700 MHz, CDCl<sub>3</sub>, 273 K): δ<sub>H</sub> = 6.23 – 6.20 (1H, m, C(3)*H*), 6.16 – 6.15 (1H, m, C(4)*H*), 3.95 (1H, d, <sup>3</sup>J<sub>HH</sub> = 4.9 Hz, C(5)*H*), 3.86 (1H, d, <sup>3</sup>J<sub>HH</sub> = 4.9 Hz, C(2)*H*), 3.71 (1H, s, C(8/8')*H*), 3.71 (1H, s, C(8/8')*H*) ppm; <sup>2</sup>H-NMR (108 MHz, CH<sub>2</sub>Cl<sub>2</sub>): δ<sub>D</sub> = 1.35 (s) ppm; <sup>13</sup>C{<sup>1</sup>H}-NMR (176 MHz, CDCl<sub>3</sub>, 273 K): δ<sub>C</sub> = 177.7 (C(1)), 172.0 (C(7/7')), 171.1 (C(7/7')), 139.3 (C(4)), 134.2 (C(3)), 54.0 (C(6)), 52.9 (C(8/8')), 52.7 (C(8/8')), 50.7 (C(5)), 48.1 (C(2)), 17.1 (sept, <sup>1</sup>J<sub>CD</sub> = 19.9 Hz, C(10)) ppm; HRMS (ESI<sup>+</sup>): C<sub>11</sub>H<sub>11</sub>D<sub>3</sub>O<sub>6</sub> [M+H]<sup>+</sup> requires 246.1051, found 246.1052 (Δ = 0.1 ppm). For characterization of [D<sub>3</sub>]-*trans*-**3a**, see its selective preparation according to general procedure D.

**(1S,4S)-4-(1,3-dimethoxy-2-methyl-1,3-dioxopropan-2-yl-3,3,3-*d*<sub>3</sub>)cyclobut-2-ene-1-carboxylic acid ([D<sub>3</sub>]-*trans*-3a)**



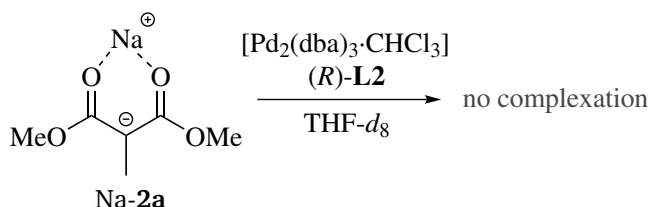
**JOP01-181**

The title compound was obtained according to general procedure D, using dimethyl (methyl-*d*<sub>3</sub>)malonate ([D<sub>3</sub>]-**2a**) as pronucleophile. The reaction was quenched after 11 h. Characterization of the crude product obtained after work-up gave a d.r. of 99:1 and quantitative deuteration at C(9) (> 99% D). The e.e. of the main product *trans*-**3a** was found to be 98%. The crude product contained only traces (< 1%) of unconverted substrate *cis*-**1**.

End-point analysis of the reaction mixture by <sup>1</sup>H-, <sup>2</sup>H- and <sup>13</sup>C-NMR as well as ESI-HRMS before quenching did not provide any evidence for the formation of β-deuteride elimination products [*trans*-5-D]-**85** and [D<sub>2</sub>]-**86**. Neither did analysis of the crude products using the same methods.

[D<sub>3</sub>]-*trans*-**3a**: <sup>1</sup>H-NMR (700 MHz, CDCl<sub>3</sub>, 273 K): δ<sub>H</sub> = 6.20–6.18 (1H, m, C(3)H), 6.18–6.16 (1H, m, C(4)H), 3.75 (1H, s, C(8/8')H), 3.73 (1H, s, C(8/8')H), 3.57 (1H, br. s, C(5)H), 3.54 (1H, br. s, C(2)H) ppm; <sup>2</sup>H-NMR (108 MHz, CH<sub>2</sub>Cl<sub>2</sub>): δ<sub>D</sub> = 1.38 (s) ppm; <sup>13</sup>C{<sup>1</sup>H}-NMR (176 MHz, CDCl<sub>3</sub>, 273 K): δ<sub>C</sub> = 177.0 (C(1)), 172.2 (C(7/7')), 171.8 (C(7/7')), 139.3 (C(3)), 135.2 (C(4)), 54.6 (C(6)), 53.1 (C(8/8')), 53.1 (C(8/8')), 50.5 (C(5)), 47.4 (C(2)), 16.8 (sept, <sup>1</sup>J<sub>CD</sub> = 19.8 Hz, C(10)) ppm; HRMS (ESI<sup>+</sup>): C<sub>11</sub>H<sub>11</sub>D<sub>3</sub>O<sub>6</sub> [M+H]<sup>+</sup> requires 246.1051, found 246.1054 (Δ = 0.9 ppm). For characterization of [D<sub>3</sub>]-*cis*-**3a**, see its selective preparation according to general procedure C.

**Attempt to prepare a Pd–malonate complex using sodium dimethyl methylmalonate (Na-2a)**



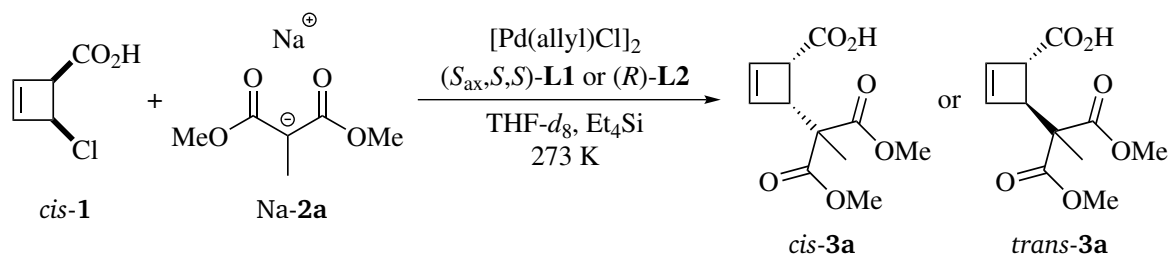
**PM01-6**

[Pd<sub>2</sub>(dba)<sub>3</sub>·CHCl<sub>3</sub>] (25.9 mg, 25 μmol, 0.5 equiv.) and ligand (R)-L2 (20.4 mg, 50 μmol, 1.0 equiv.) were dissolved in anhydrous THF-*d*<sub>8</sub> (0.5 mL) and stirred at RT for 10 min. A solution of sodium dimethyl methylmalonate Na-**2a** (ca. 95 w% purity, 8.8 mg, 50 μmol, 1.0 equiv.)

in anhydrous THF- $d_8$  (0.5 mL) was added dropwise upon stirring vigorously. After further 10 min of stirring, one drop of the reaction mixture was taken for subsequent MS analysis, and the residual solution was transferred into a precooled NMR tube. The tube was sealed with a rubber septum and parafilm<sup>®</sup>, and centrifuged (2000 rpm, 1 min) prior to NMR analysis.

$^1\text{H}$ -,  $^{13}\text{C}$ - and  $^{31}\text{P}$ -NMR,  $^1\text{H}$ - $^1\text{H}$ -COSY,  $^1\text{H}$ - $^{13}\text{C}$ -HSQC,  $^1\text{H}$ - $^{13}\text{C}/^{31}\text{P}$ -HMBC and  $^1\text{H}$ - $^1\text{H}$ -ROESY experiments as well as ESI-HRMS in positive and negative ion mode did not provide any evidence for a complexation of [Pd-L2] by Na-2a.

## 7.4 Kinetic Analysis



### JOP01-129, JOP01-130, JOP01-145

For kinetic analysis, a series of catalytic allylic alkylation reactions with substrate *cis*-1, nucleophile Na-2a and ligand  $(S_{\text{ax}}, S, S)\text{-L1}$  or  $(R)\text{-L2}$  was performed in NMR tubes sealed with a rubber septum and parafilm<sup>®</sup>. Reaction conditions were adopted from the literature,<sup>[56]</sup> with the total volume of the reaction mixture being 1.0 mL. Four stock solutions A (125 mM *cis*-1 and 125 mM  $\text{Et}_4\text{Si}$ ), B (375 mM Na-2a), C1 (3.75 mM  $[\text{Pd}(\text{allyl})\text{Cl}]_2$  and 15 mM  $(S_{\text{ax}}, S, S)\text{-L1}$ ) and C2 (12.5 mM  $[\text{Pd}(\text{allyl})\text{Cl}]_2$  and 75 mM  $(R)\text{-L2}$ ) were prepared in anhydrous THF- $d_8$ , using volumetric flasks. To the desired aliquot of stock solution A was carefully added the desired aliquot of stock solution B at 0 °C, followed by the amount of THF- $d_8$  necessary to reach a final total volume of 1.0 mL. The NMR tube was sealed and loaded into the NMR spectrometer, with the temperature set to 273 K. After wobbling on  $^1\text{H}$  and shimming, a single-scan  $^1\text{H}$ -NMR spectrum was recorded. The tube was ejected and the desired aliquot of stock solution C1 or C2 was added rapidly upon shaking. After shaking vigorously for about 5 s and additionally inverting one time, the sample was loaded into the NMR spectrometer again, and a series of  $^1\text{H}$ -NMR spectra was recorded with an interval of 60 s until reaching full conversion of deprotonated substrate *cis*-Na-1. The composition of the reaction monitoring runs performed is given in Table 7.1. For full signal assignment of products 3a, reaction mixtures 1.1 and 2.1 were subsequently analyzed by  $^{13}\text{C}$ -NMR,  $^1\text{H}$ - $^1\text{H}$ -COSY,  $^1\text{H}$ - $^{13}\text{C}$ -HSQC and  $^1\text{H}$ - $^{13}\text{C}$ -HMBC experiments.

All spectra were first treated with an automatic phase correction in *TopSpin* (version 3.5pl7, Bruker BioSpin, 2017). The spectral series were then imported to *MestReNova* (version 14.2.1, Mestrelab Research, 2021) using the directory spectra stack tool, followed by referencing<sup>[532]</sup> and a Whittaker Smoother baseline correction. The signals of interest were integrated employing the integrals graph function, and integration vs time data were transferred into

**Table 7.1:** Reaction monitoring runs performed with ligands **L** = ( $S_{ax}, S, S$ )-**L1** (top) and **L** = (*R*)-**L2** (bottom), with the volumes of stock solution A ( $V_A$ ), B ( $V_B$ ) and C1/2 ( $V_C$ ), the volume of pure THF- $d_8$  ( $V_\Delta$ ), and the resulting (attempted) starting concentrations of substrate *cis*-Na-**1**, nucleophile Na-**2a** (after protonation of 1.0 equiv.) and catalyst Pd-**L** given.

Run	$V_A / \mu\text{L}$	$V_B / \mu\text{L}$	$V_C / \mu\text{L}^{[a]}$	$V_\Delta / \mu\text{L}$	[ <i>cis</i> -Na- <b>1</b> ] / mM	[Na- <b>2a</b> ] / mM <sup>[b]</sup>	[Pd- <b>L</b> ] / mM
1.1	400	400	100	100	50	100	0.75
1.2	400	400	20	180	50	100	0.15
1.3	400	400	60	140	50	100	0.45
1.4	400	400	140	60	50	100	1.05
1.5	400	400	200	0	50	100	1.50
1.6	400	200	100	300	50	25	0.75
1.7	400	250	100	250	50	43.75	0.75
1.8	400	300	100	200	50	62.5	0.75
1.9	400	500	100	0	50	137.5	0.75
1.10	100	300	100	500	12.5	100	0.75
1.11	175	325	100	400	21.875	100	0.75
1.12	250	350	100	300	31.25	100	0.75
1.13	325	375	100	200	40.625	100	0.75
1.14	250	300	100	350	31.25	81.25	0.75
2.1	400	400	100	100	50	100	2.5
2.2	400	400	20	180	50	100	0.5
2.3	400	400	60	140	50	100	1.5
2.4	400	400	140	60	50	100	3.5
2.5	400	400	200	0	50	100	5.0
2.6	400	200	100	300	50	25	0.75
2.7	400	250	100	250	50	43.75	2.5
2.8	400	300	100	200	50	62.5	2.5
2.9 <sup>[c]</sup>	400	500	100	0	50	137.5	2.5
2.10	100	300	100	500	12.5	100	2.5
2.11	175	325	100	400	21.875	100	2.5
2.12	250	350	100	300	31.25	100	2.5
2.13	325	375	100	200	40.625	100	2.5
2.14	250	300	100	350	31.25	81.25	2.5

[a] stock solution C1 (containing ligand ( $S_{ax}, S, S$ )-**L1**) used for runs 1.*n*, stock solution C2 (containing ligand (*R*)-**L2**) used for runs 2.*n*

[b] not corrected for activation of  $[\text{Pd}(\text{allyl})\text{Cl}]_2$  by allylation of Na-**2a** reducing [Na-**2a**] by  $[\text{Pd}-\text{L}]$ , as this effect was found to be small compared to experimental deviations of starting concentrations

[c] different batches of stock solutions used as for runs 2.1 and 2.6–2.8, and therefore not included into initial rate analysis

temporal concentration profiles using *Microsoft Excel* (package Microsoft Office Professional Plus 2019).

The reaction monitoring data were subjected to initial rate analysis<sup>[440]</sup> and RPKA.<sup>[441]</sup> Initial rates were extracted by linear regression to the first 4–5 data points of each run, excluding  $t = 0$ . The experimental starting concentrations of deprotonated substrate *cis*-Na-1 and nucleophile Na-2a, which tended to be somewhat lower than the attempted concentrations, were determined from the <sup>1</sup>H-NMR spectrum at  $t = 0$  by integration against Et<sub>4</sub>Si, assuming [Et<sub>4</sub>Si] = 50 mM. The starting concentration of active Pd<sup>0</sup> was determined by quantifying the initiation by-product dimethyl 2-allyl-2-methylmalonate **87** in the first <sup>1</sup>H-NMR spectrum after addition of solution C1/2, using the resonance  $\delta_{\text{H}} = 2.55$  (2H, d, <sup>3</sup>J<sub>HH} = 7.4 Hz)<sup>[533]</sup> for integration. The initial rates extracted were plotted against the starting concentration varied ([*cis*-Na-1], [Na-2a], or [Pd-L]) and fitted with a linear regression. A proportional dependence was interpreted as a rate order of one, whereas initial rates which were independent of the starting concentration varied indicated a zero-order behavior.</sub>

For RPKA, the temporal concentrations of *cis*-Na-1 determined at reaction time  $t_n$  were transformed into approximated turnover rates  $\nu$  according to

$$\nu(t_n) \approx -\frac{1}{2} \left( \frac{[\textit{cis-Na-1}](t_n) - [\textit{cis-Na-1}](t_{n-1})}{t_n - t_{n-1}} + \frac{[\textit{cis-Na-1}](t_{n+1}) - [\textit{cis-Na-1}](t_n)}{t_{n+1} - t_n} \right), \quad (7.1)$$

i.e. by averaging the slope triangle to the previous and to the subsequent data point [*cis*-Na-1]( $t_{n-1}$ ) and [*cis*-Na-1]( $t_{n+1}$ ), respectively. The rate order in catalyst was probed by plotting the TOF, calculated by

$$\text{TOF}(t_n) = \frac{\nu(t_n)}{[\text{Pd-L}]}, \quad (7.2)$$

against [*cis*-Na-1]( $t_n$ ) for the three highest catalyst loadings (run 1.1–1.3 with L1 and 2.1–2.3 with L2), with superimposing graphs indicating a first-order dependence on [Pd-L]. The rate order in substrate was explored by plotting  $\nu(t_n)$  and  $\frac{\nu(t_n)}{[\textit{cis-Na-1}](t_n)}$  against [Na-2a]( $t_n$ ) for different [excess] concentrations

$$[\text{excess}] = [\text{Na-2a}](t = 0) - [\textit{cis-Na-1}](t = 0), \quad (7.3)$$

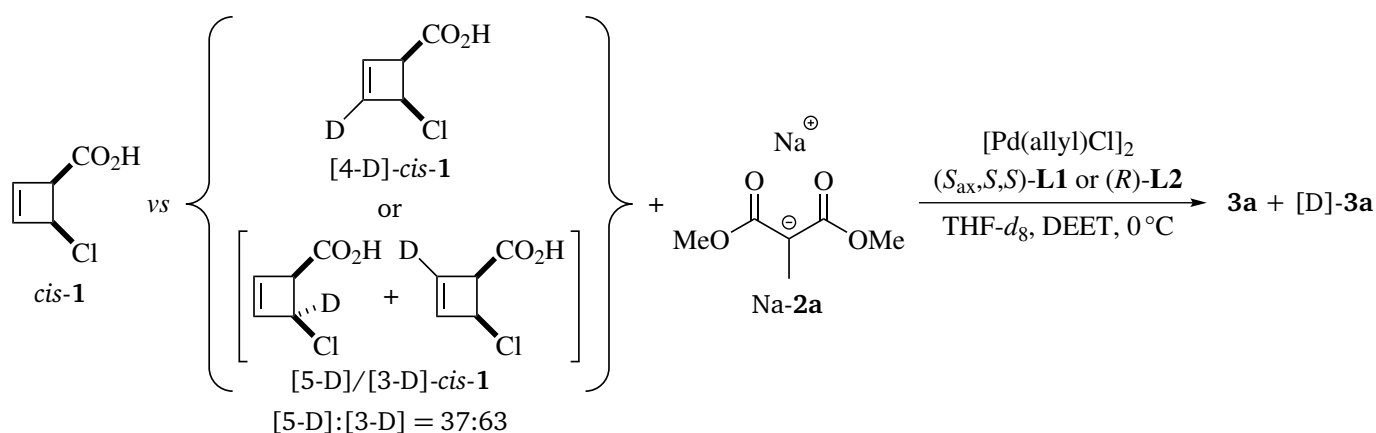
using the data from run 1.1 and 1.8–1.12 with ligand L1, and run 2.1, 2.9 and 2.11–2.13 with L2, respectively. An overlay in the former plot would show the reaction to be zero order in substrate, whereas superimposition in the latter plot would indicate a first-order dependence. Analogously, the rate order in nucleophile was probed using the reaction monitoring data from the same runs by plotting  $\nu(t_n)$  and  $\frac{\nu(t_n)}{[\text{Na-2a}](t_n)}$  against [*cis*-Na-1]( $t_n$ ) for different [excess] values, with an overlay in the former plot reflecting a zero-order behavior and superimposition in the latter plot indicating a rate order of one in nucleophile.

In order to examine for potential catalyst deactivation during turnover, the TOF was plotted against  $[cis\text{-Na-1}](t_n)$  for two reactions performed under identical conditions with equal [excess], but different initial concentrations of *cis*-Na-1 and Na-2a (run 1.1 and 1.14 with L1, run 2.1 and 2.14 with L2). In case of a deterioration of catalyst activity during turnover, the reaction with higher initial concentrations would be expected to display lower TOFs, whereas a stable catalyst performance would be indicated by the curves falling on top of one another.

## 7.5 Determination of KIEs

KIEs for the Pd-catalyzed allylic alkylation of substrate *cis*-1 with nucleophile Na-2a were generally extracted by means of intermolecular kinetic competition experiments according to the procedures reported below. From the reaction monitoring data obtained, fractional conversions  $F$  with respect to the limiting reaction partner as well as isotopologue or isotopomer ratios  $R$  (for substrate analysis) and/or  $R_p$  (for product analysis) were calculated. KIE plots were prepared with *OriginPro* (version 9.9.0.225, OriginLab Corporation, 2022) by plotting  $R$  and  $R_p$ , respectively, against  $F$ . The experimental data were fitted using equation (4.4) for substrate analysis and equation (4.6) for product analysis, with the initial substrate ratio  $R_0$  and the KIE of interest as regression parameters.

### 7.5.1 <sup>2</sup>H-KIEs by offline LC-MS Monitoring



#### JOP01-225, JOP01-227, JOP01-228, JOP01-237

The reaction was performed in a sealed 5 mL vial equipped with a magnetic stirrer bar and a rubber septum. Deuterated solvent was used to allow for determining quantitative conversion by NMR. In order to compensate for isotopic impurities in the deuterated substrates [D]-*cis*-1 used, competition runs were performed with a slight excess of [D]-*cis*-1 over unlabeled *cis*-1. For initiation, the same stock solutions C1 (3.75 mM [Pd(allyl)Cl]<sub>2</sub> and 15 mM (S<sub>ax</sub>,S,S)-L1) and C2 (12.5 mM [Pd(allyl)Cl]<sub>2</sub> and 75 mM (R)-L2) were used as in section 7.4. Sampling for subsequent LC-MS analysis was performed at the time points given below by taking 50 μL samples from



the reaction mixture. These were directly quenched in HPLC vials containing a mixture of TFA (10  $\mu$ L) and MeCN (200  $\mu$ L) at  $-45\text{ }^{\circ}\text{C}$  (MeCN cold bath).

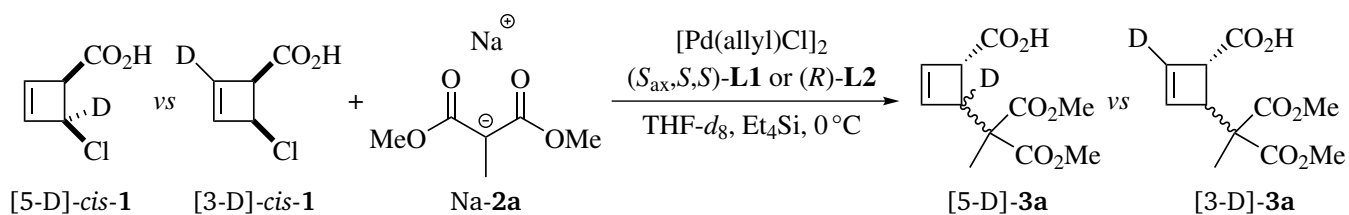
To a stirred solution of sodium dimethyl methylmalonate Na-**2a** (ca. 95 w% purity, 61.0 mg, 350  $\mu$ mol, 3.5 equiv.) and DEET (0.8 mg, 4  $\mu$ mol, 4 mol%) in anhydrous THF- $d_8$  (1.0 mL) was carefully added a solution of *cis*-4-chlorocyclobutene-2-enecarboxylic acid *cis*-**1** (6.2 mg, 47  $\mu$ mol, 0.47 equiv.) and its deuterated isotopologue [4-D]-*cis*-**1** or [5-D]/[3-D]-*cis*-**1** (94% D, 7.1 mg, 53  $\mu$ mol, 0.53 equiv.) in anhydrous THF- $d_8$  (0.8 mL) at  $0\text{ }^{\circ}\text{C}$ . After taking an initial sample in the way described above, the reaction was initiated by rapid addition of stock solution C1 (200  $\mu$ L, corresponding to 0.75  $\mu$ mol, 0.75 mol% [Pd(allyl)Cl] $_2$  and 3.0  $\mu$ mol, 3.0 mol% ( $S_{ax}, S, S$ )-**L1**) or C2 (300  $\mu$ L, corresponding to 3.75  $\mu$ mol, 3.75 mol% [Pd(allyl)Cl] $_2$  and 22.5  $\mu$ mol, 22.5 mol% (*R*)-**L2**). Samples were taken after 30 s, 1 min, 2 min, 3 min, 5 min, 7 min, 10 min, 15 min, 20 min, 25 min, 30 min, 35 min, 40 min, 50 min, 60 min, 70 min, 80 min, 100 min and 120 min when using ligand **L1**, and after 1 min, 3 min, 6 min, 10 min, 15 min, 20 min, 30 min, 40 min, 50 min, 60 min, 70 min, 80 min, 100 min, 120 min, 150 min, 180 min, 220 min and 260 min for the reaction with **L2** as ligand. After the last LC-MS sample, an additional 200  $\mu$ L sample was taken and quenched in a mixture of TFA (10  $\mu$ L) and THF- $d_8$  (500  $\mu$ L) at  $-45\text{ }^{\circ}\text{C}$ .  $^1\text{H-NMR}$  analysis of this sample confirmed that all reactions had reached nearly quantitative conversion.

LC-MS analysis was carried out by TIM HEYMANN. Measurements were performed on a  $2.1 \times 150$  mm, 2.7  $\mu$ m Proshell 120 reversed-phase pentafluorophenyl (RP-PFP) column with an Agilent 1260 Infinity II system. The latter consists of an automated vialsampler, a flexible quaternary UHPLC pump, a diode array detector (DAD), and a multicolumn compartment, which is coupled to a 6125B LC-MSD single quadrupole mass spectrometer equipped with an ESI source. The column temperature was kept constant at  $40\text{ }^{\circ}\text{C}$  and the sample was eluted with H $_2$ O:MeCN containing 0.1% formic acid at a flow rate of  $0.6\text{ mLmin}^{-1}$ . 20  $\mu$ L of each quenched reaction monitoring sample was diluted with water (30  $\mu$ L, mass spectrometry grade), and the diluted samples were cooled at  $4\text{ }^{\circ}\text{C}$  in the vialsampler until injection. 5  $\mu$ L of diluted sample was injected and elution was initiated with an eluent composition of 95:5 for 0.5 min, followed by a gradient to 70:30 over 2 min, a further gradient to 0:100 over 1 min, an isocratic hold for 2.5 min and re-equilibration to 95:5 for 3.5 min. The fractional conversion was determined by UV detection at 198 nm against DEET as internal standard. Ions were detected in negative ion mode by selected ion monitoring (SIM) at  $m/z = 131$  (*cis*-**1**) and  $m/z = 132$  ([D]-*cis*-**1**) with a dwell time of 100 ms.

The isotopologue ratios calculated from the ion intensities were corrected for the  $^{13}\text{C}$  content of unlabeled *cis*-**1**, which was ascertained by triplicate LC-MS analysis of a reference sample of *cis*-**1**, using the same method. The corrected isotopologue ratios  $R = \frac{[\text{D}]-\text{cis-1}}{[\text{cis-1}]}$  and the corresponding conversions determined were subjected to regression analysis as described above (substrate analysis only), giving the KIE of interest as relative reactivity of unlabeled over labeled substrates, i.e.  $\text{KIE} = \frac{k(\text{H})}{k(\text{D})}$ .



## 7.5.2 Relative $^2\text{H}$ -KIEs by offline $^1\text{H}$ -NMR Monitoring



### JOP01-238, JOP01-241

The reaction was performed in a sealed 5 mL vial equipped with a magnetic stirrer bar and a rubber septum. For the reaction using ligand **L1**, the same stock solution C1 (3.75 mM  $[\text{Pd}(\text{allyl})\text{Cl}]_2$  and 15 mM  $(S_{\text{ax}}, S, S)\text{-L1}$ ) was used for initiation as in section 7.4. Sampling for subsequent NMR analysis was performed at the time points given below by taking 250  $\mu\text{L}$  samples from the reaction mixture. These were directly quenched in NMR tubes containing a mixture of TFA (20  $\mu\text{L}$ ) and  $\text{CDCl}_3$  (300  $\mu\text{L}$ ) at  $-45^\circ\text{C}$  (MeCN cold bath).

To a stirred solution of sodium dimethyl methylmalonate **Na-2a** (ca. 95 w% purity, 123.9 mg, 700  $\mu\text{mol}$ , 3.5 equiv.) and  $\text{Et}_4\text{Si}$  (8.7 mg, 60  $\mu\text{mol}$ , 0.3 equiv.) in anhydrous  $\text{THF-}d_8$  (2.6 mL) was carefully added a solution of deuterated substrate [5-D]/[3-D]-cis-1 ([5-D]:[3-D] = 37:63, overall 94% D, 26.7 mg, 200  $\mu\text{mol}$ , 1.0 equiv.) in anhydrous  $\text{THF-}d_8$  (1.0 mL) at  $0^\circ\text{C}$ . After taking an initial sample in the way described above, the reaction was initiated by rapid addition of stock solution C1 (400  $\mu\text{L}$ , corresponding to 1.5  $\mu\text{mol}$ , 0.75 mol%  $[\text{Pd}(\text{allyl})\text{Cl}]_2$  and 6.0  $\mu\text{mol}$ , 3.0 mol%  $(S_{\text{ax}}, S, S)\text{-L1}$ ) or a solution of  $[\text{Pd}(\text{allyl})\text{Cl}]_2$  (3.4 mg, 9.0  $\mu\text{mol}$ , 4.5 mol%) and  $(R)\text{-L2}$  (22.5 mg, 54.0  $\mu\text{mol}$ , 27 mol%) in  $\text{THF-}d_8$  (0.4 mL). Samples were taken after 1 min, 3 min, 7 min, 12 min, 18 min, 26 min, 35 min, 50 min, 70 min, 100 min and 150 min when using ligand **L1**, and after 30 s, 3 min, 9 min, 16 min, 24 min, 34 min, 45 min, 57 min, 70 min, 85 min, 105 min, 135 min, 180 min and 280 min for the reaction with **L2** as ligand. All quenched samples were centrifuged (2000 rpm, 1 min) prior to  $^1\text{H}$ -NMR analysis, which was performed at 700 MHz and 288 K with  $90^\circ$  excitation, 16 accumulated scans, 16 dummy scans and an interscan delay of 30 s. The spectra obtained were treated with a Whittaker Smoother baseline correction, and the fractional conversion was determined by integration against  $\text{Et}_4\text{Si}$  as internal standard, using the signal at  $\delta_{\text{H}} = 0.52$  ppm (8H, q,  $^3J_{\text{HH}} = 8.0$  Hz,  $\text{CH}_2$ ) as reference integral. These spectra did, however, not allow for extraction of sufficiently accurate isotopomer ratios due to spectral overlap with unidentified impurities.

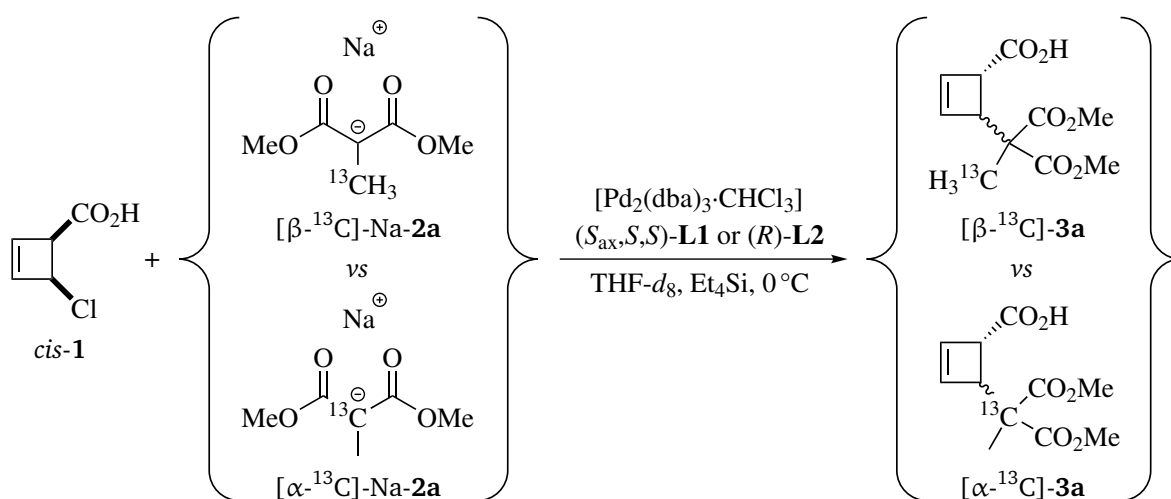
In order to improve the purity, all quenched samples apart from the initial sample were subjected to the work-up described in the following. The samples were concentrated *in vacuo* and the residue was dissolved in cold THF (1 mL), whereupon satd.  $\text{Na}_2\text{CO}_3$  (0.2 mL) and brine (3 mL) were added at  $0^\circ\text{C}$ . The aqueous layer was washed with  $\text{Et}_2\text{O}$  ( $3 \times 3$  mL), carefully acidified with 1 M HCl ( $\text{pH} \leq 2$ ) and extracted with  $\text{CH}_2\text{Cl}_2$  ( $6 \times 3$  mL). The combined organic layers were dried over  $\text{Na}_2\text{SO}_4$  and concentrated *in vacuo* to give the crude product, which was dissolved in  $\text{CDCl}_3$

and analyzed by  $^1\text{H-NMR}$  at 288 K. For each sample, two independent  $^1\text{H-NMR}$  measurements were conducted, one at 700 MHz ( $90^\circ$  excitation, 64 accumulated scans, 16 dummy scans, 30 s interscan delay) and one at 950 MHz ( $90^\circ$  excitation, 16 accumulated scans, 4 dummy scans, 30 s interscan delay), respectively. The spectra obtained were treated with a Whittaker Smoother baseline correction. The ratio of [3-D]- and [5-D]-isotopomers of both substrate *cis-1* and product **3a** (only main diastereomer) was determined according to

$$R_i = \frac{[3\text{-D}]}{[5\text{-D}]} = \frac{I_{\text{total}} - I_{\text{H3}}}{I_{\text{total}} - I_{\text{H5}}}, \quad (7.4)$$

using the integral of a suitable undeuterated position  $I_{\text{total}}$  and the integrals of partially deuterated positions  $I_{\text{H3}}$  and  $I_{\text{H5}}$ , respectively. The experimental isotopomer ratios and the corresponding conversions determined were subjected to regression analysis as described above (both substrate and product analysis), giving the KIE of interest as relative reactivity of [5-D] over [3-D], i.e.  $\text{KIE} = \frac{k(5\text{-D})}{k(3\text{-D})}$ .

### 7.5.3 $^{13}\text{C}$ -KIEs by offline $^{13}\text{C}$ -NMR Monitoring



#### JOP01-270, JOP01-271

The reaction was performed in a 10 mL Schlenk flask equipped with a magnetic stirrer bar and a rubber septum. Sampling for subsequent NMR analysis was performed at the time points given below by taking 300  $\mu\text{L}$  samples from the reaction mixture. These were directly quenched in NMR tubes containing a mixture of TFA (20  $\mu\text{L}$ ) and  $\text{CDCl}_3$  (300  $\mu\text{L}$ ) at  $-45^\circ\text{C}$  (MeCN cold bath).

To a stirred solution of *cis*-4-chlorocyclobutene-2-enecarboxylic acid *cis-1* (37.1 mg, 280  $\mu\text{mol}$ , 1.4 equiv.),  $\text{Et}_4\text{Si}$  (144 mg, 1.0 mmol, 5.0 equiv.) and dimethyl methylmalonate isotopomers [ $\beta$ - $^{13}\text{C}$ ]-**2a** (14.7 mg, 100  $\mu\text{mol}$ , 0.5 equiv.) and [ $\alpha$ - $^{13}\text{C}$ ]-**2a** (14.7 mg, 100  $\mu\text{mol}$ , 0.5 equiv.) in anhydrous  $\text{THF-}d_8$  (4.0 mL) was carefully added a solution of NaHMDS (99.0 mg, 540  $\mu\text{mol}$ ,

2.7 equiv.) in anhydrous THF- $d_8$  (1.0 mL) at 0 °C. After taking an initial sample in the way described above, the reaction was initiated by rapid addition of a solution of either  $[\text{Pd}_2(\text{dba})_3 \cdot \text{CHCl}_3]$  (10.4 mg, 10  $\mu\text{mol}$ , 5 mol%) and ( $S_{\text{ax}}, S, S$ )-**L1** (21.6 mg, 40  $\mu\text{mol}$ , 20 mol%) or  $[\text{Pd}_2(\text{dba})_3 \cdot \text{CHCl}_3]$  (20.7 mg, 20  $\mu\text{mol}$ , 10 mol%) and (*R*)-**L2** (48.9 mg, 120  $\mu\text{mol}$ , 60 mol%) in THF- $d_8$  (1.0 mL). With ligand **L1**, samples were taken after 30 s, 2 min, 4 min, 7 min, 11 min and 15 min. Subsequent samples, taken after up to 4 h, did not display any further increase in conversion of  $[\text{C}^{13}]$ -Na-**2a**. For the reaction with **L2** as ligand, samples were taken after 30 s, 3 min, 10 min, 20 min, 35 min, 55 min, 80 min, 110 min, 150 min, 200 min, 260 min, 340 min, 450 min and 22 h, after which no further conversion was detected. All quenched samples were centrifuged (2000 rpm, 1 min) prior to quantitative  $^{13}\text{C}$ -NMR analysis, which was performed at 176 MHz and 283 K with inverse-gated decoupling, 90° excitation, 600–2720 accumulated scans (depending on the measurement time available), 8 dummy scans and an interscan delay of 80 s. The latter was chosen according to the most slowly relaxing carbon of interest in the system, which was found to be the quaternary all-carbon center of product **3a** with a  $T_1$  relaxation time of approximately 17.3 s for  $[\alpha\text{-}^{13}\text{C}]$ -*cis*-**3a** and 14.4 s for  $[\alpha\text{-}^{13}\text{C}]$ -*trans*-**3a**, as determined by 1D inversion recovery experiments. The  $^{13}\text{C}$ -NMR spectra obtained were treated with a Whittaker Smoother baseline correction, and the fractional conversion was determined by integration against  $\text{Et}_4\text{Si}$  as internal standard, using the signal at  $\delta_{\text{C}} = 8.0$  ppm (4C,  $\text{CH}_3$ ) as reference integral. The ratio of  $[\beta\text{-}^{13}\text{C}]$ - and  $[\alpha\text{-}^{13}\text{C}]$ -isotopomers was determined by comparison of the respective integrals, both for nucleophile  $[\text{C}^{13}]$ -Na-**2a** (detected as its corresponding acid  $[\text{C}^{13}]$ -**2a**) and for product  $[\text{C}^{13}]$ -**3a** (only main diastereomer). The experimental isotopomer ratios  $R_i = \frac{[\alpha\text{-}^{13}\text{C}]}{[\beta\text{-}^{13}\text{C}]}$  and the corresponding conversions determined were subjected to regression analysis as described above (both substrate and product analysis), giving the KIE of interest as relative reactivity of  $[\beta\text{-}^{13}\text{C}]$  over  $[\alpha\text{-}^{13}\text{C}]$ , i.e.  $\text{KIE} = \frac{k(\beta\text{-}^{13}\text{C})}{k(\alpha\text{-}^{13}\text{C})}$ .



---

# Bibliography

- [1] L. A. Nguyen, H. He, C. Pham-Huy, *Int. J. Biomed. Sci.* **2006**, *2*, 85–100.
- [2] P. Jeschke, *Pest Manag. Sci.* **2018**, *74*, 2389–2404.
- [3] J. Knabe, H. P. Büch, G. A. Kirsch, *Arch. Pharm. (Weinheim)* **1987**, *320*, 323–328.
- [4] J. M. Walshe, *The Lancet* **1992**, *339*, 254.
- [5] J. Clayden, N. Greeves, S. Warren, P. Wothers, *Organic Chemistry*, Oxford University Press, Oxford, **2001**.
- [6] K.-C. Lin, *J. Chem. Educ.* **1988**, *65*, 857–860.
- [7] Z. G. Brill, M. L. Condakes, C. P. Ting, T. J. Maimone, *Chem. Rev.* **2017**, *117*, 11753–11795.
- [8] G. Casiraghi, F. Zanardi, G. Rassu, P. Spanu, *Chem. Rev.* **1995**, *95*, 1677–1716.
- [9] H. U. Blaser, *Chem. Rev.* **1992**, *92*, 935–952.
- [10] E. Vedejs, M. Jure, *Angew. Chem. Int. Ed.* **2005**, *44*, 3974–4001.
- [11] H. B. Kagan, J. C. Fiaud in *Topics in Stereochemistry, Vol. 18* (Eds.: E. L. Eliel, S. H. Wilen), John Wiley & Sons, Hoboken, **1988**, pp. 249–330.
- [12] E. Fogassy, M. Nógrádi, D. Kozma, G. Egri, E. Pálovics, V. Kiss, *Org. Biomol. Chem.* **2006**, *4*, 3011–3030.
- [13] R. E. Gawley, J. Aubé, *Principles of Asymmetric Synthesis*, 2<sup>nd</sup> ed., Elsevier, Amsterdam, **2012**.
- [14] G.-Q. Lin, Y.-M. Li, A. S. C. Chan, *Principles and Applications of Asymmetric Synthesis*, John Wiley & Sons, Hoboken, **2001**.
- [15] D. J. Ager, M. B. East, *Asymmetric Synthetic Methodology*, CRC Press, Boca Raton, **1995**.
- [16] F. J. Sardina, H. Rapoport, *Chem. Rev.* **1996**, *96*, 1825–1872.
- [17] S.-M. Paek, M. Jeong, J. Jo, Y. M. Heo, Y. T. Han, H. Yun, *Molecules* **2016**, *21*, 951–963.
- [18] N. Chida, T. Sato in *Comprehensive Chirality, Vol. 2* (Eds.: E. M. Carreira, H. Yamamoto), Elsevier, Amsterdam, **2012**, pp. 207–239.
- [19] M. D. Argade, A. P. Riley, *Synlett* **2022**, *33*, 1209–1214.

- 
- [20] M. Christmann, S. Bräse (Eds.), *Asymmetric Synthesis: More Methods and Applications*, Wiley-VCH, Weinheim, **2012**.
- [21] J. M. Keith, J. F. Larrow, E. N. Jacobsen, *Adv. Synth. Catal.* **2001**, *343*, 5–26.
- [22] H. Pellissier, *Adv. Synth. Catal.* **2011**, *353*, 659–676.
- [23] B. M. Matute, J.-E. Bäckvall, *Curr. Opin. Chem. Biol.* **2007**, *11*, 226–232.
- [24] B. M. Trost, F. D. Toste, *J. Am. Chem. Soc.* **1999**, *121*, 3543–3544.
- [25] R. He, X. Huo, L. Zhao, F. Wang, L. Jiang, J. Liao, W. Zhang, *J. Am. Chem. Soc.* **2020**, *142*, 8097–8103.
- [26] D. N. Tran, N. Cramer, *Angew. Chem. Int. Ed.* **2013**, *52*, 10630–10634.
- [27] P.-J. Yang, L. Qi, Z. Liu, G. Yang, Z. Chai, *J. Am. Chem. Soc.* **2018**, *140*, 17211–17217.
- [28] J. Steinreiber, K. Faber, H. Griengl, *Chem. Eur. J.* **2008**, *14*, 8060–8072.
- [29] K. Faber, *Chem. Eur. J.* **2001**, *7*, 5004–5010.
- [30] J. Wencel-Delord, F. Colobert, *Synthesis* **2016**, *48*, 2981–2996.
- [31] D. A. Evans, J. Bartroli, T. L. Shih, *J. Am. Chem. Soc.* **1981**, *103*, 2127–2129.
- [32] D. A. Evans, M. D. Ennis, D. J. Mathre, *J. Am. Chem. Soc.* **1982**, *104*, 1737–1739.
- [33] D. A. Evans, K. T. Chapman, J. Bisaha, *J. Am. Chem. Soc.* **1984**, *106*, 4261–4263.
- [34] D. A. Evans, M. D. Ennis, T. Le, N. Mandel, G. Mandel, *J. Am. Chem. Soc.* **1984**, *106*, 1154–1156.
- [35] D. A. Evans, K. T. Chapman, J. Bisaha, *J. Am. Chem. Soc.* **1988**, *110*, 1238–1256.
- [36] D. A. Evans, J. T. Shaw, *Actual. Chim.* **2003**, *2003*, 35–38.
- [37] Y. Gnas, F. Glorius, *Synthesis* **2006**, *2006*, 1899–1930.
- [38] P. T. Anastas, N. Eghbali, *Chem. Soc. Rev.* **2010**, *39*, 301–312.
- [39] P. J. Dunn, *Chem. Soc. Rev.* **2012**, *41*, 1452–1461.
- [40] B. M. Trost, *Science* **1991**, *254*, 1471–1477.
- [41] M. Hall, *RSC Chem. Biol.* **2021**, *2*, 958–989.
- [42] J. Seayad, B. List, *Org. Biomol. Chem.* **2005**, *3*, 719–724.
- [43] B. M. Trost, M. L. Crawley, *Chem. Rev.* **2003**, *103*, 2921–2944.

- 
- [44] X. Jianhua, Z. Qilin, *Acta Chim. Sinica* **2012**, *70*, 1427–1438.
- [45] N. U. D. Reshi, V. B. Saptal, M. Beller, J. K. Bera, *ACS Catal.* **2021**, *11*, 13809–13837.
- [46] J. Hu, M. Ferger, Z. Shi, T. B. Marder, *Chem. Soc. Rev.* **2021**, *50*, 13129–13188.
- [47] T. Akiyama, I. Ojima (Eds.), *Catalytic Asymmetric Synthesis*, 4<sup>th</sup> ed., John Wiley & Sons, Hoboken, **2022**.
- [48] O. Pàmies, J. Margalef, S. Cañellas, J. James, E. Judge, P. J. Guiry, C. Moberg, J.-E. Bäckvall, A. Pfaltz, M. A. Pericàs, M. Diéguez, *Chem. Rev.* **2021**, *121*, 4373–4505.
- [49] B. M. Trost, R. C. Bunt, R. C. Lemoine, T. L. Calkins, *J. Am. Chem. Soc.* **2000**, *122*, 5968–5976.
- [50] J.-B. Langlois, A. Alexakis, *Adv. Synth. Catal.* **2010**, *352*, 447–457.
- [51] T. Hayashi, A. Yamamoto, T. Hagihara, *J. Org. Chem.* **1986**, *51*, 723–727.
- [52] M. E. Hoke, M.-R. Brescia, S. Bogaczyk, P. DeShong, *J. Org. Chem.* **2002**, *67*, 327–335.
- [53] M. Moreno-Mañas, J. Ribas, *30*, 3109–3112.
- [54] B. M. Trost, D. L. Van Vranken, *Chem. Rev.* **1996**, *96*, 395–422.
- [55] M. Luparia, M. T. Oliveira, D. Audisio, F. Frébault, R. Goddard, N. Maulide, *Angew. Chem. Int. Ed.* **2011**, *50*, 12631–12635.
- [56] D. Audisio, M. Luparia, M. T. Oliveira, D. Klütt, N. Maulide, *Angew. Chem. Int. Ed.* **2012**, *51*, 7314–7317.
- [57] D. Audisio, G. Gopakumar, L.-G. Xie, L. G. Alves, C. Wirtz, A. M. Martins, W. Thiel, C. Fars, N. Maulide, *Angew. Chem. Int. Ed.* **2013**, *52*, 6313–6316.
- [58] L.-G. Xie, V. Bagutski, D. Audisio, L. M. Wolf, V. Schmidts, K. Hofmann, C. Wirtz, W. Thiel, C. M. Thiele, N. Maulide, *Chem. Sci.* **2015**, *6*, 5734–5739.
- [59] B. M. Trost, *J. Org. Chem.* **2004**, *69*, 5813–5837.
- [60] Z. Lu, S. Ma, *Angew. Chem. Int. Ed.* **2008**, *47*, 258–297.
- [61] S. Hansson, P.-O. Norrby, M. P. T. Soegren, B. Åkermark, M. E. Cucciolito, F. Giordano, A. Vitagliano, *Organometallics* **1993**, *12*, 4940–4948.
- [62] C. Breutel, P. S. Pregosin, R. Salzmänn, A. Togni, *J. Am. Chem. Soc.* **1994**, *116*, 4067–4068.
- [63] P. S. Pregosin, R. Salzmänn, A. Togni, *Organometallics* **1995**, *14*, 842–847.

- 
- [64] L. Barloy, S. Ramdeehul, J. A. Osborn, C. Carlotti, F. Taulelle, A. De Cian, J. Fischer, *Eur. J. Inorg. Chem.* **2000**, 2000, 2523–2532.
- [65] G. Gatti, J. A. López, C. Mealli, A. Musco, *J. Organomet. Chem.* **1994**, 483, 77–89.
- [66] P. Fristrup, M. Ahlquist, D. Tanner, P.-O. Norrby, *J. Phys. Chem. A* **2008**, 112, 12862–12867.
- [67] J. Powell, B. L. Shaw, *J. Chem. Soc. A* **1967**, 1967, 1839–1851.
- [68] C. Amatore, A. Jutand, G. Meyer, L. Mottier, *Chem. Eur. J.* **1999**, 5, 466–473.
- [69] L. A. Evans, N. Fey, J. N. Harvey, D. Hose, G. C. Lloyd-Jones, P. Murray, A. G. Orpen, R. Osborne, G. J. J. Owen-Smith, M. Purdie, *J. Am. Chem. Soc.* **2008**, 130, 14471–14473.
- [70] D. A. Singleton, C. F. Christian, *Tetrahedron Lett.* **2005**, 46, 1631–1634.
- [71] P. B. Mackenzie, J. Whelan, B. Bosnich, *J. Am. Chem. Soc.* **1985**, 107, 2046–2054.
- [72] S. Norsikian, C.-W. Chang, *Curr. Org. Synth.* **2009**, 6, 264–289.
- [73] C. G. Frost, J. Howarth, J. M. J. Williams, *Tetrahedron: Asymmetry* **1992**, 3, 1089–1122.
- [74] O. Hoarau, H. Aït-Haddou, J.-C. Daran, D. Cramailère, G. G. A. Balavoine, *Organometallics* **1999**, 18, 4718–4723.
- [75] S.-L. You, X.-Z. Zhu, Y.-M. Luo, X.-L. Hou, L.-X. Dai, *J. Am. Chem. Soc.* **2001**, 123, 7471–7472.
- [76] S. Jansat, M. Gómez, K. Philippot, G. Muller, E. Guiu, C. Claver, S. Castellón, B. Chaudret, *J. Am. Chem. Soc.* **2004**, 126, 1592–1593.
- [77] A. Hazari, V. Gouverneur, J. Brown, *Angew. Chem. Int. Ed.* **2009**, 48, 1296–1299.
- [78] M. Fañanás-Mastral, M. Pérez, P. H. Bos, A. Rudolph, S. R. Harutyunyan, B. L. Feringa, *Angew. Chem. Int. Ed.* **2012**, 51, 1922–1925.
- [79] H.-J. Gais, H. Eichelmann, N. Spalthoff, F. Gerhards, M. Frank, G. Raabe, *Tetrahedron: Asymmetry* **1998**, 9, 235–248.
- [80] Z.-T. He, J. F. Hartwig, *Nat. Chem.* **2019**, 11, 177–183.
- [81] N. Kaiser, U. Bremberg, M. Larhed, C. Moberg, A. Hallberg, *Angew. Chem. Int. Ed.* **2000**, 39, 3595–3598.
- [82] X. Huo, G. Yang, D. Liu, Y. Liu, I. D. Gridnev, W. Zhang, *Angew. Chem. Int. Ed.* **2014**, 53, 6776–6780.
- [83] K. Manabe, S. Kobayashi, *Org. Lett.* **2003**, 5, 3241–3244.



- 
- [84] S.-B. Tang, X. Zhang, H.-F. Tu, S.-L. You, *J. Am. Chem. Soc.* **2018**, *140*, 7737–7742.
- [85] R. Mukai, Y. Horino, S. Tanaka, Y. Tamaru, M. Kimura, *J. Am. Chem. Soc.* **2004**, *126*, 11138–11139.
- [86] X. Huo, M. Quan, G. Yang, X. Zhao, D. Liu, Y. Liu, W. Zhang, *Org. Lett.* **2014**, *16*, 1570–1573.
- [87] S. Mukherjee, B. List, *J. Am. Chem. Soc.* **2007**, *129*, 11336–11337.
- [88] X.-S. Wu, Y. Chen, M.-B. Li, M.-G. Zhou, S.-K. Tian, *J. Am. Chem. Soc.* **2012**, *134*, 14694–14697.
- [89] N. A. Butt, W. Zhang, *Chem. Soc. Rev.* **2015**, *44*, 7929–7967.
- [90] B. Sundararaju, M. Achard, C. Bruneau, *Chem. Soc. Rev.* **2012**, *41*, 4467–4483.
- [91] J. M. J. Williams in *Advanced Asymmetric Synthesis* (Ed.: G. R. Stephenson), Springer Science+Business Media, Dordrecht, **1996**, pp. 299–312.
- [92] J. Tsuji in *Handbook of Organopalladium Chemistry for Organic Synthesis* (Ed.: E. Negishi), Wiley-Interscience, New York, **2003**, pp. 1669–1687.
- [93] J. F. Hartwig, M. J. Pouy in *Iridium Catalysis* (Ed.: P. G. Andersson), Springer, Berlin, **2011**, pp. 169–208.
- [94] Q. Cheng, H.-F. Tu, C. Zheng, J.-P. Qu, G. Helmchen, S.-L. You, *Chem. Rev.* **2019**, *119*, 1855–1969.
- [95] O. Belda, C. Moberg, *Acc. Chem. Res.* **2004**, *37*, 159–167.
- [96] C. Moberg in *Transition Metal Catalyzed Enantioselective Allylic Substitution in Organic Synthesis* (Ed.: U. Kazmaier), Springer, Berlin, **2012**, pp. 209–234.
- [97] B. W. H. Turnbull, P. A. Evans, *J. Org. Chem.* **2018**, *83*, 11463–11479.
- [98] T. Kondo, T. Mitsudo in *Ruthenium in Organic Synthesis* (Ed.: S.-I. Murahashi), Wiley-VCH, Weinheim, **2005**, pp. 129–151.
- [99] C. A. Falciola, A. Alexakis, *Eur. J. Org. Chem.* **2008**, 3765–3780.
- [100] B. Plietker in *Iron Catalysis in Organic Chemistry: Reactions and Applications* (Ed.: B. Plietker), Wiley-VCH, Weinheim, **2008**, pp. 197–215.
- [101] D. Ghorai, A. Cristòfol, A. W. Kleij, *Eur. J. Inorg. Chem.* **2022**, *2022*, e202100820.
- [102] J.-F. Han, P. Guo, X.-G. Zhang, J.-B. Liao, K.-Y. Ye, *Org. Biomol. Chem.* **2020**, *18*, 7740–7750.

- 
- [103] M. L. Clarke, *Polyhedron* **2001**, *20*, 151–164.
- [104] I. G. Ríos, A. Rosas-Hernandez, E. Martin, *Molecules* **2011**, *16*, 970–1010.
- [105] P. C. J. Kamer, P. W. N. M. van Leeuwen, J. N. H. Reek, *Acc. Chem. Res.* **2001**, *34*, 895–904.
- [106] M. P. Carroll, P. J. Guiry, *Chem. Soc. Rev.* **2014**, *43*, 819–833.
- [107] M. Braun, T. Meier, *Angew. Chem. Int. Ed.* **2006**, *45*, 6952–6955.
- [108] S. R. Harutyunyan, T. den Hartog, K. Geurts, A. J. Minnaard, B. L. Feringa, *Chem. Rev.* **2008**, *108*, 2824–2852.
- [109] K. Geurts, S. P. Fletcher, A. W. van Zijl, A. J. Minnaard, B. L. Feringa, *Pure Appl. Chem.* **2009**, *80*, 1025–1037.
- [110] J. Tsuji, H. Takahashi, M. Morikawa, *Tetrahedron Lett.* **1965**, *49*, 4387–4388.
- [111] B. M. Trost, T. J. Fullerton, *J. Am. Chem. Soc.* **1973**, *95*, 292–294.
- [112] T. Hayashi, A. Yamamoto, Y. Ito, E. Nishioka, H. Miura, K. Yanagi, *J. Am. Chem. Soc.* **1989**, *111*, 6301–6311.
- [113] T. Ohmura, J. F. Hartwig, *J. Am. Chem. Soc.* **2002**, *124*, 15164–15165.
- [114] B. M. Trost, F. D. Toste, *J. Am. Chem. Soc.* **1998**, *120*, 815–816.
- [115] H. Miyabe, K. Yoshida, M. Yamauchi, Y. Takemoto, *J. Org. Chem.* **2005**, *70*, 2148–2153.
- [116] T. Kondo, Y. Morisaki, S. Uenoyama, K. Wada, T. Mitsudo, *J. Am. Chem. Soc.* **1999**, *121*, 8657–8658.
- [117] H.-J. Gais, T. Jagusch, N. Spalthoff, F. Gerhards, M. Frank, G. Raabe, *Chem. Eur. J.* **2003**, *9*, 4202–4221.
- [118] P. Butti, R. Rochat, A. D. Sadow, A. Togni, *Angew. Chem. Int. Ed.* **2008**, *47*, 4878–4881.
- [119] B. M. Trost, T. Zhang, J. D. Sieber, *Chem. Sci.* **2010**, *1*, 427–440.
- [120] P. Zhang, H. Le, R. E. Kyne, J. P. Morken, *J. Am. Chem. Soc.* **2011**, *133*, 9716–9719.
- [121] B. M. Trost, J. E. Schultz, T. Chang, M. R. Maduabum, *J. Am. Chem. Soc.* **2019**, *141*, 9521–9526.
- [122] A. Misale, S. Niyomchon, M. Luparia, N. Maulide, *Angew. Chem. Int. Ed.* **2014**, *53*, 7068–7073.
- [123] B. Böttcher, V. Schmidts, J. Raskatov, C. Thiele, *Angew. Chem. Int. Ed.* **2010**, *49*, 205–209.

- 
- [124] C. P. Butts, E. Filali, G. C. Lloyd-Jones, P-O. Norrby, D. A. Sale, Y. Schramm, *J. Am. Chem. Soc.* **2009**, *131*, 9945–9957.
- [125] S. K. Mandal, G. N. Gowda, S. S. Krishnamurthy, C. Zheng, S. Li, N. S. Hosmane, *J. Organomet. Chem.* **2003**, *676*, 22–37.
- [126] M. A. Pericàs, C. Puigjaner, A. Riera, A. Vidal-Ferran, M. Gómez, F. Jiménez, G. Muller, M. Rocamora, *Chem. Eur. J.* **2002**, *8*, 4164 – 4178.
- [127] G. C. Lloyd-Jones, S. C. Stephen, M. Murray, C. P. Butts, Š. Vyskočil, P. Kočovský, *Chem. Eur. J.* **2000**, *6*, 4348–4357.
- [128] J. Sprinz, M. Kiefer, G. Helmchen, M. Reggelin, G. Huttner, O. Walter, L. Zsolnai, *Tetrahedron Lett.* **1994**, *35*, 1523–1526.
- [129] B. Åkermark, B. Krakenberger, S. Hansson, *Organometallics* **1987**, *6*, 620–628.
- [130] B. E. Mann, R. Pietropaolo, B. L. Shaw, *J. Chem. Soc. D* **1971**, *1971*, 790–791.
- [131] S. Ramdeehul, L. Barloy, J. A. Osborn, A. D. Cian, J. Fischer, *Organometallics* **1996**, *15*, 5442–5444.
- [132] B. Crociani, S. Antonaroli, M. Burattini, P. Paoli, P. Rossi, *Dalton Trans.* **2010**, *39*, 3665–3672.
- [133] N. H. Sherden, D. C. Behenna, S. C. Virgil, B. M. Stoltz, *Angew. Chem. Int. Ed.* **2009**, *48*, 6840–6843.
- [134] M. Kollmar, G. Helmchen, *Organometallics* **2002**, *21*, 4771–4775.
- [135] P. Braunstein, J. Zhang, R. Welter, *Dalton Trans.* **2003**, *2003*, 507–509.
- [136] A. Q. Cusumano, B. M. Stoltz, W. A. Goddard III, *J. Am. Chem. Soc.* **2020**, *142*, 13917–13933.
- [137] T. Cantat, E. Génin, C. Giroud, G. Meyer, A. Jutand, *J. Organomet. Chem.* **2003**, *687*, 365–376.
- [138] B. Åkermark, G. Åkermark, L. S. Hegedus, K. Zetterberg, *J. Am. Chem. Soc.* **1981**, *103*, 3037–3040.
- [139] N. Solin, J. Kjellgren, K. J. Szabó, *J. Am. Chem. Soc.* **2004**, *126*, 7026–7033.
- [140] M. García-Iglesias, E. Buñuel, D. J. Cárdenas, *Organometallics* **2006**, *25*, 3611–3618.
- [141] P. A. Evans, J. D. Nelson, *J. Am. Chem. Soc.* **1998**, *120*, 5581–5582.

- 
- [142] B. Wucher, M. Moser, S. A. Schumacher, F. Rominger, D. Kunz, *Angew. Chem. Int. Ed.* **2009**, *48*, 4417–4421.
- [143] B. Plietker, A. Dieskau, K. Möws, A. Jatsch, *Angew. Chem. Int. Ed.* **2008**, *47*, 198–201.
- [144] B. Plietker, *Angew. Chem. Int. Ed.* **2006**, *47*, 198–201.
- [145] M. Braun, T. Meier, *Angew. Chem. Int. Ed.* **2006**, *45*, 6952–6955.
- [146] S.-L. You, L.-X. Dai, *Angew. Chem. Int. Ed.* **2006**, *45*, 5246–5248.
- [147] A. Y. Hong, B. M. Stoltz, *Eur. J. Org. Chem.* **2013**, *2013*, 2745–2759.
- [148] B. M. Trost, N. R. Schmuff, *Tetrahedron Lett.* **1981**, *22*, 2999–3000.
- [149] G. Poli, G. Prestat, F. Liron, C. Kammerer-Pentier in *Transition Metal Catalyzed Enantioselective Allylic Substitution in Organic Synthesis* (Ed.: U. Kazmaier), Springer, Berlin, **2012**, pp. 1–64.
- [150] E. Keinan, M. Sahai, *J. Chem. Soc., Chem. Commun.* **1984**, *1984*, 648–650.
- [151] M. Prat, J. Ribas, M. Moreno-Mañas, *Tetrahedron* **1992**, *48*, 1695–1706.
- [152] V. Branchadell, M. Moreno-Mañas, F. Pajuelo, R. Pleixats, *Organometallics* **1999**, *18*, 4934–4941.
- [153] M. P. T. Sjögren, S. Hansson, B. Åkermark, A. Vitagliano, *Organometallics* **1994**, *13*, 1963–1971.
- [154] J. W. Faller, M. E. Thomsen, M. J. Mattina, *J. Am. Chem. Soc.* **1971**, *93*, 2642–2653.
- [155] J. Lukas, J. E. Ramakers-Blom, T. G. Hewitt, J. J. de Boer, *J. Organomet. Chem.* **1972**, *46*, 167–177.
- [156] B. Åkermark, S. Hansson, A. Vitagliano, *J. Am. Chem. Soc.* **1990**, *112*, 4587–4588.
- [157] M. P. T. Sjögren, S. Hansson, P.-O. Norrby, B. Åkermark, M. E. Cucciolito, A. Vitagliano, *Organometallics* **1992**, *11*, 3954–3964.
- [158] U. Kazmaier, D. Stolz, K. Krämer, F. Zumpe, *Chem. Eur. J.* **2008**, *14*, 1322–1329.
- [159] B. M. Trost, M. Lautens, *Tetrahedron* **1987**, *43*, 4817–4840.
- [160] R. Takeuchi, M. Kashio, *J. Am. Chem. Soc.* **1998**, *120*, 8647–8655.
- [161] R. Takeuchi, N. Shiga, *Org. Lett.* **1999**, *1*, 265–268.
- [162] R. Jiang, L. Ding, C. Zheng, S.-L. You, *Science* **2021**, *371*, 380–386.

- 
- [163] R. Jiang, Q.-R. Zhao, C. Zheng, S.-L. You, *Nat. Catal.* **2022**, *5*, 1089–1097.
- [164] M. Kawatsura, Y. Uozumi, T. Hayashi, *Chem. Commun.* **1998**, 1998, 217–218.
- [165] B. M. Trost, T. R. Verhoeven, *J. Am. Chem. Soc.* **1980**, *102*, 4730–4743.
- [166] M. Kranenburg, P. C. J. Kamer, P. W. N. M. van Leeuwen, *Eur. J. Inorg. Chem.* **1998**, 1998, 25–27.
- [167] S. T. Madrahimov, Q. Li, A. Sharma, J. F. Hartwig, *J. Am. Chem. Soc.* **2015**, *137*, 14968–14981.
- [168] F. Glorius, A. Pfaltz, *Org. Lett.* **1999**, *1*, 141–144.
- [169] D. L. Hughes, M. Palucki, N. Yasuda, R. A. Reamer, P. J. Reider, *J. Org. Chem.* **2002**, *67*, 2762–2768.
- [170] B. M. Trost, P. L. Fraise, Z. T. Ball, *Angew. Chem. Int. Ed.* **2002**, *41*, 1059–1061.
- [171] R. Hermatschweiler, I. Fernández, F. Breher, P. S. Pregosin, L. F. Veiros, M. J. Calhorda, *Angew. Chem. Int. Ed.* **2005**, *44*, 4397–4400.
- [172] J. C. Fiaud, J. L. Malleron, *Tetrahedron Lett.* **1980**, *21*, 4437–4440.
- [173] I. Bauer, H.-J. Knölker, *Chem. Rev.* **2015**, *115*, 3170–3387.
- [174] C. Nájera, I. P. Beletskaya, M. Yus, *Chem. Soc. Rev.* **2019**, *48*, 4515–4618.
- [175] M. Bovens, A. Togni, L. M. Venanzi, *J. Organomet. Chem.* **1993**, *451*, C28–C31.
- [176] G. C. Lloyd-Jones, S. C. Stephen, *Chem. Commun.* **1998**, 1998, 2321–2322.
- [177] C. Amatore, A. Jutand, M. A. M'Barki, G. Meyer, L. Mottier, *Eur. J. Inorg. Chem.* **2001**, *2001*, 873–880.
- [178] T. Cantat, N. Agenet, A. Jutand, R. Pleixats, M. Moreno-Mañas, *Eur. J. Org. Chem.* **2005**, *2005*, 4277–4286.
- [179] A. Jutand, *Appl. Organomet. Chem.* **2004**, *18*, 574–582.
- [180] N. Svensen, P. Fristrup, D. Tanner, P.-O. Norrby, *Adv. Synth. Catal.* **2007**, *349*, 2631–2640.
- [181] P. Fristrup, T. Jensen, J. Hoppe, P.-O. Norrby, *Chem. Eur. J.* **2006**, *12*, 5352–5360.
- [182] S. Kozuch, C. Amatore, A. Jutand, S. Shaik, *Organometallics* **2005**, *24*, 2319–2330.
- [183] S. Kozuch, S. Shaik, A. Jutand, C. Amatore, *Chem. Eur. J.* **2004**, *10*, 3072–3080.
- [184] C. Amatore, A. Jutand, A. Suarez, *J. Am. Chem. Soc.* **1993**, *115*, 9531–9541.

- 
- [185] C. Amatore, M. Azzabi, A. Jutand, *J. Am. Chem. Soc.* **1991**, *113*, 8375–8384.
- [186] C. Amatore, A. Jutand, *Acc. Chem. Res.* **2000**, *33*, 314–321.
- [187] C. Amatore, A. Jutand, *J. Organomet. Chem.* **1999**, *576*, 254–278.
- [188] P. Kočovský, Š. Vyskočil, I. Císařová, J. Sejbal, I. Tišlerová, M. Smrčina, G. C. Lloyd-Jones, S. C. Stephen, C. P. Butts, M. Murray, V. Langer, *J. Am. Chem. Soc.* **1999**, *121*, 7714–7715.
- [189] I. J. S. Fairlamb, G. C. Lloyd-Jones, Š. Vyskočil, P. Kočovský, *Chem. Eur. J.* **2002**, *8*, 4443–4453.
- [190] L. Gouriou, G. C. Lloyd-Jones, Š. Vyskočil, P. Kočovský, *J. Organomet. Chem.* **2003**, *687*, 525–537.
- [191] B. M. Trost, T. R. Verhoeven, *J. Am. Chem. Soc.* **1976**, *98*, 630–632.
- [192] B. M. Trost, T. R. Verhoeven, *J. Am. Chem. Soc.* **1976**, *41*, 3215–3216.
- [193] J.-C. Fiaud, J.-L. Malleron, *J. Chem. Soc., Chem. Commun.* **1981**, *1981*, 1159.
- [194] Y. Hayasi, M. Riediker, J. S. Temple, J. Schwartz, *Tetrahedron Lett.* **1981**, *22*, 2629–2632.
- [195] H. Matsushita, E. Negishi, *J. Chem. Soc., Chem. Commun.* **1982**, *1982*, 160–161.
- [196] T. Hayashi, T. Hagihara, M. Konishi, M. Kumada, *J. Am. Chem. Soc.* **1983**, *105*, 7767–7768.
- [197] J. C. Fiaud, J. Y. Legros, *J. Org. Chem.* **1987**, *52*, 1907–1911.
- [198] B. Bartels, C. García-Yebra, F. Rominger, G. Helmchen, *Eur. J. Inorg. Chem.* **2002**, *2002*, 2569–2586.
- [199] S. T. Madrahimov, J. F. Hartwig, *J. Am. Chem. Soc.* **2012**, *134*, 8136–8147.
- [200] M. L. Spera, R. M. Chin, M. D. Winemiller, K. W. Lopez, M. Sabat, W. D. Harman, *Organometallics* **1996**, *15*, 5447–5449.
- [201] B. L. Ashfeld, K. A. Miller, A. J. Smith, K. Tran, S. F. Martin, *J. Org. Chem.* **2007**, *72*, 9018–9031.
- [202] P. A. Evans, L. J. Kennedy, *Org. Lett.* **2000**, *2*, 2213–2215.
- [203] A. Bayer, U. Kazmaier, *Chem. Eur. J.* **2014**, *20*, 10484–10491.
- [204] P. A. Evans, D. Uraguchi, *J. Am. Chem. Soc.* **2003**, *125*, 7158–7159.
- [205] D. N. Lawson, J. A. Osborn, G. Wilkinson, *J. Chem. Soc. A* **1966**, *1966*, 1733–1736.
- [206] M. McPartlin, R. Mason, *Chem. Commun.* **1967**, *1967*, 16–17.

- 
- [207] B. Plietker, *Angew. Chem. Int. Ed.* **2006**, *45*, 6053–6056.
- [208] B. M. Trost, C. A. Merlic, *J. Am. Chem. Soc.* **1990**, *112*, 9590–9600.
- [209] B. M. Trost, M. Lautens, *J. Am. Chem. Soc.* **1987**, *109*, 1469–1478.
- [210] G. C. Lloyd-Jones, S. W. Krska, D. L. Hughes, L. Gouriou, V. D. Bonnet, K. Jack, Y. Sun, R. A. Reamer, *J. Am. Chem. Soc.* **2004**, *126*, 702–703.
- [211] D. L. Hughes, G. C. Lloyd-Jones, S. W. Krska, L. Gouriou, V. D. Bonnet, K. Jack, Y. Sun, D. J. Mathre, R. A. Reamer, *Proc. Natl. Acad. Sci.* **2004**, *101*, 5379–5384.
- [212] D. Dvořák, I. Starý, P. Kočovský, *J. Am. Chem. Soc.* **1995**, *117*, 6130–6131.
- [213] J. W. Faller, D. Linebarrier, *Organometallics* **1988**, *7*, 1670–1672.
- [214] Y. D. Ward, L. A. Villanueva, G. D. Allred, L. S. Liebeskind, *J. Am. Chem. Soc.* **1996**, *118*, 897–898.
- [215] A. Kuhl, J. A. Christopher, L. J. Farrugia, P. J. Kocienski, *Synlett* **2000**, *2000*, 1765–1768.
- [216] M. T. Oliveira, D. Audisio, S. Niyomchon, N. Maulide, *ChemCatChem* **2013**, *5*, 1239–1247.
- [217] K. L. Granberg, J. E. Bäckvall, *J. Am. Chem. Soc.* **1992**, *114*, 6858–6863.
- [218] I. Shimizu, Y. Matsumoto, M. Nishikawa, T. Kawahara, A. Satake, A. Yamamoto, *Chem. Lett.* **1998**, *27*, 983–984.
- [219] B. M. Trost, E. Keinan, *J. Am. Chem. Soc.* **1978**, *100*, 7779–7781.
- [220] C. N. Farthing, P. Kočovský, *J. Am. Chem. Soc.* **1998**, *120*, 6661–6672.
- [221] H. Kurosawa, S. Ogoshi, Y. Kawasaki, S. Murai, M. Miyoshi, I. Ikeda, *J. Am. Chem. Soc.* **1990**, *112*, 2813–2814.
- [222] H. Kurosawa, H. Kajimaru, S. Ogoshi, H. Yoneda, K. Miki, N. Kasai, S. Murai, I. Ikeda, *J. Am. Chem. Soc.* **1992**, *114*, 8417–8424.
- [223] I. Starý, P. Kočovský, *Tetrahedron* **1992**, *48*, 7229–7250.
- [224] L. M. Wolf, W. Thiel, *J. Org. Chem.* **2014**, *79*, 12136–12147.
- [225] I. Starý, P. Kočovský, *J. Am. Chem. Soc.* **1989**, *111*, 4981–4982.
- [226] B. M. Trost, T. R. Verhoeven, J. M. Fortunak, S. M. McElvain, *Tetrahedron Lett.* **1979**, *20*, 2301–2304.
- [227] J.-E. Bäckvall, R. E. Nordberg, E. E. Björkman, C. Moberg, *J. Chem. Soc., Chem. Commun.* **1980**, *1980*, 943–944.



- 
- [228] J.-E. Bäckvall, R. E. Nordberg, *J. Am. Chem. Soc.* **1981**, *103*, 4959–4960.
- [229] J.-E. Bäckvall, R. E. Nordberg, D. Wilhelm, *J. Am. Chem. Soc.* **1985**, *107*, 6892–6898.
- [230] H. Grennberg, V. Langer, J.-E. Bäckvall, *J. Chem. Soc., Chem. Commun.* **1991**, *1991*, 1190–1192.
- [231] S. Shekhar, B. Trantow, A. Leitner, J. F. Hartwig, *J. Am. Chem. Soc.* **2006**, *128*, 11770–11771.
- [232] B. M. Trost, P. E. Strege, *J. Am. Chem. Soc.* **1977**, *99*, 1649–1651.
- [233] B. M. Trost, *Chem. Pharm. Bull.* **2002**, *50*, 1–14.
- [234] D. Polet, A. Alexakis, K. Tissot-Croset, C. Corminboeuf, K. Ditrich, *Chem. Eur. J.* **2006**, *12*, 3596–3609.
- [235] B. M. Trost, M. Osipov, G. Dong, *Org. Lett.* **2012**, *14*, 2254–2257.
- [236] W. Guo, A. Cai, J. Xie, A. W. Kleij, *Angew. Chem. Int. Ed.* **2017**, *56*, 11797–11801.
- [237] Q.-L. Liu, W. Chen, Q.-Y. Jiang, X.-F. Bai, Z. Li, Z. Xu, L.-W. Xu, *ChemCatChem* **2016**, *8*, 1495–1499.
- [238] B. M. Trost, E. J. Donckele, D. A. Thaisrivongs, M. Osipov, J. T. Masters, *J. Am. Chem. Soc.* **2015**, *137*, 2776–2784.
- [239] C. Margarita, P. G. Andersson, *J. Am. Chem. Soc.* **2017**, *139*, 1346–1356.
- [240] S. Kraft, K. Ryan, R. B. Kargbo, *J. Am. Chem. Soc.* **2017**, *139*, 11630–11641.
- [241] Q.-H. Xia, H.-Q. Ge, C.-P. Ye, Z.-M. Liu, K.-X. Su, *Chem. Rev.* **2005**, *105*, 1603–1662.
- [242] C. Wang, H. Yamamoto, *Chem. Asian J.* **2015**, *10*, 2056–2068.
- [243] A. B. Zaitsev, H. Adolfsson, *Synthesis* **2006**, *2006*, 1725–1756.
- [244] H. C. Kolb, M. S. VanNieuwenhze, K. B. Sharpless, *Chem. Rev.* **1994**, *94*, 2483–2547.
- [245] J. F. Teichert, B. L. Feringa, *Angew. Chem. Int. Ed.* **2010**, *49*, 2486–2528.
- [246] B. L. Feringa, *Acc. Chem. Res.* **2000**, *33*, 346–353.
- [247] B. M. Trost, Z. Shi, *J. Am. Chem. Soc.* **1996**, *118*, 3037–3038.
- [248] B. M. Trost, R. Madsen, S. D. Guile, B. Brown, *J. Am. Chem. Soc.* **2000**, *122*, 5947–5956.
- [249] B. M. Trost, R. Madsen, S. G. Guile, A. E. H. Elia, *Angew. Chem. Int. Ed.* **1996**, *35*, 1569–1572.



- 
- [250] B. M. Trost, M. Osipov, P. S. J. Kaib, M. T. Sorum, *Org. Lett.* **2011**, *13*, 3222–3225.
- [251] M. T. E. Gihani, H. Heaney, *Synthesis* **1998**, *1998*, 357–375.
- [252] E. B. Benetskiy, C. Bolm, *Tetrahedron: Asymmetry* **2011**, *22*, 373–378.
- [253] M. Majdecki, J. Jurczak, T. Bauer, *ChemCatChem* **2015**, *7*, 799–807.
- [254] K. N. Gavrilov, S. V. Zheglov, I. M. Novikov, I. V. Chuchelkin, V. K. Gavrilov, V. V. Lugovsky, I. A. Zamilatskov, *Russ. Chem. Bull.* **2015**, *64*, 1595–1601.
- [255] K. N. Gavrilov, S. V. Zheglov, E. A. Rastorguev, N. N. Groshkin, M. G. Maksimova, E. B. Benetsky, V. A. Davankov, M. T. Reetz, *Adv. Synth. Catal.* **2010**, *352*, 2599–2610.
- [256] A. ping Xing, Z. bo Pang, H. feng Li, L. lai Wang, *Tetrahedron* **2014**, *70*, 8822–8828.
- [257] F. Fernández, A. Gual, C. Claver, S. Castellón, G. Muller, M. Gómez, *Eur. J. Inorg. Chem.* **2010**, *2010*, 758–766.
- [258] Z. Qiu, R. Sun, D. Teng, *Org. Biomol. Chem.* **2018**, *16*, 7717–7724.
- [259] L.-Y. Mei, Z.-L. Yuan, M. Shi, *Organometallics* **2011**, *30*, 6466–6475.
- [260] J. Kraft, K. Milland, T. Ziegler, *Molecules* **2016**, *21*, 1704–1715.
- [261] W.-H. Deng, F. Ye, X.-F. Bai, Z.-J. Zheng, Y.-M. Cui, L.-W. Xu, *ChemCatChem* **2014**, *7*, 75–79.
- [262] X.-F. Yang, W.-H. Yu, C.-H. Ding, Q.-P. Ding, S.-L. Wan, X.-L. Hou, L.-X. Dai, P.-J. Wang, *J. Org. Chem.* **2013**, *78*, 6503–6509.
- [263] T. Song, X. Zhao, J. Hu, W. Dan, *Eur. J. Org. Chem.* **2018**, *2018*, 1141–1144.
- [264] X. Wei, D. Liu, Q. An, W. Zhang, *Org. Lett.* **2015**, *17*, 5768–5771.
- [265] C. Hethcox, S. E. Shockley, B. M. Stoltz, *Angew. Chem. Int. Ed.* **2016**, *55*, 16092–16095.
- [266] I. P. Beletskaya, C. Nájera, M. Yus, *Chem. Rev.* **2018**, *118*, 5080–5200.
- [267] M. T. Oliveira, M. Luparia, D. Audisio, N. Maulide, *Angew. Chem. Int. Ed.* **2013**, *52*, 13149–13152.
- [268] S. Krautwald, D. Sarlah, M. A. Schafroth, E. M. Carreira, *Science* **2013**, *340*, 1065–1068.
- [269] S. Krautwald, M. A. Schafroth, D. Sarlah, E. M. Carreira, *J. Am. Chem. Soc.* **2014**, *136*, 3020–3023.
- [270] X. Huo, R. He, X. Zhang, W. Zhang, *J. Am. Chem. Soc.* **2016**, *138*, 11093–11096.

- 
- [271] P. B. Armstrong, E. A. Dembicer, A. J. DesBois, J. T. Fitzgerald, J. K. Gehrman, N. C. Nelson, A. L. Noble, R. C. Bunt, *Organometallics* **2012**, *31*, 6933–6946.
- [272] J. S. Cannon, S. F. Kirsch, L. E. Overman, H. F. Sneddon, *J. Am. Chem. Soc.* **2010**, *132*, 15192–15203.
- [273] R. Zalubovskis, A. Bouet, E. Fjellander, S. Constant, D. Linder, A. Fischer, J. Lacour, T. Privalov, C. Moberg, *J. Am. Chem. Soc.* **2008**, *130*, 1845–1855.
- [274] M. Kollmar, H. Steinhagen, J. P. Janssen, B. Goldfuss, S. A. Malinovskaya, J. Vázquez, F. Rominger, G. Helmchen, *Chem. Eur. J.* **2002**, *8*, 3103–3114.
- [275] A. Saitoh, K. Achiwa, K. Tanaka, T. Morimoto, *J. Org. Chem.* **2000**, *65*, 4227–4240.
- [276] S. Ramdeehul, P. Dierkes, R. Aguado, P. C. J. Kamer, P. W. N. M. van Leeuwen, J. A. Osborn, *Angew. Chem. Int. Ed.* **1998**, *37*, 3118–3121.
- [277] J. D. Oslob, B. Åkermark, P. Helquist, P.-O. Norrby, *Organometallics* **1997**, *16*, 3015–3021.
- [278] B. M. Trost, D. L. Van Vranken, C. Bingel, *J. Am. Chem. Soc.* **1992**, *114*, 9327–9343.
- [279] B. M. Trost, B. Schöffner, M. Osipov, D. A. A. Wilton, *Angew. Chem. Int. Ed.* **2011**, *50*, 3548–3551.
- [280] H. Danjo, M. Higuchi, M. Yada, T. Imamoto, *Tetrahedron Lett.* **2004**, *45*, 603–606.
- [281] D. S. Clyne, Y. C. Mermet-Bouvier, N. Nomura, T. V. RajanBabu, *J. Org. Chem.* **1999**, *64*, 7601–7611.
- [282] J. C. Anderson, R. J. Cubbon, J. D. Harling, *Tetrahedron: Asymmetry* **1999**, *10*, 2829–2832.
- [283] B. M. Trost, D. L. Van Vranken, *Angew. Chem. Int. Ed.* **1992**, *31*, 228–230.
- [284] B. M. Trost, M. R. Machacek, A. Aponick, *Acc. Chem. Res.* **2006**, *39*, 747–760.
- [285] B. M. Trost, *Acc. Chem. Res.* **1996**, *29*, 355–364.
- [286] B. Trost, B. Breit, M. Organ, *Tetrahedron Lett.* **1994**, *35*, 5817–5820.
- [287] J. K. Whitesell, *Chem. Rev.* **1989**, *89*, 1581–1590.
- [288] B. M. Trost, G. M. Schroeder, *Chem. Eur. J.* **2005**, *11*, 174–184.
- [289] C. W. Lim, S.-G. Lee, *Tetrahedron* **2000**, *56*, 5131–5136.
- [290] B. M. Trost, A. C. Krueger, R. C. Bunt, J. Zambrano, *J. Am. Chem. Soc.* **1996**, *118*, 6520–6521.
- [291] B. M. Trost, F. D. Toste, *J. Am. Chem. Soc.* **1999**, *121*, 4545–4554.

- 
- [292] B. M. Trost, R. C. Bunt, *J. Am. Chem. Soc.* **1994**, *116*, 4089–4090.
- [293] B. Dominguez, N. S. Hodnett, G. C. Lloyd-Jones, *Angew. Chem. Int. Ed.* **2001**, *40*, 4289–4291.
- [294] J. M. Longmire, B. Wang, X. Zhang, *Tetrahedron Lett.* **2000**, *41*, 5435–5439.
- [295] B. J. Lüssem, H.-J. Gais, *J. Am. Chem. Soc.* **2003**, *125*, 6066–6067.
- [296] M. Frank, H.-J. Gais, *Tetrahedron: Asymmetry* **1998**, *9*, 3353–3357.
- [297] H.-J. Gais, N. Spalthoff, T. Jagusch, M. Frank, G. Raabe, *Tetrahedron Lett.* **2000**, *41*, 3809–3812.
- [298] G. Helmchen, A. Pfaltz, *Acc. Chem. Res.* **2000**, *33*, 336–345.
- [299] A. Pfaltz, W. J. Drury, *Proc. Natl. Acad. Sci.* **2004**, *101*, 5723–5726.
- [300] G. Helmchen, *Journal of Organometallic Chemistry* **1999**, *576*, 203–214.
- [301] T. R. Ward, *Organometallics* **1996**, *15*, 2836–2838.
- [302] P. von Matt, A. Pfaltz, *Angew. Chem. Int. Ed.* **1993**, *32*, 566–568.
- [303] M. S. Anson, A. R. Mirza, L. Tonks, J. M. J. Williams, *Tetrahedron Lett.* **1999**, *40*, 7147–7150.
- [304] J. Sprinz, G. Helmchen, *Tetrahedron Lett.* **1993**, *34*, 1769–1772.
- [305] R. N. Constantine, N. Kim, R. C. Bunt, *Org. Lett.* **2003**, *5*, 2279–2282.
- [306] H. Steinhagen, M. Reggelin, G. Helmchen, *Angew. Chem. Int. Ed.* **1997**, *36*, 2108–2110.
- [307] P. B. Armstrong, L. M. Bennett, R. N. Constantine, J. L. Fields, J. P. Jasinski, R. J. Staples, R. C. Bunt, *Tetrahedron Lett.* **2005**, *6*, 1441–1445.
- [308] L. P. Hammett, *J. Am. Chem. Soc.* **1937**, *59*, 96–103.
- [309] C. Hansch, A. Leo, R. W. Taft, *Chem. Rev.* **1991**, *91*, 165–195.
- [310] C. G. Swain, E. C. Lupton, *J. Am. Chem. Soc.* **1968**, *90*, 4328–4337.
- [311] C. G. Swain, S. H. Unger, N. R. Rosenquist, M. S. Swain, *J. Am. Chem. Soc.* **1983**, *105*, 492–502.
- [312] C. G. Swain, *J. Org. Chem.* **1984**, *49*, 2005–2010.
- [313] J. Junker, B. Reif, H. Steinhagen, B. Junker, I. C. Felli, M. Reggelin, C. Griesinger, *Chem. Eur. J.* **2000**, *6*, 3281–3286.

- 
- [314] C. Souris, A. Misale, Y. Chen, M. Luparia, N. Maulide, *Org. Lett.* **2015**, *17*, 4486–4489.
- [315] C. Souris, F. Frébault, A. Patel, D. Audisio, K. N. Houk, N. Maulide, *Org. Lett.* **2013**, *15*, 3242–3245.
- [316] K. C. Nicolaou, J. A. Vega, G. Vassilikogiannakis, *Angew. Chem. Int. Ed.* **2001**, *40*, 4441–4445.
- [317] Y. Chen, G. Coussanes, C. Souris, P. Aillard, D. Kaldre, K. Runggatscher, S. Kubicek, G. D. Mauro, B. Maryasin, N. Maulide, *J. Am. Chem. Soc.* **2019**, *141*, 13772–13777.
- [318] S. Antonsen, R. B. Østby, Y. Stenstrøm, *Stud. Nat. Prod. Chem.* **2018**, *57*, 1–40.
- [319] W. R. Gutekunst, P. S. Baran, *J. Am. Chem. Soc.* **2011**, *133*, 19076–19079.
- [320] B. Ranieri, C. Obradors, M. Mato, A. M. Echavarren, *Org. Lett.* **2016**, *18*, 1614–1617.
- [321] A. N. Baumann, M. Eisold, D. Didier, *Org. Lett.* **2017**, *19*, 2114–2117.
- [322] N. Winter, D. Trauner, *J. Am. Chem. Soc.* **2017**, *139*, 11706–11709.
- [323] A. Misale, S. Niyomchon, N. Maulide, *Acc. Chem. Res.* **2016**, *49*, 2444–2458.
- [324] D. Didier, F. Reiners, *Chem. Rec.* **2021**, *21*, 1144–1160.
- [325] M. Luparia, D. Audisio, N. Maulide, *Synlett* **2011**, *2011*, 735–740.
- [326] F. Frébault, M. Luparia, M. T. Oliveira, R. Goddard, N. Maulide, *Angew. Chem. Int. Ed.* **2010**, *49*, 5672–5676.
- [327] S. Niyomchon, D. Audisio, M. Luparia, N. Maulide, *Org. Lett.* **2013**, *15*, 2318–2321.
- [328] E. J. Corey, J. Streith, *J. Am. Chem. Soc.* **1964**, *86*, 950–951.
- [329] S. C. Coote, *Eur. J. Org. Chem.* **2020**, *2020*, 1405–1423.
- [330] H. Pellissier, *Coord. Chem. Rev.* **2023**, *482*, 215079.
- [331] H. W. Lam, *Synthesis* **2011**, *2011*, 2011–2043.
- [332] D. Moser, T. A. Schmidt, C. Sparr, *JACS Au* **2023**, *3*, 2612–2630.
- [333] M. Bihani, J. C.-G. Zhao, *Adv. Synth. Catal.* **2017**, *359*, 534–575.
- [334] L. Lin, X. Feng, *Chem. Eur. J.* **2017**, *23*, 6464–6482.
- [335] W. H. Pirkle, L. H. McKendry, *J. Am. Chem. Soc.* **1969**, *91*, 1179–1186.
- [336] P. Zhang, L. A. Brozek, J. P. Morken, *J. Am. Chem. Soc.* **2010**, *132*, 10686–10688.

- 
- [337] L. A. Brozek, M. J. Ardolino, J. P. Morken, *J. Am. Chem. Soc.* **2011**, *133*, 16778–16781.
- [338] K. Spielmann, G. Niel, R. M. de Figueiredo, J.-M. Campagne, *Chem. Soc. Rev.* **2018**, *47*, 1159–1173.
- [339] Y. Tamaru, A. Tanaka, S. G. Kengo Yasui, S. Tanaka, *Angew. Chem. Int. Ed.* **1995**, *34*, 787–789.
- [340] M. Kimura, M. Shimizu, K. Shibata, M. Tazoe, Y. Tamaru, *Angew. Chem. Int. Ed.* **2003**, *42*, 3392–3395.
- [341] G. Zanoni, S. Gladiali, A. Marchetti, P. Piccinini, I. Tredici, G. Vidari, *Angew. Chem. Int. Ed.* **2004**, *43*, 846–849.
- [342] G. P. Howell, A. J. Minnaard, B. L. Feringa, *Org. Biomol. Chem.* **2006**, *4*, 1278–1283.
- [343] W. Wang, T. Zhang, M. Shi, *Organometallics* **2009**, *28*, 2640–2642.
- [344] S.-F. Zhu, X.-C. Qiao, Y.-Z. Zhang, L.-X. Wang, Q.-L. Zhou, *Chem. Sci.* **2011**, *2011*, 1135–1140.
- [345] J. Ilgen, Phd thesis, Technical University of Darmstadt, **2021**.
- [346] J. H. Espenson, *Chemical Kinetics and Reaction Mechanisms*, 2<sup>nd</sup> ed., McGraw-Hill, New York, **1995**.
- [347] M. Gómez-Gallego, M. A. Sierra, *Chem. Rev.* **2011**, *111*, 4857–4963.
- [348] M. Nakagawa, M. Tonozuka, M. Obi, M. Kiuchi, T. Hino, *Synthesis* **1974**, *1974*, 510–511.
- [349] M. Nakagawa, J. Saegusa, M. Tonozuka, M. Obi, M. Kiuchi, T. Hino, Y. Ban., *Org. Synth.* **1977**, *56*, 49–51.
- [350] C. Einzinger, PhD thesis, Technical University of Vienna, **2007**.
- [351] A. Wohl, *Chem. Ber.* **1919**, *52*, 51–63.
- [352] A. Wohl, K. Jaschinowski, *Chem. Ber.* **1921**, *54*, 476–484.
- [353] K. Ziegler, A. Späth, E. Schaaf, W. Schumann, E. Winkelmann, *Justus Liebigs Ann. Chem.* **1942**, *551*, 80–119.
- [354] S. C. Virgil, P. R. Jenkins, A. J. Wilson, M. D. García Romero, „N-Bromosuccinimide“ in *Encyclopedia of Reagents for Organic Synthesis* (Eds.: A. Charette, J. Bode, T. Rovis, R. Shenvi), John Wiley & Sons, Hoboken, **2006**.
- [355] I. Brown, F. Smith, *Aust. J. Chem.* **1954**, *7*, 269–272.

- 
- [356] Z. Wang, *Comprehensive Organic Name Reactions and Reagents*, John Wiley & Sons, Hoboken, **2010**, pp. 3067–3072.
- [357] C. Djerassi, *Chem. Rev.* **1948**, *43*, 271–317.
- [358] I. Saikia, A. J. Borah, P. Phukan, *Chem. Rev.* **2016**, *12*, 6837–7042.
- [359] A. T. Blomquist, F. H. Baldwin, *J. Am. Chem. Soc.* **1948**, *70*, 29–30.
- [360] M. Winkler, M. Steinbiß, M. A. R. Meier, *Eur. J. Lipid Sci. Technol.* **2014**, *116*, 44–51.
- [361] M. Mitton-Fry, A. Cullen, T. Sammakia, *Angew. Chem. Int. Ed.* **2007**, *46*, 1066–1070.
- [362] J. A. B. Laurenson, J. A. Parkinson, J. M. Percy, G. Rinaudo, R. Roig, *Beilstein J. Org. Chem.* **2013**, *9*, 2660–2668.
- [363] C. M. French, I. G. Roe, *Trans. Faraday Soc.* **1953**, *49*, 791–795.
- [364] L. J. Andrews, R. M. Keefer, *J. Am. Chem. Soc.* **1951**, *73*, 5733–5736.
- [365] H. E. Zimmerman, R. M. Paufler, *J. Am. Chem. Soc.* **1960**, *82*, 1514–1515.
- [366] H. E. Zimmerman, G. L. Grunewald, R. M. Paufler, *Org. Synth.* **1966**, *46*, 101.
- [367] P. Lu, C. Sanchez, J. Cornella, I. Larrosa, *Org. Lett.* **2009**, *11*, 5710–5713.
- [368] D. H. R. Barton, D. Crich, W. B. Motherwell, *J. Chem. Soc., Chem. Commun.* **1983**, *1983*, 939–941.
- [369] J. Zhu, A. J. H. Klunder, B. Zwanenburg, *Tetrahedron* **1995**, *51*, 5099–5116.
- [370] S. C. Döller, Master's thesis, Technical University of Darmstadt, **2020**.
- [371] J. Seo, S. Y. Lee, C. W. Bielawski, *Polym. Chem.* **2019**, *10*, 6401–6412.
- [372] J. D. Williams, Y. Otake, G. Coussanes, I. Saridakis, N. Maulide, C. O. Kappe, *ChemPhotoChem* **2019**, *3*, 229–232.
- [373] R. P. Buck, S. Singhadeja, L. B. Rogers, *Anal. Chem.* **1954**, *26*, 1240–1242.
- [374] K. Simon, D. Znidar, J. Boutet, G. Guillaumot, J.-Y. Lenoir, D. Dallinger, C. O. Kappe, *Org. Process Res. Dev.* **2023**, *27*, 322–330.
- [375] E. B. Corcoran, F. Lévesque, J. P. McMullen, J. R. Naber, *ChemPhotoChem* **2018**, *2*, 931–937.
- [376] A. Mata, D. N. Tran, U. Weigl, J. D. Williams, C. O. Kappe, *Chem. Commun.* **2020**, *56*, 14621–14624.

- 
- [377] L. D. Elliott, M. Berry, B. Harji, D. Klauber, J. Leonard, K. I. Booker-Milburn, *Org. Process Res. Dev.* **2016**, *20*, 1806–1811.
- [378] P. Maibach, Master's thesis, Technical University of Darmstadt, **2021**.
- [379] W. H. Pirkle, M. Dines, *J. Am. Chem. Soc.* **1968**, *90*, 2318–2323.
- [380] K. Afarinkia, G. H. Posner, *Tetrahedron Lett.* **1992**, *33*, 7839–7842.
- [381] M. V. Vinader, K. Afarinkia, *Curr. Med. Chem.* **2013**, *20*, 3797–3801.
- [382] B. Bak, *J. Org. Chem.* **1956**, *21*, 797–798.
- [383] W. Wang, D. D. Simovic, M. Di, L. Fieber, K. S. Rein, *Bioorg. Med. Chem. Lett.* **2013**, *23*, 1949–1952.
- [384] F. Bellina, A. Carpita, L. Mannocci, R. Rossi, *Eur. J. Org. Chem.* **2004**, *2004*, 2610–2619.
- [385] H. Finkelstein, *Chem. Ber.* **1910**, *43*, 1528–1532.
- [386] R. B. Bates, C. A. Ogle, *Carbanion Chemistry*, Springer, Berlin, **1983**.
- [387] P. Knochel, *Comprehensive Organic Synthesis*, Vol. 3, 2<sup>nd</sup> ed., Elsevier, Amsterdam, **2014**.
- [388] J. Rodriguez, M. S. M. Holmsen, Y. García-Rodeja, E. D. S. Carrizo, P. Lavedan, S. Mallet-Ladeira, K. Miqueu, D. Bourissou, *J. Am. Chem. Soc.* **2021**, *143*, 11568–11581.
- [389] D. S. Masterson, B. L. Kedrowski, A. Blair, *Synlett* **2010**, *2010*, 2941–2943.
- [390] S. Chaudhury, W. A. Donaldson, *J. Am. Chem. Soc.* **2006**, *128*, 5984–5985.
- [391] R. Shintani, W.-L. Duan, S. Parka, T. Hayashi, *Chem. Commun.* **2006**, *2006*, 3646–3647.
- [392] C. G. Kruse, A. Wijsman, A. van der Gen, *J. Org. Chem.* **1979**, *44*, 1847–1851.
- [393] P. Xiao, C. Ni, W. Miao, M. Zhou, J. Hu, D. Chen, J. Hu, *J. Org. Chem.* **2019**, *84*, 8345–8359.
- [394] A. Meguellati, A. Ahmed-Belkacem, A. Nurisso, W. Yi, R. Brillet, N. Berqouch, L. Chavoutier, A. Fortune, J.-M. Pawlotsky, A. Boumendjel, M. Peuchmaur, *Eur. J. Med. Chem.* **2016**, *115*, 217–229.
- [395] A. Kamimura, R. Takeuchi, K. Ikeda, T. Moriyama, M. Sumimoto, *J. Org. Chem.* **2012**, *77*, 2236–2245.
- [396] L. Yao, H. Nie, D. Zhang, L. Wang, Y. Zhang, W. Chen, Z. Li, X. Liu, S. Zhang, *ChemCatChem* **2017**, *10*, 804–809.
- [397] T. Noël, K. Bert, E. Van der Eycken, J. Van der Eycken, *Eur. J. Org. Chem.* **2010**, *2010*, 4056–4061.



- 
- [398] M.-J. Jin, V. B. Takale, M. S. Sarkar, Y.-M. Kim, *Chem. Commun.* **2006**, 2006, 663–664.
- [399] O. Pàmies, M. Diéguez, C. Claver, *J. Am. Chem. Soc.* **2005**, 127, 3646–3647.
- [400] A.-M. Carroll, M. McCarthy, P. M. Lacey, C. P. Saunders, D. J. Connolly, A. Farrell, B. V. Rokade, R. Goddard, P. Fristrup, P.-O. Norrby, P. J. Guiry, *Tetrahedron* **2019**, 76, 130780.
- [401] R. A. Arthurs, D. L. Hughes, C. J. Richards, *Eur. J. Inorg. Chem.* **2022**, 2022, e202101077.
- [402] G. Kang, M. Yamagami, S. Vellalath, D. Romo, *Angew. Chem. Int. Ed.* **2018**, 57, 6527–6531.
- [403] S. B. Undre, M. Singh, R. K. Kale, M. Rizwan, *J. Appl. Polym. Sci.* **2013**, 130, 3537–3554.
- [404] E. M. Arnett, K. D. Moe, *J. Am. Chem. Soc.* **1991**, 113, 7288–7293.
- [405] S. Kiyooka, T. Kodani, K. Suzuki, *Bull. Chem. Soc. Jpn.* **1980**, 53, 2318–2321.
- [406] Á. Puente, S. He, F. Corral-Bautista, A. R. Ofial, H. Mayr, *Eur. J. Org. Chem.* **2016**, 2016, 1841–1848.
- [407] B. T. Watson, H. Lebel, „Sodium Hexamethyldisilazide“ in *Encyclopedia of Reagents for Organic Synthesis* (Eds.: A. Charette, J. Bode, T. Rovis, R. Shenvi), John Wiley & Sons, Hoboken, **2005**.
- [408] H. H. Keah, I. D. Rae, D. G. Hawthorne, *Aust. J. Chem.* **1992**, 45, 659–669.
- [409] W. B. S. van Liemt, W. F. Steggerda, R. Esmeijer, J. Lugtenburg, *Recl. Trav. Chim. Pays-Bas* **1994**, 113, 153–161.
- [410] J. Beyer, S. Lang-Fugmann, A. Mühlbauer, W. Steglich, *Synthesis* **1998**, 1047–1051.
- [411] M. Lang, S. Lang-Fugmann, W. Steglich, *Org. Synth.* **2002**, 78, 113.
- [412] J. M. Fevig, „Trimethyl Phosphate“ in *Encyclopedia of Reagents for Organic Synthesis* (Eds.: A. Charette, J. Bode, T. Rovis, R. Shenvi), John Wiley & Sons, Hoboken, **2001**.
- [413] M. Shibuya, S. H. S.-U. K. H.-M. Chou, M. Fountoulakis, K. Kobayashi, H. Otsuka, E. Rogalska, J. M. Cassady, H. G. Floss, *J. Am. Chem. Soc.* **1990**, 112, 297–304.
- [414] C. Winkel, E. G. Buitenhuis, J. Lugtenburg, *Recl. Trav. Chim. Pays-Bas* **1989**, 108, 51–56.
- [415] G. A. Ropp, *J. Am. Chem. Soc.* **1950**, 72, 2299.
- [416] I. J. S. Fairlamb, G. C. Lloyd-Jones, *Chem. Commun.* **2000**, 2000, 2447–2448.
- [417] G. C. Lloyd-Jones, S. C. Stephen, I. J. S. Fairlamb, A. Martorell, B. Dominguez, P. M. Tomlin, M. Murray, J. M. Fernandez, J. C. Jeffery, T. Riis-Johannessen, T. Guerziz, *Pure Appl. Chem.* **2004**, 76, 589–601.



- [418] C. Johansson, G. C. Lloyd-Jones, P.-O. Norrby, *Tetrahedron: Asymmetry* **2010**, *21*, 1585–1592.
- [419] B. M. Trost, Y. Zhang, *J. Am. Chem. Soc.* **2007**, *129*, 14548–14549.
- [420] B. Trost, Y. Zhang, *Chem. Eur. J.* **2010**, *16*, 296–303.
- [421] B. Jiang, Q.-J. Liang, Y. Han, M. Zhao, Y.-H. Xu, T.-P. Loh, *Org. Lett.* **2018**, *20*, 3215–3219.
- [422] J. E. Wilent, G. Qabaja, K. S. Petersen, *Org. Synth.* **2016**, *93*, 75–87.
- [423] J. Wilent, K. S. Petersen, *J. Org. Chem.* **2014**, *79*, 2303–2307.
- [424] G. R. Newkome, V. K. Gupta, H. C. R. Taylor, F. R. Fronczek, *Organometallics* **1984**, *3*, 1549–1554.
- [425] G. R. Newkome, T. Kawato, D. K. Kohli, W. E. Puckett, B. D. Olivier, G. Chiari, F. R. Fronczek, W. A. Deutsch, *J. Am. Chem. Soc.* **1981**, *103*, 3423–3429.
- [426] T. Kawato, T. Uechi, H. Koyama, H. Kanatomi, Y. Kawanami, *Inorg. Chem.* **1984**, *23*, 764–769.
- [427] K. Hiraki, M. Onishi, H. Matsuo, *J. Organomet. Chem.* **1980**, *185*, 111–116.
- [428] J. P. Wolkowski, J. F. Hartwig, *Angew. Chem. Int. Ed.* **2002**, *41*, 4289–4291.
- [429] J. Ruiz, V. Rodríguez, N. Cutillas, M. Pardo, J. Pérez, G. López, P. Chaloner, P. B. Hitchcock, *Organometallics* **2001**, *20*, 1973–1982.
- [430] B. F. Straub, F. Rominger, P. Hofmann, *Inorg. Chem. Commun.* **2000**, *3*, 358–360.
- [431] P. J. Chung, H. Suzuki, Y. Moro-Oka, T. Ikawa, *Chem. Lett.* **1980**, *9*, 63–64.
- [432] X.-Q. Han, L. Wang, P. Yang, J.-Y. Liu, W.-Y. Xu, C. Zheng, R.-X. Liang, S.-L. You, J. Zhang, Y.-X. Jia, *ACS Catal.* **2022**, *12*, 655–661.
- [433] F.-Q. Yuan, F.-S. Han, *Org. Lett.* **2012**, *14*, 1218–1221.
- [434] J. Sun, H. Ye, H. Zhang, X.-X. Wu, *J. Org. Chem.* **2023**, *88*, 1568–1577.
- [435] M. L. O’Duill, K. M. Engle, *Synthesis* **2018**, *50*, 4699–4714.
- [436] J. A. Keith, D. C. Behenna, N. Sherden, J. T. Mohr, S. Ma, S. C. Marinescu, R. J. Nielsen, J. Oxgaard, B. M. Stoltz, W. A. Goddard III, *J. Am. Chem. Soc.* **2012**, *134*, 19050–19060.
- [437] D. C. Behenna, J. T. Mohr, N. H. Sherden, S. C. Marinescu, A. M. Harned, K. Tani, M. Seto, S. Ma, Z. Novák, M. R. Krout, R. M. McFadden, J. L. Roizen, J. A. Enquist Jr., D. E. White, S. R. Levine, K. V. Petrova, A. Iwashita, S. C. Virgil, B. M. Stoltz, *Chem. Eur. J.* **2011**, *17*, 14199–14223.

- 
- [438] J. A. Keith, D. C. Behenna, J. T. Mohr, S. Ma, S. C. Marinescu, J. Oxgaard, B. M. Stoltz, W. A. Goddard III, *J. Am. Chem. Soc.* **2007**, *129*, 11876–11877.
- [439] D.-C. Bai, F.-L. Yu, W.-Y. Wang, D. Chen, H. Li, Q.-R. Liu, C.-H. Ding, B. Chen, X.-L. Hou, *Nat. Commun.* **2016**, *7*, 11806.
- [440] J. Casado, M. A. Lopez-Quintela, F. M. Lorenzo-Barral, *J. Chem. Educ.* **1986**, *63*, 450–452.
- [441] D. G. Blackmond, *Angew. Chem. Int. Ed.* **2005**, *44*, 4302–4320.
- [442] G. Bertuzzi, M. K. Thøgersen, M. Giardinetti, A. Vidal-Albalat, A. Simon, K. N. Houk, K. A. Jørgensen, *J. Am. Chem. Soc.* **2019**, *141*, 3288–3297.
- [443] F. Zhang, H. Song, X. Zhuang, C.-H. Tung, W. Wang, *J. Am. Chem. Soc.* **2017**, *139*, 17775–17778.
- [444] P. Boehm, P. Müller, P. Finkelstein, M. A. Rivero-Crespo, M.-O. Ebert, N. Trapp, B. Morandi, *J. Am. Chem. Soc.* **2022**, *144*, 13096–13108.
- [445] D. W. Cunningham, J. Y. Yang, *Chem. Commun.* **2020**, *56*, 12965–12968.
- [446] L. J. Sewell, M. A. Huertos, M. E. Dickinson, A. S. Weller, G. C. Lloyd-Jones, *Inorg. Chem.* **2013**, *52*, 4509–4516.
- [447] A. Gordillo, G. C. Lloyd-Jones, *Chem. Eur. J.* **2012**, *18*, 2660–2665.
- [448] H.-Y. Sun, S. I. Gorelsky, D. R. Stuart, L.-C. Campeau, K. Fagnou, *J. Org. Chem.* **2010**, *75*, 8180–8189.
- [449] Y. Li, X. M. Hong, D. M. Collard, M. A. El-Sayed, *Org. Lett.* **2000**, *2*, 2385–2388.
- [450] J. S. Mathew, M. Klussmann, H. Iwamura, F. Valera, A. Futran, E. A. C. Emanuelsson, D. G. Blackmond, *J. Org. Chem.* **2006**, *71*, 4711–4722.
- [451] C. D.-T. Nielsen, J. Burés, *Chem. Sci.* **2019**, *10*, 348–353.
- [452] S. Kozuch, J. M. L. Martin, *ACS Catal.* **2012**, *2*, 2787–2794.
- [453] W.-O. Jung, B. K. Mai, M. Yoo, S. W. J. Shields, J. R. Zbieg, C. E. Stivala, P. Liu, M. J. Krische, *ACS Catal.* **2022**, *12*, 3660–3668.
- [454] R. Shintani, T. Tsuji, S. Park, T. Hayashi, *J. Am. Chem. Soc.* **2010**, *132*, 7508–7513.
- [455] A. Martínez, S. Moreno-Blázquez, A. Rodríguez-Diéguéz, A. Ramos, R. Fernández-Galán, A. Antiñolo, F. Carrillo-Hermosilla, *Dalton Trans.* **2017**, *46*, 12923–12934.
- [456] W. Mahy, P. Plucinski, J. Jover, C. G. Frost, *Angew. Chem. Int. Ed.* **2015**, *54*, 10944–10948.

- 
- [457] D. T. Ziegler, L. Riesgo, T. Ikeda, Y. Fujiwara, G. C. Fu, *Angew. Chem. Int. Ed.* **2014**, *53*, 13183–13187.
- [458] B. Chatelet, L. Joucla, J.-P. Dutasta, A. Martinez, K. C. Szeto, V. Dufaud, *J. Am. Chem. Soc.* **2013**, *135*, 5348–5351.
- [459] N. Guimond, M. J. MacDonald, V. Lemieux, A. M. Beauchemin, *J. Am. Chem. Soc.* **2012**, *134*, 16571–16577.
- [460] B. Liu, T. Roisnel, J.-F. Carpentier, Y. Sarazin, *Angew. Chem. Int. Ed.* **2012**, *51*, 4943–4946.
- [461] X. Zhang, T. J. Emge, K. C. Hultsch, *Angew. Chem. Int. Ed.* **2011**, *51*, 394–398.
- [462] J. M. Rowley, E. B. Lobkovsky, G. W. Coates, *J. Am. Chem. Soc.* **2007**, *129*, 4948–4960.
- [463] G. M. Adams, D. E. Ryan, N. A. Beattie, A. I. McKay, G. C. Lloyd-Jones, A. S. Weller, *ACS Catal.* **2019**, *9*, 3657–3666.
- [464] A. K. Cook, M. S. Sanford, *J. Am. Chem. Soc.* **2015**, *137*, 3109–3118.
- [465] Y. Maegawa, T. Ohshima, Y. Hayashi, K. Agura, T. Iwasaki, K. Mashima, *ACS Catal.* **2011**, *1*, 1178–1182.
- [466] Y. Zhang, S. Torker, M. Sigrist, N. Bregović, P. Dydio, *J. Am. Chem. Soc.* **2020**, *142*, 18251–18265.
- [467] S. Avidan-Shlomovich, H. Ghosh, A. M. Szpilman, *ACS Catal.* **2015**, *5*, 336–342.
- [468] D. Wang, Y. Izawa, S. S. Stahl, *J. Am. Chem. Soc.* **2014**, *136*, 9914–9917.
- [469] C. Alamillo-Ferrer, G. Hutchinson, J. Burés, *Nat. Rev. Chem.* **2023**, *7*, 26–34.
- [470] K. Higashida, V. Smaïl, H. Nagae, J.-F. Carpentier, K. Mashima, *ACS Catal.* **2023**, *13*, 2156–2161.
- [471] D. Tang, X. Luo, W. Shen, M. Li, *J. Mol. Struct. (Theochem)* **2005**, *716*, 79–87.
- [472] H. J. A. Dale, A. G. Leach, G. C. Lloyd-Jones, *J. Am. Chem. Soc.* **2021**, *143*, 21079–21099.
- [473] T. Giagou, M. P. Meyer, *Chem. Eur. J.* **2010**, *16*, 10616–10628.
- [474] K. C. Westaway, *J. Labelled Compd. Radiopharm.* **2007**, *50*, 989–1005.
- [475] W. D. Jones, *Acc. Chem. Res.* **2003**, *36*, 140–146.
- [476] N. J. Christensen, P. Fristrup, *Synlett* **2015**, *26*, 508–513.
- [477] E. V. Anslyn, D. A. Dougherty, *Modern Physical Organic Chemistry*, University Science Books, Sausalito, **2006**.

- 
- [478] K. B. Wiberg, *Chem. Rev.* **1955**, *55*, 713–743.
- [479] N. Pannilawithana, B. Pudasaini, M.-H. Baik, C. S. Yi, *J. Am. Chem. Soc.* **2021**, *143*, 13428–13440.
- [480] K. W. Chan, E. Lam, V. D’Anna, F. Allouche, C. Michel, O. V. Safonova, P. Sautet, C. Copéret, *J. Am. Chem. Soc.* **2018**, *140*, 11395–11401.
- [481] W. J. Kerr, M. Reid, T. Tuttle, *ACS Catal.* **2015**, *5*, 402–410.
- [482] L. M. Geary, P. G. Hultin, *Eur. J. Org. Chem.* **2010**, *2010*, 5563–5573.
- [483] C. P. Casey, J. B. Johnson, *J. Org. Chem.* **2003**, *68*, 1998–2001.
- [484] J. Chan, N. Sannikova, A. Tang, A. J. Bennet, *J. Am. Chem. Soc.* **2014**, *136*, 12225–12228.
- [485] M. D. Aseman, M. Rashidi, S. M. Nabavizadeh, R. J. Puddephatt, *Organometallics* **2013**, *32*, 2593–2598.
- [486] K. P. Gable, F. A. Zhuravlev, *J. Am. Chem. Soc.* **2002**, *124*, 3970–3979.
- [487] J. J. Gajewski, N. L. Brichford, *J. Am. Chem. Soc.* **1994**, *116*, 3165–3166.
- [488] J. J. Gajewski, K. B. Peterson, J. R. Kagel, Y. C. J. Huang, *J. Am. Chem. Soc.* **1989**, *111*, 9078–9081.
- [489] J. F. Marlier, E. Campbell, C. Lai, M. Weber, L. A. Reinhardt, W. W. Cleland, *J. Org. Chem.* **2006**, *71*, 3829–3836.
- [490] O. Matsson, K. C. Westaway, *Adv. Phys. Org. Chem.* **1999**, *31*, 143–248.
- [491] C. Joshi, J. M. Macharia, J. A. Izzo, V. Wambua, S. Kim, J. S. Hirschi, M. J. Vetticatt, *ACS Catal.* **2022**, *12*, 2959–2966.
- [492] K.-Y. Kuan, D. A. Singleton, *J. Org. Chem.* **2021**, *86*, 6305–6313.
- [493] L. van Dijk, R. Ardkhean, M. Sidera, S. Karabiyikoglu, Özlem Sari, T. D. W. Claridge, G. C. Lloyd-Jones, R. S. Paton, S. P. Fletcher, *Nat. Catal.* **2021**, *4*, 284–292.
- [494] H. A. Sharma, K. M. Mennie, E. E. Kwan, E. N. Jacobsen, *J. Am. Chem. Soc.* **2020**, *142*, 16090–16096.
- [495] J. N. Sanders, H. Jun, R. A. Yu, J. L. Gleason, K. N. Houk, *J. Am. Chem. Soc.* **2020**, *142*, 16877–16886.
- [496] J. A. Gonzalez, O. M. Ogba, G. F. Morehouse, N. Rosson, K. N. Houk, A. G. Leach, P. H.-Y. Cheong, M. D. Burke, G. C. Lloyd-Jones, *Nat. Chem.* **2016**, *8*, 1067–1075.

- 
- [497] L. Li, V. S. Lelyveld, N. Prywes, J. W. Szostak, *J. Am. Chem. Soc.* **2016**, *138*, 3986–3989.
- [498] F. M. Wong, J. Wang, A. C. Hengge, W. Wu, *Org. Lett.* **2007**, *9*, 1663–1665.
- [499] G. Speciale, M. Farren-Dai, F. S. Shidmoosavee, S. J. Williams, A. J. Bennet, *J. Am. Chem. Soc.* **2016**, *138*, 14012–14019.
- [500] T. Humphry, S. Iyer, O. Iranzo, J. R. Morrow, J. P. Richard, P. Paneth, A. C. Hengge, *J. Am. Chem. Soc.* **2008**, *130*, 17858–17866.
- [501] D. Xie, Y. Zhou, D. Xu, H. Guo, *Org. Lett.* **2005**, *7*, 2093–2095.
- [502] K. C. Westaway, Y. Fang, S. MacMillar, O. Matsson, R. A. Poirier, S. M. Islam, *J. Phys. Chem. A* **2007**, *111*, 8110–8120.
- [503] Y. Fang, S. MacMillar, J. Eriksson, M. Kołodziejska-Huben, A. Dybała-Defratyka, P. Paneth, O. Matsson, K. C. Westaway, *J. Org. Chem.* **2006**, *71*, 4742–4747.
- [504] Z. S. Jia, J. Rudziński, P. Paneth, A. Thibblin, *J. Org. Chem.* **2002**, *67*, 177–181.
- [505] E. M. Simmons, J. F. Hartwig, *Angew. Chem. Int. Ed.* **2012**, *51*, 3066–3072.
- [506] D. A. Singleton, A. A. Thomas, *J. Am. Chem. Soc.* **1995**, *117*, 9357–9358.
- [507] G. C. Lloyd-Jones, S. C. Stephen, *Chem. Eur. J.* **1998**, *4*, 2539–2549.
- [508] S. E. Baker, A. B. Serafim, P. Morales-Agudelo, M. Vidal, A. M. Calafat, M. Ospina, *Anal. Bioanal. Chem.* **2019**, *411*, 669–678.
- [509] P. Kuklenyik, S. E. Baker, A. M. Bishop, P. Morales-A, A. M. Calafat, *Anal. Chim. Acta* **2013**, *787*, 267–273.
- [510] Z.-F. Chen, G.-G. Ying, H.-J. Lai, F. Chen, H.-C. Su, Y.-S. Liu, F.-Q. Peng, J.-L. Zhao, *Anal. Bioanal. Chem.* **2012**, *404*, 3175–3188.
- [511] A. O. Olsson, S. E. Baker, J. V. Nguyen, L. C. Romanoff, S. O. Udunka, R. D. Walker, K. L. Flemmen, D. B. Barr, *Anal. Chem.* **2004**, *76*, 2453–2461.
- [512] S. Jankowski, *Annu. Rep. NMR Spectrosc.* **2009**, *68*, 149–191.
- [513] P. A. Cox, M. Reid, A. G. Leach, A. D. Campbell, E. J. King, G. C. Lloyd-Jones, *J. Am. Chem. Soc.* **2017**, *139*, 13156–13165.
- [514] C. P. Johnston, T. H. West, R. E. Dooley, M. Reid, A. B. Jones, E. J. King, A. G. Leach, G. C. Lloyd-Jones, *J. Am. Chem. Soc.* **2018**, *140*, 11112–11124.
- [515] A. García-Domínguez, T. H. West, J. J. Primozic, K. M. Grant, C. P. Johnston, G. G. Cumming, A. G. Leach, G. C. Lloyd-Jones, *J. Am. Chem. Soc.* **2020**, *142*, 14649–14663.

- 
- [516] C. Amatore, S. Gamez, A. Jutand, G. Meyer, L. Mottier, *Electrochim. Acta* **2001**, *46*, 3237–3244.
- [517] C. Amatore, S. Gamez, A. Jutand, *Chem. Eur. J.* **2001**, *7*, 1273–1280.
- [518] C. Amatore, A. A. Bahsoun, A. Jutand, L. Mensah, G. Meyer, L. Ricard, *Organometallics* **2005**, *24*, 1569–1577.
- [519] G. Chelucci, G. A. Pinna, A. Saba, R. Valenti, *Tetrahedron: Asymmetry* **2000**, *11*, 4027–4036.
- [520] P. Dierkes, S. Ramdeehul, L. Barloy, A. D. Cian, J. Fischer, P. C. J. Kamer, P. W. N. M. van Leeuwen, J. A. Osborn, *Angew. Chem. Int. Ed.* **1998**, *37*, 3116–3118.
- [521] J. M. Brown, D. I. Hulmes, P. J. Guiry, *Tetrahedron* **1994**, *50*, 4493–4506.
- [522] B. M. Trost, K. Dogra, *J. Am. Chem. Soc.* **2002**, *124*, 7256–7257.
- [523] N. Mardirossian, M. Head-Gordon, *J. Chem. Phys.* **2016**, *144*, 214110.
- [524] J. D. Rolfes, F. Neese, D. A. Pantazis, *J. Comput. Chem.* **2020**, *41*, 1842–1849.
- [525] V. Barone, M. Cossi, *J. Phys. Chem. A* **1998**, *102*, 1995–2001.
- [526] E. Wigner, *Phys. Rev.* **1932**, *40*, 749–759.
- [527] G. M. DiRenzo, P. S. White, M. Brookhart, *J. Am. Chem. Soc.* **1996**, *118*, 6225–6234.
- [528] L. Munjanja, C. Torres-López, W. W. Brennessel, W. D. Jones, *Organometallics* **2016**, *35*, 2010–2013.
- [529] H. Ryu, J. Park, H. K. Kim, J. Y. Park, S.-T. Kim, M.-H. Baik, *Organometallics* **2018**, *37*, 3228–3239.
- [530] Y. Ping, K. Wang, Q. Pan, Z. Ding, Z. Zhou, Y. Guo, W. Kong, *ACS Catal.* **2019**, *9*, 7335–7342.
- [531] T. Xavier, S. Condon, C. Pichon, E. L. Gall, M. Presset, *Beilstein J. Org. Chem.* **2021**, *47*, 2085–2094.
- [532] G. R. Fulmer, A. J. M. Miller, N. H. Sherden, H. E. Gottlieb, A. Nudelman, B. M. Stoltz, J. E. Bercaw, K. I. Goldberg, *29*, 2176–2179.
- [533] E. H. P. Tan, G. C. Lloyd-Jones, J. N. Harvey, A. J. J. Lennox, B. M. Mills, *50*, 9602–9606.

---

# List of Abbreviations

APCI	atmospheric pressure chemical ionization
ATR	attenuated total reflection
b.p.	boiling point
br.	broad
BSA	<i>N,O</i> -bis(trimethylsilyl)acetamide
COD	1,5-cyclooctadiene
conc.	concentrated
COSY	correlation spectroscopy
d	doublet
DACH	1,2-diaminocyclohexane- <i>N,N'</i> -bis(2-diphenylphosphinobenzoyl)
dba	dibenzylideneacetone
DEET	<i>N,N</i> -diethyl- <i>meta</i> -toluamide
DFT	density functional theory
DMF	dimethylformamide
dmphen	2,9-dimethyl-1,10-phenanthroline (neocuproine)
DMSO	dimethyl sulfoxide
dppe	1,2-bis(diphenylphosphino)ethane
d.r.	diastereomeric ratio
DYKAT	dynamic kinetic asymmetric transformation
DKR	dynamic kinetic resolution
EDG	electron donating group
e.e.	enantiomeric excess
ESI	electrospray ionization
equiv.	equivalent(s)
EXSY	exchange spectroscopy
EWG	electron withdrawing group
HMBC	heteronuclear multiple bond correlation
HRMS	high resolution mass spectroscopy
HSQC	heteronuclear single quantum coherence
IR	infrared
HMDS	bis(trimethylsilyl)amide
KIE	kinetic isotope effect
LC-MS	liquid chromatography coupled with mass spectrometry

---

<b>LG</b>	leaving group
<b>m</b>	multiplet
<b>MS</b>	molecular sieve
<b>MTBE</b>	methyl <i>tert</i> -butyl ether
<b>NBS</b>	<i>N</i> -bromosuccinimide
<b>NHC</b>	<i>N</i> -heterocyclic carbene
<b>NMR</b>	nuclear magnetic resonance
<b>Nu</b>	nucleophile
<b>PEA</b>	1-phenylethylamine
<b>PHOX</b>	phosphinooxazoline
<b>ppm</b>	parts per million
<b>ψt</b>	pseudo triplet
<b>q</b>	quartet
<b>ROESY</b>	rotating frame <b>OVERHAUSER</b> effect spectroscopy
<b>RPKA</b>	reaction progress kinetic analysis
<b>RT</b>	room temperature
<b>s</b>	singlet
<b>satd.</b>	saturated
<b>sept</b>	septet
<b>t</b>	triplet
<b>TFA</b>	trifluoroacetic acid
<b>THF</b>	tetrahydrofuran
<b>TLC</b>	thin-layer chromatography
<b>TOF</b>	turnover frequency
<b>UV</b>	ultraviolet



---

# List of Figures

4.1	<sup>1</sup> H-NMR monitoring of the model reaction investigated, using ligand <b>L1</b> . . . . .	189
4.2	<sup>1</sup> H-NMR monitoring of the model reaction investigated, using ligand <b>L2</b> . . . . .	190
4.3	Typical temporal concentration profiles for the model reaction investigated . . . . .	191
4.4	Temporal concentration profiles at different Pd–ligand concentrations with <b>L1</b> as ligand and resulting initial rate plot . . . . .	192
4.5	Temporal concentration profiles at different Pd–ligand concentrations with <b>L2</b> as ligand and resulting initial rate plot . . . . .	193
4.6	Temporal concentration profiles at different initial concentrations of substrate with <b>L1</b> as ligand and resulting initial rate plot . . . . .	195
4.7	Temporal concentration profiles at different initial concentrations of substrate with <b>L2</b> as ligand and resulting initial rate plot . . . . .	196
4.8	Temporal concentration profiles at different initial concentrations of nucleophile with <b>L1</b> as ligand and resulting initial rate plot . . . . .	197
4.9	Temporal concentration profiles at different initial concentrations of nucleophile with <b>L2</b> as ligand and resulting initial rate plot . . . . .	198
4.10	Examination of rate order in catalyst by RPKA, using <b>L1</b> as ligand . . . . .	201
4.11	Examination of rate order in catalyst by RPKA, using <b>L2</b> as ligand . . . . .	202
4.12	Examination of rate order in substrate and nucleophile by RPKA, using <b>L1</b> as ligand	203
4.13	Examination of rate order in substrate and nucleophile by RPKA, using <b>L2</b> as ligand	204
4.14	Examination of catalyst deactivation by RPKA, using <b>L1</b> as ligand . . . . .	205
4.15	Examination of catalyst deactivation by RPKA, using <b>L2</b> as ligand . . . . .	206
4.16	Extraction of <sup>2</sup> H-KIE $\frac{k(H)}{k(4-D)}$ by kinetic competition of labeled substrate [4-D]- <i>cis</i> -1 against unlabeled <i>cis</i> -1 with <b>L1</b> as ligand . . . . .	210
4.17	Extraction of <sup>2</sup> H-KIE $\frac{k(H)}{k(4-D)}$ by kinetic competition of labeled substrate [4-D]- <i>cis</i> -1 against unlabeled <i>cis</i> -1 with <b>L2</b> as ligand . . . . .	211
4.18	Extraction of <sup>2</sup> H-KIE $\frac{k(H)}{k(5-D,3-D)}$ by kinetic competition of labeled substrates [5-D]/[3-D]- <i>cis</i> -1 against unlabeled <i>cis</i> -1 with <b>L1</b> as ligand . . . . .	212
4.19	Extraction of <sup>2</sup> H-KIE $\frac{k(H)}{k(5-D,3-D)}$ by kinetic competition of labeled substrates [5-D]/[3-D]- <i>cis</i> -1 against unlabeled <i>cis</i> -1 with <b>L2</b> as ligand . . . . .	213
4.20	Extraction of relative <sup>2</sup> H-KIE $\frac{k(5-D)}{k(3-D)}$ by analyzing the competing consumption of labeled substrate isotopomers [5-D]- <i>cis</i> -1 and [3-D]- <i>cis</i> -1 and the competing formation of product isotopomers [5-D]- <i>trans</i> - <b>3a</b> and [3-D]- <i>trans</i> - <b>3a</b> from labeled substrate [5-D]/[3-D]- <i>cis</i> -1 with <b>L1</b> as ligand . . . . .	215

---

4.21	Extraction of relative $^2\text{H}$ -KIE $\frac{k(5\text{-D})}{k(3\text{-D})}$ by analyzing the competing consumption of labeled substrate isotopomers [5-D]- <i>cis</i> - <b>1</b> and [3-D]- <i>cis</i> - <b>1</b> and the competing formation of product isotopomers [5-D]- <i>trans</i> - <b>3a</b> and [3-D]- <i>trans</i> - <b>3a</b> from labeled substrate [5-D]/[3-D]- <i>cis</i> - <b>1</b> with <b>L2</b> as ligand . . . . .	216
4.22	Extraction of $^{13}\text{C}$ -KIE $\frac{k(\beta\text{-}^{13}\text{C})}{k(\alpha\text{-}^{13}\text{C})}$ by kinetic competition of labeled nucleophile [ $\alpha\text{-}^{13}\text{C}$ ]-Na- <b>2a</b> against reference isotopomer [ $\beta\text{-}^{13}\text{C}$ ]-Na- <b>2a</b> with <b>L1</b> as ligand . . .	218
4.23	Extraction of $^{13}\text{C}$ -KIE $\frac{k(\beta\text{-}^{13}\text{C})}{k(\alpha\text{-}^{13}\text{C})}$ by kinetic competition of labeled nucleophile [ $\alpha\text{-}^{13}\text{C}$ ]-Na- <b>2a</b> against reference isotopomer [ $\beta\text{-}^{13}\text{C}$ ]-Na- <b>2a</b> with <b>L2</b> as ligand . . .	219

---

# List of Schemes

1.1	General strategies for the synthesis of optically active products . . . . .	1
2.1	General reaction scheme of a transition metal catalyzed allylic substitution . . . . .	5
2.2	Transition metal catalyzed decarboxylative allylic substitution . . . . .	7
2.3	Steric influence of substituents on the regioselectivity . . . . .	8
2.4	Electronic influence of substituents on the regioselectivity . . . . .	8
2.5	Influence of double bond configuration on the regioselectivity . . . . .	9
2.6	Preference for linear or branched products . . . . .	11
2.7	Regiochemical retention observed in Fe- and Rh-catalyzed allylic substitution chemistry . . . . .	11
2.8	Regiodivergent Fe-catalyzed allylic alkylation . . . . .	12
2.9	Partial regiochemical retention observed in Pd-catalyzed allylic substitutions in the presence of chloride . . . . .	13
2.10	General stereochemical mechanism of the transition metal catalyzed allylic substitution . . . . .	15
2.11	Stereochemical mechanism for the Rh-catalyzed allylic substitution . . . . .	16
2.12	Stereochemical mechanism for the Mo-catalyzed allylic substitution . . . . .	16
2.13	Isomerization of $\eta^3$ -intermediates via $S_N2$ -like displacement with free catalyst . . . . .	17
2.14	Formation of a <i>syn</i> -configured $\eta^3$ -intermediate by means of a directing group . . . . .	18
2.15	Oxidative addition under retention promoted by a coordinating leaving group . . . . .	18
2.16	Inverted stereospecificity by using a sterically biased substrate . . . . .	19
2.17	Transition metal catalyzed isomerization of allylic acetates . . . . .	20
2.18	Example for differentiation of enantiotopic olefin faces by Ir-catalyzed allylic alkylation . . . . .	23
2.19	Example for differentiation of enantiotopic leaving groups by Pd-catalyzed allylic substitution . . . . .	23
2.20	Example for differentiation of enantiotopic allylic faces by intermediate $\pi$ - $\sigma$ - $\pi$ interconversion in a Pd-catalyzed allylic substitution . . . . .	24
2.21	Example for differentiation of enantiotopic allylic termini by Pd-catalyzed allylic alkylation . . . . .	24
2.22	Pd-catalyzed asymmetric allylic alkylation of ( <i>rac</i> )-1,3-diphenylallyl acetate with various ligands . . . . .	25

2.23	Example for differentiation of enantiotopic faces of a prochiral nucleophile by Pd-catalyzed allylic alkylation . . . . .	26
2.24	Wall-and-flap model developed by TROST and coworkers rationalizing the enantioselectivity of Pd-catalyzed allylic substitutions with DACH-type ligands . . . . .	28
2.25	Structural model disclosed by LLOYD-JONES, NORRBY and coworkers rationalizing the enantioselectivity of Pd-catalyzed allylic substitutions with DACH-type ligands . . . . .	28
2.26	General model for the enantioselectivity of Pd–PHOX catalyzed allylic substitutions . . . . .	29
2.27	Summary of mechanistic studies on the enantioselectivity of Pd–PHOX catalyzed allylic substitutions, using the 1,3-diphenylallyl model system with the <i>i</i> PrPHOX ligand . . . . .	30
2.28	Pd-catalyzed asymmetric allylic alkylation of 2-oxabicyclo[2.2.0]hex-5-en-3-one . . . . .	32
2.29	Pd-catalyzed asymmetric allylic alkylation of 4-chlorocyclobut-2-ene carboxylic acid and corresponding esters . . . . .	33
2.30	Preparation of $\eta^1$ -coordinated Pd–cyclobutene complexes ligated by the PhPHOX ligand . . . . .	34
2.31	Preparation of $\eta^1$ -coordinated Pd–cyclobutene complexes ligated by phosphoramidite ligands . . . . .	35
2.32	Pd-catalyzed asymmetric allylic alkylation of cyclobutene substrates with hard nucleophiles . . . . .	36
3.1	Pd-catalyzed asymmetric allylic alkylation of cyclobutene substrates <b>1</b> as reaction of interest . . . . .	39
4.1	Synthesis of cyclobutene substrates <b>1</b> . . . . .	44
4.2	Synthesis of deuterated cyclobutene substrates [4-D]- <b>1</b> . . . . .	45
4.3	Synthesis of deuterated cyclobutene substrates [5-D]/[3-D]- <b>1</b> . . . . .	46
4.4	Isolation of malonate salts Na- <b>2</b> . . . . .	48
4.5	Synthesis of labeled malonates <b>2a</b> and transformation into their sodium salts . . . . .	48
4.6	Preliminary mechanism proposed for the Pd-catalyzed asymmetric allylic alkylation of cyclobutene substrates <b>1</b> with stabilized nucleophiles Na- <b>2</b> . . . . .	52
4.7	Unsuccessful attempt to prepare a Pd–malonate complex . . . . .	186
4.8	$\beta$ - and $\delta$ -hydride elimination as potential side reactions in allylic alkylations with malonate nucleophile Na- <b>2a</b> , provided an inner-sphere mechanism is operative . . . . .	187
4.9	Labeling studies with deuterated malonate nucleophile [D <sub>3</sub> ]-Na- <b>2a</b> . . . . .	187
4.10	Workflow for RPKA performed in this work . . . . .	199
4.11	Apparent rate orders extracted . . . . .	207
4.12	Overview of experimental <sup>2</sup> H- and <sup>13</sup> C-KIEs . . . . .	221
4.13	S <sub>N</sub> 2- and S <sub>N</sub> 2'-type oxidative addition and corresponding <sup>2</sup> H-KIEs expected for the allylic termini . . . . .	222

---

4.14	General scenarios for a DYKAT . . . . .	222
4.15	Scrambling of the allylic termini upon $\eta^1$ - $\eta^3$ - $\eta^1$ isomerization and expected magnitudes of the relative KIE $\frac{k(5-D)}{k(3-D)}$ observed . . . . .	223
4.16	Mechanistic scenarios considered for C–C bond formation with ligand <b>L1</b> . . . . .	226
4.17	Mechanistic scenarios considered for C–C bond formation with ligand <b>L2</b> . . . . .	227
5.1	Overarching mechanism proposed for the Pd-catalyzed asymmetric allylic alkylation of cyclobutene substrates <b>1</b> with stabilized nucleophiles Na- <b>2</b> . . . . .	231
6.1	Allgemeiner mechanistischer Vorschlag für die Pd-katalysierte asymmetrische allylische Alkylierung von Cyclobutensubstraten <b>1</b> mit Malonatnucleophilen Na- <b>2</b>	236



---

# List of Tables

2.1	General mechanisms for achieving enantioselectivity in allylic substitution chemistry	22
4.1	Asymmetric allylic alkylation of substrate <i>cis</i> - <b>1</b> with different malonate nucleophiles	184
4.2	Background reactivity in the allylic alkylation of substrate <i>cis</i> - <b>1</b> with different malonate nucleophiles . . . . .	185
7.1	Reaction monitoring runs performed with ligands <b>L1</b> and <b>L2</b> . . . . .	259





---

---

## **Erklärung zur Abschlussarbeit gemäß §23 Abs. 7 APB der TU Darmstadt**

---

### **§8 Abs. 1 lit. c der Promotionsordnung der TU Darmstadt**

Ich versichere hiermit, dass die elektronische Version meiner Dissertation mit der schriftlichen Version übereinstimmt und für die Durchführung des Promotionsverfahrens vorliegt.

### **§8 Abs. 1 lit. d der Promotionsordnung der TU Darmstadt**

Ich versichere hiermit, dass zu einem vorherigen Zeitpunkt noch keine Promotion versucht wurde und zu keinem früheren Zeitpunkt an einer in- oder ausländischen Hochschule eingereicht wurde. In diesem Fall sind nähere Angaben über Zeitpunkt, Hochschule, Dissertationsthema und Ergebnis dieses Versuchs mitzuteilen.

### **§9 Abs. 1 der Promotionsordnung der TU Darmstadt**

Ich versichere hiermit, dass die vorliegende Dissertation selbstständig und nur unter Verwendung der angegebenen Quellen verfasst wurde.

### **§9 Abs. 2 der Promotionsordnung der TU Darmstadt**

Die Arbeit hat bisher noch nicht zu Prüfungszwecken gedient.

Darmstadt, den 30. Oktober 2023

---

Johann J. Primožic

---